UNIVERSITY OF
BIRMINGHAM

ENHANCING PRODUCT DIFFERENTIATION THROUGH DIRECT EXTRUSION ADDITION

by

DMYTRO STRATIYCHUK-DEAR

A thesis submitted to the University of Birmingham for the degree of
DOCTOR OF ENGINEERING

School of Chemical Engineering

College of Engineering and Physical Sciences

University of Birmingham

December 2017

Abstract

The research presented herein outlines the development of *direct extrusion addition* technology for the manufacture of bi-axially oriented Polyethylene Terapthalate (PET) films. The technology enables the additives to be introduced directly into the existing extrusion process without the need to use a pre-dispersed masterbatch. Direct extrusion addition offers routes to faster new product development, improved material properties and reduced manufacturing costs. Critical to success in retrofitting the technology onto existing film lines is achieving the differing dispersion requirements of various products within the constraints of the film line operating window and conventional equipment.

An extensive experimental study was performed utilising Berstorff ZE40A and Dr Collin ZK25 twin screw extruders to manufacture numerous PET based composites. Dispersion of clay, flame retardant, silica, UV stabilising, and whitener additives in film grade (IV of 0.6 $\mathrm{dl\,g^{-1}}$), and bottle grade (IV of 0.8 $\mathrm{dl\,g^{-1}}$) PET substrates was analysed using film surface analysis and/or cross-sectional analysis of pellets (shown to adequately describe the filler dispersion in films). The analysis conducted identified the optimum operating conditions for achieving good dispersion, determined the influence of material properties and the role of machine set up/design on the level of mixing achieved, and established limitations of the powder handling process.

A model of twin screw extrusion process was proposed herein together with novel parameters which are '*residence time weighted average shear rate*, *stress* and *strain*'. These parameters can be utilised to better understand the shear and stress fields within the extruder as well as compare the extrusion processes with differing screw configurations at various operating conditions across various machine sizes.

Polymer viscosity was found to play a critical role in the dispersion of additives. In order to better understand the changes in the molecular weight (hence viscosity) induced

by the extrusion process the measured intrinsic viscosity values (indicator of molecular weight) for the extrudate were compared with those predicted through the modelling of the chemical reactions occurring within the polymer. Two separate regimes were identified with chemically driven molecular weight reduction occurring at low shear stress conditions and mechanically induced chain scission driving the molecular weight reduction at higher shear stresses.

The level of dispersion was found to increase with increasing *total residence time weighted average shear strain*. The results indicated the importance of screw speed and the minimal impact of screw configuration in determining the level of mixing achieved. A compromise between viscosity reduction via mechanically induced chain scission and high shear required for mixing was identified. These results form the basis of a design guide developed for the direct extrusion addition technology.

Acknowledgements

I want to say a huge thank you to my industrial supervisors, Kieran Looney and Paul Oliver, my academic supervisors, Stuart Blackburn and Mark Simmons as well as the course coordinator Richard Greenwood for their support and guidance on all aspects of this project. This thesis would not have been possible without their excellent supervision throughout the four years. I would also like to thank Kieran, Richard, and James Champion for encouraging me to enrol on this excellent programme as it enabled me to grow and develop both the technical and personal aspects of my life.

I want to acknowledge the support that I have received from not only the Process Development Group, lead by John Flett, but also the wider community at DuPont Teijin Films (DTF). In particular, I would like to thank Kieran for the technical support and guidance; Paul for help in composing the business cases for internal investments as well as research at external company, Nanoforce Ltd; and Pierre Moussalli for his help with mathematics of all sorts as well as providing the relaxed work environment to which I have grown so accustomed to. I acknowledge the help I received from and express my gratitude to Karl Rakos and Damian Tuffin for their guidance with white light interferometry and particle sizing; Jessica Nix for training on the optical microscopy as well as numerous electron micrographs that she has collected on my behalf; Allan Lovatt for his wisdom of the pilot scale lines; the Wilton Semi-Tech team for running the lines during my numerous experiments and collecting hand wound samples; as well as Sean Shortall and his team for generating an extensive collection of intrinsic viscosity data presented within this thesis. I also wish to thank Kieran, Paul, Karl and Stuart for being great company on numerous business trips which have enabled me to experience a wide array of technical and commercial aspects of the business.

I express my appreciation to Nanoforce Ltd. for their collaboration and allowing me to utilise their lab scale equipment to manufacture a number of polymer composites through

the course of numerous experiments. In particular, I want to thank Wei Tu for his technical guidance as well as Wei and Olivier Picot for their help in running the lab scale line.

I want to also thank DuPont Teijin Films, the University of Birmingham and the Engineering and Physical Sciences Research Council for providing we with the funding and the platform to conduct my research. I also thank the numerous suppliers who have provided samples of their materials for me to investigate.

I thank my brother, Danny, mother, Mariya, and father, Peter for providing support and encouragement through the years as well as numerous memorable weekends back down in Southampton and up in Teesside. Last but by no means least, I would like to thank the other key people in my life Kristina Blinova, Amy Seaman, Toby Meatyard, James Champion and Deryck Li for allowing me to unwind and maintain a work life balance.

Table of Contents

List of Figures

List of Tables

Abbreviations

Abbreviation	Definition
BHET	bis-hydroxyethyl terephtalate (PET monomer)
CEG	Carboxyl end group
CFD	Computational fluid dynamics
Co-TSE	Co-rotating twin screw extruder
DA	Direct to melt addition
DEG	In chain diethylene glycol
DOF	Degree of fill (within the extruder)
DMT	Dimethyl Terephthalate
DTF	DuPont Teijin Films U.K. Ltd.
EG	Ethylene glycol
FEM	Finite element method
FR	Flame retardant
GPC	Gas phase chromatography
HDPE	High density polyethylene
HEG	Hydroxyl end group
HME	Hot melt extrusion
IV	Intrinsic viscosity
KB	Kneading block (array of kneading disks)
KD	Kneading disk
LEO	Laser engravable overlay
MB	Masterbatch
PET	Polyethylene Terephthalate
PEN	Polyethylene Naphthalate
PLA	Polylactic acid
MD	Machine direction
MMD	Multi-manifold die
MW	Molecular weight
OLED	Organic light emitting diode
PIDS	Polarising intensity differential scattering
PPM	parts per million
PSD	Particle size distribution
PV	Photovoltaic
PVC	Polyvinyl chloride
RPM	Revolutions per minute
RTD	Residence time distribution
SEM	Scanning electron microscopy
SME	Specific mechanical energy
SSE	Single screw extruder
TA	Terephthalic acid
TD	Transverse direction
TEM	Transmission electron microscopy

Abbreviation	Definition
TME	Toothed mixing element
TSE	Twin screw extruder
UV	Ultraviolet
WLI	White light interferometry
2-D	Two dimensional space
3-D	Three dimensional space

Nomenclature

Extrusion parameters - geometry

Symbol	Unit	Definition
A_1	mm^2	Channel cross sectional area for unwound channel when fully filled
$A_{1,DOF}$	mm^2	Channel cross sectional area for unwound channel when partially filled
A_2	mm^2	Over the flight cross sectional area for unwound channel
$A_{t,DOF}$	mm^2	Total cross sectional area for unwound channel when partially filled, $A_{t,DOF} = A_{1,DOF} + A_2$
$A_{t,FF}$	mm^2	Total cross sectional area for unwound channel when fully filled, $A_{t,FF} = A_{1,FF} + A_2$
a	mm	Centre line distance
a_{min}	mm	Minimum centre line distance
a_1 to a_7		Constants for 6^{th} order polynomial representing channel height
b	mm	Channel width
D_b	mm	Barrel diameter
D_i	mm	Inside screw diameter
D_o	mm	Outside screw diameter
e	mm	Flight width
EF	%	Screw forwarding efficiency
$\bar{H}$	mm	Mean channel height for a partially filled channel excluding clearance
$H_{av,DOF}$	mm	Mean channel height for a partially filled channel including clearance
$H_{av,FF}$	mm	Mean channel height for a fully filled channel
H_i	mm	Intermeshing height
H_{CH}	mm	Channel height at deepest point, $H(x)$ and $H(\theta) = 0$
H_{CL}	mm	Clearance between the screw flight and barrel surface
$H(x)$	mm	Channel height as function of cross channel distance (unwound channel) in Cartesian coordinates
$H(\theta)$	mm	Channel height as function of rotation in Polar coordinates
j_{KD}	mm	Number of kneading discs in kneading block
L_{eq}	mm	Axial length of unwound channel excluding the intermeshing region
L_{KB}	mm	Length of kneading block
L_s	mm	Axial length of screw being considered
p		Number of threads on screw
SV	cm^3 per diameter of length	Specific volume

Symbol	Unit	Definition
SG		Specific gravity
t	mm	Screw pitch
t_{KB}	mm	Equivalent screw pitch in the kneading block section
V_B	$\mathrm{mm\,s^{-1}}$	Barrel velocity
x_f	mm	Location of the polymer front in the screw channel
z_w		Number of screw shafts
α	$\mathrm{m^3\,rev^{-1}}$	Constant (conveying capacity of screw element)
α_f	rad	Flight flank angle
α_i	rad	Intermeshing angle
α_r	rad	Flight root angle
α_t	rad	Flight tip angle
β	$\mathrm{m^4\,Pa\,s\,bar^{-1}\,h^{-1}}$	Constant (conveying capacity of screw element)
ϕ	$^\circ$ or rad	Helix angle
ω	rad	Kneading disk stagger angle

Extrusion parameters - process

Symbol	Unit	Definition
f		Degree of fill (expressed as a fraction)
F	%	Torque
F_{max}	N	Maximum force applied by flow
$\dot{m}$	$\mathrm{kg\,h^{-1}}$	Throughout
N	rpm	Screw speed
N_m	rpm	Maximum screw speed
P	Pa *or* bar	Pressure
P_e	Pa *or* bar	Extruder delivery pressure
P_{app}	kW	Applied power
P_w	kW	Drive rated power
$\dot{Q}$	$\mathrm{m^{-3}\,h^{-1}}$	Volumetric flow rate
SME	$\mathrm{kW\,h\,kg^{-1}}$	Overall specific mechanical energy input
SME_e	kJ	Element mechanical energy input
SME_z	kJ	Zone mechanical energy input
t	s	time
$\dot{\varepsilon}$	$\mathrm{s^{-1}}$	Extensional strain rate
$\dot{\gamma}$	$\mathrm{s^{-1}}$	Shear rate
$\dot{\gamma}_{av,DOF}$	$\mathrm{s^{-1}}$	Mean shear rate in a partially filled screw channel
$\dot{\gamma}_{av,FF}$	$\mathrm{s^{-1}}$	Mean shear rate in a fully filled screw channel
$\dot{\gamma}_{av,RTD}$	$\mathrm{s^{-1}}$	Residence time weighted average of the mean channel shear rate
$\dot{\gamma}_{min}$	$\mathrm{s^{-1}}$	Minimum shear rate in the centre of the screw channel
$\dot{\gamma}_{max}$	$\mathrm{s^{-1}}$	Maximum shear rate in the clearance between screw flight and barrel

Symbol	Unit	Definition
$\dot{\gamma}(x)$	s^{-1}	Shear rate as function of cross channel distance (unwound channel) in Cartesian coordinates
λ		Ratio of the rate of strain to vorticity tensor used as a measure of the nature of flow
σ	Pa	Shear stress
$\sigma_{av,DOF}$	Pa	Mean shear stress in a partially filled screw channel
$\sigma_{av,FF}$	Pa	Mean shear stress in a fully filled screw channel
$\sigma_{av,RTD}$	Pa	Residence time weighted average of the mean channel shear stress
σ_h	Pa	Hydrodynamic stress
σ_{min}	Pa	Minimum shear stress in the centre of the screw channel
σ_{max}	Pa	Maximum shear stress in the clearance between screw flight and barrel
$\sigma(x)$	Pa	Shear stress as function of cross channel distance (unwound channel) in Cartesian coordinates
τ	s	Overall residence time
τ_e	s	Element residence time
τ_z	s	Zone residence time
Ψ		Return fraction (number of times polymer passes though the high shear region)

Calculation of mass transfer area for degassing

Symbol	Unit	Definition
A_{front}	m^2	Area of polymer front exposed to the environment
A_{film}	m^2	Area polymer film on barrel surface exposed to the environment
A_c	m^2	Surface area of a polymer chip
A_{MT}	m^2	Mass transfer area exposed to the environment
$A_{TOT,c}$	m^2	Total surface area fur the number of polymer chips being considered
CN		Number of polymer chips being considered
L_z	m	Length of zone being considered
RN		Refresh rate of area exposed to the environment
R_c	m	Radius of a polymer chip
R_{ME}	m	Radius of a polymer chip with an equivalent mass transfer area
V_c	m^3	Volume of a polymer chip
N_a		Numerical aperture
UL	µm	Upper limit for a distribution bin
p_i		Probability of finding a particle in a given distribution bin

Symbol	Unit	Definition
λ	µm	Wavelength of light (0.55 µm mid spectrum)
σ_{sd}	µm	Standard deviation of a dataset

Image analysis

Symbol	Unit	Definition
A_agg	μm^2	Area of agglomerates
A_r		Area ratio
A_r	μm^2	Total area of image
D_f	µm	Feret diameter
D_p	µm	Projected area equivalent diameter
$\bar{D}_p$	µm	Mean projected area equivalent diameter
LL	µm	Lower limit for a distribution bin
N_a		Numerical aperture
UL	µm	Upper limit for a distribution bin
p_i		Probability of finding a particle in a given distribution bin
R_a	µm	Mean arithmetic surface roughness
λ	µm	Wavelength of light (0.55 µm mid spectrum)
σ_{sd}	µm	Standard deviation of a dataset

Material properties

Symbol	Unit	Definition
D_p	µm	Nominal particle diameter
D_{10}	µm	Diameter at 10^{th} percentile of the distribution
D_{50}	µm	Median diameter at 50^{th} percentile of the distribution
D_{90}	µm	Diameter at 90^{th} percentile of the distribution
$D_{[1,0]}$	µm	Arithmetic mean diameter
$D_{[2,0]}$	µm	Number-surface mean diameter
$D_{[3,0]}$	µm	Number-volume mean diameter
$D_{[3,2]}$	µm	Surface area moment mean diameter
$D_{[4,3]}$	µm	Volume moment mean diameter
L_p	µm	Nominal particle length
M_n	$\mathrm{g\,mol^{-1}}$	Number average molecular weight
M_w	$\mathrm{g\,mol^{-1}}$	Weight average molecular weight
r	µm	Particle radius
T_m	°C	Melting point temperature
T_g	°C	Glass transition temperature
$W_{Ad,PET}$	$\mathrm{mN\,m^{-1}}$	Work of adhesion between the additive and PET polymer

Symbol	Unit	Definition
$[\eta]$	$\mathrm{dL\,g^{-1}}$	Intrinsic viscosity (IV)
η	$\mathrm{Pa\,s}$	Shear viscosity
η_0	$\mathrm{Pa\,s}$	Zero shear viscosity
ρ	$\mathrm{kg\,m^{-3}}$	Density
ρ_b	$\mathrm{kg\,m^{-3}}$	Bulk density
$\rho_b t$	$\mathrm{kg\,m^{-3}}$	Tapped bulk density
ρ_m	$\mathrm{kg\,m^{-3}}$	Melt density
ρ_p	$\mathrm{kg\,m^{-3}}$	Particle density
ρ_s	$\mathrm{kg\,m^{-3}}$	Solid density
S_A	$\mathrm{m^2\,g^{-1}}$	Surface area
Γ	$\mathrm{mN\,m^{-1}}$	Surface tension (liquid) or surface free energy (solid)
Γ_{Ad}	$\mathrm{mN\,m^{-1}}$	Surface tension (liquid) or surface free energy (solid) of an additive
Γ^d_{Ad}	$\mathrm{mN\,m^{-1}}$	Dispersive component of surface tension (liquid) or surface free energy (solid) of an additive
Γ^p_{Ad}	$\mathrm{mN\,m^{-1}}$	Polar component of surface tension (liquid) or surface free energy (solid) of an additive
$\sigma^p_{Ad,DI}$	$^\circ$	Contact angle between the additive and diiodomethane
$\sigma^p_{Ad,W}$	$^\circ$	Contact angle between the additive and water

1 Introduction

This thesis outlines some of the challenges associated with, and provides the key learning outcomes gained from, the quest to develop retrofitable *direct extrusion addition* technology for bi-axially oriented film manufacturing lines. Successful implementation of the technology would enable the additives to be introduced directly into the polymer during film manufacture without the need for a pre-dispersed masterbatch. During the development various aspects were considered ranging from material handling to the twin screw extrusion process itself. The research focuses on understanding the different mixing mechanisms, in particular how these are affected by the material properties, operating conditions and machine set up/design. This was achieved through extensive practical research which encompassed manufacture of various polymer composites on two separate twin screw extruders as well as modelling of the twin screw extrusion process. The research has been conducted on behalf of DuPont Teijin Films Ltd. in collaboration with the University of Birmingham and Nanoforce Ltd.

1.1 Company overview

DuPont Teijin Films Ltd. (DTF) was established in the year 2000 as a 50:50 joint venture between E.I. du Pont de Nemours and Teijin Ltd. DTF is a world leading producer of polyester films and supplies various markets including *Capacitors, Cards, Digital Media & Labels, Flexible Electronics, Packaging*, and *Photovoltaics*. Trusted brands including Melinex® and Mylar® contribute to the company's vast product portfolio. DTF achieved a turnover of $1.2 billion (LTM 2Q2017), has a global production capacity of 277,000 tonnes and employs around 2,400 personnel (IVL, 2017).

The business is highly technology driven and is constantly striving to find new innovative products as well as develop its current portfolio. An innovation spend of over $30 million has resulted in over 200 patents covering film, process and propriety technologies (DTF,

2013). The company employs around 200 engineers and scientists who are based in the Global R&D facility located in Wilton U.K. and Regional Technical Centres in USA. Their success in the U.K. has been recognised with DTF being awarded Queens Award for Enterprise and Innovation in 2005, 2008 and 2011 for the development of ID card, display technology and photovoltaic backsheet films.

1.2 Project drivers and background

Manas-Zloczower and Cheng (1996) outlined how the development of polymeric materials with improved properties has become reliant on blending and compounding of polymers rather than the development of new chemical structures. This is true for DTF, with the basic chemistry of the various products being very similar; utilising *homo-* and *copolymers* of *Polyethylene Terephthalate (PET)* and *Polyethylene Naphthalate (PEN)*. The use of organic additives, inorganic colloidal particles and various coatings in/on the film allow for the modification of its bulk and/or surface properties enabling the film to be tailored to a particular application. Examples of the different applications for DTF films as well as the requirements of these are discussed *on p.39* in MacDonald (2002). Further differentiation of the products can be realised through the use of *co-extrusion* technology which enables the production of *multi-layered* films where the individual layers have a unique polymer/additive recipe.

The additives are incorporated into the film in one of two ways; via the design and manufacture of specialised polymer or by the addition of a *masterbatch*, a concentrated additive dispersed in a polymer substrate. The concentrated masterbatch can sometimes be manufactured via a batch polymer process or more commonly manufactured via compounding at a reduced cost but at the expense of lowering the molecular weight of the base polymer. It can be purchased as an 'off-the-shelf' solution based on the active ingredient or a 'bespoke' product can be compounded allowing for a degree of control over its formulation. The manufacture of a bespoke product is very time consuming and incurs an increased

cost relative to an off-the-shelf product.

As the industry is being driven to produce new products with more complex film structures; DTF needs to gain the ability to rapidly differentiate its polymers. The project aims to develop a cost-effective retrofitable technology, referred to as *direct addition technology*, that would allow the additives to be incorporated directly into the film during the filming process. By eliminating the need for specialised polymer manufacture or the use of masterbatch their associated manufacturing costs can be reduced. Further benefits of direct addition technology include elimination of low MW polymer (leading to improved mechanical properties), the removal of inappropriate dispersing aids (addressing safety concerns & end product issues) and future proofing of recipes. Direct addition could save anywhere from 1 to 3 month in product development time for each potential additive by eliminating the masterbatch manufacturing time. Up to a dozen potential additives can be tested during product development; equating to a significant time saving which can be the difference between success or failure by being the first to market or not.

The notion of direct addition technology has been explored by Leistritz GmbH, as outlined by Martin (2012) focusing on the manufacture of Polylactic Acid (PLA) sheet with calcium carbonate ($CaCO_3$) filler added at a loading of 15 and 25 % in order to improve toughness of the polymer. The company suggests many advantages to the technology including the elimination of inappropriate thermal and shear history, removal of pelletising costs and the ability of feeding higher recycle percentage. A successful process showing good dispersion of the filler and improved impact properties of the sheet was established on a pilot scale ZSE-27 MAXX extruder at a throughput, $\dot{m}$ of 40 $\mathrm{kg\,h^{-1}}$ at a screw speed, N of 160 revolutions per minute, (rpm). The machine has a length, L to diameter, D (L/D) ratio of 40. More recent publications by the company suggest a similar process for an orientated PET film line (Leistritz GmbH, 2014).

The above literature is an encouraging proof of concept for the development of technology which is being undertaken as part of this work. The novelty of this project focuses on

developing knowledge of the mixing process for miscible and immiscible blends as well as solid filler particles with varying affinity for the PET matrix. As well as establishing models for predicting the degree of mixing achieved based on additive properties and operating conditions, the work aims to develop the understanding behind the degradation of PET in the extrusion process, with particular focus on the breaking of polymer chains associated with the input of mechanical energy under high shear conditions. Unlike the purpose built technology which is being developed by Leistritz GmbH (2014), that being established in this work has to function within the constraints of the operating window of existing film lines and the limitations of more conventional equipment.

1.3 Project goals

The scope of the work has been subdivided into four sections *Material Properties, Powder Handling, Extrusion* and *Film Characterisation* each dealing with a different aspect of the overall project. The material properties section aims to identify key parameters associated with both the additive and the polymer that have a direct impact on the extent of mixing achieved as well as the extent of polymer degradation. The powder handling section, as the name suggests, will aim to develop a successful additive handling process looking at achieving accurate feeding and transport of materials. The extrusion area will focus on developing an understanding of the mixing phenomena of the different *additive-polymer* systems as well as polymer degradation during processing. Finally, the film characterisation section will aim to develop an effective way of determining the degree of mixing achieved within the film though the use of various measurement techniques. A set of key milestones has been assigned to each area; these are listed below.

1. *Material Properties:*

    (a) Quantify key additive and polymer properties in order to evaluate their impact on the processing of material and the level of mixing achieved in the composite

2. *Powder Handling:*

   (a) Establish the limitations of current feeding systems on the '*semi-tech*' pilot scale facility

   (b) Understand the additive and polymer flow characteristics and how these impact on the equipment design

   (c) Consider how to achieve stable flowrate for different additive material characteristics at a range of concentrations from sub 1 % to more than 20 % over the extruder operating window

3. *Extrusion:*

   (a) Understand the difference in the capability between single (SSE) and twin screw extruder (TSE) technology

   (b) Establish the limitations of current equipment and process design on the semi-tech pilot scale facility, consider impact of: feeding mode; location of injection points; screw design; devolatilisation capability; and filtration

   (c) Develop fundamental understanding of dispersive and distributive mixing mechanisms

      i. Consider different *additive-polymer* systems including miscible fluids, immiscible blends and solid-fluid systems

      ii. Develop models to evaluate the stress and flow fields within the extruder

   (d) Identify how to achieve the required degree of dispersive and distributive mixing under the constraints of the film line operating window

      i. Understand the impact of key material properties on the degree of mixing

      ii. Evaluate the effect of operating conditions including throughput, screw speed and temperature on the extent of mixing

      iii. Develop a screw design to give the required level of mixing

iv. Consider use of appropriate dispersive aids

(e) Understand the mechanisms behind molecular weight loss during extrusion and how to minimise this

4. *Film Characterisation:*

   (a) Identify appropriate measurement techniques for the *quantitative* evaluation of dispersive and distributive mixing in order to ensure that the direct addition is on par with or better than the current masterbatch process

   (b) Ensure that the manufactured film fulfils its core functionality to match the specification set by the customer.

It is recognised that the scope of the work is very broad, hence while the research will be limited to a few example additives discussed later in the report, it strives to lay the framework for developing the direct addition technology process for a broad range of future products.

1.4 Concluding Remarks

As the polymer industry has become more established there has been a shift away from developing novel material chemistry to modification of the existing systems via the use of additives. Currently, these are introduced in the form a bespoke or an off-the-shelf masterbatch which can be very time consuming during product development. The drive from the industry for rapid product differentiation in turn imposes the need for technological development. It is hoped that implementation of the direct extrusion technology will not only reduce the time scales for the new product development but also lead to the reduction of the manufacturing costs and improved product properties.

2 Literature review

This thesis covers a number of different process areas ranging from the film making and compounding processes to the fundamental principles governing mixing. This chapter aims to provide an overview of the areas related to the research presented herein with more specific aspects being introduced as required or provided as additional information in Appendices.

2.1 Introduction to the Polyethylene Terephthalate film making process

The base PET polymer is manufactured in a two stage batch process with the first being the esterification where dimethyl terephthalate (DMT) or terephthalic acid (TA) are reacted with ethylene glycol (EG) in order to produce the PET monomer unit. The nature of the reaction is illustrated in Figure 2.1.

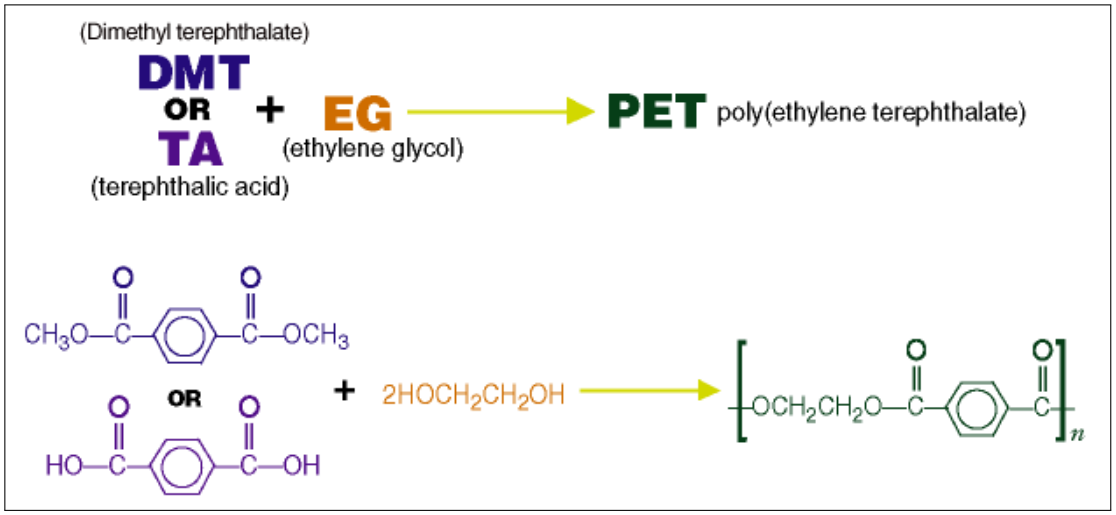

Figure 2.1: *Schematic of the esterificaion reaction (AMPEF, 2002a)*

Reaction utilising DMT as a precursor is carried out at ambient pressure in a presence of a catalyst and results in the formation of methanol which needs to be handled in downstream processing. In the more commonly used TA process, powdered acid is added

to liquid EG at elevated temperature and pressure. The reaction produces water which is distilled out of the reactor mixture resulting in the BHET monomer unit (DTF, 2011) with a viscosity of around 1×10^{-3} to 2×10^{-3} Pa s.

Post esterification the monomer is transferred to the autoclave where it undergoes a polycondensation reaction under vacuum at a temperature of around 280 °C. The reaction results in a polymer with an average chain length of around 100 monomer units with a number average molecular weight, M_n circa 20,000 g mol^{-1} and viscosity of around 150 Pa s. The rotational speed of the stirrer is monitored to evaluate the degree of polymerisation with the reaction being stopped when a certain pre-set value of the stirrer speed is achieved. During the polymerisation reaction ethylene glycol is produced; this is recycled back into the esterification vessel. The polymer is drained out of the reaction vessel though a die to form laces, which are cut into polymer chip and partially dried before blending and being used for the manufacture of film. The chip mass is around 65 mg, dependent on cutter speed, with maximum dimensions of 5 mm × 5 mm × 3 mm. These initial stages as well as the rest of the film manufacturing process can be visualised in Figure 2.2. A large scale continuous polymerisation plant can produce standard polymer at rates in excess of 30 tonnes per hour.

The nature of polymer handling prior to the extrusion process largely depends on the type of extruder being utilised. If single screw extrusion is used the polymer has to be predried at a temperature of about 160 °C for around 4 to 6 hours in order to reduce the moisture content of the chip from circa 3000 ppm to below 30 ppm (MacDonald, 2002). The removal of moisture is necessary to minimise the hydrolysis reaction during the extrusion process which results in chain scission leading to the reduction of polymer molecular weight and intrinsic viscosity (IV). Post drying the chip is often pneumatically conveyed to a hopper located above the extruder. From here the chip is *flood* fed into the feed section of the extruder; for further discussion see Section 2.2.1. Typically the film manufactured contains around 60 % virgin and 40 % recycled polymer. For single screw

extrusion processes, the recycled polymer is preprocessed in order to turn the polymer flake into polymer chip as the low density flake can not be fed directly into a single screw extruder. The selection of the hopper and extruder feed section temperature is critical in order to prevent the sintering of the polymer chip which leads to blockages in the hopper and/or feed pocket preventing the flow of material.

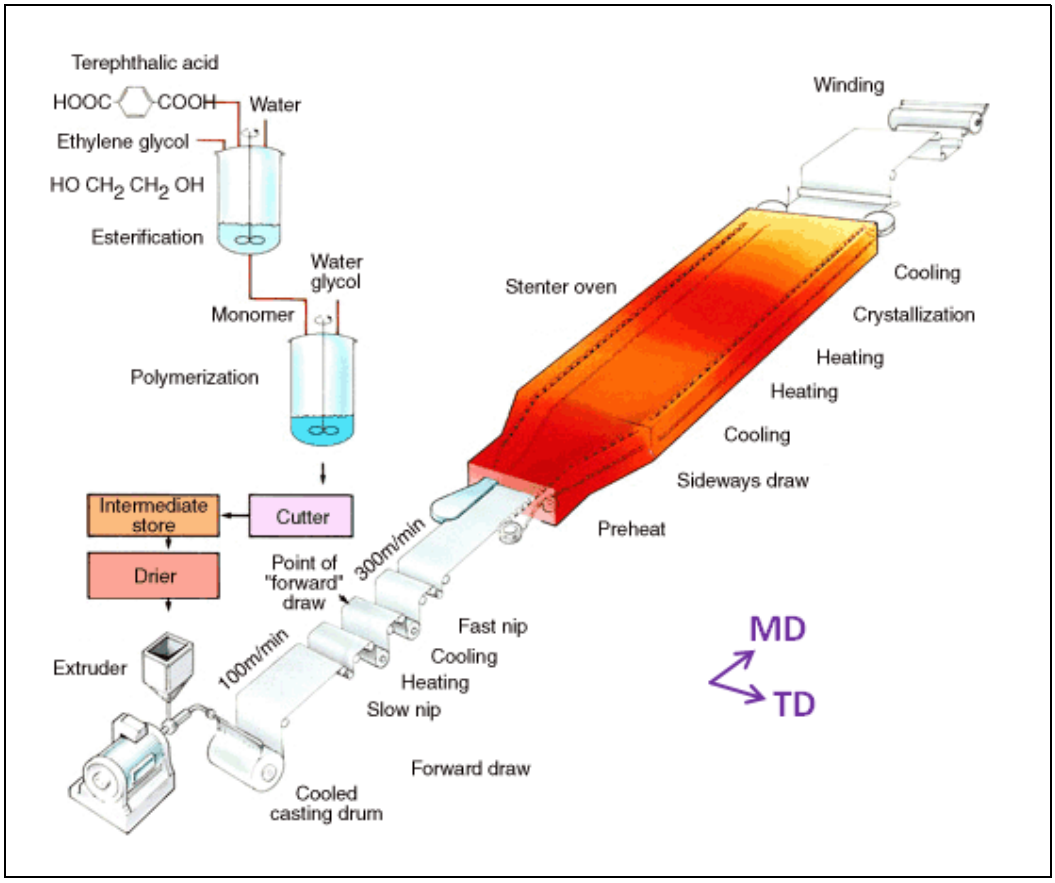

Figure 2.2: *Film process overview; adapted from AMPEF, 2002b*

The use of a twin screw extrusion process enables the processing of undried polymer chip, as the moisture can be removed from the melt through a vacuum degassing port. This type of extruder can also handle polymer flake directly; removing the need to preprocess the polymer flake thus reducing the shear and thermal history of the recycled polymer. The polymer is *starve* fed into the twin screw extrusion process at a rate less than the conveying capacity of the screw, resulting in little interdependence between throughput and screw speed.

If a standard polymer is being utilised and fillers are required to modify the bulk properties of the film, they are introduced in a form of masterbatch chip into the extrusion process. In twin screw process a separate feeding system is employed to deliver the masterbatch to the feed section of the extruder, whereas in a single screw process masterbatch is 'dry-blended' at the required ratio with the virgin polymer prior to being conveyed to the hopper or fed at the correct ratio from two silos into 1 conveying line that feeds the hopper.

Be it a single screw or a twins screw extruder, the purpose of the machine remains the same, see Section 2.2. Hensen and Bongaerts (1979) point out that typical throughput on the production line ranges from 2,000 to 3,000 $\mathrm{kg\,h^{-1}}$ with higher rates of around 3,500 $\mathrm{kg\,h^{-1}}$ being employed to manufacture thicker films (cited in MacDonald, 2002, p. 32). Such high outputs are chosen in the interest of efficiency, thus making oriented film production lines the largest in plastic processing both with respect to physical size and level of capital investment (Hensen, 1988, p.257).

More so than in other processes, film production requires a very steady output from the extruder as any throughput variations get directly translated to thickness fluctuations in the machine direction (MD) of the film. Often a gear pump is employed to produce the steady output required for the production of film thus overcoming any minor fluctuations in the extrusion output (Ellam, 2010). The extrusion systems within DTF are designed to keep the melt temperature as low as possible in order to minimise the thermal degradation of the polymer thus maintaining the molecular weight as high as possible. After leaving the extruder and gear pump (if included) the polymer travels though a filter pack which removes any unmelted or degraded material prior to the polymer entering the die. It is vital to avoid 'dead zones' within the melt system where the polymer could accumulate and degrade which in turn would lead to defects in the cast film and splitting of the film during stretching.

A die is utilised to generate a uniformly thick melt curtain; its geometry is key to effec-

tively achieving this. The melt curtain leaves the die and travels around a casting drum where it is rapidly quenched below its glass transition temperature, T_g of 78 °C for PET (MacDonald et al., 2007) in order to minimise crystallisation of the polymer and enable stretching of the film in latter processing. Electrostatic pinning is utilised to charge the film surface and ensure good contact between the polymer and the casting drum surface. This prevents a layer of air being entrained between the film and the drum surface thus enabling better heat transfer. The casting drum is maintained cold by spraying water at a temperature of around 15 °C on its internal surfaces or passing it through channels within the drum shell. MacDonald (2002) describes how an 'air-horn' can be employed to cool the air side of thicker films in order to ensure rapid cooling of the film.

The cast film now travels to the forward draw zone where the film temperature is raised above its T_g by passing it over a series of heated rollers. The film is oriented in the machine direction between two nip roll systems travelling at different speeds; typically at a ratio of around 3.5 (MacDonald, 2002). This aligns the polymer chains within the film in the direction of the draw leading to improved tensile modulus. Hensen (1988, p257) provides a detailed description of the changes in the polymer structure during film orientation. After the draw, the film is once again cooled below its glass transition temperature by a series of cooled rollers to minimise crystallisation. Now about half of the way through the filming process, see Figure 2.2 the film passes through the coating unit where aqueous based coatings of various thickness can be applied on either or both sides of the film.

It is then fed into the stenter oven where its sides are gripped by clips mounted on a chain running along the side rails of the oven. The film passes through the preheat zone of the stenter oven where, if the coating is present the water is dried from the surface of the film and the film itself is heated once again above its glass transition temperature. The film enters the sideways draw zone where it is stretched by a factor of about 4 in a transverse direction, TD by diverging rails at a temperature above 100 °C (MacDonald, 2002). This orients some of the polymer chains in the TD direction increasing the film's tensile

modulus and strength in this direction. The penultimate stage involves the heat setting or crystallisation of the film which increases the crystallinity of the polymer to around 40 % and ensures that the film does not distort or shrink when it is being processed at elevated temperatures by the customers. MacDonald (2002) describes the 'toe-in' process where the rails within the crystalliser zones of the stenter ovens are converged slightly in order to remove anisotropy from the non-crystalline regions of the film to prevent the film shrinking at elevated temperatures. The film is cooled prior to exiting the stenter, where upon exiting it is released from the clips and the thicker edges of the film are trimmed off. The edges and scrap film go on to make the recycle flake or are re-extruded to make pellets to be used with single screw extrusion processes.

The final stage involves the film travelling onto winders where the film is cut to customer specified widths and lengths and wound onto rolls prior to being shipped. Further coating can be applied in an 'off-line' process where aqueous or solvent based coatings can be utilised. It should be noted a typical process has been described here, however other processes exist and these include the stretching of the film in the TD followed by the MD direction as well as simultaneous bi-axial stretching (MacDonald, 2002). For a more in depth description of the oriented film manufacturing process as well as key influential process factors see *ch. 8* in Hensen, 1988.

As mentioned in Section 1.2, co-extrusion technology can be utilised in order to further differentiate the product lines together with the application of coatings and the addition of fillers. This technology enables structures to be created which combine the properties of different polymers. In co-extrusion two or more extruders are utilised to melt different types of polymer. These travel in separate melt systems and first come together in an injector block linked to an end fed die or a multi-manifold die (MMD). In an MMD, the polymer layers are spread to the desired width prior to the contact between different polymers which enables polymers with wider viscosity differences to be handled. For further information see Champion, 2015. A number of structures shown in Figure 2.3 can

be manufactured utilising these technologies.

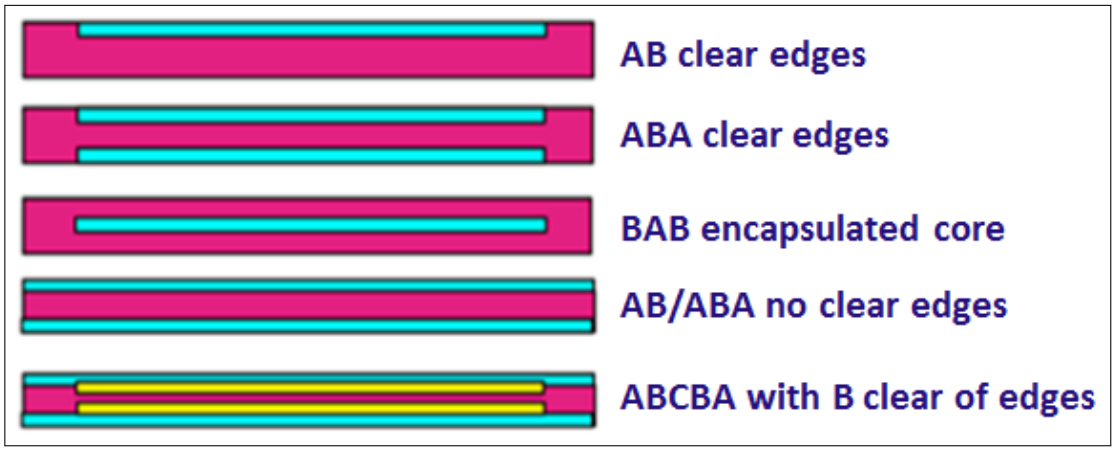

Figure 2.3: *Multi-layered film structures; adapted from Champion, 2015*

The most commonly utilised structures are AB and ABA with clear edges, where the A polymer forms the secondary layer and the B polymer forms the primary core layer. The presence of clear edges enables for effective recycling of the edge trims and prevents tacky polymer such as *co-PET* discussed in Section 3.1 sticking to the clips in the stenter oven. The thickness of individual layers as well as filler type and loading vary depending on the application of the product. Confining the additives to the surface layers can assist in maintaining optical clarity in the film.

2.2 An overview of extrusion technology

Rauwendaal (1986) provides an overview of the history of extrusion. The first extrusion machine for use with thermoplastics was built around 1935 by Paul Troester in Germany. Prior to this, mainly steam heated ram or short length screw extruders were utilised in the production of rubber. The concept of twin screw extrusion was developed by Roberto Colombo and Carlo Pasquetti, with Roberto patenting the notion of an intermeshing co-rotating twin screw extruder and Carlo developing the intermeshing counter-rotating machine. R. Colombo developed the first commercial intermeshing co-rotating machine in 1939, with the first modular design of this machine type being introduced in the 1950s

by Werner and Pfleiderer (Tang et al., 2003, p.774).

Extruders are widely utilised in a number of industries ranging from extrusion of foodstuffs and ceramics to plastics. Their generic function is to act as a pump and to generate the sufficient pressure required to force material though the die (referred to as 'diehead' pressure), which in turn will give the extrudate a particular shape. The pressure required will depend on the geometry of the die, material properties as well as the desired throughput. Within the plastic industry, plasticating extruders are of the greatest interest; these have an added requirement of melting the polymer chip as well as pumping the material. Extruders are the most common machines in the plastics sector (Rauwendaal, 2010), being utilised in pipe & profile, sheet and film extrusion lines as well as blown film, foamed plastics and compounding operations (Hensen, 1988).

2.2.1 Single screw extrusion

Single screw extruders are widely utilised in the plastic industry, they offer reliable performance at relatively low cost with the added benefit of straight forward design (Rauwendaal, 1986). The machines capacity/throughput are characterised by their diameter and the L/D ratio. Typical screw diameters range from 60 to 300 mm (Hensen, 1988) but machines of up to 600 mm exist (Rauwendaal, 1986) with L/D ratios from 20 to 30 being used with 24 being common for plastics extrusion (Eslami, 2015; Rauwendaal, 1986). In this type of machine, the screw can be subdivided into three sections: feed, transition and metering, see Figure 2.4.

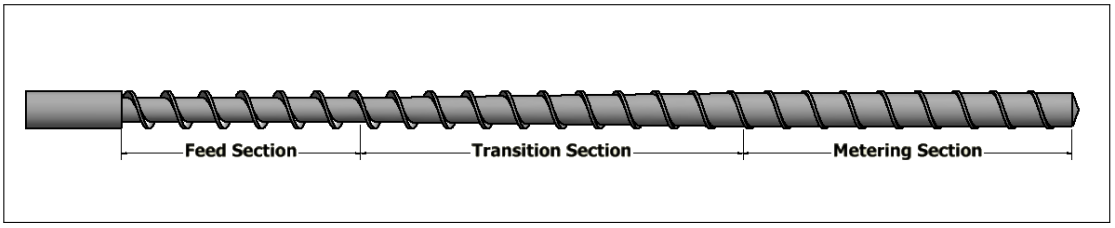

Figure 2.4: *Screw design in single screw plasticating extruder; from Eslami, 2015*

In a typical extruder the feed section ranges in length from 4 D to 8 D and the metering

section is around 6 D to 10 D with the intermediate compression section having compression ratios of 4.3:1 for PET (Kelly, 2013); although these vary depending on the material being processed. Normally the screws are solid pieces of metal, however they can have channels incorporated in them to enable the heating or cooling of the screw (Rauwendaal, 2010). Barrier flighted screws, illustrated in Figure 2.5, are also often utilised, Rauwendaal, 1986 points out their wide spread popularity in the US. These screws separate the solid pellets from the polymer melt during the compression stage ensuring complete melting of solids, improved degassing and promote dispersive mixing as the polymer has to flow through the high shear region over the barrier flight.

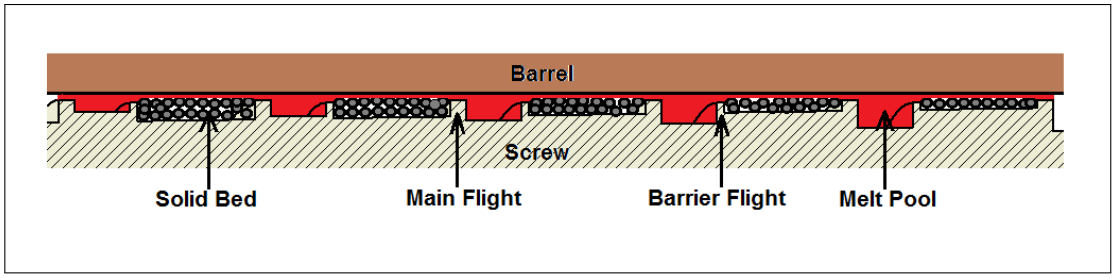

Figure 2.5: *Cross section of a barrier screw in single screw plasticating extruder; from Eslami, 2015*

The machines are typically unvented, although vented designs do exist. The devolatilisation capacity of a single screw extruder is much lower than that of a twin screw machine and vented single screw machines tend to be very long with length of up to 50 D being used (Rauwendaal, 1986). Within DTF vented designs are not utilised due to the complexities of operating and designing vented single screw machines. This means that there is a need to predry the PET prior to extrusion in order to prevent chain scission by means of the hydrolysis reaction.

Single screw extruders are normally flood fed (see Figure 2.6a), with *gravity induced conveying* ensuring the flow of material from the hopper to the extruder feed throat. This means that the extruder always operates at the maximum conveying capacity of the screw. Starve feeding of single screws, where the material is fed in at a rate less than the conveying capacity of the screw, is also possible, see Figure 2.6b. This is less common

as it reduces the effective length of the screw (Giles et al., 2005; Rauwendaal, 2010) and is only used in single screw systems to reduce the motor load or temperature build up in plastic melt. Once the material drops in the screw channel the friction between the polymer and the barrel (*drag induced conveying*) ensures the flow of the material down the axial direction of the screw. If a starve feeding mechanism is utilised, the melting mechanism differs from that proposed by Tadmor, 1966 as shown by Wilczynski et al., 2013.

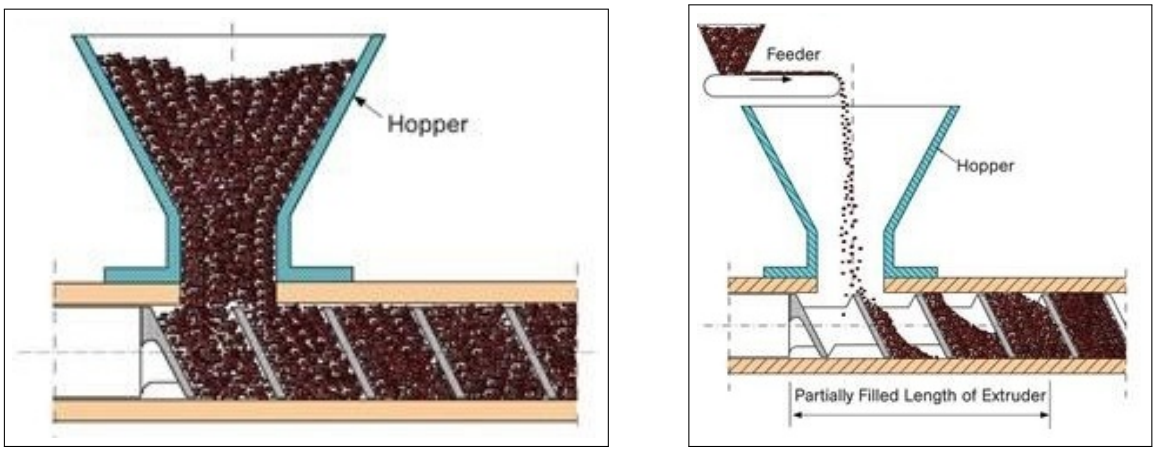

(a) *Flood fed mechanism* ***(b)*** *Starve fed mechanism*

Figure 2.6: *Feeding mechanisms in extrusion, from Rauwendaal, 2010, p.107*

Single screw machines can be operated mainly in 3 modes: as a stand alone machine, in combination with a melt pump or in tandem. Stand alone machines generally utilise a 'hard' screw profile (characterised by a long metering section and a shallow channel) which is designed for high delivery pressure (Ellam, 2010). Soft screws feature shorter metering section or deeper channels within this zone. The output of the machine and the shear rate that the polymer experiences are directly linked to the screw speed. This set up involves low capital expenditure and simple control systems. However it has little flexibility, offers low throughputs typically less than 1,600 $\mathrm{kg\,h^{-1}}$, operates with relatively high melt temperature leading to excessive polymer degradation and delivers fluctuating output which is dependant on the wear of the screw (Ellam, 2010).

Single screw machines coupled with a melt pump allow for greater flexibility by offering

higher throughputs of up to 3,000 $kg\,h^{-1}$ as well as lower polymer degradation by operating at a melt temperature 10 to 12 °C lower than a stand alone machine (Ellam, 2010). The presence of a melt pump puts the strain of delivering the required die head pressure onto the pump itself, thus enabling for the use of a 'softer' screw design. Gear pumps are typically utilised as melt pumps, which leads to potential concerns around wear of the teeth when the polymers processed contain abrasive fillers (Rauwendaal, 2010).

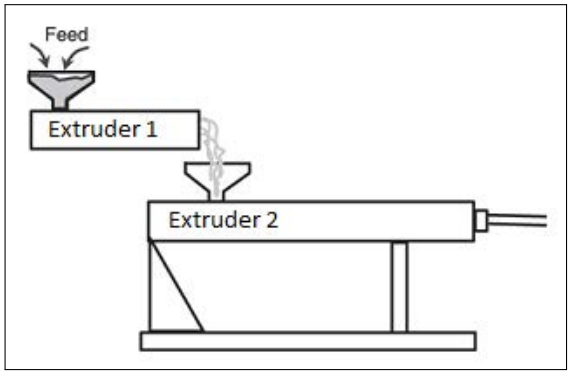

Figure 2.7: *Tandem extrusion; adapted from Giles et al., 2005, p.5*

Tandem extrusion process, see Figure 2.7 within DTF is mainly utilised in Japan. These involve the use of two single screw extruders running in series with the first machine being used to provide high shear melting and the second extruder providing cooling, mixing and metering of the flow. The machines are capable of delivering high throughputs of up to 5,000 $kg\,h^{-1}$ (Ellam, 2010) as well as very homogeneous melt. However, the design suffers from complexity, has a large foot print and requires large capital investment. This set up is difficult to control and involves large inventory of material which means that it takes longer to do polymer grade change.

2.2.2 Twin screw extrusion

A number of twin screw extruder designs exist, they differ not only by the direction and speed of rotation of the screws but also by the degree of intermeshing between the screws, see Figure 2.8. Twin screw extruders typically have barrel diameters up to 20 mm for lab scale machines, rising to circa 60 mm for pilot scale and 180 mm for production machines

(Liestritz, 2015). Typical length range from 24 to >60 L/D (Martin, 2014) and they are popular within plastics industry as they are extremely flexible due to their modular design.

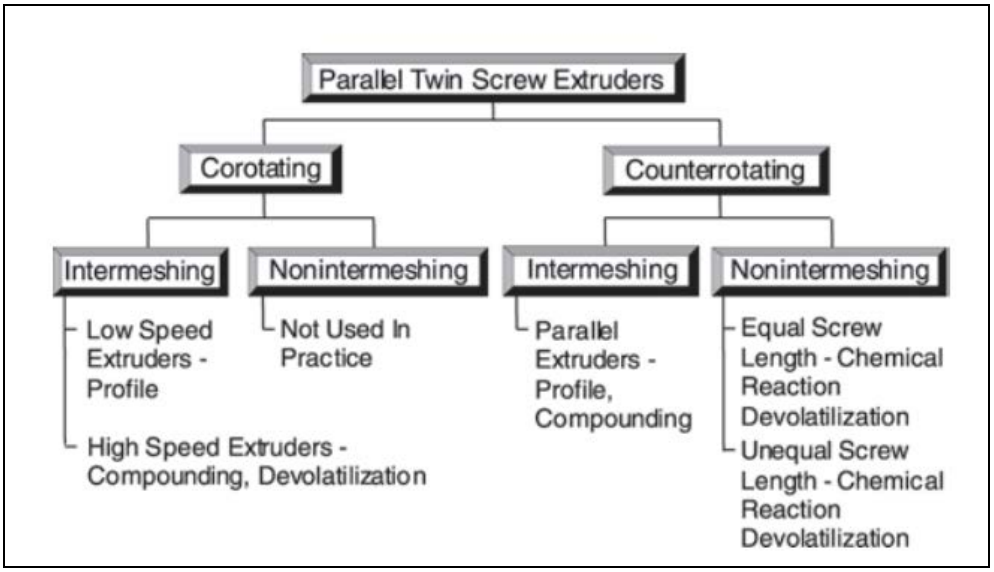

Figure 2.8: *Types of parallel twin screw extruders and their applications; from Giles et al., 2005, p.95*

A potential screw and barrel section design is illustrated in Figure 2.9. Depending on the task the machines can be configured utilising a variety of forwarding or reversing elements, kneading blocks (KB) and mixing pins to provide unique flow characteristics as well as dispersive and distributive mixing capabilities (Kalyon et al., 1991). In these extruders the flow occurs as a result of *positive displacement* rather than *drag induced conveying* meaning that limitations of single screw machines in feeding materials with poor frictional characteristics such as flake can be overcome. This also means that the machines can be operated partially filled, resulting in the ability to introduce additives directly to the melt as well as the ability to easily devolatilise the melt; thus removing the need to predry the polymer eliminating some of the operating costs. In PET processing twin screw machines also minimise gel formation resulting from predrying in air (Ellam, 2007).

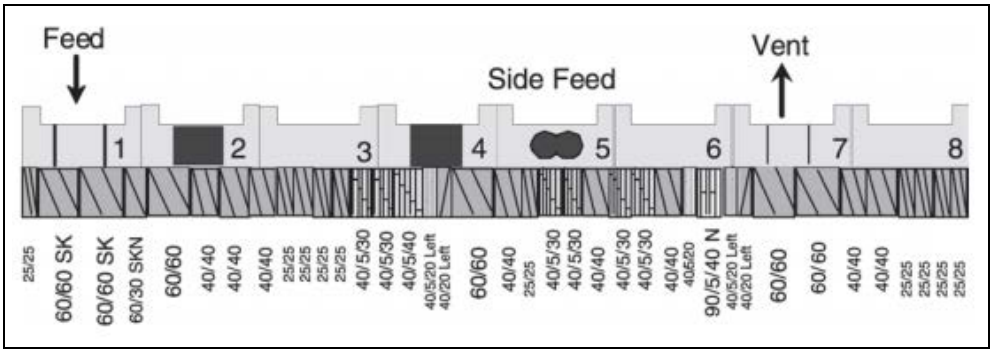

Figure 2.9: *Potential screw design; adapted from Giles et al., 2005, p.137*

In this type of machinery the screws can be fully, partially or non intermeshing, with each type having different applications. Fully intermeshing high speed co-rotating machines are widely used in compounding applications (Kelly, 2013; Kohlgrüber, 2008; Rauwendaal, 2010) due to the high dispersive mixing ability associated with high shear regions between the screws. Fully intermeshing co-rotating extruders are self wiping which permits better control of residence time distribution compared to single screws by eliminating the dead zones in front of the leading screw flight (Lawal and Kalyon, 1995; Todd, 1975). This enables much faster changeovers between different polymer grades. Non intermeshing machines have limited dispersion abilities (Rauwendaal, 2010). These can be considerably longer than their intermeshing counterparts as there is lower risk of metal to metal contact from misalignment caused by the screws bending under their own weight. These tend to be used for distributive mixing applications as well as reactive extrusion (Rauwendaal, 1986).

Co-rotating machines avoid the milling action at the conjunction of the screws and tend to be generally preferred (Morton-Jones, 1989). These machines have typical diameters of up to 130 mm with outputs of up to 3,000 $\mathrm{kg\,h^{-1}}$ (Hensen, 1988). By operating in a starve fed mode at conveying capacity less than the maximum capacity of the screw, it enables the output of the twin screw machines to be independent of the screw speed. This in turn allows control of the shear rates to which the polymer is subjected thus enabling lower melt temperatures to be achieved leading to less degradation of the polymer.

An in-depth review of co-rotating twin screw extruders focusing on the function of each extruder zone, the typical elements utilised in each of the zones as well as the flow fields within those elements is provided in Appendix A.

2.2.3 Mixing performance: single vs twin screw

Twin screw extruders operate on very different principles compared to their single screw counterparts, offering good mixing and heat transfer performance as well as melting and devolatilisation capacity. The flows within these machines are much more complex and less well defined. This makes it difficult to predict mixing performance of a set configuration or design a configuration based on the required degree of mixing from a theoretical respective for a given additive recipe. Much of the knowledge is developed in house through experimentation; although recently with the advent of more powerful computing there has been a drive to develop models of twin screw machines, see Appendix C.1.

Mixing in twin screw extruders is governed by the leakage flows in the high shear intermeshing region as well as the small clearances between the flights and the barrel. Some attempts have been made to compare the mixing performance of single and twin screw machines although this has mainly dealt with distributive mixing mechanisms. Much of the mixing analysis on twin screw extrusion has focused on determining the residence time distributions functions, such as that of Todd, 1975. Work has been undertaken to evaluate the flows and distributive mixing within twin screw extruders including that of Kalyon and Sangani, 1989a, however considerably less literature exists on dispersive mixing and even less so on quantitative comparison of single and twin screw machines.

Lawal and Kalyon (1995) describe how single screw extruders and fully filled sections of flighted elements in twin screws exhibit simple shear flows. In these types of flow when processing polymer blends the interfacial area becomes slowly oriented in the direction of flow and grows linearly with time leading to relatively poor distributive mixing, see Figure 2.10a. In twin screw extrusion the nip region allows greater interfacial area reorientation

(see Figure 2.10b) enhancing distributive mixing; although the performance depends on the type of element utilised.

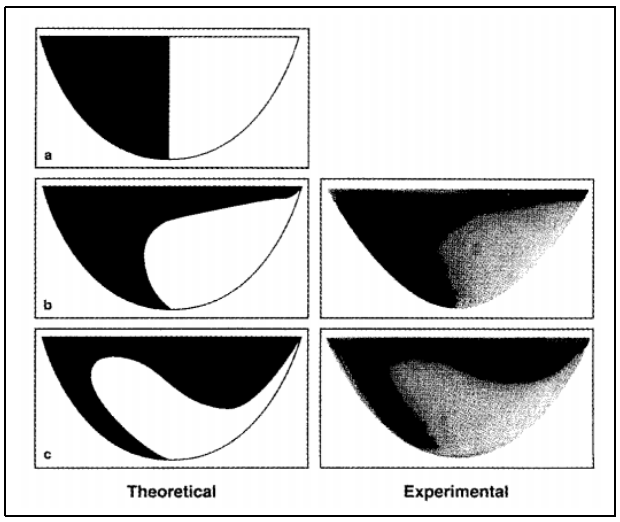

(a) *Interfacial area growth in single screw extrusion: (a) $z = 0$, (b) $z = \pi R_s$, (c) $z = \pi 2R_s$; from Lawal and Kalyon, 1995, p.1331*

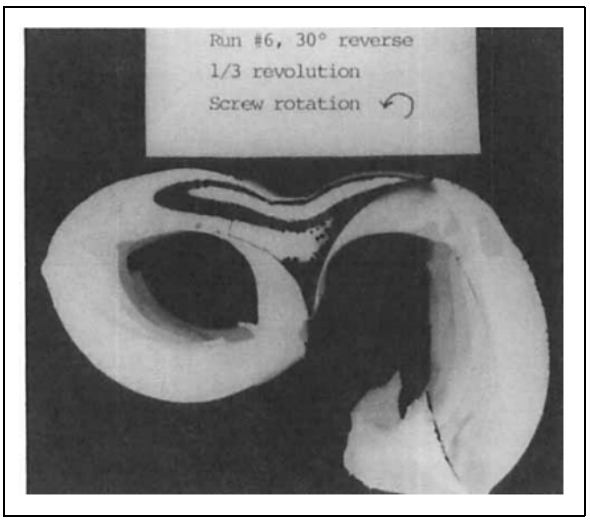

(b) *Interfacial area growth in the nip region of twin screw extruder employing 30 ° reverse KB, from Kalyon and Sangani, 1989b, p.1023*

Figure 2.10: *Distributive mixing in single and twin screw extruders*

Single screw machines can incorporate a number of different mixing sections such as '*pin*' or '*slotted flight*' sections to introduce flow reorientation improving distributive mixing and '*blister*' and '*egan*' mixing section to introduce high shear regions to aid with dispersive mixing.

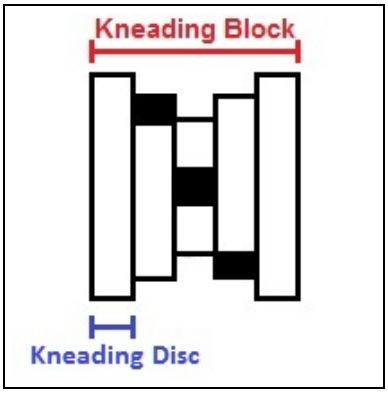

Figure 2.11: *Kneading block design; adapted from Tadmor and Gogos, 2006, p.531*

In twin screw extrusion the design of the elements, in particular the width of the individual kneading disc (KD) contained within the kneading blocks (KB) element (see Figure 2.11)

governs the degree of distributive or dispersive mixing that the arrangement is able to provide. The geometry of kneading blocks and flows within these are discussed further in Appendix A.

Manas-Zloczower and Cheng, 1996 evaluated the performance of *3.5 inch Warner & Pfleiderer single screw* extruder vs that of *2 inch Welding Engineering counter-rotating extruder* using high density polyethylene polymer (HDPE). By using Lyapunov exponents, which characterise the divergence of initial starting conditions with positive values indicating better distributive mixing, the authors were able to show that counter-rotating twin screw machine was about twice as effective as the single screw machine with exponent values of ca. 0.75 vs ca. 0.35 respectively. Similar calculations of Lyapunov exponents were performed by Lawal and Kalyon, 1995, confirming this result. By modelling the flow of 1,000 particles and analysing the average length stretch ratio, which compares the distance between two particles at time, t versus the initial distance between two particles (see Figure 2.12) Manas-Zloczower and Cheng, 1996 were able to demonstrate that a twin screw machine had much better distributive mixing performance.

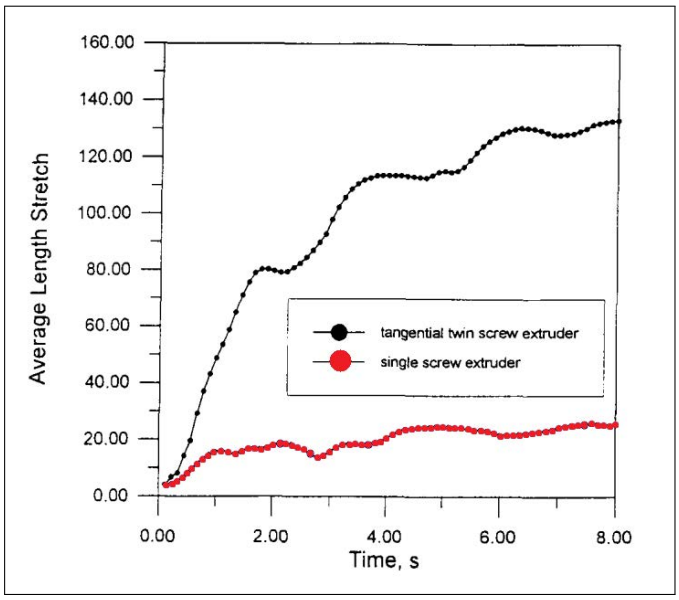

Figure 2.12: *Average length stretch for singe and counter-rotating twin screw extruder with HDPE at 60 rpm and flow of 15* $\mathrm{cm}^3\,\mathrm{s}^{-1}$*; from Manas-Zloczower and Cheng, 1996, p.82*

Similarly, Manas-Zloczower and Cheng, 1996 compared the extent of dispersive mixing achieved in the single vs twin screw machine by considering the types of flows seen in the extruder (see Figure 2.13a) and the shear stresses (see Figure 2.13b) experienced by the polymer. Parameter λ, a ratio between the rate of strain and the vorticity tensor, was utilised by the authors to describe the nature of flow; with $\lambda = 0$ representing pure rotational flow, $\lambda = 0.5$ denoting simple shear flow and $\lambda = 1$ illustrating elongational flow.

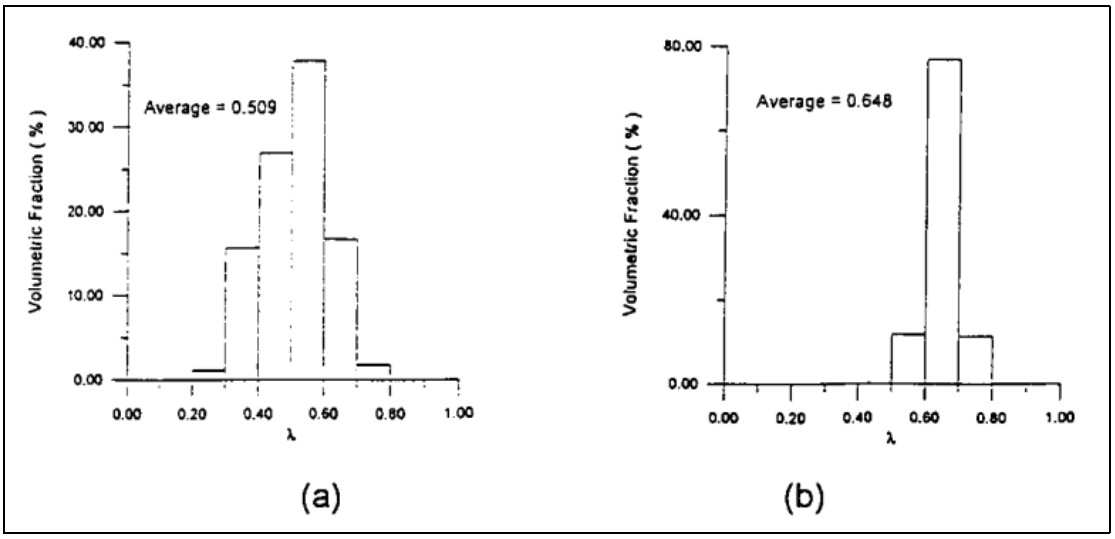

(a) *Nature of flows in single and counter-rotating twin screw extruder: (a) single screw (b) counter-rotating twin screw; from Manas-Zloczower and Cheng, 1996, p.84*

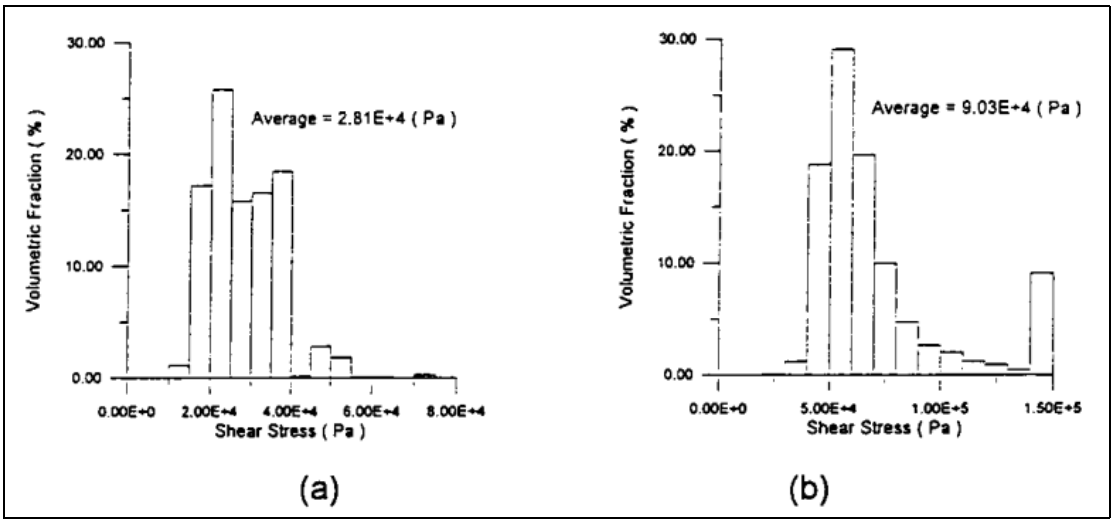

(b) *Stress distribution in single and counter-rotating twin screw extruder: (a) single screw (b) counter-rotating twin screw, from Manas-Zloczower and Cheng, 1996, p.84*

Figure 2.13: *Flow field and stress distribution analysis for single and counter-rotating twin screw extruder*

Figure 2.13a considers the volume distribution of the λ parameter, from which one can see that the flow in a single screw extruder is mainly simple shear, with only about 20 $\%_{\text{vol}}$ of flow experiencing extensional flows with $\lambda \geq 0.6$. Where as in counter-rotating twin screw machine this is close to 90 $\%_{\text{vol}}$, with almost 20 $\%_{\text{vol}}$ of polymer experiencing flow conditions of $\lambda \geq 0.7$. The importance of extensional flows in extrusion of immiscible blends has been discussed by Gogos et al., 1996 indicating that unlike in shear flow, under extensional flow there are no conditions in which a droplet of a certain size does not break up. Similarly, in composites extrusion, extensional flows are able to generate higher stresses leading to better dispersion; see Section 2.4.1.2.

By considering the stress distribution in Figure 2.13 one can see that on average the shear stress achieved within the counter-rotating twin screw extruder is three times that achieved in the single screw extruder. These higher hydrodynamic forces enable better dispersion of agglomerates in *solid-liquid* heterogeneous systems as higher cohesive forces can be overcome. A superior performance is envisaged in the co-rotating extruders since within the nip regions the screws rotate in the opposite directions to each other, unlike in the counter-rotating machines, thus generating higher shear rates and stresses.

2.3 A summary of the industrial compounding process

One approach to direct extrusion technology development is to better understand the way in which the masterbatches currently purchased by DTF are manufactured, thus enabling the principles of the compounding process to be transferred to an 'in-line' operation allowing for direct addition of powders to the film making process. Hence, it is appropriate for a brief outline of the process to be provided here. The author would like to acknowledge the works of Bart, 2006; Giles et al., 2005; Hensen, 1988; Kohlgrüber, 2008 which give a very good description of the compounding process and have been the main sources of information for this section.

In 2003, the Western Europe masterbatch market was estimated to be at 750,000 tons with engineering thermoplastics accounting for around 18 % and the colour compounds for 31 % of the market with the rest being driven by polyolefins and polyvinyl chloride (PVC) as evaluated by AMI Reynolds, 2004; (cited in Kohlgrüber, 2008, p.57). Currently, only 12 % of pigment is being introduced by direct addition (Kohlgrüber, 2008). Utilisation of the masterbatch enables the dispersive mixing step to be outsourced to the compounder, hence allowing the manufacturer of the product to focus solely on achieving adequate distributive mixing of the masterbatch within their extruder. If a highly loaded masterbatch is utilised, only a small portion of final product has been subjected to potentially extreme conditions within the extruder that allow for adequate dispersion to be achieved, hence minimising the deterioration in the properties of the final product. Issues arise when the let down ratio (a ratio of additive concentration in masterbatch to final product) is low and the loading within the masterbatch is also low. This means that much of the polymer contained within the final product has been extruded twice leading to severe deterioration in the properties of the product.

Masterbatches typically contain up to 50 $\%_{\mathrm{wt}}$ of additive with highly loaded masterbatches having concentrations up to 80 $\%_{\mathrm{wt}}$ (Murphy, 2001). As mentioned previously high speed fully intermeshing twin screw extruders are commonly utilised for compounding operations, however single screw machines fitted with special mixing elements can also be used to manufacture masterbatches with loading of up to 60 $\%_{\mathrm{wt}}$ (Rauwendaal, 2010). Challenges arise when manufacturing masterbatches with loadings greater than 20 % as it becomes increasingly difficult to establish a process that can effectively deal with the varying properties of the additives such as particle size and shape (Hensen, 1988).

Twin screw machines enable superior dispersive mixing performance due to high shear stresses in the nip region but also allow for excellent distributive mixing performance as the material is directly transferred from one screw to the other twice per revolution. The polymer is inverted between the kneading block surface and the wall during the

transfer from screw to screw leading to uniform shear history. The material experiencing high shear rates in the nip region is swiftly removed from this region allowing for greater temperature control and minimal thermal degradation (Todd and Baumann, 1978). This in turns allows for the polymer viscosity to be maintained leading to better dispersive mixing as higher shear stresses can be transferred to the agglomerates.

Achieving good mixing is vital for successful compounding operations as the properties of the compound greatly depend on the particle size, the distribution of the additive within the polymer matrix as well as the strength of the interaction between the additive and the polymer matrix. The compounders often aim to use the smallest particle size possible as this reduces the extent of dispersive mixing that has to be performed by the extruder (Bart, 2006), however this poses new challenges for material handling in particular with dust generation.

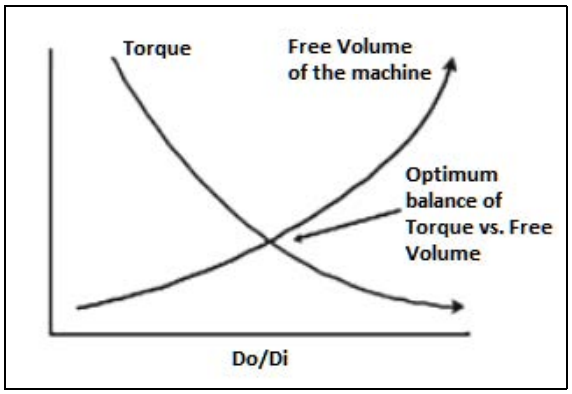

Figure 2.14: *Torque versus free volume for twin screw extruder; from Kutz, 2011, p.250*

A particular challenge for low bulk density powders is associated with appropriate screw design. This process is typically volume limited, thus one needs to design the machine to have as much free volume as possible but this results in the need to sacrifice the torque of the machine, see Figure 2.14 were D_o/D_i represents the ratio between outside and inside diameter of the screw. To overcome this limitation some powders may be added in compressed pellet form as suggested by Kohlgrüber, 2008, however this would increase the need for dispersive mixing within the extruder. The cohesive forces within such pellets

would need to be very well designed, enough to hold the pellet together during material handling operation yet enable effective dispersion within the screw.

A compounding process needs to be able to handle different varieties of additives, these may not only differ by physical characteristics such as size and density but also by their behaviour in the extrusion process. Some additives will remain solid throughout extrusion, whilst others will melt forming a fully miscible mixture and others will form an immiscible blend. It may be that the additive is in a liquid form from the start which poses completely different challenges with regards to feeding of the material. When dealing with liquid additives it is important to introduce them over a mixing element to prevent *ponding*, the separation of the melt and the liquid. Sometimes it may be possible to add the liquids directly into the feed throat of the extruder, however this can pose issues with feeding by reducing the friction coefficient between the polymer and the barrel. This can also be an issue for additives which melt rapidly upon entry into the extruder.

Solid additives can be introduced directly to the melt, although addition of loadings up to 10 $\%_{\mathrm{wt}}$ can be introduced directly to the feed pocket of the extruder together with the polymer (Kohlgrüber, 2008). If more than 30 to 40 $\%_{\mathrm{wt}}$ is introduced this should be done in two stages to enable effective wetting of the additive and to prevent the polymer from cooling too much (Kohlgrüber, 2008; Rudersdorf, 2014). Addition of waxes to the process together with the additive to aid interaction between the additive surface and the polymer matrix is common, but it is also possible for the additive surface to be modified in order to increase the affinity to the polymer or to provide steric stabilisation and prevent the formation of agglomerates.

Sometimes premixing is carried out where the additive is mixed with a powdered polymer to aid with wetting and distributive mixing, particularly in production of colour masterbatches (Kohlgrüber, 2008). However newer, high performance compounding processes rely on '*direct to melt*' addition which eliminates the time consuming step of grinding down polymer pellets and premixing with the additive (Coperion & K-tron, 2014). Direct

to melt addition allows for smaller quantities of waxes to be utilised.

2.4 Mixing mechanisms within polymer composites manufactured on twin screw extruders

In a single additive system, the introduction of the additive into a polymer matrix results in one of the three systems being formed; miscible mixture, immiscible blend and polymer composite where the additive remains solid throughout the extrusion process. It is vital to note that the mixing requirements of the three systems are starkly different. In the miscible blend system, there is no requirement for intensive (dispersive) mixing and the sole role of the extruder is to provide extensive (distributive) mixing thus enabling the polymer additive to be homogeneously distributed though space within the polymer matrix. Polymer blends require intensive dispersive mixing action to generate secondary phase droplets of the required size as well as distributive mixing to provide uniform spatial distribution. The Gogos et al., 1996, Kajiwara and Nakayama, 2011 as well as Emin and Schuchmann, 2013 provide detailed descriptions of the different mechanisms for droplet break up in extrusion of immiscible polymer blends. Although such systems were investigated, as no results are presented within this thesis are based on polymer blends this warrants no further discussion herein.

Akin to polymer blends, the mixing of polymer composites requires both dispersive and distributive actions. Intensive mixing occurs via mechanisms which significantly differ from that in polymer blends. Similarly, extensive mixing is limited to the mechanical rearrangement of the fluid elements to ensure even spatial distribution.

2.4.1 Dispersive mixing in polymer composites

Dispersive mixing induces a size reduction of the cohesive particles contained within the polymer. In addition to the change in size, the shape of the additive can also change due

to the breakage of the irregular shaped clusters and/or the attrition of long aspect ratio particles (Kalyon et al., 1988a). This in turn can change the influence of the additive on the properties of the composite. The process is strongly influenced by the flow field which the dispersed phase experiences with higher stresses yielding a more effective break down of the agglomerates. Similarly, the nature of the flow field can also impact the degree of dispersive mixing with extensional flows resulting in better dispersion (Kajiwara and Nakayama, 2011).

In composites, dispersive mixing occurs via three mechanisms *rupture*, *erosion* and *collision*. The different mixing regimes occur in parallel within a co-TSE process. Their effectiveness depends on operating conditions and the screw design. As a result at any given condition a particular mechanism will dominate. As well as break up of agglomerates, the fragments can coalesce into larger particles. Here, effective distributive mixing is required to rapidly separate the fragments and minimise re-agglomeration.

2.4.1.1 Stages of mixing in polymer composites

The overall mixing process can be described by several stages; as discussed by Bart, 2006 and Kasaliwal et al., 2010. These are as follows:

1. Filler incorporation;
2. Additive crushed/or compacted (applicable if not introduced directly to the melt);
3. Wetting and infiltration by polymer melt;
4. Dispersion (Rupture, erosion, collision);
5. Distribution (splitting and rearrangement of fluid flow elements);
6. Re-agglomeration (particularly likely in pressurised sections of the extruder).

Processes 3 to 6 occur simultaneously in the extrusion process Kasaliwal et al., 2010 and the dispersion step is considered to be the most difficult and thus the rate limiting step (Manas-Zloczower, 2009).

Although the processes run in parallel, good wetting is a prerequisite for good dispersion. It allows polymer to infiltrate the agglomerate structure which potentially disrupts the internal interactions within the agglomerate thus reducing the cohesive strength. In addition, good wetting also allows better stress transfer to the agglomerate with the external shear conditions driving the flow of the infiltrated material within the pores of the agglomerates. This in turn affects the manner in which the stresses are distributed within the agglomerate allowing better dispersion (Yamada et al., 1997). Finally, faster wetting allows the surface of the newly generated additive fragments to be coated rapidly minimizing the risk of re-agglomeration. The infiltration of the polymer is particularly important in the dispersion of the layered additives as it is a precursor to the exfoliation of the layered bundle into individual sheets.

The viscosity of the matrix and the porosity of the agglomerate affect the degree and the rate of infiltration and thus the level of dispersion achieved. Higher viscosity matrix will infiltrate slower than the lower viscosity one Yamada et al., 1997; Yamada et al., 1998. Levresse et al., 1999 showed that the decreasing agglomerate radius, agglomerate density and melt viscosity lead to increased rate of polymer infiltration. Villmow et al., 2008 also discussed how the erosion process is facilitated by the lower melt viscosity.

Three scenarios have been proposed for mixing in the extrusion process by Flecke et al., 2002 and Kasaliwal et al., 2010. The first scenario corresponds to operating conditions when the shear stress generated is larger than the critical stress for the rupture mechanism. In this case both rupture and erosion will occur, but the mixing will be dominated by the much faster rupture mechanism. In the second scenario, the shear stresses generated are above the critical stresses required for the erosion but below the critical stress for rupture resulting in the slower erosion mechanism being dominant and responsible for the size reduction of the additive. Finally, under certain conditions the generated stresses may be below the critical stress for the erosion mechanism. In this case, Flecke et al., 2002 proposes that the agglomerates will cluster to generate larger agglomerates. It is likely

that some dispersion via the collision mechanism will occur; however the proportion of collisions that generate smaller fragments as opposed to larger agglomerates will depend on the morphology of the agglomerate and how well the agglomerate is wetted.

Kasaliwal et al., 2010 proposed a model to distinguish between rupture and erosion controlled regimes and examined how the contribution from the mechanisms changes with increase in screw speed. The author reported that the proportion of mixing achieved through rupture increased from 35 to 44 and 83 % at speeds of 50, 100 and 300 rpm. Flecke et al., 2002 reports that although the mean diameter decreased along the length of the extruder indicating better mixing, the number of larger particles observed increase indicating the role of the re-agglomeration process.

2.4.1.2 Rupture mechanism

The particulate agglomerates within the polymer melt are held together by cohesive forces, the magnitude of which correspond to the critical hydrodynamic stress which has to be overcome in order to facilitate dispersion via agglomerate rupture mechanism.

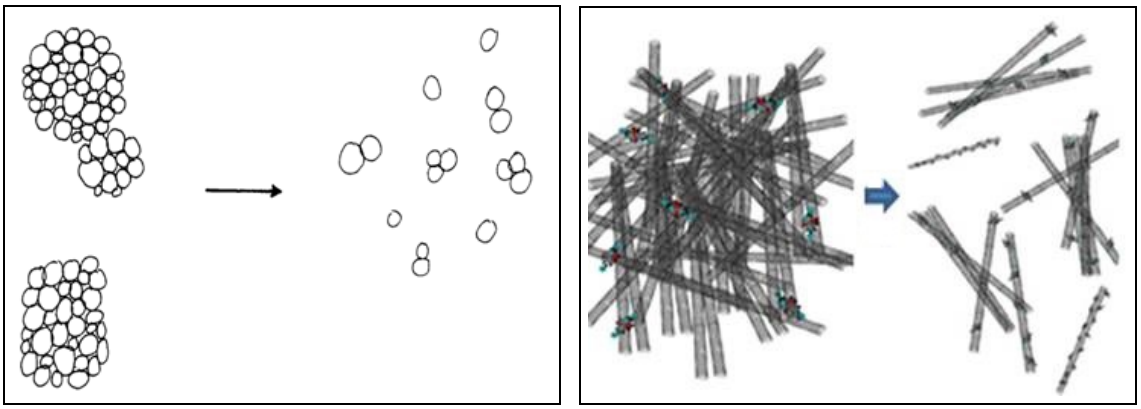

(a) *Agglomerates composed of spherical particles; Kasaliwal, 2011*

(b) *Agglomerates composed of long aspect ratio particles; Ramos et al., 2017*

Figure 2.15: *Rupture mechanism for dispersion of agglomerates*

During rupture the parent agglomerate structure is almost instantaneously broken down into a number of smaller fragments; see Figure 2.15a which then have to be rapidly wetted by the polymer to prevent re-agglomeration. Given high enough hydrodynamic stresses,

it is possible to break the agglomerates into the primary particles by repeatedly exposing the fragments to high shear thus facilitating further break down of the structure.

The ratio of the strength of the cohesive forces to the applied stress is critical in determining if rupture will occur. This ratio is often referred to as the *Fragmentation number, Fa.* If this is larger than the critical value which is set by the cohesive forces, rupture will govern dispersion and if it is less than the critical value erosion will govern dispersion. The hydrodynamic stress transferred to the agglomerate can be calculated from the equation below (from Kasaliwal et al., 2010, p.2719):

$$\sigma_h = K \cdot \eta \cdot \dot{\gamma} \tag{2.1}$$

where K is 2.5 for spheres, η is the viscosity in Pa s, $\dot{\gamma}$ is the shear rate in s^{-1} and σ_h is the hydrodynamic stress in Pa.

The magnitude of cohesive forces depends on numerous factors including particle size and filler surface characteristics (Kajiwara and Nakayama, 2011; Kasaliwal et al., 2010). Particle shape also plays a key role in determining the cohesive forces, with long aspect ratio particles being much harder to break apart due to the requirement to overcome the interlocking between different particles or to physically break the particles; see Figure 2.15b. These aspects are discussed further in Chapter 8.

The agglomerates within the additive feed vary in size and therefore will break at different critical stresses. As a result, a distribution of stresses is required to achieve effective dispersion via rupture mechanism (Lawal and Kalyon, 1995) whilst minimising the adverse effects of exposure to high stresses such as mechanical chain scission and viscous heating of the polymer. This exists within a TSE at any given screw speed; with the lowest stresses being found in the deepest portion of the channel and the highest stresses being generated in the clearances between the barrel and the screw tip as well as in the nip region; as observed by Emin and Schuchmann, 2013 in their modelling work. Fukuda

et al., 2013 examined the distribution of stresses realised within a co-rotating TSE under a number of different operating conditions by considering the rupture of spheres that were designed to break at a given stress magnitude. The peak shear stress determines the maximum size of the agglomerates within the composite. Thus, the flows though the high shear regions govern the rupture mechanism and ensuring these are present is critical for effective dispersion. Within the TSE machine the low stress regions are designed to send the material through the higher stress regions (Kajiwara and Nakayama, 2011; Kalyon et al., 1988a).

There is an optimum machine design for effective rupture which is a compromise on the size of the clearance gap. As the clearance reduces in size the peak shear stress achieved increases theoretically increasing rupture of agglomerates. However, this also has the effect of reducing material flow though the high shear region and increasing viscous heating of the polymer. Similarly, the high shear rates associated with the region can mean that the polymer chains do not have enough time to disentangle leading to mechanical scission which reduces the overall chain length and thus the viscosity of the material. All of these lead to lower hydrodynamic stresses being transmitted to the additive on average and hence a reduced rupture performance. On the other hand, as the clearance in increased although the peak stress reduces more material flows though the region which can lead to better mixing overall. However, at a certain clearance value the stresses will no longer be high enough to overcome the cohesive forces within the agglomerate and hence no rupture will take place. Importantly, although an optimum design exists it is likely to be different for every additive-polymer system due to the differences in the cohesive strength within the additive agglomerates.

It should be noted that the nature of flow plays a key role as well, with more effective dispersion achieved in extensional flow than in simple shear flow. This is due to the maximum force, F_{max} acting on the agglomerate in elongational flow being twice of that in simple shear flow (see p.61 Cullen, 2009); see Equation 2.2 and 2.3 respectively:

$$F_{max,elongational} = 6\pi\eta\dot{\varepsilon}r^2 \tag{2.2}$$

$$F_{max,simpleshear} = 3\pi\eta\dot{\gamma}r^2 \tag{2.3}$$

where $\dot{\varepsilon}$ is the elongation strain rate s^{-1}, r is the radius of the agglomerate in m.

Interestingly, the analysis of the different flow regions by Emin and Schuchmann, 2013 showed that the flows within the high shear regions tend to be dominated by simple shear flows as opposed to elongational flows. Carson et al., 2015 proposed new screw element designs to promote elongational flow.

2.4.1.3 Erosion mechanism

As the agglomerate is wetted the polymer infiltrates the outer layers of the agglomerate reducing the strength of the interaction between the surface fragments and the body of the agglomerate. Once shear is applied, the motion of the fluid on the surface generates stresses which overcome the adhesion forces holding the fragment to the body of the agglomerate. This leads to small fragments being broken off from the parent agglomerate structure; see Figure 2.16a. Erosion mechanism is much slower than the rupture mechanism but the critical stress for erosion is much less than that for rupture mechanisms. The rate at which the fragments leave the surface is proportional to the surface area of the agglomerate cluster and the residence time within the system (Kasaliwal et al., 2010).

Similar to rupture, erosion of fibrous materials with long aspect ratio is more difficult due to the interactions between the individual fibres resulting in the wetted fibre being pulled into the melt stream; see Figure 2.16b. As a result larger stresses are required to overcome this friction force or to mechanically break the fibre.

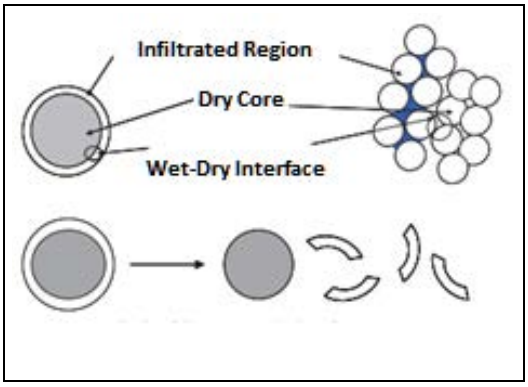

(a) *Agglomerates composed of spherical particles; Kasaliwal, 2011*

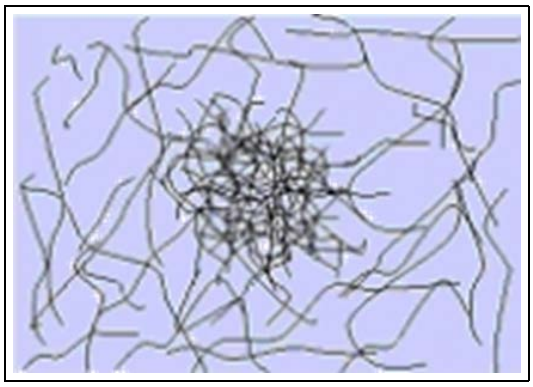

(b) *Agglomerates composed of long aspect ratio particles; Kasaliwal et al., 2010*

Figure 2.16: *Erosion mechanism for dispersion of agglomerates*

2.4.1.4 Collision mechanism

The collision mechanism was discussed by Seyvet and Navard, 2000. The authors proposed the notion of smaller fragments being generated during collisions between parent agglomerate structures; see Figure 2.17. The mechanism governed by the collision frequency, number of particles in the system, and the shear stress.

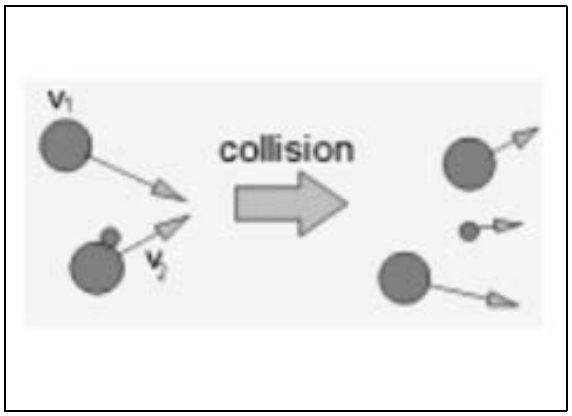

Figure 2.17: *Collision mechanism for dispersion of agglomerates; from Seyvet and Navard, 2000*

In the case of the long aspect ratio bundles, the dispersion via collision mechanism is unlikely as the two parent structures are more likely to interlock with each other leading to a larger agglomerate than generate small fragments.

2.4.2 Distributive mixing in polymer composites

Distributive mixing is responsible for uniform spatial distribution of the additive within the continuous phase. This type of mixing is highly dependant on the total strain which the material experiences. Commercial mixers typically achieve strains of 18,000 +/− 6,000 shear units Tadmor and Gogos, 2006. Akin to dispersion, the low strain regions are designed to send material though the high strain regions; that is the tip to barrel clearance and the nip regions.

Distributive mixing is typically studied in the miscible systems by examining the uniformity of the spatial distribution of the additive. Studies in polymer blends are also common where the interfacial area between the two components is considered since it acts as a representation of the total strain. Distributive mixing is also applicable in the polymer composite system, as it ensures uniform spread of the additive throughout the product. Within polymer composites manufacture, the distributive mixing is achieved through the repeated rearrangement of the fluid flow elements (Manas-Zloczower and Cheng, 1996). This process occurs around the tips of the kneading blocks or in specially designed elements; see Appendix A. These elements function particularly well with a reversing element paced directly downstream of them as this increases the residence time in the zone and thus the number of fluid element rearrangements.

Todd and Baumann, 1978 examined the distributive mixing achieved in a twin screw compounder by considering the quantity of the additive within the individual polymer pellets and reported a very good level of mixing. In manufacture of the composites, it is often assumed that this type of mixing is very good and it is only the dispersive mixing that has to be optimised. This is generally true within TSE machines due to the complex nature of flows produced by the screws. However, as the residence time within TSE is relatively short there is the need to ensure consistency of feed as the axial mixing along the extruder is relatively poor with flows tending to that of plug flow in certain screw configurations.

2.5 Concluding remarks

The initial focus of this chapter was on providing an overview of the film making process. This was followed by a brief review of the compounding process and it is envisaged that the ideas from the compounding sector can form the basis for the development of direct extrusion addition technology on the film line. It is important to realise that, unlike the compounding process which focuses on the extrusion alone, direct addition technology has to function within the bounds imposed by the the upstream and the downstream processes on the film line leading to tighter boundaries on the operating window.

Although both single and twin screw extruders are utilised on the manufacturing plants within DTF business, from the review of the two extrusion technologies it is evident that the initial work should focus on the co-rotating twin screw extrusion equipment. This has several advantages including the potential to offer greater mixing capacity, starve fed operation allowing direct to melt addition and modular design providing greater opportunity to tailor the mixing to a particular product.

From the review of the mixing mechanisms, it is evident that there is a compromise that has to be reached between the design of the machine and the operating conditions in order to achieve the desirable mixing whilst maintaining product properties. It is also clear that this compromise may be different for each of the additive-polymer systems and there is a significant challenge in designing a system that is able to process at least a similar group of additives (by a classification that is yet to be determined). The design and operation of successful process will require knowledge of the additive and polymer properties, additive to polymer interactions as well as how these coupled with the machine design and operation influence the level of mixing achieved. These challenges require the extension of existing knowledge and provide the novelty in this research project.

3 | Materials utilised

A number of polymers and additives have been utilised though the course of the research. The supplier information and the brand names are not published within this thesis in order to protect intellectual property of the sponsoring company. The materials were chosen based on the their ability to provide an insight into the fundamentals of the different mixing mechanisms, limitations of the direct to melt addition process and business drivers. The material properties as well as the research and business interests are discussed herein.

3.1 Polymers studied

A film grade *PET-A* and bottle grade *PET-B* of homopolymer PET as well as a copolymer, *co-PET* were utilised in the research. Table 3.1 illustrates the key properties of these materials including intrinsic viscosity, IV and number average molecular weight, M_n which calculated via Mark-Houwink-Sakurada equation (Wagner, 1985) as well as the apparent viscosity, η.

Table 3.1: *Physical properties of PET-A, PET-B and co-PET*

Property	**Units**	**PET-A**	**PET-B**	**co-PET**
Intrinsic viscosity, IV	$\mathrm{dl\,g^{-1}}$	~ 0.62	~ 0.80	~ 0.64
Number average molecular weight, M_n	$\mathrm{g\,mol^{-1}}$	$\sim$ 19,900	$\sim$ 27,300	$\sim$ 20,600
Zero shear viscosity, η_0	Pa s	251*	719†	371‡
Apparent viscosity, η [at 100 $\mathrm{s^{-1}}$]	Pa s	219*	626†	323‡
Chip weight	mg	60	60	60
Chip height	mm	3	3	3
Chip width	mm	3	3	3
Chip depth	mm	3	3	3
Melt density, ρ_m	$\mathrm{kg\,m^{-3}}$	1250	1250	1250
Solid density, ρ_s	$\mathrm{kg\,m^{-3}}$	1400	1400	1400
Bulk density, ρ_b	$\mathrm{kg\,m^{-3}}$	800	800	800

**at 275* °C †*at 285* °C ‡*at 265* °C

The apparent viscosity values quoted are at the standard processing temperatures for the particular polymer grade. These were calculated based on the O'Dell Model in a form

of an Arrhenius relationship which is utilised internally within DTF (Champion, 2015). The apparent viscosity is determined at a shear rate, $\dot{\gamma}$ of 100 s^{-1} as this is close to the maximum shear rate that the polymer may experience whilst flowing in deepest part of the main channel within the extruders utilised in the experiments. The shear rates experienced in the high shear nip regions as well as clearances between the screw tip and the barrel are much greater; see Chapter 6.

Although PEN films are also produced by DTF, with polymer viscosities even higher than that of *PET-B*, these polymers were considered to be beyond the scope of the work. The decision was made in order to focus on understanding the interactions between PET matrix and the additive.

3.1.1 Product Respective

PET-A is the standard grade of polymer, often utilised as a base polymer in a number of DTF's products with some products requiring the use of a higher molecular weight substrate *PET-B*. Such products include the flame retardant films where higher viscosity of the polymer helps to minimise dripping of the polymer during burning of the film.

Co-PET contains less than 20$\%_{wt}$ of copolymer. It is utilised for the manufacture of a heat sealable secondary layers (layer A) in an AB or an ABA structure. The use of the copolymer inhibits crystallisation of the film during the *casting* process. In addition as the film passes though the *stenter oven* at temperatures of ca. 220 °C the secondary layer melts, resulting in an amorphous tacky layer on the outside of the finished film. The different film structures, the casting process as well as the use of the stenter oven is covered in Section 2.1.

3.1.2 Research Respective

The difference in molecular weigh of the *PET - A* and *PET - B* allows for the impact of polymer viscosity onto the extent of dispersive mixing to be evaluated. Varying degree

of polymerisation of these two grades, and hence average chain length, is useful in understanding the effect of these parameters on the extent of polymer degradation during the extrusion process. The use of a copolymer grade, *co-PET* enabled the investigation into the influence of polymer wetting behaviour on the extent of dispersive mixing achieved within a given polymer-additive system.

3.2 Additives studied

As part of this project several types of additives have been considered, which all serve a different purpose within the film. Initial candidates were selected by examining the usage of different masterbatches within the U.K. region in order to evaluate the potential impact that direct addition of these additives could have on the business. In addition to product drivers, the additives were also selected based on their suitability for the direction of this research.

3.2.1 Product perspective

As well as looking at existing products, several additives were selected by the new product development team. These where driven by the difficulty in obtaining an appropriate masterbatch. The additives include several whiteners, flame retardant (FR) additives, ultraviolet (UV) stabilisers, fillers and a clay. These are discussed next, together with their properties and applications.

3.2.1.1 Whiteners

Whiteners are incorporated into the film in order to promote the scattering of light and hence generate the white appearance of the film. The process is enhanced by the high refractive index of the additive and a nominal particle size being around half that of the wavelength of visible light, ranging from 200 to 350 nm (TDSC, 2012). There are numerous types of whiteners available on the market. These differ by crystalline structure,

particle size, particle shape and the nature of surface coatings applied to the particle.

Within DTF several grades are utilised, with the first grade under consideration being referred to as *W-1* for the purpose of this report and the second being referred to as *W-2*. The aforementioned grades are supplied by different manufacturers. They have the same crystalline structure but differ in the nature of organic coating applied to them. The exact composition of these is unknown being the intellectual property of the supplier. The physical properties for these materials are given in Table 3.2.

Table 3.2: *Physical properties of W-1 and W-2 whitener grades; data collated from manufacturers' literature unless otherwise indicated*

Property	**Units**	**W-1**	**W-2**
Alumina coating	$\%_{\mathrm{wt}}$	0.6	1.7
Organic coating	$\%_{\mathrm{wt}}$	0.4	0.3
Nominal particle diameter, D_p	µm	0.21	0.22
Solid density, ρ_s	$\mathrm{kg\,m^{-3}}$	4,100	ca. 4,000
Bulk density, ρ_b	$\mathrm{kg\,m^{-3}}$	$1{,}095 \pm 15^{\dagger}$	$950^{\ddagger}$
Tapped bulk density, ρ_{bt}	$\mathrm{kg\,m^{-3}}$	1400	-
Specific surface area, S_A	$\mathrm{m^2\,g^{-1}}$	6.5	-

† *Measured value, error indicates 90 % CI for Student's T distribution*
‡ *From Bell and Bloom, 2014*

W-1 and *W-2* whitener grades have applications in motor films at a loading of ca. 0.5 $\%_{\mathrm{wt}}$ as well as photovoltaic (PV) backsheet film at a loading of ca. 4.5 $\%_{\mathrm{wt}}$. A desire to incorporate these whiteners in excess of 10 $\%_{\mathrm{wt}}$ exists within the new product development team.

Addition of acicular whitener was also examined as part of this project. This additive is being tested for application in the outcoupling film at a loading of less than 1 $\%_{\mathrm{wt}}$. These films are utilised in the manufacture of Organic Light Emitting Diodes (OLEDs). There are three grades of the additive available, referred to *W-3, W-4* and *W-5* from now on in this report. These additives have the same crystalline structure as *W-1* and *W-2* but differs in particle size and shape. For physical properties of these grades refer to Table 3.3.

Table 3.3: *Physical properties of W-3a, W-3b and W-3c whitener grades; data from manufacturer's literature*

Property	**Units**	**W-3**	**W-4**	**W-5**
Nominal particle diameter, D_p	µm	0.13	0.21	0.27
Nominal particle length, L_p	µm	1.68	2.86	5.15
Aspect ratio		13	14	19
Solid density, ρ_s	$\mathrm{kg\,m^{-3}}$	4,200	4,200	4,200
Specific surface area, S_A	$\mathrm{m^2\,g^{-1}}$	10 - 15	7 - 10	5 - 7

3.2.1.2 Flame retardants

DTF currently manufactures flame retardant (FR) films for sale in Japan. However there is a strong driver to develop a product that can be sold in the European market. Several applications are available for such a product including labels on electronic devices. There are a number of additives being considered as part of the new product development, however the direct addition project focuses on additives referred to as *FR-1* to *FR-4*. Grades *FR-1* to *FR-3* have the same chemical structure and differ by particle size only. Grade *FR-4* is supplied by the same manufacturer but differs in its chemical structure. Table 3.4 shows the physical properties of the FR additives. It should be noted that the FR materials are non hygroscopic, thus making storage of the material easier and removing the need to predry the powder. The additive *FR-4* melts at 208 °C, thus it will melt during extrusion process resulting in a non composite system.

Table 3.4: *Physical properties of FR-1, FR-2, FR-3 and FR-4 additives; data obtained from the supplier*

Property	**Units**	**FR-1**	**FR-2**	**FR-3**	**FR-4**
Diameter†, D_{10}	µm	0.845	2.050	1.352	80.099
Diameter†, D_{50}	µm	2.538	26.747	41.290	349.359
Diameter†, D_{90}	µm	8.996	47.382	76.826	1002.52
Distribution span	-	3.212	1.695	1.828	2.640
Solid density, ρ_s	$\mathrm{kg\,m^{-3}}$	1,350	1,350	1,350	1,300
Bulk density, ρ_b	$\mathrm{kg\,m^{-3}}$	100 - 250	400 - 600	400 - 600	~ 600
Surface area, S_A	$\mathrm{m^2\,g^{-1}}$	3.21	1.00	1.21	0.0367
Moisture content	$\%_{\mathrm{wt}}$	≤ 0.5	≤ 0.2	≤ 0.2	≤ 0.25

† *Diameters indicated are the percentiles for the volume-number weighted distribution*

3.2.1.3 UV stabilisers

Some applications such as that in the photovoltaic backsheet market require the film to withstand exposure to sunlight over several decades. In order to prevent the degradation of PET via exposure to UV light, contained within sunlight, UV stabilisers are introduced into the film. These preferentially absorb ultraviolet light, hence prolonging the lifetime of the PET film. Several types of additives are utilised to achieve this, these shall be referred to as *UV-1* and *UV-2*. The additive *UV-1* is currently introduced into the film in the form of masterbatch. In its natural form the additive is a very fine powder, however it is also supplied as 'Easy Dosible' granules and these shall be referred to as *UV-1ED*. *UV-1* and *UV-2* are chemically different additives, with the supplier claiming that *UV-2* is twice as effective as *UV-1* and thus can be added into the film at half the concentration.

Table 3.5: *Physical properties of UV-1, UV-1ED and UV-2 additives; data obtained from the supplier*

Property	**Units**	**UV-1**	**UV-1ED**	**UV-2**
Nominal particle diameter, D_p	µm	1 - 128	$\sim$ 4,000	3.4†
Solid density, ρ_s	kg m^{-3}	1,191	1,191	400 - 600
Bulk density, ρ_b	kg m^{-3}	-	450 - 500	-
Melting point temperature, T_m	°C	148.8	149	120 - 130
Surface tension, Γ	mN m^{-1}	72 - 73	72 - 73	73.8

† *Diameters indicated is the 10th percentile* D_{10}

3.2.1.4 Silica

Silicas are used as fillers in the film to generate designed texture on the surface which helps with the winding of the film when it is being processed by DTF and handled by our customers. In this application the surface quality is critical as any agglomerates on the surface can lead to defects in the coatings applied by DTF's customers in further processing. Several different silicas were considered here with the different grades being referred to as *S-1* to *S-5*. Their physical properties are provided in Table 3.6. Typically, these are introduced into the film at loadings below 5 %$_{\mathrm{wt}}$. More recently, there is a drive to incorporate higher loadings leading to a much higher volume fraction of the filler

increasing the likelihood of agglomeration.

Table 3.6: *Physical properties of S-1 and S-5 silica grades; data collated from manufacturers' literature*

Property	**Units**	**S-1**	**S-2**	**S-3**	**S-4**	**S-5**
Nominal diameter, D_p	µm	6.2	6.2	6	5	5
Solid density, ρ_s	$kg\,m^{-3}$	2,200	2,200	2,200	2,200	2,200
Particle density, $\rho_p^{\dagger}$	$kg\,m^{-3}$	444	604	688	948	1170
Bulk density, $\rho_b^{\dagger}$	$kg\,m^{-3}$	267	363	413	494	703
Surface area, S_A	$m^2\,g^{-1}$	300	600	500	700	700
Pore volume	$ml\,g^{-1}$	1.8	1.2	1	0.6	0.4

† *Calculated based on particle density and loose random packing density*

Interestingly, the specific surface area reduces with increase in particle porosity which is counter-intuitive, but can be explained by the growth in the number of closed pores.

3.2.1.5 Clays

Tubular clay, referred to as *C-1* is a development additive with a potential application within laser engravable overlay (LEO) films, where it would enhance the colour of the charring in the film. These films are used as a final layer in the composite printed card structure. The material physical properties are provided in Table 3.7.

Table 3.7: *Physical properties of C-1 clay; data from manufacturer*

Property	**Units**	**C-1**
Nominal particle diameter, D_p	µm	0.05
Nominal particle length, L_p	µm	0.5 - 1
Aspect ratio	-	10 - 20
Solid density, ρ_s	$kg\,m^{-3}$	2,530
Bulk density, ρ_b	$kg\,m^{-3}$	$420 \pm 14^{\dagger}$
Surface area, S_A	$m^2\,g^{-1}$	35 - 65
Pore volume	%	20

† *Measured value, error indicates 90 % CI for Student's T distribution*

It should be noted that the materials are hygroscopic and pick up moisture from the atmosphere adding an extra challenge with regards to material handling operations. It

typically contains around 3 % of free moisture and thus there is a potential need to predry the material given the sensitivities of PET to hydrolitic degradation.

3.2.2 Research perspective

The vast differences in the physical and chemical properties of the additives will allow for several different aspects to be studied. These are discussed below.

3.2.2.1 Different additive-polymer systems

Although the majority of the results presented within this research focus on polymer composites, the additives discussed in Section 3.2.1 behave very differently within the extruder. This coupled with the varying degree of additive-polymer interaction enabled different additive-polymer systems to be studied; see Table 3.8.

Table 3.8: *Types of additive-polymer systems studied*

Additive	System	Additive behaviour within the polymer
UV-1	Miscible system	Melts during processing and is fully incorporated within the polymer matrix
FR-4	Immiscible blend	Melts during processing and is immiscible with the polymer resulting in droplets of the secondary phase within the matrix
W-1	Polymer composite (good affinity)	Remains solid during extrusion and has good affinity with the polymer resulting in non-voided bi-axially oriented films
FR-1	Polymer composite (poor affinity)	Remains solid during extrusion and has poor affinity with the polymer resulting in voided bi-axially oriented films

3.2.2.2 Effect of particle size and shape on mixing

FR-1 additive is supplied in several grades differing by particle size, making this additive the most suitable for evaluating the effect of particle size onto the extent of mixing observed in the finished film. By maintaining the same additive other factors that potentially influence the degree of mixing are maintained constant. One aspect that can not be

controlled is the increase in the specific surface area of the additive, due to the reduction in size of the additive.

The additives in Table 3.9, are ideal for analysing the effects of particle shape on the degree of dispersion. Some of the whiteners have similar aspect ratio but differ in dimensions whilst others differ only in aspect ratio. These can be compared with the 'spherical' grades (Table 3.2) to determine the effect of shape. Since, the clay *C-1* has similar dimensions to the fibrous whiteners, it enables the study into the affect of additive-polymer interactions.

Table 3.9: *Additives used to examine the impact of particle shape on mixing*

Property	**Units**	**W-3**	**W-4**	**W-5**	**C-1**
Nominal diameter, D_p	µm	0.13	0.21	0.27	0.05
Nominal length, L_p	µm	1.68	2.86	5.15	0.5 - 1
Aspect ratio		13	14	19	10 - 20

3.2.2.3 Influence of surface area and porosity on mixing and polymer degradation

The aforementioned silica additives are excellent candidates for evaluating the effect of surface area on the extent of mixing observed, with increase in surface area leading to the requirement of rapid wetting kinetics in order to ensure that agglomerates are not formed. These additives have comparably narrow particle size distributions and do not contain any surface coatings on the particles eliminating any potential differences in the strength of additive-polymer interactions.

Similarly, it is vital to consider the effect of porosity especially in hygroscopic materials that retain moisture given how sensitive PET is to degradation via hydrolitic mechanisms. Increased porosity may result in limited moisture being removed in the vacuum degassing section of the extruder thus leading to excessive degradation.

3.2.2.4 Development of powder handling process

The different properties of each of the additives considered will enable for the development of an effective powder handling process. This will need to handle the feeding of particles that are considerably different in size and shape. Similarly, the effect of particle porosity and bulk density has to be considered, especially when dealing with fine particles that could lead to significant generation of dust. Such scenarios could not only result in contamination issues but has the potential to lead to unsafe working environment. There is a need to understand how the compressibility and flowability of the powders impact the powder handling process and whether any special measures such as modified hopper design will be required.

3.3 Concluding Remarks

A number of polymers and additives have been selected based on the product, business and research drivers for this work. By considering such a broad range of materials it was possible to evaluate the role of polymer properties and the additive properties on the level of dispersion achieved in PET composites manufactured on a co-rotating twin screw extruder. The differences within the range of additives studied allowed the requirements of the powder handling process to be specified; this is something that is completely new to the company. Different pairings between the additives and polymer grades enabled the importance of the interactions between the two phases to be considered.

4 | Analysis methods utilised

One of the main challenges in evaluating the level of mixing lies in establishing a scale of scrutiny; that is the level of mixing required by the product in order for it to fulfil its function. For example if one was to extrude coloured sheets the size of A4 paper and package 100 of them together for retail, then any variation in colour within a single sheet would be unacceptable. Although variation between the 100 sheets would be undesirable, it is likely that a slight differences would be acceptable. The challenge lies in scale of scrutiny varying with the product. In the case of DuPont Teijin Films (DTF) the level of mixing required for UV additive in stabilised film is different to that for flame retardant additive in its protected films portfolio. One of the ways to address this would be to have a separate test for each product that determines whether the level of mixing is suitable for product needs. Although this is the ideal solution for the development of products, it would place strict limitations on using the analysis to better understand the fundamentals of mixing. This is a direct result of not being able to compare the mixing of different additives in various products due to varying test methods.

Within the compounding sector which has to ensure that the level of mixing is consistent within the tonnes of masterbatch supplied in any order as well as between orders the filter pressure test is commonly utilised. For the test, a screen changer of a certain size is chosen depending on the product needs or base additive size. In the test initially an unfilled polymer is passed through the filter to obtain a steady operating pressure, P_1 after which the filled sample is processed for a given period of time to obtain a maximum pressure, P_{max} followed by the base polymer to determine the steady state pressure P_2; see Figure 4.1 for a graphical representation. The difference in pressure $(P_2 - P_1)$ provides information on the number of agglomerates deposited on the filter surface and hence the level of dispersion between different samples can be visualised.

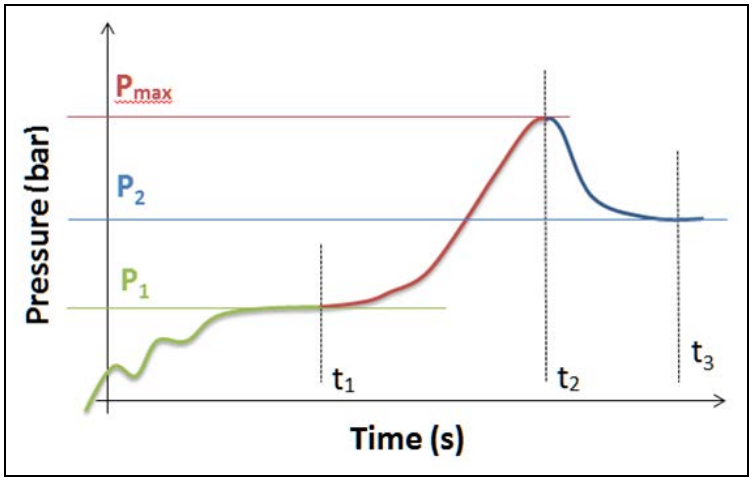

Figure 4.1: *Pressure test utilised by compounding industries*

The test is good for understanding the mixing within the bulk as significant quantity of material is processed. However, it is not suitable to determine the size of agglomerates and thus gain detailed information on the mixing mechanisms. With regards to DTF, such a test would be unsuitable in the long run as chip is required and film samples are produced. The film lines are fitted with filtration devices, and the rate of pressure increase across these could be monitored however this would require running over a large number of hours and hence would not be suitable for screening a large number of conditions; as is the goal of this work.

Within literature, the studies on dispersion focus mainly on microscopy techniques ranging from optical microscopy, scanning electron microscopy (SEM) and transmission electron microscopy (TEM). These can be used to analyse the level of dispersion for different additives but generally have the drawback of only small samples being examined and thus they may not represent the bulk of the material. Image analysis is typically used to size the particles/agglomerates observed. As is common, Domenech et al., 2013 utilised the area ratio to compare the differences in mixing observed with smaller area ratio representing better dispersion, see below:

$$A_r = \frac{\sum A_{agg}}{A_{tot}} \times 100 \tag{4.1}$$

where A_r is the area ratio, A_{agg} is the area of agglomerates and A_{tot} is the total area of the image. Typically, the authors decide upon the minimum cut off (typically around 10 µm) which determines the size of the agglomerates that are acceptable and thus are not counted in A_{agg}. This varies with the product and puts a limitation on drawing conclusions from a variety of different products.

Some authors promote the use of rheology to overcome the drawback arising from a small areas being considered in the image analysis. Rheology is sensitive to the microstructures within the sample (Domenech et al., 2013) and the increases in viscosity can be associated with formation of networks and hence good dispersion (Ammala et al., 2008). Although more rare, others have drawn on the analysis of distributive mixing and utilised a dispersive mixing index (Lafleur et al., 2000). The issue with the utilisation of a dispersion indices is similar to that with area ratio where the use of a single number, although useful for sample comparison, leads to a loss of information and thus proves poor in understanding mixing mechanisms.

4.1 Dispersion analysis

The method of analysis utilised for this work aims to mitigate some of the drawbacks reported above. Todd and Baumann, 1978 specified that for compounding the scale of scrutiny that is important for distributive mixing is a pellet (typically 10 to 60 mg in size), as the same amount of additive should be present in each one. A similar scale of scrutiny was taken for analysis of dispersive mixing as the level of mixing should be the same within each pellet as well as across different pellets.

4.1.1 Microscopy analysis

Microscopy was chosen as the preferred technique for the analysis as it can yield comparable results for both the pellet samples produced on the *Dr Collin ZK25* machine and the film samples manufactured on the *Berstorff ZE40A* machine. With regards to the

films produced, samples from the casting drum prior to the stretching were selected for analysis in order to ensure that any potential break up of agglomerates during stretching was not taken into account. This also helped with cases where the interactions between the additive and the matrix are poor which leads to voiding around the particles often making the samples more opaque as a result. As the cast film samples produced are typically < 1 mm in thickness, it was possible to undertake the analysis directly on the film.

Direct analysis on the chip was also performed, however due to the curvature of the chip only a small portion of the image was suitable for image analysis; outlined in red in Figure 4.2a. In order to overcome this and better visualise the agglomerates within the polymer pellets, the pellet was melted between a glass slide to generate a thin film (ca. 60 µm) allowing light to pass through the sample much more easily. This was done on a hot plate set to a temperature of ca. 285 °C; yielding specimens shown in Figure 4.2b. By rapidly quenching the pressed sample in cold water, crystallisation of the polymer was minimised allowing the sample to maintain its transparency.

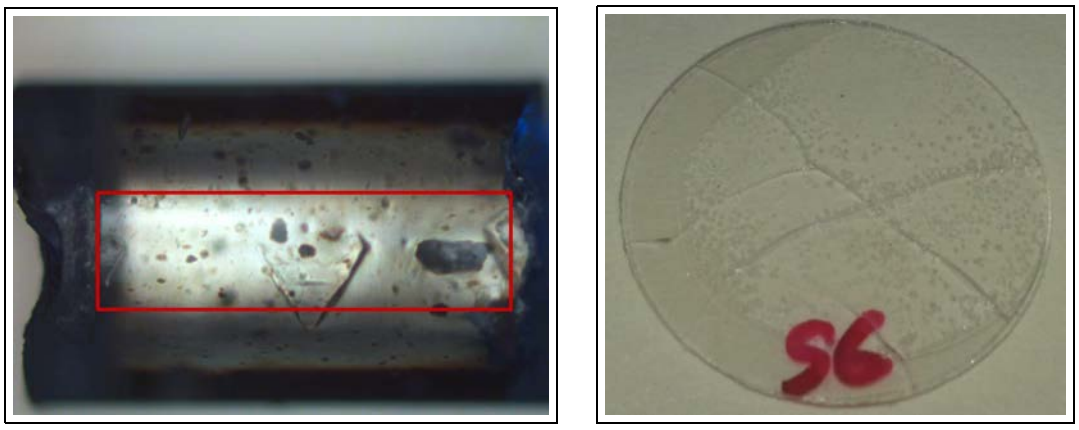

(a) *Reflected light microscopy on pellet* ***(b)*** *Pressed pellets*

Figure 4.2: *Microscopy sample preparation*

The transmitted and reflected light microscopy images were captured utilising a Leica DMR microscope. A number of objectives were available including 2.5X, 5X, 10X, 20X and 50X each offering an increasing level of detail with a reducing field of view. Typically, four images were captured for each pellet at random locations with a total of three randomly

selected pellets being tested; leading to 12 images per sample condition being analysed. There was some variation in the number of images captured, however the aim was to keep the number of particles detected and sized above the guidelines of ISO 13322-1. By examining 6,100 particles the mean of the particle size distribution can be estimated with a 95 % confidence interval and the percentiles of the distribution can be estimated to ±10 % through the analysis of 15,200 particles.

4.1.2 Image analysis

The images obtained through microscopy were analysed using *FiJi* distribution of ImageJ open source software that is commonly utilised for image analysis by research institutions across the globe. A useful guide for image analysis was produced by Ross, 2009. Although sometimes modified depending on the image, a typical procedure involved:

1. Importing the image into software
2. Applying a Gaussian Blur filter (ca. 2 pixel) to remove inherent noise in the image
3. Converting the image into 8-bit grayscale image
4. Removing the background via median subtraction tool provided in BioVoxell plug-in
5. Thresholding the image in order to convert the image into black and white binary image; this was performed through ImageJ automatic thresholding algorithm to ensure reproducibility between images
6. Analysing the particles with the minimum detection limit set at 2X the resolution of the microscope, particles located on the edge of the image were excluded and any holes within the particle included in the calculation of the particle area

   Note: The minimum resolution was established from equation below, where λ *is the wavelength of light (0.55* µm *mid-spectrum) and NA is the objective numerical aperture (Davidson, 2017)*:

$$Resolution = \frac{\lambda}{NA}$$

A number of characteristic diameters for the additive can be generated with image analysis, with the two most commonly used being the *projected area equivalent diameter*, D_p and *feret diameter*, D_f. The projected area diameter is calculated based on the assumption that the particle is a sphere and therefore the detected area in image analysis is said to equal to the area of a circle, from which the diameter is calculated. The feret diameter on the other hand is the longest distance observed across the particle; see Figure 4.3a. The feret diameter is more accurate in the case when particles are partially thresholded; as illustrated by yellow areas in Figure 4.3b. However, the projected area equivalent diameter is less sensitive when two or more particles overlap each other; see Figure 4.3c. As a monolayer of particles is not being considered in the analysis, the chances of particles overlapping is quite high and therefore the projected area equivalent diameter was chosen as a more suitable option.

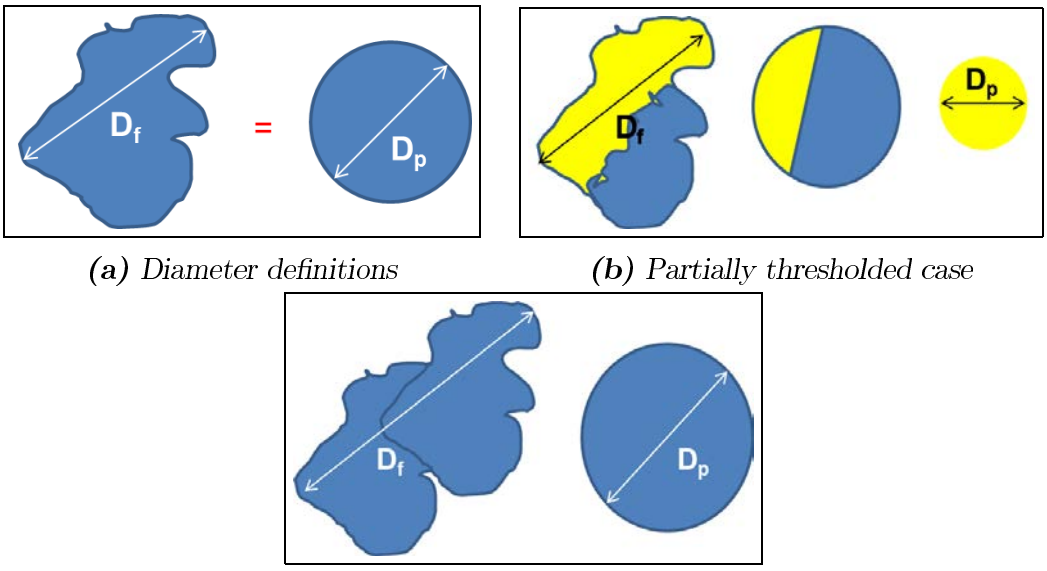

(a) *Diameter definitions* ***(b)*** *Partially thresholded case*

(c) *Overlapping particle case*

Figure 4.3: *Projected area equivalent versus feret diameter*

4.1.3 Generating particle size distributions

Once, the particles were sized and counted the number, area and volume discrete probability distributions were generated. The number distribution was obtained as follows:

$$For \quad D_{min} \leq D_p \leq D_{max}: \quad p_i = \frac{\sum_{D_p<LL}^{D_p \leq UL} x_i}{x_{tot}} \tag{4.2}$$

where D_{min} and D_{max} are the minimum and maximum particle sizes observed, D_p is the particle size, p_i is the probability of finding a particle in a given bin size, LL and UL are the lower and upper limit of bin sizes, x_i is the particle number, and x_{tot} is the total particle count. From this a cumulative distribution was be obtained.

The mean and the standard deviations were calculated for the distributions as follows:

$$\bar{D_p} = \sum_{min}^{max} D_i \cdot p_i \quad where \quad D_i \quad is\ the\ size\ for\ a\ given\ bin \tag{4.3}$$

$$\sigma_{s.d.} = \sqrt{\sum_{min}^{max} \left[D_i - \bar{D_p}\right]^2 \cdot p_i} \tag{4.4}$$

In a similar manner the area weighted distribution was obtained where percentage of total area occupied by particles in each bin size was calculated as:

$$For \quad D_{min} \leq D_p \leq D_{max}: \quad A_i\,(\%) = \frac{\sum_{D_p<LL}^{D_p \leq UL} A_i}{A_{tot}} \tag{4.5}$$

Similarly, the volume percent occupied by particles in a given bin size as established as:

$$For \quad D_{min} \leq D_p \leq D_{max}: \quad V_i\,(\%) = \frac{\sum_{D_p<LL}^{D_p \leq UL} V_i}{V_{tot}} \tag{4.6}$$

As well as the mean and the standard deviation, D_{10}, D_{50} and D_{90} were calculated representing to the 10^{th}, 50^{th} and 90^{th} percentiles of the distribution i.e. in a volume distribution, D_{50} represents the upper limit for the particle size of the particles that cumulatively would occupy 50 % of the total volume; see Figure 4.4. This enabled numerical comparisons between various distributions whilst maintaining information about the shape of the distribution itself. Most importantly, by selecting the same bin sizes as utilised on the particle analyser, it is possible to directly compare the distribution of the powder additive

(black line in Figure 4.4) and that obtained within the polymer composite (red line). In the ideal case, the two distributions would overlap, however as the sample line moves closer to the base powder (as represented by green arrow) better mixing is obtained. By comparing the distance between the sample and the base powder, the degree of mixing can be evaluated irrespective of the additive/polymer combination being utilised.

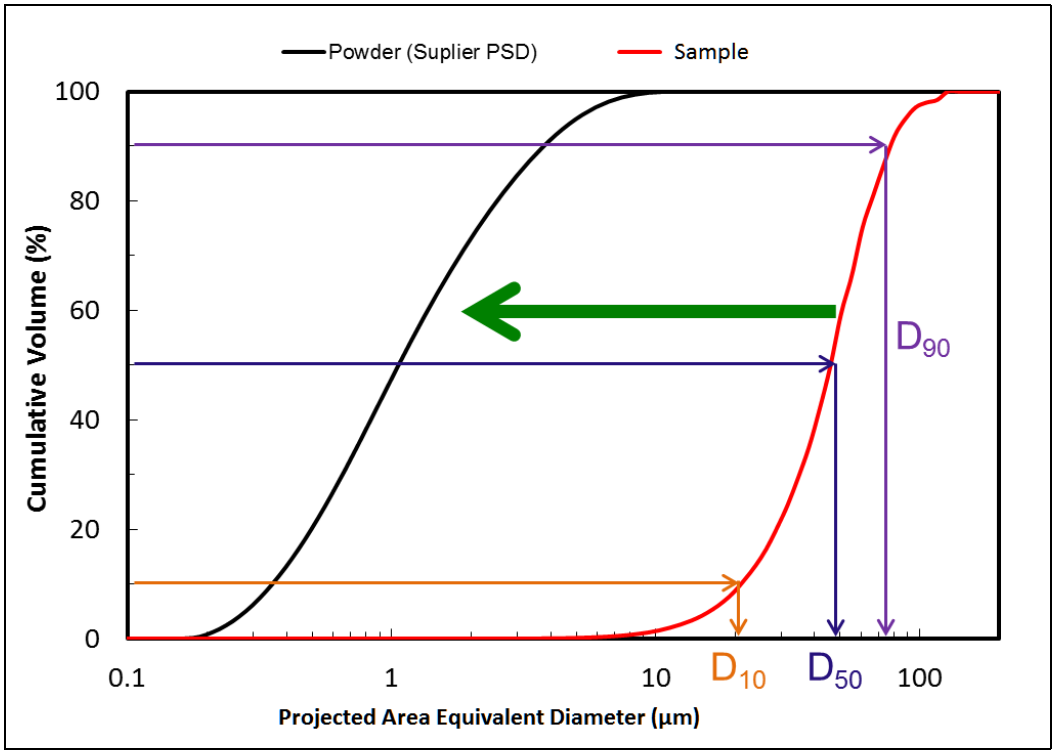

Figure 4.4: *Cumulative volume vs particle size distribution*

The number, area and volume weighted distributions demonstrate various aspects of the process. The number distribution is good for establishing the quantity of the dispersed particles. However, as the additive becomes better dispersed these become more difficult to detect. The area weighed distribution is particularly useful for products where surface finish is critical; as the area occupied by the agglomerates can be determined and hence one can examine aspects such as number of defects per million opportunities. As the aim of this work is to achieve the best possible dispersion, the volume weighted distribution allows the easiest tracking of larger particles since the volume of one large particle may equate to thousands of small ones depending on the respective sizes.

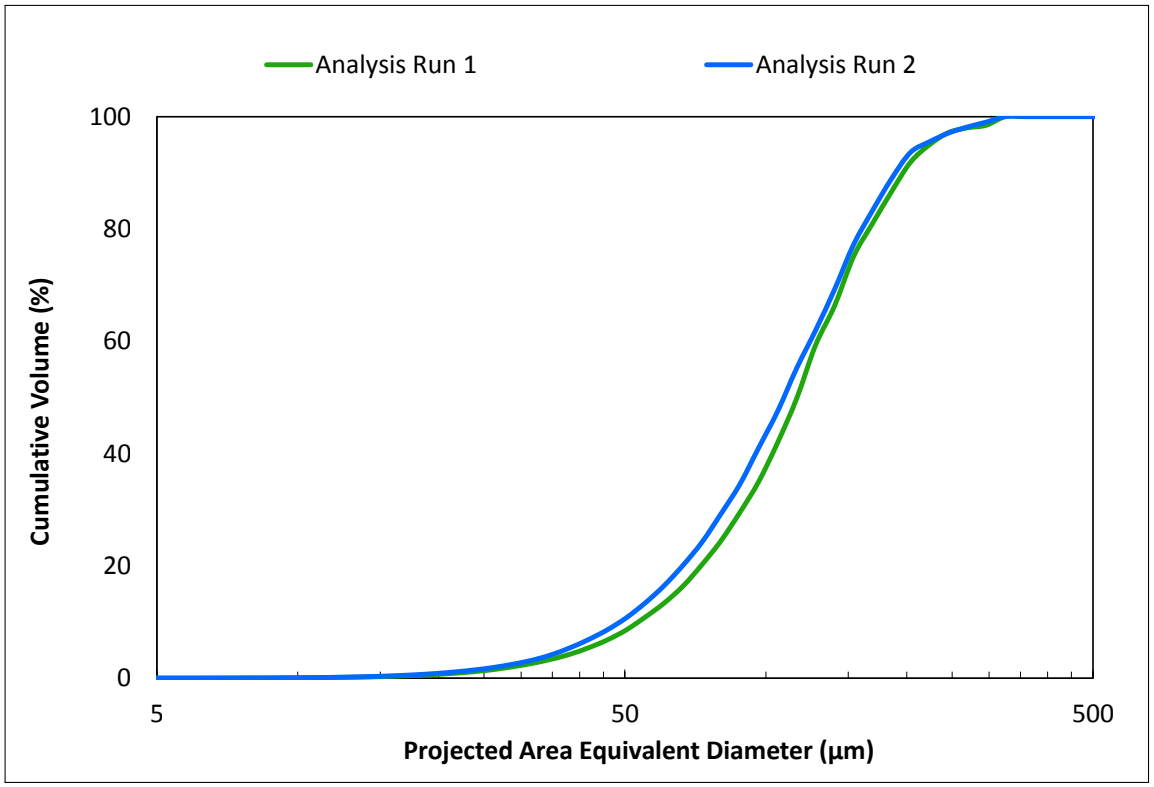

(a) FR-1 in H-PET manufactured on Berstorff ZE40A machine at 122 rpm *and 60* $\mathrm{kg\,h^{-1}}$

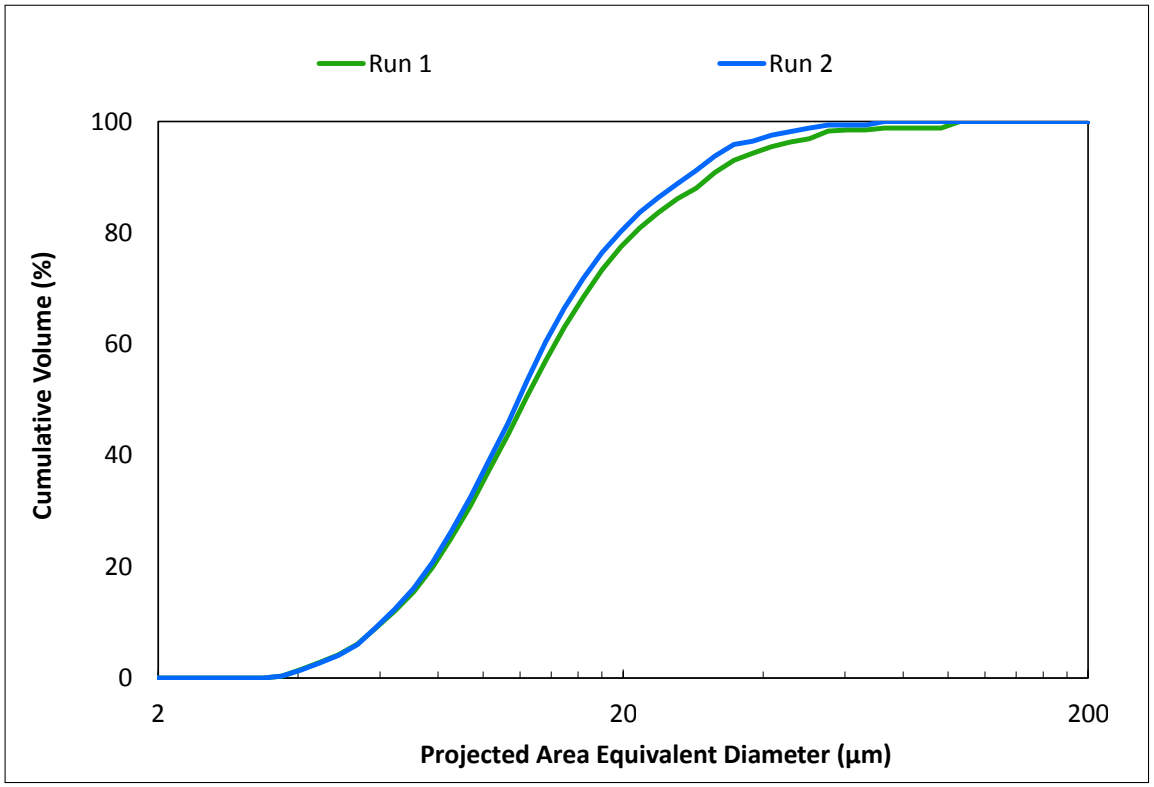

(b) FR-1 in H-PET manufactured on Dr Collin ZK25 machine at 290 rpm *and 6* $\mathrm{kg\,h^{-1}}$

Figure 4.5: *Repeatability and reproducibility of particle size distributions*

Figure 4.5a illustrates the reproducibility of the analysis method proposed. Here, run 1 represents initial analysis of 3 randomly selected chips for a sample manufactured on the *Berstorff ZE40A* machine. Run 2 corresponds to analysis on another set of 3 randomly selected chips from the same batch of material. It can be seen that the reproducibility of analysis is good with only small differences between the two distribution curves being observed.

Figure 4.5b focuses on the repeatability. It shows particle size distributions for FR-1 composites in H-PET matrix. Here, run 1 represents an analysis of a sample manufactured at a given set of conditions. Run 2 represents the results of the analysis on a sample manufactured at the same set of conditions but later in the day. Similarly, it can be seen that good agreement between the two curves exists.

In the cases where the film sample was too opaque or the particles too small to be sized by optical microscopy, scanning electron microscopy (SEM) analysis was undertaken. These were performed on a Hitachi table top SEM, model TM3030. The machine is capable of delivering 15X to 30,000X magnification under 5 and 15 kV electron beam that can be coupled with EDX for elemental composition analysis. It should be noted that for samples containing long aspect ratio particles the orientation of the surface being examined plays a crucial role in determining the visibility of the particles. Initial analysis was performed on a cross section perpendicular to the direction of flow achieved through microtoming the polymer chip; this was later adapted by setting the chip in resin and grinding down top layers to expose a surface parallel to the direction of flow. In the latter, the particles were much more prominent with much better contrast between the particles and the matrix being achieved, thus making image analysis much more accurate. The particle size distributions were generated in the same manner as those for microscopy analysis.

4.1.4 White light interferometry analysis

Some drawbacks of microscopy analysis include a constricted field of view, limited applicability in opaque materials and very poor performance in composites with high loading of filler on a volume basis as it becomes difficult to distinguish individual particles. Surface analysis via white light interferometry (WLI) has potential to overcome these issues with the ability to examine 1 cm^2 area and detect features larger than 0.4 microns. Equipment available at DTF, has the potential to examine 35 by 35 cm area at slight loss of resolution; now detecting ca. 2 micron features. An example of the surface topography information gathered can be observed in Figure 4.6. This was obtained with a Wyko NT3300 optical profiling system at 20 times magnification.

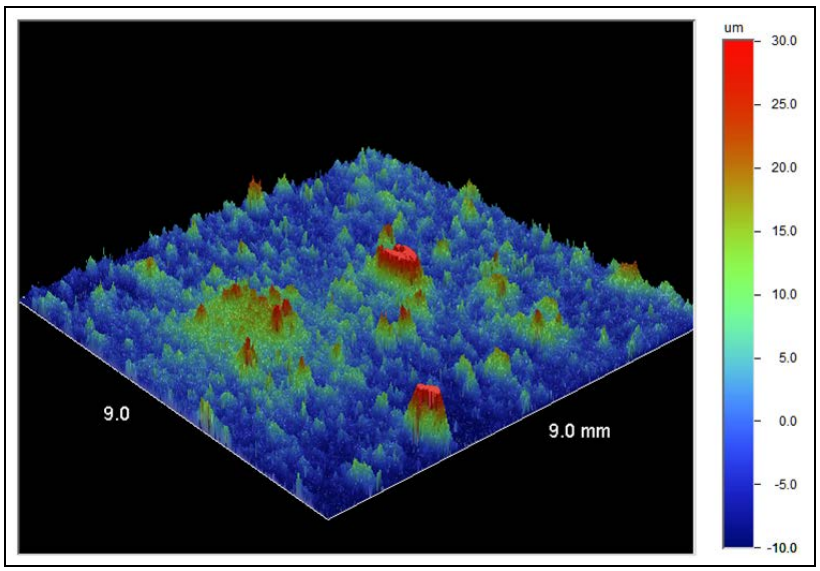

(a) Finished film

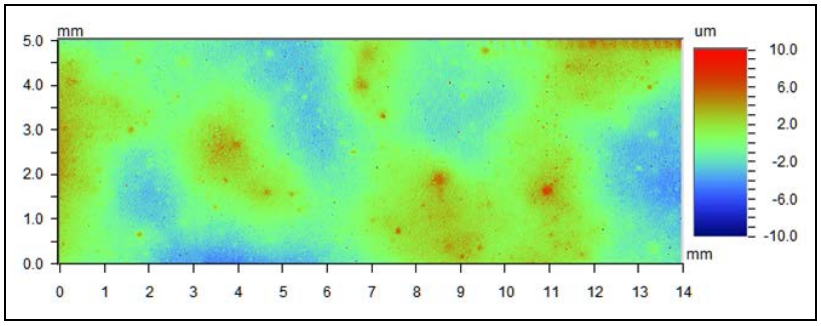

(b) Cast film

Figure 4.6: *White light interferometry analysis of the air side surface for FR-1/S-PET composites manufactured on Berstorff ZE40A machine at 360* rpm *and 122* $kg\,h^{-1}$

It is vital to understand whether the surface analysis is representative of the bulk of the film. In order to evaluate the performance of the technique, the particle size distributions obtained from WLI analysis were compared to the reflected light analysis performed on the cross section of the film (through the film depth). An example cross section for the sample shown in Figure 4.6 is given in Figure 4.7. A total of 12 images through various depth of the film were examined, for a number of samples.

Figure 4.7: *Reflected light microscopy analysis of the cast film cross section for FR-1/S-PET composites manufactured on Berstorff ZE40A machine at 360* rpm *& 122* $\mathrm{kg\,h^{-1}}$

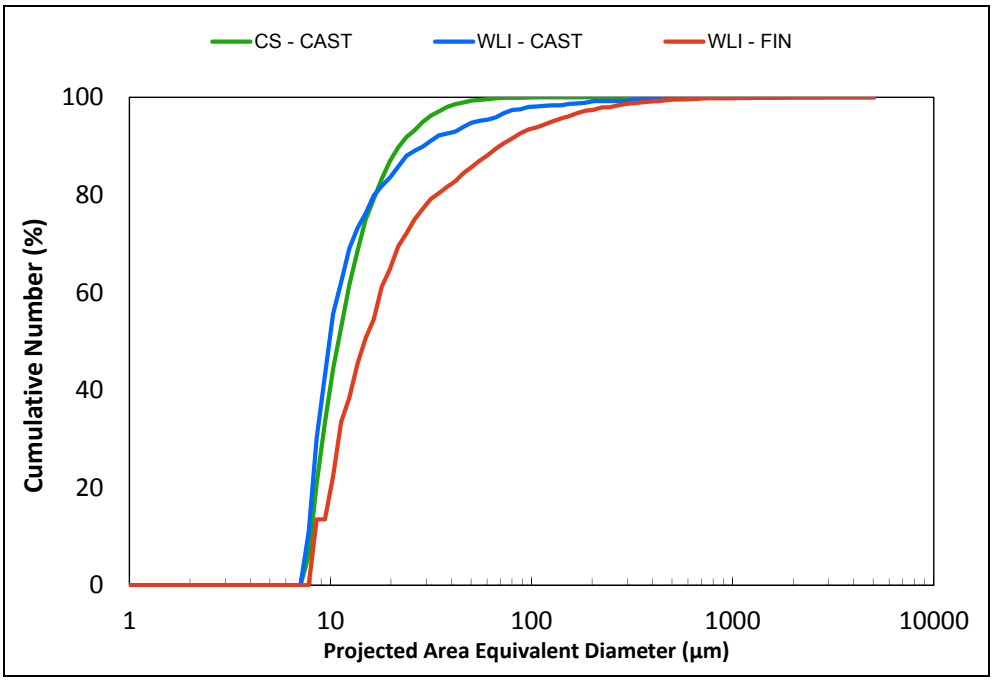

Figure 4.8: *Comparing WLI and reflected light microscopy for FR-1/S-PET composites manufactured on Berstorff ZE40A machine at 360* rpm *& 122* $\mathrm{kg\,h^{-1}}$

Figure 4.8 shows the particle size distribution obtained. It is evident that there is good agreement between the particle size distributions generated, as the distribution obtained via white light interferometry on the cast film sample matches well with that obtained through the reflected light microscopy of the cross sections. The slightly larger tail end of the distribution is likely due to the larger field of view resulting in more of the larger particles being detected. A discrepancy between the cast and the finished film analysis exists. Further research showed this is due to the voiding of the polymer around the additive due to the weak interaction between the additive and the polymer matrix; see Figure 4.9.

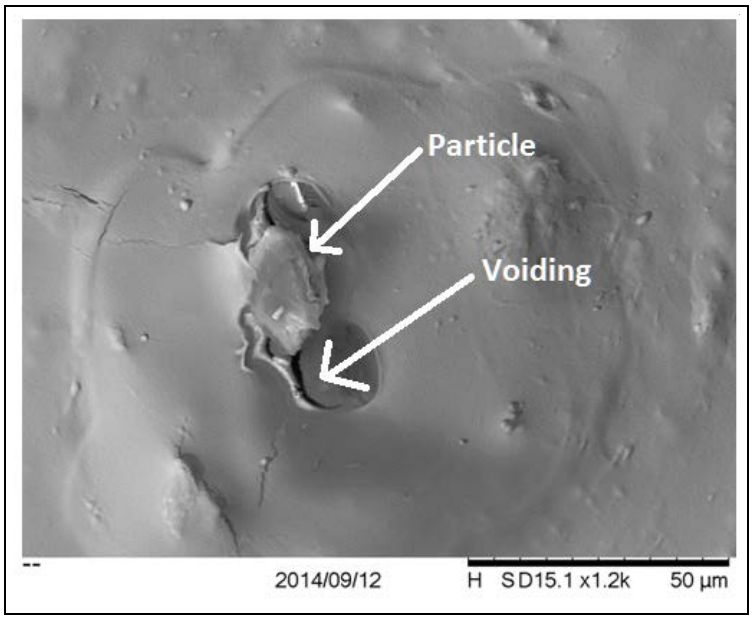

Figure 4.9: *Cumulative volume vs particle size distribution*

One of the challenges with WLI analysis is described by Wicksell's corpuscle problem where it is not known how far the agglomerate is protruding from the surface therefore it is not necessarily the maximum diameter of the particle which is being measured; as represented by the sliding plane in Figure 4.10. A number of potential solutions exist, including that proposed by Williams et al., 2008 who states that the measured diameter corresponds to 79 % of the true 3-D diameter. A more comprehensive statistical solution for unfolding a particle size distribution was proposed by Saltikov, 1967. The method derives the 3-D distribution based on the 2-D particle size distribution and the probability

distribution of where the particle is likely to be sectioned. A *Python* script was utilised to implement Saltikov's method. The script can be obtained from Lopez-Sanchez, 2016 together with the supporting documentation from Lopez-Sanchez, 2017.

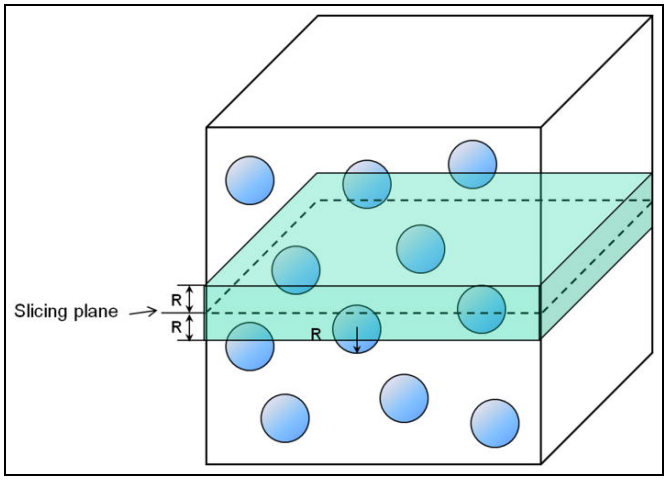

Figure 4.10: *Wicksell corpuscle problem; from Liang and Enright, 2012*

Figure 4.11 shows the shift from the measured cumulative distribution to larger sizes in the Saltikov's cumulative distribution approximates the true 3-D sizes of the particles. An increase of ca. 10 % in the volume occupied by the largest of the particles can be seen.

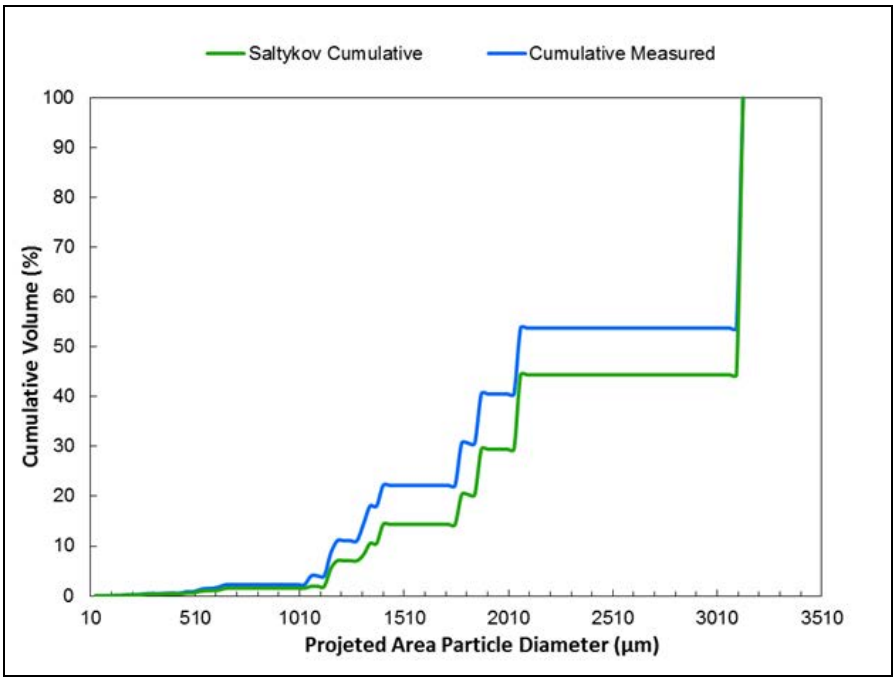

Figure 4.11: *3-D distribution derived via Saltikov method using the Python script*

As well as providing information on the degree of mixing and results which are more representative of the bulk material achieved by inspecting a larger field of view, the use of surface analysis leads to the use of surface statistics. Tools such as quadrant test, nearest neighbour and empty space functions have the potential to improve surface design capabilities of the products. Although some initial exploration of the area has been undertaken, these are not reported here.

4.2 Other analysis

A number of complementary analysis techniques have been utilised throughout this work in order to gain further information about the raw materials and samples manufactured.

4.2.1 Laser diffraction particle size analysis

The particle size distributions of the additives in powder form were obtained via laser diffraction particle size analysis. Beckman Coulter LS 13 320 analyser fitted with polarising intensity differential scattering (PIDS) was used allowing particles in the range from 0.017 to 2,000 µm to be measured (Beckman Coulter, 2009). Mie theory of light scattering model was utilised which takes account of absorption as well as diffraction of light. For the analysis the powder was mixed with water at 10 $\%_{\mathrm{wt}}$ loading and then high shear mixed for 20 min at 400 rpm. The reported distributions are an average of 5 measurements.

4.2.2 Solution viscometry

Intrinsic viscosity of the polymer matrix was determined though solution viscometry using a Viscotek Y501C dilute solution viscometer. Repeatability studies show that an error band of $\pm$ 0.005 $\mathrm{dL\,g^{-1}}$ for the determined IVs corresponds to a 95 % confidence interval (Shortall, 2015). The data reported in this work represents an average of 2 measurements with the errors reported being determined from *student t* distribution to

a 95 % confidence interval. The analysis was performed by dissolving the polymer in Phenol/1,1,2,2-tetrachloroethane solution at 110 °C. Any additive contained within the PET films was accounted for by the computer software and corrections to the viscosity were made based on this.

4.2.3 Melt phase rheology

Melt phase rheology was performed as a complementary technique to solution IV. TA Instruments Discovery Hybrid Rheometer was utilised for analysis using 40 mm parallel plate geometry. The instrument was fitted with the environmental test chamber which allows temperatures ranging from -160 to 600 °C at rates of up to 60 °C min^{-1}. The complex viscosity of the polymer was determined via oscillatory technique with angular velocity of 10 rad s^{-1} and 2 % strain. In order to prevent hydrolysis of the PET during the measurement, the polymer sample was pre-dried overnight in a vacuum oven at 90 °C prior to analysis to remove any moisture contained within the material. In addition, the test was performed under a dry nitrogen atmosphere in order to prevent moisture pick up by the polymer from the air and degradation by thermo-oxidative reactions.

4.2.4 Contact angle

In order to determine the surface free energy of the additive powders a VCA 2500 XE goniometer produced by AST Products was utilised. The surface free energy was calculated from Fowke's expression based on the measured contact angles between the additive powder and two liquids (water and diiodomethane). The theory behind the calculations is addressed in Appendix G. The technique requires a flat surface for the solid phase. This was achieved by using a hydraulic press (kindly provided free of cost by Intertek, Wilton) to compact the powders into disks with 10 t cm^{-2} of force. By removing the air and minimising the porosity within the solid phase in the majority of cases it was possible to place a liquid droplet on the surface without it permeating into the solid.

4.3 Concluding remarks

There are numerous approaches in evaluating the level of mixing achieved by an extrusion process; as discussed in Appendix B. In this work the degree of mixing was examined by considering the end product of the extrusion process; that is the polymer pellets and/or film. A number of analysis techniques were utilised during the course of the project to evaluate the level of mixing achieved within polymer composites and thus develop a better understanding of the fundamental mixing processes. A commonly used combination of optical microscopy and image analysis was utilised to determine the size of additive within polymer matrix. However, unlike in the literature, the degree of dispersion was specified relative to the particle size distribution of the additive in its raw form in order to be able to better compare different additive/polymer systems. The notion of utilising surface analysis via white light interferometry to effectively size the additive within the polymer composite is proposed. This allows for a much larger area to be examined than that achieved via optical microscopy thus generating results that are more representative of the bulk material. The technique appears to be suitable for composite and blend systems.

A number of auxiliary techniques were used to provide further information on the systems being studied. As well as initial attempts to characterise the degree of interaction between the additive and the polymer, techniques enabling the properties of the polymer matrix and that of the powder additive to be examined such as solution viscometry and laser diffraction were also used.

5 Equipment specifications, layout and limitations

The research presented in this thesis involved a large number of experiments to examine the impact of material properties, operating conditions as well as equipment configuration on the level of mixing achieved in PET based polymer composites. Initially, the practical work was carried out on the larger of the two pilot scale facilities at DuPont Teijin Films U.K. Ltd. (DTF) at Wilton. This facility is based around a sequential draw process to manufacture bi-axially oriented film ranging in thickness from tens to hundreds of microns and over a metre in width. There is a possibility to manufacture multilayer films either through *injector block* or *multi-layered die* technologies that are coupled to three extruders; two single screw machines and a twin screw machine.

As discussed in Section 2.2.3, twin screw machines offer a superior mixing performance to single screw machines. Based on this, the twin screw extruder on the pilot plant was utilised for the initial experiments. For simplicity, this twin screw extruder hereinafter shall be referred to as the *Berstorff ZE40A* machine. The limitations of the *Berstorff ZE40A* machine resulted in a collaboration between DTF and Nanoforce Technology Ltd. who are based at Queen Mary University of London, Mile End being established. As part of this collaborative work DTF gained access to a laboratory scale twin screw extruder hereinafter referred to as the *Dr Collin ZK25* machine and the expertise of Dr. Wei Tu and Olivier Picot.

5.1 *Berstorff ZE40A* extruder specifications and layout

The *Berstorff ZE40A* machine was manufactured in 1989 by is a KraussMaffei Berstorff. Key specification is given in Table 5.1. Each of the individual zones is water cooled with heating also being possible through 'cuff' heaters. The chute to the feed pocket can be vibrated to prevent accumulation of materials. The extruder is fitted with a 'gentle' screw configuration providing 1.5 $^{L}/_{D}$ of mixing post melt section which itself is 3 $^{L}/_{D}$.

Table 5.1: *Specification for the Berstorff ZE40A (KraussMaffei Berstorff GmbH, 1989)*

Berstorff	ZE40A
Barrel Diameter (mm)	42.6
$^{L}/_{D}$	28
Number of zones	7
Motor power (kW)	30
Maximum torque (N m)	130
Maximum screw speed (rpm)	460
Maximum output (kg h^{-1})	ca. 160*

* *depending on polymer viscosity*

The extruder is equipped with a vacuum extraction system capable of reaching pressures of ca. 10 mbar which is located immediately post the melting section in zone 4; see Figure 5.1. The figure also provides the function of each zones, location of thermocouples and pressure transducers.

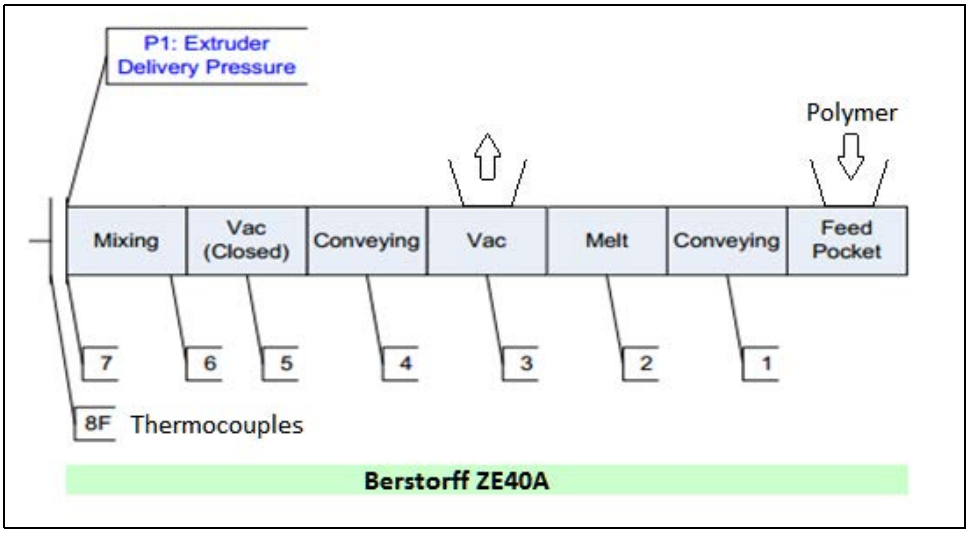

Figure 5.1: *Berstorff ZE40A extruder layout*

In a standard process un-dried polymer is pneumatically conveyed to the hopper located above the extruder. The hopper supplies a Brabender feeder which has an inventory of ca. 40 kg. The machine is operated in starve fed mode with the feeder enabling the polymer throughput to be independently controlled from the extruder screw speed.

Upon exiting the extruder the polymer flow is stabilised with the use of a melt pump which also generates the required pressure to push the material through the rest of the melt system. Post melt pump the material passes through a screen changer. A variety of sizes are available with typically a 40 µm mesh being selected. However, for this work no screen changer was utilised in order to make sure that any large agglomerates would be visible within the film. It is important to note that the pressure drop across the screen changer correlates with the build up of a filter cake, which in itself can act as an indicator of additive dispersion. After the filter the polymer flows towards the die where it is extruded into a melt curtain. This is rapidly cooled in order to minimise crystallisation. The overview of the film making process is provided in Section 2.1.

5.1.1 Additive feeding

Starve feeding of the *Berstorff ZE40A* machine also allows for the additives to be independently introduced into the feed pocket of the machine via three separate feeders. The first is a volumetric Posimax cone feeder by Ktron which is capable delivering outputs ranging from grams per hour up to a maximum of ca. 1 $\mathrm{kg\,h^{-1}}$. Although this feeder is able to deliver very low outputs, the geometry of the feeder requires the additive to be free flowing in nature; otherwise bridging of the additive occurs. A single screw gravimetric Brabender feeder is also available. This is capable of generating outputs from hundreds of grams per hour up to ca. 15 $\mathrm{kg\,h^{-1}}$. The feeder is fitted with a spiral or a blade screw and is generally used to feed masterbatch pellets. The geometry of the screws and that of the hopper also made the feeder unsuitable for feeding cohesive materials.

In addition to the single screw feeder, a twin screw gravimetric Brabender feeder is also available and is capable of delivering outputs from ca. 0.5 to 25 $\mathrm{kg\,h^{-1}}$. This feeder can be equipped with blade or concave screws as well as a mechanical agitator theoretically making it suitable for feeding cohesive powders. The different screws types are shown in Figure 5.2.

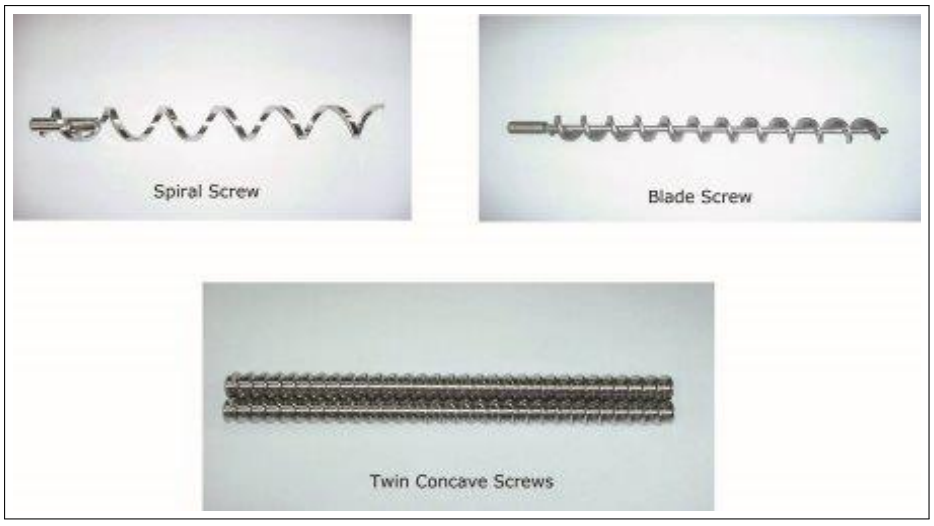

Figure 5.2: *Feeder screw types; from Powder and Bulk Solids, 2016*

As well as feeding the additives separately, it is possible to premix the powder with the

polymer manually and feed this with the main polymer feeder or via the single and/or the twin screw feeder. Care must be taken in order to prevent segregation of the additive and the polymer due to differences in size between the chip and the polymer pellets (Stevens and Covas, 1995), particularly when there is poor interaction between the two materials. Segregation is most likely when the additive particles are large enough for their weight to dominate the interaction forces. Bart, 2006 highlights that segregation is likely when $D_p > 75\mu m$ and should not occur if $D_p < 10\mu m$. In practice, when utilising an additive premix once the number of particles exceeds that which completely cover the surface of the polymer pellets some segregation is likely to occur even in strongly interacting systems.

5.1.2 Limitations of the twin screw Brabander feeder

The accuracy of the feeder was established by verifying the experimentally determined output with the feedback value from the control system. The experimental values were determined by collecting and weighing the material delivered by the feeder over a period of 3 min at each set point. The sample was taken once the feeder has reached a steady state and the measurements were repeated at least twice. By monitoring the errors regarding 'overspeed' and 'underspeed' within the control system the minimum and maximum stable outputs possible for a given additive were determined. An example results plot is shown in Figure 5.3 where the first and last point on the plot represent the minimum and maximum outputs obtained.

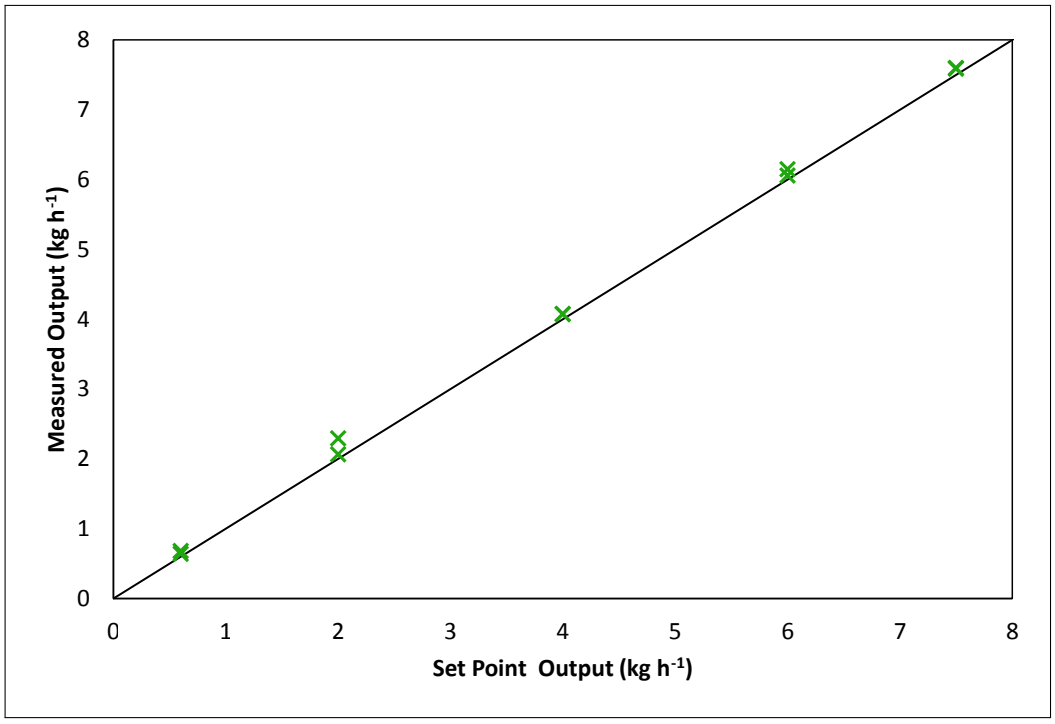

Figure 5.3: *Feeding accuracy of W-1 whitener on Brabander twin screw gravimetric feeder fitted with concave screws and mechanical agitator*

It should be noted that the concave screws were not the optimum solution for feeding of all powders. In the case of flame retardant additive FR-4, the material was compacted onto the screw (see Figure 5.4) at outputs above 4 $\mathrm{kg\,h^{-1}}$, which is roughly half of the maximum value observed when feeding whitener W-1. The compaction of material resulted in severe noise being generated by the machine. Although less critical in the case of FR-4 as the material melts within the extruder, such compaction of material in the feeder means that extra work has to be done by the extruder in order to disperse the additive. This is particularly critical with the additives that remain as a solid throughout the extrusion process. The issues were overcome by utilising the blade screws coupled with the mechanical agitator. These allowed for a maximum output of 6 $\mathrm{kg\,h^{-1}}$ whilst maintaining the accuracy of feed at a similar level to that obtained with the concave screws; see Figure 5.5. Experiments showed that typically the blade screws provide poorer accuracy and maximum output when compared to the concave screws.

Figure 5.4: *Compaction of FR-4 additive onto the feeder screws*

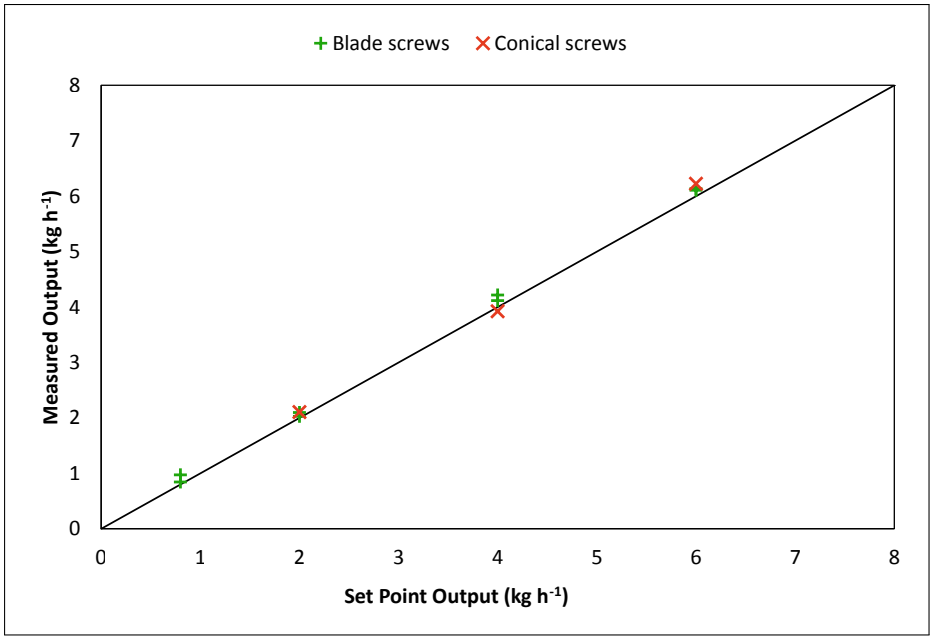

Figure 5.5: *Feeding accuracy of FR-4 flame retardant on Brabander twin screw gravimetric feeder fitted with concave or blade screws and a mechanical agitator*

Feeding of friable additives such as the UV-1ED ultraviolet additive grade also presented several challenges. Whilst using the blade screws the maximum output was significantly

higher, however the feed was less stable and the maximum output reduced with time as the additive broke up and accumulated in the clearance between the screw flight and the barrel; see Figure 5.7. The concave screws on the other hand provided a lower maximum but a much more stable delivery of feed; see Figure 5.8. As the flows within a co-rotating TSE tend to resemble plug flow this results in poor axial mixing, especially on configurations with fewer mixing elements. As a result the stability of the feed is critical in order to ensure that a uniform product is generated with no variation in the additive concentration along the length of the film. Figure 5.6 shows the extent of additive build up between the screw flight and the barrel surface.

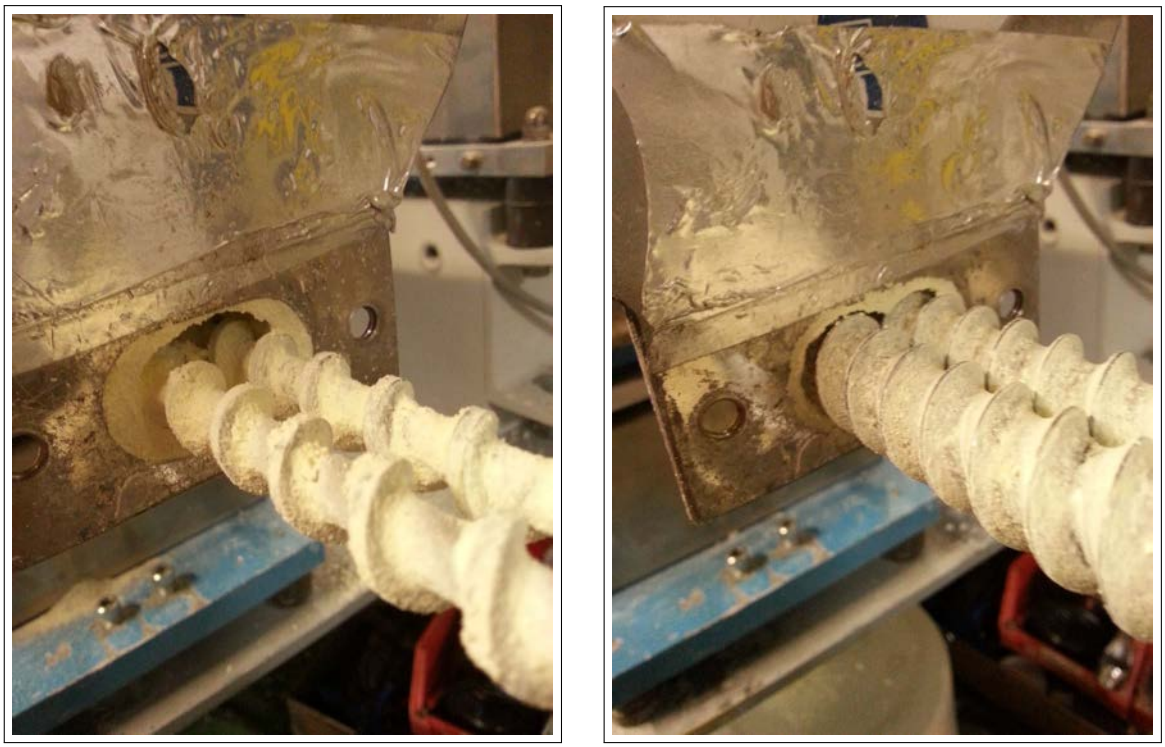

(a) *Blade screws* ***(b)*** *Concave screws*

Figure 5.6: *Generation and build up of powder on Brabander twin screw feeder processing UV-1ED additive*

The fine powder generated in the feeder does not only influence the performance of the feeder, but in layouts such as that around the *Berstorff ZE40A* extruder where the feeder is not directly supplying the feed pocket, the fines have a tendency to build up in the conveying system downstream of the feeder. Eventually this leads to clumps of material

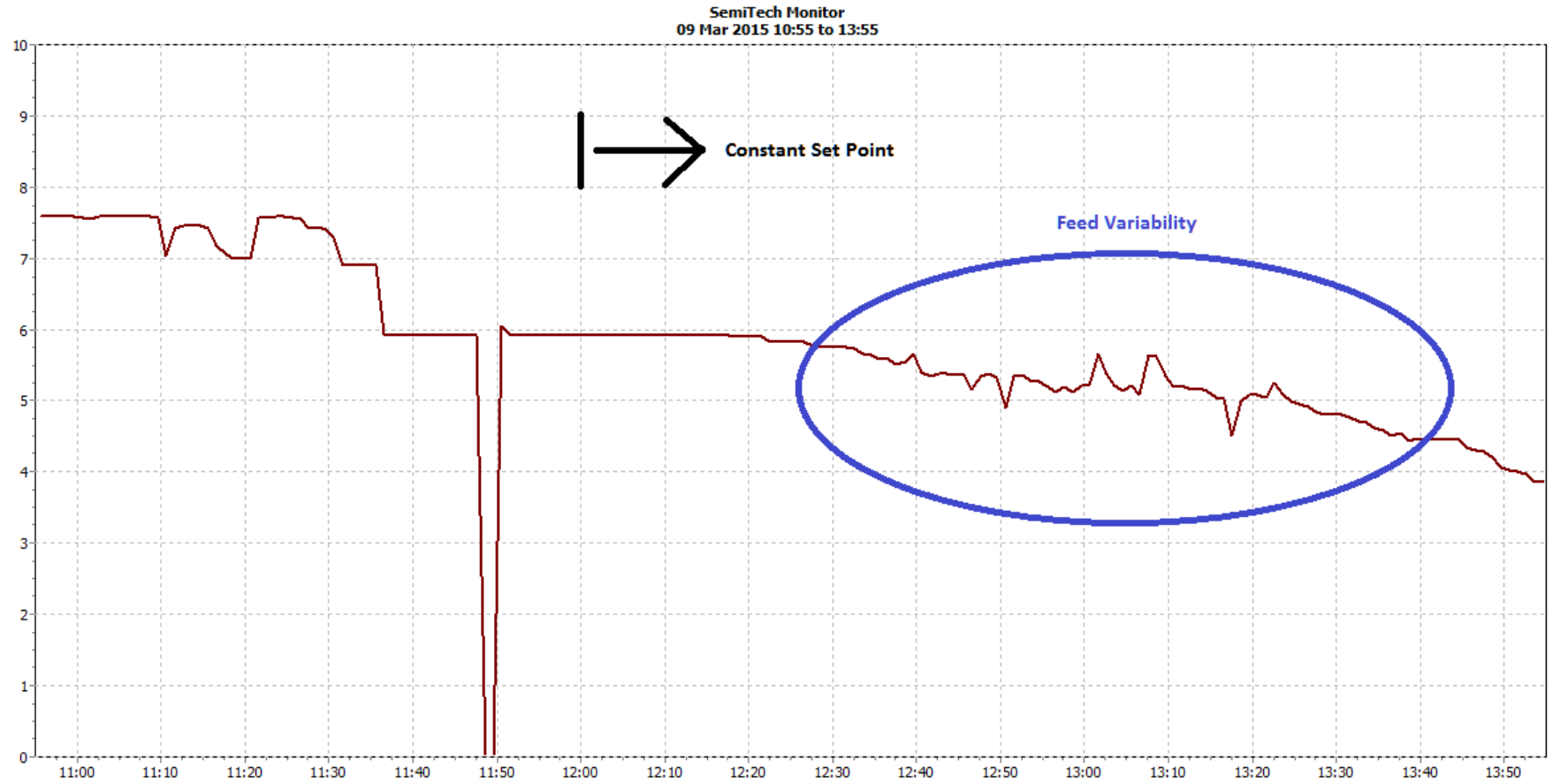

Figure 5.7: *Feedback value for output in* $\mathrm{kg\,h^{-1}}$ *on twin screw Brabender feeder fitted with blade screws (UV-1ED additive)*

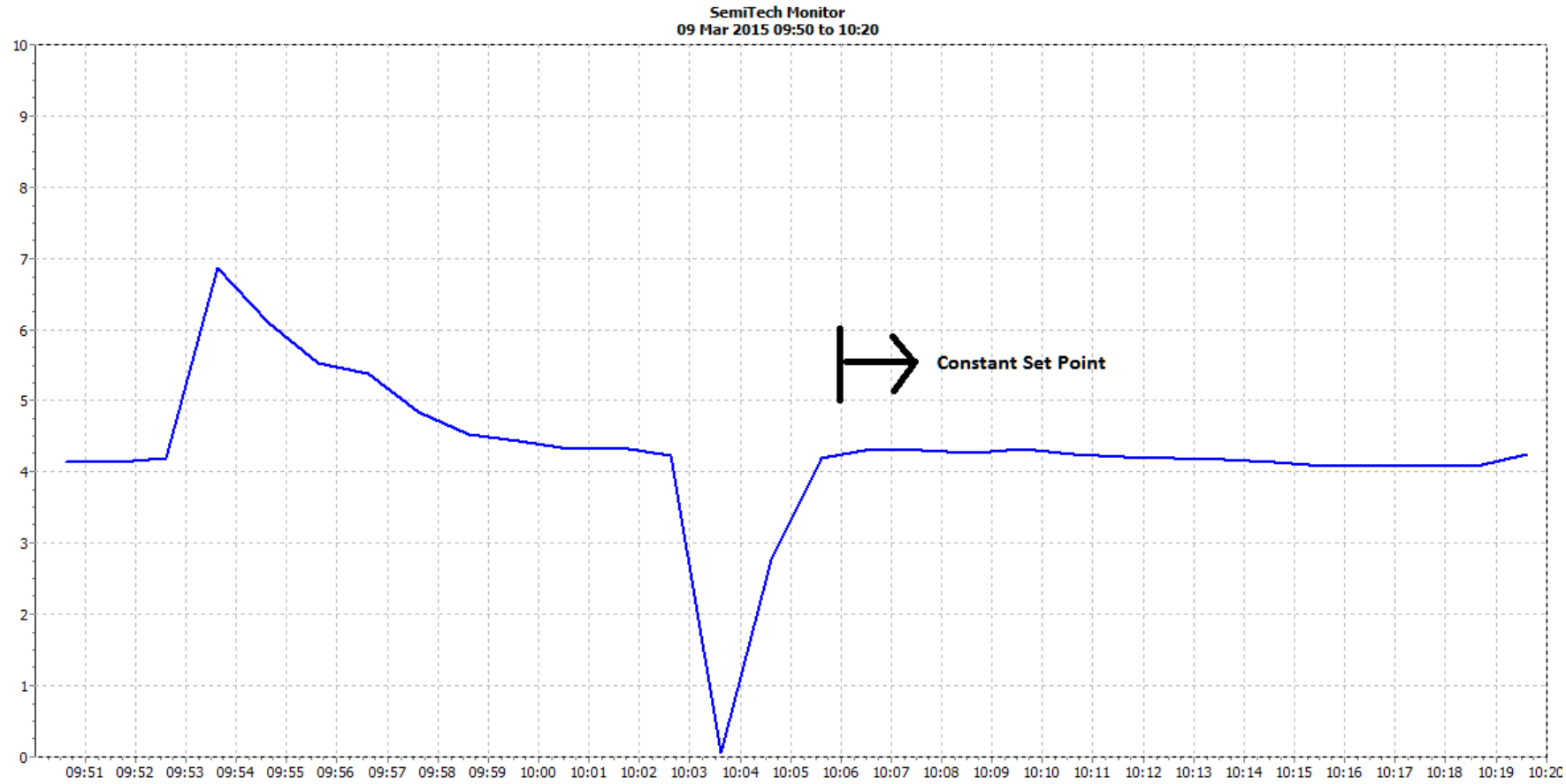

Figure 5.8: *Feedback value for output in* $\mathrm{kg\,h^{-1}}$ *on twin screw Brabender feeder fitted with concave screws (UV-1ED additive)*

breaking off which then produces concentration spikes within the product. Therefore it is clear, that other layouts or feeder technologies such as belt feeders should be considered for the conveying of friable materials.

5.2 Limitations of the *Berstorff ZE40A* layout

Both Giles et al., 2005 and Rauwendaal, 2010 outline the importance of additive bulk density on feeding of the materials and equipment design particularly regarding the injection points. Rauwendaal, 2010 reports that feeding issues may prevail when the bulk density of the material is less than 30 % of its solid density. Giles et al., 2005 states that materials with bulk density below 320 $\mathrm{kg\,m^{-3}}$ may be difficult to feed; particularly as the powders begin to have a tendency to bridge in the hopper. Bridging can also occur in heavier materials that are cohesive; this was the experience when feeding the W-1 whitener grade.

The split feed process, such as that on the *Berstorff ZE40A* machine, where the additive is introduced into the feed pocket of the extruder via a separate stream to the polymer has a very limited applicability when dealing with low bulk density materials. Here, the air escaping from the feed pocket has the tendency to fluidise the powder (Stevens and Covas, 1995). This results in the particles that are entrained in the air flow being carried out from the extruder which not only produces inconsistent feed but also generates a significant quantity of dust. This is particularly critical in screw configurations where significant back mixing is present or when operating at high screw speed. Typically within the compounding industry such materials would be incorporated using a stuffer feeder (Rauwendaal, 2010) with atmospheric vents allowing the air which has entered together with the additive to be removed once the material is wetted out by the polymer.

Such issues in feeding were experienced when introducing FR-1 flame retardant grade which has a bulk density of 100 - 250 $\mathrm{kg\,m^{-3}}$. Figure 5.9 shows the extent of dust

accumulation. The feeding of silica grades which have porous particles and therefore the particles are considerably lighter was not attempted and the alternatives were found in the *Dr Collin ZK25* machine with the use of a stuffer feeder.

This set up also poses challenges for the feeding of the long aspect ratio filler as the high shear stresses in the melt section can lead to the attrition of the filler. The flowability of the fibrous material decreases with increasing aspect ratio (Schulze, 2008) and in order to minimise attrition twin screw feeders are often replaced with vibrating feeders Giles et al., 2005. The feeders should be selected to ensure that under typical operating conditions they are not operating close to the minimum speed in order to provide a consistent feed of material.

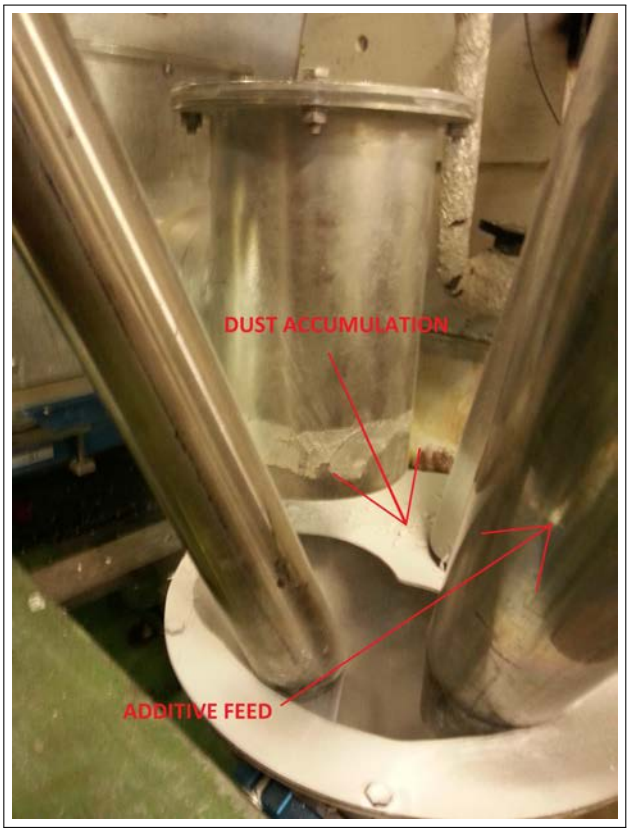

Figure 5.9: *Feeding accuracy of FR-4 flame retardant on Brabander twin screw gravimetric feeder fitted with concave or blade screws and a mechanical agitator*

5.3 *Dr Collin ZK25* extruder specifications and layout

The specification for the *Dr Collin ZK25* twin screw extruder is given in Table 5.2. The extruder consists of 7 zones, with each individual zone being electrically heated and pneumatically cooled. The overall set up includes two Ktron feeder, one for feeding the polymer chip and the other for dispensing the additive. These can be fitted with either blade or conical screws. The additive is injected directly into the melt with the use of a Ktron stuffer feeder that is fitted with blade screws. The air entrained with the additive can either be removed via the atmospheric vent ports or be allowed to escape back via the side feeder which is operated partially full. As the machine is not fitted with a capacity for vacuum extraction the PET polymer had to be pre-dried prior to the experiments. This was done in order to ensure that any moisture present within the material was removed and did not lead to hydrolysis which in turn reduces the viscosity of the material.

Table 5.2: *Specification for the Dr Collin ZK25 (Dr Collin GmbH, 2018)*

Dr Collin	ZK25
Barrel Diameter (mm)	25
$^{L}/_{D}$	42
Number of zones	7
Motor power (kW)	9.7
Maximum torque (N m)	180
Maximum screw speed (rpm)	460
Maximum output ($kg\,h^{-1}$)	ca. 10*

* *depending on polymer viscosity*

The extruder is fitted with a lace die generating a single strand of polymer. This is cooled in a water bath with the air knife removing the excess moisture prior to the strand being cut with a pelletiser. Figure 5.10 illustrates the layout.

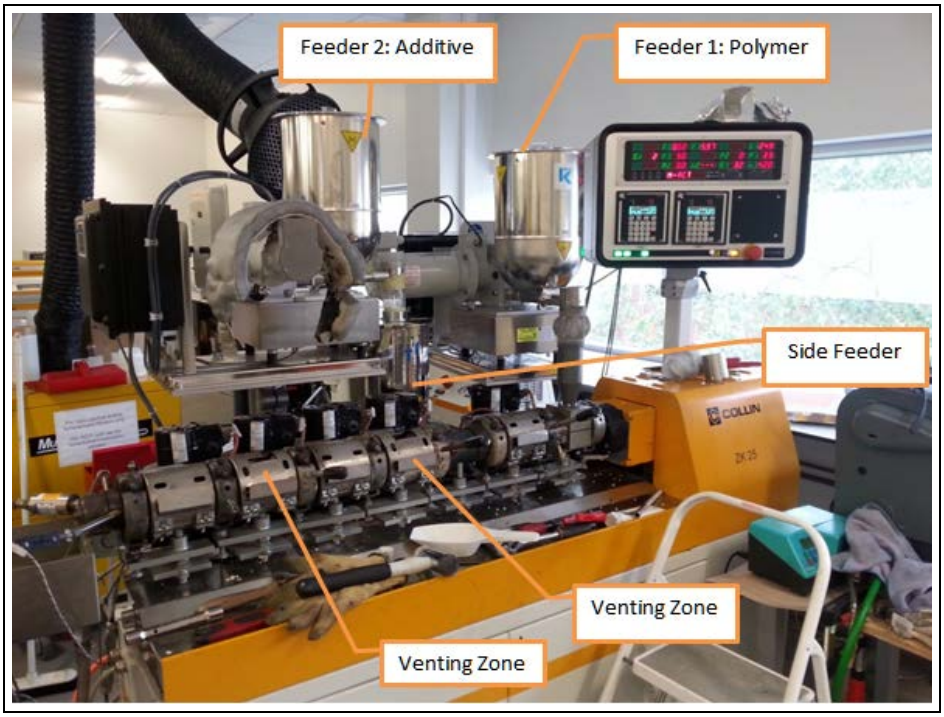

(a) Dr Collin ZK25 set up

(b) Overall layout of equipment

Figure 5.10: *Layout of Dr Collin ZK25 extruder and auxiliary equipment*

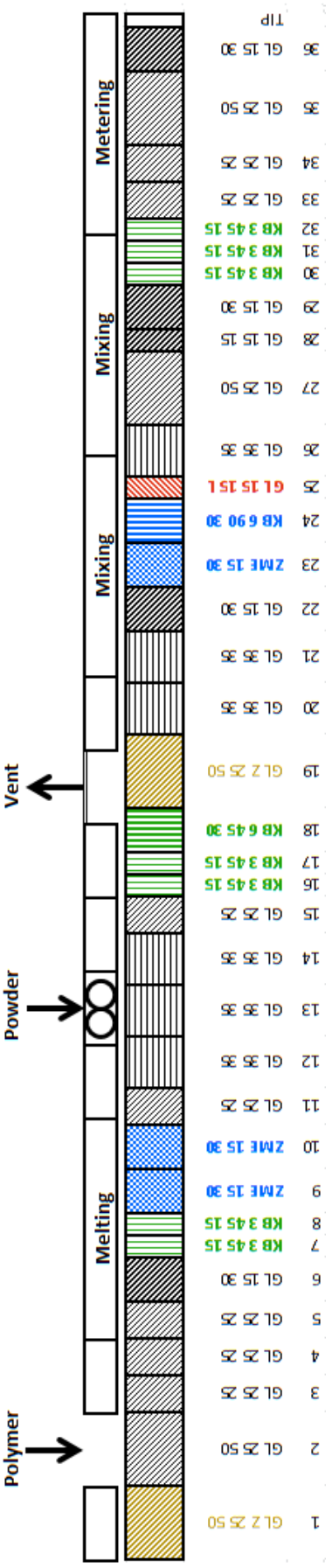

Figure 5.11: *Existing screw geometry on the Dr Collin ZK25 machine*

The *existing* configuration, illustrated in Figure 5.11, is set up to allow the additive to be introduced directly to the melt in zone 3 with the use of large pitched conveying elements. These are followed with narrow kneading blocks with equipped with narrow disks in order to distribute and wet out the powder as well as wider disks to provide dispersive mixing. Further mixing section is located in zone 5 where a slotted mixing element is used to provide dispersive mixing and a kneading block fitted with wide disks coupled to a reverse conveying element to deliver dispersive mixing. Further narrow disk kneading blocks are utilised at end of zone 6 to redistribute the additive within the melt one more time prior to it exiting the extruder in zone 7. Spaces between the various mixing sections are filled with large pitch conveying elements that promote the rapid conveying of material and the reduction in the degree of fill which results in increased shear stresses being delivered into the system.

5.4 Concluding remarks

The *Dr Collin ZK25* set up has several key advantages over the *Berstorff ZE40A* layout as it provides the ability to introduce additives directly into the polymer melt. This in turn enables additives with very low bulk density to be incorporated into the polymer. This smaller lab scale unit will act as a proof of concept for potential investments on the larger *Berstorff ZE40A* machine. In addition, due to *Dr Collin ZK25* machine being a stand alone unit it is much easier to explore the impact of different screw configurations as the process of swapping screws is considerably quicker. Similarly, the longer length of the *Dr Collin ZK25* machine will help determine if the 28 $^{L}/_{D}$ is sufficient to achieve good dispersion of the additives or if a longer machine is required. One disadvantage of the *Dr Collin ZK25* layout is the lack of cast film die resulting in the need to process the pellet samples in order to analyse the level of dispersion.

6 | Modelling of the shear and flow fields inside the co-rotating twin screw extruder

Increasingly the industry is relying on modelling of the TSE process to allow rapid development of the optimal screw configurations for a given application. Modelling is much quicker than experimental trials and is much more cost effective. If utilised correctly the models can be used to develop an understanding of flow and shear conditions which have a direct impact on the mixing of additives and polymers.

6.1 Development of an 'in-house' TSE model

This chapter focuses on extending the capability of a 1-D extrusion model inherited from M. Ellam (2013) which is used in-house by DTF to calculate the flow velocity, pressure, degree of fill and residence time within each element for a given screw profile at set operating conditions. The pressure drop calculations are based on the Hoffman alpha, α and beta, β constants provided by DuPont Corporate Labs; see equation 6.1:

$$\frac{\partial P}{\partial z} = \frac{\eta\left(\alpha 60N - \frac{\dot{m}}{\rho}\right)}{\beta} \tag{6.1}$$

where P is pressure in bar, z is the axial distance along the extruder in m, η is the melt viscosity in Pa s, N is screw speed in rpm, $\dot{m}$ is the throughput in $\mathrm{kg\,h^{-1}}$, ρ is density in $\mathrm{kg\,m^{-3}}$. Constants α & β with units of $\mathrm{m^3\,rpm^{-1}}$ and $\mathrm{m^4\,Pa\,s\,bar^{-1}\,h^{-1}}$ respectively are element dependent and are discussed in White, 1990.

Appendix D provides the details of the calculations performed in the existing model. Within the experience of DTF, the pressure and fill profiles calculated are known to

be accurate in the melt sections; but are only approximations for non molten material (Ellam, 2013a).

The extended functionality is based on the ideas proposed in Potente et al., 1994 including the ideology of modelling kneading block sections as a pseudo conveying channel. Unlike the model proposed by Potente et al. which simply calculates the average shear rate and stress in the cross section of the channel, this development proposes the use of a new parameters: the 'residence time weighted average shear rate' and the 'residence time weighted average shear stress'. These parameters account for the average shear rate and stress conditions in each element within the screw configuration thus allowing for the shear conditions across the whole screw geometry to be represented by a single number. They allow rapid comparison between different operating conditions and screw designs. It is also hoped that these average shear conditions in the extruder as a whole can be related to the level of mixing observed in a polymer blend/composite system.

6.1.1 Geometry of Twin Screw Extruders

Although the geometry of TSEs is complex, it can be described mathematically once several key parameters are set; such as the screw diameter and the centreline distance. Booy, 1978, Potente et al., 1994, Rauwendaal, 1986 (see p.459-476) and 1996 provide detailed descriptions for the geometry of TSEs; a brief summary of the most important equations is provided here.

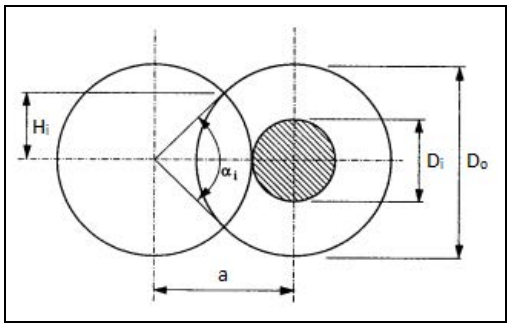

Figure 6.1: *Key parameters defining the geometry of TSEs; from Rauwendaal, 1996b, see p.128*

Figure 6.1 shows a cross section of the TSE machine and acts as a basis for the definition of the machine's geometry. Typically the outside screw diameter, D_o and the centreline distance, a would be set during the design process; allowing the other parameters describing TSE geometry to be calculated. As discussed by Rauwendaal, 1996b, once the outside screw diameter is set the minimum value for the centreline distance is governed by the geometry of the self-wiping profile. For a double flighted design this is given by:

$$\frac{a_{min}}{D_o} = 0.5\sqrt{2} \approx 0.707 \tag{6.2}$$

The root diameter, D_i is calculated from D_o and a as below.

$$D_i = 2a - D_o \tag{6.3}$$

From this, the D_o/D_i ratio can be established whose magnitude is an indicator of the free volume within the machine.

The D_o and a parameters also determine the degree of intermeshing; defining the intermeshing angle, α_i and the intermeshing height, H_i. These can be evaluated as:

$$\alpha_i = 2\arccos\left(\frac{a}{D_o}\right) \tag{6.4}$$

$$H_i = \frac{1}{2}D_o \sin\left(\frac{1}{2}\alpha_i\right) \tag{6.5}$$

Delving deeper into the design of TSEs, one can focus on the cross section of the screw. A double flighted design is discussed here as it is by far the most common for co-rotating TSEs; see Figure 6.2. It can be divided into three areas: the flight tip, flight flank and flight root with the width of the sections determining the corresponding angles α_t, α_f and α_r.

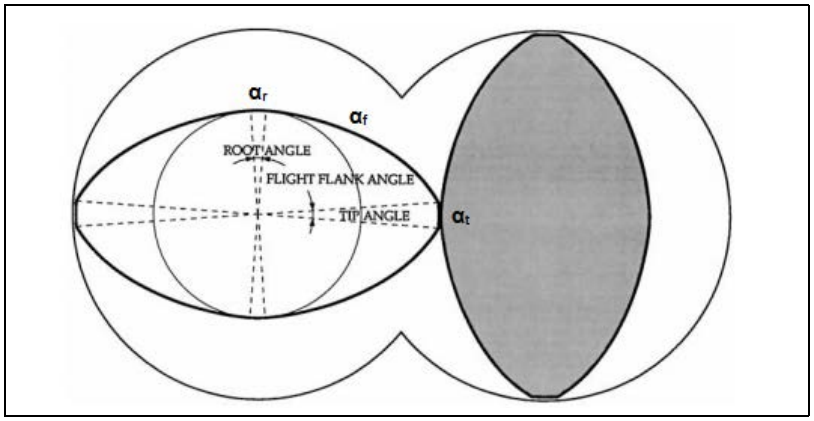

Figure 6.2: *Geometry for double flighted TSE; from Rauwendaal, 1996b, see p.129*

Considering the left hand screw in the Figure 6.2, the sum of these angles for all flights on the screw (p) should equal to 2π radians.

$$p\alpha_t + 2p\alpha_f + p\alpha_r = 2\pi \tag{6.6}$$

The left and right hand screws have the same self wiping profile so the root angle should equal the flight angle. Therefore the flight tip angle and the flank angle can be related as follows:

$$p\alpha_t + p\alpha_f = \pi \tag{6.7}$$

The rotation of the screws can be visualised as a right hand screw (B) rolling around a stationary left hand screw (A). As B moves relative to A, it cuts a path from root to tip, extending over an angle equal to the intermeshing angle. Thus the *intermeshing angle* α_i *equals the flank angle* α_f; (Rauwendaal, 1996b). Hence one can write, where the angles are in radians:

$$\alpha_t = \frac{\pi}{p} - \alpha_i \tag{6.8}$$

One other important parameter is the helix angle, ϕ (sometimes referred to as pitch angle) which describes the forward conveying capacity of the screw; see Figure 6.3.

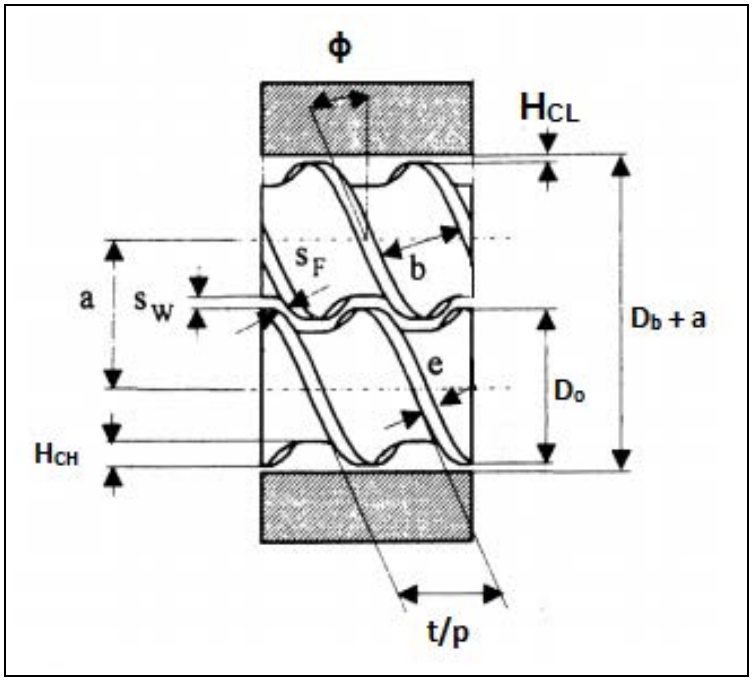

Figure 6.3: *Geometry of TSE; from Potente et al., 1994, see p.14*

The helix angle can be related to the pitch, t and the circumferential distance, πD_o around the screw.

$$\phi = \arctan\left(\frac{t}{\pi D_o}\right) \tag{6.9}$$

The flight width, e and the channel width, b are calculated from the helix and flight tip angle; as follows:

$$e = \frac{t \cdot \alpha_t \cdot \cos(\phi)}{2\pi} \tag{6.10}$$

$$b = \frac{t \cdot \cos(\phi)}{p} - e \tag{6.11}$$

The channel depth (root to screw tip), H_{CH} at the centre of the channel can also be calculated from the outside diameter and the centreline distance.

$$H_{CH} = D_o - a \tag{6.12}$$

This value represents the maximum channel depth, H($\theta = 0$). However, if one would like to know how this changes with the rotation of the screw then its cross section needs to be considered, see Figure 6.4.

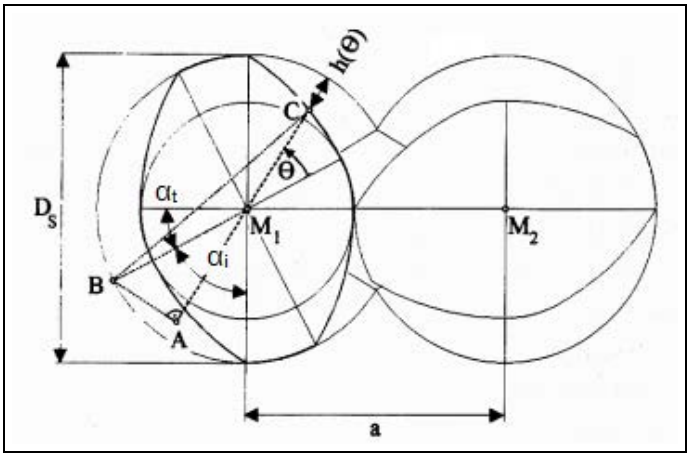

Figure 6.4: *Geometry of TSE cross section; from Potente et al., 1994, see p.12*

The change in height as a function of the angular coordinate, θ can be described as follows:

$$H(\theta) = \frac{D_o}{2}\left[1 + cos(\theta)\right] - \sqrt{a^2 - \left(\frac{D_o}{2}\right)^2 \sin^2(\theta)} \tag{6.13}$$

Potente et al., 1994, (see p. 12) found that this can be approximated by the 4^{th} order polynomial where c_1 and c_2 are constants as follows:

$$H(\theta) = c_1 \cdot \theta^4 + c_2 \cdot \theta^2 + D_o - a \tag{6.14}$$

where

$$c_1 = -\left[\frac{1}{24} \cdot \frac{D_o}{a} - \frac{1}{128} \cdot \left(\frac{D_o}{a}\right)^2 - \frac{1}{48}\right] \quad \text{and} \quad c_2 = -\left[\frac{1}{4} - \frac{1}{128} \cdot \left(\frac{D_o}{a}\right)\right] \cdot D_o$$

It is often useful to consider a co-rotating TSE machine in a similar manner to a SSE by 'unwinding' the screw channel and the barrel; see Figure 6.5a. Kinematic reversal is applied such that the barrel surface moves relative to the screw. It is assumed that no flow occurs in the intermeshing region, hence the equivalent length of the barrel, L_{eq} for each screw can be calculated as:

$$L_{eq} = (2\pi - \alpha_i) \cdot D_o \cdot \cos(\phi) \tag{6.15}$$

In such cases, it is important to understand how the height changes in Cartesian coordinates (x, y, z); see Figure 6.5b. This can be achieved by applying the following transformation to Equation 6.13:

$$\theta = \frac{2x}{D_o \cdot \sin(\phi)} \tag{6.16}$$

The resultant equation is valid for $-b/2 \leq x \leq -e/2$ and $e/2 \leq x \leq b/2$ for axis definition employed in Figure 6.5b where the origin is located at the centre of the channel.

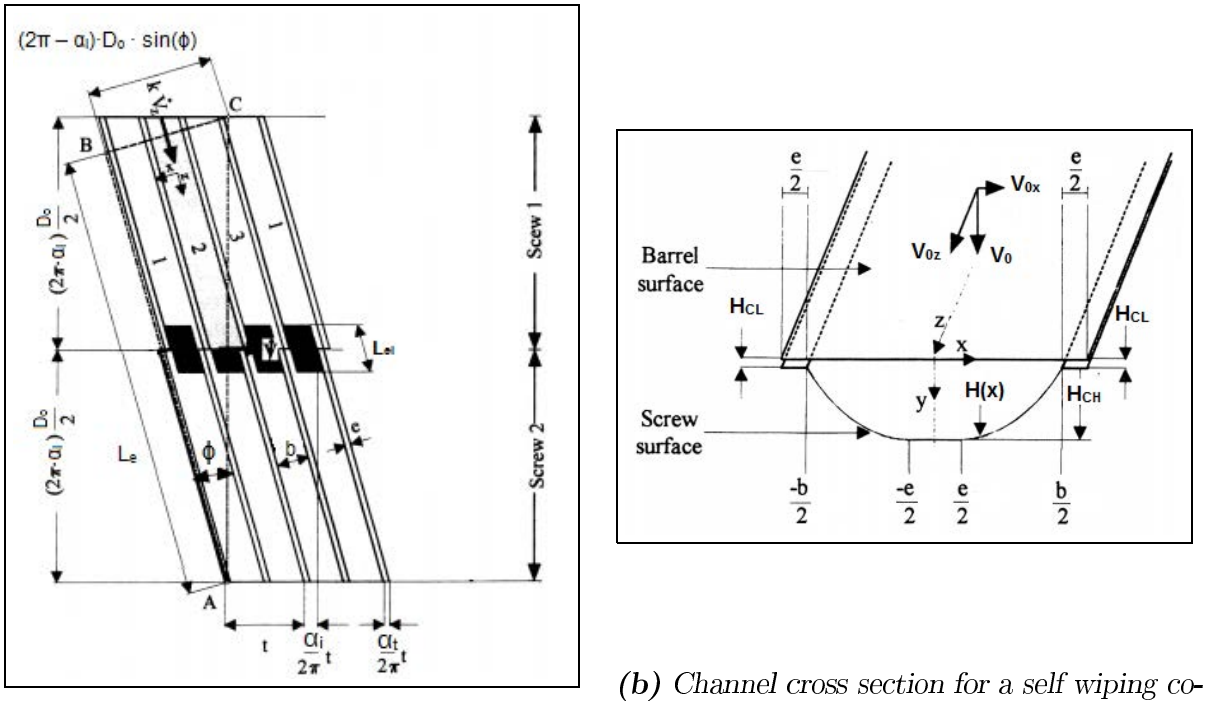

(a) *Unwound channel geometry for a TSE*

(b) *Channel cross section for a self wiping co-rotating TSE*

Figure 6.5: *TSE channel geometry;from Potente et al., 1994*

Both Equation 6.12 and 6.13 rely solely on the outside screw diameter, D_o and hence ignores the clearance, H_{CL} between the screw and the barrel diameter, D_b; this is calculated as follows:

$$H_{CL} = \frac{D_b - D_o}{2} \tag{6.17}$$

The clearance could be significant depending on the mechanical tolerances to which the machine has been designed; and more importantly on the wear of the machine. Thus, the value for H_{CL} should be added on to the calculated values for $H_{CH}, H(\theta)$ and $H(x)$ (as defined in Figure 6.5b).

In a similar manner to the conveying elements, the kneading block sections can also be '*unwound*' and treated as pseudo conveying sections; see Figure 6.6b. The procedure for this is described in detail by Potente et al., 1994.

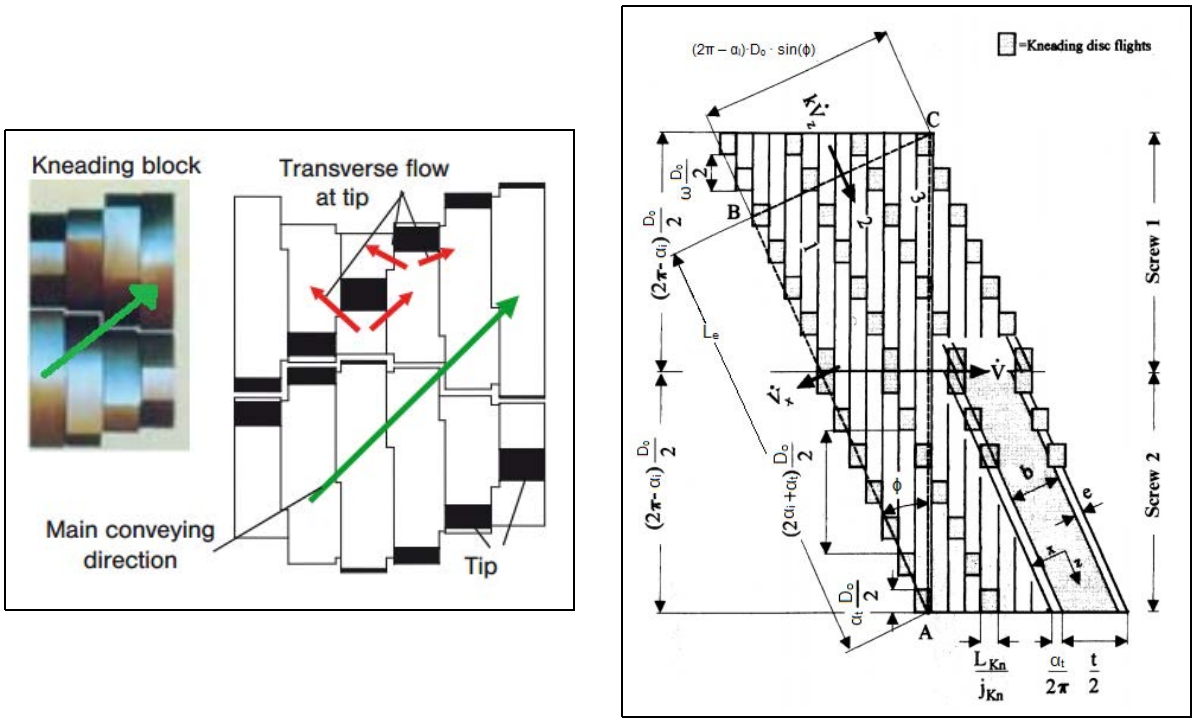

(a) *Flow in kneading blocks for a TSE; from Kohlgrüber, 2008, see p.164*

(b) *Unwound kneading block channel model; from Potente et al., 1994, see p.15*

Figure 6.6: *TSE Kneading block channel geometry*

The method assumes that the tips of the kneading disks unwind in a manner where the tips form an equivalent foot print to a screw flight and the rest of the kneading disk body goes on to form the channel for the polymer to flow in; see Figure 6.6a. The pitch of this equivalent channel can be calculated as follows:

$$t_{KB} = \frac{2\pi \cdot L_{KB}}{\omega \cdot j_{KD}} \tag{6.18}$$

where L_{KB} is the length of the kneading block section and j_{KD} is the number of kneading disks in the kneading block section and ω (see Figure 6.9) is the kneading disk stagger angle in radians. The rest of the of the parameters can be calculated from this equivalent pitch; as described previously.

6.1.2 Key Assumptions for the Model

The model aims to calculate how the shear rate and shear stress experience by the polymer change as a function of degree of fill, hence operating conditions and screw design within the extruder. It relies on several key assumptions which are discussed below.

The first key principle of the model assumes that the figure '8' cross section of the TSE extruder can be unwound into a flat plane; similar to a model of SSE. Secondly is the assumption that the polymer does not flow directly between the two screws and is instead passed from one screw to the other. As a result it experiences minimum shear in the nip region which is ignored as the short residence time in this region means that the exposure to these conditions is minimal. The majority of 'high shear' history is attributed to flow over the trailing flight of the screw channel and the tips of the kneading disks. This is in agreement with the work of Murphy, 2001 who proposes that the dominant area for dispersive mixing is in the elongational flow which occurs in the clearance between the screw flight and the barrel. The flow mechanisms in different elements are discussed in detail within Section A.2 of the literature review which supports this assumption.

Lawal and Kalyon, 1995 claimed that flow in the nip region is important. This is due to the high shear in the nip which is caused by the higher velocity that the polymer flow experiences as two screws move in opposite directions to one another. However, utilising positron emission particle tracking Diemert et al., 2011 showed that the majority of the material is passed from one screw to another meaning that almost no material passes through the nip region. This coupled with the short residence time in this region means that the exposure to these high shear conditions is minimal.

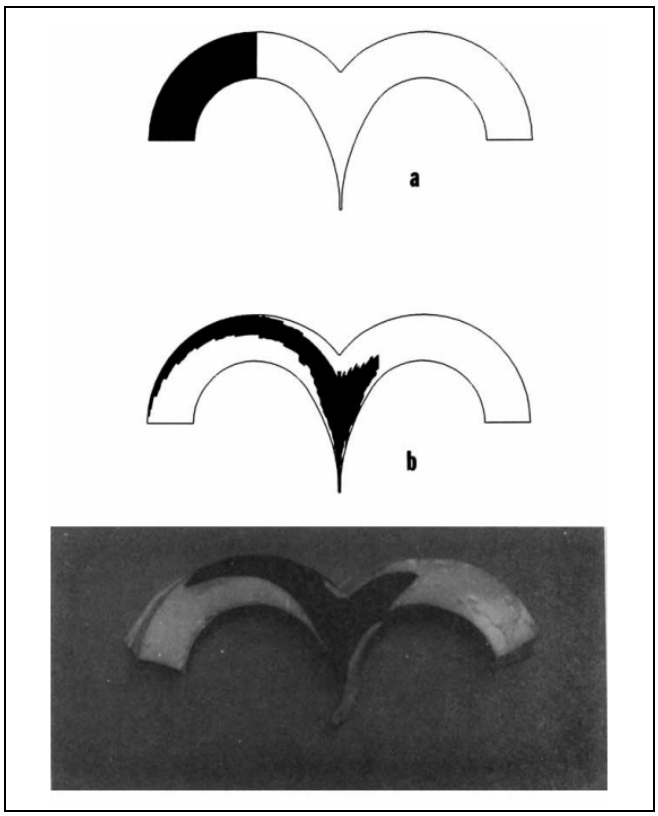

(a) *Experimental validation of flow in the nip region (Kalyon et al., 1988a, p.349)*

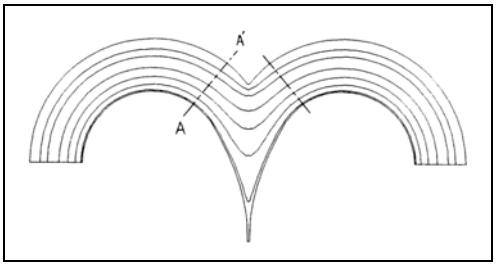

(b) *Streamlines in co-TSE inter mesh region (Kalyon et al., 1988a, p.348)*

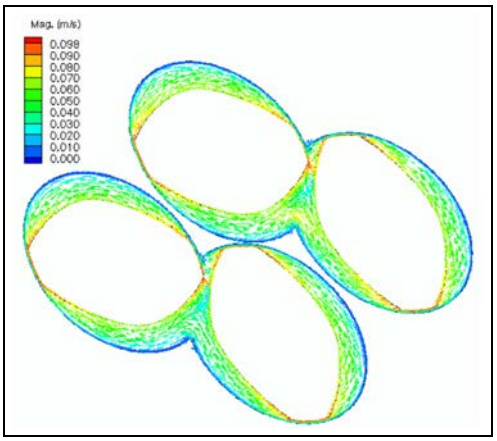

(c) *Velocity vectors in co-TSE nip region (Shah and Gupta, 2004, p.446)*

Figure 6.7: *Flow through the nip region in co-TSE*

Figure 6.7a shows the experimental results where a dye was used to visualise flow through the intermeshing regions. These are in good agreement with the streamlines of material flow through the intermeshing region generated with 2-D FEM modelling by Kalyon et al., 1988a as shown Figure 6.7b. The nip region was modelled in detail using a 3-D simulation by Shah and Gupta, 2004 in PELDOM software. The results (shown in Figure 6.7c) demonstrate velocity streamlines which do not pass through the intermeshing region. The author's own observations of TSE operating with the barrel removed demonstrate the transfer of material from one screw to another; see Figure 6.8.

Figure 6.8: *Material transfer in TSE nip region*

The author accepts that there are some limitations in the assumption that the kneading blocks can be '*unwound*' and treated as a pseudo-conveying channel. This assumption is a 'sufficiently accurate' for narrow kneading disks that are staggered by a small angle; see Figure 6.9b. Increasing the width of the kneading disk will require higher pressure to force material to flow over the tip resulting in more material flowing around the disks. In a similar manner, an increase in the stagger angle of the disk will decrease its conveying capacity by allowing more material to flow around the disks; see Figure 6.9c. In both of these cases the flow pattern will therefore deviate from that in the conveying channel reducing the validity of the assumption. However, the magnitude of the error is mitigated by the fact that the increase in the disk width is accounted for by a larger equivalent flight width within the model so the result of both the model and reality, is that a higher proportion of the polymer will be subjected to a higher shear rate.

Similarly, as the stagger angle is increased the conveying capacity of a kneading disk is reduced; changing the flow pattern and increasing the residence time in the zone. The modelling results using the *Semi-Tech* machine have shown that increasing stagger angle from 30 to 90 degrees increased the residence time from 0.53 to 5.79 s, at a constant throughput of 30 $\mathrm{kg\,h^{-1}}$ and 300 rpm. Since the ultimate output of the model is average shear rate or stress which are weighted by residence time, the model should be represen-

tative in accounting the changes in the kneading block geometry. In fact, it is likely that the model underestimates the shear that the polymer sees, hence in its final application, it will not over predict the mixing performance as the higher shear in reality should only increase mixing.

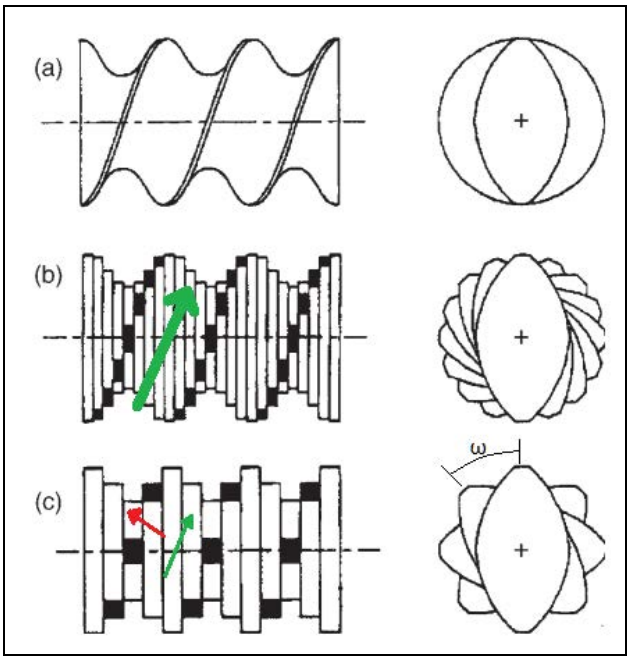

Figure 6.9: *Geometry of kneading blocks (Tadmor and Gogos, 2006, see p.530)*

The other inaccuracy regarding the kneading block model is the lack of a reduction in their self wiping ability. This reduction would increase the probability of material flowing through the nip region and thus experiencing higher shear. This region is ignored by the proposed model. However, work undertaken by various authors to quantify the flows in the kneading block sections shows that little/no flow travels through the nip region, see Figure 6.10a (Gotsis and Kalyon, 1989). In addition Lawal et al., 1993 identified a formation of a stagnant point in flow during a certain orientation of disks; see Figure 6.10b. Connelly and Kokini, 2007 also investigated the flows in kneading disks using 2-D analysis where they showed that minimal flow passed through the nip region; see Figure 6.10c . This was further confirmed by the work of Diemert et al., 2011 who tracked a radioactive particle in twin screw granulation process using Positron Emission Particle Tracking to show that in majority of cases the particle travels in a figure '8' motion. An

exception was identified when the particle got stuck at the surface of the screw. These results were discussed further in Section A.2.

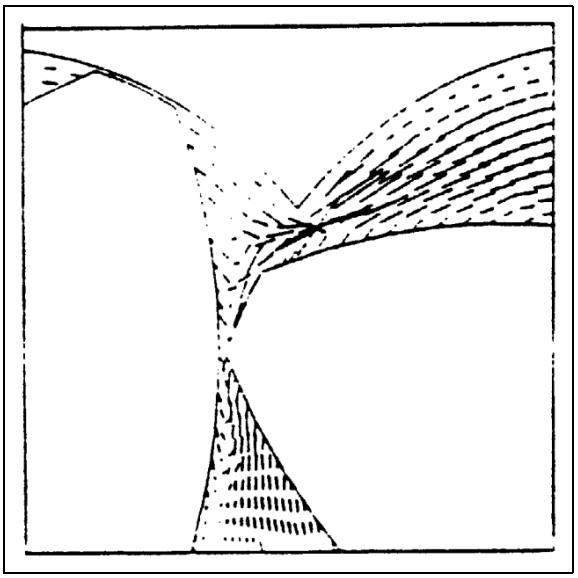

(a) *Streamlines in co-TSE KB region (Gotsis and Kalyon, 1989, p.48)*

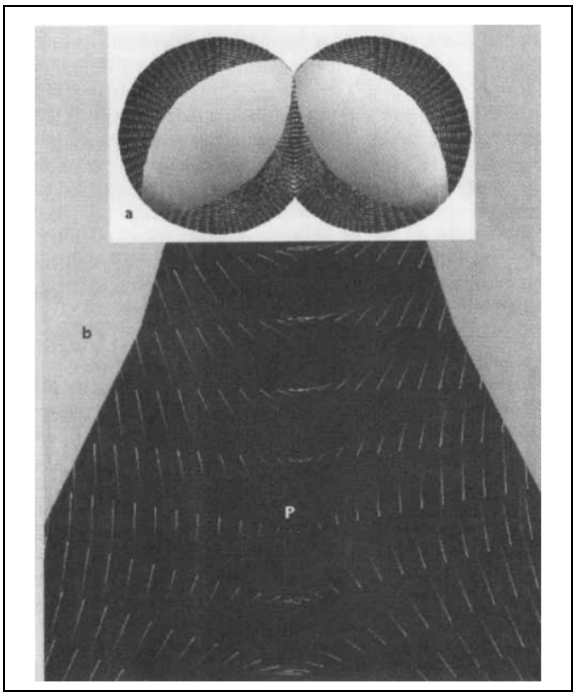

(b) *Streamlines in co-TSE KB region (Lawal et al., 1993, p.146)*

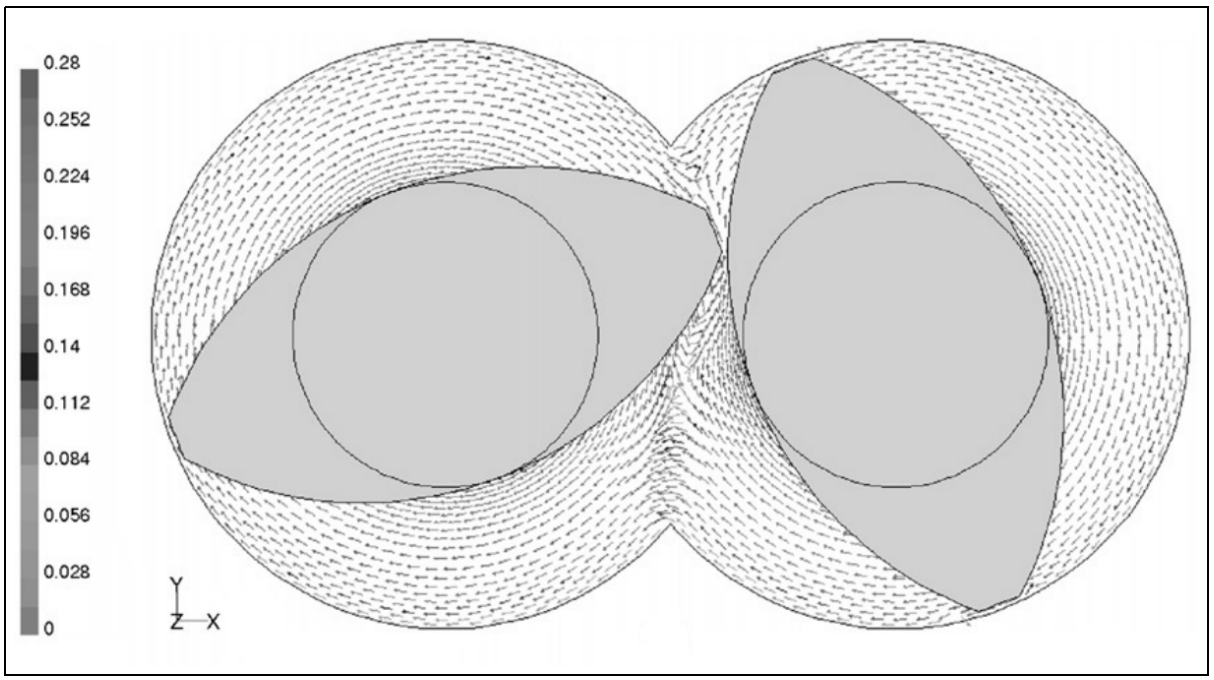

(c) *2-D FEM analysis of nip region for KB in a co-TSE (Connelly and Kokini, 2007, p.961)*

Figure 6.10: *Flow through the nip in kneading block region in a co-TSE*

Based on these works as well as understanding the pressure distribution in a co-TSE as shown in Figure A.11a (previously discussed) the author would propose that the majority of polymer flow travels in a figure '8' type motion with only a minimal fraction of the material being exposed to high shear in the nip between two kneading disks. There is potential for these proportions to change as the kneading blocks become worn and the gap in the nip region increases making it easier for material to flow through it. In such case the model would misrepresent the amount of shear to which the polymer is exposed. The rate of wear can be minimised by selecting materials of construction appropriate to the application and monitored via regular screw inspections.

The model relies on another key assumption which describes the nature of flow within the conveying channel and the pseudo conveying channel associated with the kneading block sections. The principle is akin to that which occurs in SSE. As the barrel surface moves at an angle (the helix angle, ϕ) to the flow channel the polymer is pushed towards the leading edge of the trailing flight where the material accumulates; see Figure 6.11a. Some material escapes from the zone by leakage flow through the clearance between the flight tip and the barrel. Such is true along all sections of the screw apart from directly under any degassing zone where there is no contact with the barrel hence polymer coats the surface of the screw; see Figure 6.11b.

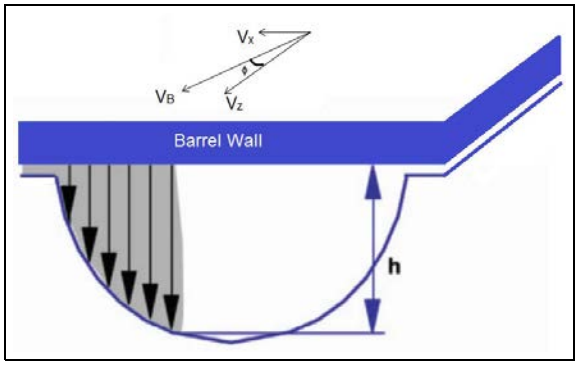

(a) Polymer flow in conveying and pseudo conveying channel (cross section view); adapted from Weinmann, 2007, p.36.

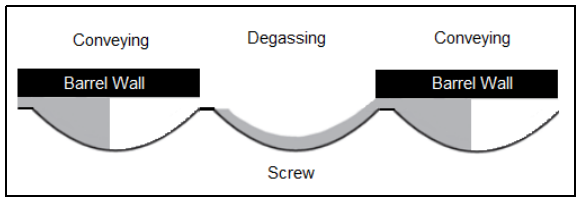

(b) Polymer flow under a degassing zone

Figure 6.11: *Polymer flow in co-TSE*

This is an underpinning assumption for the model, evidence for which can be seen in Figure 6.8 where the flow of polymer can be visualised on the screws. Perhaps a better representation (another of author's observations) is in Figure 6.12 where a high viscosity cleaning compound was passed through the extruder and solidified rapidly on the screw upon exiting the barrel. This demonstrates the flow described in Figure 6.11a.

Figure 6.12: *Polymer flow in co-TSE resembles that of SSE*

Currently, no adjustment is made in the model to account for the proportion of the elements that are exposed directly to the empty space in a degassing section. As a result the shear is slightly overestimated; however as the surface area of the degassing port relative to the rest of the barrel is very small, the inaccuracy should be minimal. This is an acknowledged limitation, which will be addressed at a later date once the concept behind the model has been demonstrated.

To conclude, several key assumptions had to be made in order to extend the current in-house model in order to estimate the average shear rate and stress that the polymer experiences when being processed in a co-TSE. These include assumptions about the ability to model a TSE extruder as an unwound channel, no flow through the nip region and the nature of flow in the conveying and pseudo-conveying channels proposed. These have been discussed and addressed using research carried out by other authors working

in the field and by author's own observations.

At the time of writing the model accounts for flow in conveying and kneading elements only. The flow in slotted mixing elements and toothed mixing elements elements is not accounted for. Currently these are modelled as flow in fully filled conveying elements, which is a misrepresentation due to the elevated shear which back flow of polymer that passes through the slots in these elements would experience; see Section A.2 for discussion on nature of flows. However, a decision was made to focus on the 'principle' elements first to prove the concepts behind the model at this stage.

6.1.3 Model Calculations

An understanding of the TSE geometry coupled with assumptions discussed above allow the residence time weighted shear rate and stress to be calculated. A high level summary of the calculations performed in the model is shown in Figure 6.13 with a in depth flowchart illustrated in Figure 6.14 where the different columns indicate separate 'sheets' in the Excel model.

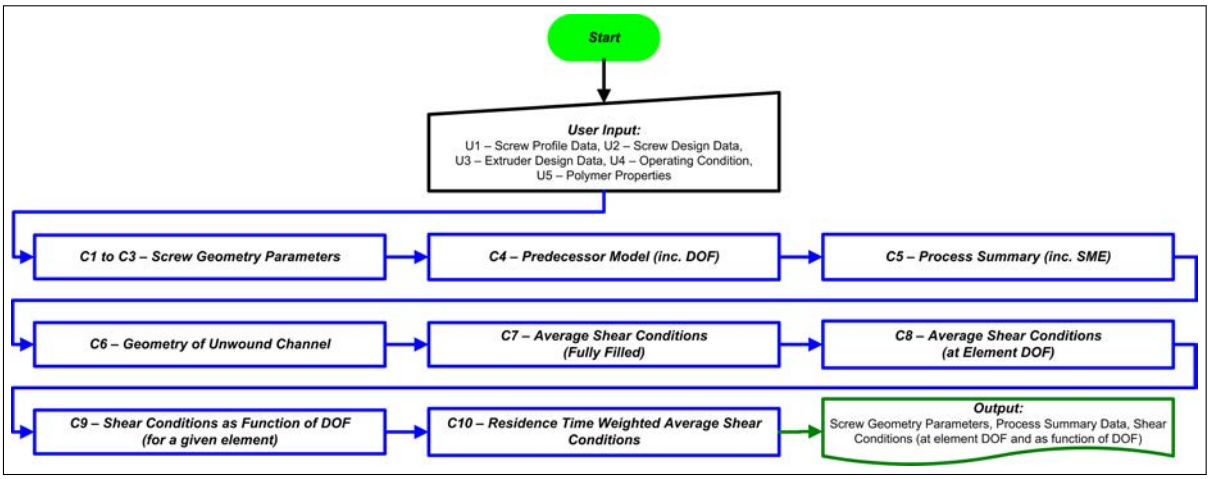

Figure 6.13: *Summary of model calculations*

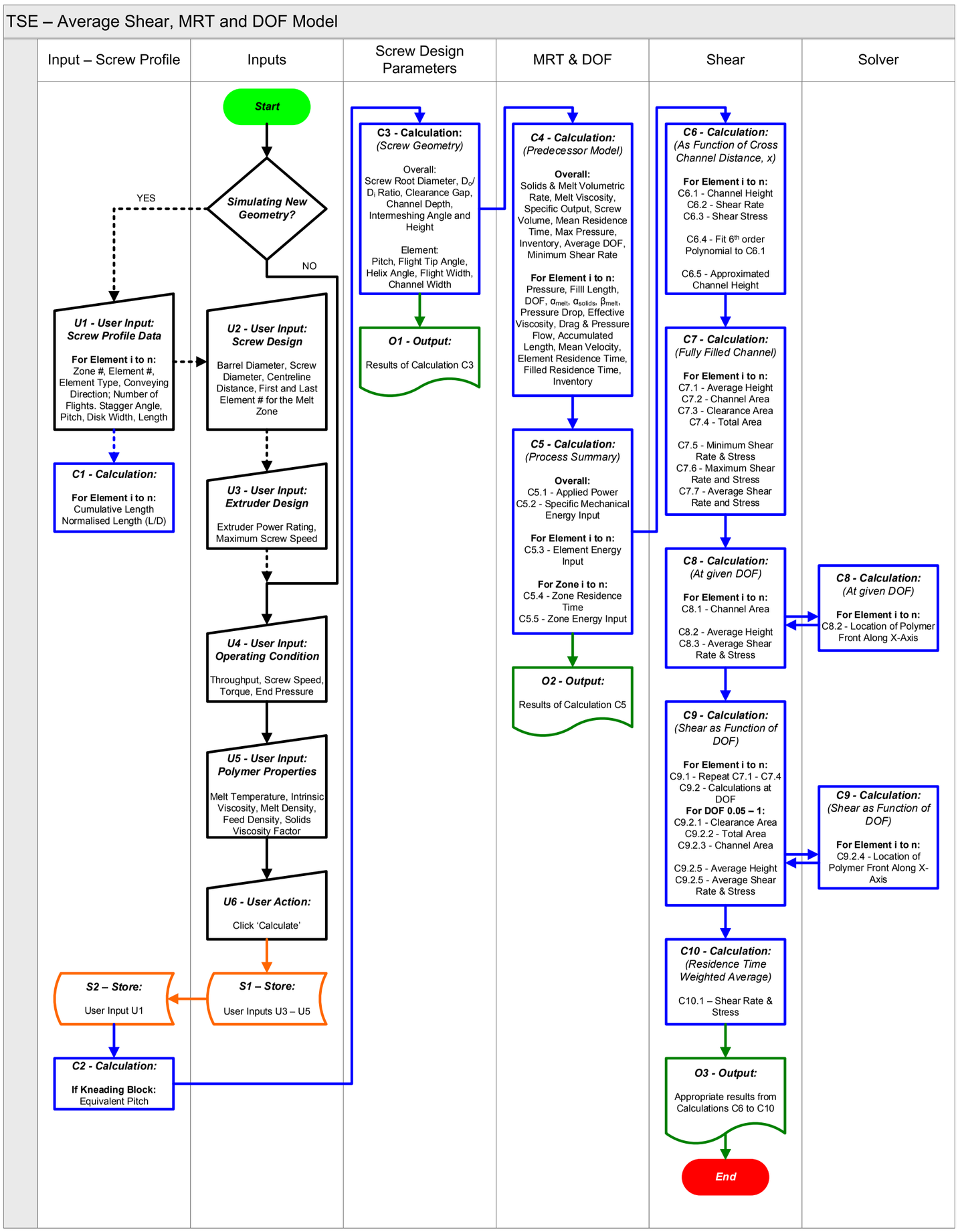

Figure 6.14: *Flowchart of model calculations*

6.1.3.1 Calculation C1-C4

Calculations **C1-C3** deal with establishing the key parameters associated with the geometry of the screw; as listed in Figure 6.14. The equations for these were discussed in Section 6.1.1. Calculation **C4** is the current in-house model and acts as a basis for the added functionality. The list of parameters calculated is also described in 6.14. However, the equations for these are not discussed here as they are considered to be outside the scope of this work although they are provided in Appendix D. As discussed previously the principle equation for this model is shown in Equation 6.1.

6.1.3.2 Calculation C5

Calculation **C5** is a section which summarises the extrusion process in a few key parameters such as Specific Mechanical Energy (SME) input. For the purpose of the model SME in $\mathrm{kW\,h\,kg^{-1}}$ is calculated in terms of the machine applied power P_{app} in Equation H.2 where P_w is the drive rating in kW, N and N_m are screw speed and maximum screw speed respectively, F is the running torque of the machine in percent. A gearbox efficiency factor of 0.97 is also applied, however no adjustment is made for the '*free running torque*' of the machine which represents the power required to turn the screw in an empty machine at given screw speed.

$$P_{app} = 0.97 \cdot P_w \cdot \frac{N}{N_m} \cdot \frac{F}{100} \tag{6.19}$$

thus

$$SME = \frac{P_{app}}{\dot{m}} \tag{6.20}$$

An attempt has been made to separate the work done by the TSE into sections; either by element or zone with SME_e and SME_z being defined (see below) where τ_e and τ_z are element and zone residence time respectively. These however, are relatively poor indicators of the actual work done in each zone as the majority of the energy applied by

the TSE will be utilised to heat up and melt the material as opposed to conveying and mixing it.

$$SME_e = P_{app} \cdot \tau_e \qquad \text{and} \qquad SME_z = P_{app} \cdot \tau_z \tag{6.21}$$

If one sets aside the energy required for melting and heating of the polymer then the residence time within an individual zone is a good indicator of the work induced to the polymer by that particular zone. It is calculated as follows; where i and j are the start and end elements of a given zone:

$$\tau_z = \sum_{n=i}^{n=j} \tau_e \tag{6.22}$$

6.1.3.3 Calculation C6

Calculation **C6** deals with establishing the height of the 'unwound' channel as a function of x in Cartesian co-ordinates and the coresponding shear rate and stresses experienced by the polymer. Applying the transformation given in Equation 6.16 to 6.13 yields the equation below to describe the 'varying part' of the channel as a function of x:

$$H\left(x\right) = \frac{D_o}{2}\left(1 + cos\frac{2x}{D_o \cdot \sin\left(\phi\right)}\right) - \sqrt{a^2 - \left(\frac{D_o}{2}\right)^2 \sin^2 \frac{2x}{D_o \cdot \sin\left(\phi\right)}} \tag{6.23}$$

The details of the overall geometry for the channel have been discussed in Section 6.1.1. By performing the calculations for each part of a channel it is possible to establish how the height changes across the whole width of the channel.

In order to efficiently calculate the area occupied by the polymer within the channel (see calculation C8), a continuous function was needed for the $H(x)$. A 6^{th} order polynomial was used to describe $H(x)$; see below.

$$H(x) = a_1x^6 + a_2x^5 + a_3x^4 + a_4x^3 + a_5x^2 + a_6x + a_7 \tag{6.24}$$

For each element within the configuration, the constants a_1 to a_7 were determined by fitting the polynomial to the calculated heights using a '*least squares*' method with the help of '*WorksheetFunction.LinEst*' VBA function within Excel. $H(x)$ was then calculated from Equation 6.24, for comparison with heights generated from the well established equations. It was found that the 6^{th} order polynomial provided a good fit for both small and large pitched screw elements; see Figure 6.15.

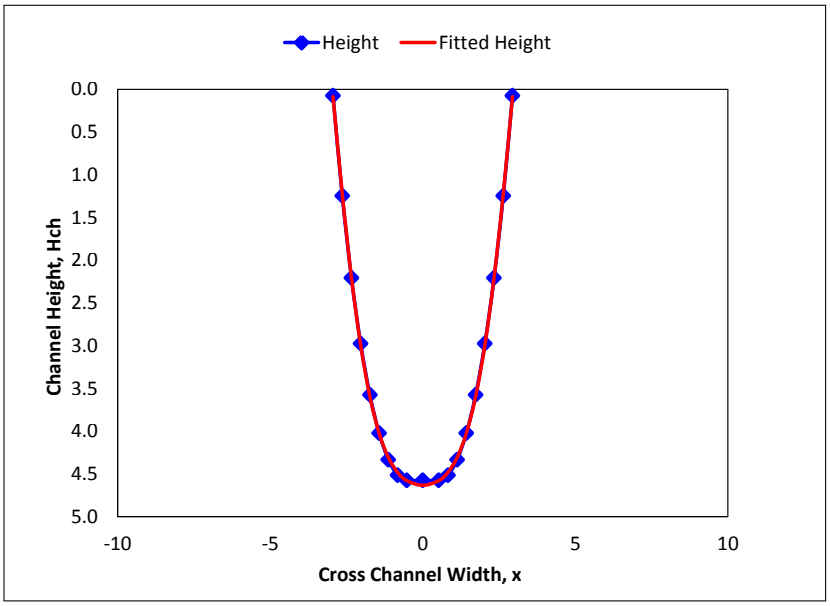

(a) *Pitch 14* mm, $D_b = 30.85$ mm *&* $a = 26.2$ mm

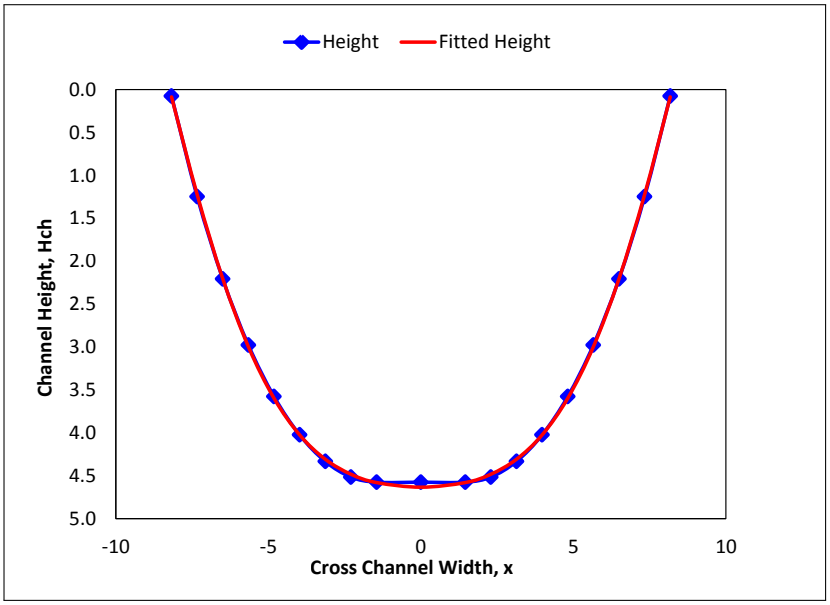

(b) *Pitch 42* mm, $D_b = 30.85$ mm *&* $a = 26.2$ mm

Figure 6.15: *Continuous function for H(x) vs calculated H(x)*

The shear rate (in s^{-1}) and stress (in Pa) are calculated as a function of the cross channel distance, x as follows:

$$\dot{\gamma}(x) = \frac{\pi \cdot {}^{D_b}/_{\cos(\phi)} \cdot {}^{N}/_{60}}{H(x)} \tag{6.25}$$

thus

$$\sigma(x) = \eta \cdot \dot{\gamma}(x) \tag{6.26}$$

6.1.3.4 Calculation C7

These calculations deal with establishing average shear conditions for a fully filled channel. For the purpose of the analysis the channel has been split into two sections; the channel area A_1 and over the flight tip area A_2 which is assumed to always be fully filled. These are shown in Figure 6.16.

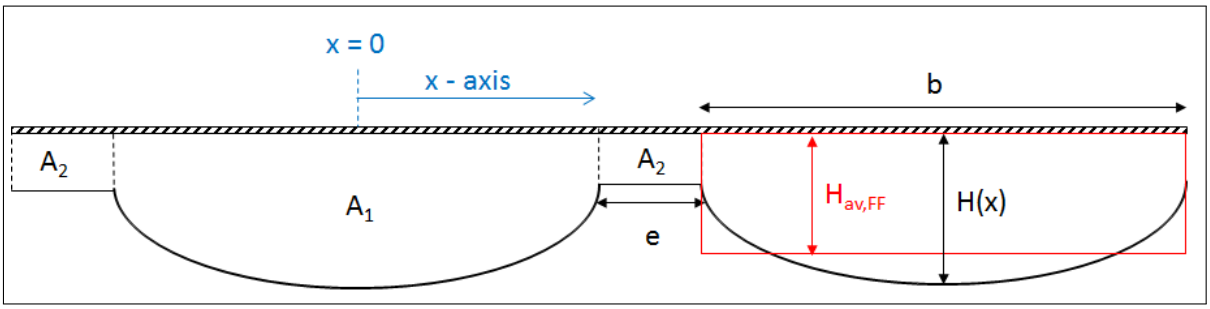

Figure 6.16: *TSE channel cross section*

The average shear conditions within the area A_1 can be approximated by and average height of the channel $H_{av,FF}$. This is calculated by assuming that the flow passes through a rectangular channel with an area equivalent to A_1 of width b and height $H_{av,FF}$. The average height of the channel can be calculated as follows:

$$H_{av,FF} = \frac{1}{b}\int_{-b/2}^{b/2} H(x)dx \tag{6.27}$$

Potente et al., 1994 shows that excluding the clearance height, H_{CL} this can be estimated by the following equation; where constants c_1 and c_2 are as defined in Equation 6.14:

$$H_{av,FF} = \left[2 \cdot \frac{c_1 \cdot \alpha_i^5/5 + c_2 \cdot \alpha_i^3/3}{2\alpha_i + \phi} + D_o - a\right] + H_{CL} \tag{6.28}$$

A number of shear conditions can be calculated for various positions across the channel. The minimum shear is experienced in the centre of the channel, $x = 0$ where the height is the greatest, defined by $H_{CH} = H(0)$.

$$\dot{\gamma}_{min} = \frac{\pi \cdot {}^{D_b}/_{\cos(\phi)} \cdot {}^{N}/_{60}}{H_{CH}} \tag{6.29}$$

thus

$$\sigma_{min} = \eta \cdot \dot{\gamma}_{min} \tag{6.30}$$

The maximum shear is experienced when the polymer passes over the flight and the clearance is the smallest; resulting in:

$$\dot{\gamma}_{max} = \frac{\pi \cdot {}^{D_b}/_{\cos(\phi)} \cdot {}^{N}/_{60}}{H_{CL}} \tag{6.31}$$

thus

$$\sigma_{max} = \eta \cdot \dot{\gamma}_{max} \tag{6.32}$$

The average shear conditions over the region A_1 and A_2 where $A_2 = H_{CL} \times e$ can be calculated as an area weighted average; where $A_{t,FF}$ is the sum of A_1 and A_2.

$$\dot{\gamma}_{av,FF} = \frac{\frac{\pi \cdot D_b/\cos(\phi) \cdot N/60}{H_{CL}} \cdot A_2 + \frac{\pi \cdot D_b/\cos(\phi) \cdot N/60}{H_{av,FF}} \cdot A_1}{A_2 + A_1} \tag{6.33}$$

thus

$$\sigma_{av,FF} = \eta \cdot \dot{\gamma}_{av,FF} \tag{6.34}$$

This is akin to an average based on mass fractions if we assume that the density of the

material does not change. The author acknowledges that in reality the density will change slightly as the result of a difference in temperature between the high shear region over the flight and the lower shear region within the channel, however the difference in density of PET between that at 280 °C (1222.4 $\mathrm{kg\,m^{-3}}$) and at 300 °C is (1211.9 $\mathrm{kg\,m^{-3}}$) is very small. A temperature difference of this magnitude is likely in the channel, but not readily verifiable. The best estimate would be achieved by CFD modelling, which is considered beyond the scope of this project.

6.1.3.5 Calculations C8

This subset of calculations calculates the average shear conditions for a partially filled channel; specifically at the degree of fill calculated for the element by the model. Diagrammatically, this can be visualised in Figure 6.17.

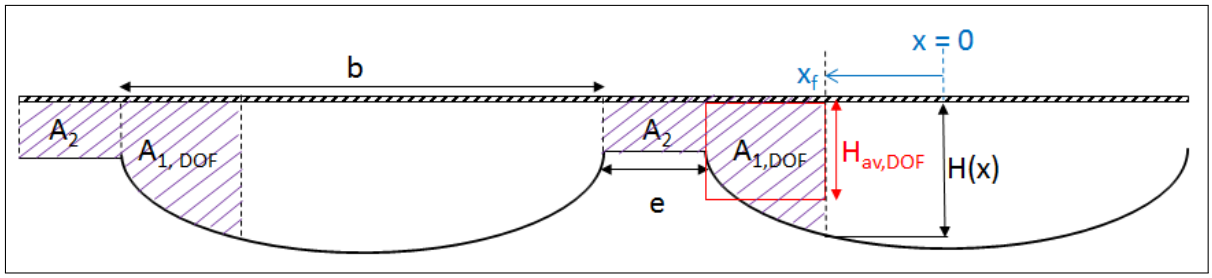

Figure 6.17: *TSE channel cross section*

The procedure in this case is slightly different to that in calculations C7. Here, the degree of fill is a known parameter and the location of the polymer front, denoted by x_f in the above figure is an unknown. Initially the total area at a given % fill level, DOF, is established as follows:

$$A_{t,DOF} = A_{t,FF} \cdot \frac{DOF}{100} \tag{6.35}$$

Since the area directly over the flight, A_2 is assumed to always be fully filled, its value remains constant; thus the area occupied by the polymer in the channel can be established.

$$A_{1,DOF} = A_{t,DOF} - A_2 \tag{6.36}$$

Next the '*Solver*' functionality within Excel was utilised to establish the value of x_f within the limits of $^{-b}/_2 \leq x_f \leq {}^{-b}/_2$ which would satisfy the value of the integral below where $H(x)$ is represented by the Equation 6.24.

$$A_{1,DOF} = \int_{-b/2}^{x_f} H(x) \tag{6.37}$$

From this the average height for the channel at a given degree of fill can be established as follows:

$$H_{av,DOF} = \frac{A_{1,DOF}}{x_f} \tag{6.38}$$

The maximum shear rate and stress are established in the same way as in calculation C7 (see Equations 6.33 and 6.34). The average shear rate and stress experienced by the polymer are calculated as follows:

$$\dot{\gamma}_{av,DOF} = \frac{\frac{\pi \cdot D_b/\cos(\phi) \cdot N/60}{H_{CL}} \cdot A_2 + \frac{\pi \cdot D_b/\cos(\phi) \cdot N/60}{H_{av,DOF}} \cdot A_{1,DOF}}{A_{t,DOF}} \tag{6.39}$$

thus

$$\sigma_{av,DOF} = \eta \cdot \dot{\gamma}_{av,DOF} \tag{6.40}$$

Although not calculated within the model, the theoretical minimum shear rate and stress can be calculated in a similar manner to that for a fully filled channel where the H_{CH} is replaced by the $H\left(x_f\right)$.

6.1.3.6 Calculations C9

Calculations C9 establish how the average shear conditions which the polymer experiences change as a function of degree of fill within a given screw element. The actual calculations

are the same as that in calculations C8. These are performed repeatedly to develop a function for DOF ranging from 5 to 100 %.

6.1.3.7 Calculations C10

This section delivers the main output of the model, the residence time weighted average shear rate and stress. Here, $i = 1$ and n represent the initial and final element in the screw profile and τ_e is the element residence time.

$$\dot{\gamma}_{av,RTD} = \frac{\sum_{i=1}^{n} [\dot{\gamma}_{av,DOF} \cdot \tau_e]}{\sum_{i=1}^{n} \tau_e} \tag{6.41}$$

thus

$$\sigma_{av,RTD} = \eta \cdot \dot{\gamma}_{av,RTD} \tag{6.42}$$

Although not currently implemented, the author accepts that the next obvious development would be to calculate the residence time weighted average shear stress, $\sigma_{av,RTD}$ as a function of varying viscosity. In reality the viscosity changes along the screw profile as a result of solid to melt transition, temperature changes and molecular weight reduction. This has not been undertaken as no accurate data is available for how the viscosity would change. However, as the model aims to represent the direct to melt addition process it can be assumed that the viscosity would not change too drastically within melt sections of the extruder which is being operated with a constant barrel temperature profile. It is assumed that the majority of the molecular weight reduction occurs within the melting section; see Chapter 7 for further discussions.

6.1.4 Validation of the Model

An attempt has been made to validate the results of the model with the results from the model published by Potente et al., 1994. However, this has proven difficult as the authors were not very forthcoming with the specification of the equipment nor the full set of the

operating conditions. The presented results were obtained using a ZSK 30 TSE machine at a throughput of 10 $\mathrm{kg\,h^{-1}}$ and an unknown screw speed. Some other results presented in the paper were obtained at output of 15 $\mathrm{kg\,h^{-1}}$ and screw speed of 150 and 250 rpm; based on this a screw speed of 100 rpm was selected as initial estimate for the shear rate results. With regards to the machine specification, an estimate was made based on publications of Jaffer, 1998 who reported the values denoted in Table 6.1.

Table 6.1: *Design parameters for WP-ZSK 30; from (Jaffer, 1998)*

Parameter	**Value**
Barrel diameter, D_b	30.85 mm
Screw outside diameter, D_o	30.70 mm
Screw root diameter, D_i	21.30 mm
Centreline distance, a	26.20 mm
Channel height, H_{CH}	4.70 mm
Clearance between screw and barrel, H_{CL}	0.075 mm

An overview of the results from author's model and that of Potente et al., 1994 are shown in Figure 6.18a and 6.18b respectively. Some stark differences can be observed in the results presented. The first major difference is the variation in how quickly the mean shear rate increases with reducing DOF for the elements of different pitch. The author's model indicates little difference between the various pitched elements, whereas there is significant difference observed by Potente et al., 1994. It appears that these do not reach the same asymptotic minimum indicating that potentially a different screw speed (at the 10 $\mathrm{kg\,h^{-1}}$) has been used by the author to generate the graphs since the channel height would be constant for all elements. Intriguingly, there seems to be an offset in the inflection point (the DOF at which the shear rate drastically increases) for the elements of different pitch. This was further investigated below (see 6.1.4.1). The other major difference is in the prediction of the minimum shear rate achieved, with the author's model generating higher values. Presuming the assumptions for the geometry of the machine are correct, then the screw speed of 100 rpm appears to be too high. The impact of this has been investigated in Section 6.1.4.2.

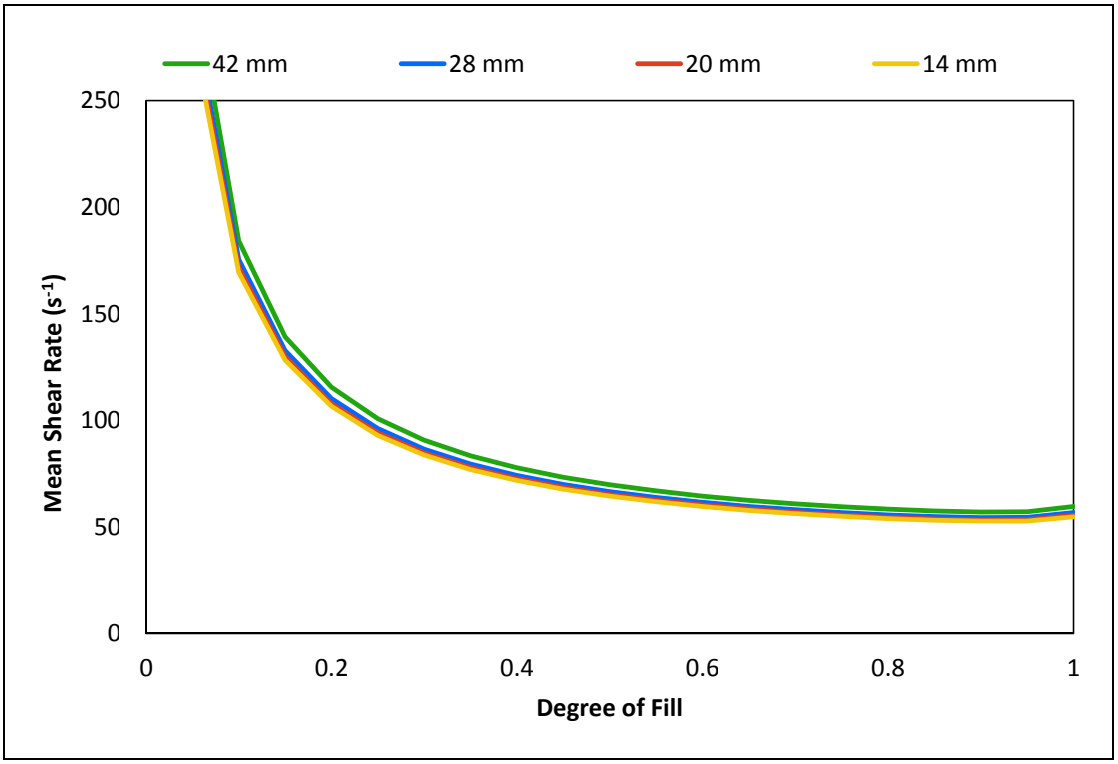

(a) Model results for various elements of different pitch (mm)

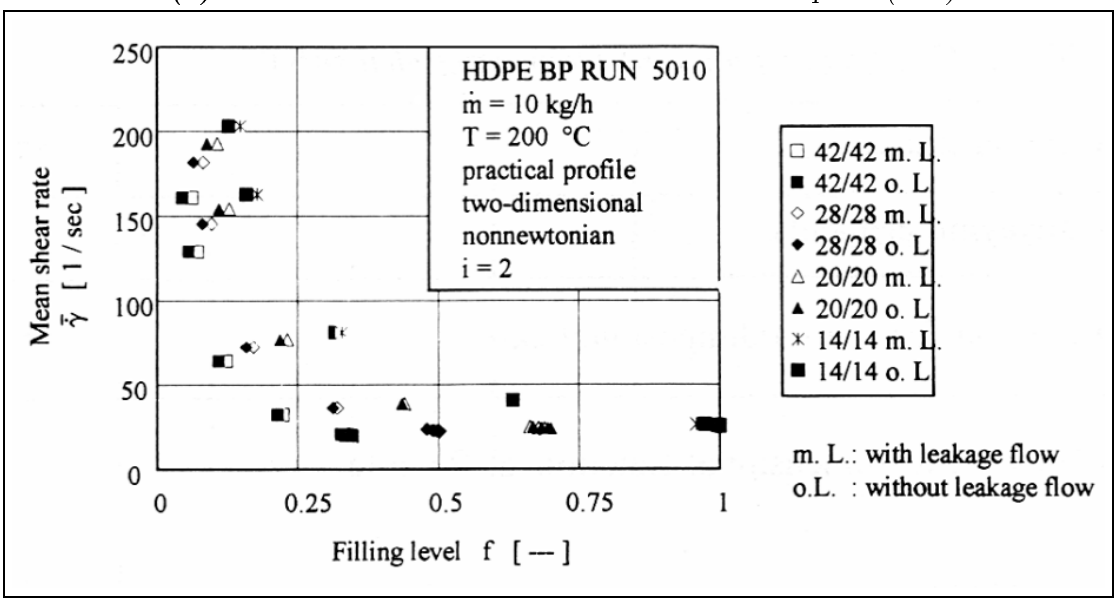

(b) Results by Potente et al., 1994, see p.18

Figure 6.18: *Shear rate as function of DOF*

6.1.4.1 Effect of Element Pitch

In order to better understand the differences between the results of the two models, initially the role of element geometry was investigated. The model proposed here indicates a weak relationship between the mean shear rate and DOF for the elements of different pitch; this is contrary to results of Potente et al., 1994. For the investigation two extreme cases were selected, the 14 and 42 mm; which were compared at screw speed of 50 rpm and 10 $\mathrm{kg\,h^{-1}}$.

Instinctively one might expect that as the DOF changes, the location of the polymer front would be different in the elements with pitch of 14 and 42 mm thus leading to different average shear rates for the two elements. Although this is true with respect to the absolute value of x_f, it is not the case when considering the polymer front location relative to the element geometry. If the polymer front location x_f is normalised by the width of the channel b, and plotted against the average height $H_{av,DOF}$ then it is evident that the rate of change in the average height is almost identical for 14 and 42 mm elements; see Figure 6.19a. As a result, the average height changes in the same manner for as function of DOF for both 14 and 42 mm pitched elements (see Figure 6.19b), meaning that the shear rate as a function of DOF should be the same both type of elements (see Equation 6.39).

From Figure 6.18a one can see that the model predicts some change in how the mean shear rate changes as a function of DOF for elements of different pitch; yet from the above these should be the same. This minor change is a result of the shear rate calculation itself, which accounts for the effects of the helix angle of the flight; see Equation 6.39. The larger pitch element has a larger helix angle, hence the barrel velocity which the polymer sees parallel to the flight is larger in magnitude; as represented by the green arrow in Figure 6.20.

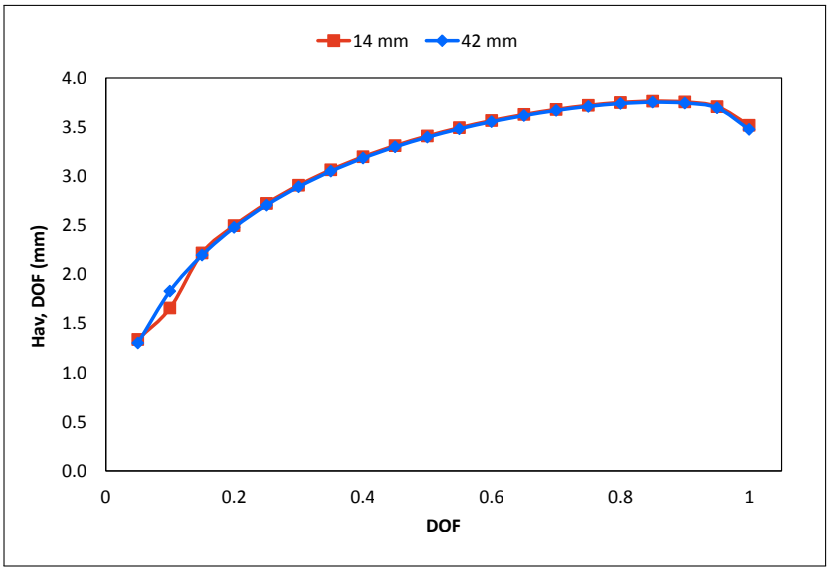

(a) $H_{av,DOF}$ *vs normalised cross channel distance.*

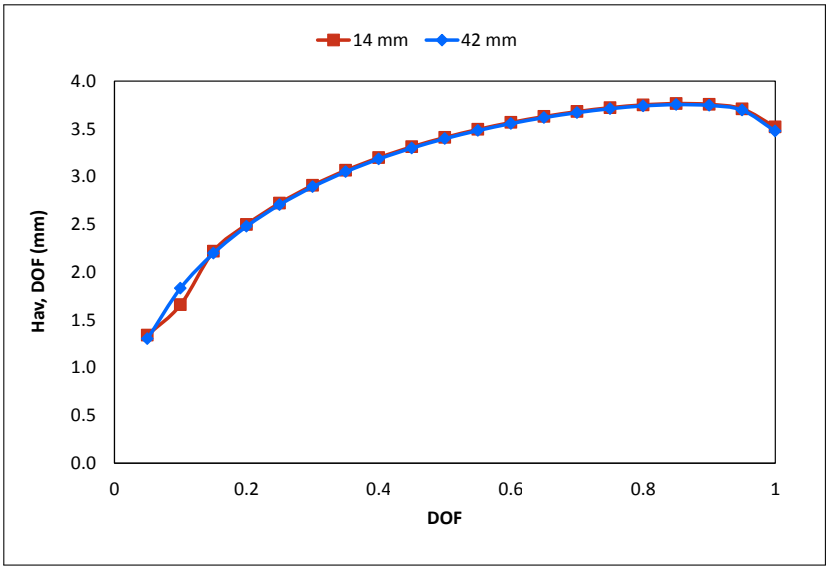

(b) $H_{av,DOF}$ *as a function of DOF*

Figure 6.19: *Impact of channel geometry on* $H_{av,DOF}$*; thus average shear rate.*

Figure 6.20: *TSE channel cross section*

Although this initial investigation did not shed any light on the difference in average shear rate predicted for elements of differing pitch in the model by Potente et al., it demonstrates the reasons as to why such small changes were evident in the model proposed here.

6.1.4.2 Effect of Screw Speed

As discussed previously, the screw speed for the results presented by Potente et al., 1994 was not supplied and initial estimate of 100 rpm was made in an attempt to validate the model presented here; however from Figure 6.18a it appears that this is too high.

A number of screw speeds were tested for each element at an output of 10 $\mathrm{kg\,h^{-1}}$, in order to best match the data supplied by Potente et al., 1994. The results are shown in Figure 6.21. Considering Figure 6.21a initially, it is evident that for the 42 mm pitch element a screw speed of 50 rpm matches the peak average shear at lower degrees of fill and the lower screw speed of 25 rpm matches the minimum shear at the higher DOF values.

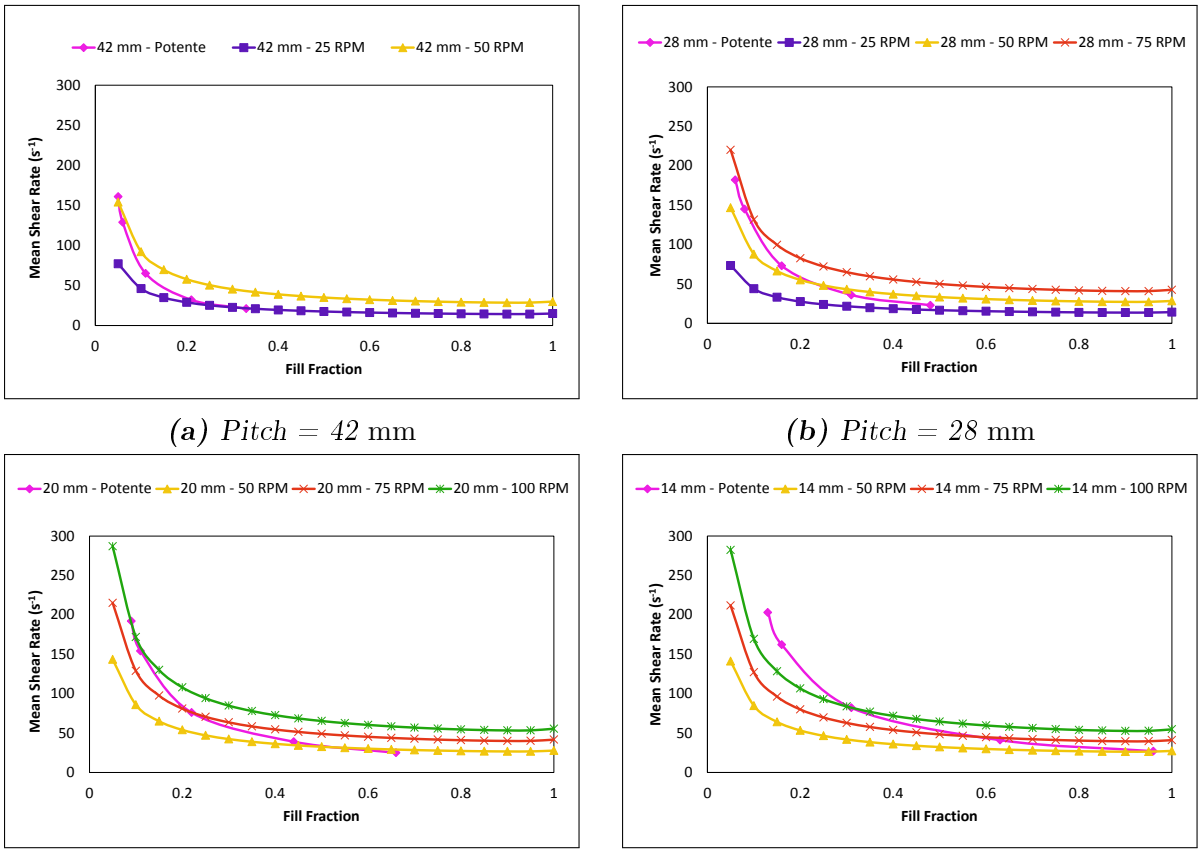

(a) Pitch = 42 mm *(b) Pitch = 28 mm*

(c) Pitch = 20 mm *(d) Pitch = 14 mm*

Figure 6.21: *Average shear rate vs DOF at various screw speeds for different pitch elements*

A similar trend can be observed with elements of other pitch, where no screw speed setting produces suitable replication of results obtained by Potente et al., 1994. The differing nature of the average shear rate curves seems to indicate that the geometry of the channel being modelled is inherently different. Factors concerning the assumed geometry of the machine are investigated below.

6.1.4.3 Effect of Geometry

As Potente et al., 1994 did not specify the geometry of the machine, an investigation was carried out into understanding the impact of some of the key parameters to see if the model results could be brought in line with the results published by Potente et al., 1994. As discussed previously one of the key parameters for TSE geometry is the centreline distance, a. This determines the degree of intermeshing of the screws, hence the channel

depth and the free volume of the machine.

The impact of the centreline distance in the average shear as a function of the DOF can be seen in Figure 6.22a. As the centreline distance is increased, the degree of intermeshing and thus the channel depth is reduced (assuming the self wiping profile is maintained). The reduction in channel depth leads to increased shear rate across the whole of the channel simultaneously. This is observed by an increase in the average shear rate for a given DOF as seen in 6.22a by the the curve shifting vertically.

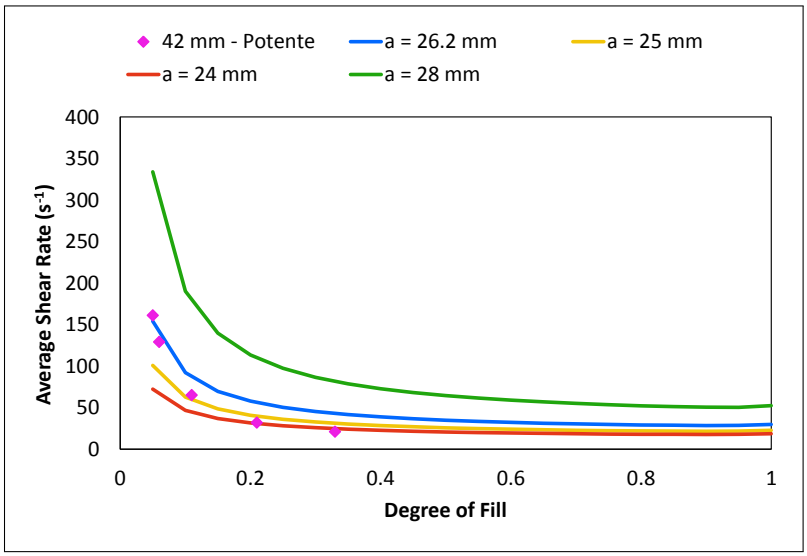

(a) Impact of centreline distance for 42 mm element at 50 rpm

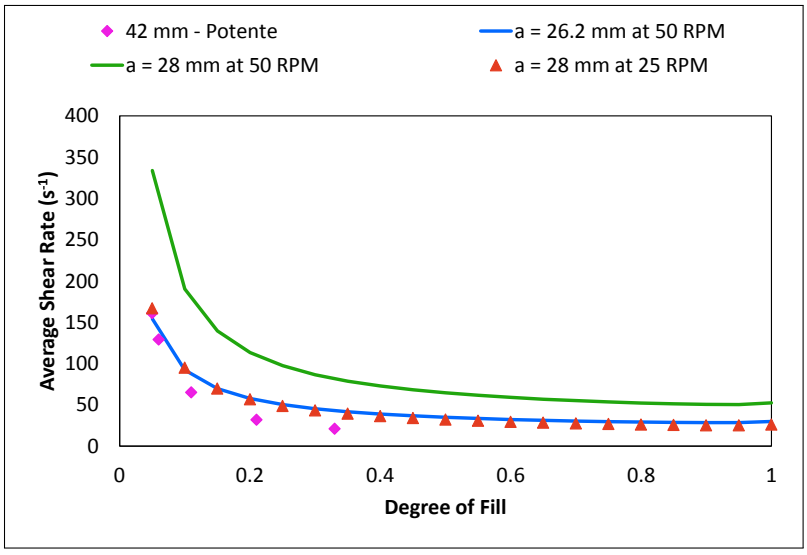

(b) Impact of screw speed at increased centreline distance for 42 mm element

Figure 6.22: *Influence of centreline distance on average shear rate as function of DOF*

It is interesting that the shape of the curve with the centreline distance of 28 mm seems to correspond most closely to that proposed by Potente et al., 1994. The average shear values for this case are roughly twice that of the values presented by the author; thus a case with half the screw speed was also run in an attempt to obtain a better match. The results are demonstrated in Figure 6.22b, where the average shear rate in this case is almost identical to the reference case (Case 3 in Table 6.2) with a centreline distance of 26.2 mm. This can be explained by the changes in geometry as result of centreline distance where in going from centreline distance of 26.2 to 28 mm reduces the channel height from 4.65 to 2.85 mm (roughly factor of 2) thus increasing average shear by a similar amount. When the screw speed was halved, the average shear is then reduced to almost the original value. Table 6.2 demonstrates the conditions for each of the cases shown in Figure 6.22.

Table 6.2: *Test cases for changes in centreline distance of the TSE being modelled; 42* mm *pitch*

Parameter	Case 1	Case 2	Case 3	Case 4	Case 5
Screw pitch, t (mm)	42	42	42	42	42
Screw Speed, N (rpm)	50	50	50	50	25
Centreline distance, a (mm)	24	25	26.2	28	25
Barrel diameter, D_o (mm)	30.85	30.85	30.85	30.85	30.85
D_o/D_i	1.80	1.61	1.43	1.23	1.23
Channel height, H_{CH} (mm)	6.85	5.85	4.65	2.85	2.85
Clearance: screw to barrel, H_{CL} (mm)	0.075	0.075	0.075	0.075	0.075

If one was to set the centreline distance at 24 mm, such that the asymptote for the minimum average shear rate matched that proposed by Potente et al., 1994, then it is evident that the model proposed here underestimates the shear rate at the lower degrees of fill. This could be an effect of the assumed values for the clearance between the barrel and the screw. Figure 6.23 shows the importance of including the clearance gap for the shear calculation.

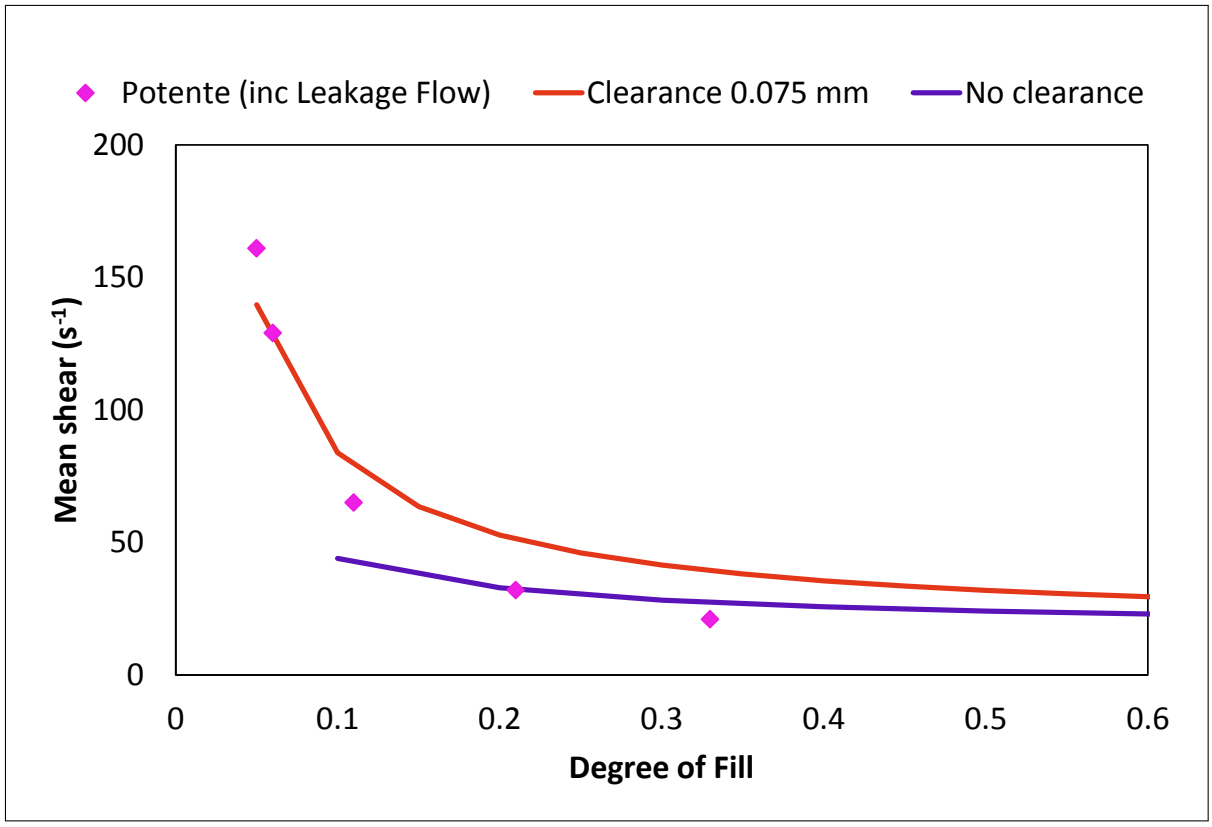

Figure 6.23: *Effect of screw tip to barrel clearance*

As seen from Figure 6.17 and Equation 6.39, the average shear rate is calculated by the shear rate over the flight area and the main channel being weighted by the corresponding areas A_2 and A_1. Increasing the over the flight clearance increases the size of the area A_2 thus increasing the 'importance' of this region, but this also has the effect of drastically reducing the shear rate. Thus increasing the over the flight clearance will initially increase the average shear rate up to an optimum point, beyond which further increase in the clearance will reduce the average shear rate; see Table 6.3.

Table 6.3: *Average shear rate at a DOF of 5 % for various clearances; centre line distance of 24* mm *and 42* mm *pitch*

Clearance: screw to barrel, H_{CL} (mm)	0.075	0.200	0.500	0.675
Average shear rate, $\dot{\gamma}_{av,DOF}$ (s^{-1})	72.27	74.37	79.50	73.95

The effect of changes in the clearance lessens as the centreline distance is increased which reduces the channel depth and increases the magnitude of shear rate within the channel

itself; see Table 6.4.

Table 6.4: *Average shear rate at a DOF of 5 % for various clearances; centre line distance of 26.2* mm *and 42* mm *pitch*

Clearance: screw to barrel, H_{CL} (mm)	0.025	0.075	0.425	0.925
Average shear rate, $\dot{\gamma}_{av,DOF}$ (s^{-1})	209.22	209.55	204.43	202.71

The is effect is much less noticeable at higher degrees of fill within the screw element.

6.1.4.4 Limitations

A number of routes have been explored in attempting to match the results of the model proposed here with the results of the paper by Potente et al., 1994. Some discrepancies in the absolute values still exist, even though the trends observed are very similar. The model proposed by Potente et al., 1994 is complex; taking account of drag flows, pressure flows, temperature changes as well as the potential for the non-Newtonian behaviour.

Although the in-house model without the added functionality considers flows resulting from the pressure gradient; the added functionality of the model solely focuses on drag induced flow. In fully filled channels if the pressure flows are included then the model will be underestimating the average shear rate. This is a direct result of the reverse flows which the pressure gradient generates within a given element; leading to a velocity profile proposed by Lawal and Kalyon, 1995; see Figure 6.24.

The author believes that the most likely reason for the discrepancy between the proposed model is with the underlying assumption of how the polymer flows. Currently, it is assumed that the polymer in over the flight region is not refreshed and simply flows along the axial direction similar to the flow in the channel. In reality, as the barrel is moving at an angle relative to the channel, a given quantity of material flows over the flight from one channel into another; commonly termed leakage flow.

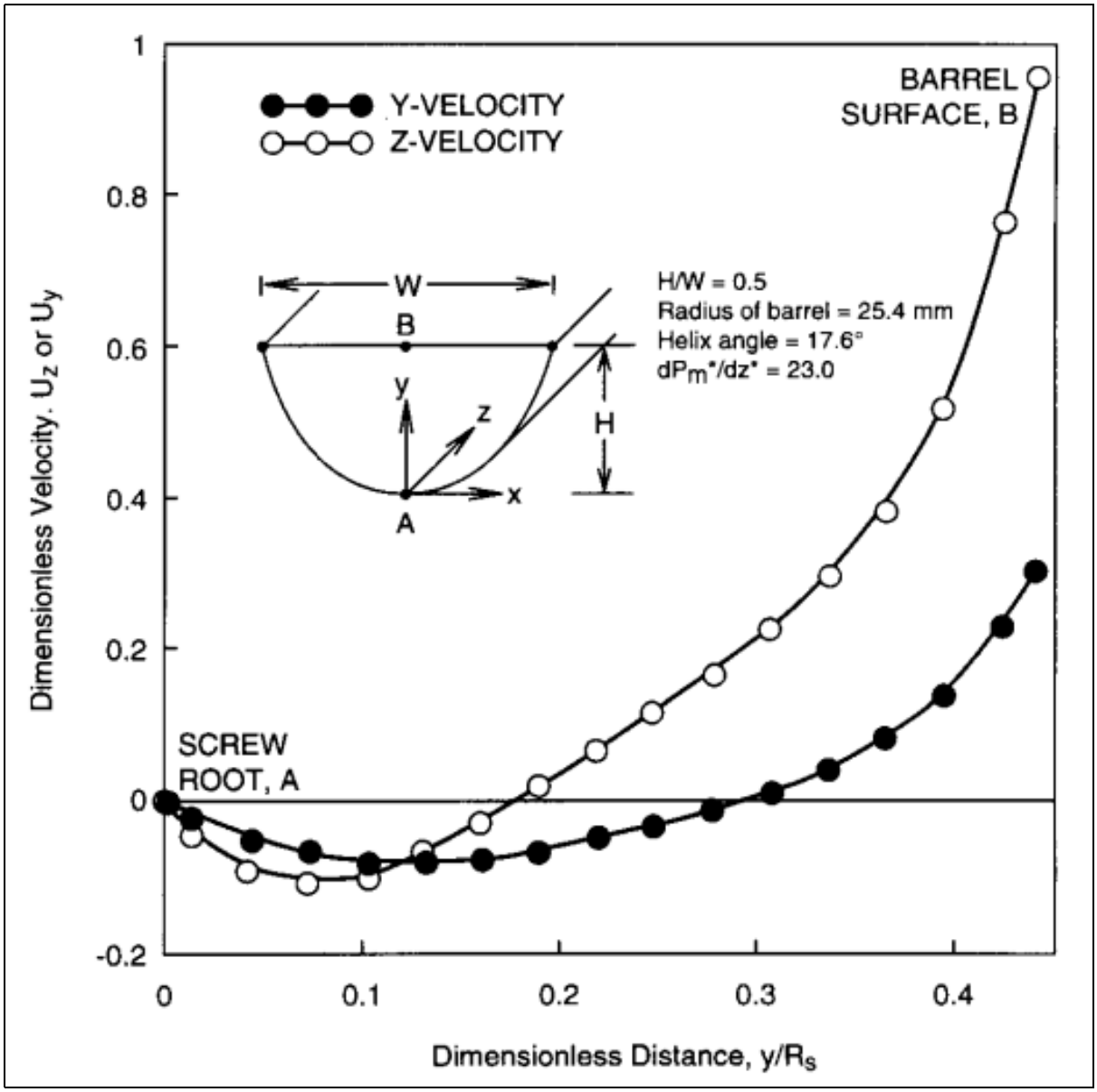

Figure 6.24: *Velocity profile in TSE channel; from Lawal and Kalyon, 1995, see p.1331.*

There are several potential ways to account for leakage flows The most complex solution would be to accurately calculate the leakage, drag and pressure flows by considering the area available for material flow across the barrel cross section; similar to Figure 6.25. This is particularly complex for the kneading block scenario or the slotted mixing elements where there are relatively large gaps for leakage flows to occur in.

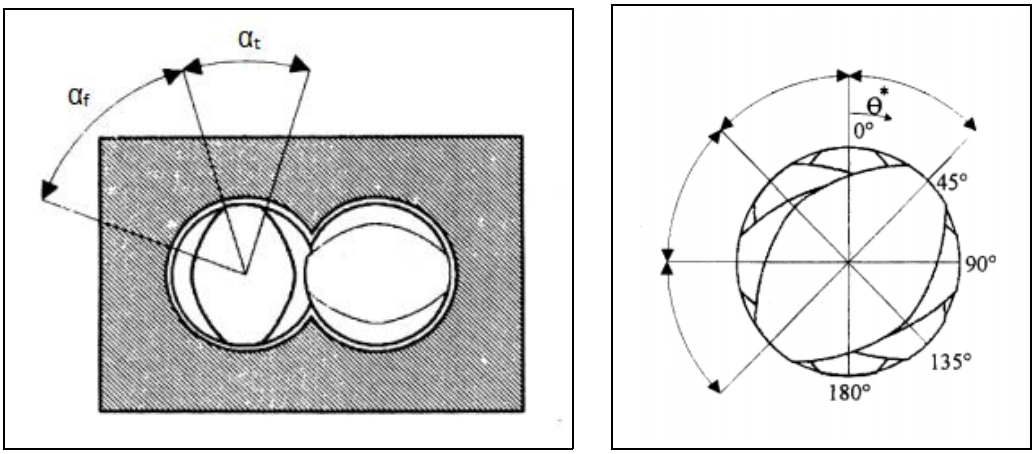

(a) *Conveying elements* ***(b)*** *Kneading elements*

Figure 6.25: *Free area available for leakage flows (Potente et al., 1994)*

A less complex modification would be possible based on a 'number of passes' function which denotes the number of times that the polymer passes through the high shear region. Such function was proposed by the Kohlgrüber, 2008, see p.174; where ψ is the return fraction, L_s is the length of screw under consideration, p is the number of flights, z_w is the number of shafts and $\dot{Q}$ is the volumetric flow through the extruder in $\mathrm{mm^3\,s^{-1}}$.

$$\Psi = \frac{0.5 \cdot \pi \cdot D_b \cdot N \cdot H_{CL} \cdot L_s \cdot p \cdot z_w}{\dot{Q}} \tag{6.43}$$

This could be utilised within the calculation for the average shear rate to increase the 'importance/weighting' of the flow in the clearance between the screw flight and the barrel. Initially, the kneading block elements and SME elements could be treated as pseudo-conveying elements where the clearance gap is adjusted to account for the extra leakage flows that occur in these elements. This would better replicate the flows occurring in reality within a TSE machine.

6.2 Concluding Remarks

The author proposes the use of new parameters 'residence time weighted average shear rate, $\dot{\gamma}_{av,RTD}$' and 'residence time weighted average shear stress, $\sigma_{av,RTD}$' as a measure of

the effectiveness of a twin screw extrusion process. It is proposed that these parameters are used to quantify the impact of the changes in operating conditions and screw geometry on the end properties of the materials being processed. Within this thesis, these parameters are utilised to understand the molecular weight reduction of PET (see Chapter 7) and degree of additive mixing achieved (see Chapter 9) during TSE processing.

This chapter covers the development of a new *in-house* model with increased functionality which allows the residence time weighted average shear rate, $\dot{\gamma}_{av,RTD}$ and the residence time weighted average shear stress, $\sigma_{av,RTD}$ to be calculated. Within the model, a TSE process is treated in a similar manner to a SSE process and the calculations are performed based on flows in an 'unwound' channel. The proposed parameters are calculated on the basis of the 'average shear rate' (a notion proposed by Potente et al., 1994), which itself is determined by the degree of fill, and the residence time within each element in a given screw configuration. The principles set out in the existing *in-house* model (details in Appendix D) were used to calculate the degree of fill and the residence time within each element. These are a function of the screw configuration itself as well as the operating conditions of the machine. It is hoped that the model can enable effective scale up by allowing the conditions within a small scale machine to be replicated effectively in the larger scale machine without the need for extensive on-line experimental trials.

An attempt was made to validate the calculation of the 'average shear rate' contained within the new *in-house* model against the data presented by Potente et al., 1994 who proposed the idea. The trends observed by the model proposed herein were very similar to that of Potente et al., although the absolute values differ. Difficulties were had in replicating the model proposed by Potente et al. due to the limited information on the operation conditions and the machine utilised by the authors. As a result, the influence of a number of operating conditions and design parameters onto the shear rate predicted by the model proposed herein have been explored. It is felt that the impact of these as well as the limitations of the model are well understood.

7 | Understanding molecular weight loss during polyethylene terephthalate extrusion

The molecular weight (M_w) of the polymer is a critical parameter as it directly determines the end properties of the film and sets the processing requirements, which are significantly different for high M_w and standard M_w material. It is vital that the molecular weight loss is minimised during polymer processing as this allows for films with improved end use properties to be manufactured efficiently. It allows for a greater proportion of recycle material to be introduced into the process or allows for a lower M_w polymer to be utilised to achieve a film with set target properties leading to reduced material costs. Critically the molecular weight also determines the viscosity of the material thus setting the stress transferred to an additive agglomerate which directly governs the dispersive mixing. Understanding where and how the molecular weight loss occurs within the extrusion process should enable better design of additive injection points and selection of operating conditions for achieving well mixed polymer composites and blends.

Within DTF, the intrinsic viscosity (IV), $[\eta]$ of the polymer acts as an indicator of the number average molecular weight, M_n (Wagner, 1985). Absolute techniques such as end group analysis and mass spectrometry as well as fractionation methods such as gel permeation chromatography (GPC) can be utilised to determine the molecular weight of the polymer and its distribution. However, these are much more costly and time consuming. Solution IV analysis provides a good representation of the mean molecular weight providing that the measurements are performed by the same operator as the technique can suffer from operator to operator induced variations. Once the IV has been determined, it can be related to the molecular weight by the Mark-Houwink-Sakurada Equation (Wagner,

1985) where K and a are constants that depend on temperature and solvent (Schöppner et al., 2014); see Equation 7.1.

$$[\eta] = KM_n^a \tag{7.1}$$

A typical film grade virgin polymer has an IV of 0.62 dL g^{-1} which corresponds to a M_n of ca. 20 000 representing an average chain length of around 100 repeating units. Hereinafter, the IV shall be discussed and used as a measure of the number average molecular weight of the polymer. A typical graphical representation of the relationship between intrinsic IV and M_w is given in Figure 7.1.

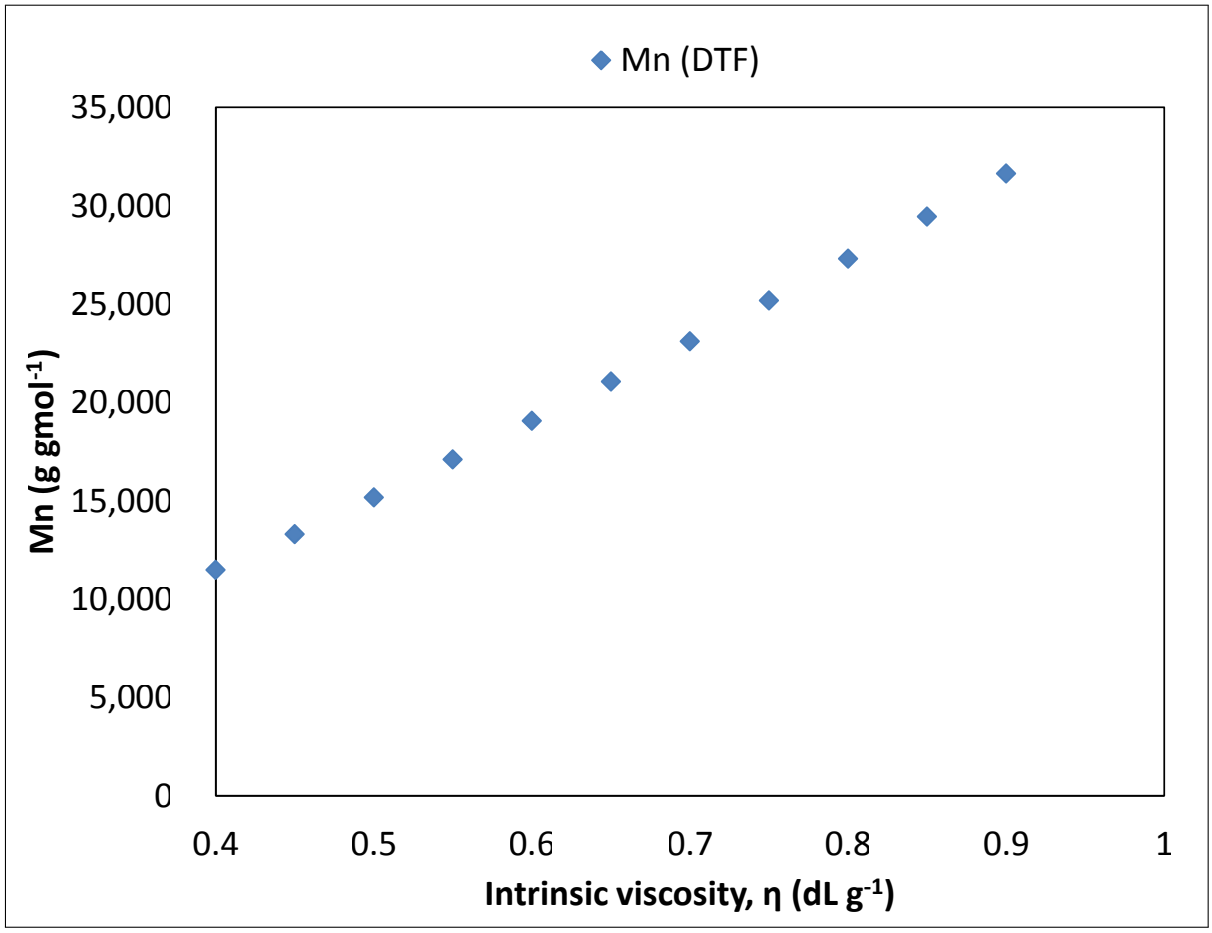

Figure 7.1: *Intrinsic viscosity vs. number average molecular weight*

The polymer chemistry of PET is well established and a knowledge of the various chemical reactions which occur at the processing conditions of the PET exists within DTF and the

literature. However, very little is known about the about the mechanically induced IV loss of the polymers, with only a handful of publications looking at the phenomenon and majority of these focusing on polymers in solutions.

7.1 Chemical reactions within PET

Within PET chemistry, the presence of moisture at extrusion processing conditions leads to the greatest reduction in the IV through the hydrolysis of PET chains (see Section 7.5.2.2). Other chemical reactions leading to a change in IV also occur including thermal esterification (reverse of hydrolysis), forward and reverse polymerisation as well as thermal and thermal - oxidative degradation. These are summarised below from Looney et al., 2016 with detailed mechanisms being available in Venkatachalam et al., 2012.

1. Hydrolysis (Acid-end catalysed or Antimony Sb^{3+} catalysed) **[⇓ in IV]**

   Di-ester chain + Water → Carboxyl end group + Hydroxyl end group

   $$-(C_6H_4)\text{-}COOC_2H_2OOC\text{-}(C_6H_4)- + H_2O \rightarrow -(C_6H_4)\text{-}COOH + HOC_2H_4OOC\text{-}(C_6H_4)-$$

2. Thermal esterification **[⇑ in IV]**

   Carboxyl end group + Hydroxyl end group → Di-ester chain + Water

   $$-(C_6H_4)\text{-}COOH + HOC_2H_4OOC\text{-}(C_6H_4)- \rightarrow -(C_6H_4)\text{-}COOC_2H_2OOC\text{-}(C_6H_4)- + H_2O$$

3. Forwards polymerisation (Antimony Sb^{3+} catalysed) **[⇑ in IV]**

   Hydroxyl end group + Hydroxyl end group → Di-ester chain + Glycol

   $$-(C_6H_4)\text{-}COOC_2H_4OH + HOC_2H_4OOC\text{-}(C_6H_4)- \rightarrow -(C_6H_4)\text{-}COOC_2H_4OOC\text{-}(C_6H_4)- + HOC_2H_4OH$$

4. Reverse polymerisation **[⇓ in IV]**

   Di-ester chain + Glycol → Hydroxyl end group + Hydroxyl end group

   $$-(C_6H_4)\text{-}COOC_2H_4OOC\text{-}(C_6H_4)- + HOC_2H_4OH \rightarrow -(C_6H_4)\text{-}COOC_2H_4OH + HOC_2H_4OOC\text{-}(C_6H_4)-$$

5. Thermal degradations **[⇓ in IV]**

   Di-ester chain → carboxyl end group + Vinyl end group

   $$-(C_6H_4)\text{-}COOC_2H_4OOC\text{-}(C_6H_4)- \rightarrow -(C_6H_4)\text{-}COOH + CH_2{=}CHOOC\text{-}(C_6H_4)-$$

6. Thermal - oxidative degradations **[⇓ in IV]**

   In chain DEG + Oxygen → peroxides

   $$\text{–COOCH}_2\text{CH}_2\text{OCH}_2\text{CH}_2\text{OCO–} + \text{O}_2 \rightarrow \text{–COOCH}_2\text{CH(OOH)OCH}_2\text{CH}_2\text{OCO}$$

   Note: there is a 60 % probability that the chain will break in the melt phase forming another carboxylic end group

Schematically these reactions can be seen in Figure 7.2

The kinetics of these reactions can be described by the rate equations given in Equation 7.2 to 7.8, where k denotes the rate constant. The concentrations of di-ester chains, hydroxyl end group, carboxyl end group, water, ethylene glycol, oxygen and in chain diethylene glycol are denoted by [Di-ester], [HEG], [CEG], [H_2O], [EG], [O_2] and [DEG] respectively.

1. Hydrolysis

   Acid - end catalysed

   $$r = k[Di-ester][H_2O]^{1.5}[CEG]^{0.5} \tag{7.2}$$

   Antimony Sb3+ catalysed

   $$r = k[Di-ester][H_2O] \tag{7.3}$$

2. Thermal esterification
   $$r = k[CEG][HEG] \tag{7.4}$$
3. Forwards polymerisation
   $$r = k[HEG]^2 \tag{7.5}$$
4. Reverse polymerisation
   $$r = k[Di-ester][EG] \tag{7.6}$$
5. Thermal degradations
   $$r = k[Di-ester] \tag{7.7}$$
6. Thermal - oxidative degradation
   $$r = k[DEG][O_2] \tag{7.8}$$

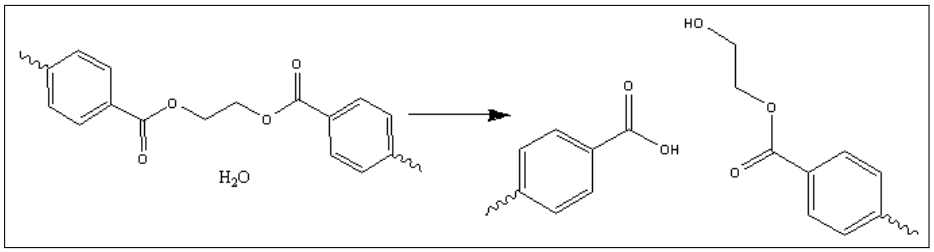

(a) *Hydrolysis (Acid-end catalysed or Antimony Sb^{3+} catalysed)*

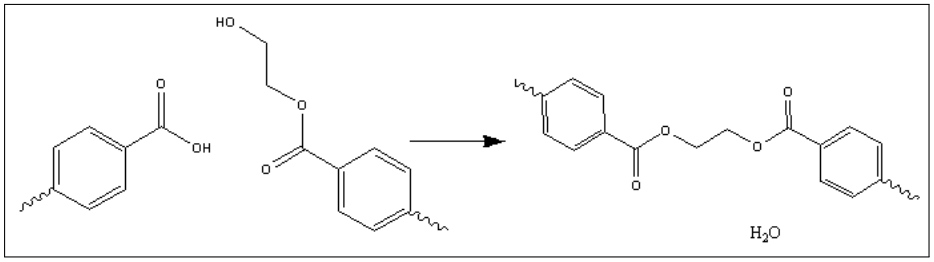

(b) *Thermal esterification*

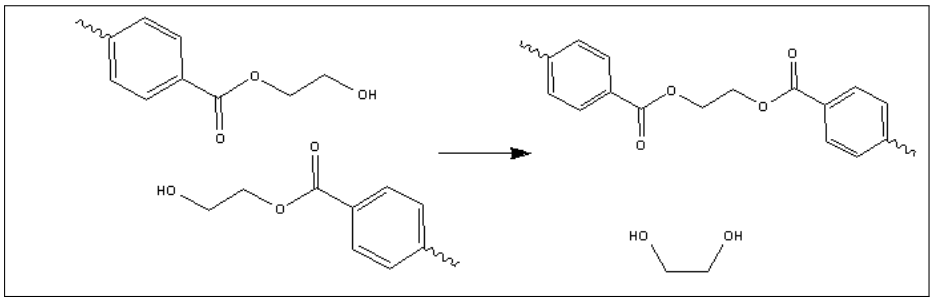

(c) *Forward polymerisation (Antimony Sb^{3+} catalysed)*

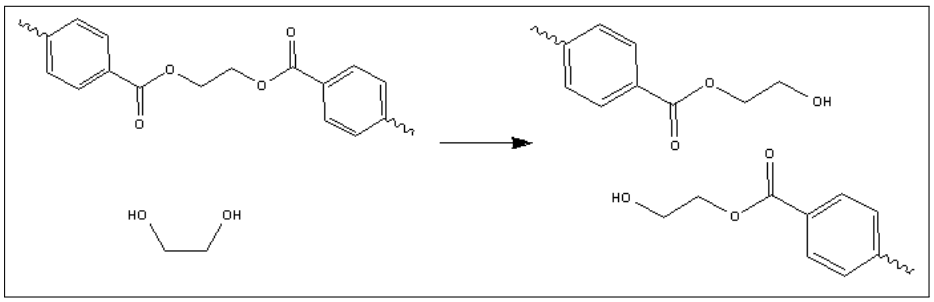

(d) *Reverse polymerisation*

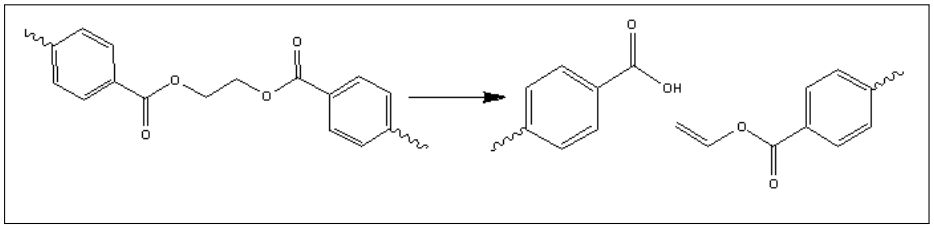

(e) *Thermal degradation*

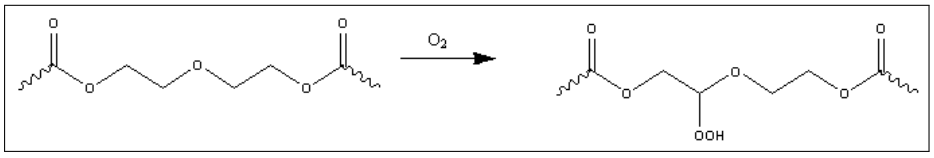

(f) *Thermal-oxidative degradation*

Figure 7.2: *Chemical reactions in PET; drawn by Sophie Pain, DTF, 2017*

It is vital to distinguish between the two different sets of kinetics available for the hydrolysis reaction. The majority of studies on hydrolysis of PET examine the rate of reaction at temperatures below the meting point. In such cases the process is described as random chain scission which is autocatalytic in nature due to the build up of acid end groups Zimmerman and Kim, 1980. However, some questions have been raised regarding the autocatalytic behaviour by Launay et al., 1994 who conducted experiments at 100 °C and preliminary concluded that the rate of reaction could be predicted by a non catalytic random chain scission process. There are few studies on the rates of hydrolysis in the melt phase, one of such is that by Campanelli et al., 1993 who examined the kinetics of the hydrolysis reaction at 250, 265 and 280 °C. Campanelli et al. determined the activation energy for the hydrolysis reaction to be 55.7 $kJ\,mol^{-1}$. The authors also identified a critical concentration of water above which further hydrolysis could not occur. This value is multiple orders of magnitude above the concentrations of water experienced in the extrusion process where 'wet' chip typically has moisture content of 3000 ppm.

Within DTF, hydrolysis occurring at temperatures below melting point is simulated by the acid end catalysed rate equation with the random chain scission reaction being utilised for the molten state. Figure 7.3 compares the rate of these reactions via the increase in CEG at different temperatures.

The results in Figure 7.3 are based on polymer with initial IV of 0.8 $dL\,g^{-1}$, initial moisture content of 2000 ppm and 0 % crystallinity and were obtained through the *in-house* reaction simulating software *Polyhand*. Times of 6 s and 30 s were investigated with the smaller representing the minimum and the larger the maximum residence time that the polymer spends in the melt section of the *Semi-Tech* extruder(as described in Chapter 5). Only the melt zone was considered here, as the vacuum degassing zone is located immediately after it in which it was assumed that any unreacted moisture would be rapidly extracted. From Figure 7.3 it is evident that at the higher temperatures the rates of the acid end and the antimony catalysed reactions are very similar, however a large discrepancy exists

at the lower temperatures whilst the polymer is in the solid state. In this work, the lower acid end autocatalytic rate has been utilised when evaluating polymer in the 'solid' state below temperatures circa 250 °C as the work presented in by Launay et al., 1994 could not draw firm conclusions to disprove the widely reported autocatalytic reaction mechanism.

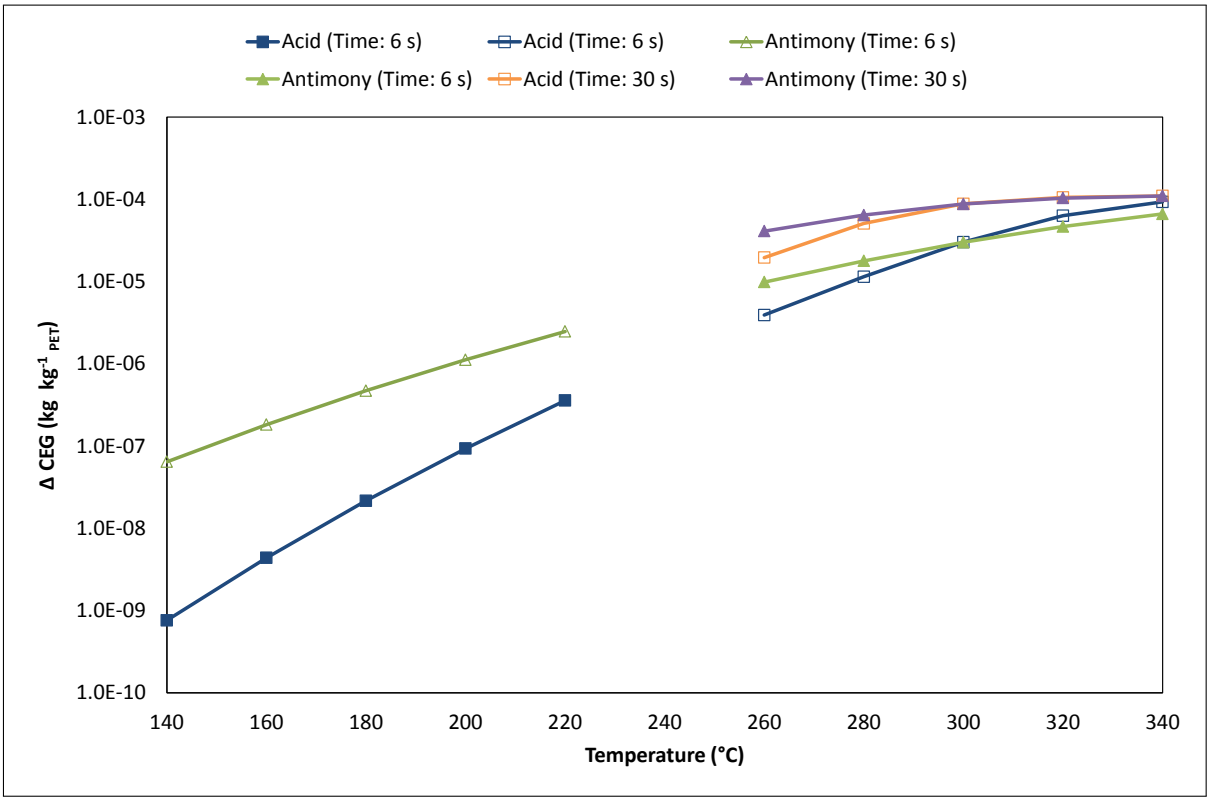

Figure 7.3: *Rate of Acid vs Antimony catalysed hydrolysis reactions in PET as function of temperature (filled markers represent estimated regions in which the literature experiments were conducted & unfilled extrapolated data)*

Recently, Schöppner et al., 2014 performed a study on degradation of PET in a co-rotating twin screw extruder where samples were taken from various sections of the machine enabling the IV changes to be monitored. This research is particularly relevant to the findings presented herein and is discussed in the relevant sections within this chapter.

7.2 Mechanically induced chain scission

Within literature some work has been reported on the topic of mechanically induced polymer chain scission. The research is often not based on PET and largely focuses on shear

induced molecular weight reduction of polymers in solution. Key works include that of Bestul, 1954; 1956; Goodman and Bestul, 1955; Goodman, 1957; Ram and Kadim, 1970 who examined the effect of shear on solutions containing polyisobutenes. Yu et al., 1979 examined the phenomenon in greater detail by considering the changes in the molecular weight distribution of polyisobutenes and comparing them with the effects on monodisperse polystyrene. D'Almeida and Dias, 1997 examined the impact of shear on solution containing polyethylene oxide and carboxymethylcelulose. The authors reported that polyethylene oxide showed a reduction in its molecular weight whereas carboxymethylcelulose did not. The research on the mechanical chain scission of polymers in solution is ongoing with recent publications such as Shanshool et al., 2011 and Brun et al., 2016 targeting the oil and gas sector.

Limited studies performed on polymers directly exist. Larsen and Drickamer, 1957 found that the amorphous regions played a much more significant role in mechanically induced chain scission of polyethylene compared to crystalline regions. Mechanical chain scission of polypropylene was investigated by Schott and Kaghan, 1963 and that of high density polyethylene by Rideal and Padget, 1976. Romão et al., 2009 considered the changes in the PET molecules during a number of reprocessing cycles. The authors reported an increase in the presence of linear low molecular weight oligomer from 0.06 $\%_{\text{wt}}$ to 4 $\%_{\text{wt}}$ following five extrusion cycles of bottle grade PET. This lead them to conclude that potentially the larger chains do not break in the middle. More recently, Schöppner et al., 2014 focused on the changes to PET following a single extrusion run. The authors reported that as the screw speed increases (the residence time decreases) the IV loss also increases which potentially indicates mechanically induced chain scission. However, the authors did not propose that scission via such mechanism indeed occurred. These and other works are explored in greater detain in Appendix E.

Molecular weight reduction of PET during melt processing as a result of chemical reactions is well defined, however this is not the case for mechanically induced chain scission. Ideas

can be carried over from the research conducted on the polymers in solution and some attempts to describe the mechanisms behind mechanically induced chain scission have been made by Bestul, 1956; Yu et al., 1979 and Brostow, 1983. Little experimental data exists which would allow the molecular weight reduction of PET via mechanical chain scission during extrusion to be accurately predicted. Internally within DTF,this mechanism is not well understood even though some evidence for it exists. It is felt that in this area the author can facilitate the development of knowledge. This improved understanding would allow the optimisation of process conditions and equipment design thus potentially improving product performance not only for new developments but also for existing products.

7.3 The experimental trials

A total of three experimental trials were undertaken to develop a better understanding of molecular weight loss during the extrusion process. Wet polymer was processed using the *Semi-Tech* extruder at various outputs and screw speeds. The details of the machine set up are described in Chapter 5. It is important to note that the machine has a vacuum degassing section located immediately after the melt zone (operated at ca. 10 mbar) in order to remove any moisture contained within the PET. Unless stated otherwise, the barrel temperatures were set at 275 °C. In some cases the viscous heating of the polymer in the zone was far more than the cooling capacity of the zone resulting in higher temperatures being recorded from the feedback loop. Upon exiting the extruder the polymer passed through a gear pump and a screen filter prior to being extruded through an end fed die onto a casting drum. Here, the film was rapidly cooled to ambient temperature and samples of cast film were collected for IV analysis.

The first trial focused on processing high IV bottle grade PET (denoted as H-PET). Initially the screw speed and the output were increased in unison to maintain the torque of the machine constant at a value of circa 80 %. This allowed the molecular weight loss

to be evaluated along the limit of the operating window for the machine. Next the screw speed was adjusted whilst the output was maintained constant (allowing the torque of the machine to drop) in order to evaluate the impact of screw speed (shear rate and stress) on IV reduction. Following this the output was reduced at a constant screw speed (allowing a reduction in machine torque) to evaluate the impact of output (residence time) on the molecular weight loss.

Trial 2 focused on processing standard IV film grade material (denoted as S-PET) with the same changes in conditions as in Trial 1. A number of output and screw speeds were set to match exactly the conditions in Trial 1 in order to evaluate the impact on the energy demand when processing two materials with significantly different starting IVs. The last trial focused on determining if running the feeding zones and the melting zone colder (at 265 °C) and hotter (at 300 °C) would significantly change the energy input into the polymer potentially allowing another means of controlling maximum output and IV losses during processing. This was done for both the standard and high IV PET.

Finally, during all the trials some pre-heated material was processed in order to see if the energy demand (torque) on the machine could be reduced allowing for higher outputs to be realised at a given screw speed. The material was preheated to a temperature of 140 °C in preheated ovens. The process took around 3 hours in which time some drying would have taken place. The wet chip was assumed to contain circa 3000 ppm of water, with the predicted values for the pre-heated chip being around 1600 ppm (as evaluated using a drying model). The polymer was loaded on trays at a depth of circa 20 mm to allow uniform heating of the material. From the ovens it was transferred by pneumatic conveying into a hopper and feeder with a combined inventory of around 50 kg from which it was fed into the twin screw extruder at a specified output.

7.4 Impact of operating conditions on IV

A hypothesis for the set of three trials has been set up based on the current understanding of the molecular weight loss during the extrusion process. Figure 7.4 shows a extruder output versus screw speed graph with a line corresponding to running the machine at 90 % torque. This is generally considered to be the limiting value, although sometimes a value of 80 to 90 % is often chosen depending on material to prevent any spikes in torque tripping the machine and causing the process to stop.

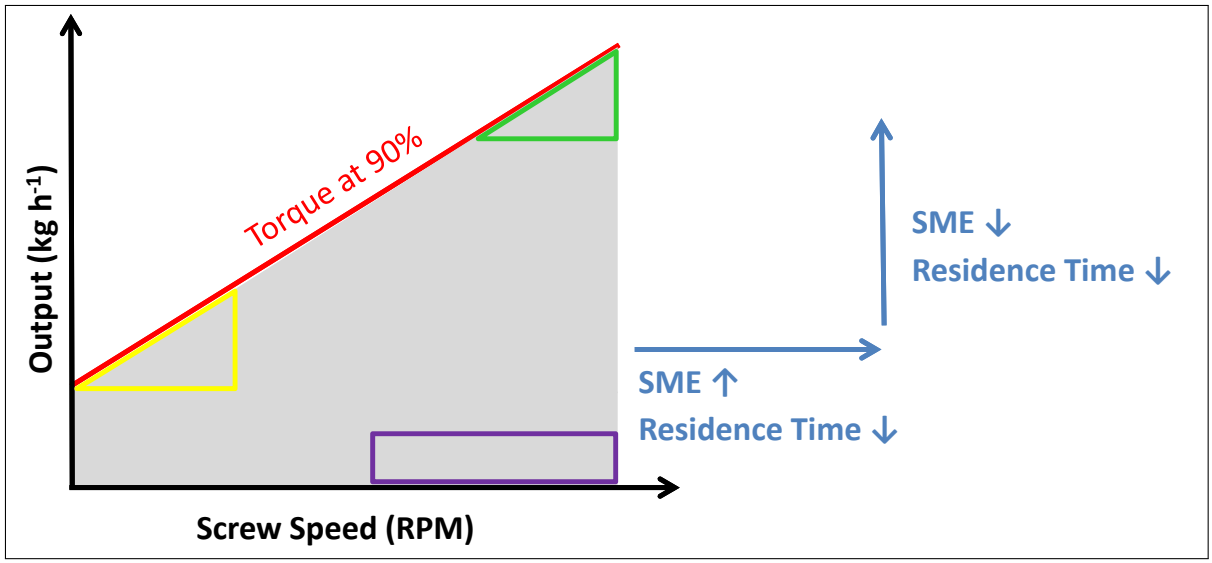

Figure 7.4: *Operating window of a twin screw extruder; triangles represent the optimum conditions for minimising IV loss by chemical reactions (green) and mechanical (yellow) means with the purple square representing optimum conditions for mixing*

From a purely economics perspective if there was no material degradation taking place the extruder should be run at the highest screw speed and thus highest output to process the most material possible reducing the production costs per unit mass of product. In film manufacture any limitations of downstream equipment are often transferred to the extruder. For example to produce a 50 µm film, the lowest casting drum speed may be x m min^{-1} which would then require the extruder to run at half the maximum capacity. In such case the screw speed would be reduced (as opposed to torque) and torque maintained constant at the limiting value to minimise the energy usage of the machine. On the other hand a compounder would select an appropriate screw speed to which gives good mixing

of the polymer composite/blend and the output would be determined from this, but the machine would still in most cases be operated at ca. 90 % torque.

In order to minimise IV loss driven by the chemical reactions, the extruder should be operated at maximum output and screw speed (a region represented by green triangle in Figure 7.4) as this is where the residence time is the smallest. It may be that a slightly lower output and screw speed may be selected (allowing a higher residence time) in order to minimise viscous heating of the material reducing the temperature and thus the rate of the chemical reactions.

On the other hand, if mechanically induced chain scission was solely responsible for the IV loss then the machine should be operated at high temperatures and low screw speeds in order to reduce the shear stress exerted on the polymer chains. As there is a need to input the smallest amount of energy into the material (per unit mass) then the machine should still be operated close to the 90 % torque limitation. This region is represented by the yellow triangle in Figure 7.4.

Finally, for the manufacture of composites or blends the material needs to be subjected to high shear rates and stresses to promote mixing of the secondary phase via the dispersive and distributive mechanisms. Dispersive mixing is an energy intensive process thus it requires high SME input. On the other hand distributive mixing is governed by the number of times flows are rearranged within the extruder hence long residence time is required to promote this. This means that the optimum mixing would be achieved at high screw speeds and low output as represented by the region towards the right side of the purple box in Figure 7.4. In practice as seen in Chapter 9, the highest screw speed may not always provide the best mixing, hence a lower screw speed may be selected as represented by the left side of the purple box.

Importantly, all three of these regions lie in completely different parts of the extruder operating window outlining a need for compromise. This is without taking into account the

economics and the limitations of upstream and downstream equipment. Although there is a middle ground, this is not suitable for all products; instead different aspects will be sacrificed to a greater extent depending on the product. Possessing a good understanding of the different mechanisms for IV loss and mixing will in turn allow the selection of optimum operating conditions for each product within both the constraints placed by product specification, equipment and economics.

Note: The IV measurements presented are an average of two measurements with error bars representing the 90 % confidence interval (student's t distribution) for the location of the mean. The error bars have not been plotted on all the graphs to make the visualisations of the trend easier due to the extensive number of data points on some of the graphs.

7.4.1 Output, screw speed and torque

The data gathered from the 3 trials has been plotted to show IV loss as a function of torque (Figure 7.5) in order to validate the earlier hypothesis.

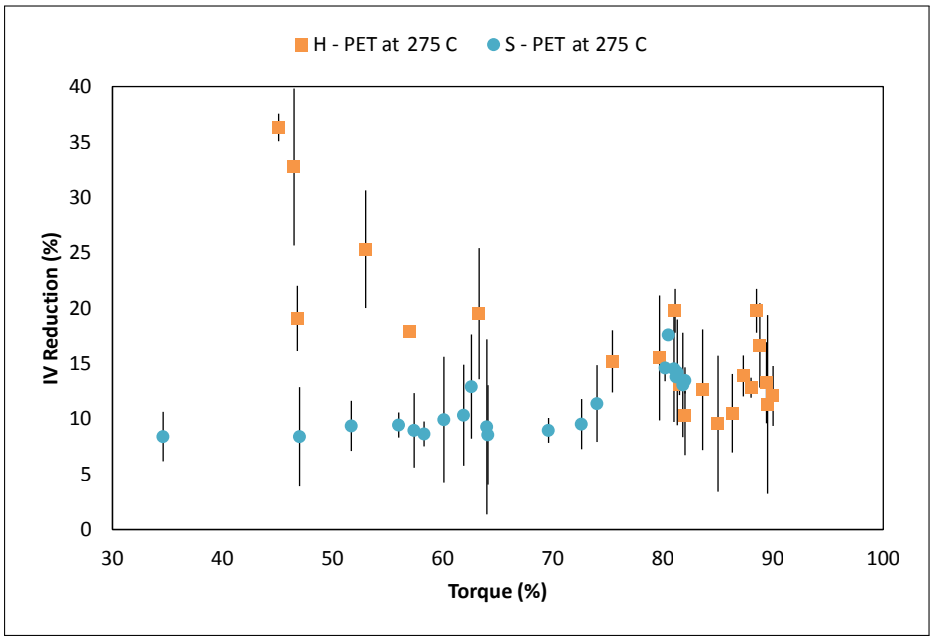

Figure 7.5: *IV Loss vs Torque for different screw speeds and outputs*

From the Figure 7.5 it is evident that H-PET conforms to the hypothesis with the majority

of samples collected at higher torque having an IV reduction circa 10 % and those at lower torques reaching values of 35 %. On the contrary for S-PET the IV loss at low torque is < 10 % as opposed to close to 20 % at higher torque. As torque is an indication of the degree of fill within the TSE, these results are a first indication of different mechanisms for IV loss.

To examine this further, the effect of shear and residence time can be considered by looking at the samples processed under constant torque as these represent a very similar degree of fill within the machine. The average DOF for the series 'H-PET: Torque ca. 85 % at 275 C' ranges from 50 to 60 %. The results for H-PET and S-PET are shown in Figure 7.6a and 7.6b. In the case of H-PET as the screw speed increases (resulting in an increase in shear rate, stress and a reduction in residence time) there is an increase in the IV loss suggesting a relationship with an increase in shear rate/stress. On the other hand the IV loss reduces with an increase in screw speed for S-PET suggesting a dependence on residence time and hence a chemically induced IV loss.

The impact of screw speed at a constant output was also considered as illustrated in Figure 7.7a and 7.7b for H-PET and S-PET respectively. In the case of H-PET there is a very strong dependence of IV reduction on screw speed. This is attributed to the reduction in the average DOF within the extruder increasing the average shear rate and stress that is seen by the polymer. For S-PET a similar trend is observed as previously with the IV loss reducing with increased screw speed. This is a likely result of the reduction in residence time, as illustrated by the residence time data in the plot which has the same trend as the IV loss.

Apart from screw speed, the output of a TSE machine is another parameter that can be directly controlled; more importantly it can be done almost independently of screw speed. The effects of output are illustrated in Figure 7.8.

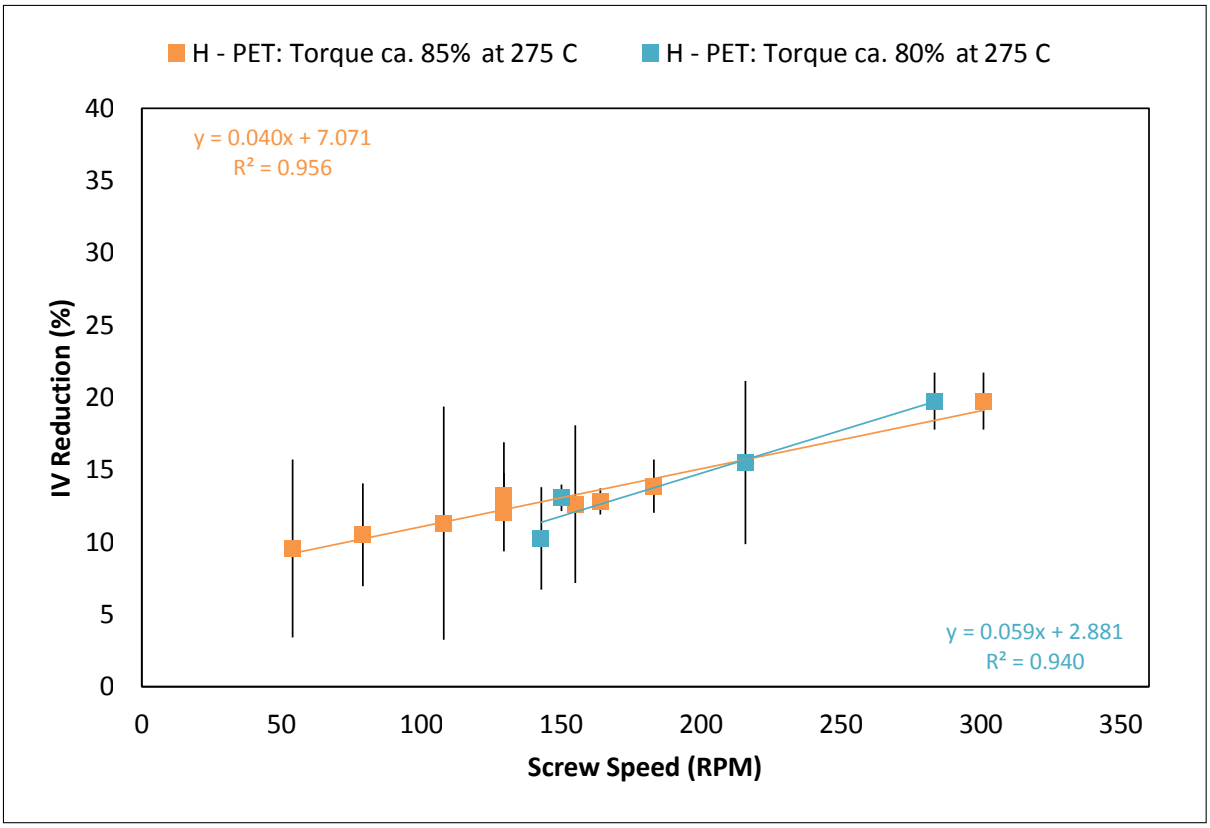

(a) H-PET

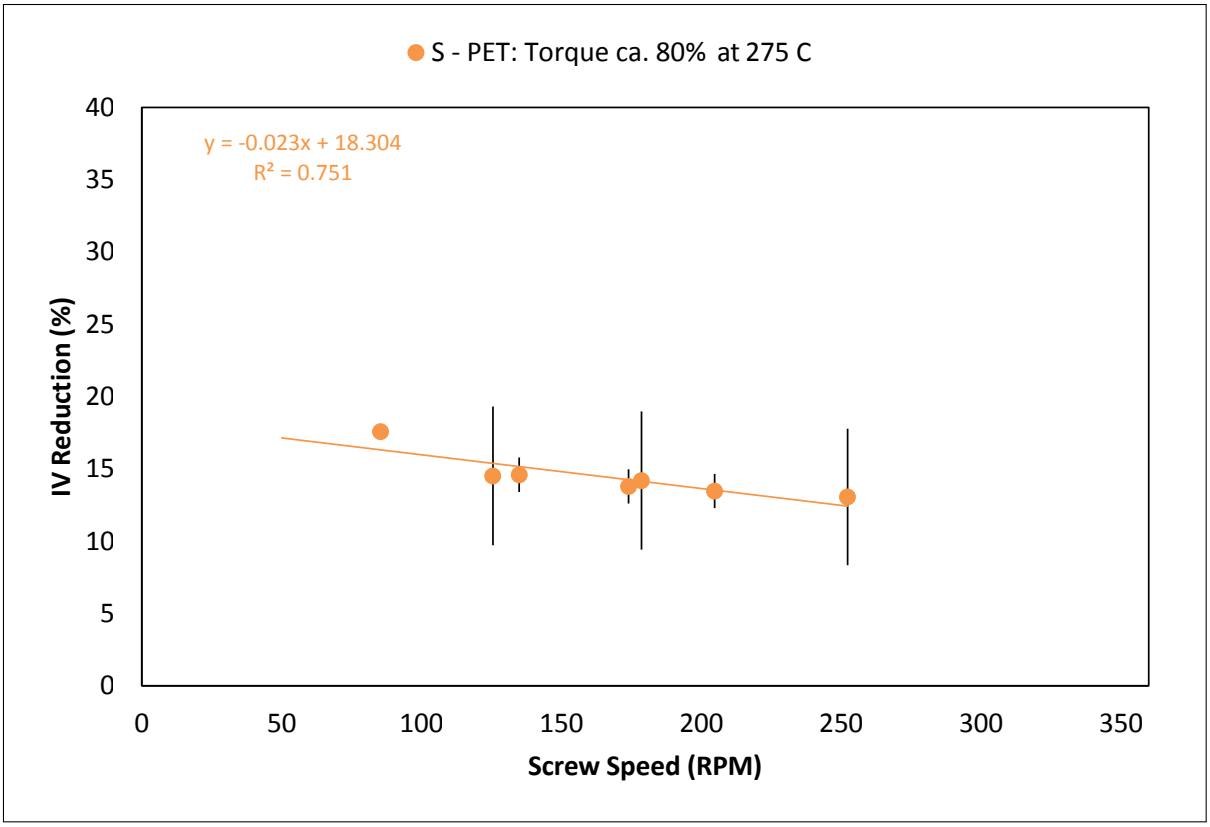

(b) S-PET

Figure 7.6: *IV reduction vs screw speed at constant torque*

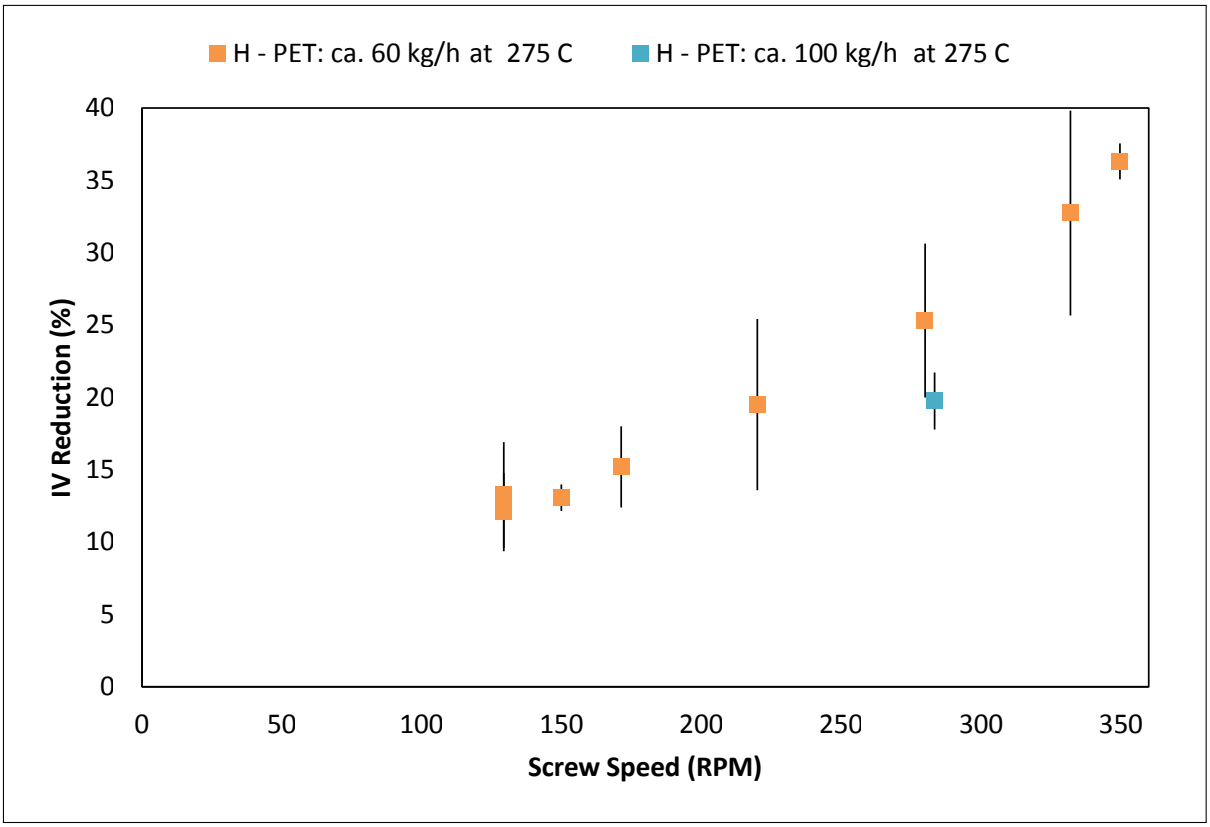

(a) H-PET

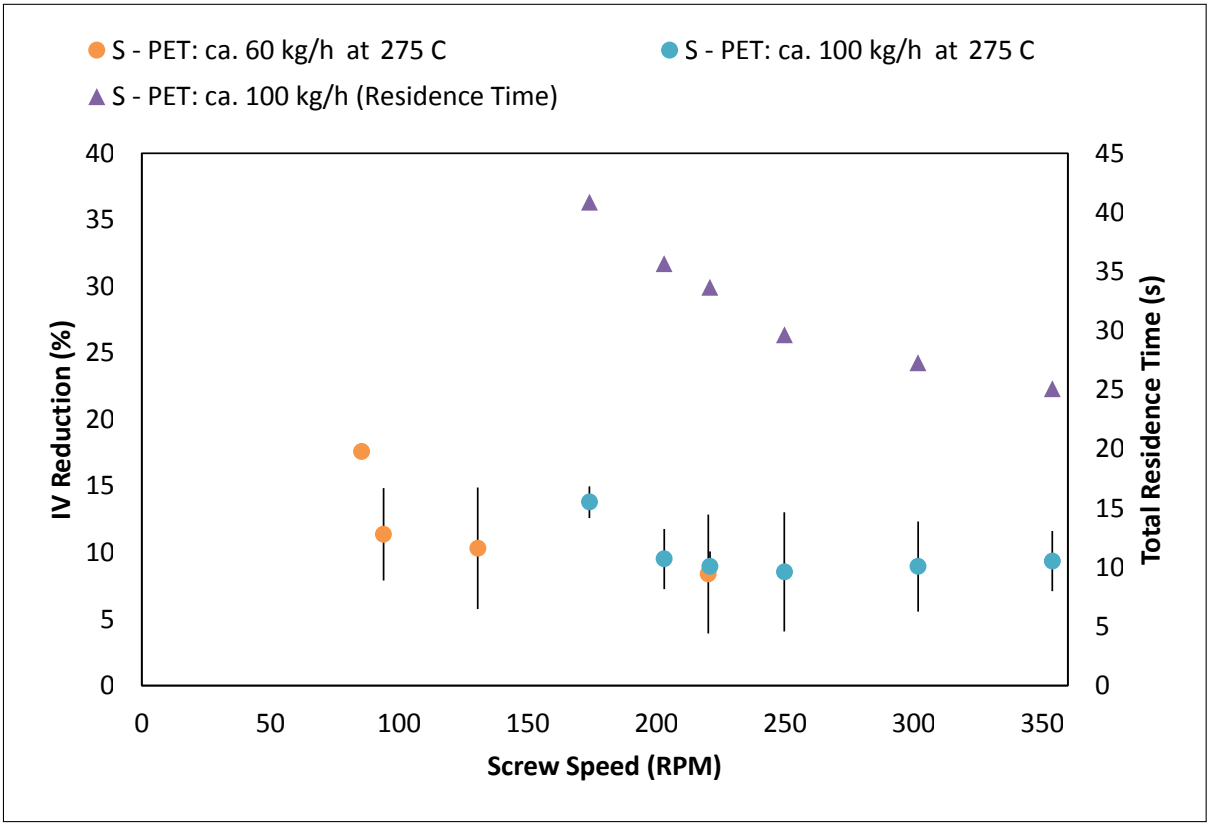

(b) S-PET; Residence time calculated from the extrusion model discussed in Chapter 6

Figure 7.7: *IV reduction vs screw speed at constant output*

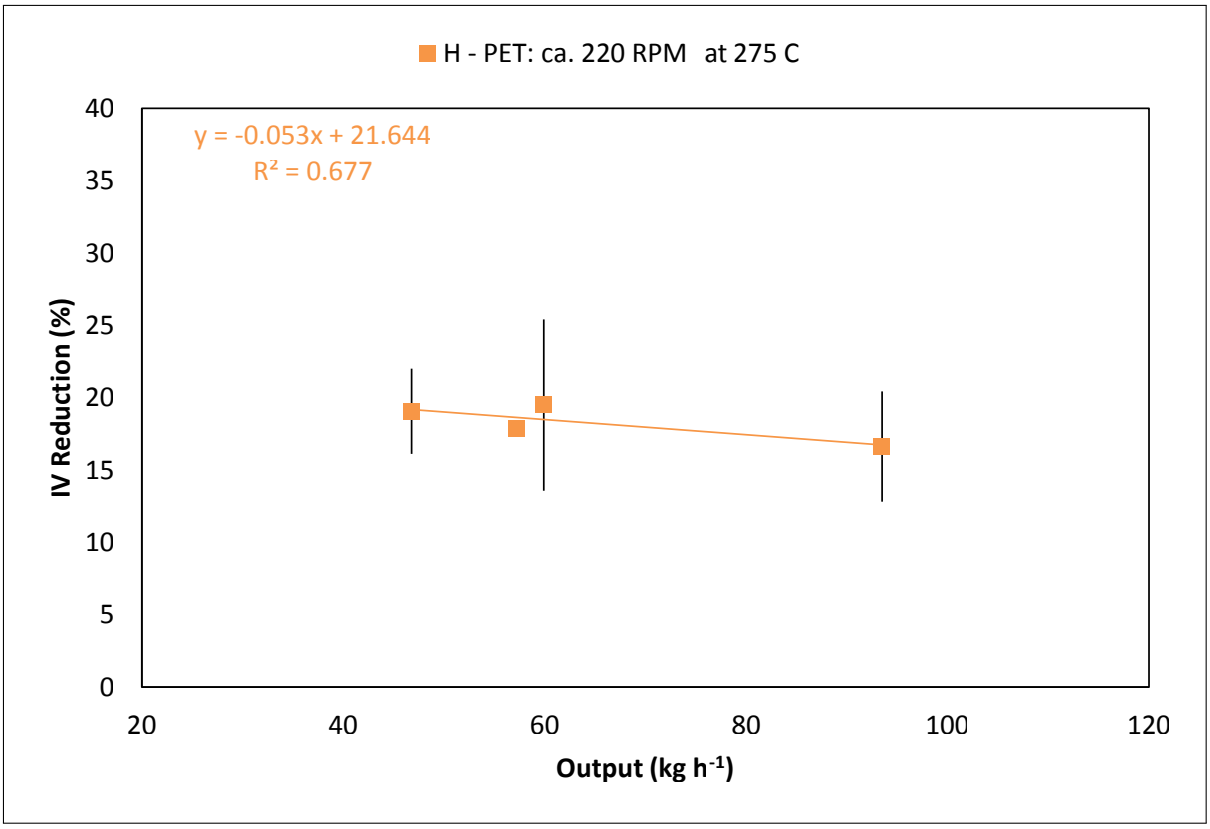

(a) H-PET

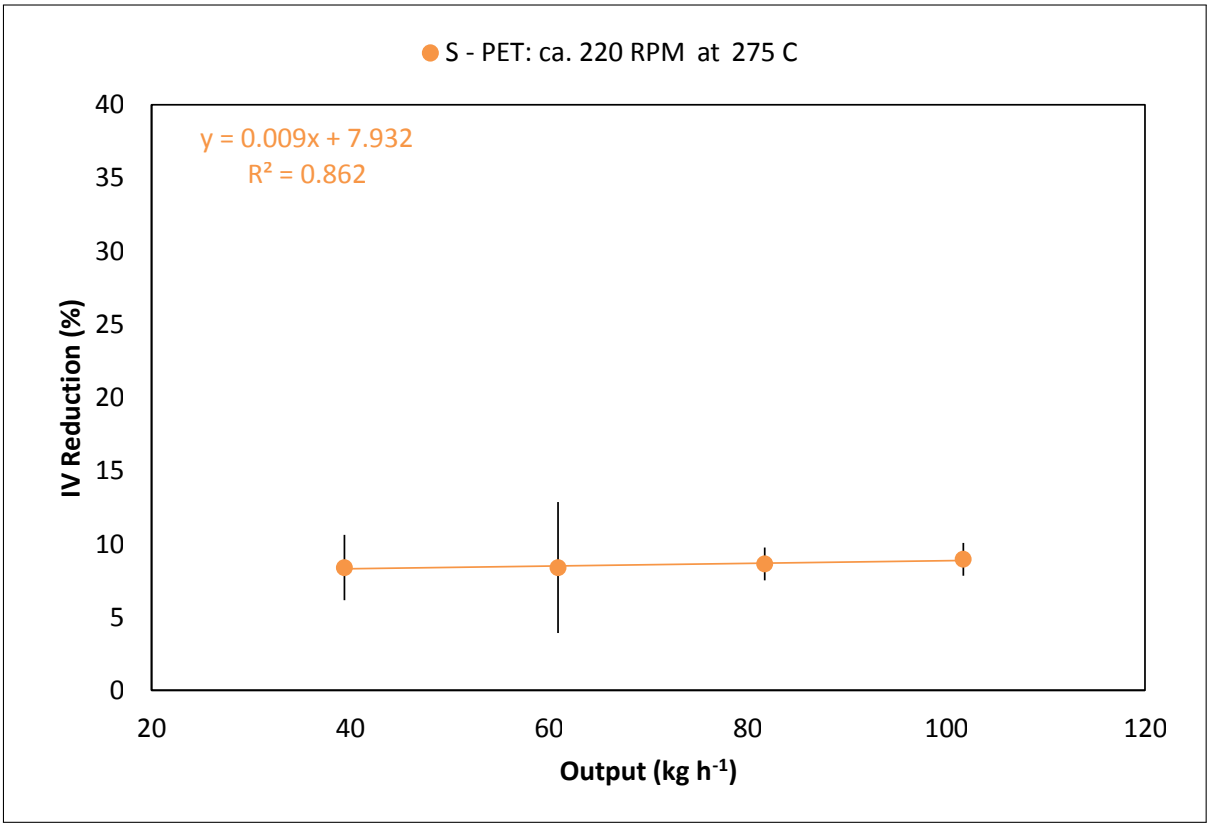

(b) S-PET

Figure 7.8: *IV reduction vs output at constant screw speed*

With respect to H-PET increasing the output from 45 to 95 $kg\,h^{-1}$ results in a very slight reduction in the IV loss of the polymer. With this change in output the average degree of fill within the machine rises from 34 to 50 %, the SME reduces from 0.140 to 0.132 $kW\,h\,kg^{-1}$ and the residence time reduces from 41 to 32 s. The rise in DOF results in slightly lower average shear rate experienced by the polymer yielding a lower IV loss. This is in agreement with Schöppner et al., 2014 who said that higher output lead to lower shear loads and a better distribution of those shear loads in addition to other benefits such as a reduction in melt temperature and residence time.

Although one may be tempted to say that there is a slight rise in IV loss of S-PET when the output is increased from 40 to 100 $kg\,h^{-1}$ in reality due to the error in measurement and with the very small change it is not possible to draw any conclusions. In the step change in output investigated the average DOF rises from 34 to 60 %, the SME reduces from 0.121 to 0.096 $kW\,h\,kg^{-1}$ and the residence time reduces from 51 to 34 s. One would expect that for IV loss process controlled by chemical reactions the reduction in residence time would give rise to a lower IV drop. In hindsight performing the output experiments at a lower screw speed would have likely yielded larger changes in the DOF, SME and residence time resulting in larger differences in IV loss measurements and thus clearer trends. This was not possible as the limitations of the machine were not known prior to the experiments.

For molecular weight loss controlled by chemical reactions melt temperature is very important as it governs the rates of those reactions with higher temperatures leading to larger IV loss. If the chain scission is mechanically induced then the higher temperatures may in fact be beneficial as they would lower the viscosity of the material resulting in lower shear stresses being applied to the polymer. During the trials two types of melt temperatures were recorded, one a direct measurement of the melt curtain with a pyrometer and the other being the feedback temperatures on barrel heaters in each zone of the extruder. These are shown in Figure 7.9 and 7.10 respectively. The pyrometer measure-

ments of the melt curtain offer a direct (non contact) measurement of the polymer melt temperature. However, as the measurement is taken after the polymer has passed through the gear pump, screen filter and the rest of the melt system, there is a question regarding how representative is the measurement of the temperature at the exit of the extruder. It is likely that the measured values are cooler than the temperatures at extruder exit since the heaters are set to lower temperatures than zone measured (in most cases). A disadvantage is that the measurement is very susceptible to operator error as it is possible to measure the temperature of surrounding metal work as opposed to the melt itself; see circled data points in Figure 7.9.

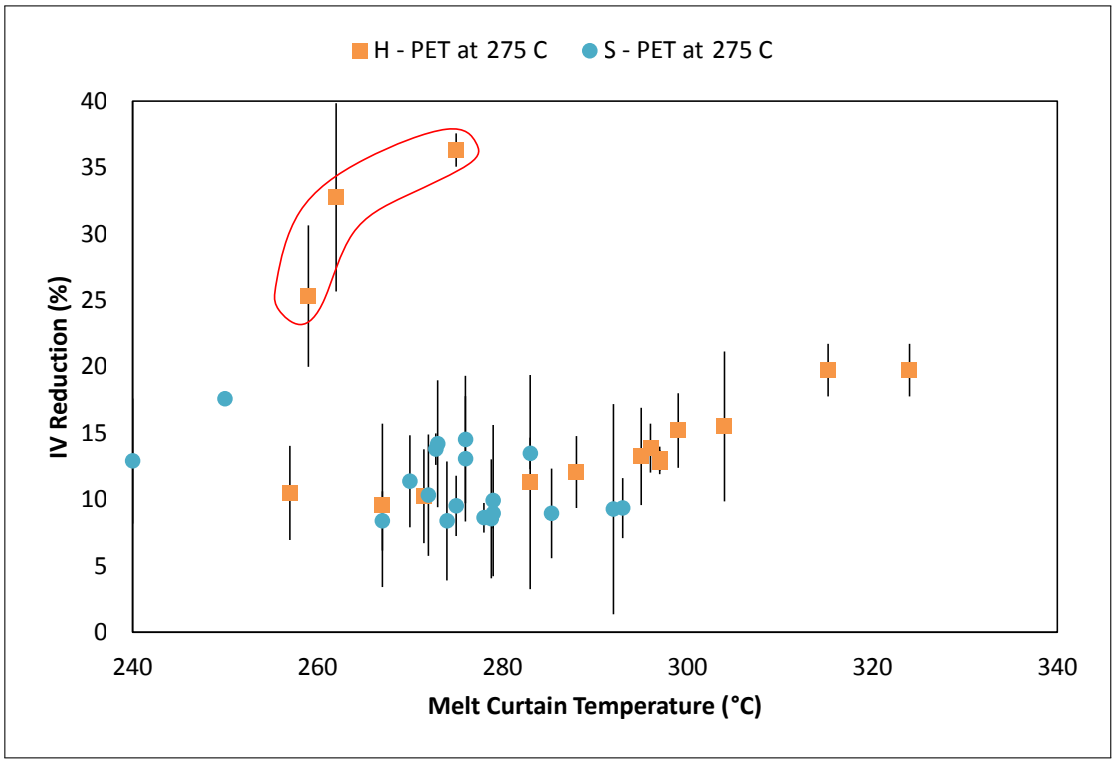

Figure 7.9: *IV Loss vs melt curtain temperature; circled data likely to represent measurement anomalies*

The feedback temperature in Zone 3 (melting zone) and Zone 7 (last zone: mixing and metering) in particular provide a good representation of the melt temperature when the viscous heating is more than the cooling capacity of the barrel zones. On the other hand they offer a very poor representation at conditions when the heaters are supplying energy to the system as the polymer may be at a temperature lower than the barrel zone.

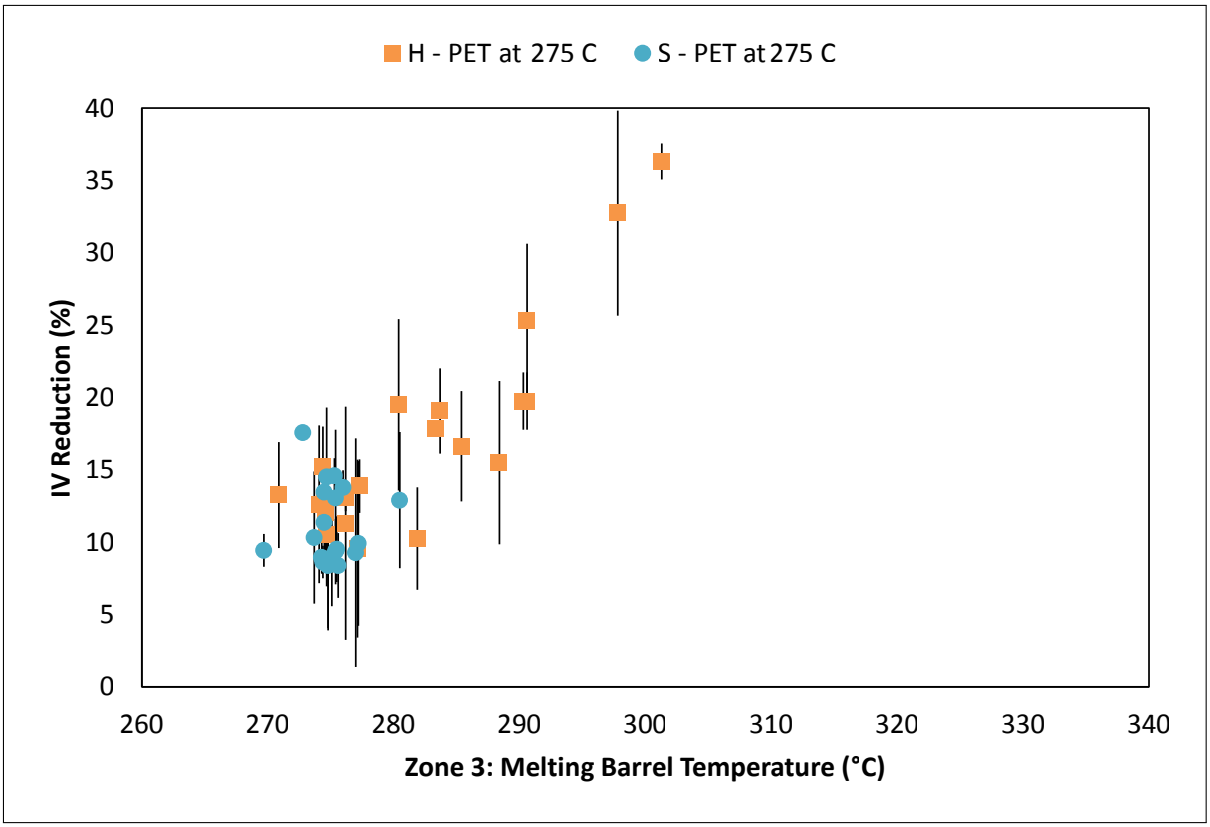

(a) Zone 3: Melt zone

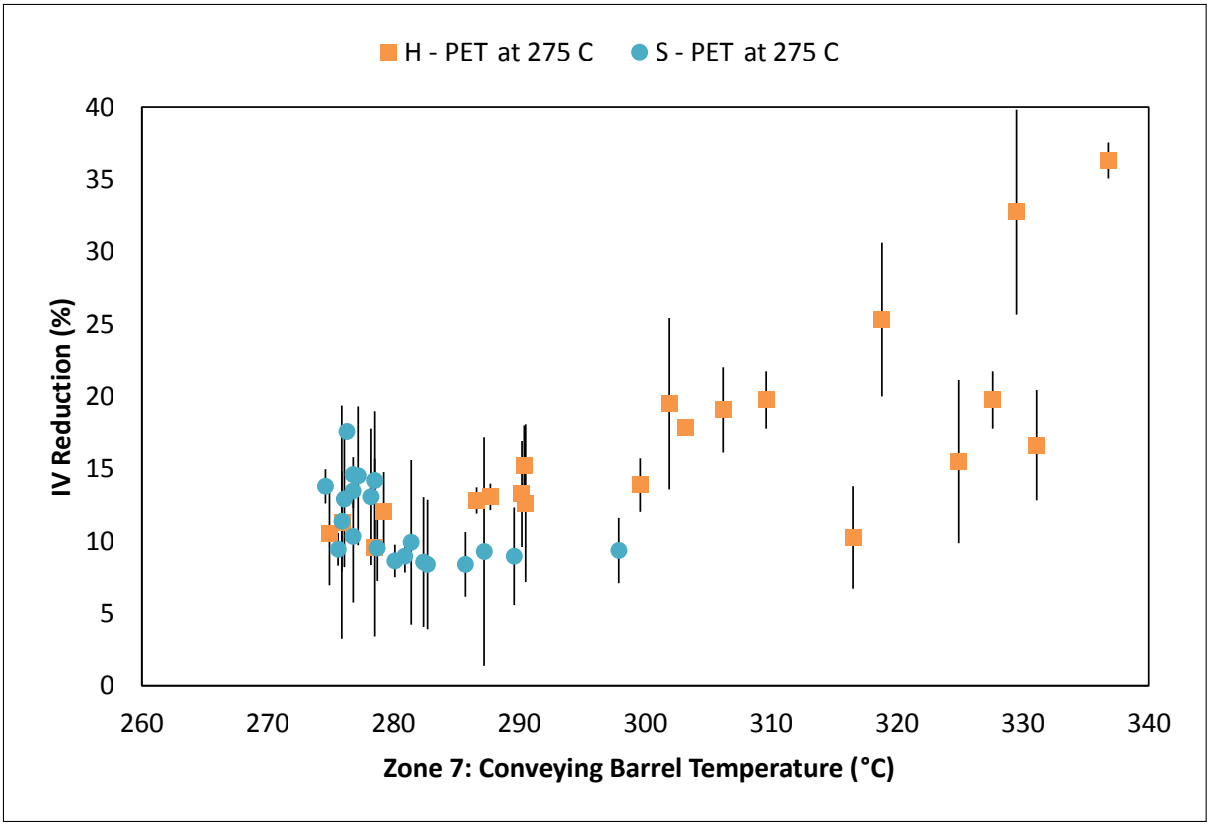

(b) Zone 7: Mixing and metering zone

Figure 7.10: *IV reduction vs barrel zone feedback temperature*

Evaluating the results of the pyrometer measurements in Figure 7.9 it is evident that for H-PET as the melt temperature increases the IV loss also increases. Although for S-PET the data is more scattered it could be concluded that there is a slight reduction in the IV loss with increasing melt temperature. In considering the feedback temperatures for Zone 3 in Figure 7.10a little can be said about S-PET as the data appears scattered. For H-PET the IV loss increases as a function of melt temperature. The feedback temperatures in Zone 7 provide a better trend as this is the last zone in the extruder; hence offering a better representation of the work put into the polymer. Here, it is evident that the IV loss for S-PET decreases with an increase in melt temperature and increases for H-PET.

In reality, even though the melt temperature influences the kinetics of the chemical reactions, it should not be used to form correlations for IV loss. The melt temperature is simply an indicator of the work put into the system. For S-PET the higher temperature readings are a result of the lower residence time (high screw speed) and for H-PET they are the result of higher shear conditions (high screw speed). The observed trends are explained if the IV loss for S-PET is chemically induced and that for H-PET is driven by mechanical chain scission.

7.4.2 Impact of calculated parameters on IV loss

As well as the parameters that directly influence the operation of the TSE, calculated parameters including specific energy input, residence time, degree of fill and specific output can provide a greater insight of the process. The impact of these is discussed in this section.

A parameter of interest is the degree of fill within the extruder, as it directly influences the average shear rate that the polymer experiences as well as the residence time distribution of the material (Martin, 2013). It can be calculated accurately (see Appendix D) or approximated by the Equation 7.9:

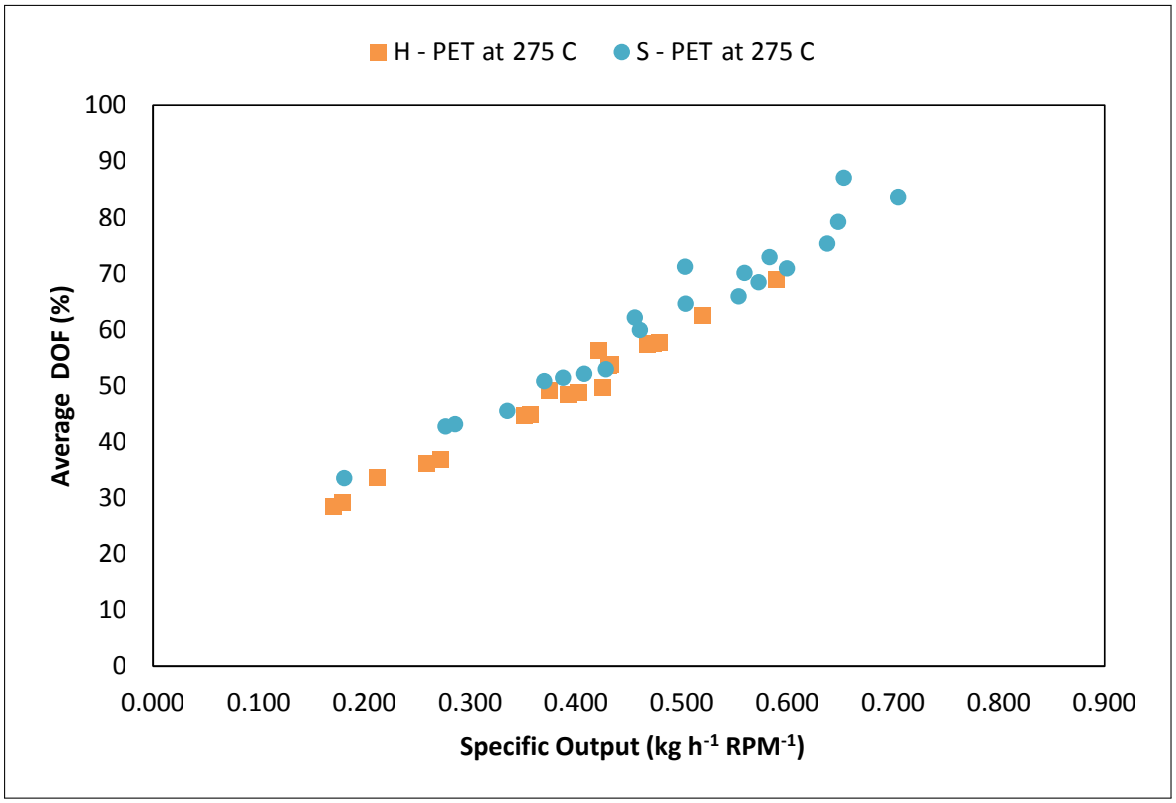

Figure 7.11: *Degree of fill vs specific output*

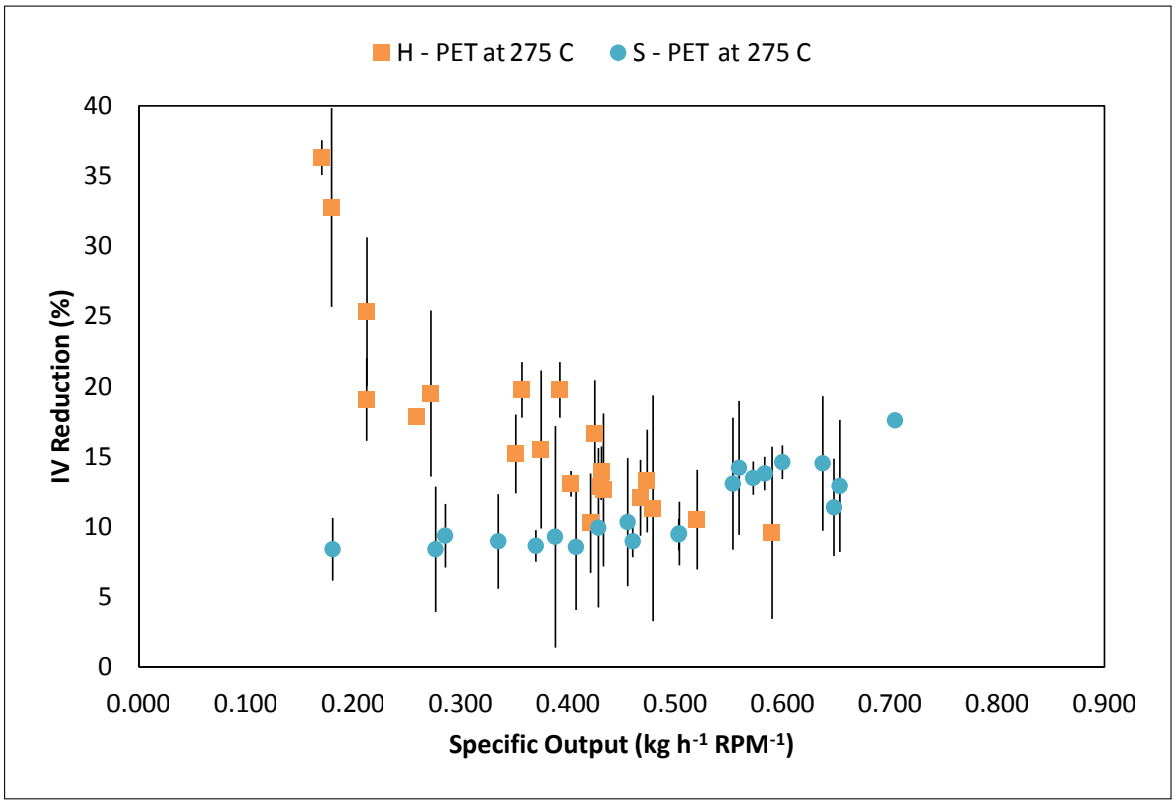

Figure 7.12: *IV loss as function of specific output*

$$DOF = \frac{0.2777\dot{m}}{SV \cdot \frac{N}{60} \cdot SG \cdot EF} \tag{7.9}$$

where $\dot{m}$ is the mass flowrate in $\mathrm{kg\,h^{-1}}$, N the screw speed in rpm, SV the specific volume in $\mathrm{cm^3}$/diameter of length , SG the specific gravity and EF the forwarding efficiency of the screw (around 35 % for a profile containing 1/3 kneading blocks) (Martin, 2013).

Specific output is much simpler to calculate and can be directly related to the average degree of fill, as illustrated in Figure 7.11. Thus, this parameter is used as a basis for correlations with the IV loss as seen in Figure 7.12. It is evident that for H-PET IV loss drastically decreases as the degree of fill in the extruder increases. This can be related to the much lower average shear rate which the polymer experiences at the higher degree of fill. From the reaction perspective, higher degree of fill results in lower melt surface area thus reducing thermal-oxidative reaction rate (Schöppner et al., 2014) and more importantly reduces the degassing efficiency in the vacuum zone leading to higher rate of hydrolysis. This is a relationship that is observed with S-PET where the IV loss increases with the rising degree of fill suggesting again that the IV loss is governed by the reactions.

Interestingly the results presented by Schöppner et al., 2014, who worked with film grade PET with an intrinsic viscosity almost identical to that of S-PET, show a different trend; a trend which resembles that of H-PET (see Figure 7.13). The experiments performed by the authors were done on a smaller machine, 25 mm in diameter compared to the 40 mm extruder used here and at much higher screw speeds. A comparison of the minimum shear rates experienced by the polymer in the centre of the channel can be made. In the experiments run by Schöppner et al. the shear rate range is from 60 to 200 $\mathrm{s^{-1}}$ compared to these results which range from 20 to 130 $\mathrm{s^{-1}}$. The combined results suggests that there is a point when even for the lower molecular weigh PET the IV loss becomes governed by the shear as opposed to the chemical reactions. This differs to the opinion of Schöppner et al. who acknowledges the importance of shear but concluded that the increased IV loss is due to the higher melt temperatures at the lower specific output conditions.

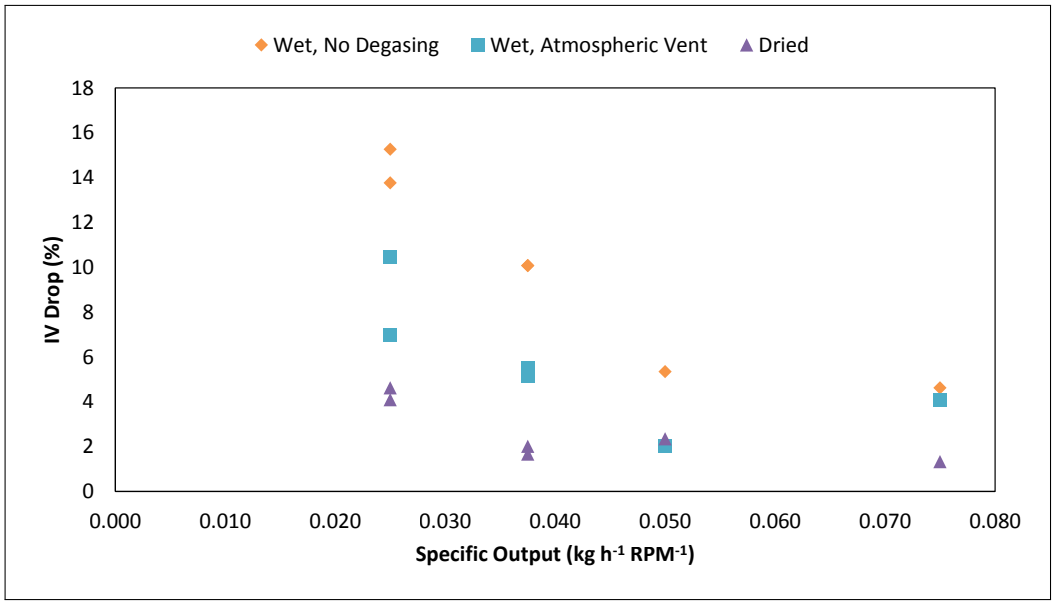

Figure 7.13: *IV loss as function of specific output from Schöppner et al., 2014*

Another parameter of interest is the residence time, which is calculated based on the throughput, free volume of the machine and the average degree of fill. The dependence of IV loss on the residence time is shown in Figure 7.14.

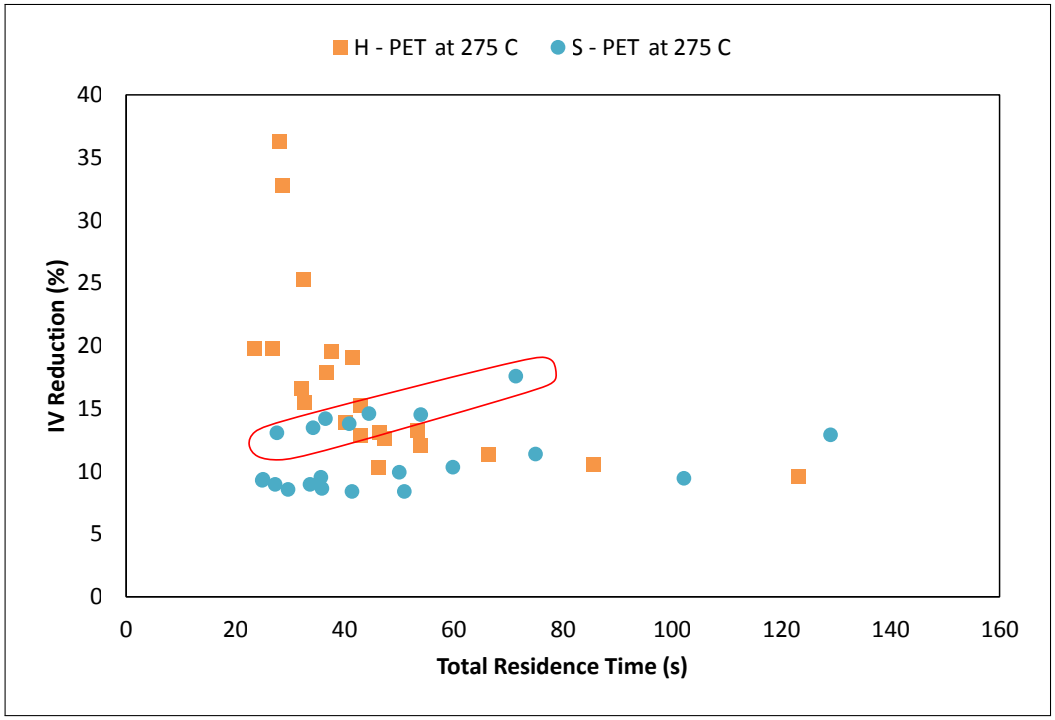

Figure 7.14: *IV loss as function of total residence time for H-PET and S-PET*

For H-PET the IV loss increases drastically at residence times below 60 s which is rep-

resentative of conditions at elevated screw speeds. This illustrates that the IV loss is not controlled by the kinetics of the chemical reactions. For S-PET a dependence on the kinetics can be seen as the IV loss increases linearly with increasing residence time. Interestingly, there appear to be two distinct groups where the group with the higher IV loss is circled in red on Figure 7.14.

The cause of this has been investigated further in Figure 7.15 which shows the different conditions for sets of data. The experiments conducted at higher torque ($>$ ca. 80 %) clearly form the distinct group. At these conditions the average degree of fill within the extruder is the highest and more importantly there is a high average degree of fill in the degassing zone (Zone 4). These results demonstrate the limitation of the degassing zone in removing the moisture leading to greater IV loss via hydrolysis reaction. This has been further examined in Figure 7.16.

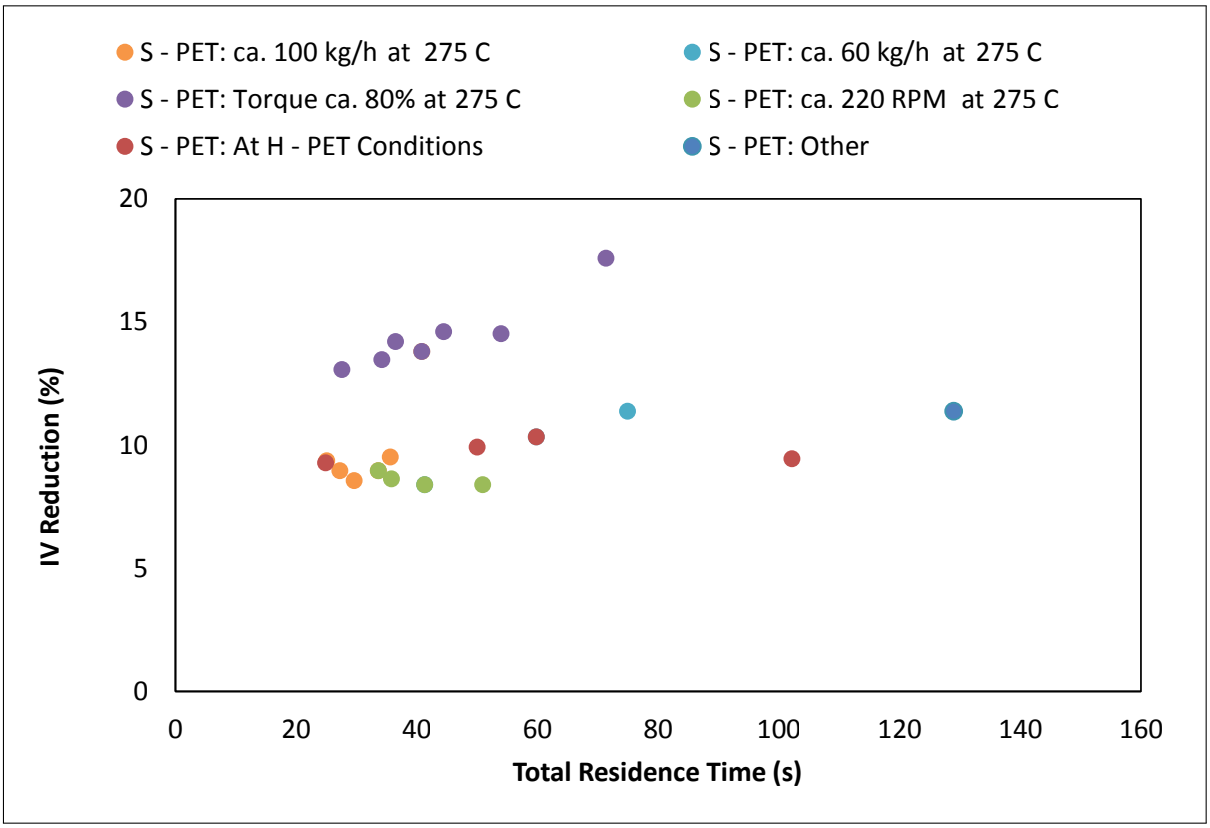

Figure 7.15: *IV loss as function of total residence time for S-PET*

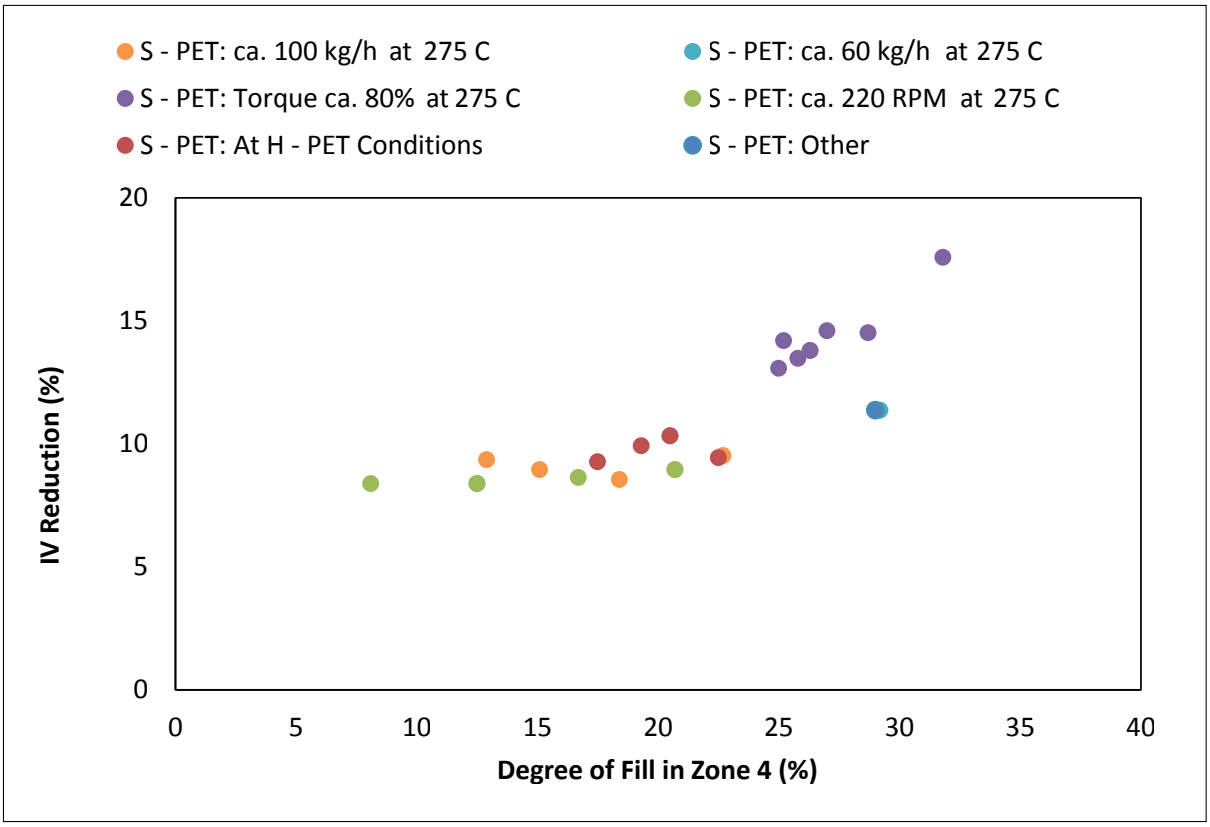

Figure 7.16: *IV loss as function of degree of fill in degassing zone for S-PET*

From Figure 7.16 it is evident that the degassing efficiency decreases when the DOF in Zone 4 reaches the value of circa 20 %, as beyond this point the increase in IV loss is observed.

Another parameter of interest is the specific mechanical energy input; particularly important when trying to establish appropriate operating conditions to achieve good mixing. It appears that the energy input can also be correlated to the IV loss. SME is particularly good calculated parameter as it utilises all three variables which describe the extrusion process: output, screw speed and machine torque. The dependence of IV loss on SME can be seen in Figure 7.17. H - PET exhibits a positive correlation where the IV loss increases with increasing energy input. On the other hand the IV loss of S-PET shows a slight reduction in the IV loss with increase in SME input, which is a direct result of the reduced residence times at the high SME conditions. There appears to be a good transition from S-PET to H-PET trends. An optimum SME can be identified in the region of

around 0.10 to 0.11 kW h^{-1} as this is where the IV loss is the smallest.

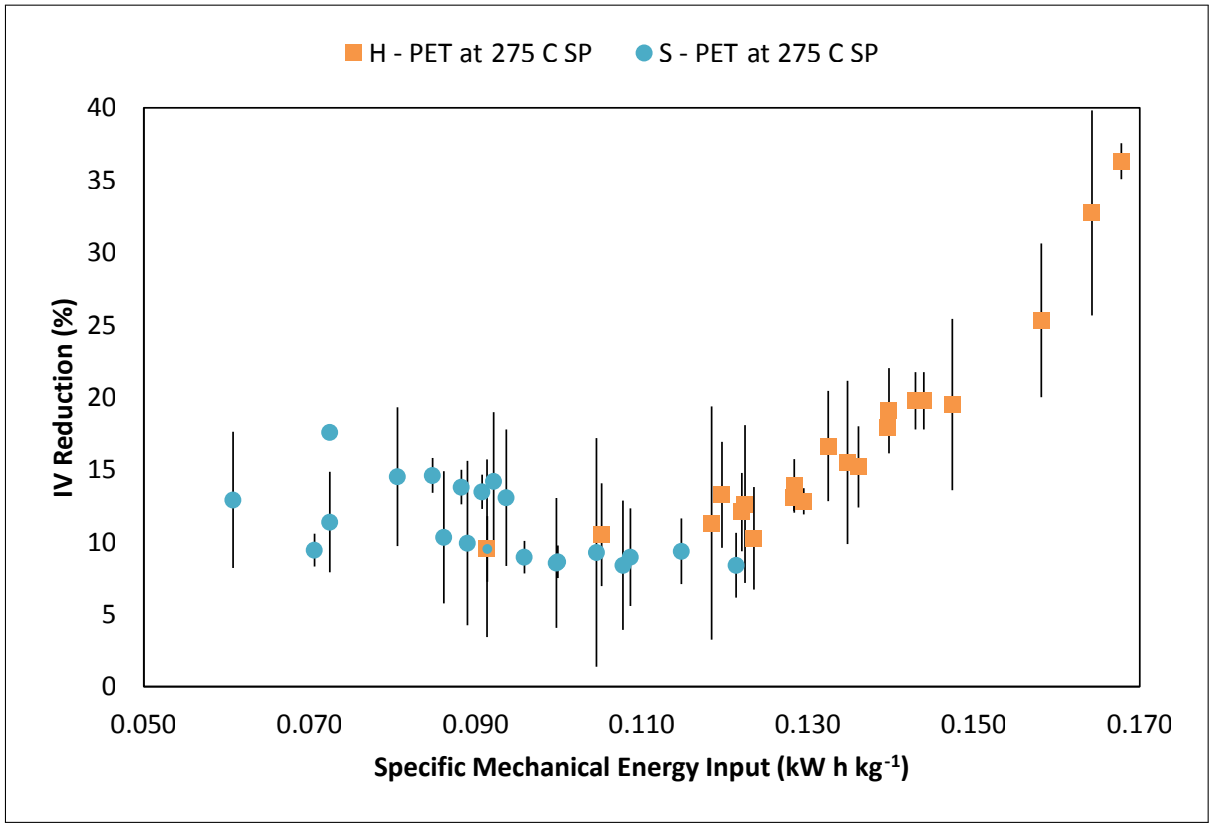

Figure 7.17: *IV loss as function of specific energy input*

7.4.3 Summary of IV loss trends

A number of relationships for IV loss have been presented, these are summarised in Table 7.1. It is clear that H-PET and S-PET exhibit opposing trends in all cases.

Table 7.1: *Summary of IV loss relationships; Note: +/− represent 0 to 5 % increase/decrease in IV, ++ / −− represent 5 to 15 % increase/decrease in IV, and +++/ −−− represent >15 % increase/decrease in IV.*

Parameter	H-PET	S-PET
Increase in torque	− − −	++
Constant torque	++	−
Increase in screw speed	+++	−−
Increase in output	−	+
Increase in specific output	− − −	++
Increase in total residence time	− − −	+
Increase in SME	+++	−−

The difference in trends for these polymers is associated with different mechanisms being responsible for the IV loss. It is proposed that the reduction in IV and hence the molecular weight for S-PET is mainly driven by the reaction kinetics with the key reaction being hydrolysis. As a result the IV loss is primarily dependant on the residence time and any parameters that effect the residence time. An increase in output and screw speed both reduce the residence time, hence lead to a reduction in the IV loss of the polymer. Torque and specific output are also indicators of the residence time. As both of these parameters reduce the residence time reduces leading to a reduction in IV loss. Similarly, increased SME is correlated with reduced residence time, hence the reduction in IV loss. Further to this, the degree of fill within the degassing zone also has an impact. A limiting value of circa 20 % was observed above which there is a limitation on the melt surface area leading to a reduction in the efficiency of moisture removal and thus increasing the IV loss.

With respect to H-PET, the IV loss appears to be driven by mechanically induced chain scission associated with high shear rates and in particular shear stresses. For this reason the factors that influence the shear rate affect the IV reduction. Increase in screw speed directly increases the shear rate and a decrease in output reduces the degree of fill thus increasing the average shear rate resulting in greater IV reduction. Similarly, a reduction in torque and an increase in SME are associated with a rise in shear rate thus causing greater IV loss. In this case the IV reduction by chemical means is considerably smaller than the mechanically induced loses, hence a reduction in residence time causes a rise in IV loss. This also means that any gains in degassing efficiency realised by running at lower DOF are over shadowed by the IV losses generated through the increase in average shear rate that the polymer experiences. The rise in melt temperature observed at the high shear conditions is simply a representation of the work to which the polymer has been subjected and thus can not be linked with the IV loss.

7.5 Understanding the onset of mechanically induced chain scission

7.5.1 Shear rate and stress relationships

In order to understand chain scission induced by mechanical work, the IV loss was considered as a function of shear rate. There are three possible shear rates which can be utilised: the minimum shear rate at the deepest part of the screw channel, the maximum shear rate in the clearance between the screw flight/kneading block tip and barrel or the residence time weighted average mean channel shear rate. The later describes the average shear rate within the extruder with one single number based on the operating conditions and degree of fill within each element of the machine. For its derivation see Chapter 6.

The effects of minimum shear rate on IV loss can be visualised in Figure 7.18a. For H-PET there is a positive correlation of IV loss with increase in shear rate. However, one of the difficulties in using the minimum shear rate is that it reflects only the screw speed and the screw geometry at a single point. This results in several data points of different IV loss at a given shear rate when for example the machine is operated at different output; as outlined in red on the figure concerned. One advantage of utilising the residence time weighted average mean channel shear rate is that it negates this issue; see Figure 7.18b. Here, the same trend for H-PET is observed with an increase in shear rate resulting in increased IV loss. For S-PET the opposite trend is observed with a reduction in IV loss as a function of increased shear rate. The two distinct groups for S-PET, the high torque and lower torque are also clearly visible.

A concern with utilising shear rate to examine the impact on IV loss is that it is still effectively a process parameter and thus negates the influence of material properties on the chain scission. As several authors have proposed previously (see Appendix E) shear stress can be a good indicator of IV loss. The shear stress takes account of material viscosity which reflects temperature, pressure and shear rate.

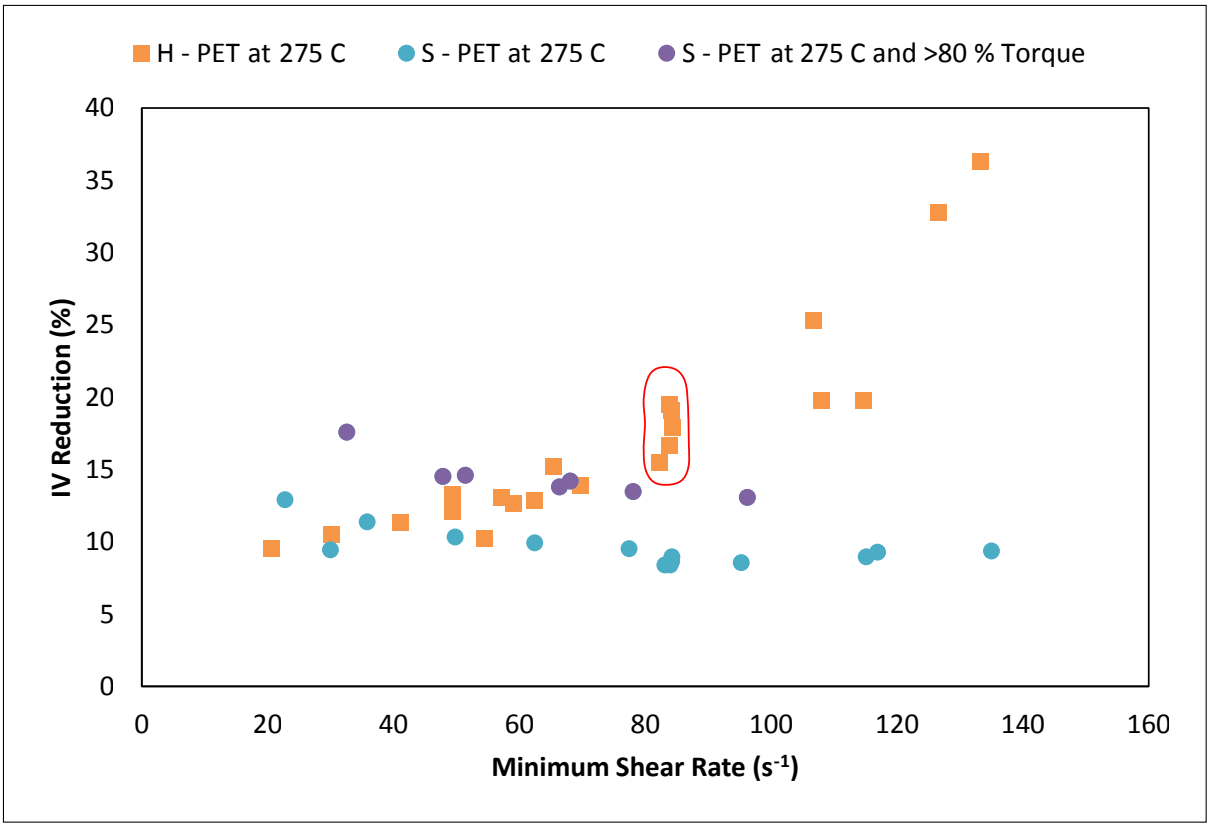

(a) Minimum shear rate in the centre of the screw channel

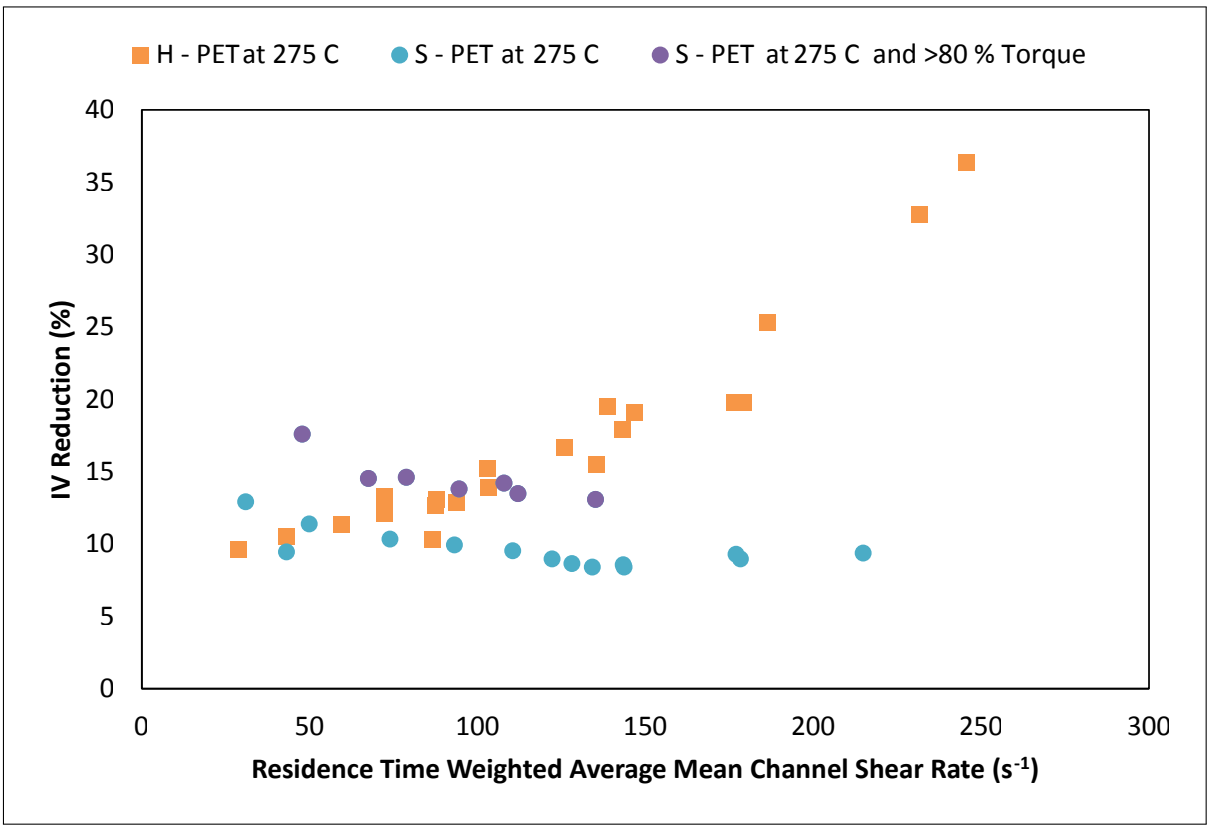

(b) Residence time weighted average mean channel shear rate

Figure 7.18: *IV reduction as function of shear rate*

The challenges in utilising the shear stress derive from selecting an appropriate melt temperature and intrinsic viscosity for the polymer to enable the calculation of the melt viscosity. For example in the case of examining shear stresses exerted on agglomerates ideally one would utilise the viscosity which reflects any chain scission which may have taken place and temperature at the point of addition.

Since the change from original material properties is of interest, then the IV of the virgin polymer should be utilised as a basis for the calculation. The temperature is more difficult to chose as several options are available:

- *Melt curtain temperature* - direct (non contact) measurement of polymer temperature. Although some concerns about reliability of the measurement and availability of data for all conditions mean that it is not possible to utilise this.
- *Zone 3 barrel temperature* - feedback temperature in the melting zone. This is the point in the extruder where the highest stresses on the polymer will be exerted as it melts.
- *Maximum barrel temperature* - the maximum temperature will give the lowest melt viscosity of the material.
- *Residence time weighted average barrel temperature* - as the temperature of the material changes through the extruder zones, this would provide an estimated average of the polymer temperature in the extruder.
- *Melting point temperature* - defines the point where the material begins to flow, yielding the highest melt viscosity and thus stress delivered to the material.

Figure 7.19a shows the dependence of IV loss on the shear stress calculated based on polymer viscosity at melting zone temperature. For S-PET the IV loss decreases and for H-PET the IV loss increases as a function of shear stress. There is a good agreement between the IV losses for H-PET and S-PET at shear stress of around 40 kPa.

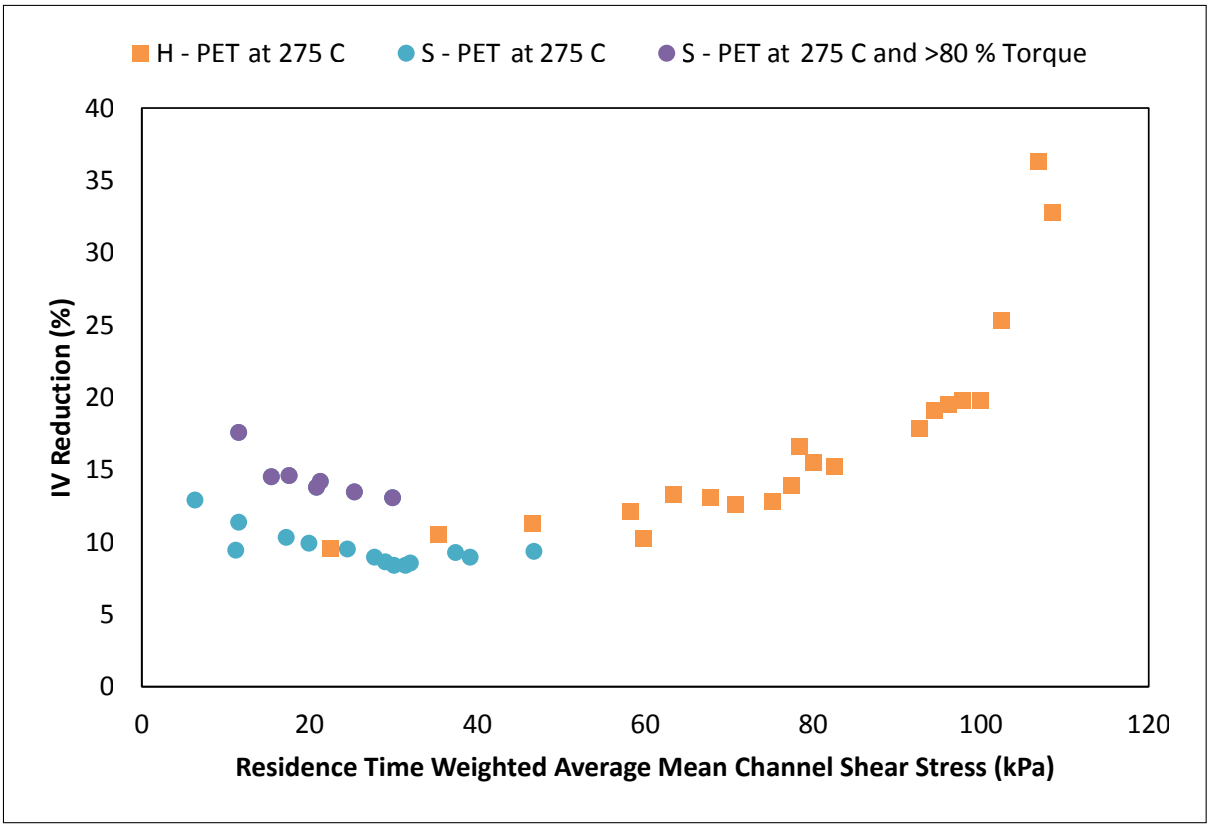

(a) Shear stress based on viscosity at Zone 3 (melting zone) barrel temperatures

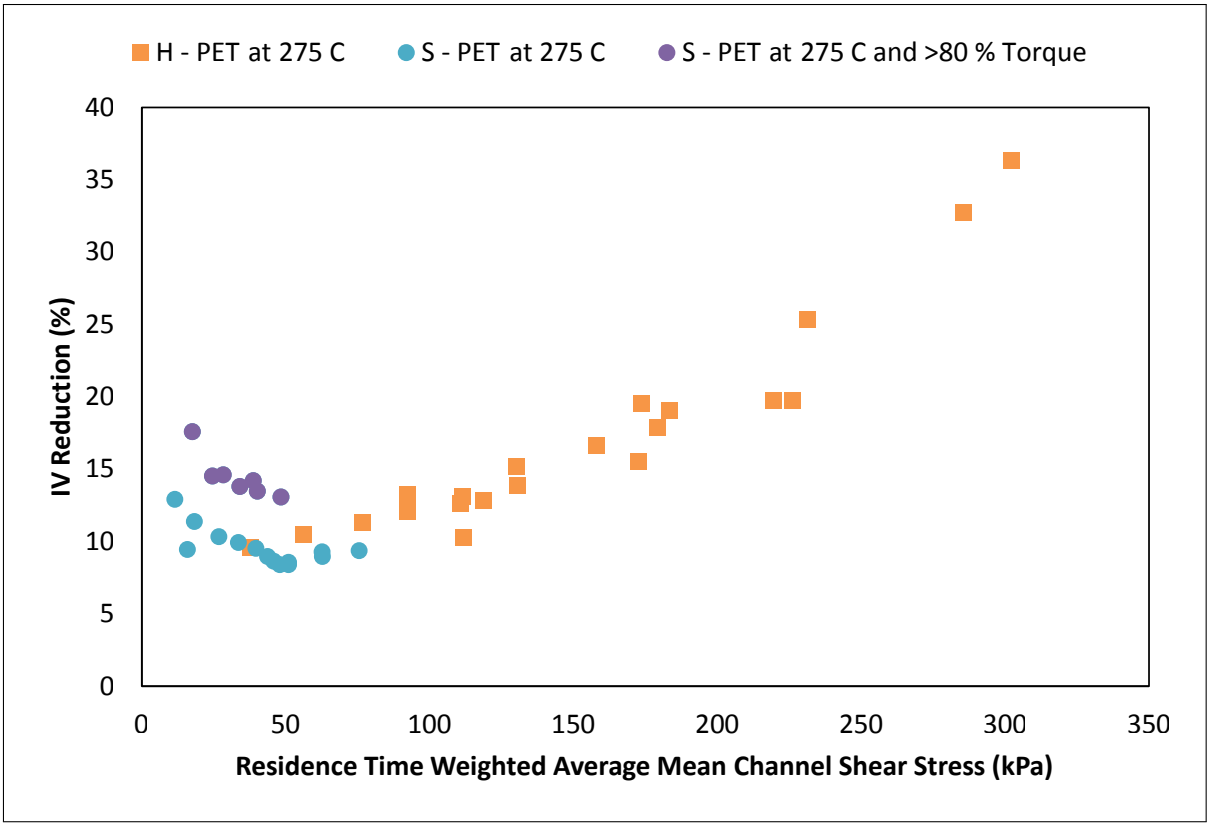

(b) Shear stress based on viscosity at 255 °C

Figure 7.19: *IV reduction as function of shear stress*

However, a 'step change' rise in IV loss between the stress of 100 and 120 kPa appears to have no theoretical explanation suggesting that this temperature is inappropriate for the calculation of melt viscosity. Barrel temperatures are useful indicators of polymer temperature when there is excessive viscous heating and the control struggles to maintain the temperature of the zone, however their applicability in other cases is doubtful.

The best correlation was obtained with the melting point temperature which was set at 255 °C for both H-PET and S-PET; see Figure 7.19b where a linear relationship between IV loss and shear stress can be observed for H-PET. There is also a clear inflection point at ca. 40 to 50 kPa, where indicating a 'critical' stress at which the IV loss process appears to become governed by mechanical chain scission as opposed to chemical reactions. It is likely that there is a critical value dependant on equipment and process set up, with parameters such as degassing efficiency greatly effecting the IV loss by chemical means.

7.5.2 Predicting IV loss through chemical reactions

Polyhand is a simulation package utilised within DTF to predict the IV loss as a result of the various chemical reactions based on the conditions which the polymer experiences. Example results based on a change in a single parameter is shown in Appendix K. The model was used to simulate the extrusion process; which was separated into sections corresponding to the different extruder zones; see Figure 7.20. The simulations were based on the actual process conditions for each experiment run considered.

The model relies on several key input parameters for its calculations. These include:

- *Chip details* - diffusion length scale, chip temperature, chip crystallinity;
- *Environment* - type of medium, pressure, temperature, humidity, polymer and air mass flow rates, residence time;
- *Polymer properties* - initial moisture content, IV, CEG, HEG, DEG, oxygen content, and ethylene glycol concentration;

- *Reactions* - selection of reactions to be simulated including chemical reactions listed in Figure 7.2 and diffusion reactions.

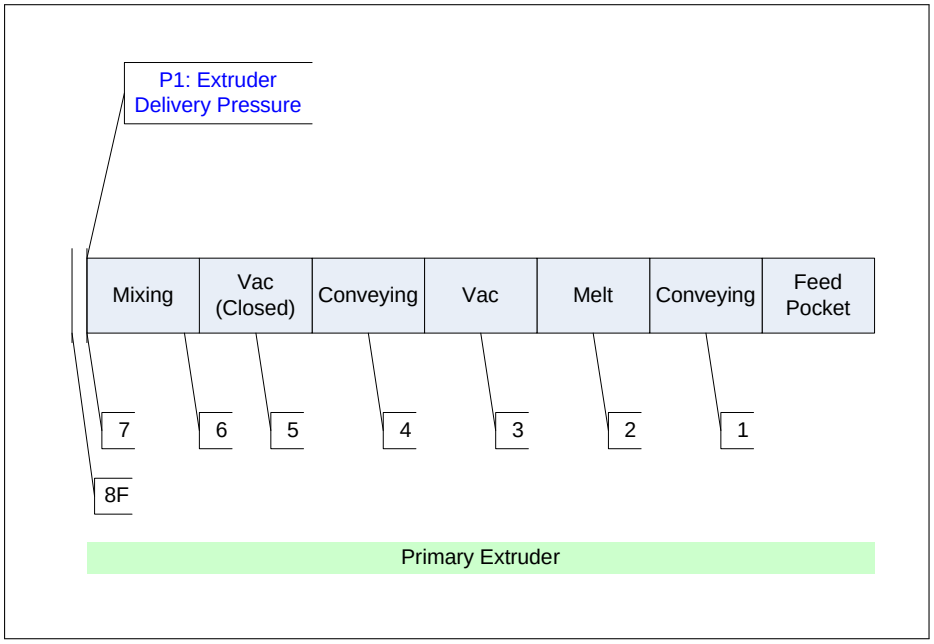

Figure 7.20: *Berstorff ZE40A extruder layout; numbers represent location of the thermocouples*

The following conditions were utilised in the different sections of the extruder.

- Zone 1: Feed
  - Initial moisture content of 2280 ppm based on moisture analysis of measurement of the polymer chip
  - Air flowrate calculated based on bulk density of chip and throughput of polymer with temperature set to the feedback temperature of the zone barrel heater
  - Chip temperature *assumed* to increase from 20 - 70 °C
  - Diffusion length scale 2.02 mm based on chip size of 35 mg, cylindrical shape and aspect ratio of 0.5
  - Diffusion reactions *turned on* as polymer is in contact with the air

- Zone 2: Conveying
  - Moisture content and polymer properties based on output of previous zone (profile across the chip)

  - Air flowrate assumed to be equal to ½ of that in zone 1, temperature set to the feedback temperature of the zone barrel heater
  - Chip temperature *assumed* to increase from 70 - 150 °C
  - Diffusion length scale same as in Zone 1
  - Diffusion reactions *turned on* as polymer is in contact with the air
- Zone 3.1: Kneading block section of melt zone
  - Moisture content and polymer properties based on output of previous zone (average values across chip due to change in diffusion length scale)
  - Air flowrate assumed to be equal to ⅓ of that in zone 1, temperature set to the feedback temperature of the zone barrel heater
  - Chip temperature *assumed* to increase from 150 - 255 °C
  - Melt equivalent diffusion length scale was calculated (see below)
  - Diffusion reactions *turned on* as polymer is in contact with the air
- Zone 3.2: Reverse conveying section of melt zone
  - Moisture content and polymer properties based on output of previous zone (profile across the chip)
  - Environment temperature set to the feedback temperature of the zone barrel heater
  - Chip temperature *assumed* to increase from 255 - feedback barrel temperature in zone 3 °C
  - Melt equivalent diffusion length scale was calculated
  - Diffusion reactions *turned off* as this is a fully filled section of the screw
- Zone 4 to 6: Conveying
  - Moisture content and polymer properties based on output of previous zone (profile across the chip)
  - Under vacuum with environment set at temperature of the corresponding zone feedback barrel heater temperature
  - Chip temperature set at the feedback temperature of the corresponding barrel zone heater
  - Melt equivalent diffusion length scale was calculated

  - Diffusion reactions *turned on* as these zones are partially filled

- Zone 7: Mixing and metering
  - Moisture content and polymer properties based on output of previous zone (profile across the chip)
  - Environment set at temperature of the corresponding zone feedback barrel heater temperature
  - Chip temperature set at the feedback temperature of the corresponding barrel zone heater
  - Melt equivalent diffusion length scale was calculated
  - Diffusion reactions *turned off* as these zones are fully filled

  Note: In all zones the residence time was calculated based on the expanded in house extrusion model as discussed in Chapter 6

One of the difficulties with this model is determining the appropriate estimate for the diffusion length scale in the melt sections of the extruder as this has not been done previously within DuPont Teijin Films. This was estimated on the basis of the area of polymer exposed to the environment and assumed geometry of the polymer chip as described in the following subsection.

7.5.2.1 Estimating the diffusion length scale

An estimate of the area of polymer exposed to the environment was based on the nature of polymer flow assumed for the extrusion model discussed in Chapter 6. Figure 7.21 shows the polymer front and the area of thin film deposited on barrel surface (denoted with green colour) within the screw channel which are assumed to represent the total area available for mass transfer. This area depends on the degree of fill within the extruder, the length of degassing section and the screw speed as it is refreshed every screw revolution.

For the purpose of the derivation it has been assumed that no mass transfer occurs in the intermeshing region; thus the equivalent length of the unwound channel L_{eq} can be calculated based on the intermeshing angle of the two screws. The height of the polymer

front $H(x_f)$ and x_f which depend on the degree of fill in the degassing section of the extruder were obtained with the use of the extrusion model. Equations for determining these parameters can be found in Chapter 6. For the purpose of the derivation discussed here the axis have been defined with reference to the extruder barrel and not the screw channel as was done in the aforementioned chapter.

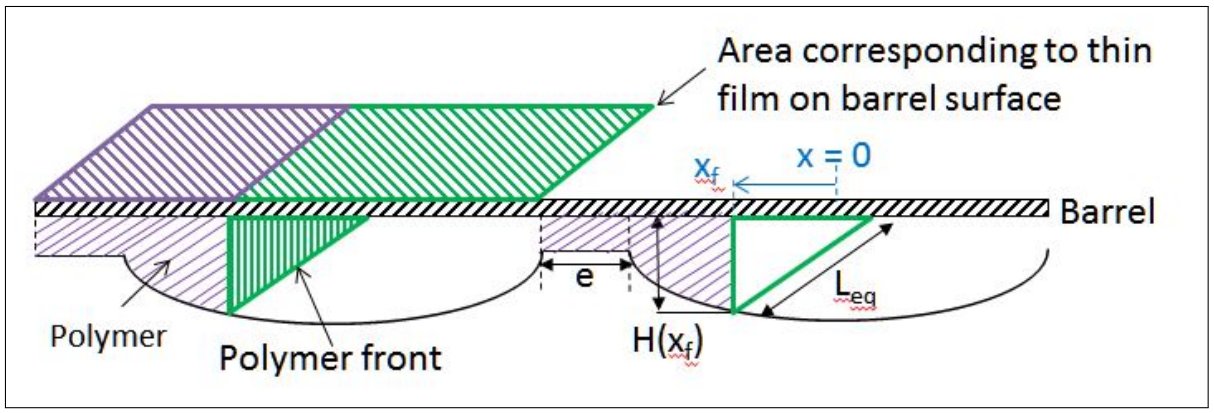

Figure 7.21: *Area available for mass transfer in degassing zone*

Initially, the area of polymer front, A_{front} was estimated for a stationary geometry as shown below; where z_w denotes the number of shafts, L_z the length of the degassing zone, t the element pitch, p the number of threads on the screw, α_i the intermeshing angle in radians, D_o the outside screw diameter, ϕ the helix angle and $H\left(x_f\right)$ height of the polymer front.

$$A_{front} = z_w \cdot \frac{L_z}{t} \cdot \left[p \cdot \frac{2\pi - \alpha_i}{2\pi} \cdot \pi \cdot \frac{D_o}{\cos\phi} \right] \cdot H\left(x_f\right) \tag{7.10}$$

The area of the polymer film deposited on the surface of the barrel, A_{film} for a stationary geometry can be calculated by subtracting the area occupied by the polymer in the channel and the area occupied by the flight from the total barrel surface area; see Equation 7.11 where e is the flight width and b the channel width.

$$A_{film} = z_w \cdot \left[\frac{2\pi - \alpha_i}{2\pi} \cdot \pi \cdot D_o \cdot L_z\right] - z_w \cdot \frac{L_z}{t} \cdot \left[p \cdot \frac{2\pi - \alpha_i}{2\pi} \cdot \pi \cdot \frac{D_o}{\cos\phi}\right] \cdot \left[e + \left(\frac{b}{2} + x_f\right)\right] \tag{7.11}$$

Thus in a stationary system the total area available for mass transfer is the sum of A_{front} and A_{film}. However, in a 'live' process this area is refreshed with every screw rotation. The number of times the area is refreshed, RN can be established from the screw speed and the residence time of the polymer in the degassing zone, τ_z.

$$RN = \frac{N}{60} \cdot \tau_z \tag{7.12}$$

The residence time itself can be estimated based on the length of the zone and the free cross sectional area available to flow; see below where D_i is the root diameter of the screw and $\dot{Q}$ is the volumetric flowrate in $\mathrm{m^3\,s^{-1}}$ as obtained from the mass flowrate and melt density.

$$\tau_z = \frac{z_w \cdot [{}^{2\pi - \alpha_i}/_{2\pi} \cdot {}^{\pi}/_{4} \cdot (D_o^2 - D_i^2)] \cdot L_z}{\dot{Q}} \tag{7.13}$$

Therefore, in the time frame that the material spends in the degassing zone, the mass transfer area, A_{MT} can be defined as follows:

$$A_{MT} = RN \cdot [A_{front} + A_{film}] \tag{7.14}$$

Now that a mass transfer area has been calculated, this can be converted into diffusion length scale based on the geometry of polymer chip in the solids state. The chip is assumed to be cylindrical with an aspect ration of 0.5 such that the radius, R_c is equal to the depth of the chip. For a single chip the surface area, A_c and volume V_c of the chip can be calculated.

$$A_c = 2 \cdot \pi R_c^2 + R_c \cdot 2\pi R_c \tag{7.15}$$

$$V_c = \pi R_c^2 \cdot R_c^2 \tag{7.16}$$

Based on this the area to volume ratio A_c/V_c can be shown to equal to $4/R_c$.

The degassing zone can be treated as if it contained solid chip. In such case the number of chips CN in the zone can be established from the volumetric flowrate, residence time and the volume of the individual chip.

$$CN = \frac{\dot{Q} \cdot \tau_z}{V_c} \tag{7.17}$$

From this the total surface area, $A_{TOT,C}$ of chip in the degassing zone for the time frame that the material spends in the degassing zone can be calculated.

$$A_{TOT,C} = CN \cdot A_c \tag{7.18}$$

The ratio of the calculated mass transfer area A_{MT} and the total chip surface area $A_{TOT,C}$ can be utilised to scale the surface area to volume ratio of the chip. From this one can establish the radius of the chip which has surface area equal to the mass transfer area, R_{ME} thus defining the new diffusion length scale.

$$R_{ME} = \frac{4}{A_c/V_c \cdot A_{MT}/A_{TOT,C}} \tag{7.19}$$

This calculation heavily depends on the calculation of the mass transfer area in the degassing zone. Albalak, 1996 utilised a similar method to that presented here with the area of polymer front and the thin film on the surface of the barrel being calculated. Wang, 2001 and Tomiyama et al., 2009 utilise a similar approach to determine the mass transfer area addressing some of the more crude assumptions in this approximation such as the

lack of thin film layer on the free screw surface. Albalak, 1996, p.364 provides charts from which the mass transfer surface area can be estimated that were developed on a 30 mm diameter machine. Since the diameter of the *Semi-Tech* machine is only 10 mm larger, a comparison was made at an output of 40 $kg\,h^{-1}$ and 79 rpm with the model proposed here yielding a mass transfer area of 0.275 m^2 and that proposed by Albalak, 1996 estimating the area at 0.259 m^2.

To obtain a good fit between the Polyhand model and the experimental results the calculated diffusion length scale had to reduced by a factor of 2. This can be explained by the area of the film deposited on the screw itself being unaccounted for. Although a factor of 2 was utilised to correct at all conditions, it is acknowledged that this factor is likely to change at least slightly with screw speed.

7.5.2.2 Comparison of modelling results with experimental data

The results of the IV loss predictions generated with Polyhand are shown in Figure 7.22. The chart demonstrates three distinct categories for the predicted IV losses: those with an error < 1 %, 1 to 2 % and those with predicted IV loss within 7 % of the experimental value. It should be noted that IV losses for the previously identified group of high torque/degree of fill experiments were predicted well. This was not the case for the low degree of fill experimental conditions where the IV loss process is unlikely to be controlled by the chemical reactions. Figure 7.23 illustrates the predicted IV losses as a function of degree of fill within the degassing zone. It is evident that the predicted IV losses show a linear dependence on the degree of fill in the zone, where as the experimental results show a plateau when the DOF drops below the critical value of around 20 %. It is likely that below this value the moisture is rapidly removed from the polymer leading to IV losses by means other than hydrolysis. To examine this further, the contribution of each individual reaction to the predicted IV loss was evaluated with the most prominent reactions being hydrolysis and thermo-oxidative reactions; see Figures 7.24 and 7.25.

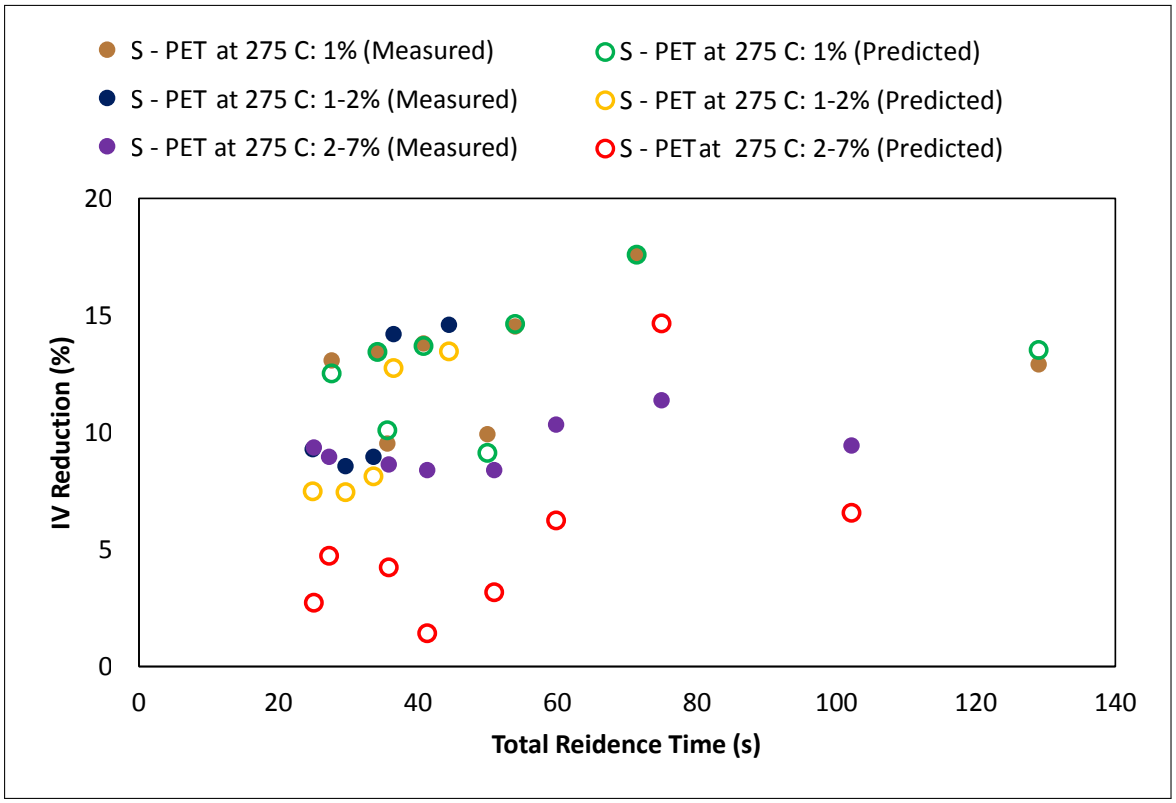

Figure 7.22: *Predicted IV loss vs total residence time*

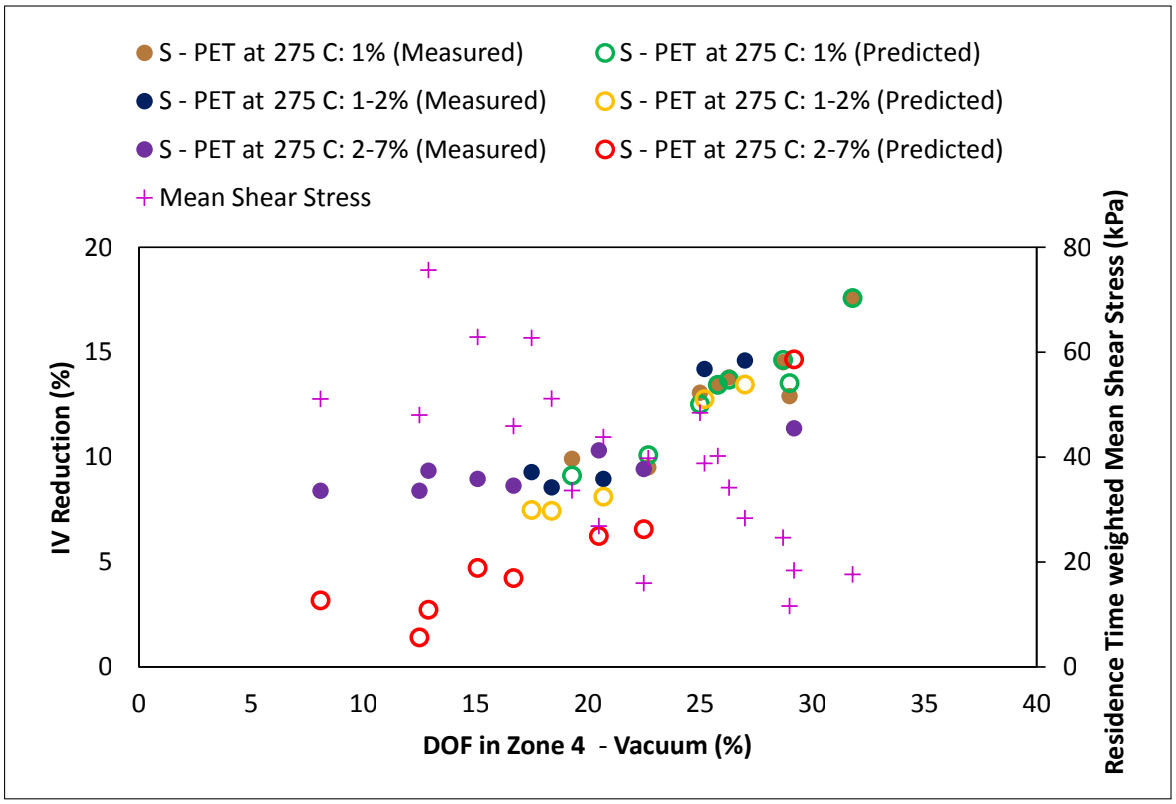

Figure 7.23: *Predicted IV loss vs degree of fill in degassing zone and mean shear stress*

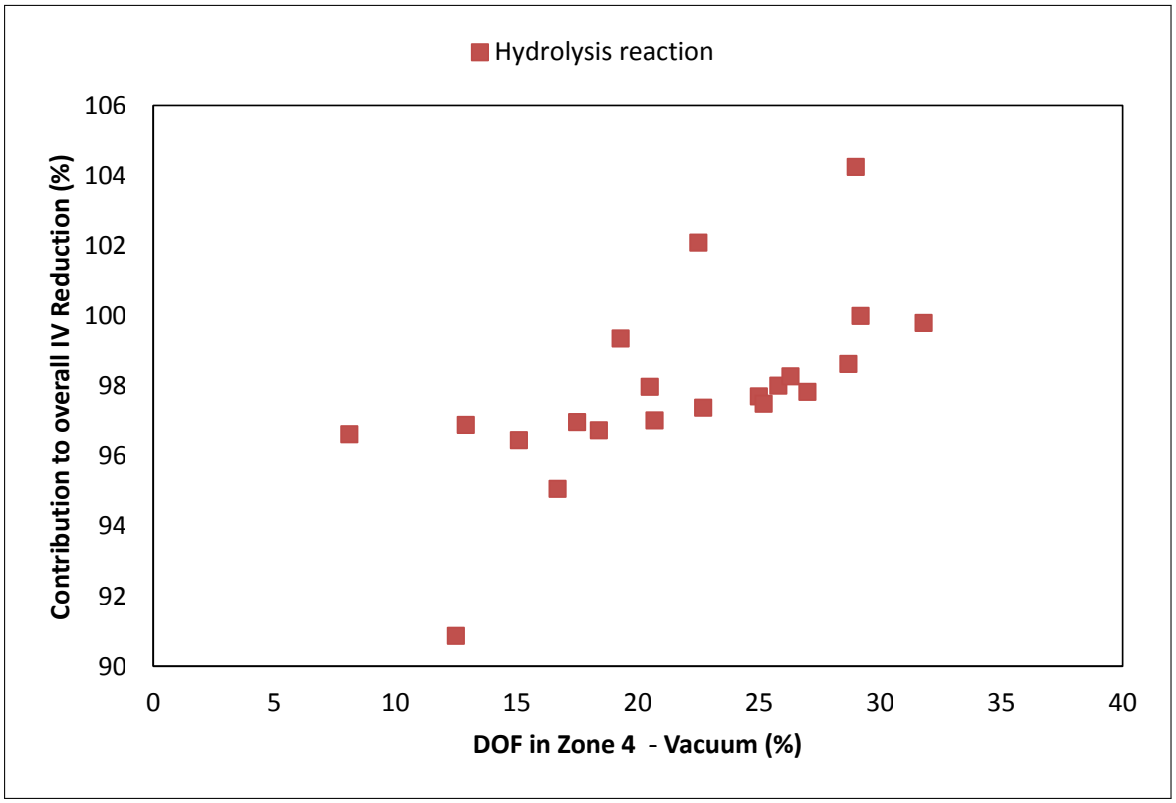

Figure 7.24: *Contribution of hydrolysis reaction to IV loss*

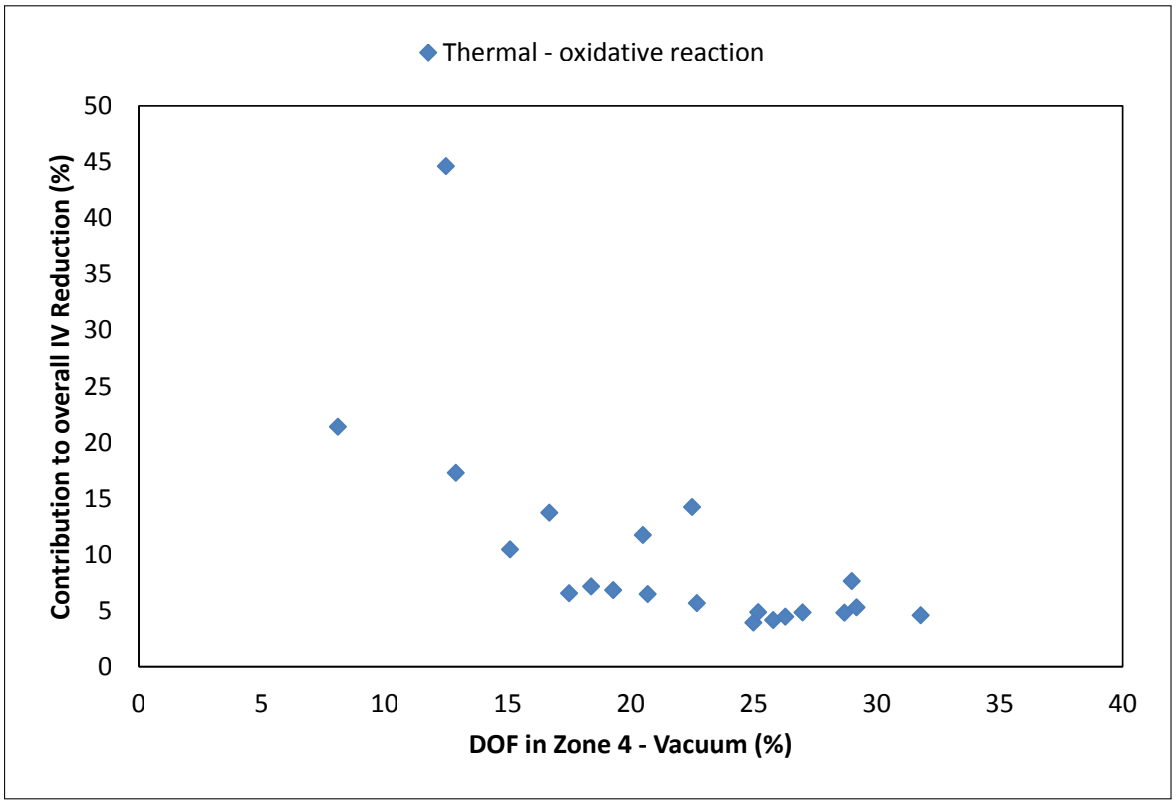

Figure 7.25: *Contribution of thermal oxidative reaction to IV loss*

It should be noted that in the case of hydrolysis reaction at some conditions a contribution of > 100 % to the overall IV loss has been reported. This is feasible as some of this IV loss is offset by the IV gain generated through thermal esterification and forward polymerisation.

Although not shown here, the IV gain provided by the thermal esterification reaction typically ranged between 5 and 10 % with an increase of up to 20 % being seen at the lower degrees of fill within the zone. Similarly, the net IV gain from the forward and reverse polymerisation reactions was in the region of 2 % with a slight increase when DOF values within the zone reduced to below 20 %.

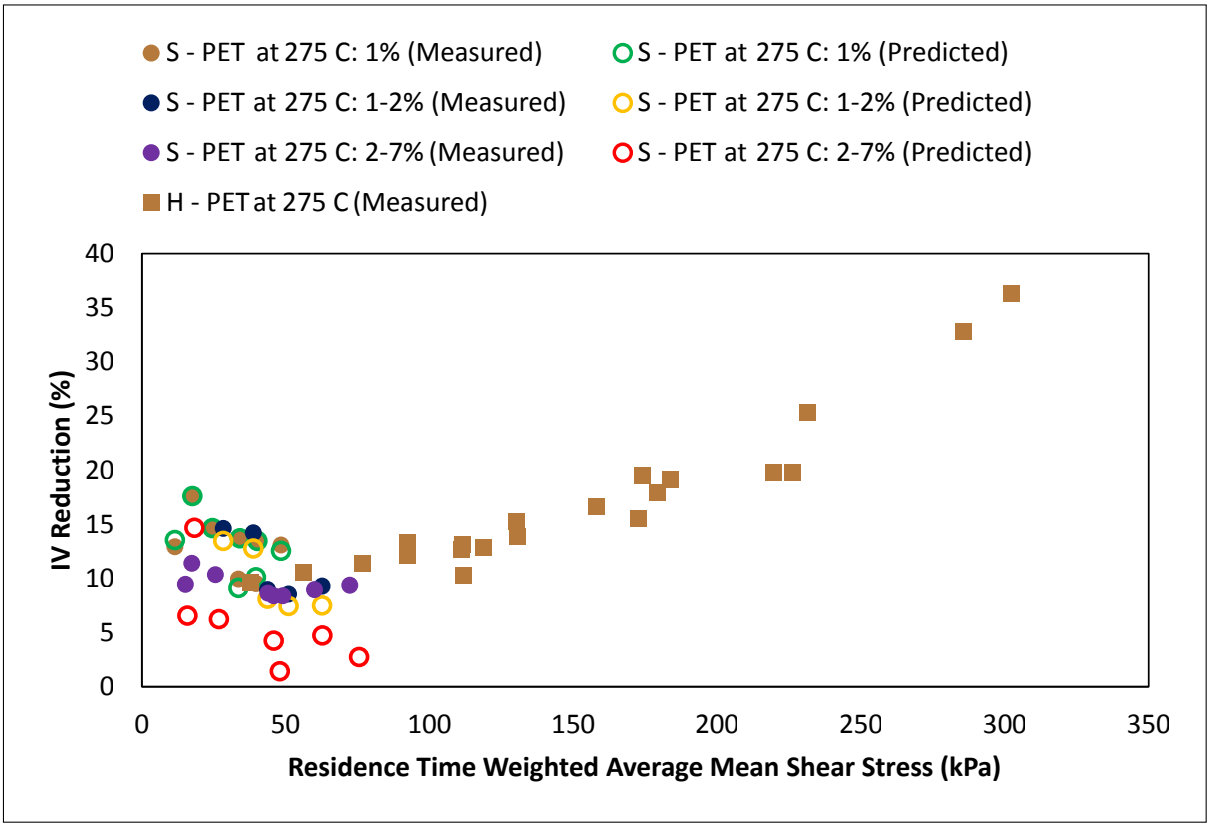

Figure 7.26: *Measured and predicted IV loss vs residence time weighted average mean shear stress*

Figure 7.26 shows the predicted IV loss and measured IV loss as a function of the shear stress to which the polymer is subjected. It is evident that there is a good agreement for the high torque S-PET samples, but poor fitting of the lower torque/DOF samples. It is also clear that as the shear stress increases there is a presence of greater error in the

IV prediction. This is a likely result of the mechanically induced chain scission having a greater influence on the IV loss. The discrepancies at the lower shear stresses are likely to be due to the limitations of the model to calculate the appropriate diffusion length scale.

7.6 Verifying IV measurements with rheology

Oscillatory rheology was carried out on a select number of samples to identify the changes induced by extrusion process on the polymer. The analysis was performed using a TA Instruments Discovery Hybrid Rheometer. The instrument was fitted with the environmental test chamber which allows temperatures ranging from -160 to 600 °C at rates of up to 60 °C min^{-1} A temperature sweep was performed from 260 to 350 °C at a strain of 5 % and an angular frequency of 10 $\mathrm{rad\,s}^{-1}$ utilising a 40 mm parallel plate geometry. The polymers were dried in the vacuum oven overnight at 90 °C prior to tests and the analysis was performed under a nitrogen atmosphere in order to prevent the viscosity loss associated with the molecular weight loss due to hydrolysis reaction. From the rheology data, it is possible to utilise the O'Dell model to calculate the IV of the polymer and hence determine the IV loss (Champion, 2015). This allows comparison of the solution method for obtaining IVs with the rheology method. Figure 7.27 shows a good agreement between the two methods with the detailed being shown in Table 7.2. The IV drops obtained via rheology are on average 1.67 % larger than those calculated from solution IVs.

Figures 7.28a and 7.28b demonstrate the complex viscosity of the samples detailed in Table 7.2. For S-PET samples T3S13 and T2S8 show considerable reduction in melt viscosity compared to T2S4 and T2S17 which were extruded at the same residence time weighted average mean shear stress but at higher torque and degree of fill. This highlights the significance of efficient degassing of moisture as the impact of hydrolysis is very high. This is particularly evident between samples T2S4 and T3S13 which were extruded at almost identical process conditions yet the melt viscosity at 260 °C is almost 40 Pa s lower. H-PET samples show considerable reduction in melt viscosity. Importantly, the

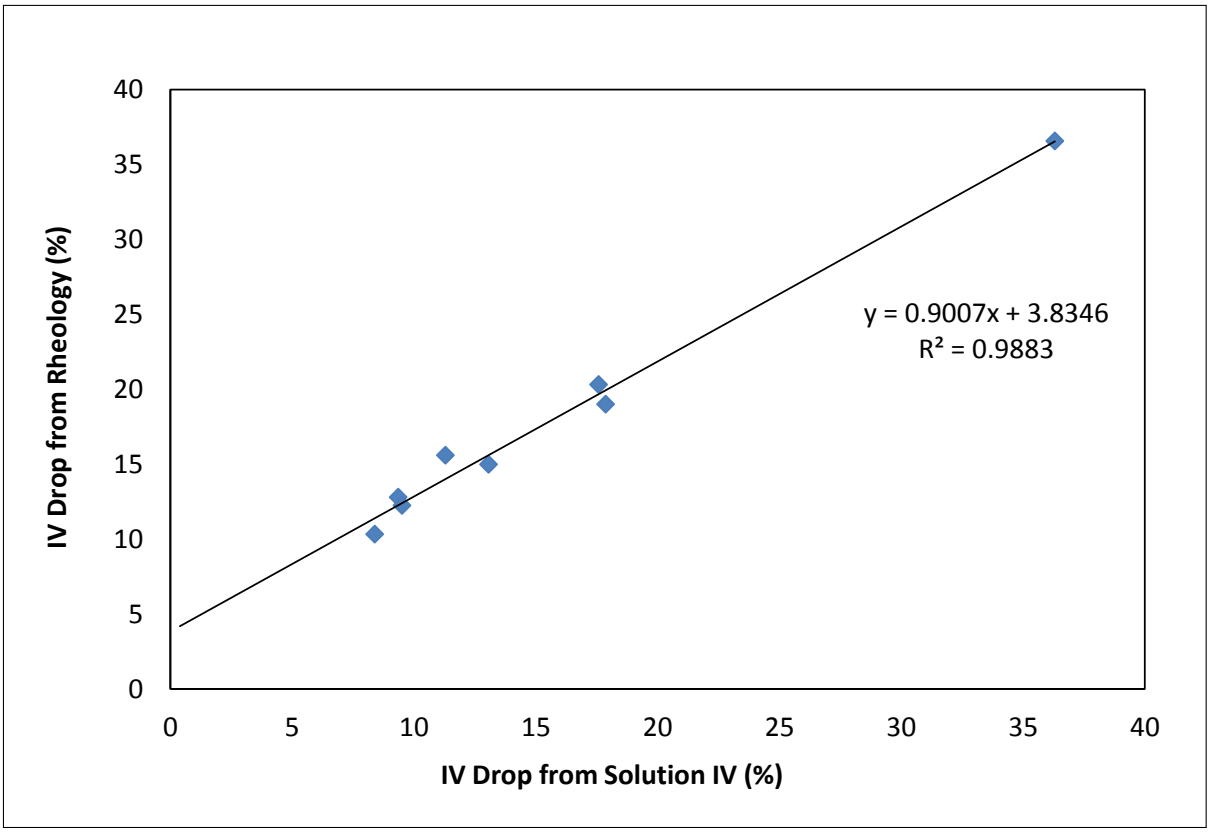

Figure 7.27: *Comparison of IV Drops obtained from solution IVs and rheology analysis*

sample extruded at high shear stress showing melt viscosity akin to the S-PET which has been processed completely negating the advantages of utilising higher molecular weight base polymer.

Table 7.2: *Comparison of IV loss obtained via solution method and via rheological analysis*

Sample	Polymer	$\dot{m}$	N	Torque	SME	DOF	Shear Stress	IV Drop - Solution	η at 260 °C	IV Drop - Rheology
-	-	$kg\,h^{-1}$	rpm	%	$kW\,h\,kg^{-1}$	%	kPa	%	Pa s	%
Virgin	S-PET	-	-	-	-	-	-	-	442	-
T2S4	S-PET	60.9	94	74	0.072	77.1	18	11.29	152	15.59
T2S17	S-PET	39.4	218	34.6	0.121	33.5	48	8.39	206	10.32
T2S13	S-PET	101.1	354	51.7	0.115	43.1	76	9.35	179	12.79
T3S13	S-PET	60.2	85	80.5	0.072	83.4	18	17.58	114	20.32
T2S8	S-PET	139.7	252	81.8	0.094	65.9	48	13.07	158	14.98
Virgin	H-PET	-	-	-	-	-	-	-	1076	-
T1S1	H-PET	31.8	53.9	85	0.091	68.8	40	9.52	661	12.24
T1S16	H-PET	57.2	221	57	0.140	36.1	178	17.88	442	19.00
T1S12	H-PET	59.6	349.7	45.1	0.168	28.5	302	36.31	130	36.57

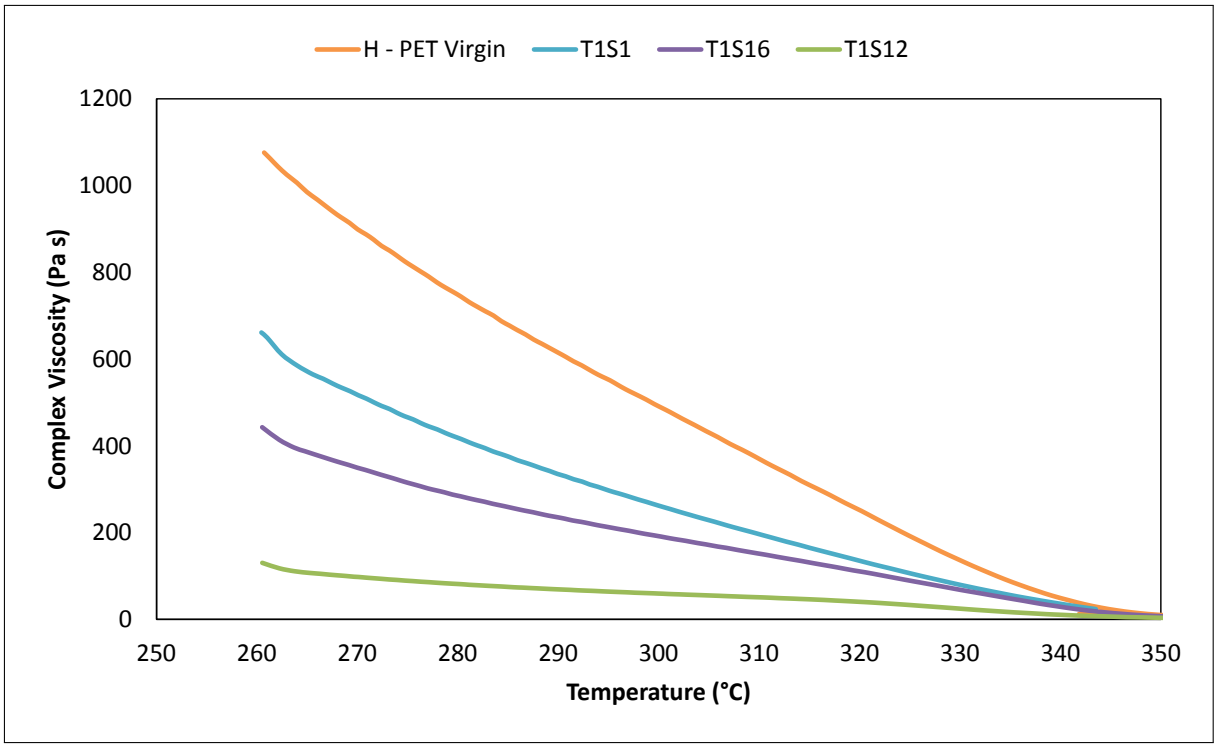

(a) Temperature sweep of H-PET samples

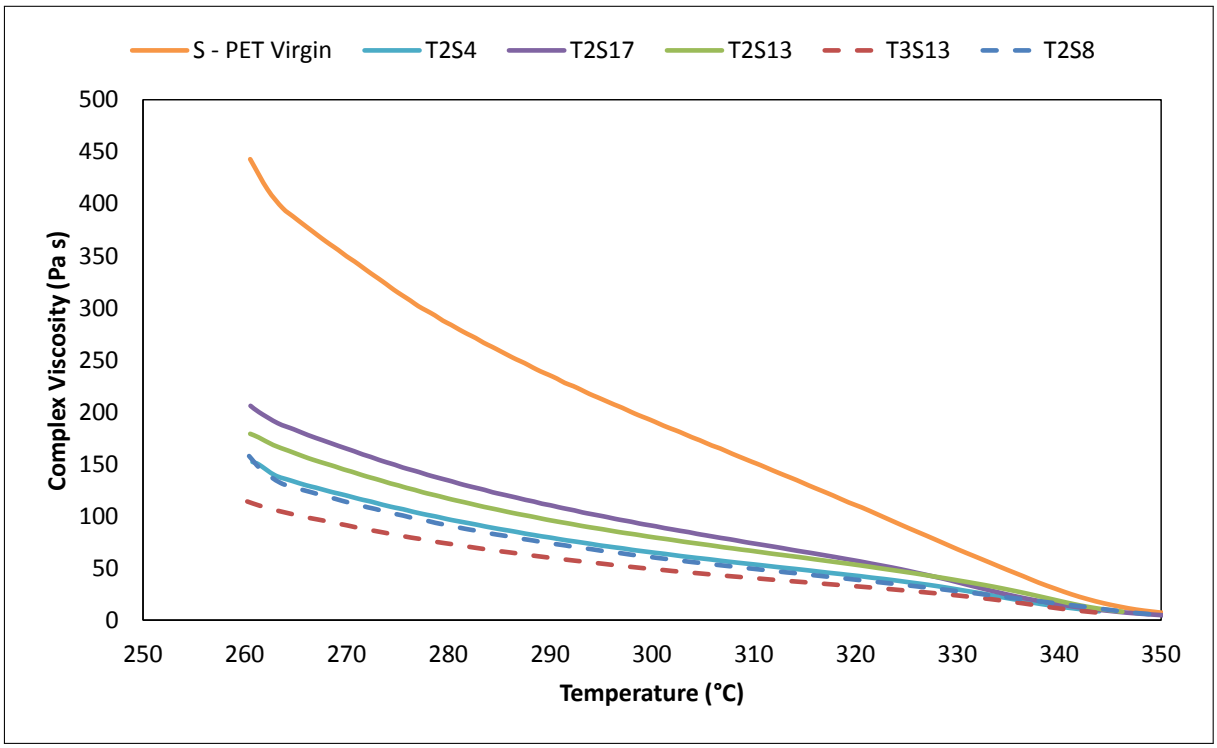

(b) Temperature sweep of S-PET samples

Figure 7.28: *Complex viscosity of processed samples as function of temperature*

7.7 Effect of pre-heating of polymer

Schöppner et al., 2014 states the same effect can be achieved with a vacuum degassing section as with pre-drying of the PET when it comes to IV loss, but there may be other advantages that can be gained by pre-drying the material. More importantly, perhaps these advantages can be realised by pre-heating the material to a given temperature as opposed to fully drying it. It is accepted that in such a process some drying will take place, however, certainly in sections of the operating window where the shear stress controls the IV loss the extra energy contained within the polymer could minimise the losses in molecular weight that the polymer experiences.

Figures 7.29a and 7.29b demonstrate the impact of pre-heating the polymer to 140 °C for H-PET and S-PET respectively. It is evident that IV loss can be minimised by circa 5 % at lower screw speeds. Although the effect is seen at the higher screw speeds circa 300 rpm the gains diminish. Similarly, in the case of S-PET the pre-heating the materials leads to IV loss being minimised by as much as 10 % in certain cases. It appears that up to circa 200 rpm the reduction in IV loss remains consistent. Higher screw speeds were not tested as these were beyond the typical operating conditions for this type of polymer.

It is envisaged that some of the reduction in IV loss is a result of reduced hydrolysis, however, a portion of this reduction is a very likely result of the reduction in work which is applied top the polymer by the extruder. By allowing the polymer to enter the extruder at a hotter temperature the material can heat up to a a hotter temperature before thin film of polymer is removed from the individual polymer chip. As can be seen from the rheology data in Figure 7.28 the changes in viscosity between 260 and 270 °C are drastic. The reduced viscosity allows the polymer chains to move more freely, but also reduces the shear stress applied to these chains.

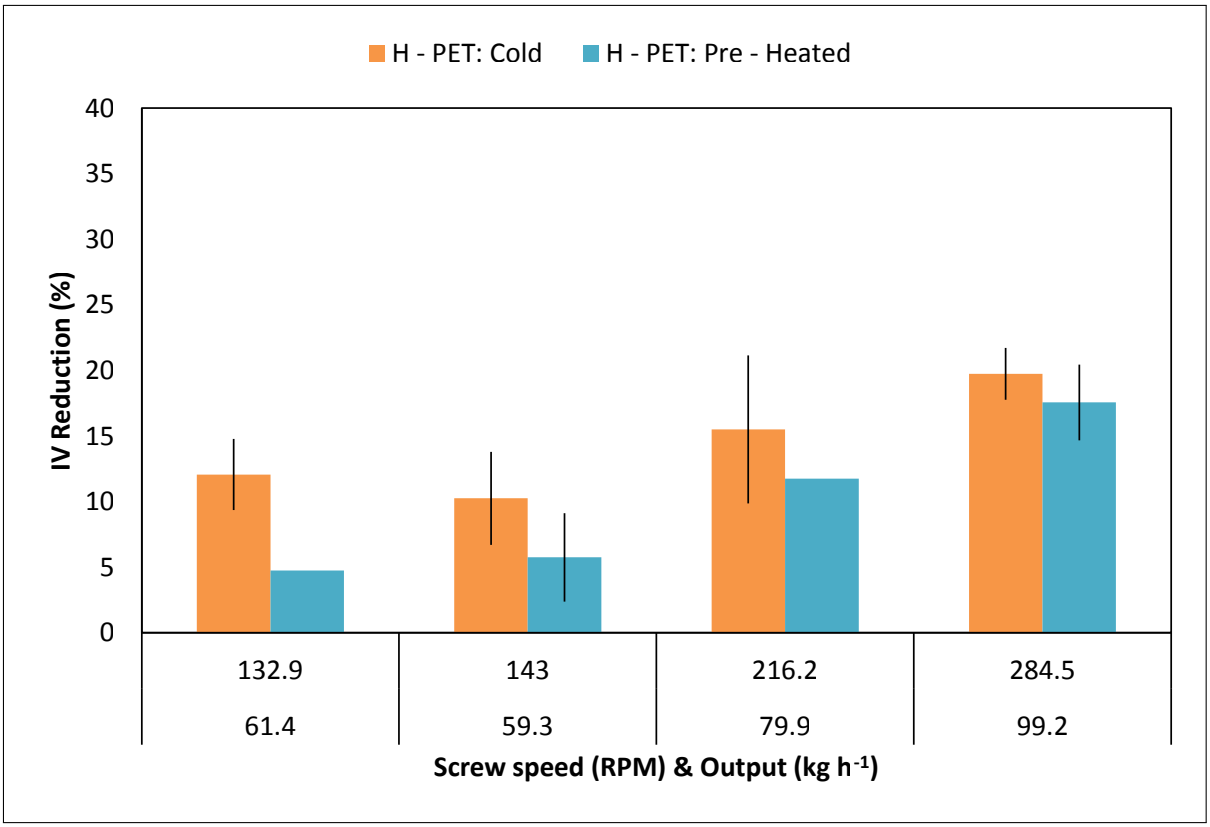

(a) H-PET

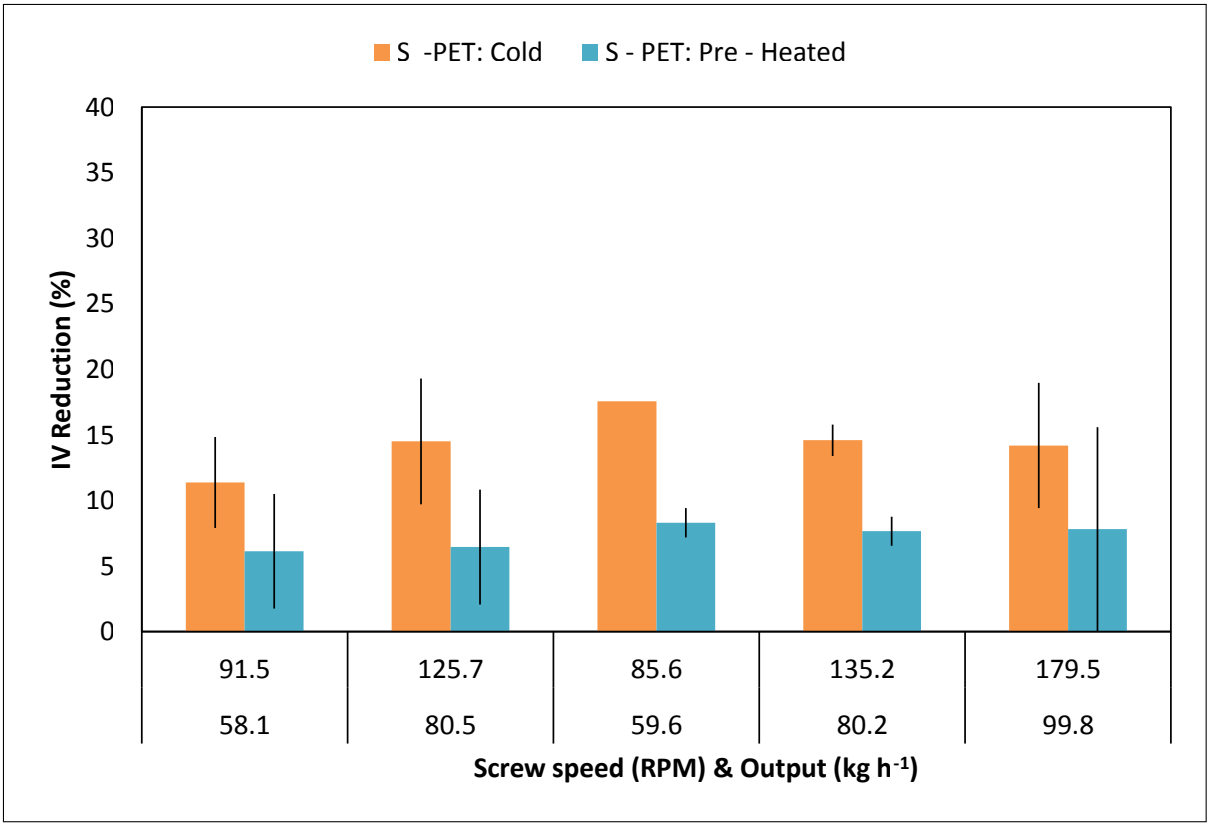

(b) S-PET

Figure 7.29: *Effect of pre-heating the material on IV loss*

7.8 Effect of barrel temperatures

The effect of running with hotter or colder barrel temperatures in the all zones prior to and including the melting zone were also examined. This was done to evaluate the hypothesis that higher temperatures in these zones would supply more energy to the polymer resulting in advantages similar to that seen with pre-heated material.

The results for H-PET and S-PET are demonstrated in Figures 7.30a and 7.30b respectively. Regarding the processing of H-PET, the barrel temperatures only appear to have a small influence at the low output and screw speed condition (high residence time). Here, there is sufficient time for the extra energy supplied by the barrel heaters to be conducted into the polymer. This leads to a reduction in IV loss with higher barrel temperatures for the same reasons as with pre-heated material. It is also important to note that the reduction in IV loss is not as significant as pre-heating the material. When the screw speed and the output is raised (residence time reduced) the barrel temperatures do not change the IV loss.

With S-PET at low output and screw speed a much smaller change in IV loss is observed between 265 and 275 °C as the viscosity change (387 to 312 Pas) is less significant compared to H-PET (984 to 813 Pas). Similarly, at higher outputs and screw speeds there is no statistical difference between temperatures of 265 and 275 °C. However, when the temperature was raised to 300 °C a significant reduction in IV loss can be seen (in 2 out of 3 samples) which is almost on par with preheating the material. It is important to point out that in this case the temperature of the vacuum degassing zone was also increased by 25 °C. It is most likely that this temperature change induced better degassing as opposed to reducing the mechanically induced chain scission. Previous results clearly demonstrate that in S-PET the IV loss depends on the rate of hydrolysis in most cases.

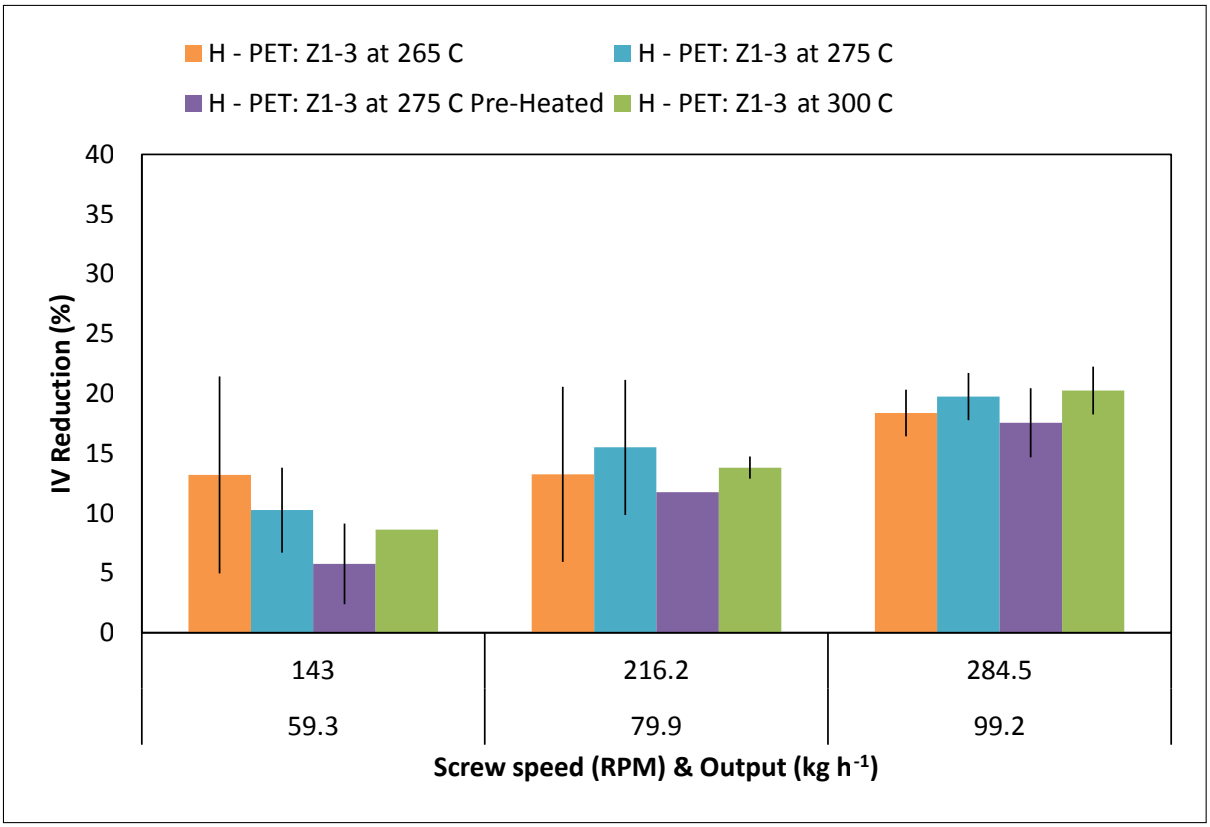

(a) H-PET

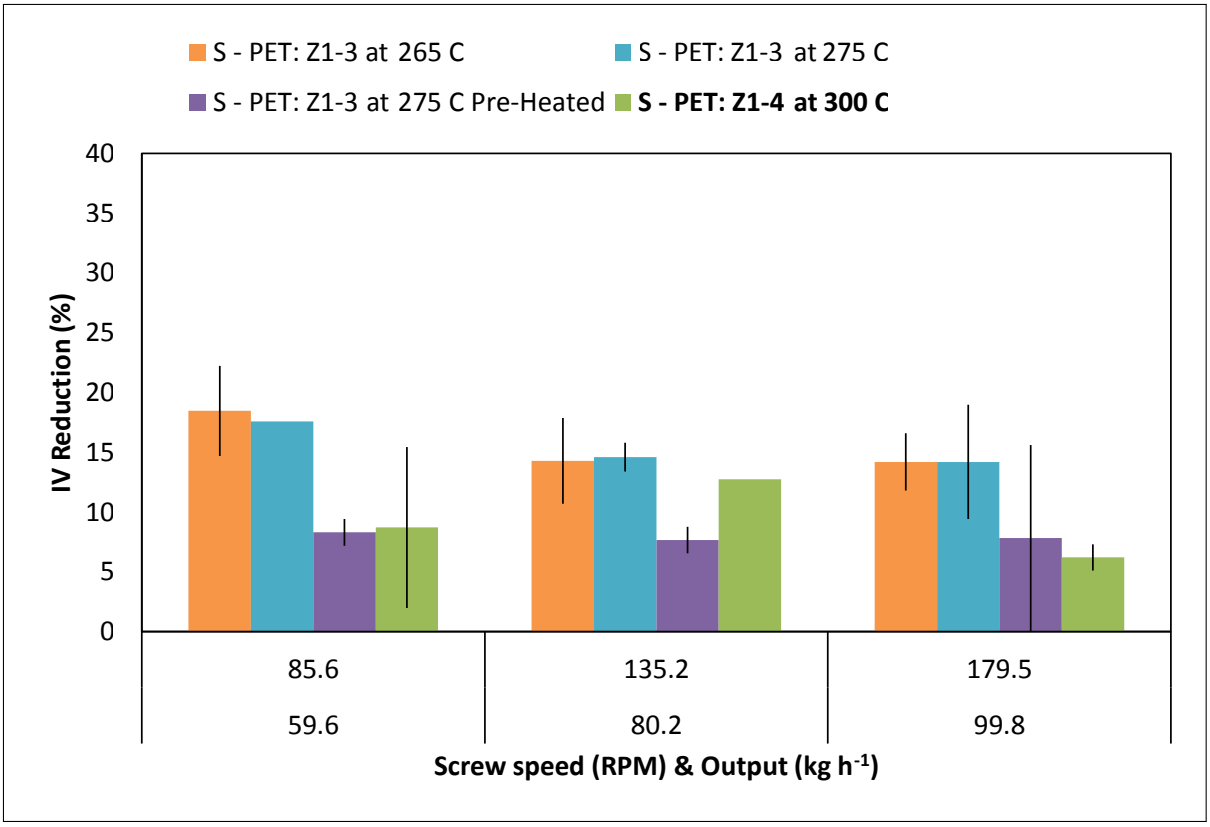

(b) S-PET

Figure 7.30: *Effect of barrel zone temperatures on IV loss*

7.9 The role of screw design in IV loss

One aspect which was not considered in this study was the impact of the screw configuration where elements such as wider kneading blocks are known to subject the materials to greater shear. It is envisaged that elements which are typically classed as dispersive mixing elements would lead to a greater reduction in the IV of the polymer. However, work undertaken by Schöppner et al., 2014 showed no significant differences between the high shear and the low shear screw configurations. This is an area where there is little published work and thus would warrant further investigations in the future.

7.10 Concluding remarks

In general the PET chemistry is well defined and there is a comprehensive understanding of the reactions leading to a reduction in the molecular weight of PET. However, there is little literature published on the molecular weight reduction in PET during extrusion processing. Importantly, studies on the molecular weight reduction (as measured by the intrinsic viscosity, IV loss) of PET such as Romão et al., 2009 and Schöppner et al., 2014 draw no comparisons between the IV losses measured post extrusion processing and those predicted from the understanding of the chemical reactions at the given process conditions.

The novelty of the work presented in this chapter lies in exactly such comparisons. The results presented herein examine the IV losses associated with the twin screw extrusion processing at various operating conditions (e.g. screw speed, machine output and torque settings) for both film grade and bottle grade PET. The measured IV losses were compared to those predicted by *Polyhand* for the corresponding processing conditions. (*Polyhand* is an *in-house* software tool utilised within DTF to model the chemical reactions occurring within PET at different conditions; details of which are discussed at the start of the chapter). The predicted IV losses matched well with the measured values when the polymer was extruded at the conditions where the degree of fill within the machine was

high and the hydrodynamic stresses generated were low. In other cases, the predicted results were significantly lower than the measured values indicating different mechanisms for the molecular weight reduction.

The dependence of the measured IV losses on the on the operating conditions e.g. screw speed and calculated parameters such as specific energy input, specific output, and residence time was examined in order to better understand the mechanisms of the molecular weight reduction. As the screw speed increases and the residence time decreases, one expects the IV loss to decrease due to the reduction in residence time. This trend was observed when processing the lower molecular weight film grade PET. However, the opposite trend of an increasing IV loss with increasing screw speed was observed when processing the higher molecular weight bottle grade PET. Unlike Schöppner et al., 2014 who observed a similar trend and attributed it to the increased melt temperature, it is proposed that the higher molecular weight PET is undergoing mechanically induced chain scission (as observed by Romão et al., 2009) as the result of much higher hydrodynamic stresses generated within the extruder compared to the lower molecular weight PET.

In examining the IV loss as a function of the newly proposed parameter the 'residence time weighted average shear stress, $\sigma_{av,RTD}$' (as defined in Chapter 6), two different regimes appear to exist. On the machine in question, a critical value for this parameter between 40 to 50 kPa s was observed. Beyond this the IV drop increases as the function of increasing shear stress (reducing residence time) indicating that the mechanically induced chain scission is the dominant mechanism for IV loss in PET. At values less than the critical value, the IV drop reduces as function of increasing shear stress (reducing residence time) indicating a chemically controlled mechanism for the molecular weight reduction.

As per hypothesis, the lowest screw speed, lowest output, and highest torque scenario, proved to deliver the lowest IV loss with respect to mechanically induced chain scission. In considering the chemically induced chain scission the proposed optimum conditions were high screw speed, high output, and hight torque. However, it was found that a lower

output, high screw speed, and lower torque setting was optimum as these delivered the benefit of short residence time, but also had a low degree of fill in the degassing section leading to better removal of moisture, reduced hydrolysis reaction (dominant process) and hence smaller IV losses. Overall, a compromise in the conditions has to be reached in order to minimise the IV losses though chemically and mechanically induced chain scission.

The impact of pre-heating the polymer and changing the temperature of all the extruder zones prior to and including the melt section on IV loss was also examined. With pre-heated material the less work has to be applied to the polymer by the extruder leading to smaller IV losses. This was true for both high and standard molecular weight staring polymer. As well as achieving better final molecular weights within the polymer other processing advantages were identified but these are discussed elsewhere. The impact of barrel zone heater temperatures proven to be not statistically significant apart from two cases. The first is with high molecular weight base polymer at low outputs and low screw speed when there is time to the heat to be conducted into the polymer chip which lead to a reduction in IV loss. The second was for standard molecular weight polymer when the barrel heater of the degassing section was also increased in temperature. In this case the efficiency of the degassing section was improved, leading lower IV losses on par with that achieved with preheated polymers. This is likely to only work when the dominant mechanism for IV loss is through chemical chain scission.

The IV losses determined through solution rheology methods were compared with IV losses calculated by oscillatory rheology performed on directly on the polymer samples. The two methods were in very good agreement with the rheology on the polymer yielding slightly larger IV drops on average. Finally, the correlations derived from the experimental results presented here will be incorporated into the 'in-house' *Polyhand* model which will enable the company to better predict the properties of the manufactured film.

8 | Importance of material properties in mixing

The properties of the compounded material depend on the particle size of the additive and its distribution through the polymer as well as the strength of adhesion to the polymer matrix (Giles et al., 2005). Therefore it is vital to achieve good dispersion and distribution of the additive through the matrix as well as to encourage strong interaction between the two entities. The dispersibility of the additive in the polymer matrix is a function of agglomerate strength, the inherent properties of the matrix, and the dispersing stress applied during processing (Kasaliwal, 2011). As a result, the material properties play a vital role in determining the mixing characteristics within the extrusion process as well as being a key consideration for determining the process limitations of direct addition extrusion; see Chapter 5.

With respect to the polymer, Kasaliwal et al., 2011; Villmow et al., 2008 have examined the role of polymer matrix viscosity on the extend of additive mixing observed. Although these provide an indication of the effect, there are no quantitative results that can be transferred to the systems in question as the experiments in literature have been performed on mainly carbon nanotubes being dispersed in non PET matrix. Gogos et al., 1996 provides a good review on the theory for quantifying the strength of the agglomerate based on the primary particle size, strength of interparticle interactions and the agglomerate porosity. However, the impact of particle shape is far more difficult to understand as no quantitative data exists for the role of aspect ratio. Some research is also available on modifying the interactions between the additive and the PET matrix by the introduction of dispersive aids (Fortunato et al., 2014) and additive surface modification (Kimura et al., 2000). Apart from Kimura et al., 2000 who evaluated the surface energy change of the additive, the research within the literature tends to be qualitative rather then quantitative

with respect to the strength of the additive - polymer interactions. These works as well as the research of others are discussed in further detail in Appendix F.

The results presented here provide quantitative data on the role of polymer viscosity and how this effects the various dispersion mechanisms. In addition, an attempt was made to determine the role of particle size, aspect ratio and porosity in determining the extend of dispersion observed within the polymer composites by directly relating the size of particles within the composite to their inherent properties. Most importantly, a method is proposed for quantifying the strength of interaction between the polymer matrix and the additive based on the surface energies of the individual entities. Dispersive aids and copolymer was utilised to modify these interactions.

8.1 Results

Composites containing various additives based on a PET substrate were produced on the *Berstorff ZE40A* and the *Dr Collin ZK25* machines. The properties of the materials utilised are given in Chapter 3 with the details of the equipment specification, limitations and set up discussed in Chapter 5.

8.1.1 Polymer viscosity

Polymer viscosity plays a critical role in determining the magnitude of the hydrodynamic stresses delivered to the agglomerates which in turn determine the effectiveness of the rupture, erosion and collision mechanisms for dispersion. The viscosity of the material was altered via changes in the molecular weight of the PET substrate; which also meant changes in the length of the polymer chains. An attempt to control the viscosity independently in various zones of the extruder by changing the barrel temperatures was made, however the results were inconclusive; see Section 9.1.3.1. The effect of polymer chain length (as its own entity) was examined by Kasaliwal, 2011 and discussed in Section F.1.1.

A typical film grade PET (S-PET) and bottle grade PET (H-PET) were utilised as two substrates to manufacture FR-1 composites. S-PET and H-PET has IV of 0.62 and 0.8 $\mathrm{g\,dL^{-1}}$ respectively with the corresponding number average molecular weight of ca. 19,850 and 27,300 g $\mathrm{gmol^{-1}}$. Table 8.1 shows the viscosity of S-PET measured at 10 $\mathrm{rad\,s^{-1}}$ and 5 % strain and that of H-PET measured at 100 $\mathrm{rad\,s^{-1}}$ and 5 % strain at three temperatures which are typical for a PET extrusion process.

Table 8.1: *Viscosity of S-PET and H-PET*

Temperature (°C)	265	275	285
Viscosity of H-PET (Pa s)	725	617	518
Viscosity of S-PET (Pa s)	226	181	144

Figure 8.1 shows the level of dispersion achieved in S-PET and H-PET composites manufactured on the *Berstorff ZE40A* machine.

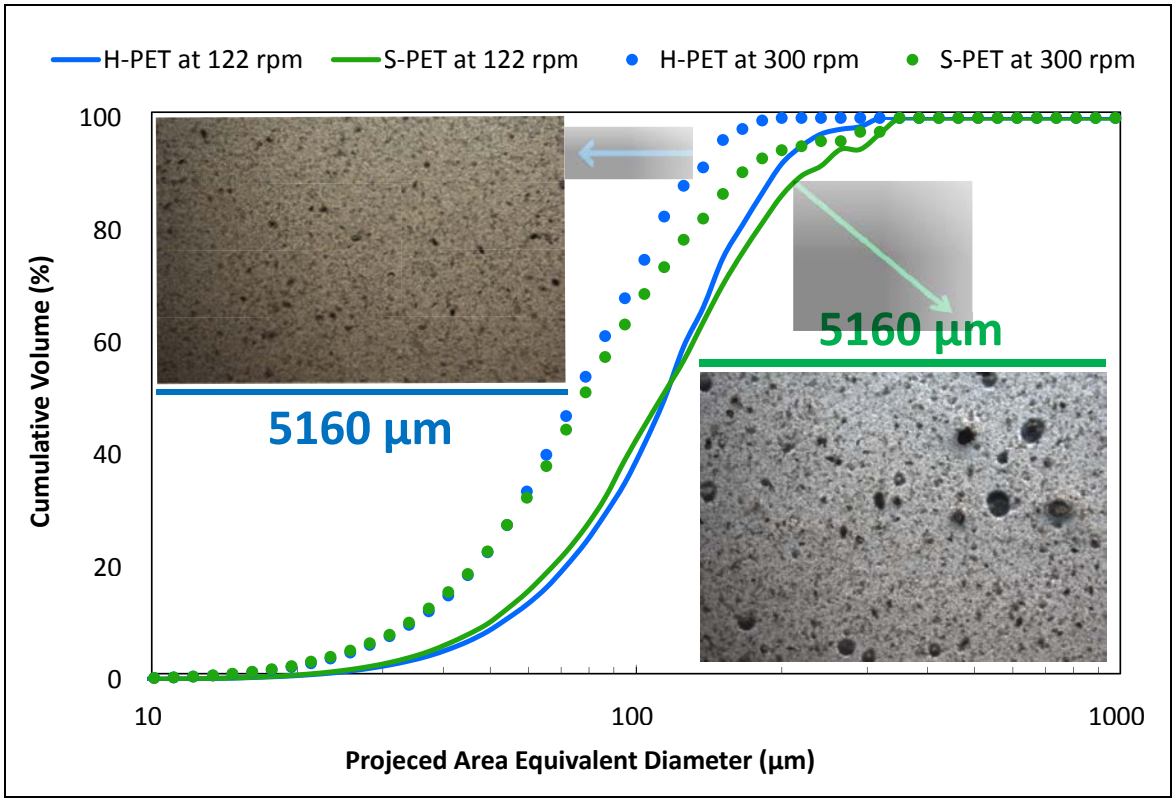

Figure 8.1: *Additive dispersion in FR-1 composites based on S-PET and H-PET manufactured at 60* $\mathrm{kg\,h^{-1}}$ *on the Berstorff ZE40A machine via the split-feed route*

At the higher screw speed there is no significant difference in the dispersion via erosion

mechanisms with the lower end of the distribution remaining almost identical. This indicates that during exposure to high shear rates and short residence time associated with these the changes in viscosity between the two polymer grades are not significant enough to influence the wetting behaviour or the extent of polymer infiltration onto the pores of the agglomerate structure. One could argue that S-PET offers slightly improved dispersion through erosion at 122 rpm (lower shear, higher residence time condition) as shown by slight shift to the left in the lower end of the distribution relative to H-PET. This is due to the lower viscosity polymer being able to infiltrate the pores of the agglomerate structure with greater ease. However, this small change is overshadowed by the impact achieved through the rise in screw speed where the lower end of the distributions drastically shifts to the left.

Unlike with erosion, a clear difference in the effectiveness of the rupture mechanism can be seen in both the low and the high screw speed cases. Here, the use of H-PET (a higher viscosity matrix) leads to increased hydrodynamic stresses being transferred to the agglomerate. These mean that the agglomerates can be broken down to a smaller size, as illustrated by the D_{90} of the H-PET distributions being smaller than that of S-PET; see Figure 8.1.

The notion of increased shear stresses leading to improved rupture can be verified by considering Figure 8.2. The figure shows that as the screws speed increases, which causes an increase in peak shear rate and thus shear stress, the D_{90} of the distribution reduces. This is true for the composites produced on both the S-PET and H-PET substrate.

Similar behaviour was observed on FR-1 composites manufactured on the *Dr Collin ZK25* machine via the masterbatch route; see Figure 8.3.

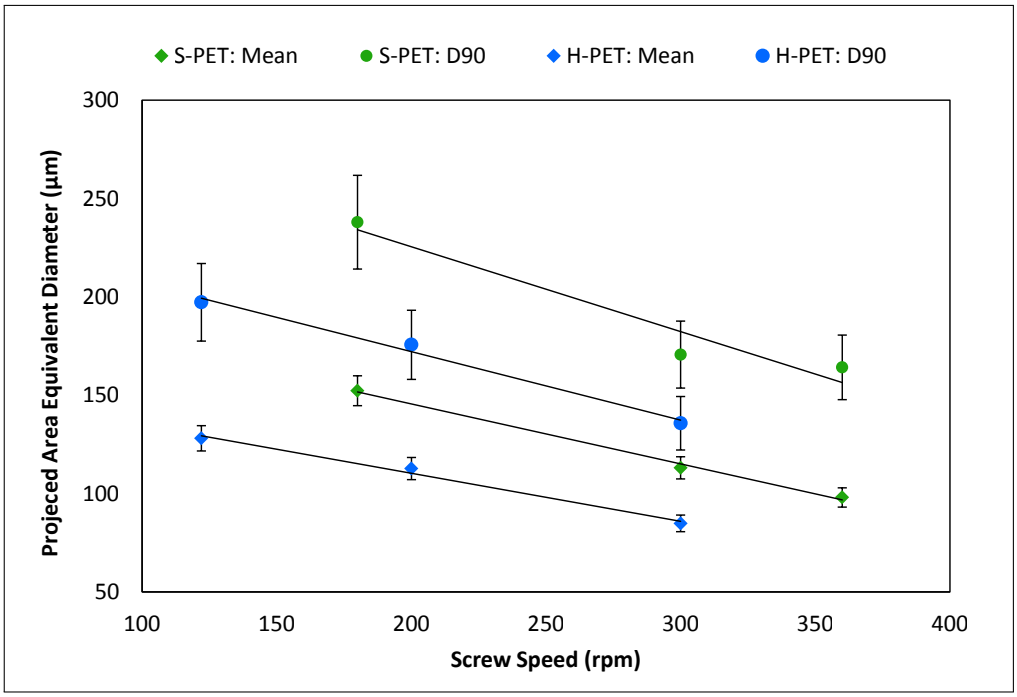

Figure 8.2: *Changes in FR-1 composite dispersion based on S-PET and H-PET substrate as function of screw speeds manufactured at 60* $\mathrm{kg\,h^{-1}}$ *on the Berstorff SE40A machine via split-feed method*

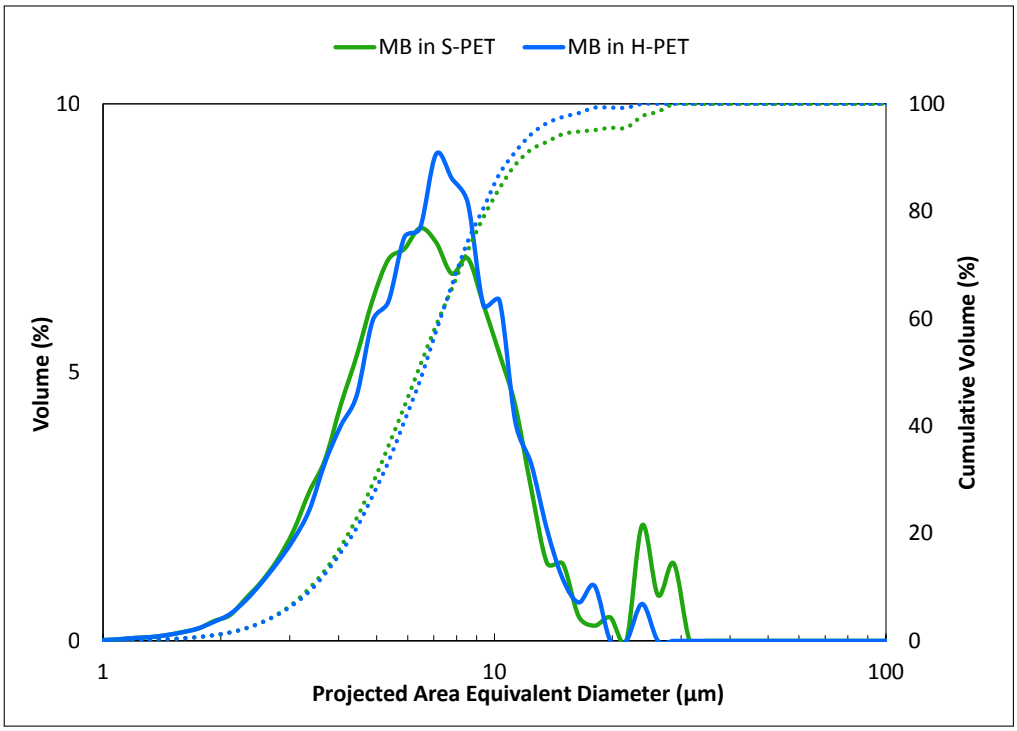

Figure 8.3: *Additive dispersion in FR-1 composites based on S-PET and H-PET substrate manufactured at 6* $\mathrm{kg\,h^{-1}}$ *and 290 rpm on the Dr Collin ZK25 machine via the masterbatch route*

8.1.2 Additive properties

As well as the properties of the polymer, the inherent properties of the additive can influence the level of mixing achieved within the composites. The results from the experiments to evaluate these are discussed within this section.

8.1.2.1 Particle size

Section F.2.1 covered how the changes in particle size (and specific surface area) lead to the change in the forces that dominate the inter-particle interactions. The effect of the differences in particle size was evaluated by considering the mixing achieved in H-PET composites produced using 3 different grades of FR additive. The additives in question have the same chemical composition and differ only by their particle size distribution (PSD) and changes in other parameters associated with this change, such as bulk density. The key markers of the PSD are shown in Table 8.2, from which it can be seen that the proposed PSDs differ significantly between the grades.

Table 8.2: *Percentiles of particle size distribution for FR-1, 2, and 3 additive; as provided by the supplier*

Additive Grade	D_{10} (µm)	D_{50} (µm)	D_{90} (µm)
FR-1	0.8	2.5	9.0
FR-2	2.1	26.7	47.4
FR-3	1.4	41.3	76.8

Figure 8.4 shows stark differences between the dispersion of the additive achieved and the PSDs of the different grades which were provided by the supplier. These initial results suggest poor dispersion of the FR-1 grade of additive and attrition of the FR-2 and FR-3 grades.

Further investigation into the particle size of the additive was carried out at DTF to better understand the observations. The details of the method for the PSD measurement can be found in Section 4.1. Figure 8.5 shows the PSDs obtained at DTF.

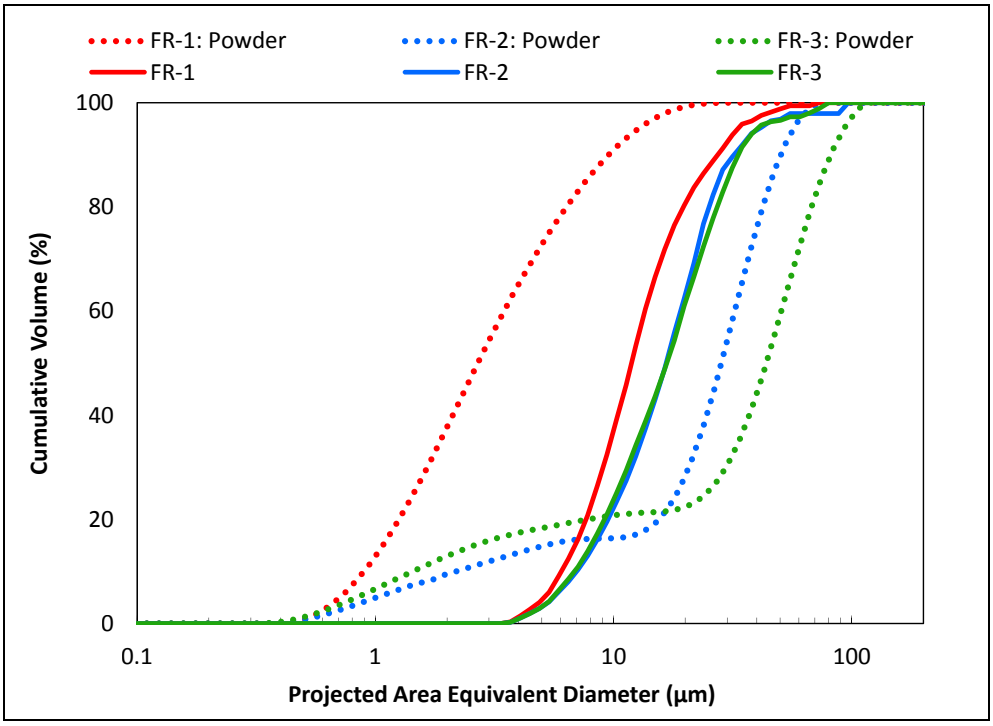

Figure 8.4: *Dispersion in FR-1, FR-2 and FR-3 composites manufactured at 6* $\mathrm{kg\,h^{-1}}$ *and 290 rpm on the Dr Collin ZK25 machine via the premix route*

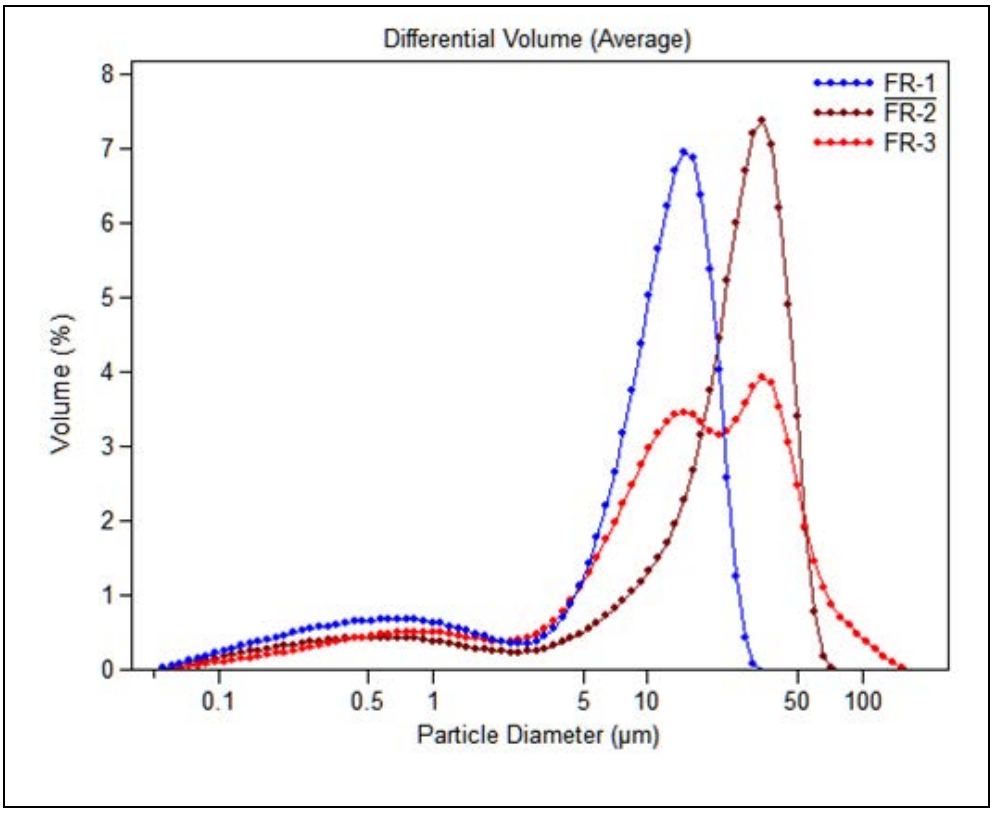

Figure 8.5: *PSD of FR-1, FR-2 and FR-3 additive; curves shown are an average of 5 runs measured at DTF using a Coulter LS13 320*

Unlike the PSDs provided by the supplier which were undertaken in acetone with the use of dispersive aids, the measurements for the PSDs obtained at DTF were conducted in demineralised water with no dispersive aids after exposing the samples to high shear mixing for 20 min. These are thought to better reflect the conditions within the polymer as the composites were manufactured without any dispersive aids. From DTF's experience, the in-house method utilised for obtaining PSDs is more extensive than that commonly used in industry due to the use of back scatter detectors in the Coulter LS13 320 laser diffraction analyser. As opposed to the Fraunhofer model that is commonly used in industry and only accounts for diffraction scatter, within DTF the Mie Scattering model is utilised for PSD analysis which accounts for the absorption of light and the refractive index of the material (Rakos, 2016). Table 8.3 shows the key markers of the distributions represented in Figure 8.5. It is evident form the Figure 8.5 that FR-1 and FR-2 grades indeed have a distinct PSD. FR-3 grade appears to almost be a blend of the FR-1 and the FR-2 grades with a slightly more larger particles than FR-2 grade.

Table 8.3: *Percentiles of particle size distribution for FR-1, 2, and 3 additive; as measured at DTF*

Additive Grade	D_{10} (µm)	D_{50} (µm)	D_{90} (µm)
FR-1	0.6	10.7	19.2
FR-2	1.2	24.5	42.7
FR-3	1.3	15.8	46.8

Figure 8.6 compares the additive PSDs measured in the composite to those of the powder additive as obtained though measurements at DTF. It is evident that in this case the FR-1 additive is generally well mixed with slight agglomeration observed at the top end as represented by the increasing D_{90} values. Around a 3 µm minimum observed in the composite PSDs is due to the resolution limit of the microscope at the magnification utilised (5 times) and explains the discrepancy in the lower end of the PSDs.

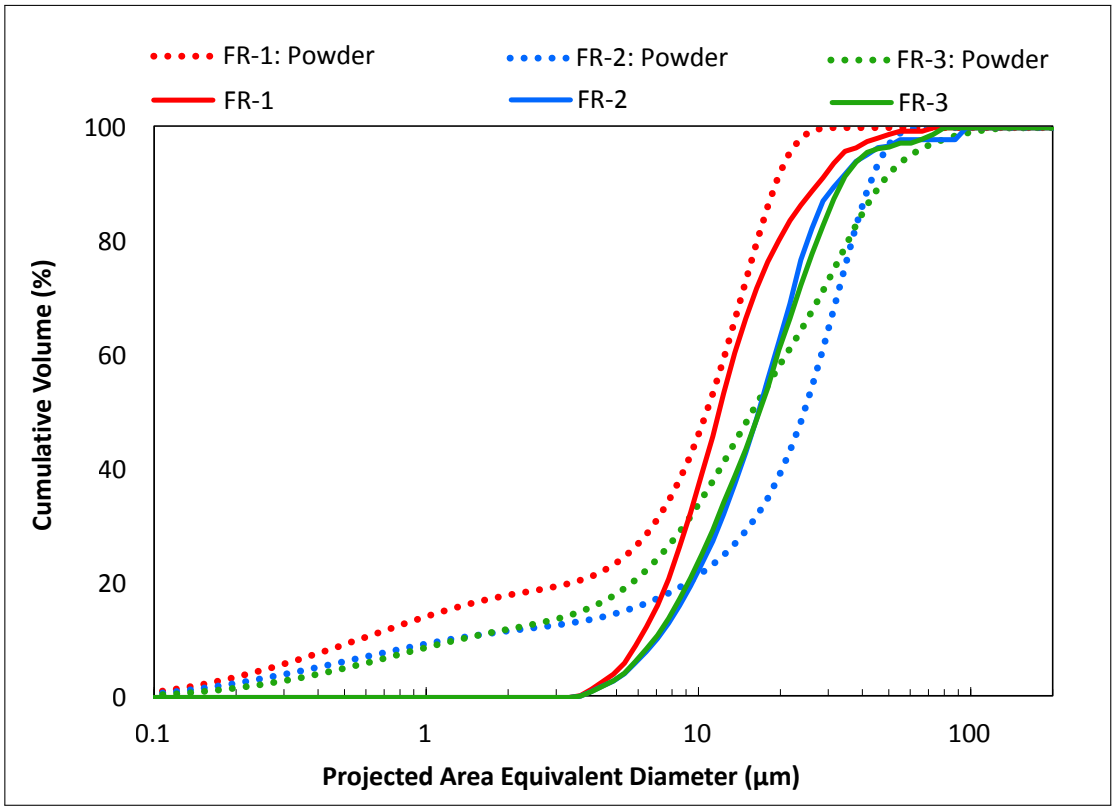

Figure 8.6: *Dispersion in FR-1, FR-2 and FR-3 composites vs additive PSDs obtained at DTF; manufactured at 6* $\mathrm{kg\,h^{-1}}$ *and 290 rpm on the Dr Collin ZK25 machine via the premix route*

Similarly, the FR-2 and the FR-3 grades are also well dispersed. It appears that the distributions observed within the composite are slightly smaller than that of the powder additive. This is a likely result of the larger particles being missed in the field of view under consideration; since on the number basis these larger particles are very infrequent. However, since the composites were manufactured via the *premix* route, it could also be argued that some attrition of the additive occurred during the exposure to high stresses in the melting section. This is unlikely as the lack of melted polymer in the melt section generally tends to lead to cold agglomeration of the additive.

Since, the additive PSDs are much closer together then suggested by the supplier it is more difficult to draw firm conclusion on the influence of particle size. It can be said that using the *existing* (severe mixing) screw configuration for the *Dr Collin ZK25* machine a good dispersion was achieved in composites containing three different additives ranging in

size from around a micron to tens of microns. It is envisages that additives with a smaller base size may be more difficult to disperse effectively; especially when the interaction between the polymer and the additive is weak.

8.1.2.2 Particle shape and aspect ratio

The influence of particle shape and aspect ratio was examined though manufacturing of H-PET composites containing two '*spherical*' grades and three long aspect ratio '*needle*' grades of whitener additive which have the same chemical composition and crystalline structure. The spherical grades (W-1 and W-2) have a base crystal size of around 0.2 µm but come from separate suppliers and hence have a different surface treatments. The needle grades W-4 and W-5 have a similar cross sectional diameter to the spherical grades with an aspect ratio of 14 and 25 respectively. W-3 material maintains an aspect ratio close to W-4 grade, however the diameter of the needle for this grade is about half that of the W-4 grade. See Section 3.2.1.1 for further details of the material properties. It is believed that these additives do not possess any surface treatment. Figure 8.7 shows example electron micrographs for the spherical and needle grades. The composites were manufactured using the *Dr Collin ZK25* machine equipped with the '*existing*' screw configuration (see Chapter 5 for details) at several different output and screw speed settings.

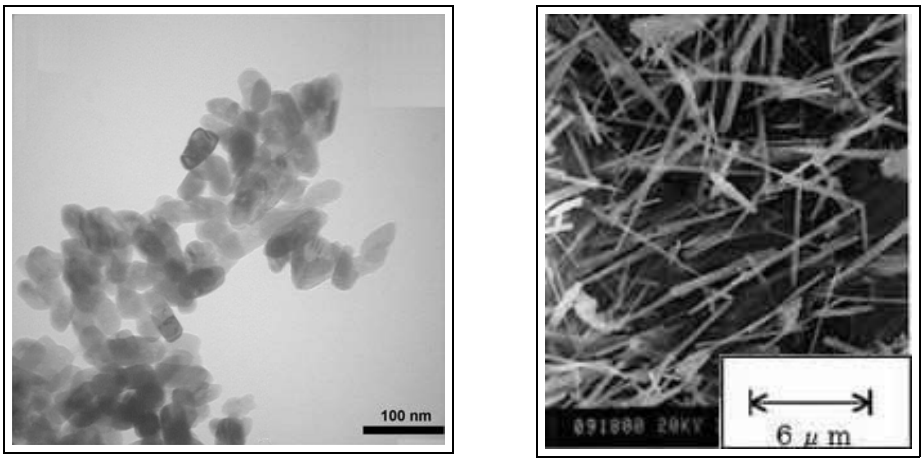

(a) *Transmission electron micrograph for a spherical grade (Natarajan et al., 2015)*

(b) *Scanning electron micrograph W-5 needle grade; from supplier*

Figure 8.7: *Electron micrographs of titanium dioxide particles*

Focusing on the effect of particle shape initially, Figure 8.8 shows the transmitted light microscopy images captured for the W-1 spherical and the W-5 needle grade composites. In order to obtain the images the polymer composite chip was melted between two glass slides to generate thin polymer film between them; more details on the method in Chapter 4. From the images, it is evident that good dispersion has been obtained in both cases with no indication of agglomerates being present. Although the highest available magnification lens (x50) was utilised, the large number of particles within the images and the interactions between them made it impossible to obtain an accurate PSD though the automatic sizing of individual particles in ImageJ.

Scanning electron microscopy (SEM) analysis was undertaken to obtain a clearer picture of the dispersion achieved. The analysis was undertaken on the composite chip which was microtomed to reveal a cross-section perpendicular to the direction of flow. This means that the needle shaped particles should be aligned in the direction of flow and the SEM images are showing their cross section. Figure 8.9 shows the level of dispersion achieved with W-1 and W-5 grades of whitener. It is evident that the level of dispersion for the spherical and the needle grade are again very similar, agreeing with the findings from the optical microscopy analysis. It is important to note that no significant difference was found in the level of dispersion between two spherical grades; also see SEM images in Figure 8.10.

The level of dispersion achieved with both the spherical and the needle grades was better than that reported by Padmanabhan and Jayanth, 2008 who showed SEM micrographs with titanium dioxide agglomerates up to 10 µm being discovered within an undisclosed polymer composites produced via the *split feed* or *premix method*. Fortunato et al., 2014 also reported agglomerates ca. 10 µm in titanium dioxide/PET composites produced via direct to *melt addition* method.

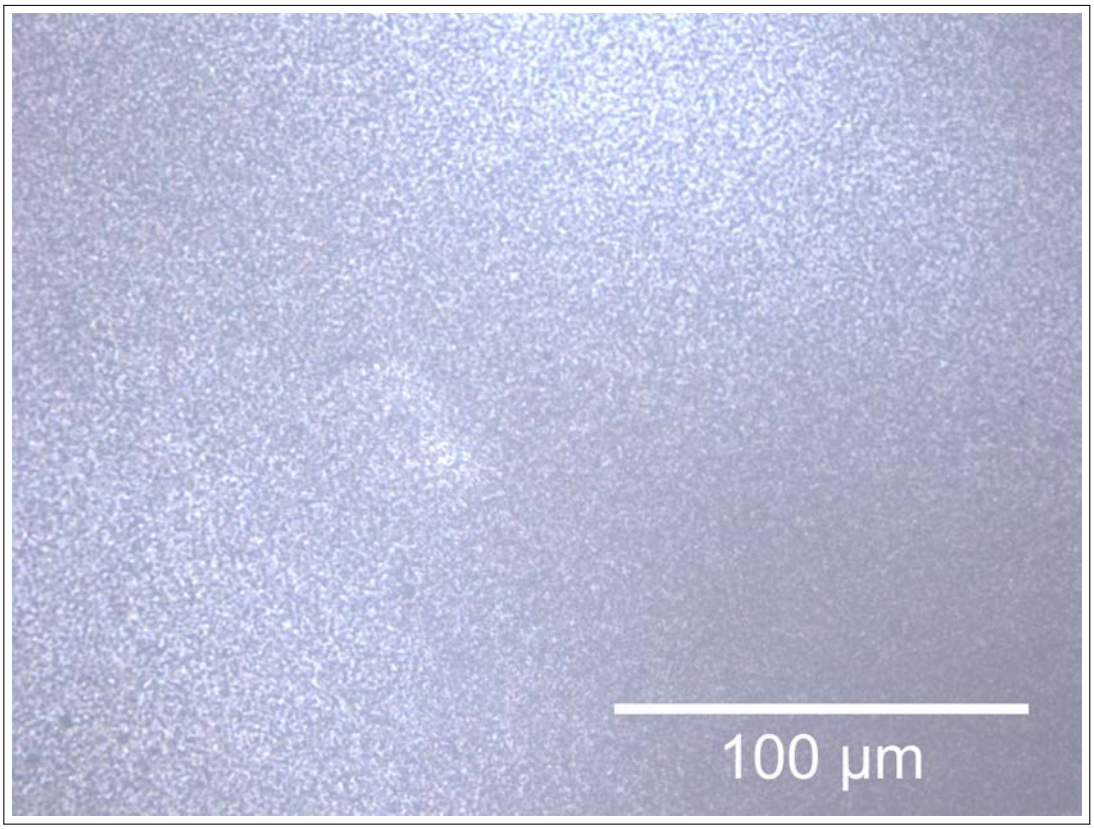

(a) *Optical microscopy: W-1 spherical grade at 6* $\mathrm{kg\,h^{-1}}$ *and 240 rpm; magnification x50*

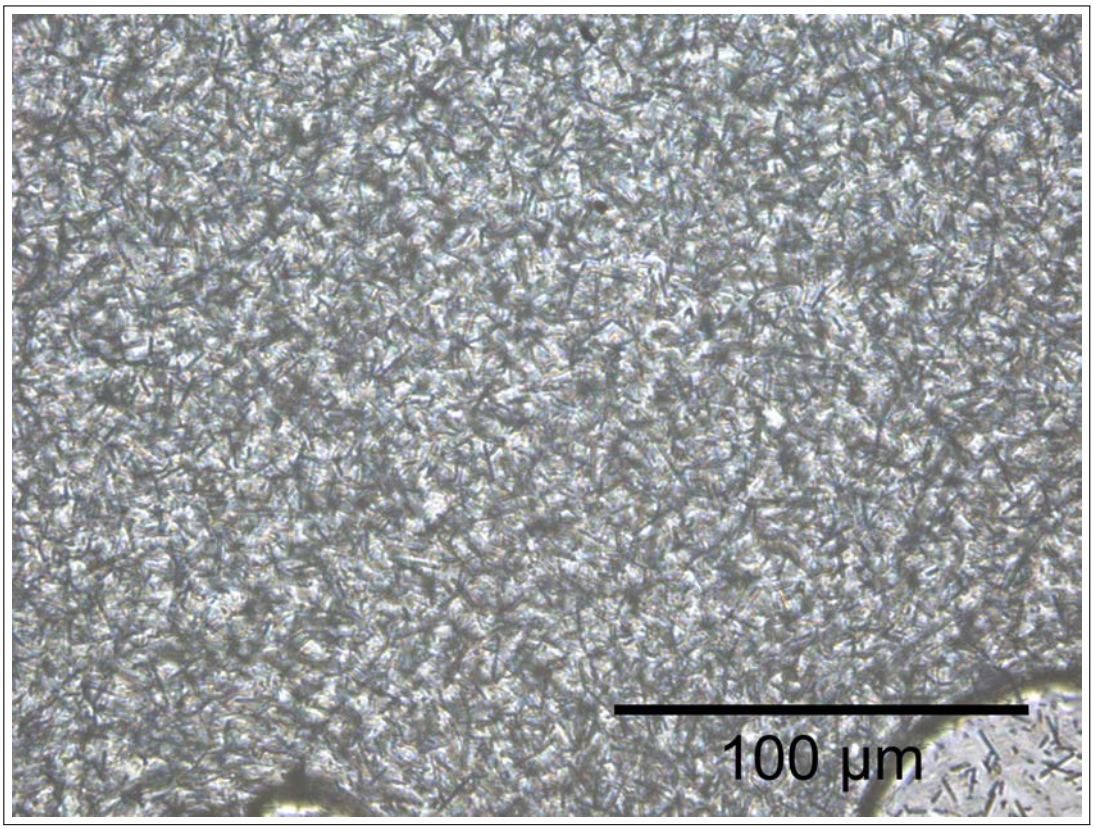

(b) *Optical microscopy: W-5 needle grade at 6* $\mathrm{kg\,h^{-1}}$ *and 400 rpm; magnification x50*

Figure 8.8: *Optical microscopy analysis comparing dispersion of spherical grade and needle grade whitener; manufactured on the Dr Collin ZK25 machine via the premix method*

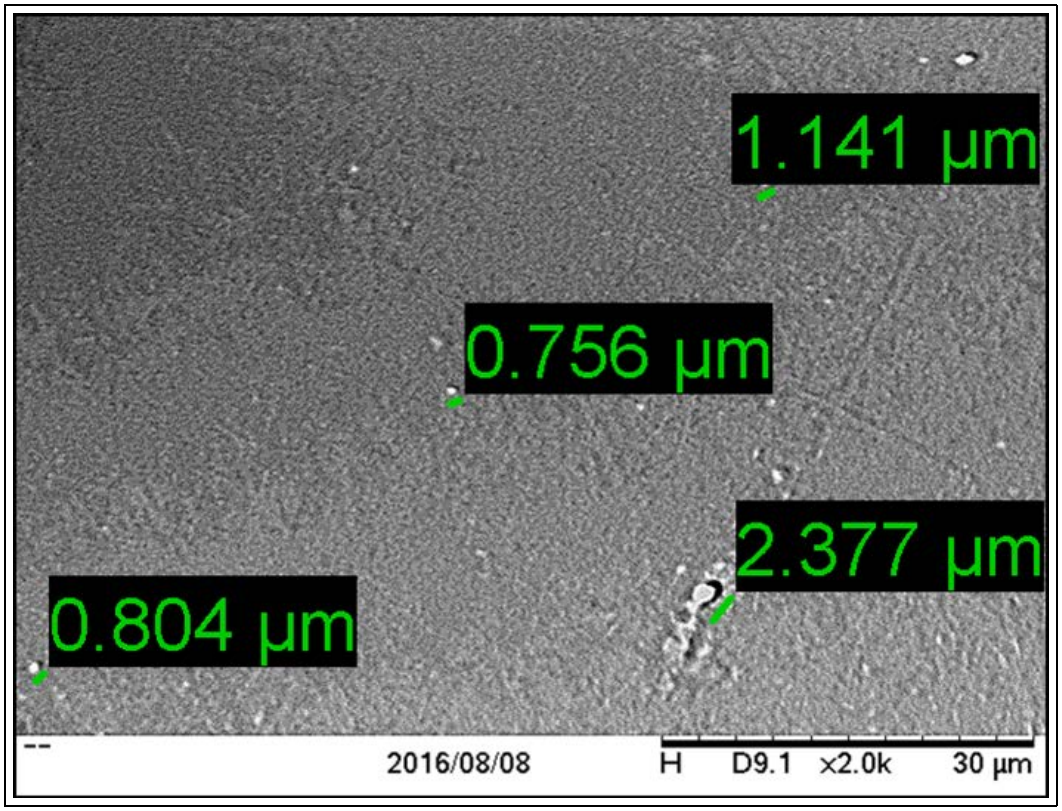

(a) *SEM: W-1 spherical grade at 3* $\mathrm{kg\,h^{-1}}$ *at 240 rpm*

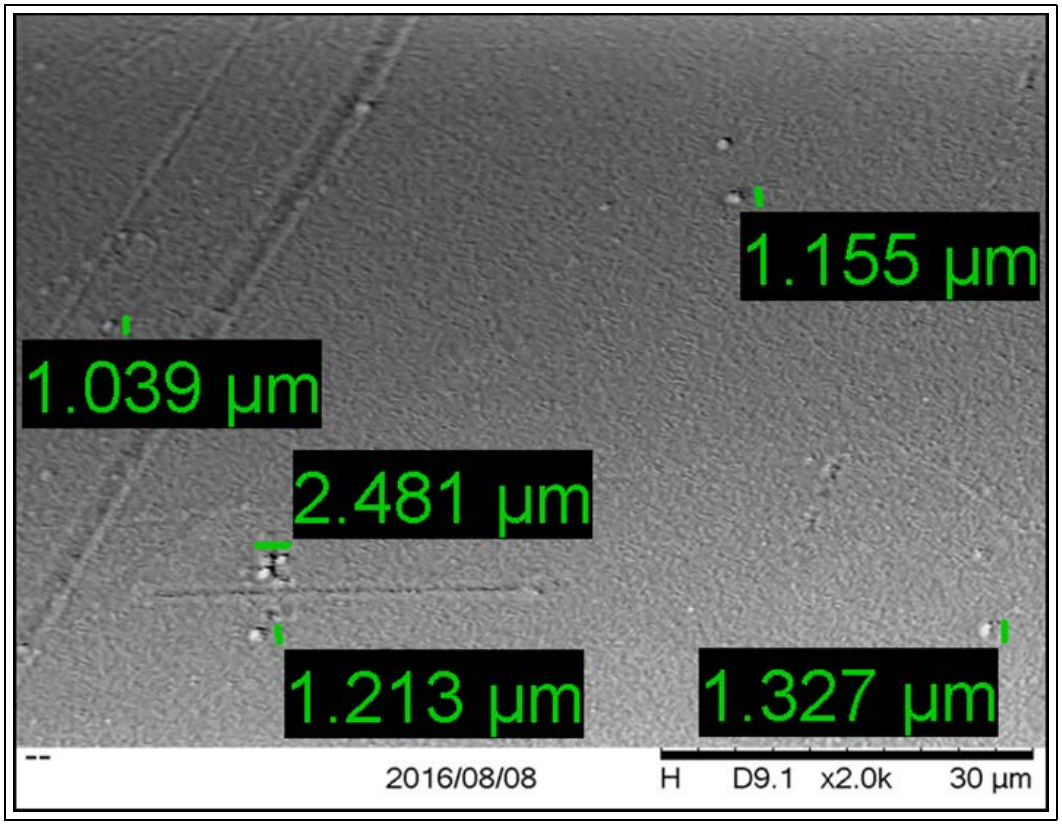

(b) *SEM: W-5 needle grade at 3* $\mathrm{kg\,h^{-1}}$ *at 240 rpm*

Figure 8.9: *Scanning electron microscopy analysis comparing dispersion of spherical and needle grade whitener in composites manufactured on the Dr Collin ZK25 machine via the premix method; images captured by Jessica Nix at DTF*

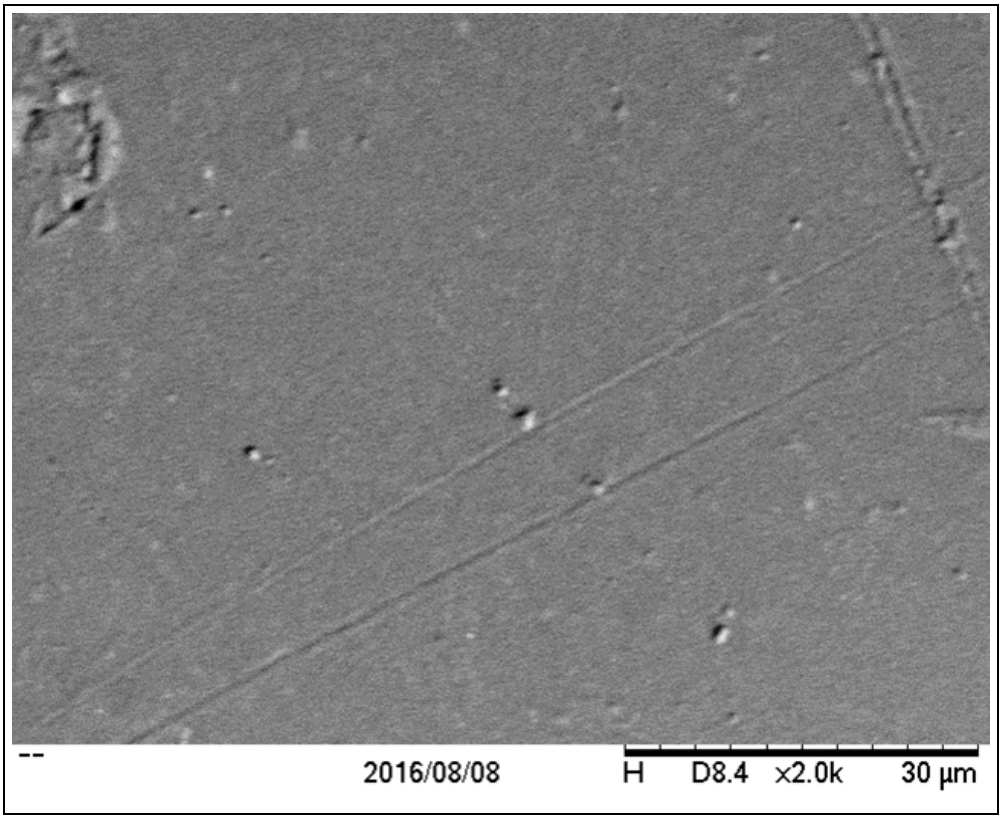

(a) W-1 spherical grade at 6 $\mathrm{kg\,h^{-1}}$ *and 240 rpm*

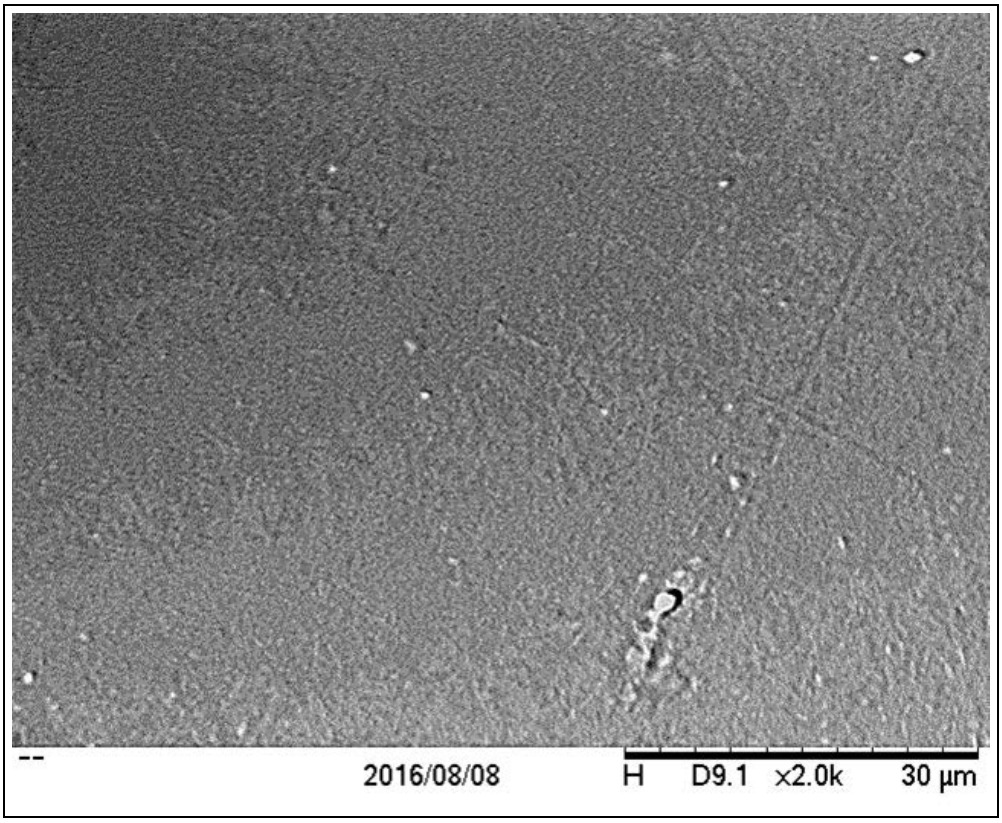

(b) W-2 spherical grade at 6 $\mathrm{kg\,h^{-1}}$ *and 240 rpm*

Figure 8.10: *Dispersion of W-1 and W-2 spherical grades manufactured on the Dr Collin ZK25 machine via the premix method; images captured by Jessica Nix at DTF*

Generally, one would expect the dispersion of the long aspect ratio needles to be more difficult then that of spherical particles due to the increased potential for interlocking between the individual particles; as discussed in Section F.2.2. This does not appear to be the case with whitener additives and has been attributed to the strong interaction between the additive and the PET polymer matrix. The role of the interactions is made clear by the composites containing the tubular clay (referred to as C-1) which has a very similar particle shape to W-5 whitener grade, but is significantly more difficult to disperse; as discussed in Section 8.1.3.

Figure 8.11, shows the level of mixing achieved in W3, W-4 and W-5 composites. The aspect ratio of the filler in Figures 8.11a and 8.11b is alike (13 vs 14), therefore it is reasonable to assume that the level of interlocking between individual needles within the agglomerate bundles should be similar resulting in similar degree of mixing. However, the level of mixing is different with W-3 grades exhibiting better mixing. This can be associated with the smaller diameter of the W-3 needles, which reduces their mechanical strength allowing the needles to be broken more easily and thus leading to improved dispersion of the bundles.

Comparing Figures 8.11b and 8.11c shows that the W-4 grades exhibits better mixing with smaller features being detected on the SEM image. This result agrees with theory and can be explained by the lower aspect ratio (14 vs 25) of the W-4 grade compared to the W-5. As the aspect ratio increases this leads to more interactions between the individual needles within the agglomerate bundles. As a result larger stresses are required to overcome this extra resistance to the relative movement between the individual needles reducing the effectiveness of the rupture and the erosion mechanism at a given set of operating conditions. The effectiveness of the collision mechanism is also reduced as the probability of two agglomerates (bundled structures) colliding and generating small fragments is considerably smaller than that of them fusing together into a single larger structure.

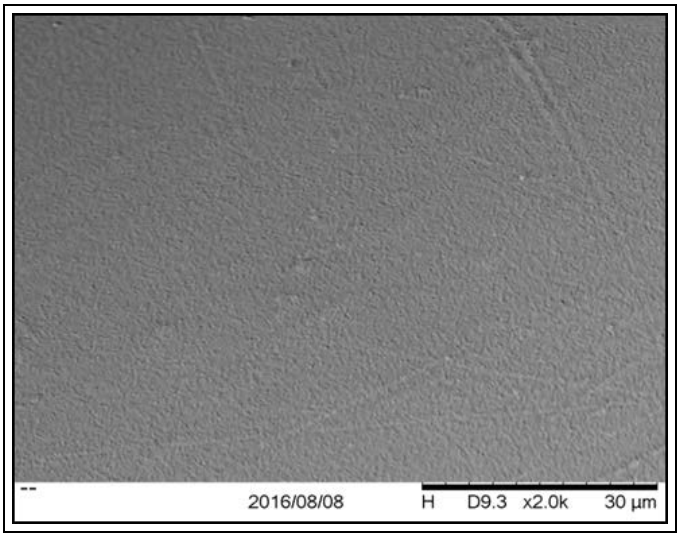

(a) W-3: aspect ratio of 13

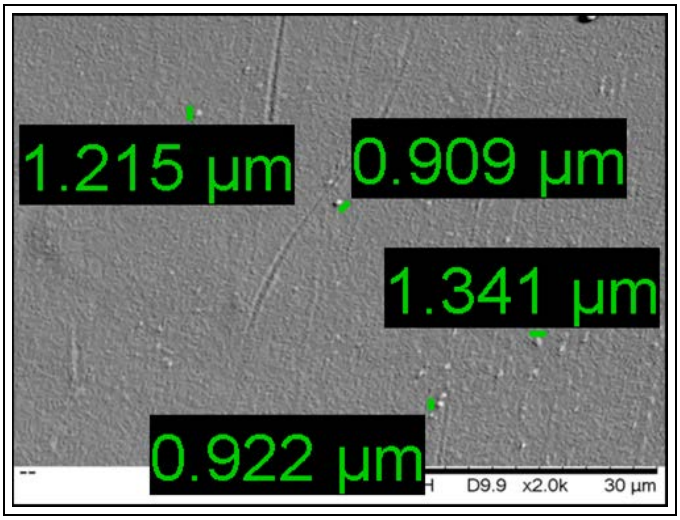

(b) W-4: aspect ratio of 14

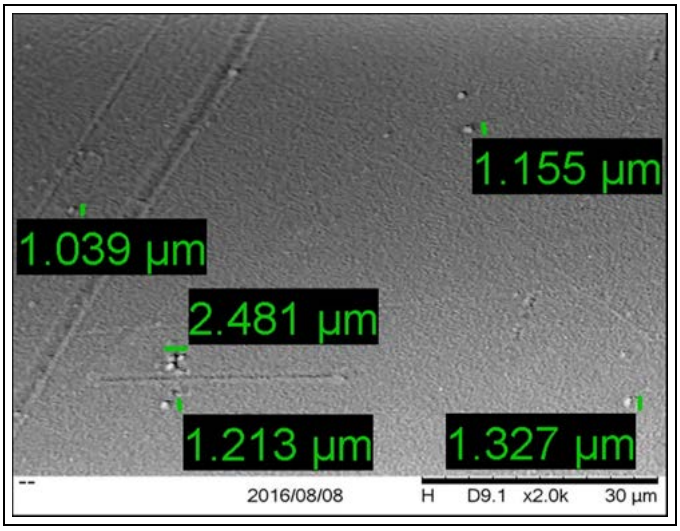

(c) W-5: aspect ratio of 25

Figure 8.11: *Dispersion of needle grade whiteners in composites manufactured on the Dr Collin ZK25 machine via the premix method at 3* $\mathrm{kg\,h^{-1}}$ *and 400 rpm; images captured by Jessica Nix at DTF*

8.1.2.3 Porosity and bulk density

The following hypotheses are proposed for the affect of additive porosity on the level of mixing achieved. It is thought that higher porosity of the additive would have two competing effects. Firstly, the rise in the number of open pores within the additive structure would lead to an increased wetting demand as the polymer penetrates into the pores. This is likely to enable more efficient transfer of forces from the fluid to the agglomerate enhancing dispersion. A competing effect would originate from the moisture contained within the open pores. If the additive is not effectively dried, the moisture will lead to increased hydrolysis of the PET polymer chains, reducing the matrix viscosity and lowering the hydrodynamic stresses transferred to the agglomerate; thus reducing effectiveness of dispersion processes. In addition, the increased wetting demand is likely to enforce a constraint on the direct addition process by limiting the amount of filler that can be incorporated into the composite.

The impact of porosity was evaluated by considering the mixing of co-PET and S-PET composites containing several grades of silica (referred to as S-1 to S-5). The additives were carefully chosen to have a similar average particle size of circa 5 to 6 µm and only differ by the level of porosity (from 0.4 to 1.8 $\mathrm{ml\,g^{-1}}$), specific surface area (from 300 to 700 $\mathrm{m^2\,g^{-1}}$) and the associated parameters such as bulk density. Detailed additive properties can be found in Section 3.2.1.4.

S-5 grade of the silica has porosity of 0.4 $\mathrm{ml\,g^{-1}}$ and specific surface area of 700 $\mathrm{m^2\,g^{-1}}$, which represents the minimum porosity and the maximum surface area values considered. On the contrary, S-1 grade has a maximum porosity of 1.8 $\mathrm{ml\,g^{-1}}$ and the minimum surface area of 300 $\mathrm{m^2\,g^{-1}}$. It may be expected that as the porosity increases the specific surface area should also increase. This is not the case and is explained by the nature of the pores within the material. The high porosity silica has a large number of closed pores which contributes to changes in the density of the particle and not the surface area.

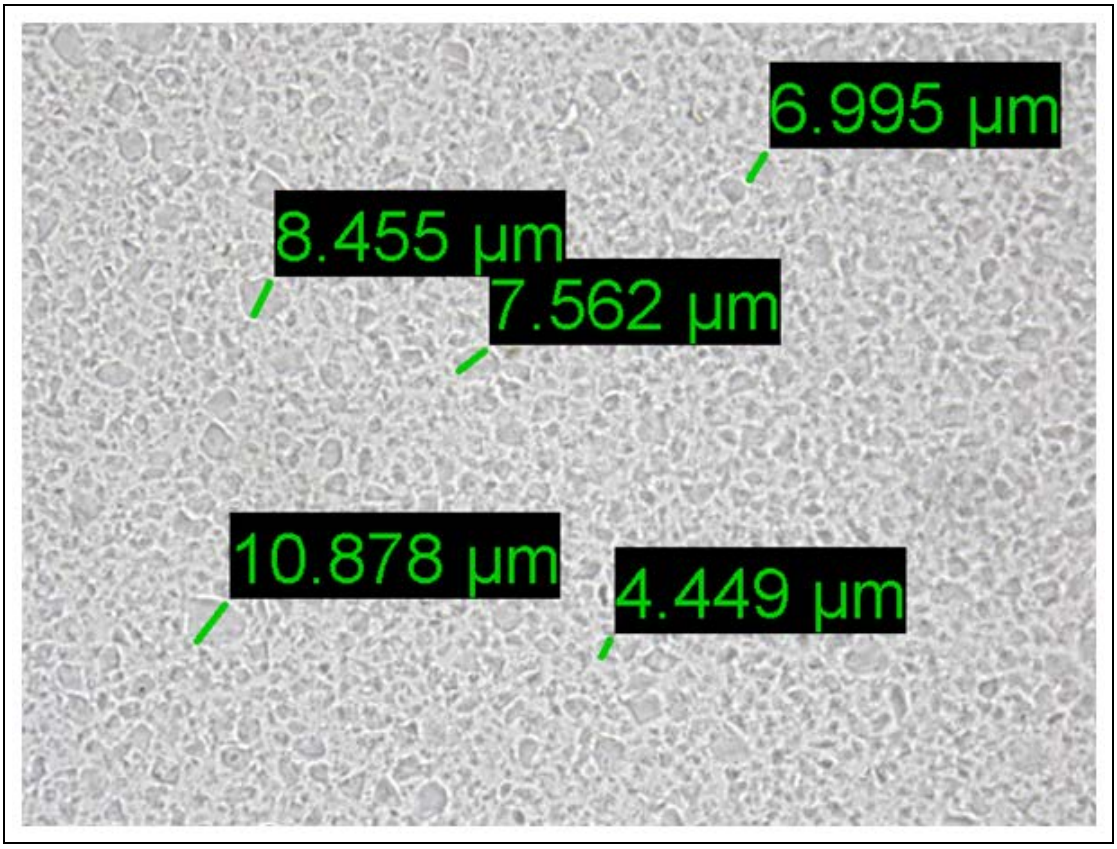

(a) *S-5 at 13.1* $\%_{wt}$*: porosity of 0.4* $\mathrm{ml\,g^{-1}}$ *and specific surface area of 700* $\mathrm{m^2\,g^{-1}}$

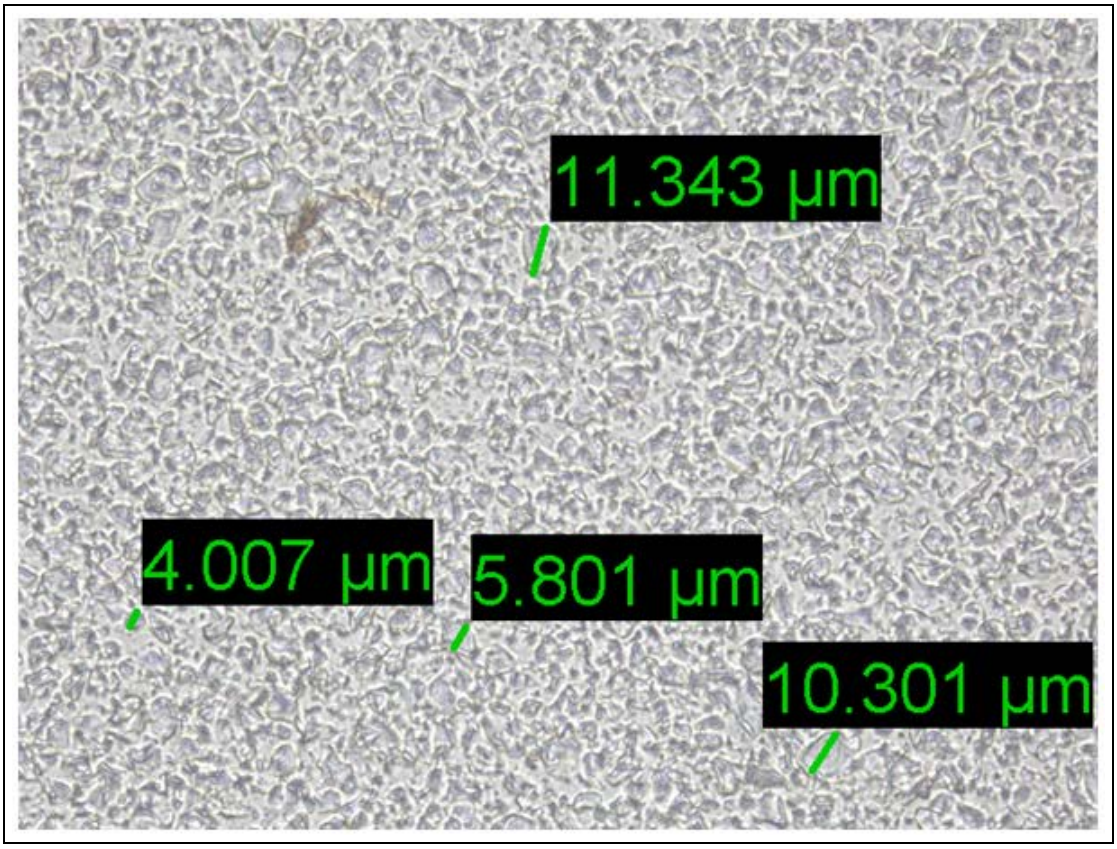

(b) *S-1 at 10.5* $\%_{wt}$*: porosity of 1.8* $\mathrm{ml\,g^{-1}}$ *and specific surface area of 300* $\mathrm{m^2\,g^{-1}}$

Figure 8.12: *Dispersion of S-1 and S-5 silica grade in co-PET composites manufactured on the Dr Collin ZK25 machine via the direct to melt addition method at 4* $\mathrm{kg\,h^{-1}}$ *and 300* rpm

On the other hand the lower porosity grade has a larger proportion of open pores into which material can enter increasing the specific surface area of the material whilst minimising the impact on the density of the particle. As the open pores are of interest in evaluating the wetting demand, it can be concluded that the specific surface area provides a better representation. The surface area is determined through gas adsorption (Brunauer-Emmett-Teller theory) with the values in this case being provided by material suppliers.

From Figure 8.12, it is evident that the surface area (or porosity) does not impact on the level of dispersion achieved as in S-1 and S-5 composites as the silica is dispersed to its primary particle size of ca 6 µm; potentially disproving the first part of the hypothesis. The lack of differentiation in the level of mixing has been attributed to the very high strength of interaction between the silica additive and the polymer matrix. It is felt that more work can be done in this area with a different additive which has a weaker interaction with the polymer matrix to either prove or disprove the hypothesis.

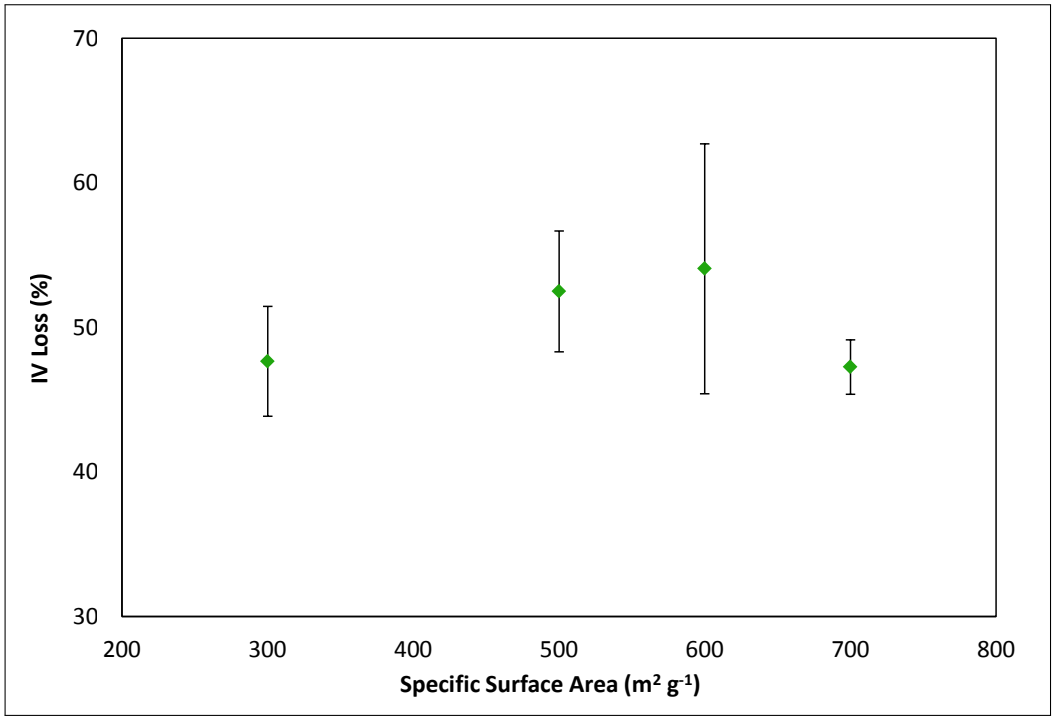

Figure 8.13: *Dependence of IV loss on specific surface area of silica in silica/co-PET composites manufactured on the Dr Collin ZK25 machine via the direct to melt addition method at 4* $\mathrm{kg\,h^{-1}}$ *and 300* rpm

Figure 8.13 does show that there is some dependency on the level of IV loss experienced by the PET matrix as a function of specific surface area (open pores) potentially confirming the second part of the hypothesis. A more in-depth statistical analysis involving a larger sample population would have to be undertaken to develop a prediction with a high level of confidence since the error bars in the current analysis are quite large due to a small sample number.

Although the specific surface area is potentially better for correlating with the level of mixing, the porosity of the additive controls the density of the particles. This influences several key factors and thus plays a critical role in determining the process limitations.

Firstly, for a given mass fraction it determines the volume fraction of the additive within the composite. For a constant particle size, an additive with a lower particle density will occupy more space and thus the composite will contain a larger number of particles. This is particularity important in surface applications, where it is the volume fraction and more precisely the number of particles at the surface that determine the surface properties. Secondly, the particle density determines the likelihood that the particle will be entrained in the airflow exiting the extruder through the feed pocket or the degassing ports. This puts a limit on the applicability of a *split feed* method of addition and determines how close to the addition point the degassing ports can be located. Lastly, a decreasing particle density reduces the bulk density of the material. This in turn determines the amount of air entering the extruder together with the additive thus setting the maximum amount of filler that can be incorporated via a single addition point.

During the manufacture of the co-PET composites containing porous silica, two types of process limits were found. The first directly relates to discussions above and is a function of the ability of the extruder screws to convey the material forward and thus the free space within the machine. Figure 8.14 shows the target silica content compared to actual content within the composites (as obtained though ash analysis) for different extruder screw speeds when all the other parameters were maintained constant. Actual

silica content decreases with decrease in the speed of the extruder screws. This is due to the increase in degree of fill within the extruder with decreasing screw speed leaving less space available for additive material. The analysis corresponds well to the observations on the day of the experiment, where the silica powder accumulated in the side feeder at the reduced extruder speed conditions even though the side feeder was operating close to the maximum speed. Potentially such a limitation could be overcome by the use of a different screw design for the side feeder or a less restrictive profile for the extruder screws.

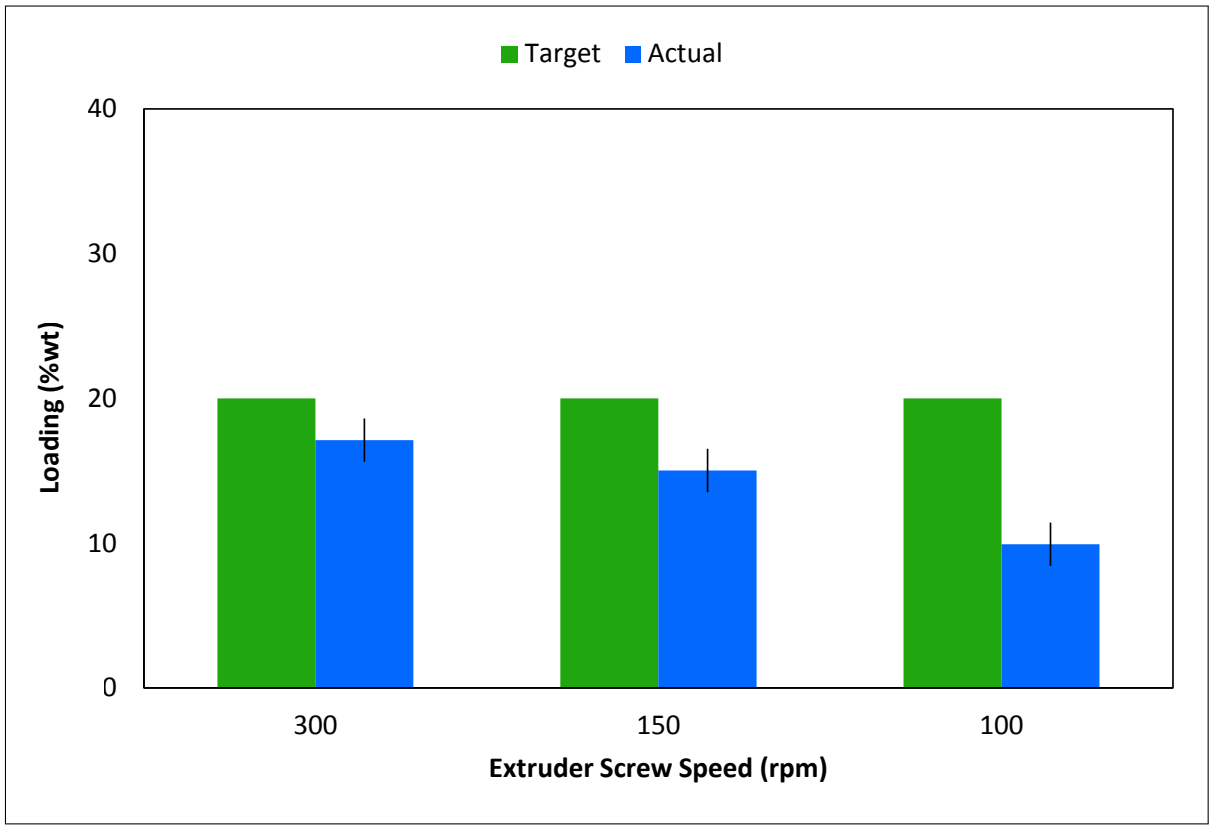

Figure 8.14: *Actual vs target loading of silica achieved in co-PET composites manufactured at various screw speeds on the Dr Collin ZK25 machine via the direct to melt addition method at 4* $\mathrm{kg\,h^{-1}}$*; side feeder screw speed maintained constant*

The second limitation is illustrated in Figure 8.15, which shows the loading at which the lace became very brittle. This hindered the ability of the cutter to cut the lace in order to produce the chip and hence a stable manufacturing process was not possible. This limit is likely to hold true in the manufacture of film where the brittleness of the film would cause splits around the casting drum, forward or sideways draw processes.

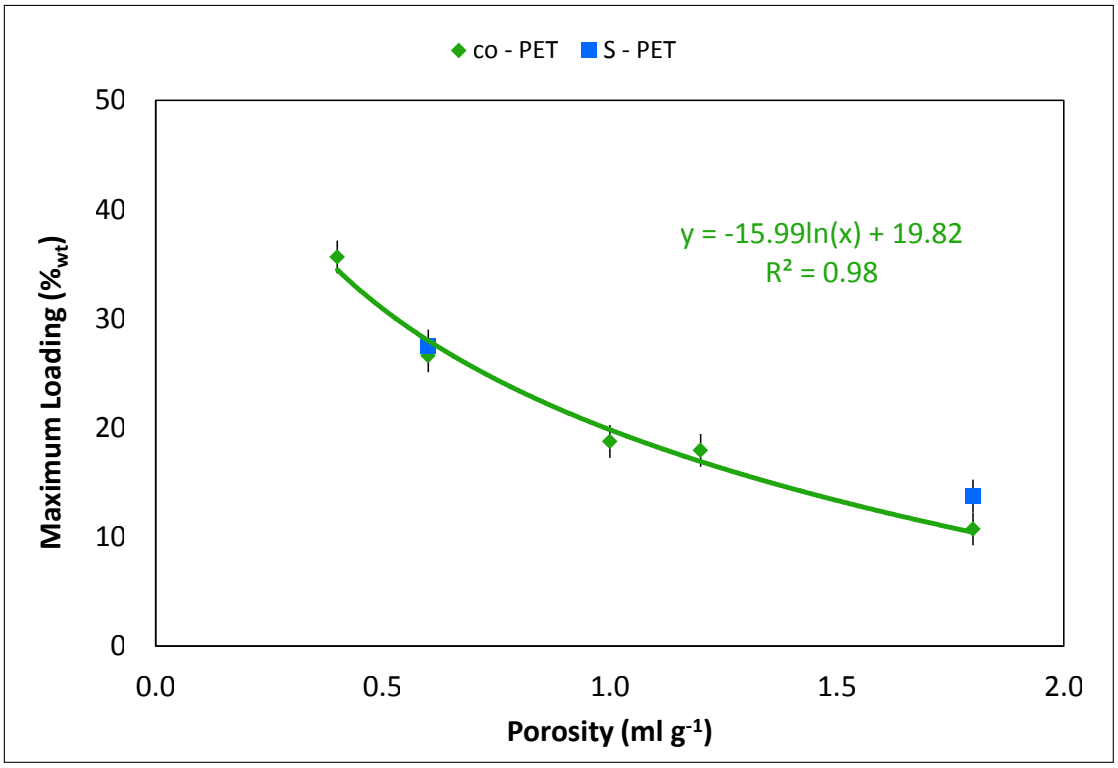

(a) Maximum loading as $\%_{wt}$

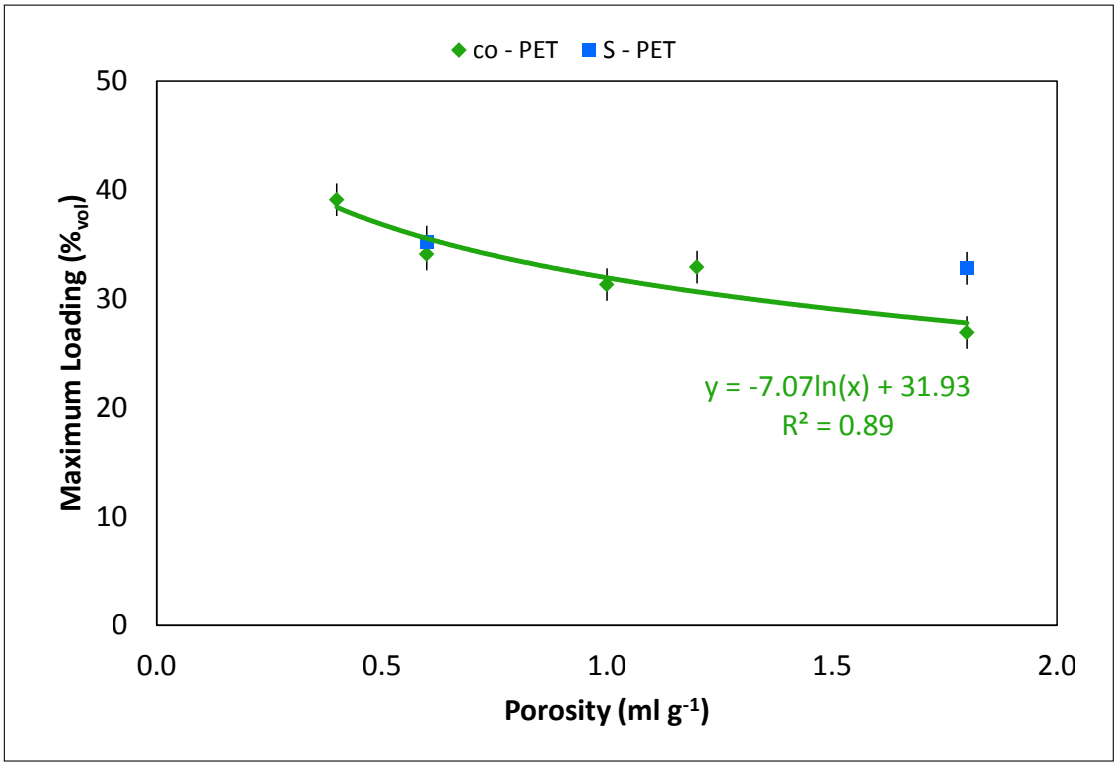

(b) Maximum loading as $\%_{vol}$

Figure 8.15: *Maximum loading achieved in silica/co-PET composites manufactured on the Dr Collin ZK25 machine via the direct to melt addition method at 4* $\mathrm{kg\,h^{-1}}$ *and 300* rpm

The loading within the composites on the mass basis decreases drastically with the increase in the porosity of the material. On the volume basis the loading within the composites decreases only slightly with increasing porosity with the limiting value dropping from ca. 40 to 30 $\%_{vol}$. For the same shape of particle, one would expect that the limiting volume fraction would remain the same. This is potentially explained by the loss in the ability of more porous additive to conduct heat. This in turn would allow a higher degree of crystallinity to be formed within the polymer phase in the lace as it was being cooled in the water bath leading to the lace becoming more brittle. Further investigation into how the limiting volume fraction changes particularly with particle shape would be of great interest.

8.1.3 Interactions between the additive and polymer

As discussed, the long aspect ratio whitener grades W-3, W-4 and W-5 with ratios of 13 and 14 and 25 respectively all showed a very good mixing with only a few small agglomerates being present. On the contrary, similarly shaped long aspect ratio (10 to 20) tubular clay referred to as C-1 showed a very poor level of dispersion with large agglomerates being visible to the naked eye within the polymer chip when processed at the same extrusion conditions.

Figure 8.16 provides an indication of the level of dispersion achieved in both cases. The stark difference in mixing achieved suggests that the level of interaction between the additive and the polymer has a key role to play in determining the level of dispersion. Two methods of altering the interactions were tested which were the use of co-polymer (co-PET) and the use of dispersive aids.

The composites were manufactured on the *Dr Collin ZK25* machine fitted with screw configurations entitled the '*Base Case*' and '*Configuration 3*'; for details of the set up see Chapter 5 and Appendix J respectively.

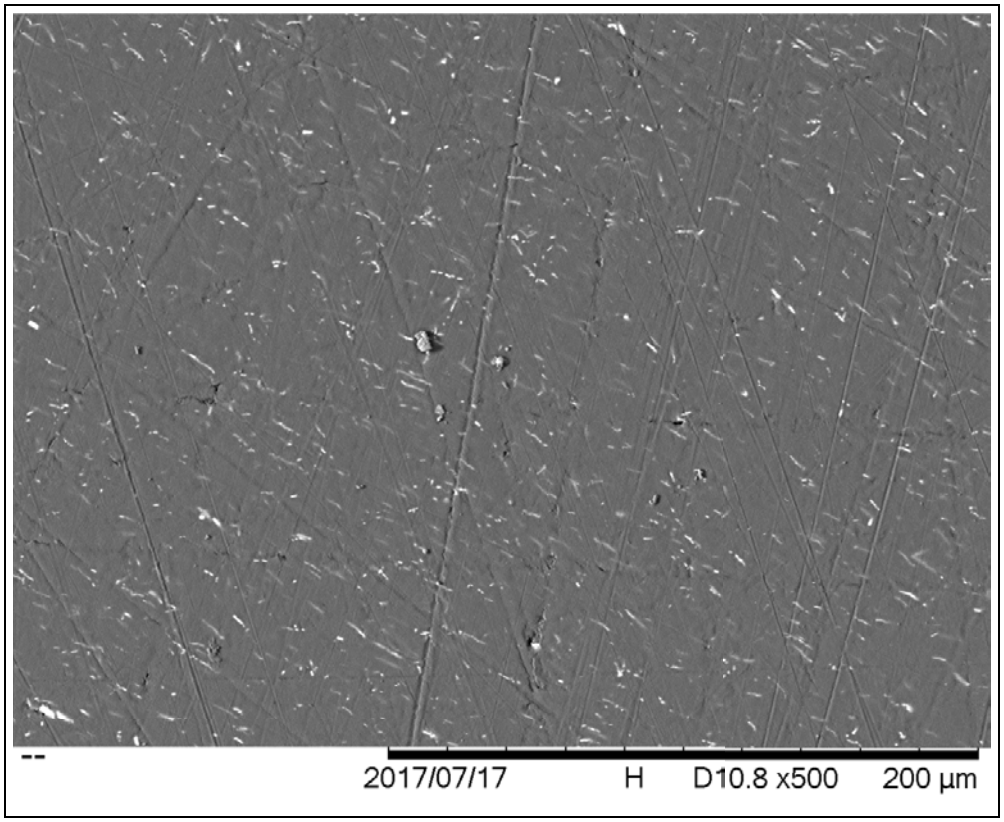

(a) *SEM analysis on cross section of chip (cut in the direction of flow) showing whitener (W-5) at 5* $\%_{wt}$

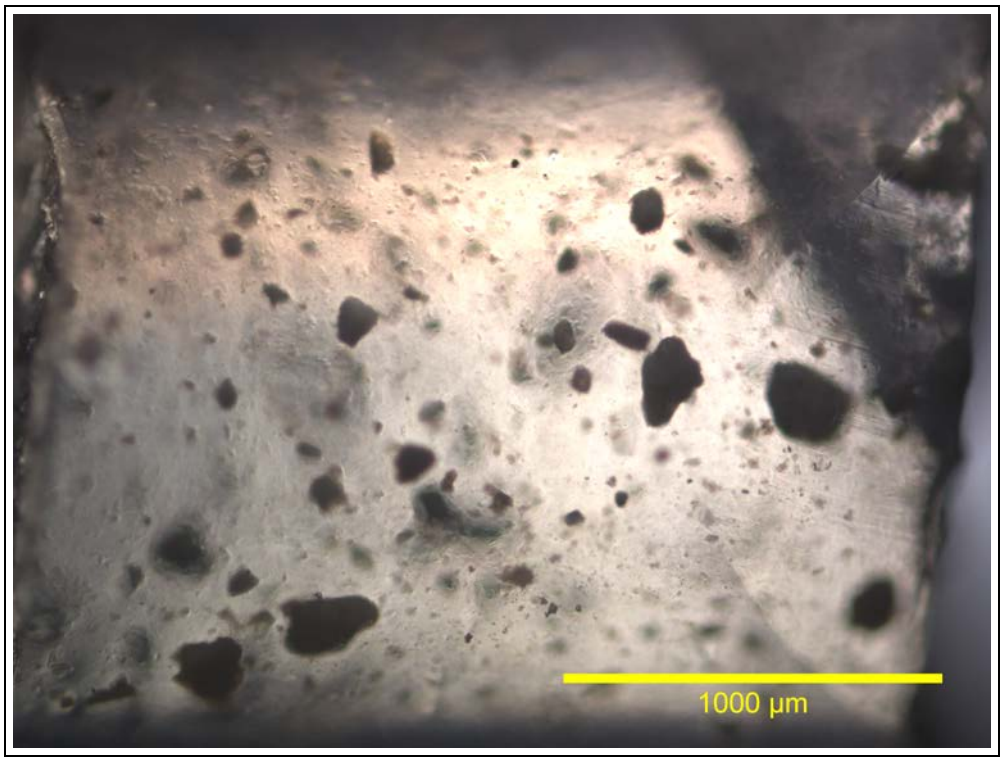

(b) *Reflected light microscopy of the chip surface showing tubular clay (C-1) at 5* $\%_{wt}$

Figure 8.16: *Dispersion of whitener and tubular clay in H-PET composites manufactured on the Dr Collin ZK25 machine fitted with Base Case screw configuration at 240* rpm *and 6* $\mathrm{kg\,h^{-1}}$ *via direct to melt addition route.*

8.1.3.1 Modifying additive-polymer interactions with a co-Polymer

By introducing a co-polymer into the overall polymer matrix a number of properties can be altered. A co-polymer grade, referred to as co-PET, is commonly utilised within DTF. This grade of material contains $\leq$20 $\%_{wt}$ of co-polymer which inhibits the crystallization of material, lowers the viscosity of the matrix and leads to a very 'tacky' polymer once it is exposed to temperatures greater than 220 °C. It was hypothesised that the presence of a co-polymer in in the polymer matrix during the tubular clay dispersion process would alter the interactions between to the clay and the matrix leading to much more effective dispersion.

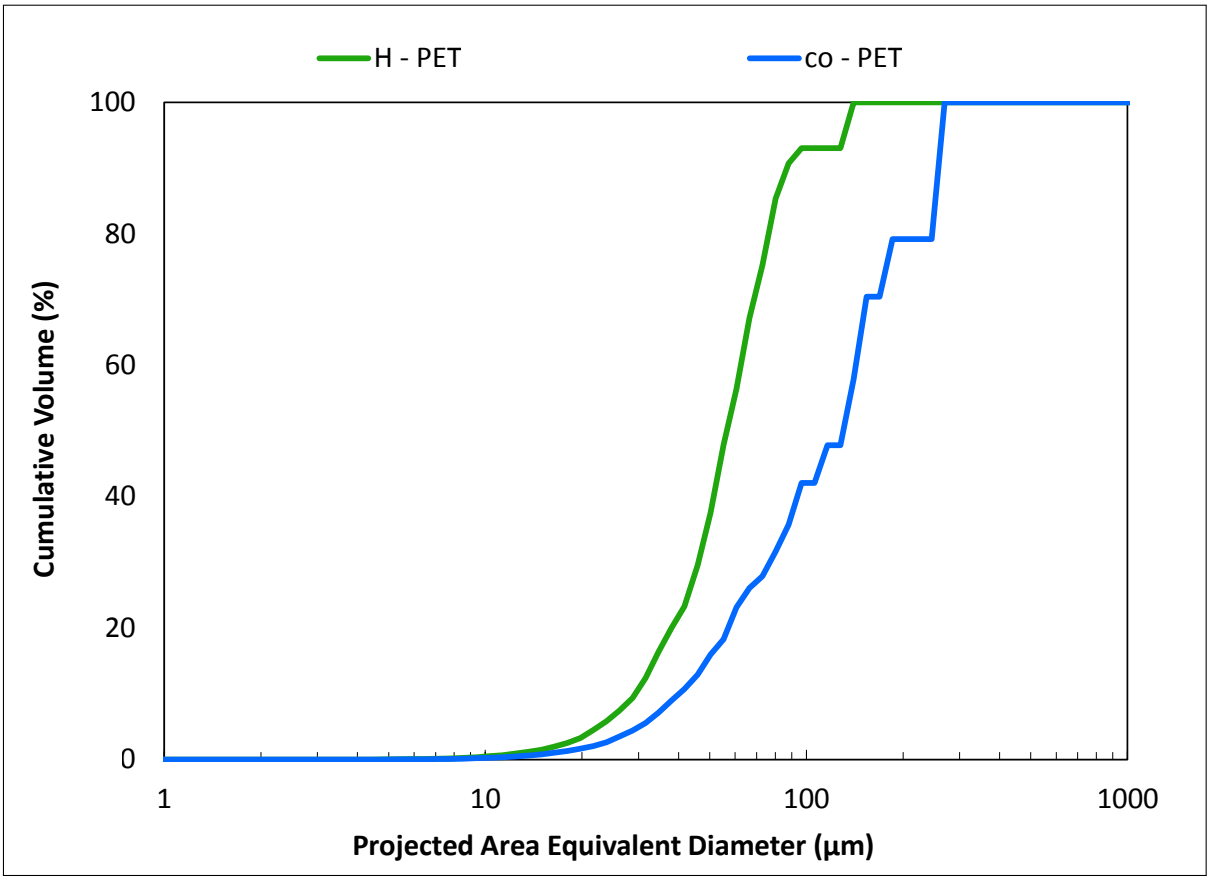

Figure 8.17: *Dispersion of 5 $\%_{wt}$ tubular clay (C-1) in H-PET and co-PET composites manufactured on the Dr Collin ZK25 machine fitted with Configuration 3 screw configuration via the direct to melt addition method at 6* kg h^{-1} *and 240* rpm

Figure 8.17, shows that the level of dispersion achieved in the H-PET matrix was much better than that in the co-PET matrix. As the viscosity of H-PET is considerably higher

than that of co-PET (see Table 8.4), the proportionally higher shear stresses achieved during the extrusion are the likely reason that the dispersion in H-PET composites is significantly better. This is supported by the significantly lower values for the D_{90} of the distributions suggesting that the additive experienced higher stresses.

Table 8.4: *Viscosity of H-PET, S-PET and co-PET; S-PET measured at 10* $\mathrm{rad\,s^{-1}}$ *and 5 % strain, H-PET measured at 100* $\mathrm{rad\,s^{-1}}$ *and 5 % strain, and co-PET measured at 100* $\mathrm{rad\,s^{-1}}$ *and 10 % strain*

Temperature (°C)	265	275	285
Viscosity of H-PET (Pa s)	725	617	518
Viscosity of S-PET (Pa s)	226	181	144
Viscosity of co-PET (Pa s)	126	109	96

It is acknowledge that a fairer comparison would have been between that of S-PET processed at 285 °C and co-PET at 265 °C as the viscosities of the polymer matrix would have been more evenly matched in such an experiment. However, the research is in part driven by business needs and an improvement on the level of dispersion achieved in H-PET polymer was sought. It was already shown that H-PET delivers higher dispersion than S-PET in Section 8.1.1.

8.1.3.2 Modifying additive-polymer interactions with dispersive aids

A number tertiary components can be introduced into a binary additive/polymer composites system to modify the interactions between the additive and the polymer matrix; see Section F.3. Both, wetting agents and compatibilisers require considerable knowledge of the additive and polymer chemistry in order to select a component which would correctly interact and link the two phases; this was deemed beyond the scope of this work. Dispersive aids function in a different manner, by simply providing a third lower viscosity phase which forms around the additive and enhances the transfer of stress from the main polymer matrix to the agglomerate. As a result a simpler criteria is utilised in the selection process, such as ease of handling.

Overall three dispersive aids were tested including Tegomer H-Si 6440 P, Tegomer DA 626

and TOTM. Tegomer H-Si 6440 P (supplied by Evonic) is a polyester modified with siloxane and was thought to be compatible with the external siloxane surface found on the tubular clay. The material was supplied in pellet form and has a melting point of 54 °C. Tegomer DA 626 on the other hand is a relatively high viscosity liquid with viscosity of 50 to 150 mPa s at 25 °C which was used to test a different method of addition. TOTM (supplied by Eastman) had even higher viscosity of 200 mPa s and was tested prior to Tegomer DA 626.

In all of the cases the composites were manufactured via the *premix* route on the *Dr Collin ZK25* machine. Tegomer H-Si 6440 P pellets were dry blended with the polymer and the tubular clay prior to being fed into the extruder. Both of the liquid dispersive aids were preheated to around 60 °C in order to reduce the viscosity of the material and enable easier handling. The tubular clay was then mixed into the liquid at the required ratio. The mixture was then blended with the polymer pellets aiming for an even distribution of the mix around each of the polymer pellets. The results are shown in Figure 8.18.

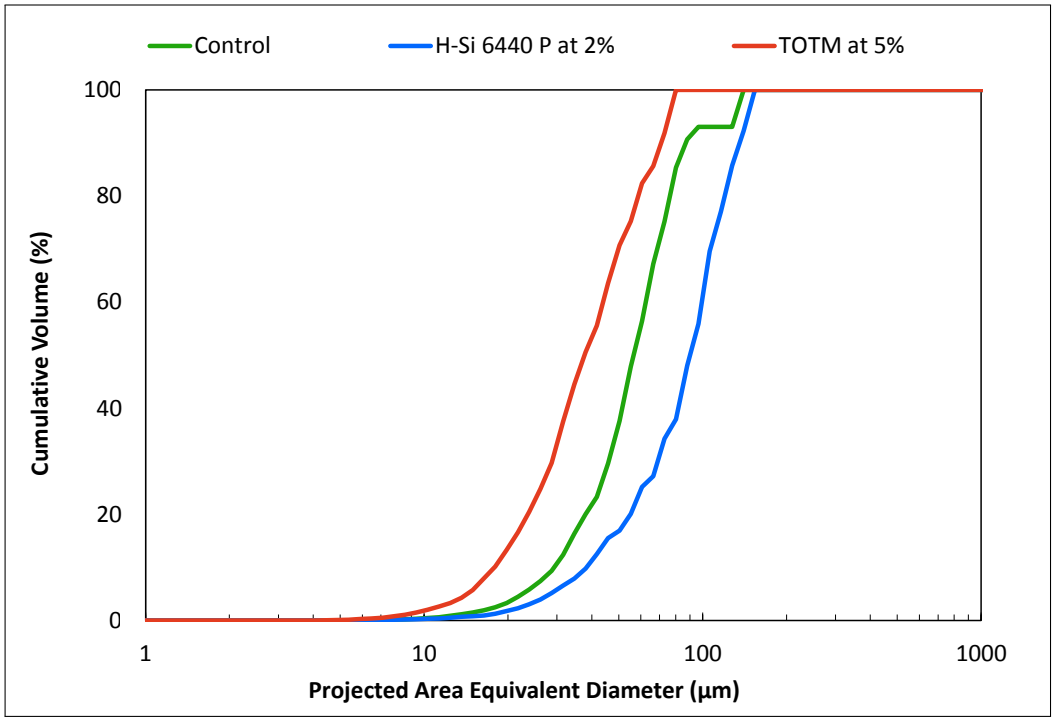

Figure 8.18: *Dispersion of 5 $\%_{wt}$ tubular clay (C-1) with Tegomer H-Si 6440 P and TOTM in H-PET composites; manufactured on the Dr Collin ZK25 machine fitted with Configuration 3 screw configuration via the premix method at 6* kg h^{-1} *and 240* rpm

It is evident that addition of TOTM leads to significant improvement in dispersion when compared to the control sample with no dispersive aids. This suggests that a lower viscosity tertiary phase can be effectively utilised to aid with dispersion of difficult to disperse (incompatible) additives. Interestingly, the use of a low viscosity dispersive aid in pellet form has lead to a reduction in the level of dispersion. This result suggests that upon addition H-Si 6440 P mixes in with the PET matrix significantly lowering the overall viscosity of the polymer matrix leading to worse dispersion. Another potential explanation involves the C-1 tubular clay preferentially locating in the PET continuous phase as opposed to the discontinuous phase. However, in this case one would expect the same level of mixing as the control and not the worsening in dispersion observed. In addition as no secondary phase was observed in the microscopy analysis, this theory is less likely.

During manufacture of these composites some issues were identified with processing for each of the additives. Low melting point of the H-Si 6440 P meant that the additive melted in the feed zone of the extruder once it hit the screws and the barrel. This prevented the material from being conveyed forwards resulting in the accumulation of the material in the feed throat causing inconsistent feeding. The use of TOTM caused similar feeding issues, however there is a scope to control this by optimising the additive to tubular clay ratio. A major issue with TOTM was the fuming at the die which poses a significant health and safety risk. These issues make both additives unsuitable for application in the film making process.

The suitability of a third additive, Tegomer DA 626, was evaluated on a different screw configuration with the results shown in Figure 8.19. Similarly to TOTM, an improvement in dispersion was observed with the use of Tegomer DA 626 dispersive aid. In order to improve material handling and minimise the risk of feeding issues the loading of the tubular clay was doubled to 10 $\%_{\mathrm{wt}}$.

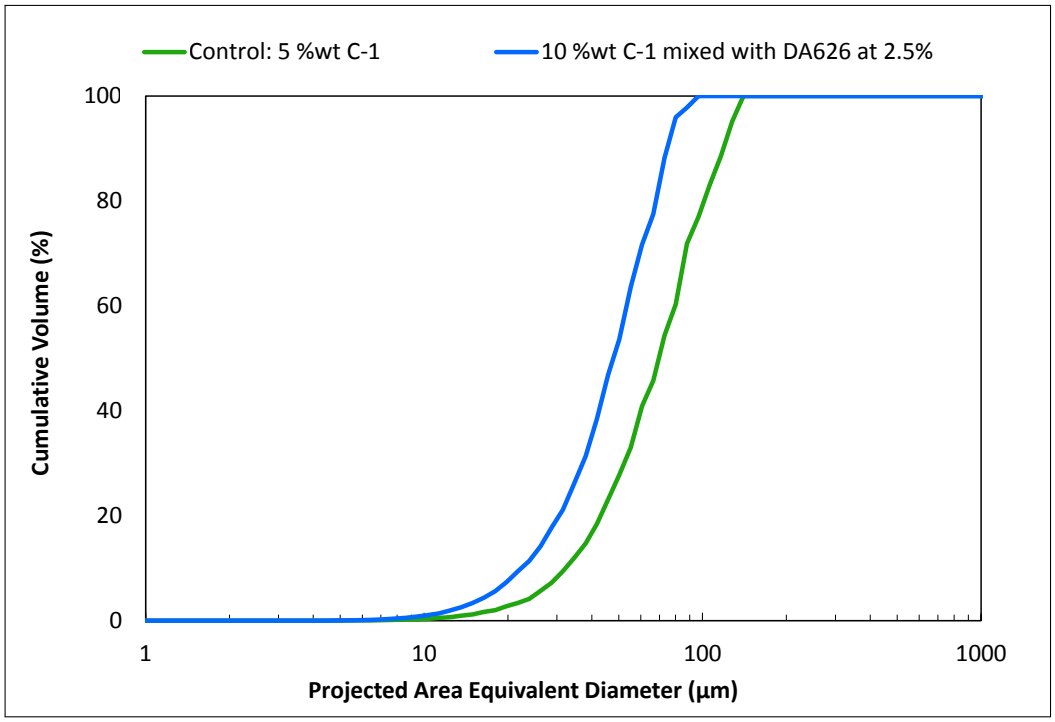

Figure 8.19: *Dispersion of 10 $\%_{wt}$ tubular clay (C-1) with Tegomer DA 626 in H-PET composites; manufactured on the Dr Collin ZK25 machine fitted with Configuration 5 screw configuration via the premix method at 6* $\mathrm{kg\,h^{-1}}$ *and 240* rpm

Although this additive did not cause any fuming and offered stable feeding, there were some changes in the product including colour. There is also significant concern about the stability of such additives within the system. A risk that with time the low viscosity dispersive aids may migrate to the film surface leading to the failure in product function does exist. A more in depth study would have to be run to identify if any dispersive aid could be used without compromising the function of the product. As such research would have to be undertaken for each additive/polymer system, the current business preference lies in optimising the screw profile to obtain the correct level of dispersion. This has been addressed in Appendix J.

8.1.3.3 Quantifying the strength of interactions

In addition to modifying the interaction between the additive and the polymer, an attempt was made to quantify the strength of these interactions. The work of adhesion between the additive and the polymer was estimated based on the polar and dispersive components

of the surface energy for the polymer and the additive. The thermodynamic parameter is a measure of work required to separate an interface between substances A and B into independent surfaces A and B. The background theory for wetting and surface energies is provided in Appendix G.

The polar and dispersive components for the surface energy of the powder additives were calculated based on Fowke's method. The powders were initially pressed into disk form with a powder press applying 10 $\mathrm{t\,cm^{-2}}$ of force to generate a flat surface whilst removing the porosity contained within the poured powder; see Figure 8.20.

Figure 8.20: *Example of disks produced though powder pressing*

The dispersive component of the surface energy was calculated on the basis of the value of the contact angle formed when a drop of liquid which only has a dispersive component to the surface energy, in this case diiodomethane, was placed onto the additive surface. The contact angle was measured with the use of a goniometer and based on an average of 3 measurements. As the dispersive component of the surface energy for diiodomethane is known to be $\Gamma_{DI} = \Gamma^d_{DI} = 50.8\ \mathrm{mN\,m^{-1}}$ (Zenkiewicz, 2007), the dispersive component for the additive could be calculated from Equation 8.1:

$$\Gamma_{Ad} = \Gamma^d_{Ad} = 0.25 \cdot \Gamma_{DI} \left(1 + \cos\theta_{Ad,DI}\right)^2 \tag{8.1}$$

where Γ^d_{Ad} is the dispersive component of the surface tension for the additive in $\mathrm{mN\,m^{-1}}$,

Γ_{DI} surface tension of diiodomethane in $\mathrm{mN\,m^{-1}}$, and $\theta_{Ad,DI}$ is the contact angle formed between drop of diiodomethane and the additive surface in degrees.

Once the dispersive component of the surface energy was obtained for the additive, the polar component could be calculated from Equation 8.2 though the measurement of contact angle with a liquid which has both a polar and a dispersive component to the surface tension, in this case water. The polar and dispersive components for water were reported as $\Gamma^p_W = 50.7$ and $\Gamma^d_W = 22.1\ \mathrm{mN\,m^{-1}}$ by Wu, 1971 yielding an overall surface tension of $\Gamma_W = 72.8\ \mathrm{mN\,m^{-1}}$.

$$\Gamma^p_{Ad} = \frac{\left[0.5 \cdot \Gamma_W \left(1 + \cos\theta_{Ad,W}\right) - \left(\Gamma^d_{Ad}\Gamma^d_W\right)^{0.5}\right]^2}{\Gamma_W} \tag{8.2}$$

where Γ^p_{Ad} and Γ^d_{Ad} are the polar and dispersive components of surface tension for the additive in $\mathrm{mN\,m^{-1}}$, Γ^d_W and Γ^d_W is the dispersive component and the overall surface tension for water in $\mathrm{mN\,m^{-1}}$ and $\theta_{Ad,W}$ is the contact angle formed between drop of water and the additive surface in degrees.

The work of adhesion between the additive and the polymer can be estimated based on harmonic mean equation proposed by Wu, 1971 or the geometric mean proposed by Owens and Wendt, 1969. The harmonic mean is reported here, although both were determined in the analysis; see Equation 8.3. Once the work of adhesion is known, the contact angle formed when a droplet of polymer is placed on the additive can be estimated and used as an indication of wetting.

$$W_{Ad,PET} = 4\left[\frac{\Gamma^d_{Ad}\Gamma^d_{PET}}{\Gamma^d_{AdV} + \Gamma^d_{PET}} + \frac{\Gamma^p_{Ad}\Gamma^p_{PET}}{\Gamma^p_{Ad} + \Gamma^p_{PET}}\right] \tag{8.3}$$

The polar and dispersive components for the surface energy of PET are well known with values of $\Gamma^p_{PET} = 4.1\ \mathrm{mN\,m^{-1}}$ and $\Gamma^d_{PET} = 43.2\ \mathrm{mN\,m^{-1}}$ being reported by Owens and Wendt, 1969.

This method does have some errors associated with it. These can arise either from the measurement of the powder surface tension components or the assumed temperature independence of the parameter for both the polymer and the additive.

Errors in the measurement of the additive surface tension occur if all the porosity is not removed during pressing. As a result with hydrophilic additives the liquid can be rapidly drawn into the powder disk making the contact angle measurement very difficult and inaccurate. There is also a smaller concern associated with fine particles being drawn up into the liquid droplet and thus influencing the interactions between the additive and the liquid. Other methods are available such as the Washburn method, which is discussed in Appendix G, which relies on liquid being drawn up into a column of powder with the rate or the final height achieved being related to the contact angle. This method relies on having similar packing density between various samples and requires specialised equipment for preparing the samples and measurement of the rate of liquid rise which were not available at DTF. A more novel technique of inverse gas phase chromatography can also be utilised to obtain the surface tension components. Both of these techniques were deemed too complex for the initial proof of concept work carried out here.

The second level of complexity arises from the temperature dependence of the surface tension, particularly the polar component. To account for this the measurements would need to be performed at the temperature of interest, which for 285 °C would require very specialised equipment. Another possibility is to account for the change post measurement as proposed by Cardinaud, 2013. Although this could be done for PET, it would be very difficult to account for the changes in the surface tension of the additives as the critical parameters would not be available in the cases of novel additives.

Table 8.5 shows the estimated work of adhesion between the whitener and PET matrix as well as the tubular clay and the polymer matrix. Surprisingly, the estimated values were very similar and thus did not explain the differences in mixing observed.

Table 8.5: *Estimated work of adhesion between polymer matrix and whitener, tubular clay and silica additives*

Additive Grade	C-1	W-5	Silica
Work of Adhesion ($mN\,m^{-1}$)	88	86	110[†]

[†]from Γ values reported in Kimura et al., 2000

Further investigation into potential differences between the two systems found that the measured IV losses for composites manufactured at ca. 400 rpm and 6 $kg\,h^{-1}$ on the *Dr Collin ZK25* machine were far more significant in the tubular clay system. The IV loss for tubular clay was around 46 % and for the whitener system approximately 16 % which at a shear rate of 100 s^{-1} translate to shear stress of 0.8 kPa and 7.2 kPa. As a result of the higher shear stresses in the whitener system the dispersion in is much more effective. The excessive IV losses are associated with the high level of moisture in the tubular clay.

This should not disregard the importance of the work of adhesion does in determining the level of mixing. Typically during manufacture of PET composites filled with silica, a similar level of IV losses can be realised; see Figure 8.13. However, the much higher work of adhesion (see Table 8.5) combined with a easier to disperse spherical shape of the particles means that effective dispersion of the silica can be achieved within PET composites.

8.2 Concluding Remarks

Additive and polymer properties both play a critical role in determining the level of additive mixing achieved within the polymer composite produced. Publications exist around the role of polymer viscosity e.g. Vaia et al., 1995, Villmow et al., 2008, and Kasaliwal et al., 2011, however there is limited information on the role of additive properties e.g. Bart, 2006. This is especially true for PET based composites manufactured via a twin screw extrusion process. In this chapter the results of an extensive compounding study are presented; focusing on the dispersion of flame retardants, silica, tubular clays, and

whiteners in a high molecular weight PET and a lower molecular weight PET substrate.

The work presented here showed that good dispersion of the FR additives was achieved for particles ranging from 1 to 10s of microns in size. The impact of particle shape was also considered, with little difference being observed between the spherical and the longest aspect ratio whitener additives. In agreement with Bart, 2006, an increased difficulty in dispersing the additive was seen with increasing aspect ratio of the filler. No direct affect from the additive porosity on the level of dispersion was found. However, the porosity was significant in determining some critical process limitations such a the maximum loading of the additive and nature of the additive injection point.

Polymer viscosity was found to be an critical parameter which had a significant impact on the level of dispersion achieved. Kasaliwal et al., 2011; Vaia et al., 1995 reported better dispersion of nanoclays and MWCNTs respectively in lower viscosity polymers due to improved polymer infiltration of the agglomerate structure. In the case of the flame retardant additive in the PET matrix, higher viscosity lead to the generation of larger hydrodynamic stresses and a more effective dispersion via rupture mechanism.

Lastly the interactions between the additive and the polymer matrix were also considered. Dispersive aids were evaluated as a potential method of modifying the interactions in order to facilitate better dispersion. This was shown to be effective by Fortunato et al., 2014 for the dispersion of TiO_2 in PET. Although the use of liquid dispersive aids premixed with the additive powder proved promising in delivering better mixing there are some significant drawbacks in their use. Dispersive aids in pellet form were found to decrease the mixing efficiency of the system. Gao et al., 2011 showed the significance of the interactions between $BaSO_4$ and the PET matrix through the surface modification of the additive. In this chapter, a method was proposed to quantify and estimate the strength of the interaction between the additive and the polymer through the calculation of the work of adhesion. Further developments to the method can be made, however the initial work showed the potential use of such a technique.

9 | Impact of operating conditions on degree of mixing

The intrinsic properties of the polymer and the additive determine the interactions between the two components as well as those within the components themselves. Thus, the properties of the two components directly influence the ease with which the two will mix; as discussed in Chapter 8. Similarly, the design of the co-TSE geometry is the intrinsic property of the mixing equipment, thus defining its capacity for delivering effective mixing. The operating conditions on the other hand define a process window and provide a level of control over the degree of mixing within this operating space. This allows for slight adjustments in the mixing quality to be made depending upon product requirements. It should be noted that as a result of upstream and/or downstream equipment limitations the actual operating window may be significantly smaller than the extrusion equipment process window.

Changes in the *directly controllable* machine parameters i.e. throughput, screw speed, machine torque and barrel temperatures, directly induce changes in the *calculated* parameters. These are specific throughput, degree of fill, specific mechanical energy input, residence time and corresponding distribution, as well as the shear rate and stress; and can be much more easily related to the different stages of mixing as well as the mixing mechanisms discussed in Section 2.4. The other parameters include the set up of the machine, namely the nature of the additive injection method as well as parameters set by the recipe of the product e.g. additive loading within the polymer composite/blend.

The works of Donoian and Christiano, 1999; Fortunato et al., 2014; Villmow et al., 2008 and particularly that of Domenech et al., 2011; Kasaliwal, 2011 provide a good overview for the role of the individual parameters in determining the degree of dispersion achieved. The findings reported in these and others are discussed in detail within Appendix H.

The research presented here, focuses on the understanding which of these parameter can offer the greatest amount of control over the level of mixing achieved in the PET matrix. This system poses additional challenges due to the potential viscosity reduction along the length of the extruder as a result of moisture induced hydrolysis and more importantly mechanically induced chain scission; see Chapter 7. The reduction in the viscosity leads to a lower hydrodynamic stresses being transferred to the agglomerates and thus limit the dispersion via the likely dominant rupture mechanism. As a result, a limit on the degree of control over the level of dispersion that achieved as a result of the changes in the operating conditions is almost certain.

9.1 Results

A number of experiments were undertaken on the *Berstorff ZE40A* and the *Dr Collin ZK25* machines with various additive/polymer combinations; some of the relevant results are discussed here. For the purpose of this section, it is vital to acknowledge that the *Dr Collin ZK25* machine is smaller in diameter (25 mm vs 40 mm), longer (42 $^{L}/_{D}$ vs 28 $^{L}/_{D}$) and most importantly has much more severe screw configuration with total mixing element length of 11.5 vs 4.5 $^{L}/_{D}$ over *Berstorff ZE40A* machine. Further information on equipment set up and materials used is given in Chapter 5 and 8 respectively. Where possible, for continuity, the reported results are from the same equipment set up and are based on the same additive-polymer composite, with the additional results appearing in the Appendices.

9.1.1 Effect of controllable parameters on mixing

As previously discussed, changes in controllable parameters can be used on the manufacturing line to fine tune the mixing performance of a particular screw configuration. The effectiveness of each of these parameters is discussed below.

9.1.1.1 Screw speed

Screw speed is the most important parameter as it offers the greatest degree of control over the twin screw extrusion process, influencing the minimum, average and peak shear rate as well as the residence time. All of these have an impact on mixing as well as the polymer matrix itself. Film grade (S-PET) and bottle grade (H-PET) composites containing FR-1 additive were manufactured on the *Berstorff ZE40A* and *Dr Collin ZK25* equipment to examine the degree of control that this parameter offers over mixing.

Figure 9.1a shows the cumulative volume weighted particle size distributions for FR-1 in H-PET composites manufactures on the *Berstorff ZE40A* machine (via *split feed* method) at different screw speeds. As the speed increases from 122 to 300 rpm the PSD shifts to the left indicating smaller particles and thus superior dispersion at higher screw speeds.

Figure 9.1b shows how the mean (which is influenced by the larger agglomerates, unlike the D_{50}) and the 90^{th} percentile (D_{90}) of the volume weighted PSDs change with increasing screw speed for FR-1 composites based on the S-PET and H-PET substrate. In both substrates the increase in screw speed leads to a reduction of the mean and D_{90} of the distributions indicating improved dispersion at higher speeds. Interestingly, the rate of particle size reduction with speed appears to be very similar for both S-PET and H-PET indicating the dependence of the dispersion mechanism on shear rate. H-PET composites consistently have smaller particle size showing the importance of material viscosity in dispersion of particles and hence shear stress achieved within the system. This effect will be discussed elsewhere.

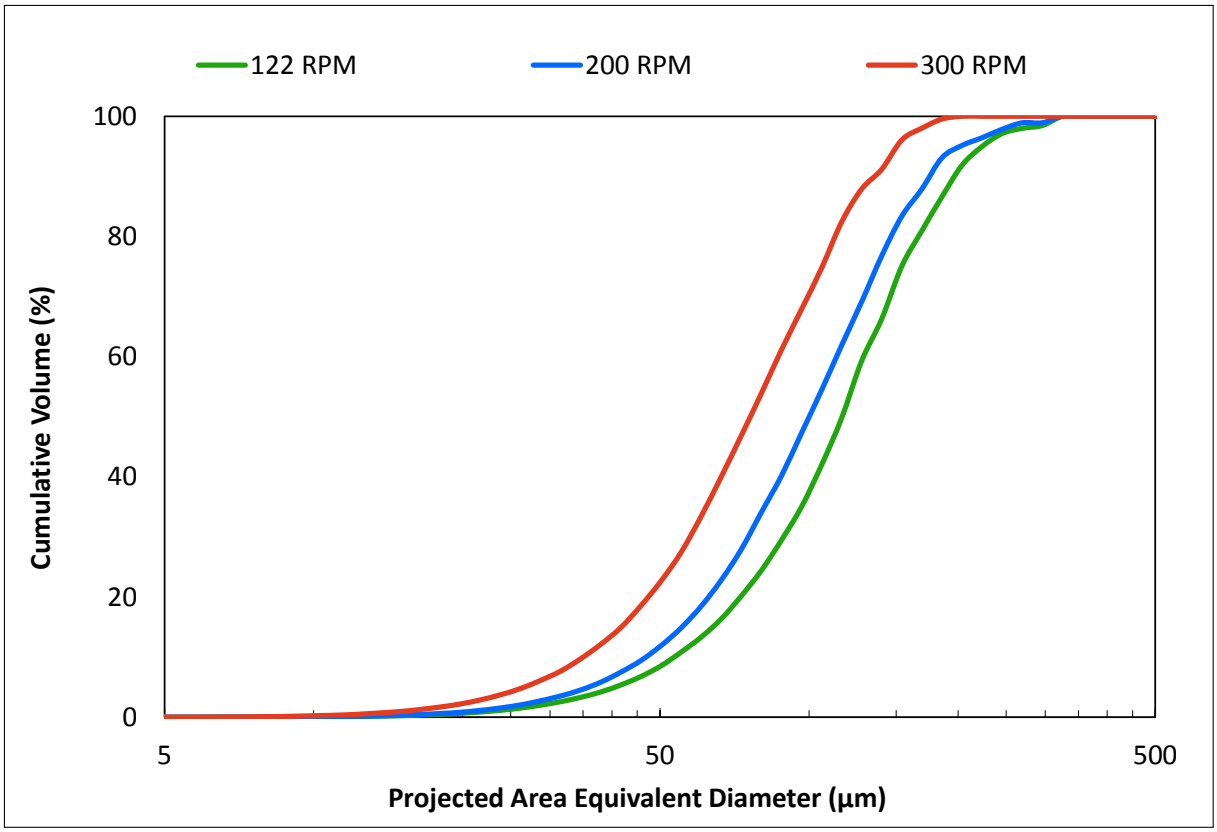

(a) PSDs of FR-1 at 5 $\%_{wt}$ in H-PET composite extruded at 60 $\mathrm{kg\,h^{-1}}$

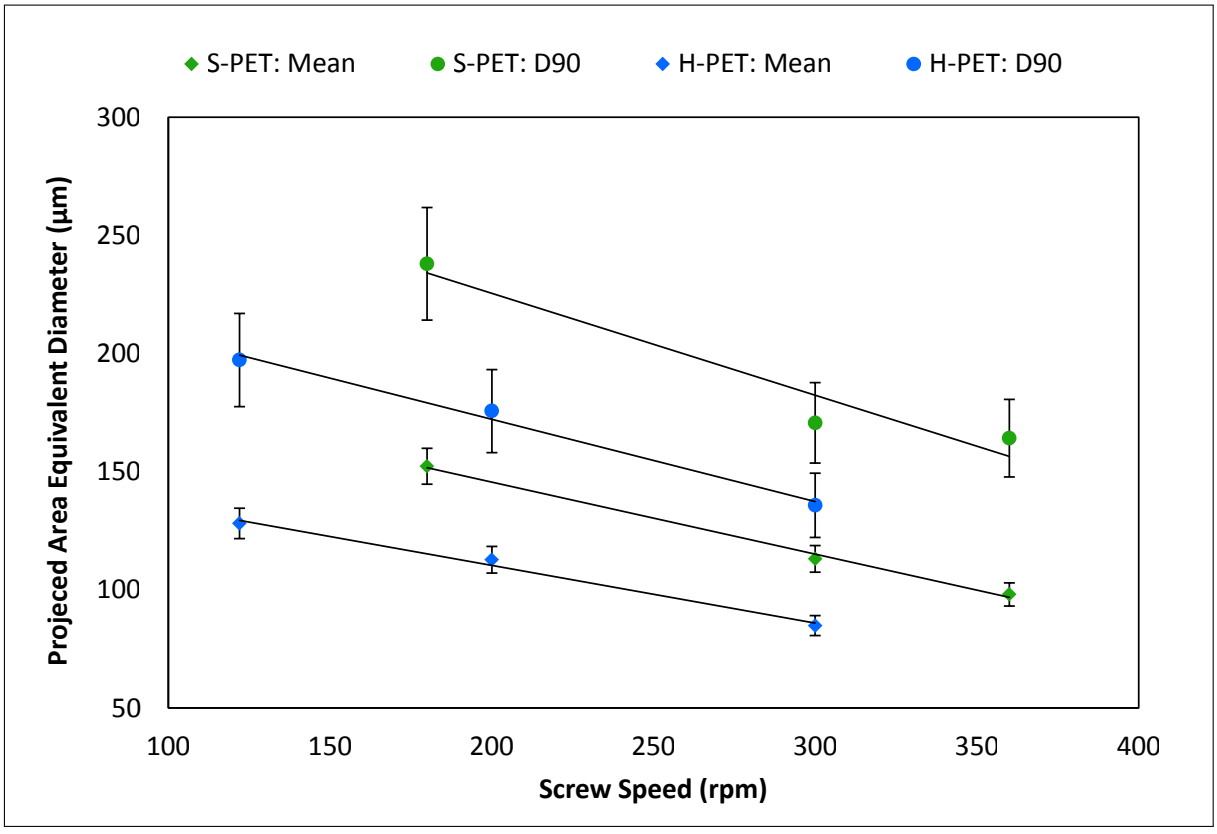

(b) Mean and D_{90} of volume distribution for FR-1 at 5 $\%_{wt}$ in S-PET and H-PET composites extruded at 60 and 90 $\mathrm{kg\,h^{-1}}$ respectively

Figure 9.1: *Effect of screw speed on FR-1 composites manufactures on Berstorff ZE40A machine; PSDs obtained by by transmitted light microscopy at x2.5 magnification.*

From Figure 9.2 it is evident that the increase in screw speed leads to increased molecular weight loss of the polymer substrate. This not only reduced the dispersive mixing efficiency by lowering the viscosity of the material and limiting the stress which can be transferred to agglomerates, but also leads to a reduction in the mechanical properties of the composite. It is interesting that the rate of IV loss appears similar for both S-PET and H-PET substrate suggesting a dependence on shear rate. This combined with the increased losses for H-PET indicating a dependence on initial material viscosity suggests that the IV losses are occurring as a result of shear stress applied to the polymer. These aspects are discussed further in Chapter 7.

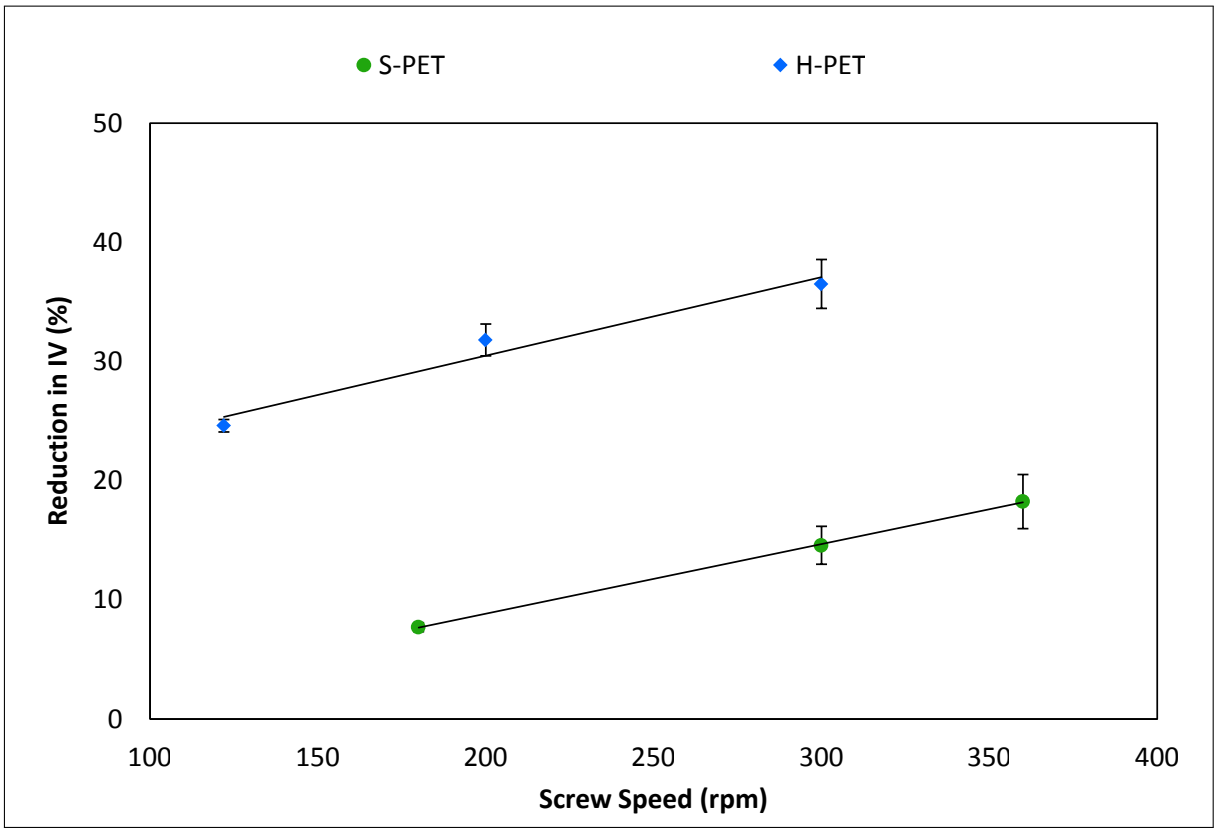

Figure 9.2: *Effect of screw speed on polymer IV in S-PET and H-PET composites containing FR-1 at 5 $\%_{wt}$.*

A more extensive investigation was undertaken on the *Dr Collin ZK25* equipment. Here, the H-PET composites containing FR-1 additive at 5 $\%_{wt}$ loading were run at 5 different screw speeds. Figures 9.3a and 9.3b show how the discrete and cumulative volume distributions change as a result of increased screw speed.

As the screw speed is increased two different yet simultaneous changes are occurring. Firstly, there is an increase in the volume fraction (and hence the number) of the smaller sized particles ($<$ 10 µm); see Figure 9.3a. This is a direct result of the increased minimum, average and peak shear rates which lead to increased dispersion via the *erosion* mechanism. Here, the drastic increase in shear rate overrules the affect of reduction in residence time associated with increase in screw speed which should theoretically lead to a reduction in the slower erosion process. Secondly, there is a reduction in the number of the larger sized agglomerates illustrated by the shift in the top end of the cumulative distribution to the left; see Figure 9.3b. This indicates increased effectiveness of dispersion via *rupture* mechanism, also caused by the increase in minimum, average and most importantly peak shear rate; see Table 9.1 for shear rate data.

Table 9.1: *Calculated shear rates for Dr Collin ZK25 machine at different screw speeds; calculated via the model derived in Chapter 6*

Screw speed (rpm)	100	190	290	350	420
Minimum shear rate, $\dot{\gamma}_{min}$ (s^{-1})	47	89	136	164	196
Residence time weighted average shear rate, $\dot{\gamma}_{av,RTD}$ (s^{-1})	70	173	304	387	484
Maximum shear rate, $\dot{\gamma}_{max}$ (s^{-1})	262	497	759	916	1100

As the shear rate increases, the shear stresses increases accordingly allowing for the larger cohesive forces of the smaller agglomerates to be overcome leading to their rupture. However the reduction in D_{90} ceases at 290 rpm showing a small increase going from 350 to 420 rpm. A closer examination of the 420 rpm PSD shows a cross over point at around 15 µm particle size, with the lower end of the distribution shifting to the left due to increased effectiveness of the erosion mechanism and the top end of the distribution shifting to the right indicating decreasing effectiveness of the rupture mechanism. This decreased effectiveness is a likely result of the of the mechanically induced polymer chain scission (discussed in Chapter 7) which leads to a reduction in polymer viscosity. This process is thought to take place in the melt zone where the shear stresses are the highest meaning that an additive is introduced into a lower viscosity polymer at the higher screw speeds.

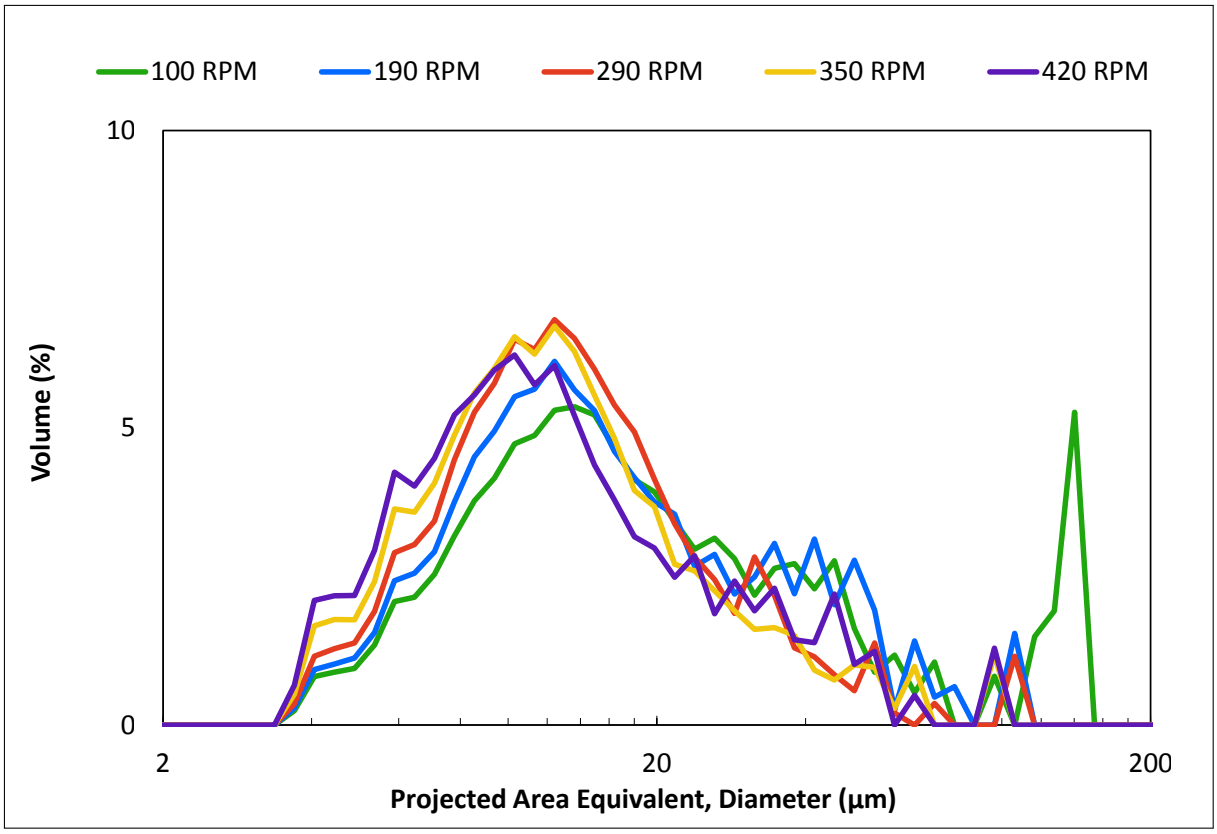

(a) Discrete volume weighted PSD

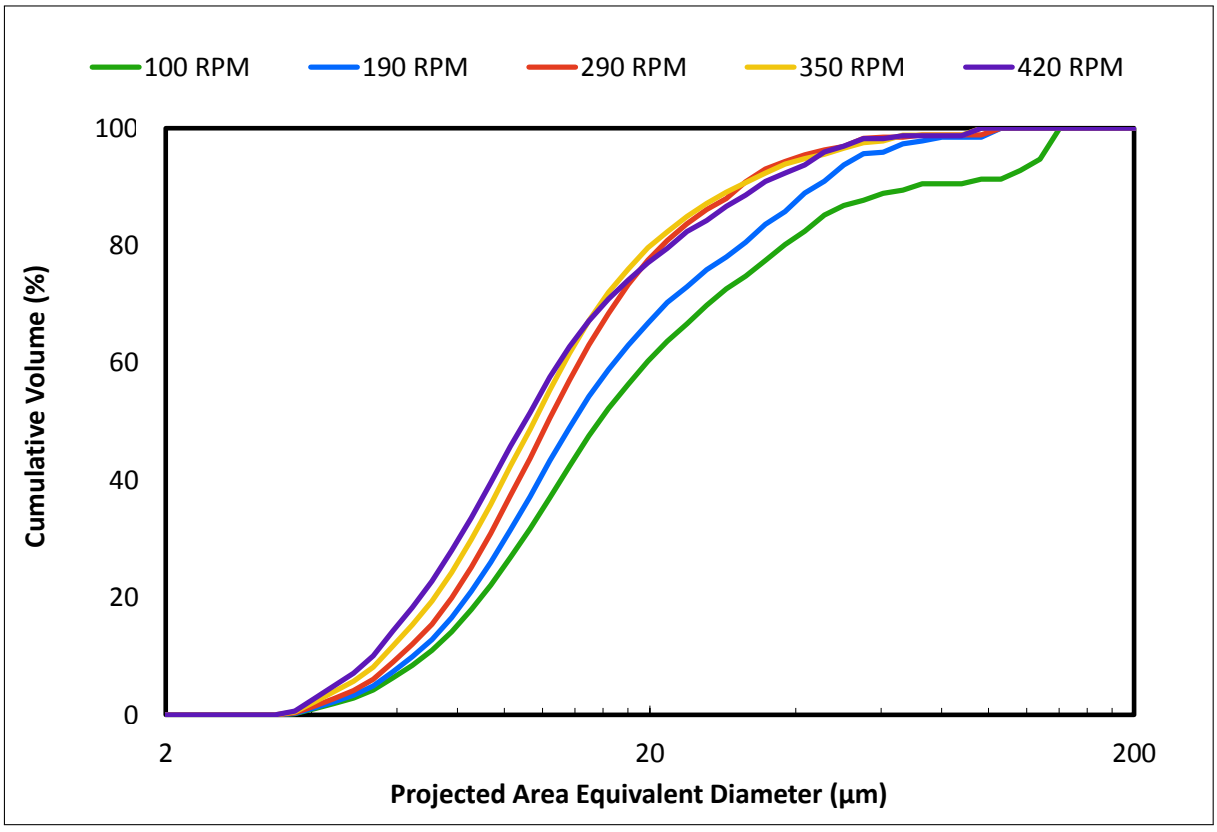

(b) Cumulative volume weighted PSD

Figure 9.3: *Effect of screw speed on FR-1 composites (5 $\%_{wt}$ in H-PET) manufactured on Dr Collin ZK25 machine at 6 $\mathrm{kg\,h^{-1}}$ via the premix method; PSDs obtained by transmitted light microscopy at x5 magnification.*

As a result, even though the screw speed increase raises the shear rate, the shear stresses delivered to the particles are lower reducing the effectiveness of dispersion via a rupture mechanism.

Figure 9.4a shows the measured IV losses corresponding to the results discussed. The results do not show a clear trend, apart from the three higher screw speeds delivering a higher IV loss and hence melt viscosity loss. Figure 9.4b shows the IV as a function of screw speed for unfilled PET processed on the *Berstorff ZE40A* machine. Here a linear trend is evident, which would support the theory proposed to explain the diminishing effectiveness of the rupture mechanism at higher screw speeds. There are two possible explanations for the reason why no clear trend exists in Figure 9.4a. Firstly, the polymer had to be pre-dried in order to be processed on the *Dr Collin ZK25* machine as there is no venting which could potentially mean that the polymer entered the process with varying moisture content, with hydrolysis leading to different IV losses. Secondly and most likely, the lack of trend is due to the accuracy of the IV measurement which is sensitive to additive content within the sample. Here, poor distributive mixing leading to slight variations would lead to different IV losses as a result of the wrong correction factor being used to calculate the results for the polymer alone.

The same trend was observed in H-PET composites containing the flame retardant FR-3 additive. The effects of screw speed on S-PET composites containing S-3 silica additive were more difficult to distinguish as the additive is very well mixed and therefore any changes in screw speed had minimal effects. The results can be found in Figures I.1 and I.2 contained within the Appendix I.

Furthermore, the work presented in Appendix J shows an existence of a limiting state which appears to be consistent over different screw configurations which occurs at differing screw speeds. This suggests that once a certain size is reached the stresses required to break these agglomerates can not be generated or effectively transferred to the agglomerate within the machine.

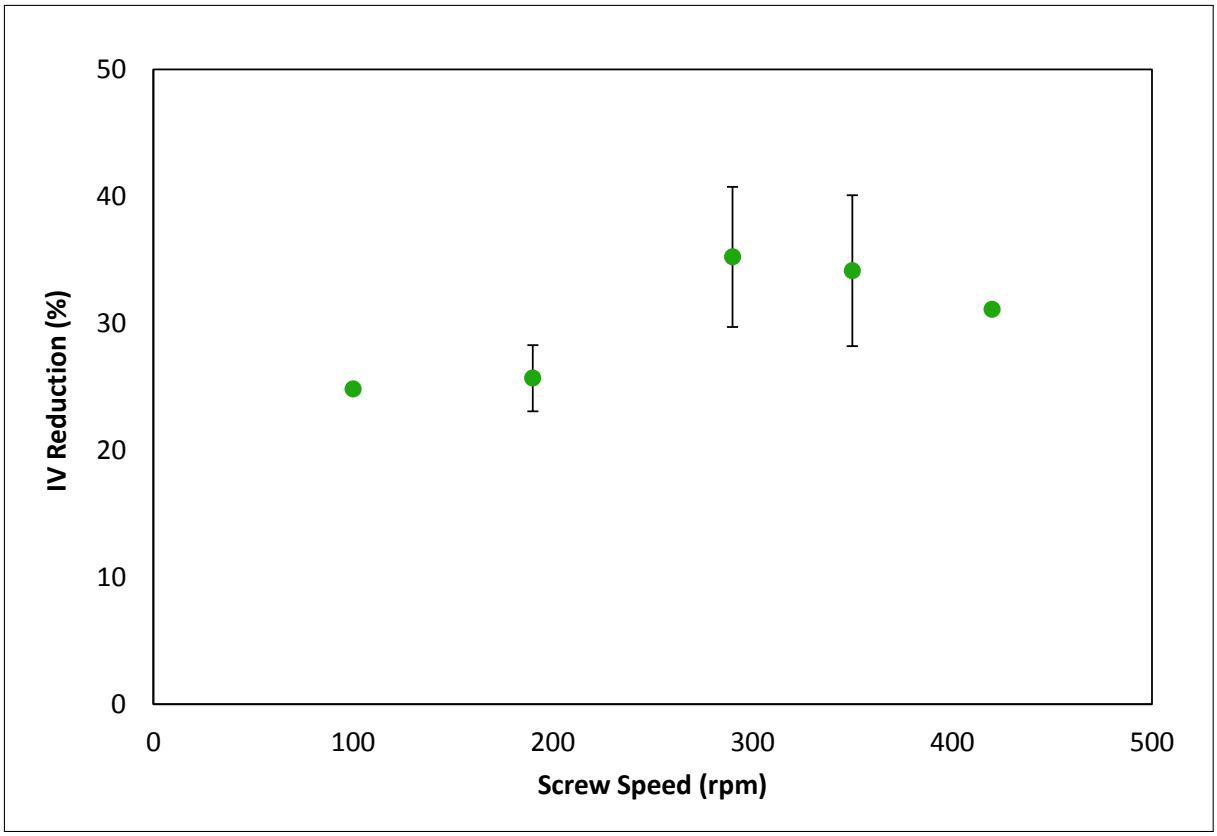

(a) IV vs screw speed for H-PET/FR-1 composites manufactured at 6 $\mathrm{kg\,h^{-1}}$ *via premix method*

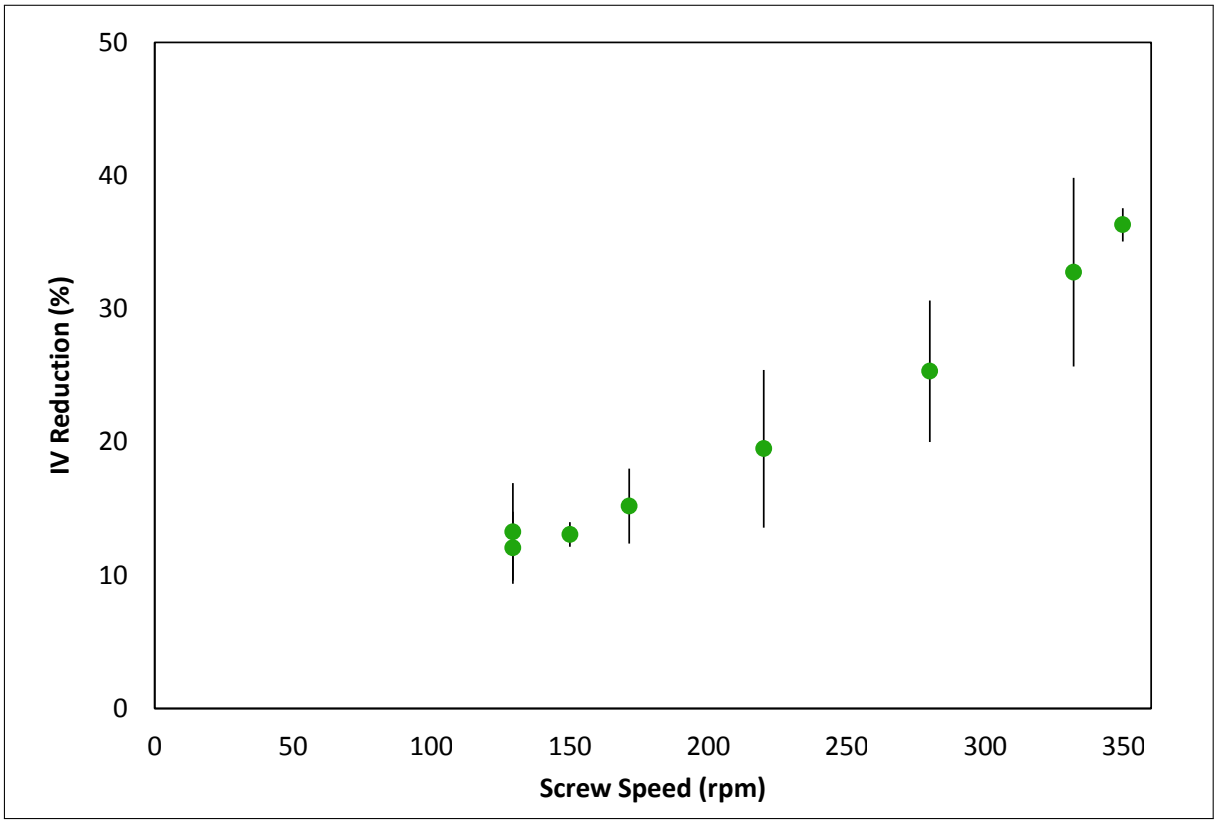

(b) IV vs screw speed for unfilled H-PET manufactures on the Berstorff ZE40A machine at 60 $\mathrm{kg\,h^{-1}}$

Figure 9.4: *IV vs screw speed; error bars denote 90 % confidence interval based on student t distribution*

9.1.1.2 Output

Several experiments were undertaken to investigate the impact of extruder output on the degree of mixing within polymer composites. Figure 9.5 shows how changes in output on the *Berstorff ZE40A* machine affected the mixing in S-PET/FR-1 composites. It is evident that in this case reducing the extruder output increased the level of dispersive mixing with the PSD shifting towards the left; indicating the increased number of smaller particles. Interestingly the D_{90} remained relatively similar in all cases showing that the peak shear stress achieved was not significantly different; see associated polymer IVs in Table 9.2 which remained almost identical at all conditions. Hence, the dispersion via rupture mechanism was not improved significantly.

Table 9.2: *IV results for the extruder output experiments conducted on Berstorff ZE40A machine*

Screw speed rpm	**Output** $kg\,h^{-1}$	**Specific output** $kg\ h^{-1}\ rpm^{-1}$	**Residence time** s	**IV loss** %
300	60	0.20	33.9	19.45 ± 1.5
300	90	0.30	28.0	14.57 ± 1.6
360	90	0.25	24.5	18.24 ± 2.3
360	120	0.33	22.5	19.51 ± 2.4

Based on this it can be said that the improvements in mixing can be associated with increased effectiveness of the erosion mechanism. This can be associated with two aspects. The first (but the least likely) explanation is it increased as a result of the increased residence time. As can be seen in Table 9.2 the mean residence times, as predicted by the model discussed in Chapter 6, are relatively short and the relatively small change in output does not significantly change it. That is not to say that the residence time does not have an effect, since although the mean does not change significantly the change in the fully filled sections of the extruder would be much greater. Here, an increase in output would reduce the dwell time reducing the number of times the polymer passes through the high shear region and thus reducing the number of particles being dispersed.

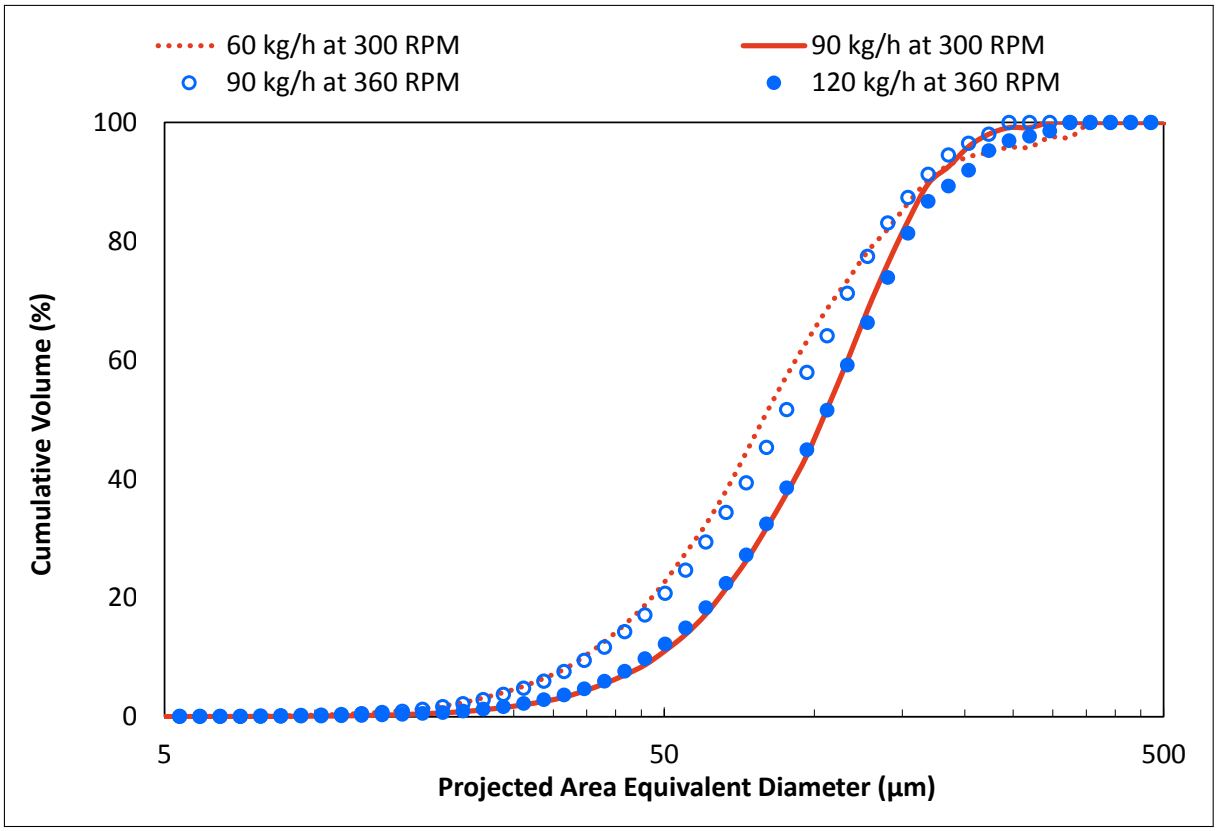

Figure 9.5: *Effect of extruder output on mixing in S-PET composites containing FR-1 at 5 $\%_{wt}$ extruded at 300 and 360 rpm on the Berstorff ZE40A machine.*

The most likely reasoning behind the increased effectiveness of the erosion mechanism is the change in the average degree of fill within the extruder which in turn changes the average shear rate to which the polymer is exposed. At 300 rpm, a 30 $\mathrm{kg\,h^{-1}}$ reduction in output reduces the specific output by 0.1 $\mathrm{kg\,h^{-1}\ rpm^{-1}}$, which corresponds to average degree of fill reducing from 42.3 to 32.9 %. Similarly, the same reduction in output leads to ca. 0.1 $\mathrm{kg\,h^{-1}\ rpm^{-1}}$ in specific output at 360 rpm, corresponding to the average degree of fill reducing from 43.8 to 35.6 %. These two similar changes in the degree of fill, together with their absolute values explain why the resultant PSDs at different screw speeds are so similar.

A similar result was obtained when examining the impact of output on the manufacture of H-PET composites containing FR-1 additive at 5 $\%_{\mathrm{wt}}$ produced on the *Berstorff ZE40A* machine and in the manufacture of S-PET composites containing S-3 additive on the *Dr*

Collin ZK25 machine (see Appendix I).

The opposite trend was observed in the case of H-PET composites containing FR-3 additive at 5 $\%_{wt}$ which were manufactured on the *Dr Collin ZK25* machine. Here, increased extruder output leads to better mixing results especially in the high screw speed scenario; see Figure 9.6.

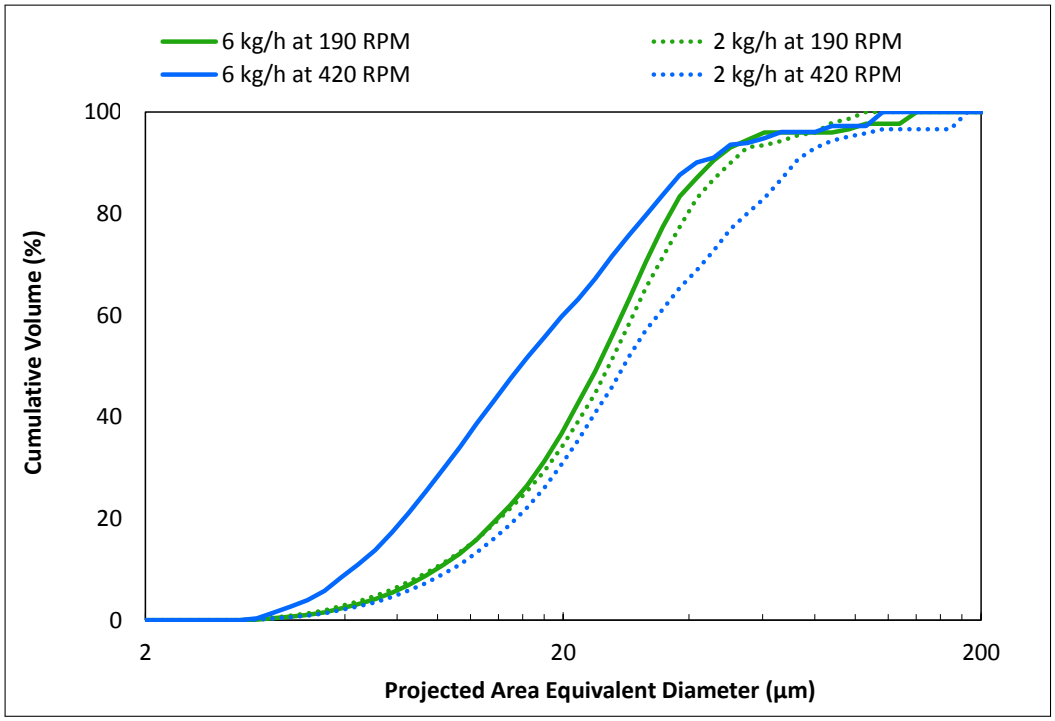

Figure 9.6: *Effect of extruder output on mixing in H-PER composites containing FR-3 additive at 5 $\%_{wt}$ manufactured on the Dr Collin ZK25 machine using premix method*

This can be explained by IV loss. Unlike with composites produced on the *Berstorff ZE40A* machine, the composites manufactured on the *Dr Collin ZK25* machine have considerable differences in the final polymer IV values with greater output reducing the IV loses significantly; see Table 9.3.

Although, the improved final IVs explain the lower D_{90} on the higher output samples, they do not account for the improved erosion mechanism and higher numbers of smaller particles. The poorer mixing at the lower outputs is a probable result of very low degree of fill in the side feeder addition zone, which leads to incomplete wetting of the filler and

Table 9.3: *IV results for the H-PET composites containing FR-3 additives manufactured at different extruder outputs on Dr Collin ZK25 machine*

Screw speed rpm	**Output** $kg\,h^{-1}$	**Specific output** $kg\ h^{-1}\ rpm^{-1}$	**IV loss** %
190	2	0.011	27.0 ± 1.7
190	6	0.032	20.7 ± 1.4
420	2	0.005	39.8 ± 4.4
420	6	0.014	26.3 ± 1.3

results in larger agglomerates which have to be broken down in the extrusion process. This is most evident in the case of higher screw speeds where the specific output of 0.005 and 0.014 $kg\,h^{-1}\ rpm^{-1}$ correspond to an average degree of fill of only 9 and 18 %.

9.1.2 Effect of calculated parameters on mixing

Based on the data presented investigating the impact of controllable parameters the effect of calculated parameters was also considered in order to better understand the fundamental principles of mixing.

9.1.2.1 Specific output and degree of fill

As disused, one of the key calculated parameters is the specific output of the TSE machine. It can be correlated to the average degree of fill within the extruder which in turn influences the average shear rate that the polymer sees during processing. See Figure 7.11 and Chapter 6 for details. Figure 9.7, shows the mean projected area equivalent diameter of particles within the PET composites linearly decrease with decreasing specific output. Such a trend is true for both S-PET and H-PET composites, and most interestingly the results from both can be approximated by the same line of best fit. This is surprising, as Figure 9.1b clearly showed that at the same screw speed better dispersion was achieved using a H-PET substrate for the composite.

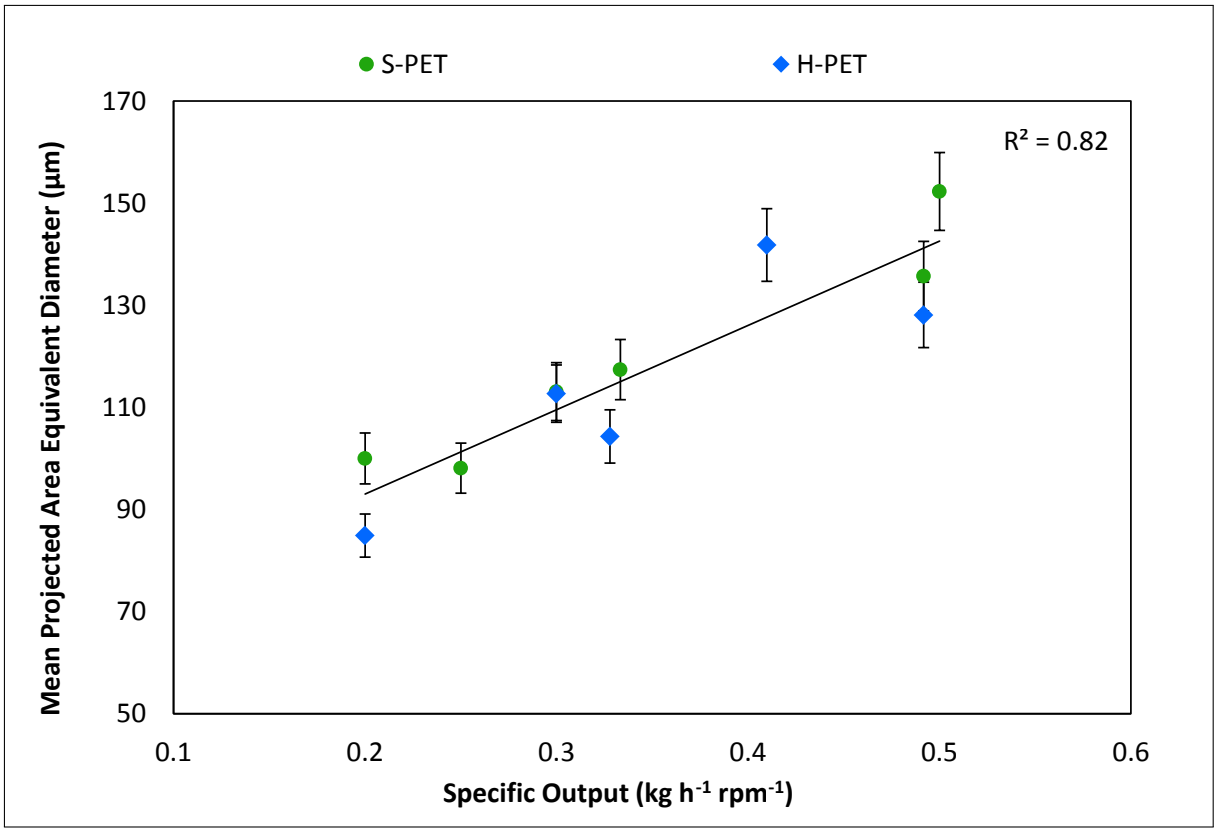

Figure 9.7: *Effect of specific output on mixing in S - PET and H-PET composites containing FR-1 additive at 5 $\%_{wt}$ manufactured on the Berstorff ZE40A machine using split feed addition method*

This exaggerated difference in performance is a result of the different outputs used to generate the screw speed correlations. While the viscosity of the polymer does have an effect, the output also plays a role. In H-PET, a projected area equivalent volume weighted mean diameter of 85 µm was achieved at 300 rpm and 60 kg h^{-1} (specific output of 0.2 kg h^{-1} rpm^{-1}). Under the same conditions a mean diameter of 100 µm was achieved in S-PET. Unfortunately this is the only data point with the specific outputs being identical; a consequence of the limitations in the operating window of the machine.

More revealing results about the impact of specific output were obtained through the analysis of experiments conducted on the *Dr Collin ZK25* machine. Figure 9.8a and 9.8b shows the results for H-PET composites containing FR-1 and FR-3 additives respectively.

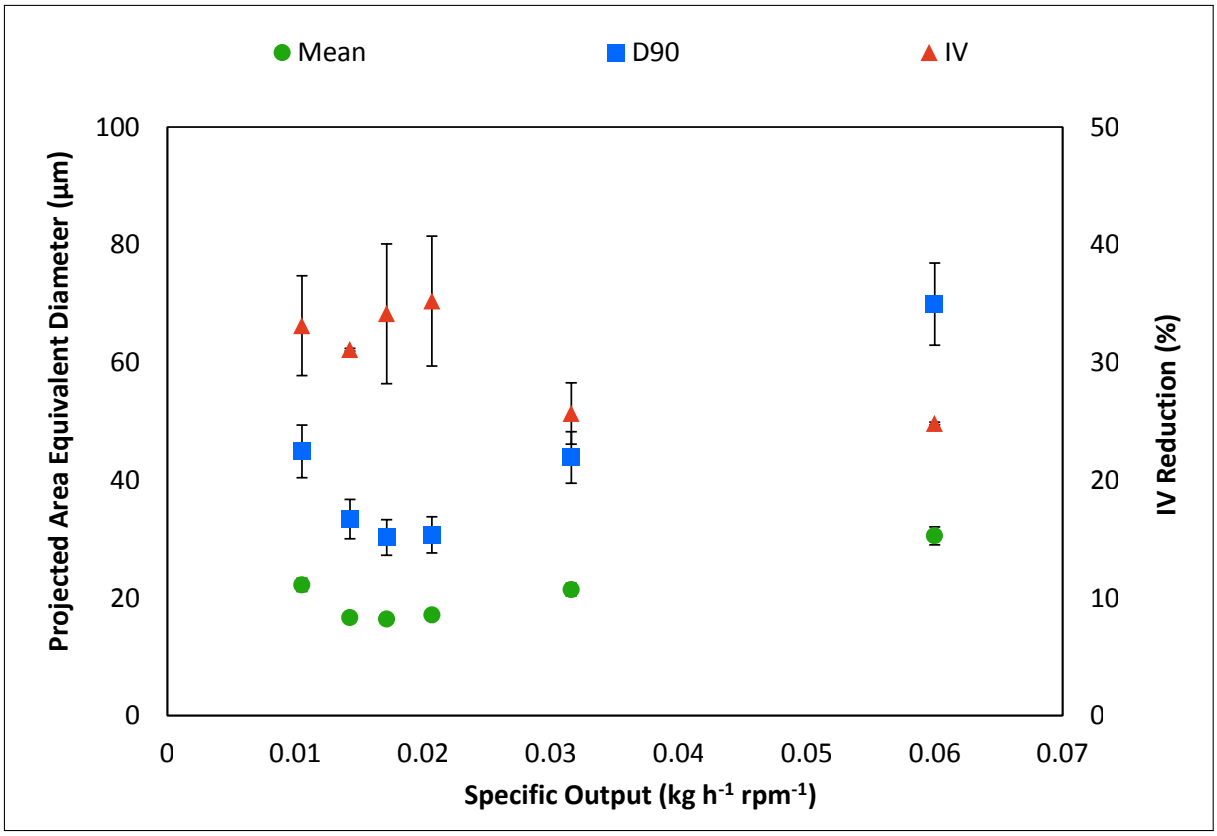

(a) H-PET/FR-1 composites

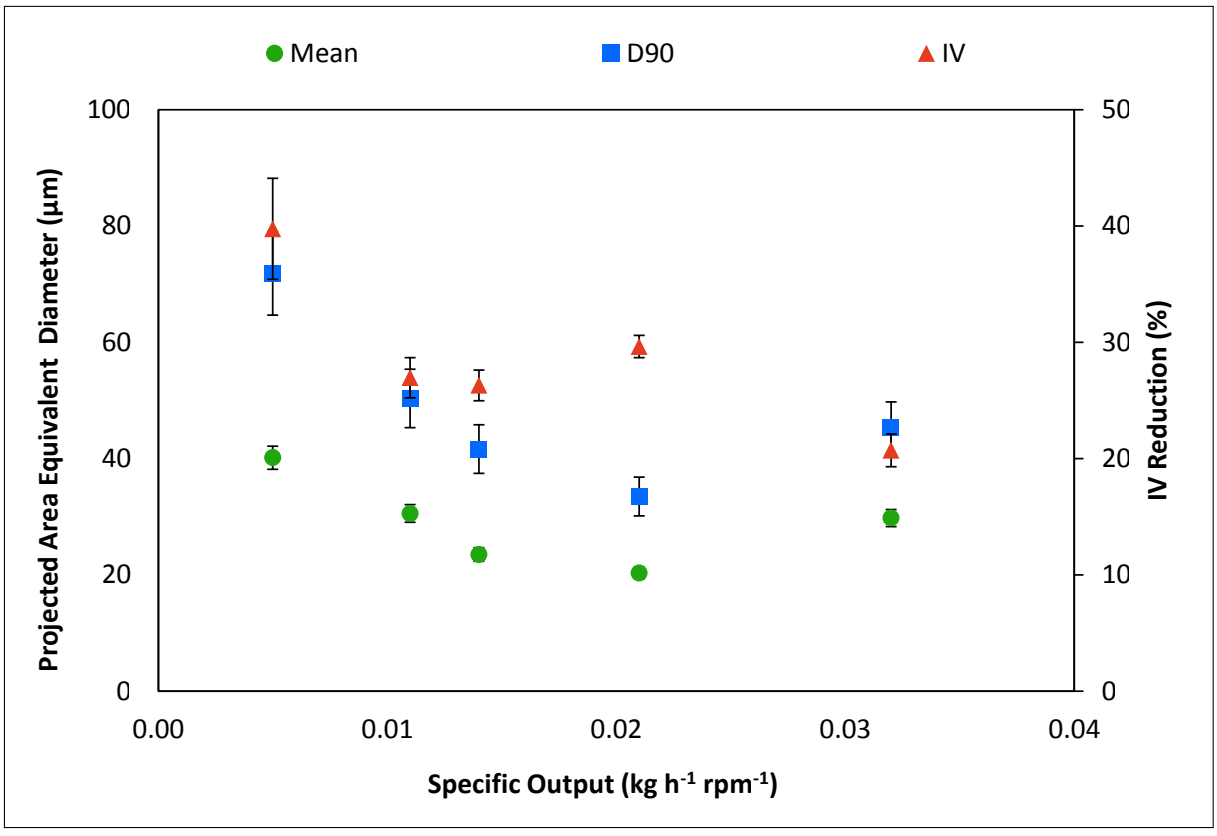

(b) H-PET/FR-3 composites

Figure 9.8: *Impact of specific output on mixing in H-PET composites containing FR-1 and FR-3 additives manufactured on Dr Collin ZK25 machine using premix method*

In both cases, a specific output of ca. 0.02 $kg\,h^{-1}\,rpm^{-1}$, corresponding to an average degree of fill of 22 %, appears to give the optimum dispersion. This can be explained through the consideration of shear rate. As the degree of fill within the screw channel decreases from fully filled state, the average shear rate and stress delivered to the polymer increase with the increase becoming most prominent at low specific outputs; see Figure 9.9.

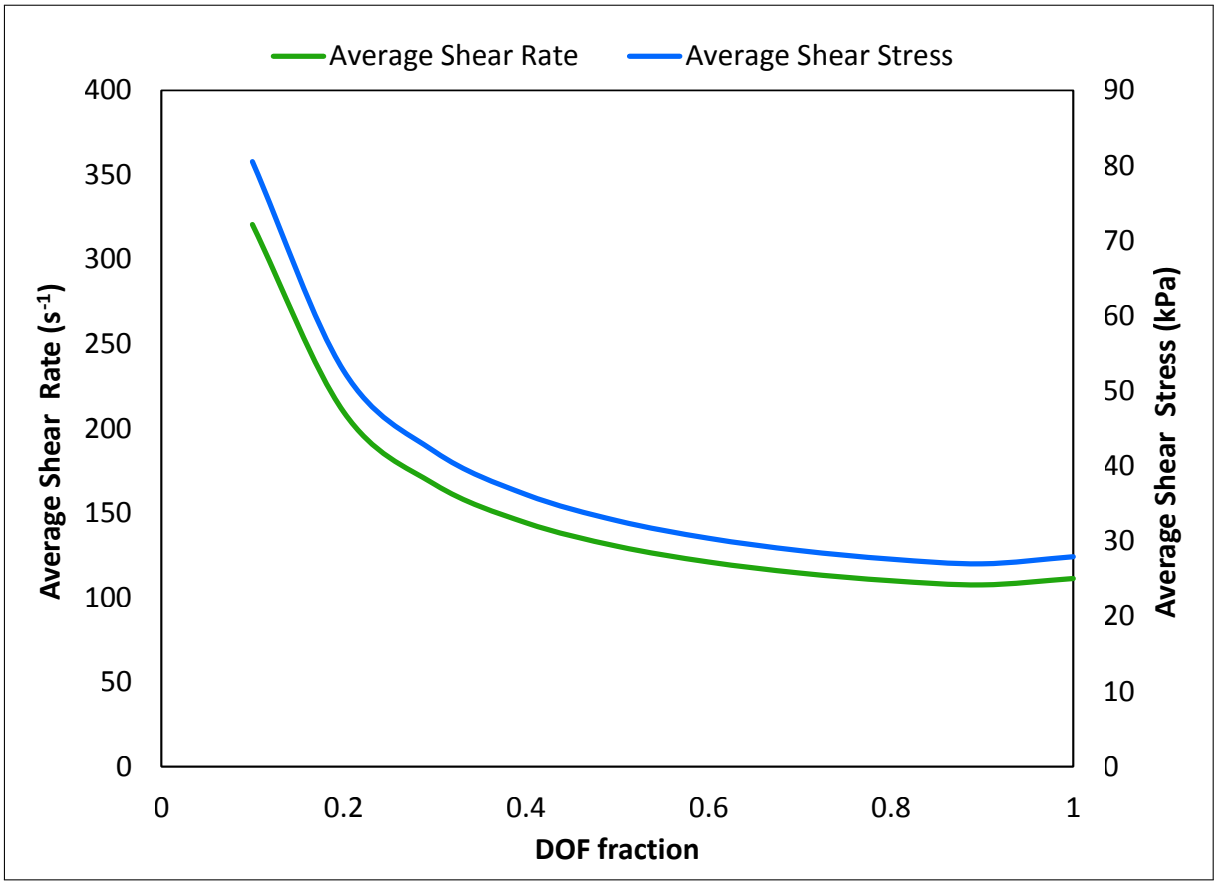

Figure 9.9: *Shear rate and stress vs degree of fill in Dr Collin ZK25 conveying element; pitch of 25* mm

Initially, the increase in average shear rate which the polymer sees increases the shear stress delivered to the agglomerates aiding dispersion via rupture and erosion mechanisms, thus reducing the measured mean diameters. In this initial stage the polymer IV loses remains relatively constant; see Figure 9.8. As the degree of fill is reduced further to very low values (obtained at high screw speed and low output) the polymer is subjected to high shear rates (and importantly stresses) for increased period of time leading to the increased reduction of the molecular weight of the material itself. This in turn lowers the

material viscosity, lowering the shear stress delivered to the agglomerates (even at these elevated speeds) resulting in a poorer dispersion process via the rupture mechanism. It is the rupture mechanism, that predominately governs the maximum size of agglomerates (which in a volume weighted distribution heavily influencing the mean) due to the rupture mechanism being considerably faster then the erosion mechanism.

Although at the very low specific outputs dispersion via erosion mechanism is improved due to increased shear rate and residence time (as result of low output) it is not enough to overcome the shortfall caused by the loss in the effective rupture mechanism. The optimum conditions for erosion mechanism are also unlikely to be at the highest screws speed as at this condition the residence time within the extruder is very short. However, it is likely to be reasonably close to the maximum speed as the increased shear rate is likely to have a bigger affect on the effectiveness of the mechanism compared to increased residence time.

9.1.2.2 Residence time

Unlike in the micro-compounder used by Kasaliwal, in the TSE the residence time can not be directly controlled. Instead it is influenced as a result of changes in the throughput or the screw speed of the machine. A decrease in screw speed leads to an increase in residence time, as well as a decrease in peak, minimum and average shear rates and stresses to which the polymer is subjected. Similarly, the residence time can be increased by reducing the output of the machine which maintains the peak and the minimum shear rate the same, but shear stresses are likely to decrease as result of increased polymer molecular weight loss and thus reduction in viscosity. The average shear rate increases as a result of a reduction in the degree of fill in the partially filled zones as well as the length of fully filled sections.

As the residence time increases it promotes better dispersion through the enhanced erosion mechanism increasing the number of smaller particles. Similarly, the increased dwell time

results in the increased number of passes through the high shear region increasing the probability of larger agglomerates being broken via the rupture mechanism. However, as it is not an independent parameter it does not generate reliable overall trends to predict mixing; see Figure 9.10.

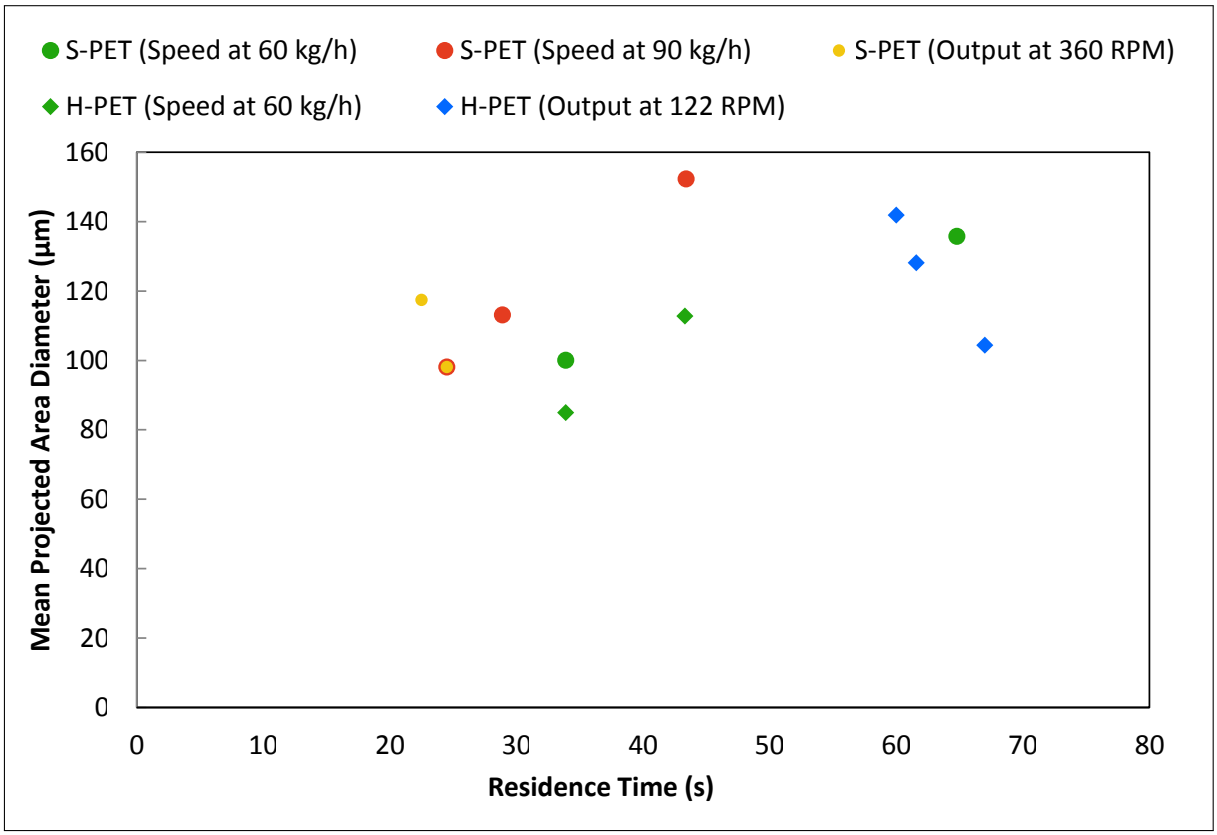

Figure 9.10: *Mean diameter vs residence time in FR-1 composites manufactured on the Berstorff ZE40A machine through split feed method*

Figure 9.10 shows that for both substrates (S-PET and H-PET) when the screw speed is increased, the mean diameter decreases with reducing residence time as a result of drastically increased shear rates and stresses. On the other hand when the output is reduced, the mean diameter decreases with increasing residence time as a result of higher average shear rates as well as the increased number of passes through the high shear region.

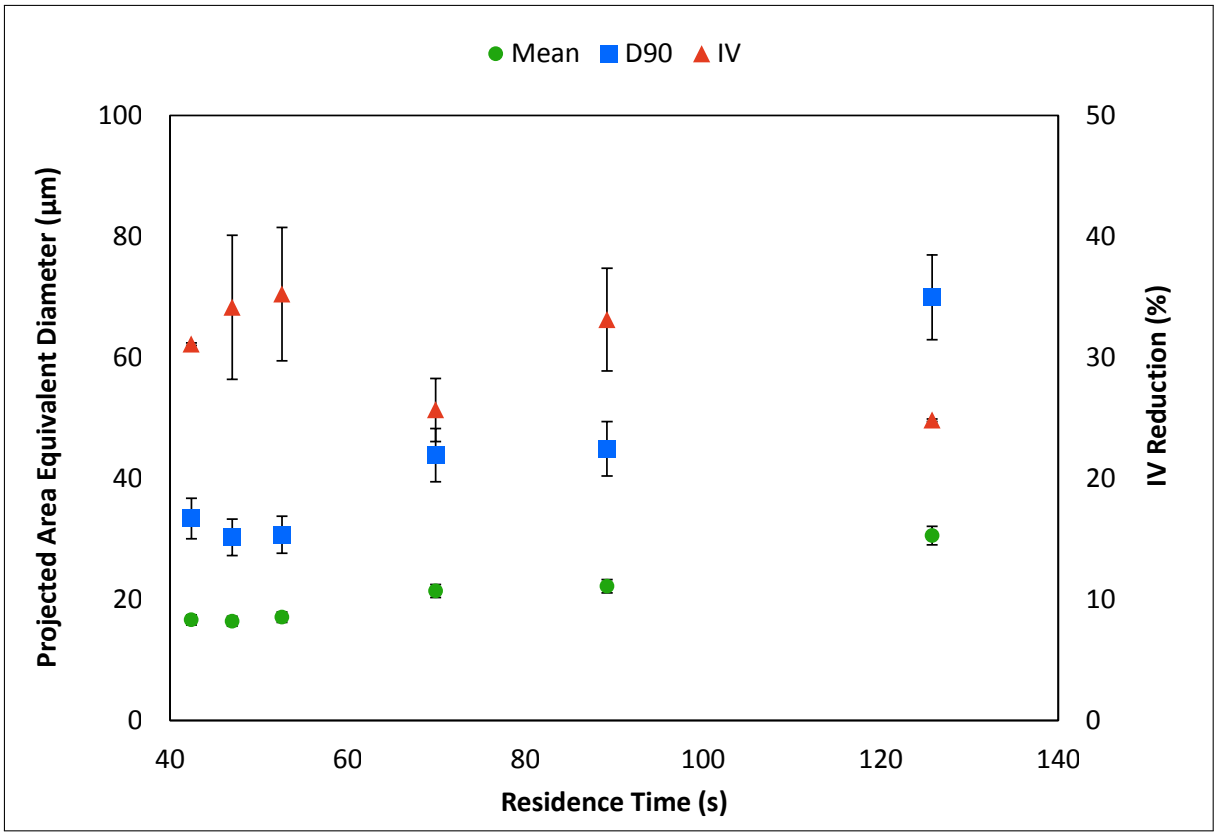

Figure 9.11: *Mean diameter vs residence time in FR-1 composites manufactured on the Dr Collin ZK25 machine through premix method*

In agreement with the above, Figure 9.11 shows how the mean particle diameter reduces with reduced residence time when the screw speed is increased for FR-1 composites manufactured in H-PET substrate on the *Dr Collin ZK25* machine through the *premix* method. In the similar manner the D_{90} is seen to decrease by circa 30 µm. The loss in the intrinsic viscosity of the polymer increases as a function of decreasing residence time showing its dependence on shear rate and stress as opposed to the dwell time which would be expected in a purely chemically driven reaction.

9.1.2.3 Specific mechanical energy input

As discussed, specific mechanical energy has been shown to be an effective way of predicting the level of mixing in a polymer composite system. The parameter encompasses machine screw speed, output and torque (function of degree of fill) providing a single value for comparing a number of different conditions. In the results presented here a strong

dependence of mean particle size is observed on SME.

Figure 9.12, shows how the mean diameter of the particles within FR-1 composites manufactured in S-PET and H-PET substrate on the *Berstorff ZE40A* machine decreases with increasing energy input. Perhaps most interestingly, the data for S-PET and H-PET composites lies on broadly the same line of best fit. In this case the correlation is not as clear as that observed by other authors, however the overall trend is evident.

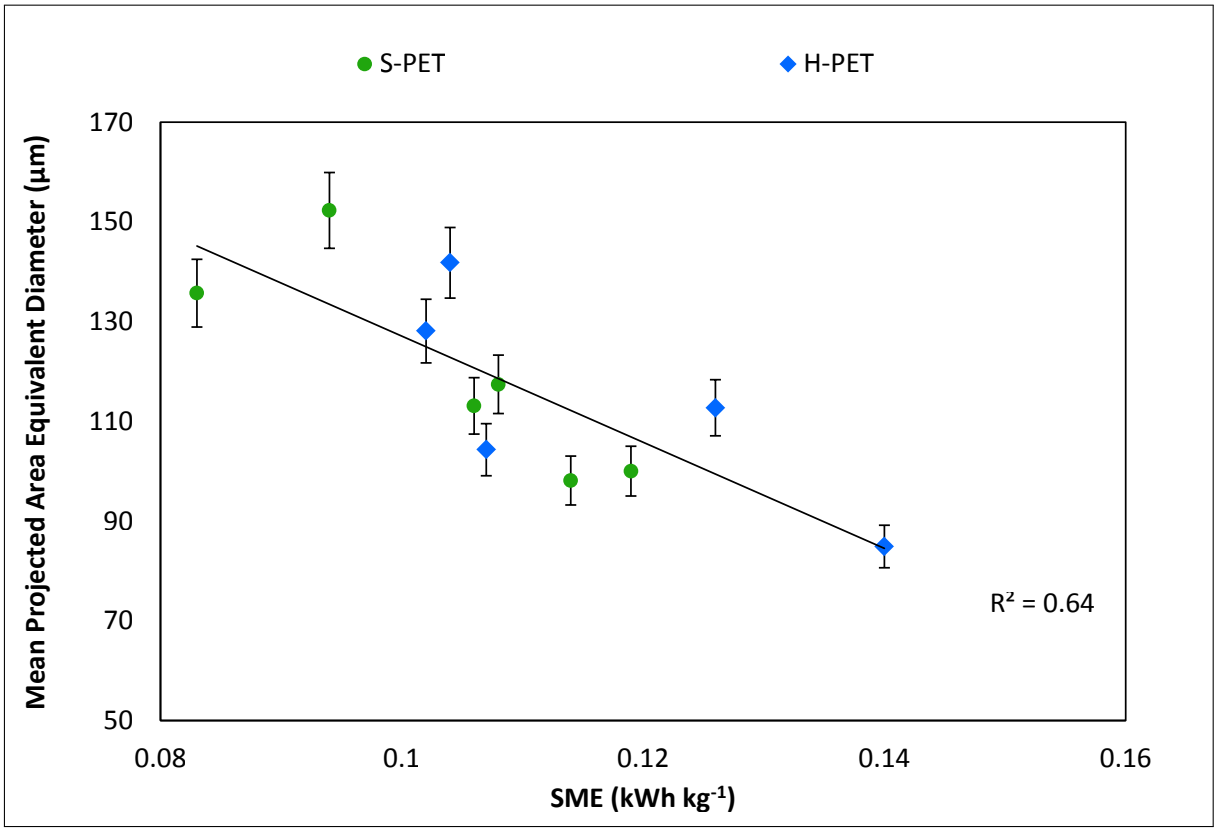

Figure 9.12: *Mean diameter vs SME in FR-1 composites manufactured on the Berstorff ZE40A machine through split feed method*

Figure 9.13a and 9.13b show the mean and D_{90} values for FR-1 and FR-3 composites manufactured on the *Dr Collin ZK25* machine using a *premix* method. The trend observed in FR-1 composites is in good agreement with that observed on the *Berstorff ZE40A* machine and shows a decrease in the mean and D_{90} of the particle size with increasing SME.

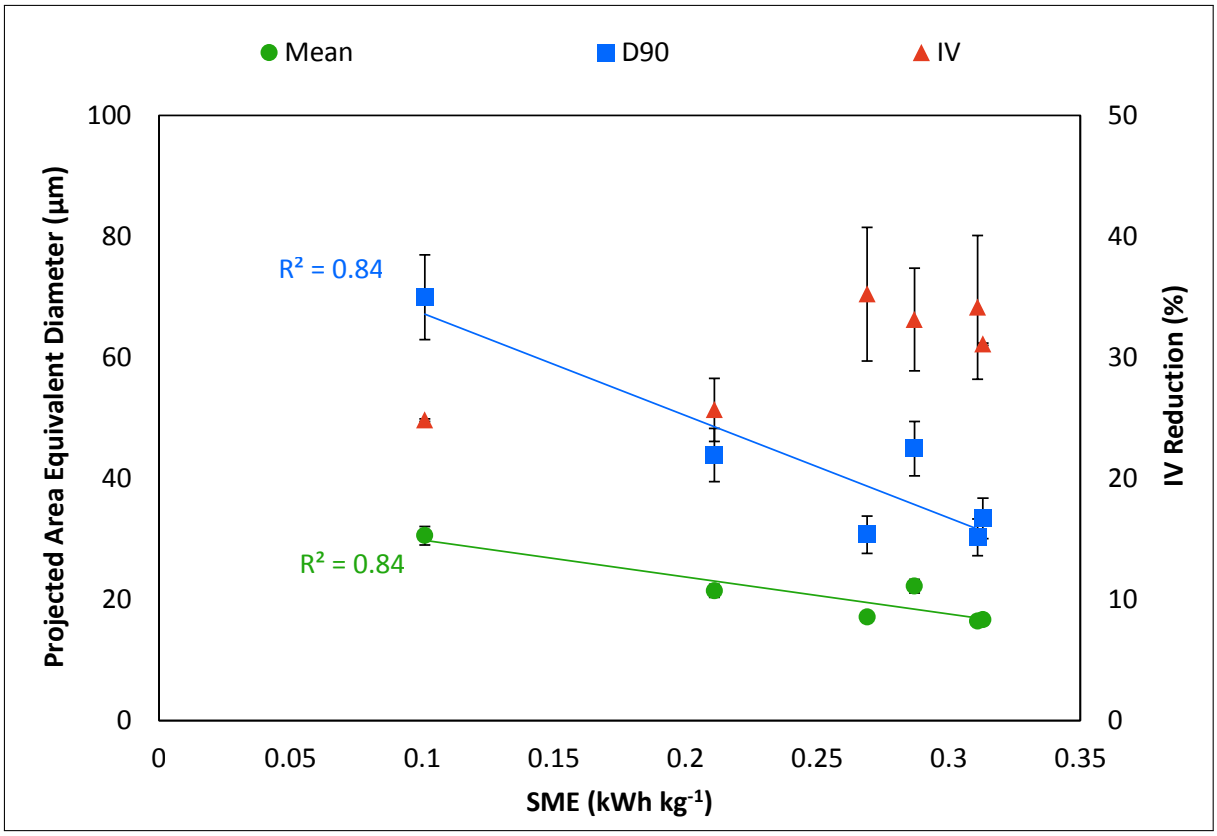

(a) H-PET/FR-1 composites (predominantly screw speed changes)

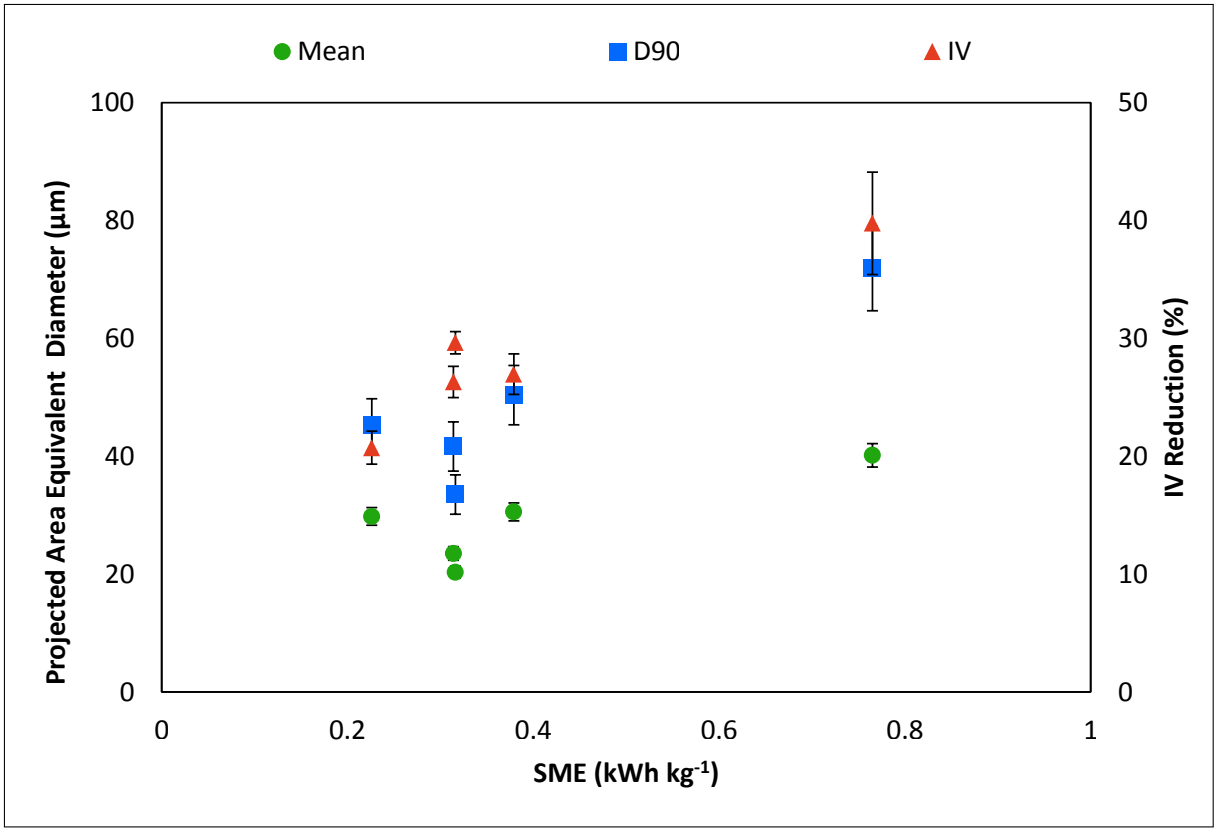

(b) H-PET/FR-3 composites (screw speed and output changes)

Figure 9.13: *Impact of specific energy input on mixing in H-PET composites containing FR-1 and FR-3 additives manufactured on Dr Collin ZK25 machine using premix method*

The results in Figure 9.13b are different to that reported in the literature and promote greater discussion. There appears to be an optimum value of ca 0.3 kW h kg^{-1}. Prior to this the mean diameter decreases with rising SME and after this value the mean diameter rises as SME increases. In Chapter 7, a link between increasing SME and decreasing intrinsic viscosity (hence molecular weight and melt viscosity) is made; see Figure 7.17. In combination with the dependence of melt viscosity on the SME, a probable explanation for the increase in the mean particle diameter is that the increase in shear rate was offset by the decrease in the melt viscosity leading to smaller shear stresses being transmitted to the agglomerates and thus the existence of larger particle sizes.

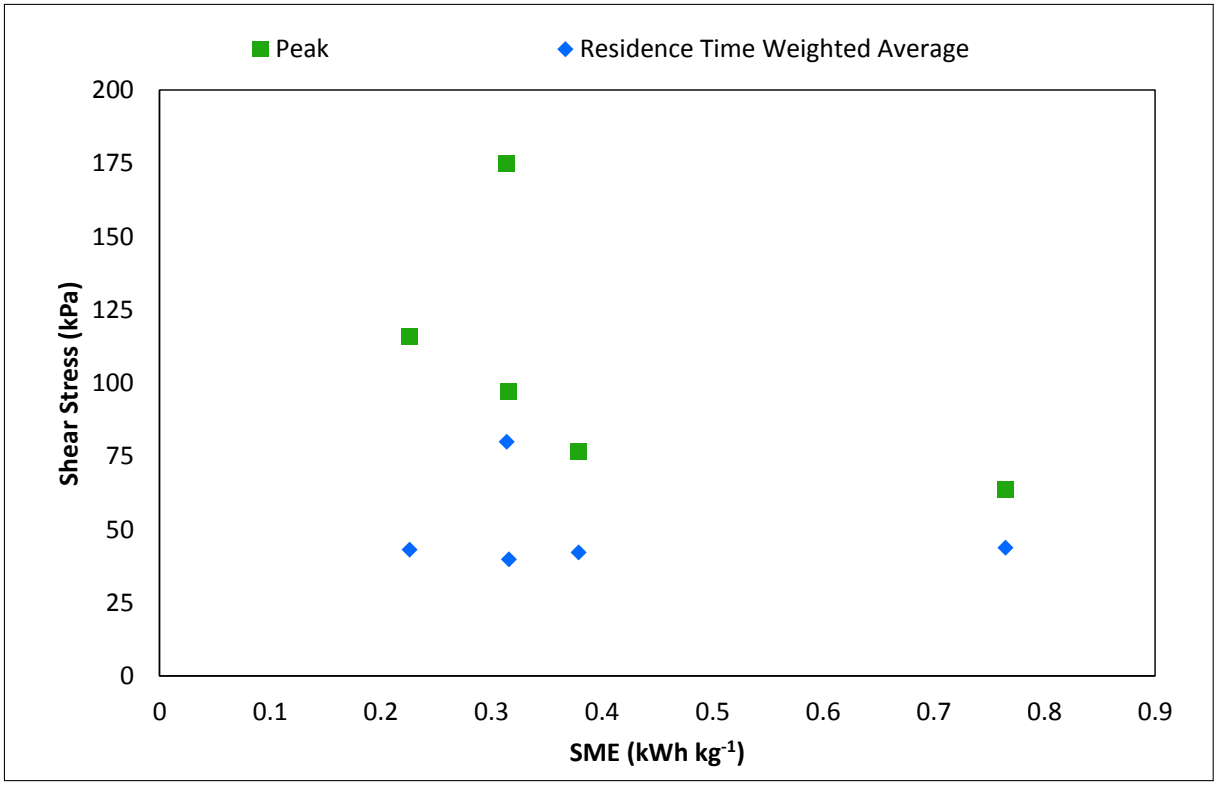

Figure 9.14: *Peak and residence time weighted average shear stress as function of SME for FR-3 composites manufactured on the Dr Collin ZK25 machine through premix method; calculated on basis of the extrudate molecular weight at temperature of 275* °C

Figure 9.14 shows the peak and the residence time weighted shear stress as the function of SME. The residence time weighted average stress was calculated based on the final molecular weight of the extrudate using the model discussed in Chapter 6. It is evident that under the conditions examined here, the residence time weighted average shear stress

does not change significantly, whereas the peak shear stress found in the clearance region between the barrel and the screw flight decreases with increasing SME. The decreasing peak shear stress value results in worsening performance of the rupture mechanism for dispersion yielding larger average values for the particle size.

9.1.2.4 Shear rate and stress

Changes in the operating conditions of the machine lead to changes in the peak, average and the minimum shear rate and stress that the polymer experiences. This in turn influences the dispersion mechanisms, with the rupture mechanism being driven by shear stress and erosion and collision mechanisms by shear rate; see Section 2.4 for further detail. It is difficult to separate the effects of the individual mechanism in a TSE as a result of changes in directly controllable parameters leading to the question: *Is there a single parameter or a best parameter to correlate with the level of dispersion?*.

An understanding of the role of each mechanism helps to provide the answer. The collision mechanism is likely to produce few very small fragments and/or re-agglomeration in a polymer TSE process due to the very high viscosity of the melt inhibiting rapid separation of particles in the event of collision thus its effects can be neglected. Given the right conditions, the erosion mechanism can have a significant role to play in increasing the number of smaller fragments by peeling off the outer layers of the overall agglomerate structure. However, in a highly agglomerated system where the surface area of the particles is small this mechanism is unlikely to be dominant due to the very small residence times within a typical TSE machine. Once some initial dispersion has taken place the role of this mechanism should be more obvious. As a result the use of shear rate to correlate the level of dispersion seems inappropriate.

The initial dispersion in a composite system would occur as a result of the rupture mechanism; leading to almost instantaneous breakage of the parent agglomerate into a number of smaller structures. This mechanism is dominated by very high shear stresses, suggest-

ing that the peak shear stress occurring in the clearance between the barrel and the screw tip could be an appropriate parameter to correlate with dispersion. However, the stress in this region is very difficult to calculate as the magnitude of polymer viscosity in this region is difficult to determine.

Since, the majority of the high shear regions are located close to the barrel wall one could argue that the barrel temperature would provide a good estimate of the polymer viscosity. However, that is not the case, as in these high shear regions there is likely to be some significant viscous shear heating; see Kalyon et al., 1988b. Although PET is often assumed to be Newtonian, there is a potential for some shear thinning behaviour as a result of the very high shear rates (over 1000 s^{-1} at high screw speeds) that can be found in these regions. Similarly, there is a flow distribution within a TSE with no guarantee that a fluid element will pass though the high shear region. Although a high degree of pipeline flow (channelling) is unlikely certain conditions and screw designs can promote this (Lawal and Kalyon, 1995). Residence time weighted average shear stress could be an alternative to the peak shear stress as a parameter to correlate with degree of dispersive mixing. Unlike peak shear it takes count of changes in output and addresses the limitations discussed.

In order to calculate the shear stress it is important to consider which value of molecular weight (represented by IV) should be utilised in the polymer viscosity prediction. As the virgin (unprocessed) IV is the only parameter known prior to extrusion it would be beneficial to utilise this in any predictive model. Since the molecular weight of the polymer changes during extrusion as a result of chemically and mechanically induced chain scission, the viscosity of the virgin polymer could arguably only be utilised in the cases of *premix* or *split feed* method. In *direct to melt* addition the additive will be introduced past the melting section, which is the most severe on the molecular weight of the PET. It is in the melt section where the majority of the mechanically induced chain scission will occur due to the highest material viscosity, and the majority of chemically induced scission due to

high moisture content within the polymer in the zone. As a result,a decision to use the extrudate intrinsic viscosity value was utilised. In future cases this could be predicted through other experimental results and models; see Chapter 7.

Figure 9.15 shows that there is no correlation between the residence time weighted average shear stress calculated on the basis of extrudate IV and measured melt temperature and dispersion. This suggests that the rupture mechanism dominating dispersion is occurring much earlier in the extrusion process. As material is added via a *split feed* method, it is likely that this is occurring in the melt section when the viscosity is the greatest and hence the shear stress applied is also the highest.

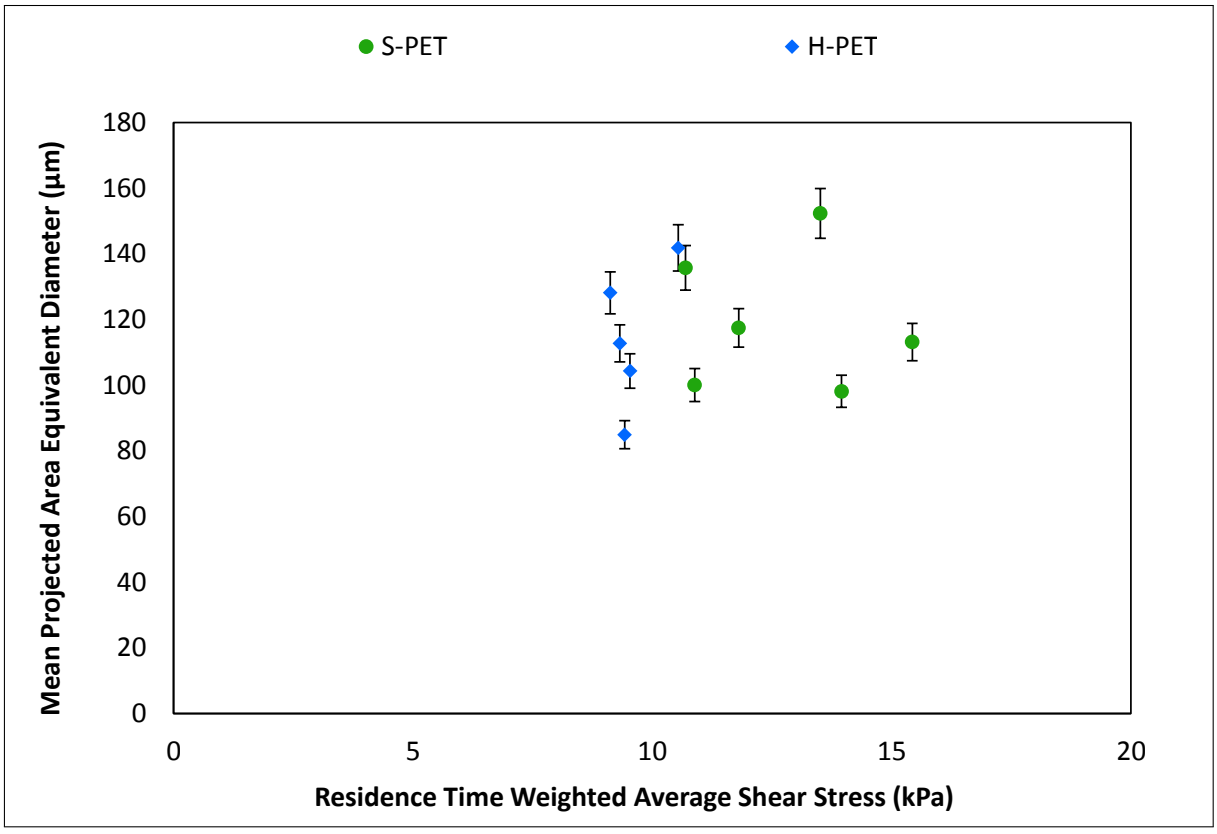

Figure 9.15: *Residence time weighted average shear stress vs mean particle diameter calculated on the basis of extrudate IV and measured melt temperature for FR-1 composites manufactured on Berstorff ZE40A machine via split feed method*

Figure 9.16, shows the same data plotted as a function of residence time weighted average shear stress which was calculated on the basis of virgin polymer IV. The Figure shows

a linear trend with the mean projected area equivalent diameter reducing as a function of increasing shear stress confirming that the majority of the agglomerate rupture is occurring in the melt zone of the extruder before the viscosity loss seen in the extrudate reduces the magnitude of the stress. Similarly, the role of polymer viscosity in infiltrating the agglomerate is clearly shown by the better dispersion being achieved in lower viscosity polymer at the same shear stress. This is in agreement with the findings of Kasaliwal et al., 2011.

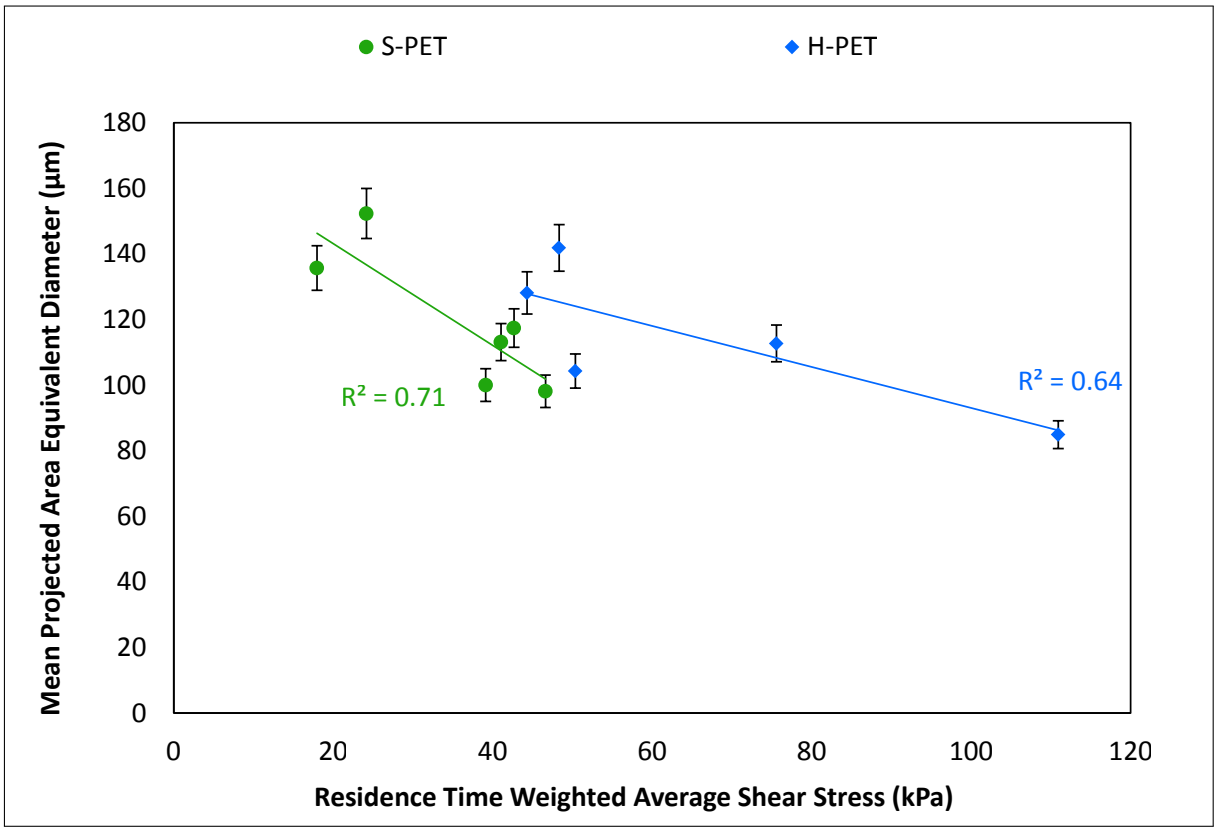

Figure 9.16: *Residence time weighted average shear stress vs mean particle diameter calculated on the basis of virgin polymer IV and measured melt temperature for FR-1 composites manufactured on Berstorff ZE40A machine via split feed method*

One could assume that the rupture takes place in the melt zone only, and thus base the shear stress calculation on the temperature of melt in that zone or the melting temperature of the polymer which would yield the highest shear stress values. Although this is possible with the *Berstorff ZE40A* machine due to the very gentle nature of the screw it seems highly unlikely that this would be true in the case of a much more severe screw

configuration where a number of different mixing elements were used. Such a relationship was tested, yielding R^2 values that match that of the residence time weighted average shear rate.

Although plotting the mean diameter against shear stress yields a trend, a quantification of the trend is difficult due to the uncertainties in calculating the shear stress involved. In short these are caused by variation in temperature within the screw channel and along the length of the screw, variation in shear rate within the flow channel and reduction in the molecular weight of the polymer along the length of the screw. Figure 9.17 shows the mean particle diameter as a function of the residence time weighted average shear rate. This encompasses all of the dispersion mechanisms and shows that for a given shear rate the dispersion is generally better in the H-PET substrate due to the higher shear stresses achieved.

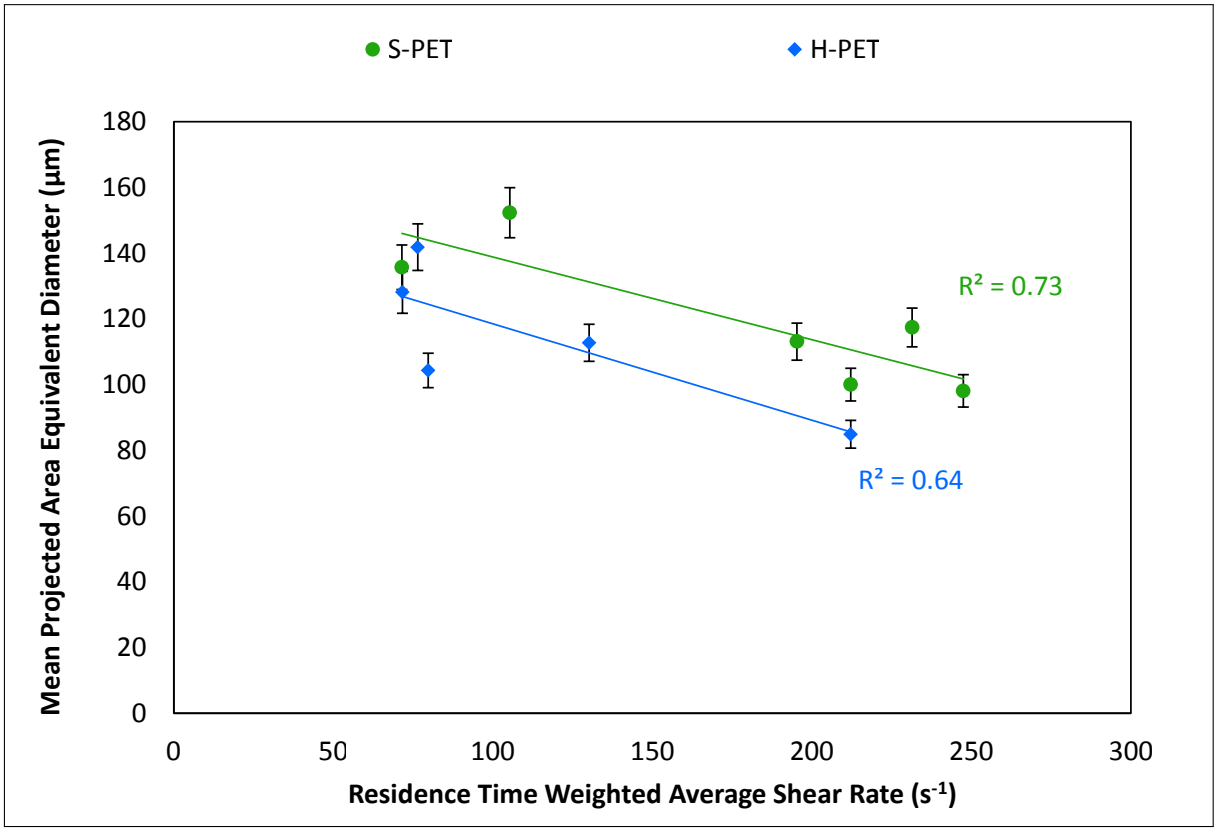

Figure 9.17: *Residence time weighted average shear rate vs mean particle diameter for FR-1 composites manufactured on Berstorff ZE40A machine via split feed method*

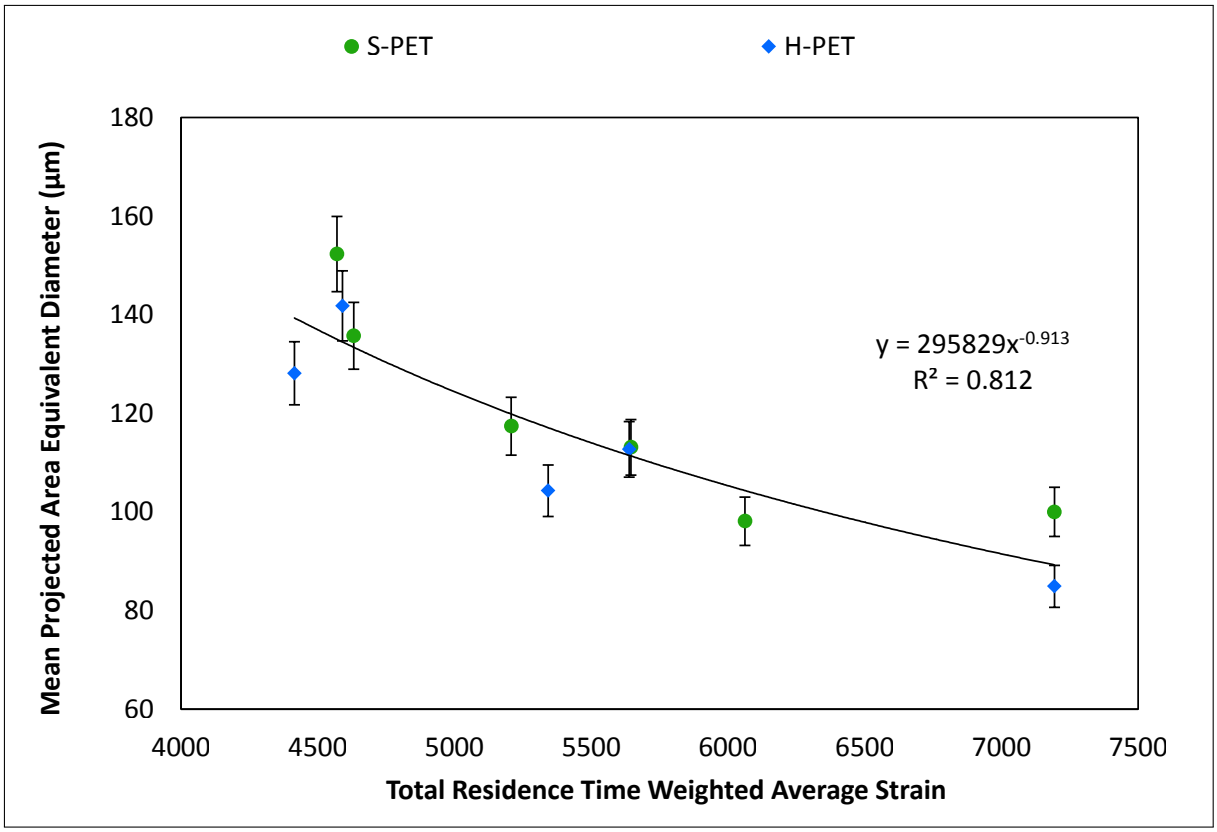

Figure 9.18: *Residence time weighted average shear stress vs mean particle diameter calculated on the basis of virgin polymer IV and measured melt temperature for FR-1 composites manufactured on Berstorff ZE40A machine via split feed method*

Whilst dispersion via rupture mechanism is seen as a very rapid process, it is still governed by the length of time that the polymer spends in the extruder as this determines the number of passes that the polymer has through the high shear regions. Similarly the erosion mechanism is also governed both by the shear rate and the residence time in the system. Kasaliwal et al., 2010 proposed the product of applied stress and time as a measure for rate of mixing achieved. In the PET system examined here, there are challenges in assessing the applied shear stress, as a result strain is used as an indicator of this parameter. The residence time weighted average total strain was calculated as the product of residence time and the residence time weighted average shear rate. When plotted against the mean particle diameter, this yields a strong correlation showing the decay in the mean diameter described by a power law relationship; see Figure 9.18.

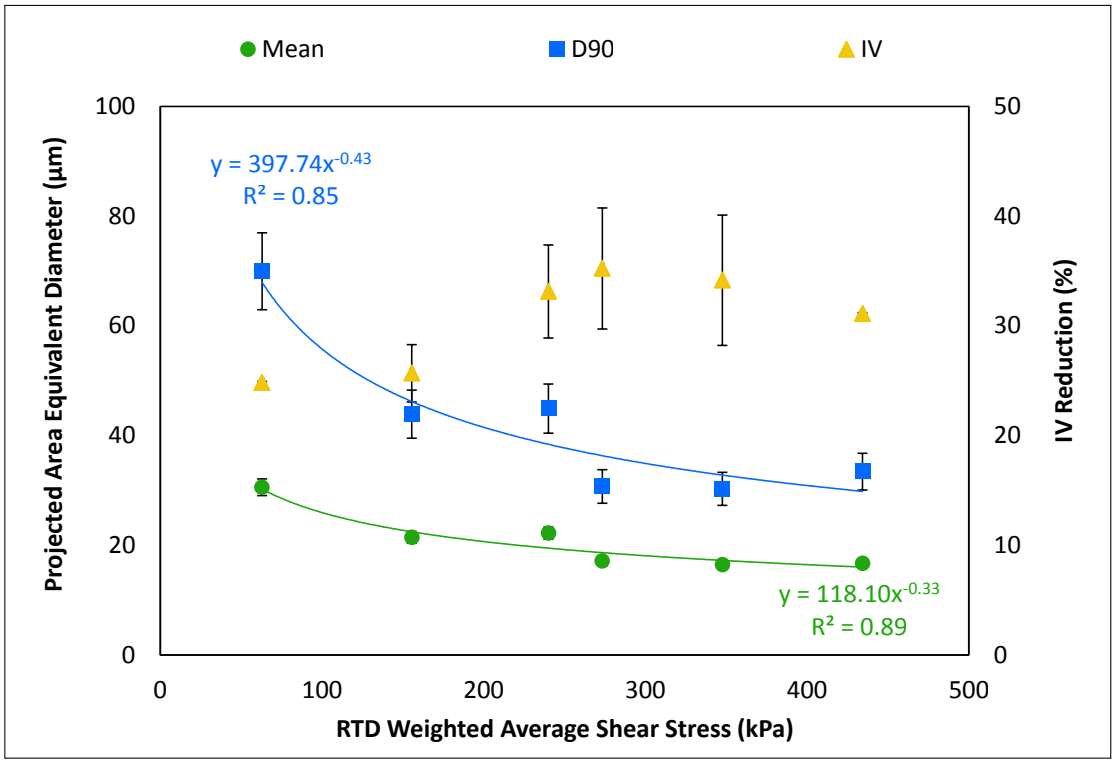

Figure 9.19: *Residence time weighted average shear stress vs mean particle diameter for FR-1 composites manufactured on Dr Collin ZK25 machine via premix method*

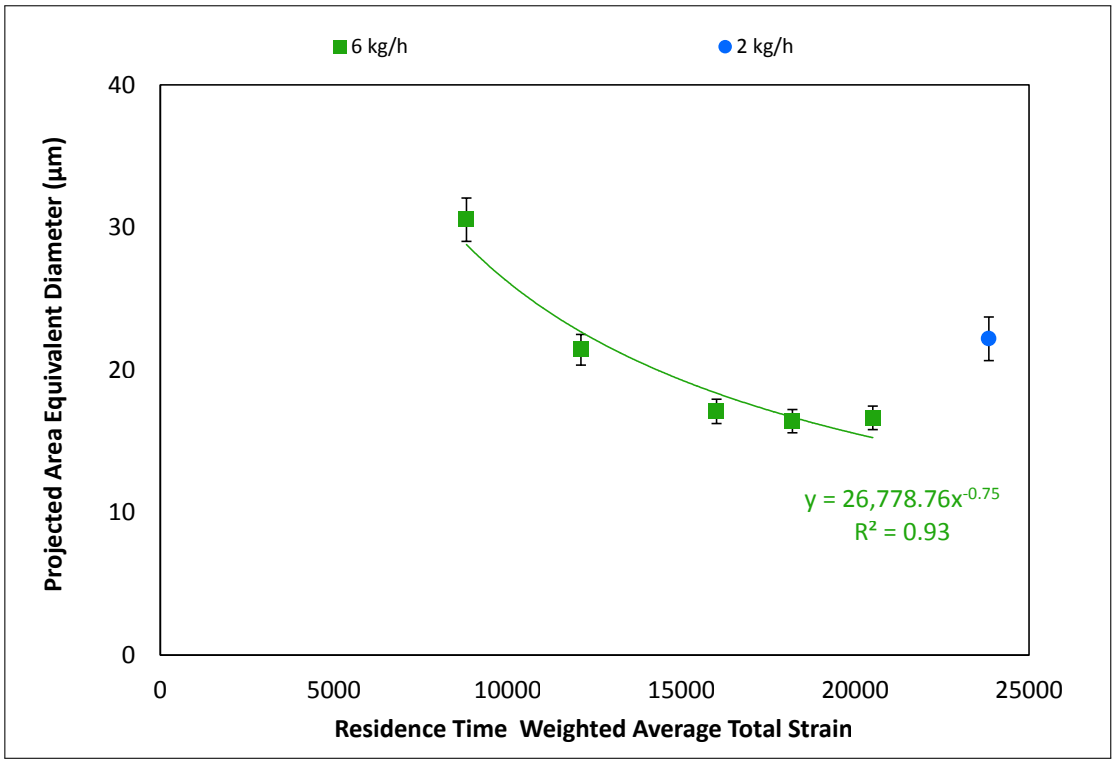

Figure 9.20: *Residence time weighted average shear strain vs mean particle diameter for FR-1 composites manufactured on Dr Collin ZK25 machine via premix method*

Figures 9.19 and 9.20 show the mean particle size diameter as a function of the residence time weighted average shear stress and strain respectively for experiments conducted on the *Dr Collin ZK25* machine. Figure 9.19 demonstrates a stronger correlation with residence time weighed average shear stress than that which was seen in the composites manufactured on the *Berstorff ZE40A* machine. The level of dispersion tends to a plateau as the IV loss increases at the higher stresses. The likely explanation for this is that all but one of the points were obtained by maintaining throughput the same and changing the screw speed. This is particularly evident in the Figure 9.20, where the low output sample has the highest total strain, but the mixing is relatively poor due to the much smaller peak shear stress delivered at this condition. This perhaps brings into question the possibility of using the total shear strain as a single parameter to relate to the degree of mixing; a further more detailed investigation is warranted here.

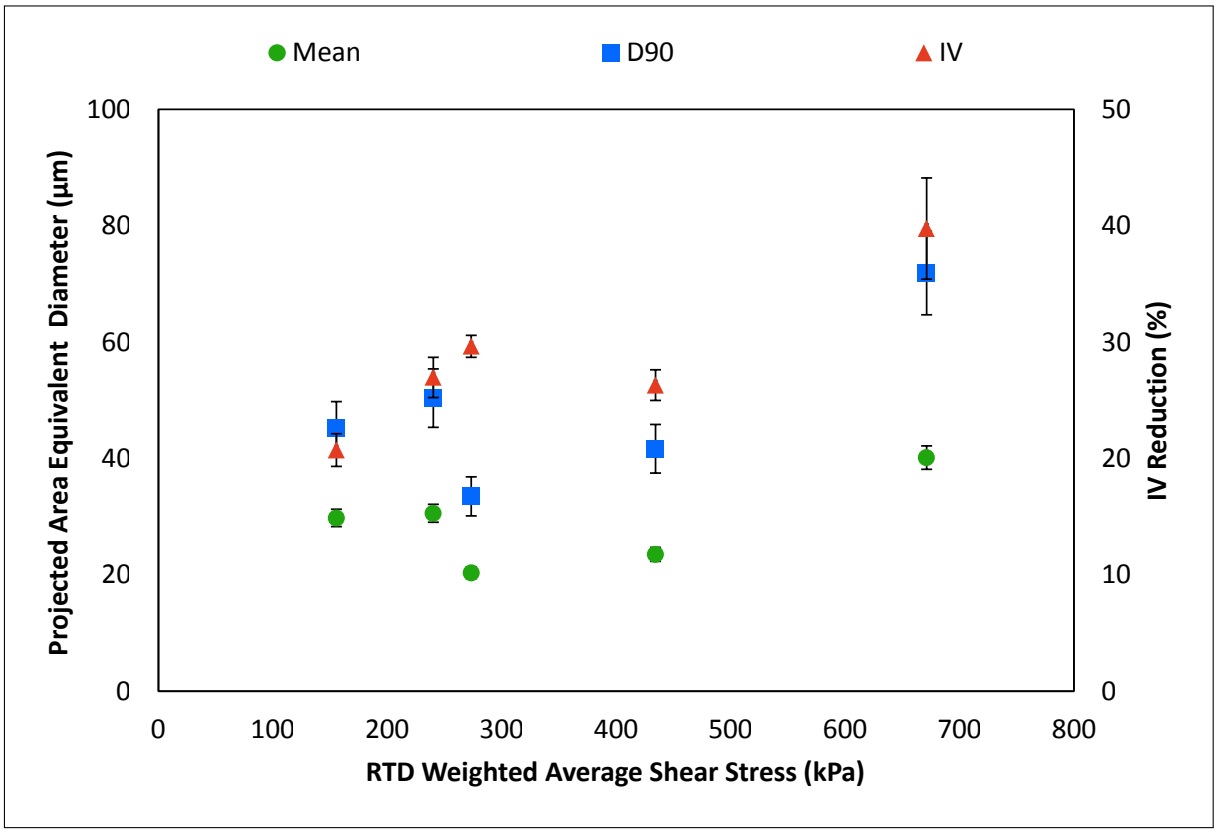

Figure 9.21: *Residence time weighted average shear stress calculated on basis of virgin polymer IV vs mean particle diameter for FR-3 composites manufactured on Dr Collin ZK25 machine via premix method*

Figure 9.21 illustrates the mean particle diameter as a function of the residence time weighted shear stress for FR-3 composites manufactured at different output and screw speed combinations on the *Dr Collin ZK25* machine via the *premix* method. In this case the trends are not very clear. Considering the values at 700 kPa it could be argued that there is a slight reverse trend with the mean particle size increasing with increasing shear stress. The most probable explanation for such results is high molecular weight loss of the polymer in the initial length of the extruder leading to lower viscosity and thus poor transfer of the shear forces to the agglomerates. It is also possible that some cold agglomeration of the particles took place in the melting zone for the high screw speed and very low output condition represented by the average shear stress value ca 700 kPa on the graph leading to the anomalous result.

9.1.3 Effect of operating set up and recipe on mixing

As well as changes in directly controllable parameters other aspects can have a significant impact on the level of mixing. These include the recipe of the product and the TSE set up. Aspects associated with the recipe include the properties of the additive and the polymer (see Chapter 8) as well as additive loading discussed below. Machine set up can be subdivided into additive injection points, barrel temperature and screw design.

9.1.3.1 Barrel temperatures

Theoretically barrel temperatures can also play an important role in enabling mixing by controlling the viscosity of the material to either aid wetting or to promote higher shear stresses and aid dispersion of the additive. A hypothesis of higher temperature in the zone directly post addition (no temperature control on the injection zone) would lower the melt viscosity enabling the polymers to better infiltrate the outer layers of agglomerate promoting erosion mechanism later in the process. Similarly, the lowering of the temperature in the latter mixing zones would raise the viscosity allowing for transfer

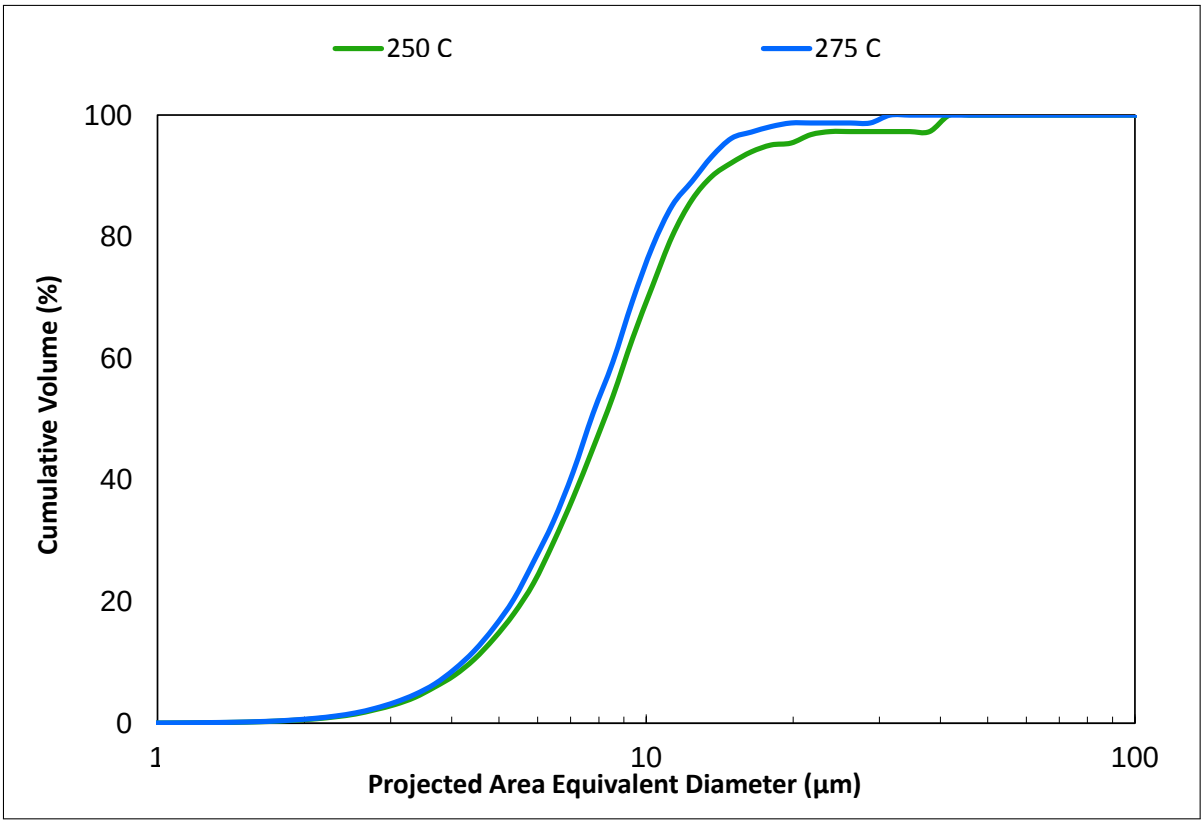

(a) Zone 4: 1st zone post injection

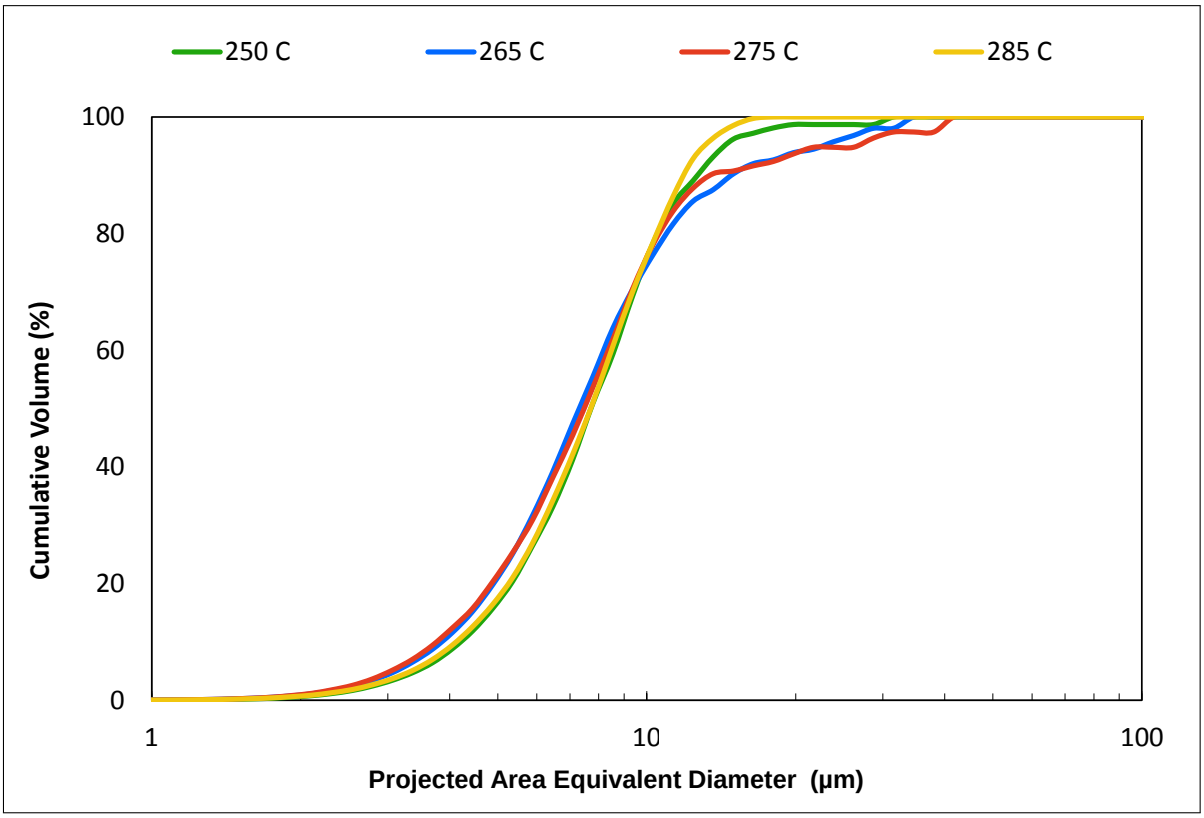

(b) Zone 5 to 7: latter mixing and conveying zones

Figure 9.22: *Impact of barrel temperatures on mixing in FR-1/H-PET composites manufactured on Dr Collin ZK25 machine using direct to melt method; microscopy images used for the distributions were captured at x20 magnification*

of larger stresses to the agglomerates enabling rupture of smaller agglomerates.

Figure 9.22a shows that a higher temperature of the zone directly post additive injection yields a very small improvement in the degree of mixing achieved. There is a small shift to smaller sizes in the lower end of the distribution showing an improvement in the erosion mechanism. This improvement transcends to the rupture mechanism as the better wetting enables more effective transfer of shear stresses and as a result there is a lowering in the D_{90} value. Figure 9.22b shows the results for the changes in barrel temperature of the latter mixing zones. No clear trend is observed here, even though there is some variability in the D_{90} of the distribution. Both the highest and the lowest temperature of 285 °C and 250°C seem to yield better dispersion than 265 and 275 °C. The analysis method is discussed in Section 4.1.

These results are broadly in agreement with that of Fortunato et al., 2014 who also found no significant link between the barrel temperatures and the level of mixing achieved. The minute difference in mixing observed here on the small scale 25 mm diameter *Dr Collin ZK25* machine draws into question the possibility of such type of control on the larger diameter machines where the surface area to throughput ratio would mean that the barrel heaters/chillers would be less effective.

9.1.3.2 Additive loading

The impact of additive loading has been investigated on several occasions utilising different additives and machines. Initial investigations were undertaken on FR-2 composites based on the S-PET substrate manufactured at 90 $\mathrm{kg\,h^{-1}}$ and 160 rpm via the *split feed* method. White light interferometry was utilised to analyse the dispersion of the additive on the surface of the finished film produced. Small area (min resolution ca. 0.4 µm) and large area (min resolution ca. 2 µm) analysis was undertaken on the finished film, with the latter providing the clearest results; see Figure 9.23. It is evident that as the loading of the additive increases the surface roughness of the film increases with arithmetic roughness,

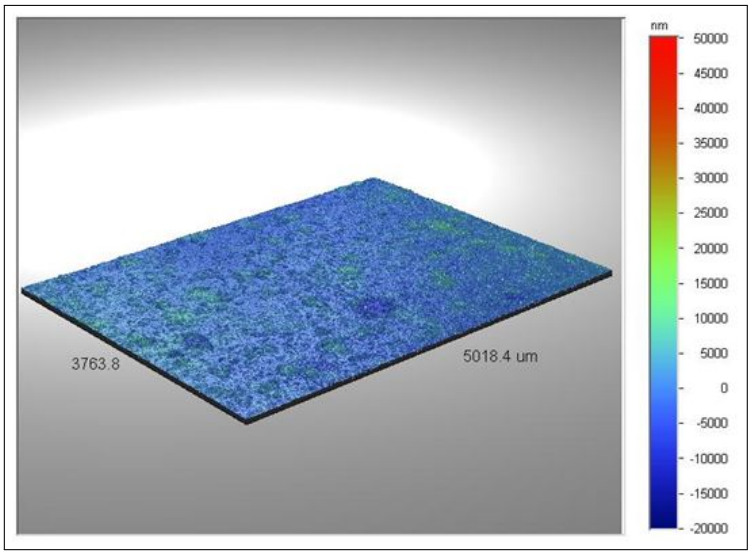

(a) 3 $\%_{wt}$

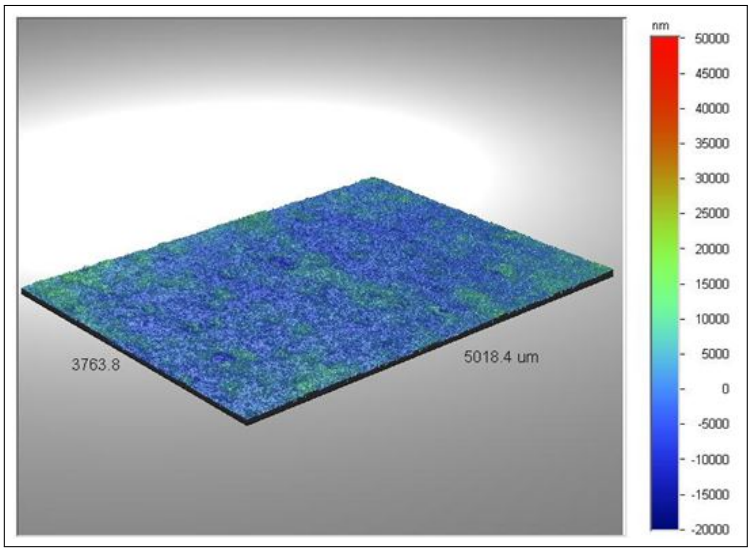

(b) 5 $\%_{wt}$

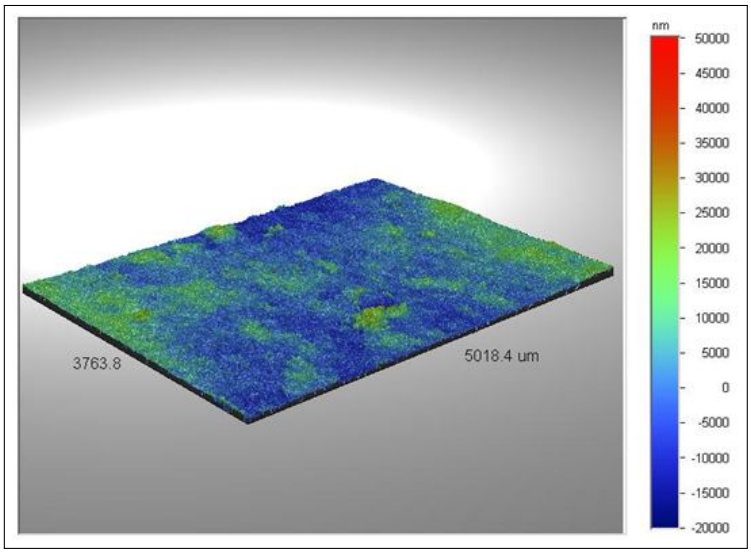

(c) 7 $\%_{wt}$

Figure 9.23: *Impact of additive loading on mixing in S-PET composites containing FR-2 additive manufactured on Berstorff ZE40A machine using split feed method*

R_a values rising from 1.9 to 2.9 and 6.1 µm with loading increase from 3 to 5 and 7 $\%_{wt}$ respectively. This is a likely result of decreasing wetting efficiency.

Further investigations were undertaken on H-PET composites containing FR-1 additive manufactured on the *Berstorff ZE40A* machine at 60 $kg\,h^{-1}$ and 122 rpm. The mixing efficiency was evaluated through analysis of transmitted light microscopy images of the film samples to obtain particle size distribution of the additive within the composite.

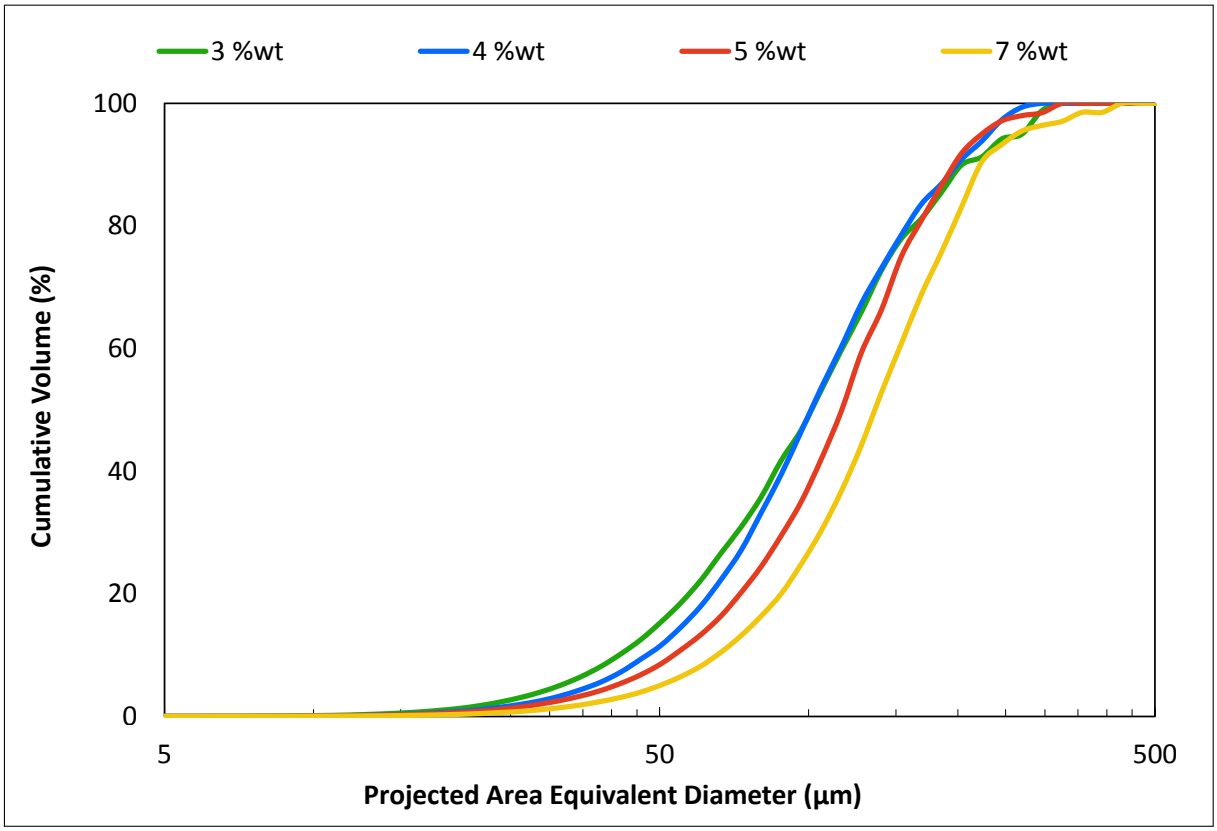

Figure 9.24: *Impact of additive loading on mixing in H-PET composites containing FR-1 additive manufactured on Berstorff ZE40A machine using split feed method; captured at magnification x2.5*

Figure 9.24 shows the particle size distribution at concentrations of 3, 4, 5 and 7 $\%_{wt}$. It is clear that increasing the loading of the additive shifts the particle size distribution to the right indicating larger sized particles. The most evident shift in the lower end of the distribution with D_{10} values increasing from 41.4, 47.1, 53.7, and 65.3 µm. This change shows the decreasing efficiency of the additive wetting which in turn reduces the

available surface area and in turn decreases dispersion via the erosion mechanism which is responsible for the generation of very fine particles. The top end of the distribution remains very similar with D_{90} values ca. 200 µm for 3, 4, 5 $\%_{wt}$. An increase in the D_{90} value is seen for 7 $\%_{wt}$ distribution this is a likely result of either additive re-agglomeration further down the extrusion process or increased cold agglomeration caused by compaction of material in and prior to the melt zones or both.

Figure 9.25 shows the how the level of dispersion changes with increasing loading in H-PET composites containing FR-1 additive manufactured on *Dr Collin ZK25* machine at ca. 6.5 $kg\,h^{-1}$ and 290 rpm using the *direct to melt* addition method.

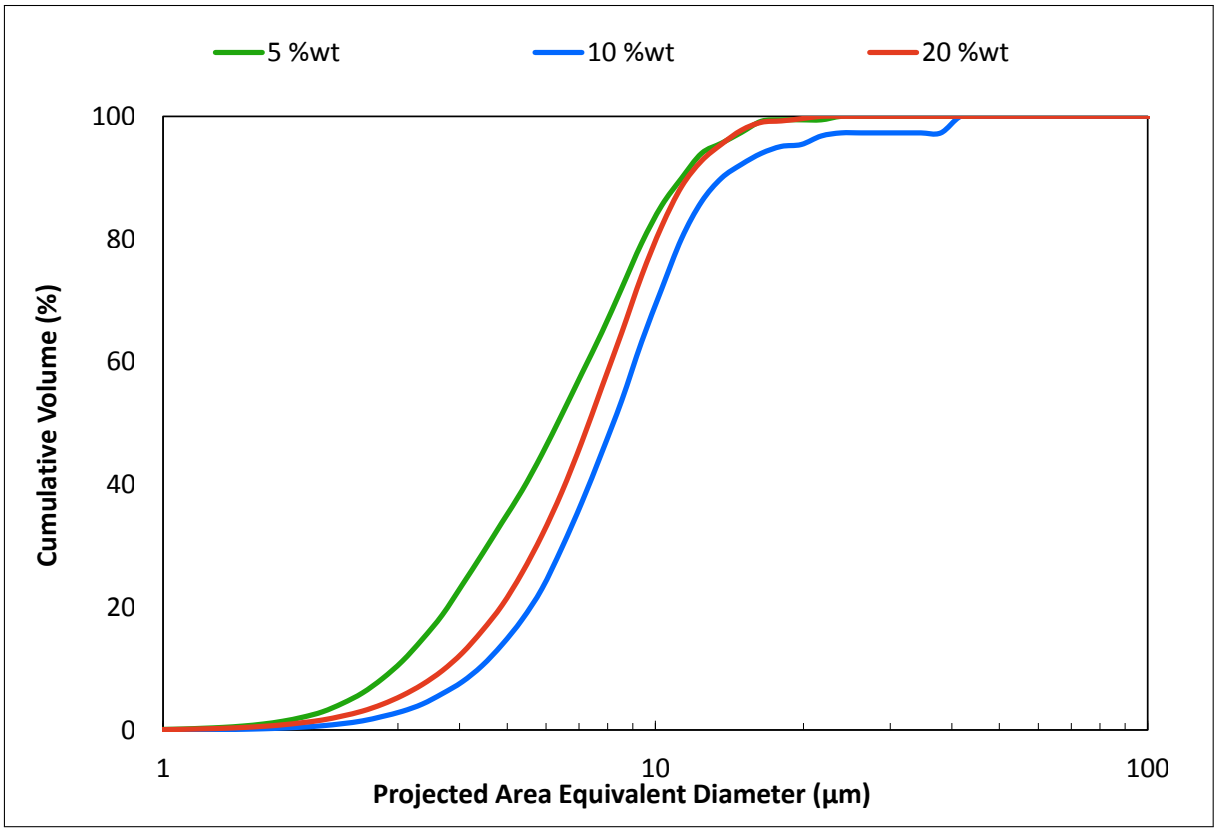

Figure 9.25: *Impact of additive loading on mixing in H-PET composites containing FR-1 additive manufactured on Dr Collin ZK25 machine using direct to melt addition method; captured at magnification x20*

As the loading increases from 5 to 10 $\%_{wt}$ there is a shift in the PSD to a larger particle size as previously seen with the samples manufactured on the *Berstorff ZE40A* machine.

Interestingly the D_{90} also increases slightly perhaps indicating greater compaction in the feeding equipment (side feeder and supplying gravimetric feeder) or poorer wetting of the additive at the point of addition leading to worse dispersion. However, as the addition rate increases further to 20 $\%_{wt}$ the PSD shifts again to smaller size. There are two possible explanations, an increase in the effectiveness of the collision mechanism or most likely the increased volume fraction of the additive leads to an increase in the viscosity of the overall composite and thus higher shear hydrodynamic stresses being transferred to the agglomerates enabling more effective rupture. The change in viscosity can be approximated with the Einstein equation for volume fraction up to 10 % or Krieger-Dougherty equation for more concentrated systems (Remmler, 2015). For the FR-1 additive the viscosity increase for virgin H-PET at 275 °C is in the region of 400 Pa s according to Krieger-Dougherty equation which can translate to a significant shear stress increase depending on the shear rate.

9.1.3.3 Additive injection point

Across the *Berstorff ZE40A* and *Dr Collin ZK25* machines several additive injection options were evaluated in accordance with the possibilities of each piece of equipment. The level of mixing was determined comparing the particle size distribution of the additive and an equivalent masterbatch process. An initial investigation was carried out on the *Berstorff ZE40A* machine with the *split feed* method of addition being considered. Although the *premix* method would be possible on this machine it is undesirable due to the high throughputs (up to 160 $kg\,h^{-1}$) which would require significant quantity of dry blending which was not possible.

Figure 9.26 shows the level of mixing achieved in FR-1/H-PET composites manufactured at various levels of addition. Interestingly the particle size distribution supplied by the manufacturer differs significantly to that obtained internally at DTF on a Coulter LS1320 laser diffraction instrument. The PSDs captured by supplier used acetone as carrier and dispersive aids, whereas PSDs captured at DTF utilised demilitarised water with no

dispersive aids. Two PSDs were obtained at DTF, one with the powder in its raw form and the other with the powder being high shear mixed for 20 min in T25 Ultra Turrax machine. The method utilised at DTF is believed to be superior due to the use of the Mie Scattering model for PSD analysis which accounts for the absorption of light and the refractive index of the material as opposed to the Fraunhofer model that is commonly used in industry and only accounts for diffraction scatter (Rakos, 2016). On the basis of this any comparison in mixing will be made against this method.

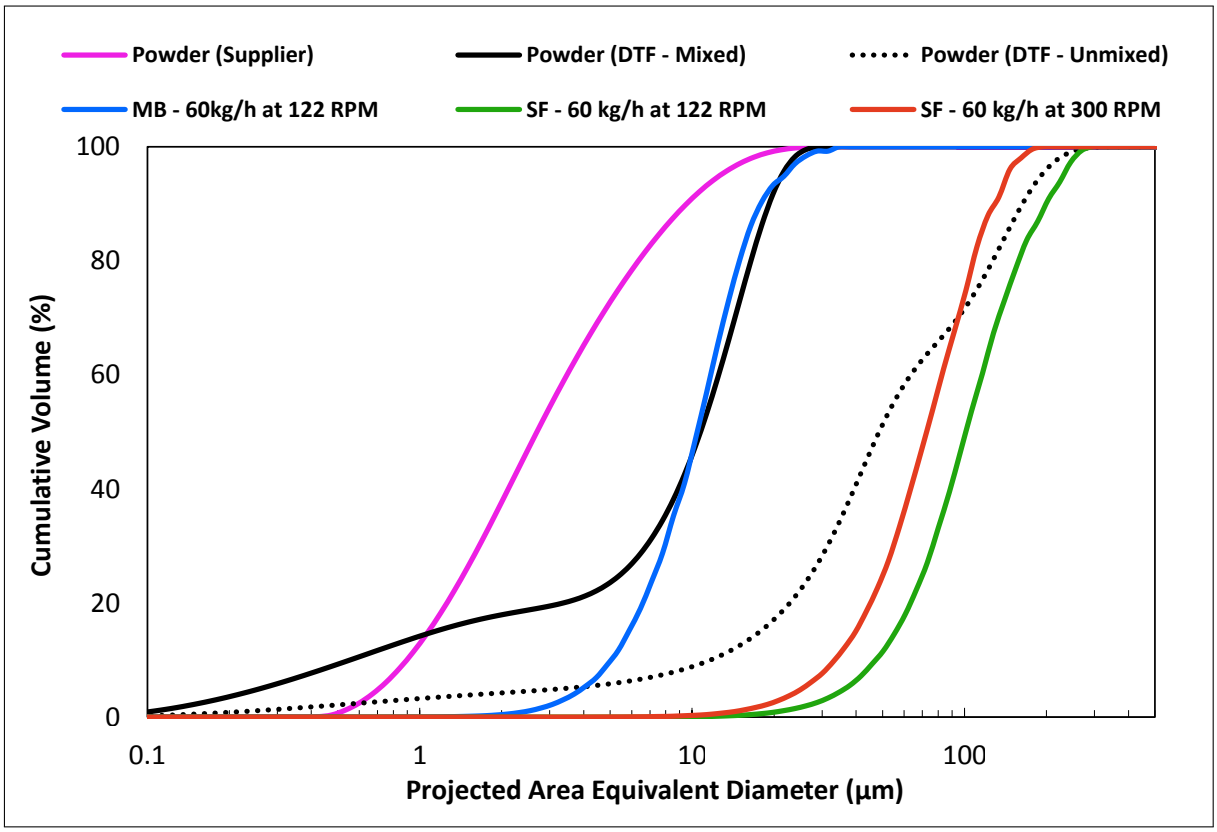

Figure 9.26: *Comparing additive injection method for H-PET composites containing FR-1 additive manufactured on Berstorff ZE40A machine using split feed method at a loading of 4 $\%_{wt}$; captured at magnification x2.5*

It is evident from the Figure 9.26 that the composites manufactured via the current masterbatch route achieve very good dispersion, reducing the agglomerates to the base particle size of the powder especially at the top end of the distribution. There is some discrepancy at below ca. 30 % cumulative volume where the powder is much smaller. This is a direct result of the water being able to penetrate dipper into the agglomerate during the high

shear mixing process than the polymer in the extrusion process leading to the break down to smaller sizes. The *split feed* method of addition lead to very poor degree of mixing, with the PSD obtained being much larger indicating some further agglomeration during the feeding and/or extrusion process. Although the PSD of the sample manufactured at a higher screw speed (loading of 5 $\%_{wt}$) yields improvement in mixing it is still very far away from the PSD of well dispersed powder. There are several potential causes with the first being cold agglomeration of the powder prior to and in the melt zone during material compression making it much harder to disperse. The most likely reason is that the very gentle nature of the screw configuration utilised within the *Berstorff ZE40A* machine which has a total mixing element length equating to 4.5 $^{L}/_{D}$ not being sufficient to deliver full dispersion in the extrusion process.

Further investigations were carried out on the *Dr Collin ZK25* machine which has a much more severe screw profile with the total length of the mixing elements equalling 11.5 $^{L}/_{D}$; see Figure 9.27. It is evident that in this case very good mixing is observed. Overall the *masterbatch* process route leads to slightly smaller particle size compared to the *premix* and the *direct to melt* (DA) addition methods. This can be accounted for by the additive being processed twice through severe extrusion mixing processes. The *premix* route seems to generate more smaller particles as can be seen though the lower end of the distribution being further to the left than the *direct to melt* addition method (red line in Figure 9.27). This is a likely result of the increased residence time that the additive experiences via this method enabling more effective erosion. On the other hand the greater compaction forces in the melt section seem to induce few more larger agglomerates increasing the D_{90} slightly.

All three methods appear to lead to slightly smaller particle size compared to the base additive powder suggesting some attrition of the additive. However, a more likely explanation is that the magnification utilised to obtain was set to high. This is illustrated with a direct to melt addition sample from a separate trial where the $\times 5$ magnification was

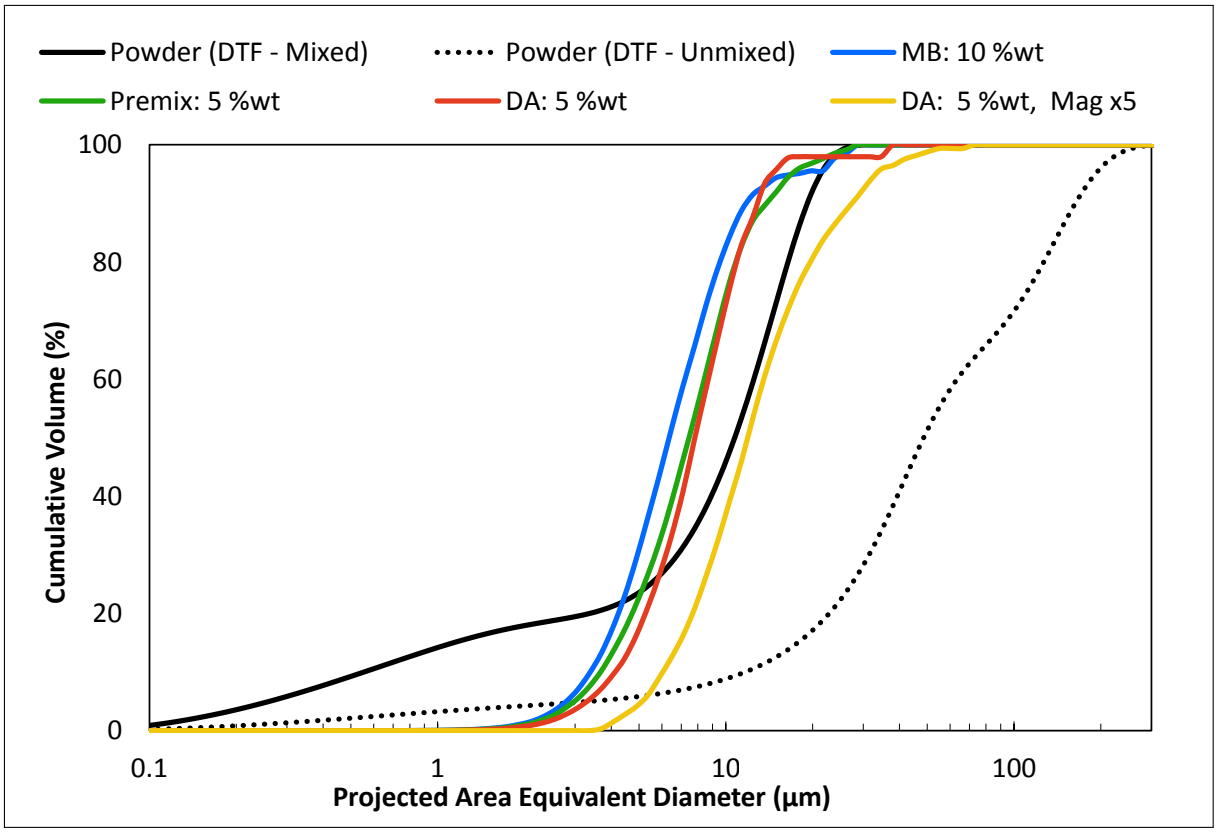

Figure 9.27: *Comparing additive injection method for H-PET composites containing FR-1 additive manufactured on Dr Collin ZK25 machine at ca. 6.5* $\mathrm{kg\,h^{-1}}$ *and 290* rpm *using premix and direct to melt methods at a loading of 10* $\%_{wt}$*; captured at magnification x20*

utilised instead of ×20 to obtain the PSD, leading to a particle size distribution which closely resembles that of the additive powder itself. There are some larger agglomerates present, however this is far from the poor level of mixing which was achieved on the *Berstorff ZE40A* machine. These results illustrate that although the operating conditions offer a level of control over the mixing, a well configured screw design is vital for the good dispersion of the additive.

9.2 Concluding Remarks

Changes in the operating conditions and the set up of the extrusion process offer a direct control over the level of mixing achieved during the polymer composite manufacture. Within this field, there is limited literature on the dispersion of additives in the PET

matrix. This chapter addresses this gap in knowledge by examining how the level of dispersion in bottle grade and film grade PET based composites (containing several grades of FR additives) was influenced by the changes in the operating conditions and the set up of a twin screw extruder. Several parameters were considered, including directly controllable and calculated parameters as well as impact of the product recipe and machine set up. The observed changes in dispersion were related to the different dispersion mixing mechanisms.

Under the controllable parameters umbrella the screw speed had the most significant impact. The level of mixing was seen to increase with speed. This is in agreement with Kasaliwal et al., 2010; Villmow et al., 2008 who investigated the dispersion of MWCNTs. Critically, this was only true up to a certain speed, beyond which the mechanical chain scission of the polymer lead to a drastic reduction in the viscosity of material and much poorer dispersion through the rupture mechanism. In their findings Fortunato et al., 2014 reported better dispersion of titanium dioxide in PET with increasing speed, but the authors did not observe a limiting screw speed value. A reduction in output was also shown to lead to better dispersion of the additive. In this case the reduced level of fill which resulted in higher average shear rate promoted the erosion mechanism and significantly increased the number of fine particles.

The changes in controllable parameters influence the calculated parameters. These offer a level of insight into the changes in the mixing mechanisms. Specific output (which represents the degree of fill within the extruder) was one of the critical parameters, with a reduction in the parameter leading to better mixing. This is in agreement with Donoian and Christiano, 1999 who also observed improved mixing at a lower specific output. However, when the degree of fill decreases so much that the higher shear transfers more energy into the polymer it leads to a worsening of mixing below a certain value of the degree of fill. This was related to the energy input which exhibited a similar trend. Initially an increase in the energy input promotes better mixing, but beyond a critical value

(which likely is system specific) the level of dispersion achieved decreased with increasing energy input.

Kasaliwal et al., 2010 observed improved dispersion of MWCNTs in polycarbonate matrix with increasing residence time. The results presented here show that the residence time had no strong correlation with the level of dispersion. Unlike Kasaliwal et al., 2010, who examined the role of residence time in a batch extrusion process, the results presented here are for experiments performed on a continuous twin screw extrusion process. In this case the residence time can not be controlled directly and is a function of changes in other parameters such as screw speed and output. No relationship between the residence time and mixing was observed on the *Berstorff ZE40A* machine and increase in mixing with decreasing residence time trend was observed on the *Dr Collin ZK25* machine which was related to the increased shear under these conditions. Due to the short residence time in a TSE, the erosion mechanism (residence time controlled) has a much lower influence compared to the rupture mechanism which is largely shear stress dependent.

In this chapter, an attempt to relate the level of mixing to a set of newly proposed parameters was made. '*The residence time weighted average shear stress*' based on the extrudate polymer viscosity showed no correlation with the level of dispersion achieved. However, there was a trend between the level of mixing and the same parameter calculated on the basis of the virgin polymer melt viscosity. As the shear stress is notoriously difficult to calculate due to the distribution of shear rates as well as the changing melt viscosity, a relationship with shear rate was examined. In particular '*the total residence time weighted shear strain*' which showed promising trends in the majority of cases. This parameter accounts indirectly for the shear stress which the polymer sees as well as relates this to the residence time of the material in the extruder. Some indication of poor fitting at very low output (high residence time) was observed as these conditions yielded very high strain values and yet the mixing was poor due to the viscosity reduction of the polymer.

Investigations into the effects of product recipe revealed that the level of dispersion de-

creased with increasing loading, in particular on the *Berstorff ZE40A* machine which has a gentle screw configuration. Similarly, the influence of additive injection point was also evaluated. On the same machine, the dispersion of the additive was very poor with the composites manufactured via the *split feed* method. Here, some agglomeration was seen when compared to the powder in its 'stored' state. Here the existing masterbatch route provided a much better level of dispersion, achieving particles size in the composite very similar to the powder itself. Much more promising results were obtained on the *Dr Collin ZK25* machine which has a more severe screw profile showing the masterbatch route to be comparable with the direct to melt addition and premix method of manufacture. This shows the importance of having an appropriate screw configuration; effects of which were examined in Appendix J.

Lastly, the impact of barrel zone temperatures was also examined. Changes in temperature directly post additive injection yielded minute gains. Changes in temperature in the latter zones of the extruder yielded inconclusive results. In either case, this would not be an appropriate method of mixing control on the larger scale machine as the surface area to throughput ratio decreases drastically with increasing machine diameter which in turn reduces the efficiency of barrel cooling/heating process. This is still an important parameter to consider during a novel process set up in order to prevent processing issues such as polymer un-melts caused by the localised reduction in temperature in highly loaded systems.

10 | Concluding Remarks

Although, the bi-axially oriented PET films market is a rapidly expanding one with numerous new potential applications being proposed year on year, the changing nature of the sector leads to the requirement for rapid product differentiation capability. This promotes the use of the direct addition technologies within the film manufacturing process. The research presented within this thesis focuses on the development of such technology which enables additives to be introduced into the film making process without the need for a pre-dispersed masterbatch.

During the development various aspects associated with the manufacture of PET based composites on twin screw extruders, such as operating conditions and machine set up, were studied and the results presented can be transferred to other applications including compounding of PET. In the process a number of polymer-additive systems were considered in order to investigate the effects of the material properties as well as the interactions between the additive and the polymer on the level of mixing achieved.

The key outcomes of the thesis include:

1. Proposal of novel parameters the '*residence time weighted average shear rate, stress* and *strain*' which can be utilised to compare various twin screw extrusion processes and assess the impact of the changes in the operating conditions, screw geometry and machine size on the flow and stress fields within the extruder. These parameters were used to better understand the dispersion process as well as the mechanisms behind the molecular weigh loss during extrusion processing and can be calculated via the model developed in Chapter 6.

2. Comparison between the measured values for molecular weight loss achieved during extrusion processing at various operating conditions with those predicted from the understanding of the chemical reactions occurring during melt processing. Such

study is novel and has led to the identification of two different regimes that govern the molecular weight loss. The first is driven by the chemical reactions (controlled by the residence time) which occurs at low screw speeds and the second is driven by the mechanical chain scission (controlled by the shear stress) which occurs at higher screw speeds. A strong correlation between the residence time weighed average shear stress seen by the polymer and the IV loss under operating conditions that result in the high energy input to the polymer was identified; see Chapter 7. From the experiments, it is evident that pre-heating the polymer reduces the demand placed on the extruder, allows gentler heating of the melt and thus minimises the IV loss.

3. Identification of the polymer viscosity as the critical material parameter which influences the level of dispersion achieved. The polymer viscosity ultimately determines the shear stress transmitted to the agglomerates and thus the effectiveness of agglomerate dispersion via the rupture mechanism. This is in agreement with study by Kasaliwal et al., 2011 on dispersion of MWCNTs in polycarbonate matrix. Unlike in existing literature which either considers the properties of the polymer or the additive, the role of additive properties was also considered within this study. Longer aspect ratio additive particles were harder to mix due to the increased mechanical interlocking between the particles. Additive porosity proved critical in determining the bulk density and thus the optimum feeding method. In addition, a limiting volume fraction of the additive was identified above which the material became to brittle; see Chapter 8.

4. Proposal of a method to quantify the strength of the additive - polymer interactions via the contact angle measurement and the calculation of the work of adhesion. Strong interactions between the additive and the polymer are critical in encouraging wetting and thus enabling dispersion by facilitating the transfer of energy. Dispersive aids were utilised to modify these interactions with varying degree of success; see Chapter 8.

5. Identification of the key extrusion process parameters that influence the degree of dispersion achieved. Screw speed was shown to have the greatest affect; similar to Kasaliwal et al., 2010. However, beyond a critical speed the high shear starts to induce mechanical chain scission of the polymer which leads to decrease in viscosity and hence reduction in the effectiveness of mixing. Degree of fill and specific mechanical energy input are vital parameters for determining the role of individual mixing mechanisms. Interestingly, no correlation between the degree of mixing and the residence time was observed. This is due to the rupture mechanism being dominant method of dispersion in the systems studied and the difficulty in isolating the residence time from other parameters such as the shear stress. A promising correlation between the increasing total residence time weighted average shear strain and improving dispersive mixing was observed.

6. Analysis of impact of the different screw configurations on the level of dispersion achieved. Within this research a number of configurations were tested, showing a minimal impact on dispersion and yielding inconclusive results. Majority of the changes in dispersion observed as result of screw configuration alterations were smaller than that achieved by changes in the operating conditions. As the residence time does not have a significant effect on the level of mixing achieved and the screw configuration mainly changes the residence time distribution under the same operating conditions, this could potentially explain the low impact that the screw configuration had on mixing. Critically, this in turn suggests that the screw profile should be maintained as gentle as possible in order to minimise IV loss and hence viscosity reduction. The results contradict that of Villmow et al., 2010 who saw better dispersion of MWCNTs with TME elements when compared to kneading block elements.

Lastly, a different approach for determining the level of mixing achieved was proposed. This was based on the comparison between the size distribution of the additive within the polymer matrix and that of the additive powder which enables for the role of the

different mechanisms to be studied. This is deemed not possible with the commonly used methods within the literature such as area fraction which allow a comparison between different samples, but do not indicate the nature of changes that occur to the particle size distribution. Further more, in film manufacture a the representative sample for the particle size distribution of the additive can be obtained by examining the surface of the cast film. This was shown to be a representative of the particle size distribution within the bulk of the material.

11 | Future Work

Following the work presented here some further research can be recommended; this includes the following areas:

1. *Extrusion model* - Although the model presented here has proven useful in comparing different operating conditions, helped to better understand the fundamental mixing mechanisms and the molecular weight loss PET suffers during extrusion, improvements can be made. These include modifying the model to account for the number of polymer passes through the high shear clearance regions as well as including calculations for the slotted and toothed mixing elements.

2. *Quantifying additive-polymer interactions* - An attempt has been made to quantify the strength of the interaction between the polymer and the additive. Improvements to the method should focus on better characterisation of the contact angle for the additive powders. This may be achieved through the use of Washburn method or inverse gas phase chromatography. However, these would only yield more accurate estimates of the interactions. It may be possible to measure the interactions directly by monitoring the forces involved with the use of hot stage atomic force microscopy and functionalised tips.

3. *Material properties* - Since it turned out that the grades of the additive utilised in trying to understand the role of particle size on the level of dispersion had overlapping distributions it was hard to reach definitive conclusions. Instead of relying on a supplier to provide significantly differing grades of material it may be possible to separate these by different size exclusion techniques which would yield a more monodisperse distribution of the additive. A comparison between the size of the additive in the composites manufactured with these monodispersed fractions would yield a much better indication of the role of particle size in a governing dispersion.

4. *Screw configuration* -

(a) The results presented on the role of screw design in determining the degree of mixing yielded mixed results. In all of these the differences in dispersion obtained between the different configurations were very small, which were attributed to the negligible impact of residence time in the extruder on mixing. However only standard kneading block and mixing elements were tested. It would be of great interest to examine the dispersive capacity of other elements, including those that generate extensional flows.

(b) Similarly, the significance that the polymer viscosity played in determining degree of dispersion was clear. This warrants further research into the impact of different screw configurations on the IV loss seen by the polymer and hence its final viscosity when processed with differing screw configurations. Specifically, it may be possible to optimise the screw profile to reduce the mechanically induced chain scission within the polymer in the melting section, particularly during high screw speeds, which would then enable much higher stresses to be transferred to the agglomerates further down the extruder thus facilitating much better dispersion of the additive.

A | A review of the intermeshing co-rotating twin screw extruders

Padmanabhan and Jayanth (2008) describes the key criteria for defining a successful extrusion process as being energy consumption, production capacity and uniformity of the melt produced. Unlike in single screw extruders (SSEs) where output of the machine is directly related to the screw speed, in twin screw extruders (TSEs) these are independent allowing for greater control of the energy input and mixing quality.

The added benefit of TSE is in its modular design, which theoretically allows for the screw profile to be reconfigured based on the demands of an individual product. This can be achieved without the expense of an extra set of screws that would be required for a SSE process. Considerably different performance potentially can be delivered through reconfiguring the layout of the existing screw elements, or with little investment into another type of mixing elements. In reality, such changes are rarely done in practice with companies utilising the same profile for numerous applications.

Discussions in this thesis will focus on 2 threaded designs of twin screw extruders, since the earlier 3 threaded design is rarely used due to its limitation on free volume of the extruder and hence the output of the machine (Giles et al., 2005; Kohlgrüber, 2008).

A.1 Extruder zones

A twin screw extruder consists of several key zones: *intake/feed, melting, degasing (primary and secondary; based on application), downstream feeding, mixing* and *metering*, with each zone having a specific function. Selected screw profile design has to maintain the effectiveness of each zone whilst ensuring that the process delivers the correct amount of work to the material allowing complete melting and mixing to be achieved. One of the

key aspects to be considered is the free volume within the machine, in particularly when dealing with low bulk density additives as discussed in section 2.3.

A.1.1 Intake zone

The primary function of the *intake* zone of the extruder is to accept the materials being fed onto the screws of the extruder and convey them to the melting zone whilst allowing the air entrained within the material to escape back via the feed pocket opening. TSE processes are typically operated starve fed allowing the output to be determined by the feed rate of the material while the screw speed controls the degree of fill within the machine and hence the residence time.

The polymer can be fed into the extruder either in pellet or low bulk density flake form resulting in the need to select the appropriate screw element to ensure that there is enough free volume within this section to handle the volumetric flow rate of material. When dealing with low bulk density materials, there is an added challenge of the material potentially being fluidised by the escaping air, especially when operating at high outputs. This effect can be minimised by operating the melt zone partially filled and allowing the degassing section to remove the air introduced with the feed (Kohlgrüber, 2008).

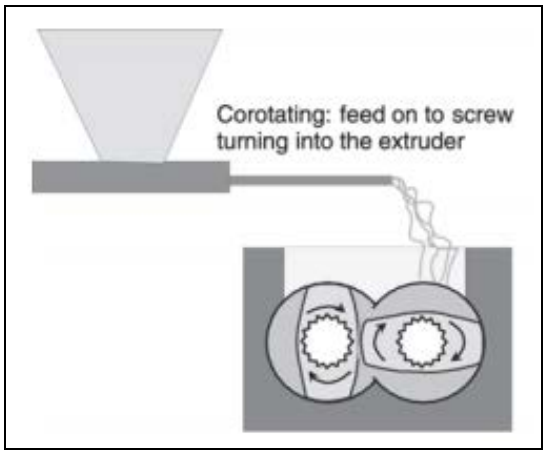

Figure A.1: *Polymer feeding in intermeshing corotating TSEs; from Giles et al. (2005, p.104)*

Intake zone length of around 4 to 6 D is enough to ensure effective feeding of the product. Kohlgrüber (2008) advises the use of elements with a pitch of 1.5 D directly below the feed pocket to convey the material forward and then reduce this to 0.75 or 1 D in order to compress the material and raise the degree of fill prior to the melting zone. Typical elements used in the intake zone are illustrated in Figure A.2.

Ideally the feed is introduced on top of the screw which is rotating toward the barrel wall allowing for the material to be rapidly conveyed beneath, see figure A.1. If the material is fed onto the other screw, there is a need for material to be transferred from one screw to another which increases the risk of polymer pellets or additive bouncing out of the feed throat at high screw speeds reducing the accuracy of the process.

TABLE OF INTAKE ZONE ELEMENTS

ELEMENTS		CHARACTERISTICS			POTENTIAL USE
NOMENCLATURE	GEOMETRY & PROFILES	CONVEYING EFFICIENCY	FREE VOLUME	TENDENCY TO BREAKUP AND COMPACT	
Single Flight 'V' Element		Highest	Medium	Medium	All Types
Forward Screw Element		Low	Medium	Medium	Pellets
Deep Flight Schubkanten		Low	Highest	Medium	Tri-lobed Force-fed Extruders
Schubkanten Element		High	High	High	Powders, Mix of Powders and Granules
Special Schubkanten Element		Low	Highest	Medium	Bi-lobed Force-fed Extruders
Single Flight Elements		Medium	Low	Low	Alloys & Blends with different melt characterization

Figure A.2: *Typical screw elements in intake zone for corotating TSE; from Padmanabhan and Jayanth (2008, p.31)*

The intake zone of the extruder is normally water cooled to ensure that the polymer does not begin to melt and adhere to the feed throat or the screw thus limiting the feeding capacity. If the recipe contains a small loading of additive, this can be introduced into the feed pocket either as premix with the polymer or via a separate feeder; benefits of each method are discussed in Section H.8. It is vital to understand the tendency of the screw elements to compact the material if a powdered additive is being introduced here, as this will increase the dispersive mixing requirement of the mixing section.

Liquids can be introduced here too, although preferentially they would be added directly to the melt later in the extrusion process in order to eliminate any risk of the liquid allowing polymer to slip on the barrel thus causing issues in feeding.

A.1.2 Melting zone

Polymer melting is commonly imagined as a phase transformation from a solid to a liquid state. In reality, semi-crystalline polymers such as PET undergo partial melting with the crystalline regions melting out and the amorphous regions undergoing glass transitions. The melting zone of the extruder is designed to generate enough heat for such transition to occur. Viscous heating of the polymer is achieved as a result of inter-pellet friction as well as friction between the pellets and the extruder barrel. Some heat is transferred from the barrel wall, but this is small in comparison to viscous heating with (Morton-Jones, 1989) reporting the ratio as 33 % to 67 % respectively. Typical elements utilised in the section are shown in Figure A.3. Large pitch conveying elements are used post melt zone to transport the material to the next processing section whilst minimising the work on the polymer. Depending on the application, extra large pitch (6 D) elements can be utilised to homogenise the melt (Kohlgrüber, 2008).

TABLE OF MELTING ZONE ELEMENTS						
ELEMENTS		CHARACTERISTICS				POTENTIAL USE
NOMENCLATURE	GEOMETRY & PROFILES	MELTING ABILITY		DISPERSIVE MIXING ABILITY	SHEAR UNIFORMITY *	
		AMORPHOUS	CRYSTALLINE			
Fractional Kneading Element		Highest	Highest	Highest	High	All types of Melting and Dispersive Mixing
Forward Kneading Element		Low	Medium	Low	Medium	Easy to Melt Crystalline Material
Reverse Kneading Element		Medium	High	Medium	Medium	Crystalline Material
3KB Kneading Elements		High	Highest	High	Medium	Amorphous
Neutral Kneading Elements		Medium	High	High	Low	Not usually recommended for Melting Used for Mixing

Figure A.3: *Typical screw elements in melting zone for corotating TSE; from Padmanabhan and Jayanth (2008, p.32)*

Melting in the SSEs occurs via well defined and understood mechanisms of *Continious Solids Melting* proposed by Tadmor (1966) and *Disperse Solids Melting* (DSM) modelled by Huang and Peng (1993) (as sited in Cunha et al., 2008, p.505), with a good comparison between the two models being given in Rauwendaal (1996a). In TSEs the melting mechanisms are less well defined and much more complex. Rauwendaal (1996a; 2010) simply states that in TSEs melting occurs via the DSM model, with work of Linjie and Xiaozheng (2000) pointing out the complexities of the process (see Figure A.4); especially how it depends on screw configuration, operating conditions as well as the material properties. Linjie and Xiaozheng analysed the melting mechanisms of HDPE in a co-rotating twin screw extruder via a glass visualisation window to determine 10 substages of melting as well as the conditions in which they occur.

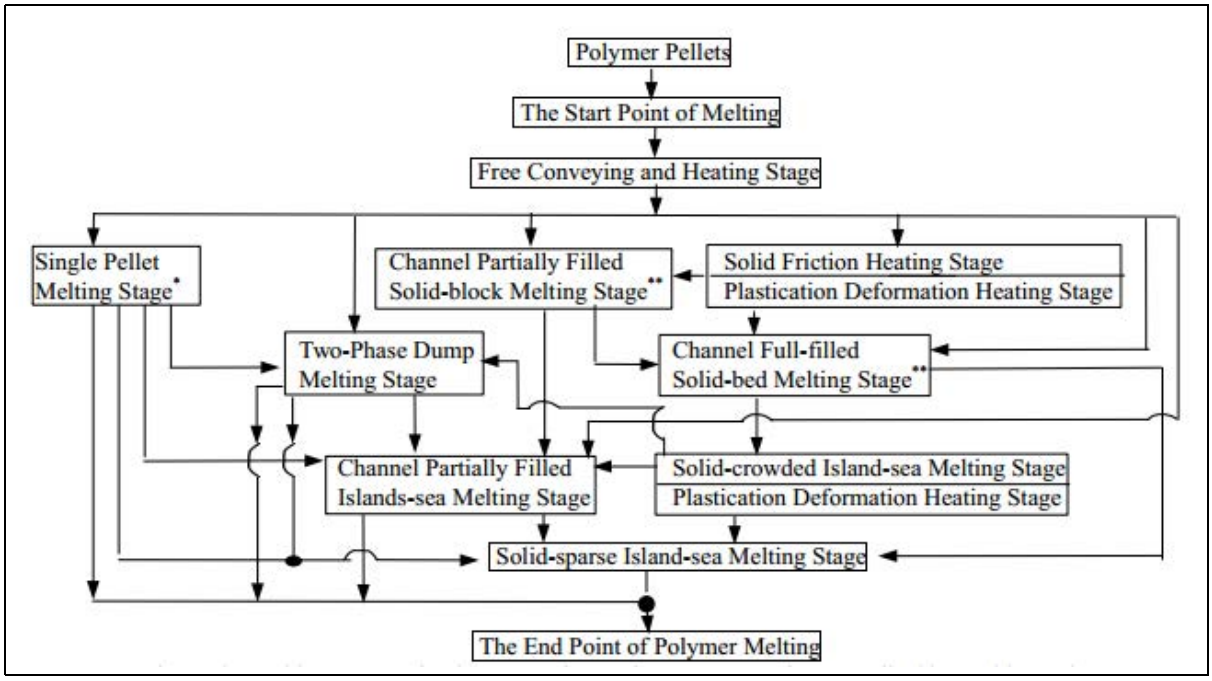

Figure A.4: *Stages of polymer melting in corotating TSE; from Linjie and Xiaozheng (2000, p. 151)*

Melting in the TSE is highly influenced by the degree of fill and residence time, hence throughput, screw speed and the geometry of the screw are vital parameters to consider in this section. One should also be aware of the heat flux into the zone from the barrel, pellet size, specific heat capacity and the enthalpy of melting for the material which is being processed. The length of the melting zone can be made shorter by increasing the degree of fill, utilising smaller pellets as well as using narrow kneading blocks (Kohlgrüber, 2008) with higher compression promoting melting of crystalline polymers (Padmanabhan and Jayanth, 2008).

The length of the zone can be further reduced by introducing solid additives (fillers). This increases the viscosity of the matrix leading to higher viscous heating, hence a higher melting rate as well as reducing the amount of energy required in the process by reducing the quantity of polymer being processed at a given output (Stevens and Covas, 1995). The additive also increases the energy dissipation rate leading to a reduced melting length (Tadmor and Gogos, 2006). However, this increased rate may lead to overheating of the melt and thus polymer degradation. The use of liquid additives, or additives which melt

into a liquid of a lower viscosity (such as waxes) may lead to the additive migrating to the barrel surface and preventing the formation of a melt film hindering the melting process and thus increasing the melting length (Kohlgrüber, 2008).

If additive is introduced together with the polymer into the feed zone, then the melting section acts as the first mixing section for the additive. The zone promotes dispersive mixing due to the high polymer viscosities involved in the section, which in turn allow higher shear stresses to be reached and promote the possibility of elongational flows (Padmanabhan and Jayanth, 2008).

A.1.3 Degasing zone

Degasing zones can be either atmospheric or run under applied vacuum and are utilised in TSEs to facilitate the removal of moisture, volatile components and any air that is introduced together with the feed. A second zone is often used post the additive side feeder zone to remove air that is forced into the extruder together with the additive.

Within DTF, twin screw PET extrusion processes are operated with degassing zones being subjected to a strong vacuum in order to promote rapid removal of moisture, which is so critical in preventing the hydrolysis of PET molecules. This allows for the use of un-dried PET in the process. The devolatilisation process is driven by the superheating of volatile components and exposure of the melt pool to rapid decompression under the vent. In order to achieve a strong vacuum an effective melt seal is critical both post and prior to the zone, with a length of up to 1D being required (Padmanabhan and Jayanth, 2008) to prevent leakage flows. The seal can be achieved by reducing the pitch of the conveying elements, or a more robust seal can be generated by utilising reversing elements (conveying or kneading block) in order to generate a fully filled section. The elements in the vacuum zone are selected to continuously expose a thin film of polymer and allow for continual surface regeneration. Typically long forwarding or schubkanten elements are utilised, with the undercut elements giving 20 % increase in the free volume

(Padmanabhan and Jayanth, 2008). This increases the surface area and promotes the devolatilisation process.

Martin (2014) provides a good overview of the vacuum system design which includes the following components:

- *Vent stack* is located directly on top of the barrel, typically incorporating glass or an 'o' ring seal, a pipe connection for the vacuum hose; in PET process this is often heated to ensure the self cleaning of the stack.
- *Interconection plumbing* typically consisting of rubber piping pitched downwards to allow material to flow to the knock-out pot.
- *Knock-out pot* should be located as close to the extruder as possible and is the first vessel that the gas stream encounters, which will collect most of the solids and liquids removed by the stream. Baffles are often added to the pot to promote the change in direction of the flow allowing the material to settle.
- *Liquid condencer* may be required depending on the composition of the stream leaving the extruder.
- *Dry filter* is the last line of defence protecting the vacuum pump.
- *Vacuum pump* is used to generate the required suction, typically leading to pressures of around 130 to 60 mbar, with PET process often running at higher levels by utilising a two stage pump.
- *Vent stuffer* is sometimes utilised to force low viscosity material back into the extruder, allowing the machine to be operated at a higher degree of fill and hence throughput.

The vent is normally located around 6 L/D from the discharge, or sooner to promote increased stability in melt pressure. In PET processing the first vacuum vent is located as soon as the material has melted in order remove the moisture.

Degree of fill is a key parameter for this zone, with low degree of fill being targeted in order to prevent material escaping though the vent and to increase the surface area. A number of baffles can be utilised in the vent to prevent the polymer from being ejected into the vent; see Figure A.5. Type B and C is used with polymers that adhere to the screw, such as PET, with type C insert being preferred when a large volume of gas needs

to be removed. In order to enable higher throughput, and hence running at a higher degree of fill a stuffer screw can be used to force the polymer back into the extruder.

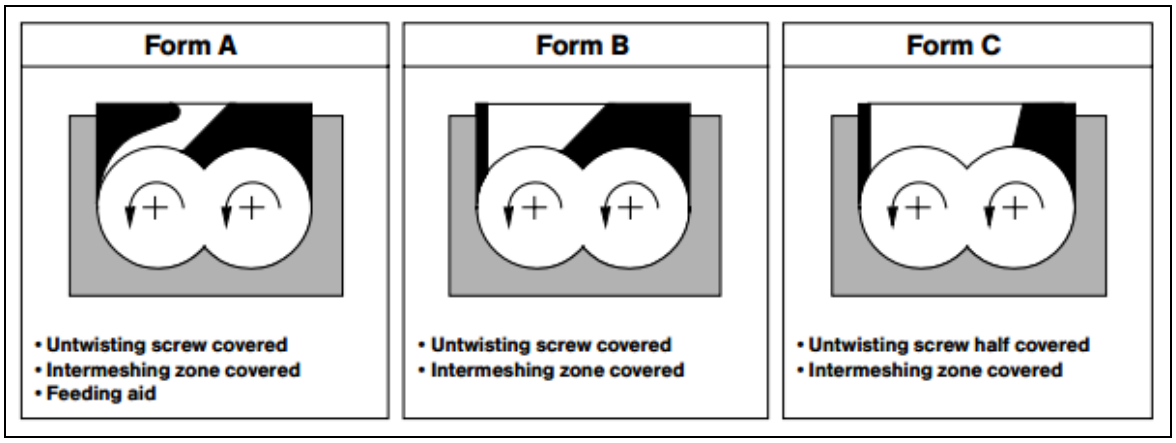

Figure A.5: *Types of degasing vent inserts; from Kohlgrüber (2008, p.70)*

Degree of fill is a function of the operating conditions (throughput, screw speed), element design and screw configuration. Figure A.6 illustrates the effect of Degree of fill and screw design on available surface area. Experiments on removing methanol from active pharmaceutical ingredients by Martin (2014) showed that the devolatilisation depends linearly on screw speed and feed rate. The use of vacuum significantly improved the devolatilisation capacity.

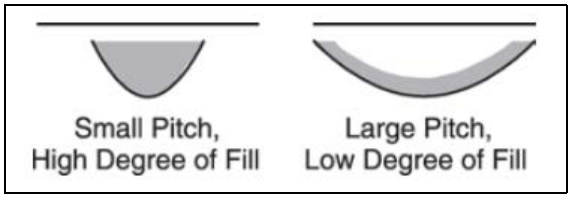

Figure A.6: *Influence of degree of fill and screw pitch on the surface area; from Giles et al. (2005, p.123)*

The optimum operation of a degassing vent can be achieved under the following conditions, as described by (Kohlgrüber, 2008; Martin, 2014):

- *High vacuum level* promoting low equilibrium concentration.
- *High screw speed* allowing increased surface renewal of the melt and lower degree of fill leading to increased surface area of the melt.
- *High residence time* to facilitate removal of volatiles; however excessive exposure to shear, temperature and oxygen may introduce degradation of the polymer.

- *High melt temperature* leading to high diffusion constant and low equilibrium concentration.
- *Bubbles (froth generation)* help devolatilisation; sometimes stripping agents may be added.

It is vital that the volatiles being extracted do not condense on the stack and fall back into the extruder, as this will lead to contamination issues. In PET processing the build up of oligomers is a key concern, and this can be prevented by appropriate vent design. Oligomers are deposited in the vent if the surface temperature is less than 200 °C, so the temperature must be maintained higher than this. However, it needs to be maintained lower than 255 °C in order to prevent any polymers from falling back down into the extruder (Ellam, 2007).

A.1.4 Downstream feeding zone

Downstream feed sections are used to introduce additives directly to the polymer melt as opposed to adding them together with the polymer into the intake zone of the extruder. The advantages of this method is discussed in Section H.8. It is possible to have the additives gravity fed directly onto the screw as long as there is the capacity within the system to accept the extra volume (Giles et al., 2005). More often, the additives are fed from a gravimetric feeder into a side feeder (sometimes referred to as stuffer feeder) which forces the additives into the extruder. The side feeders are operated in a *starve fed* mode to ensure control over the additive flow rate (Giles et al., 2005). This has several advantages especially in handling of lower bulk density additives which may become fluidised by the escaping air in the direct feed method. For comparison see Figure A.7.

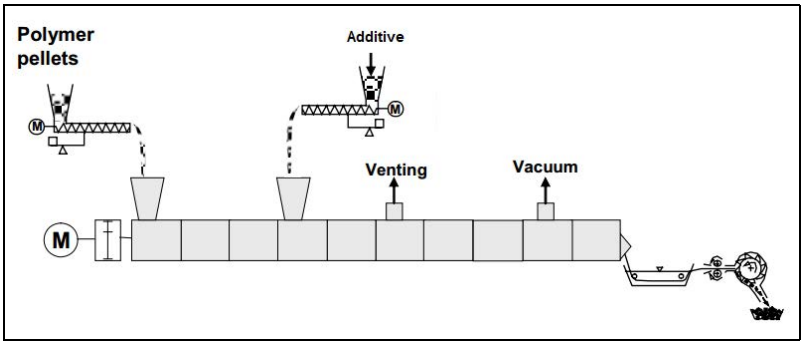

(a) Direct Feed Process

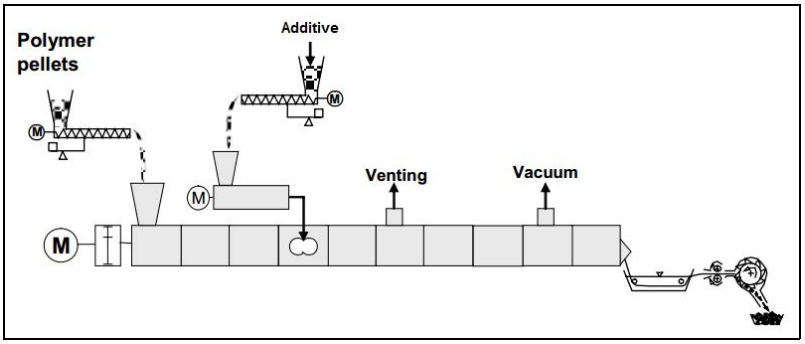

(b) Side Feed Process

Figure A.7: *Downstream feeding proceses; addapted from Kohlgrüber (2008, p.81)*

Multiple downstream feeding zones can be utilised in a compounding process when high proportions of filler are being added. This ensures that the additive is fully wetted out after each zone reducing agglomerate formation and the need for dispersive mixing. The incorporation of powdered additive via this method is typically a volume limited process, thus one needs to ensure that the screws provide the greatest free volume and conveying capacity possible. Typically a kneading block section will be utilised just prior to side feed to inhibit the polymer flow and generate the free space required for the additive.

Undercut or double undercut elements (see Figure A.8) are used within the zone for very low bulk density material. These offer 15 % to 30 % increase in free volume (Kohlgrüber, 2008), however they loose some of the self wiping ability increasing the risk of product building up next to the flanks of the screw. Such dead spots have the potential to lead to polymer degradation within the extruder. It should also be noted that as the free volume increases the conveying efficiency of the element decreases. If possible for the application,

standard large pitch elements should be utilised within the zone to ensure material is rapidly conveyed forwards, whilst maintaining the self wiping ability of the screw.

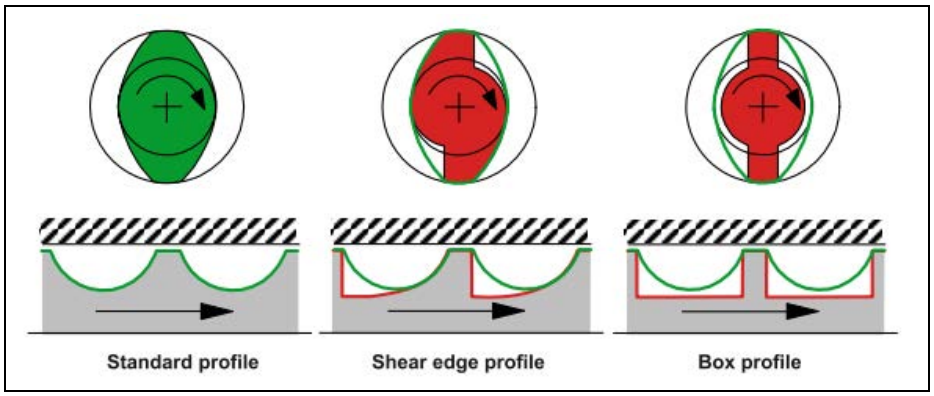

Figure A.8: *Profile of undercut and double undercut elements; from Kohlgrüber (2008, p. 222)*

The mixing is performed in partially filled sections to ensure that the air which enters into the extruder with the additive can escape via the degassing port adjacent to the additive entry point (Kohlgrüber, 2008). It is important that the additive is fully wetted out before it reaches the degassing zone to ensure that the additive is not removed by the escaping air, especially in the case of low bulk density materials. As the filler content increases more energy is required to wet the additive.

Temperature of the polymer in this zone is a key parameter. When introducing the filler in large volumes one has to ensure that the temperature of the polymer does not drop below its melting temperature; particularly important in semi-crystalline and crystalline polymers. As the temperature reduces polymer viscosity will increase and the polymer may begin to crystallise and solidify increasing the load on the extruder. For large loadings the additive may be preheated to ensure that the reduction in polymer temperature is minimised. A balance has to be achieved between maintaining a low polymer viscosity in the side feeding section to facilitate the wetting of the additive and then increasing the viscosity of the polymer in the later mixing stage. The increase in viscosity will increase the stresses being transferred to the agglomerates thus promoting the dispersive mixing of the additive.

In cases where the polymer is sensitive to the moisture contained within the additive and moisture extraction in the extruder is not sufficient then the additive may have to be pre-dried. This is particularly important if the additive is low bulk density, so there may not be a possibility to apply a vacuum to the degassing section post additive addition as this may in turn remove the non wetted additive.

A.1.5 Mixing zone

The aim of the mixing zone is to deliver a homogeneous mixture of the additive incorporated within the polymer. Padmanabhan and Jayanth (2008) provide a good overview of the functions within the mixing zone of the extruder. The nature of the mixing required depends on the type of system that is being mixed, for detailed discussion see Section G.3. If the additive is miscible with the polymer then the sole task of the mixing zone is to deliver good distributive mixing. That is, achieving a uniform spatial distribution of the dispersed phase in the continuous phase.

If the additive is incompatible with the polymer forming a '*blend*', then the mixing section has to provide good dispersive as well as distributive mixing. The same applies for the mixing of solid additives into the polymer matrix. Dispersive mixing is the break up of large dispersed phase droplets or the agglomerated particles to smaller size units achieved by applying a high shear stress. The dispersive mixing can be improved under the same operating conditions by lowering the cohesive strength of the dispersed phase as well as by changing the nature of flow from simple shear to elongational flow; more detail in Section 2.4.

Another layer of complexity is added when a solid additive (filler) is being incorporated into the polymer matrix, as initial length of the mixing zone is also now responsible for ensuring that good wetting of the additive has taken place. The wetting of the additive within the extruder is caused by the '*kneading*' action which refers to the folding, stretching and pressing of the material. *Complete wetting* is achieved when the additive particle

is fully incorporated into the polymer matrix with the polymer bonding to the particle. In *incomplete wetting*, the polymer can surround the particle, but not be physically bound to it. Complete wetting can be either as a result of *natural* affinity of the polymer for the additive, *facilitated* through the use of a wetting agent such as waxes or *forced* through the use of a coupling agent.

It is important to note, that some of DTF's products specifically rely on incomplete wetting, where the additive particles are dispersed to their primary particle size, and are fully surrounded by the polymer yet there is no bond between the additive and the polymer. This leads to the formation of voiding around the particles upon stretching of the film which leads to changes in the optical properties of the film.

The types of mixing elements typically utilised in the mixing zone are illustrated in Figure A.9. Fractional kneading elements are used to deliver increased wetting functionality, which is a result of the design delivering uniform shear as well as increased elongation flows. Erdmenger or Sakagami elements are also effective in creating good wetting; these are used when kneading is not desirable.

TABLE OF MIXING ZONE ELEMENTS							
		CHARACTERISTICS					POTENTIAL USE
ELEMENTS	GEOMETRY & PROFILES	UNIFORMITY IN SHEAR	ELONGATIONAL MIXING ABILITY	DISPERSIVE NATURE	CLEANING ACTION	WETTING ACTION	
Fractional Kneading Elements		High	Highest	High	High	Highest	Kneading of highly filled materials with Talc, Mica
Forward Kneading Elements		Medium	Low	Low	Highest	Low	General purpose mixing requirement
Reverse Kneading Elements		Medium	Low	Medium	Medium	Medium	Kneading under Compression
Neutral Kneading Elements		Low	Low	Highest	Low	Medium	Intense localised shear or dispersion of agglomerated Pigments
3KB Kneading Elements		High	Medium	Medium	High	High	A better substitute of RKB for general Purpose Mixing Requirement
Screw Mixing Elements		High	Low	Low	Low	Low	Use for Fiber dispersion with reduced attrition
Toothed Block		Medium	Medium	High	Low	Medium	Used for distributive Mixing in shallow flighted extruders
Tooth Mixing Elements		High	High	High	Low	High	Used for high stirring action while blending two or three different polymers
CME:* Erdmenger Type		Highest	Medium	Medium	Low	High	Generally with high clearances between elements, Effective in introducing uniform high intensity shear action
CME:* Sakagami Type		Highest	Highest	Low	High	Highest	

*CME: Continuous Mixing Elements

Figure A.9: *Typical screw elements in mixing zone for corotating TSE; from Padmanabhan and Jayanth (2008, p.34)*

A.1.6 Metering zone

The metering zone of the extruder is the last zone prior to the melt exiting the machine. It is the function of this zone to generate the pressure required to feed the melt pump stably or overcome the pressure drop associated with the die and the rest of the melt system. Here, the melt is transported by the displacement caused by the rotation of the

screws. Narrow pitch screw elements are best for this zone due to the increased degree of fill that is associated with them.

A.2 Understanding flow and shear fields in co-rotating TSEs

Studies on the extrusion process itself began with the 1950's with Darnell and Mol (1956) publishing the first quantitative study looking at the solids conveying mechanism within single screw extruders. A decade later Tadmor (1966) developed on qualitative work of Maddock (1959) to establish a melting mechanism within single screw extruders. A history of research in the area of twin screw extrusion is provided by (Tang et al., 2003). Initial analysis was initiated by R. Erdmenger in 1964 who proposed the figure of '*8*' flow path in the co-rotating intermeshing twin screw machine. The modelling work to understand the flow of material in the screw elements and kneading blocks began in the mid 1970s with M. L. Booy developing the mathematics describing the self wiping profile in 1980.

Flows within the extrusion process are located in the creeping flow regime due to the high viscosities associated with the polymers being processed. This means that there is no turbulence to consider and thus any inertial forces can be neglected in analysis of flow in twin screws extruders.

A good review of flows within co-rotating TSEs is given in Giles et al. (2005) and Kohlgrüber (2008). Simple shear flows are predominant within co-rotating twin screw extruders and are found in the low shear regions within the screw channels; that is away from the nip and over the flight region. The nip and the over the flight clearance regions are characterised by high shear, with high degree of compression and extension of the polymer flow. These occur as a result of the polymer having to flow through a narrow gap leading to a drastic increase in velocity, as demonstrated in Figure A.10.

When considering additives in the molten state, pure shear and elongational flows result in an increase of interfacial area between the two components, however these do not involve cross mixing. Thus good distributive mixing (mechanism discussed in Section 2.4) is achieved through the splitting and recombining of fluid elements leading to macroscopic rearrangements within the overall flow. Extensional flows are very good in dispersing the secondary phase droplets formed when the additive is incompatible with the polymer matrix (blend system). In extensional flow there is no fluid recirculation occurring within the drop and hence no forces that can completely resist the break up of the droplet.

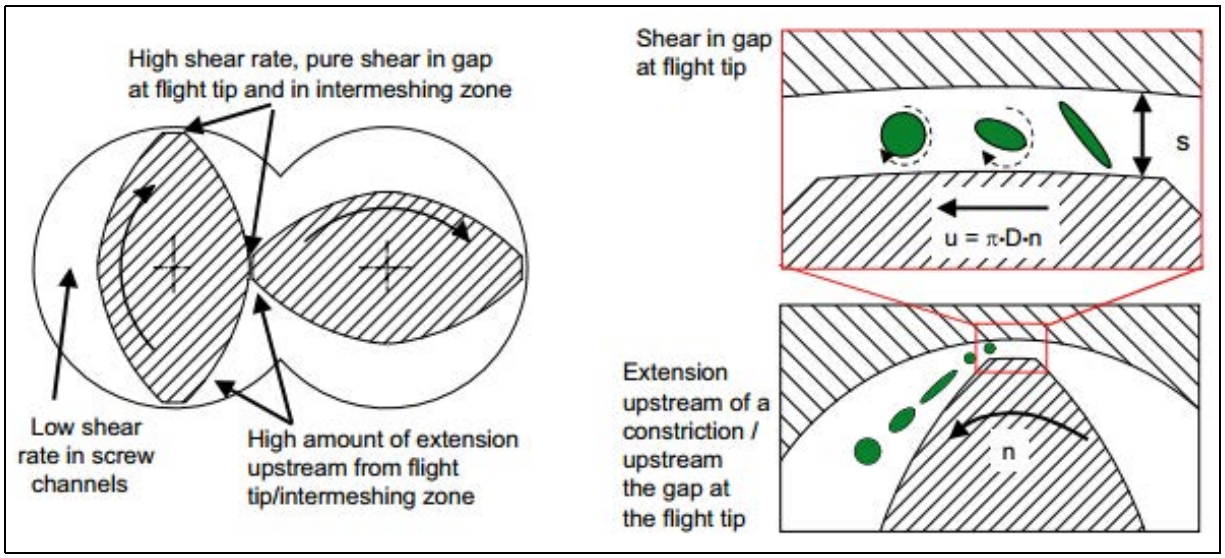

Figure A.10: *Typical screw elements in mixing zone for co-rotating TSE; from Kohlgrüber (2008, p.172)*

The high shear rates and shear stresses combined with extensional flow found in the flight clearances and nip regions form good conditions for dispersive mixing of particulate additives distributed within the polymer matrix; see Section 2.4 for discussion on the mixing mechanism.

A.2.1 Flow pattern in conveying elements

In the counter rotating twin screw extruder the polymer is effectively forced though the intermeshing region by the rotation of the screws resulting in a high pressure region at the entrance to the nip and a low pressure region upon the exit of the nip. In a co-rotating

TSE the screws effectively work against each other, with the donating shaft pushing the polymer against the receiving shaft. This reduces the volume available to the polymer leading to a zone of high pressure on the donating shaft. On the receiving shaft the polymer is taken away rapidly from the nip region into the emptiness of the partially filled flight leading to a zone of low pressure. The exact nature of these pressure regions was modelled by Shah and Gupta, 2004; an illustration can be seen in Figure A.11.

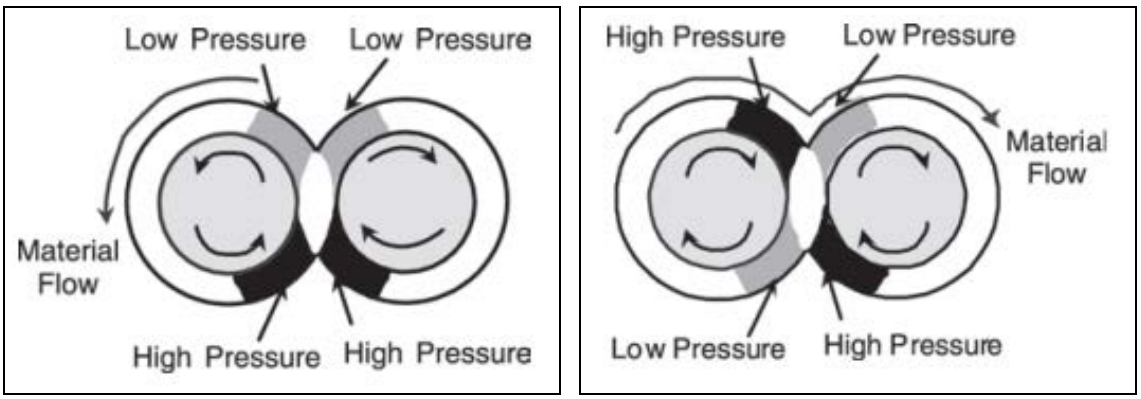

(a) *Counter-rotating TSE* ***(b)*** *Co-rotating TSE*

Figure A.11: *Flow in TSEs; from Giles et al. (2005, p.96)*

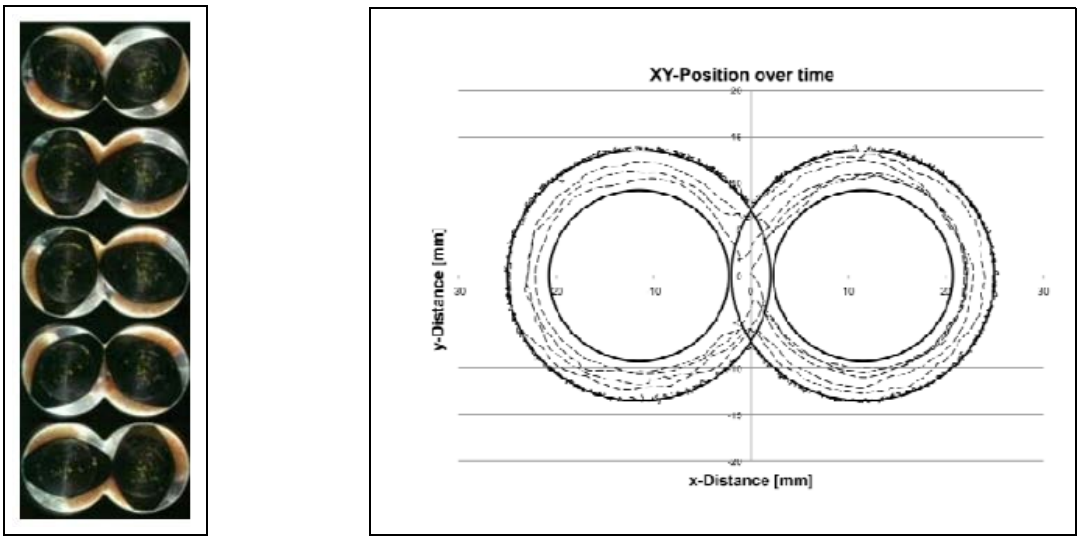

(a) *Flow in co-TSE; from Giles et al. (2005, p.96)* ***(b)*** *Flow in co-TSE, as visualised by PEPT; from Diemert et al., 2011*

Figure A.12: *Transfer of materials in co-TSE*

As one screw is rotating downwards and the other is rotating upwards the cross flow of material through the intermeshing region is prevented. Instead the material is transferred

from one screw onto another, resulting in a figure of '*8*' flow pattern as described by R. Erdmenger. This can be visualised in Figure A.12a and was confirmed by Diemert et al., 2011 in his positron emission particle tracking experiments; see Figure A.12b. Outside the intermeshing zones the drag flow follows the rules for the conveying found in single screw machines. In this region, the conveying efficiency depends on the friction between the polymer and the barrel surface as well as the friction between the polymer and the screw.

The degree of intermeshing in co-rotating machines will determine the quantity of the material that flows through the nip region. In fully intermeshing machines it is assumed that no material flows through the nip, as the gap between the screws is the minimum required for mechanical clearance (assumed to be zero in calculations); hence allowing for completely self wiping design. Figure A.13 shows a the flow in the nip region of a single flighted TSE and its the geometry of the nip if unravelled into a plane.

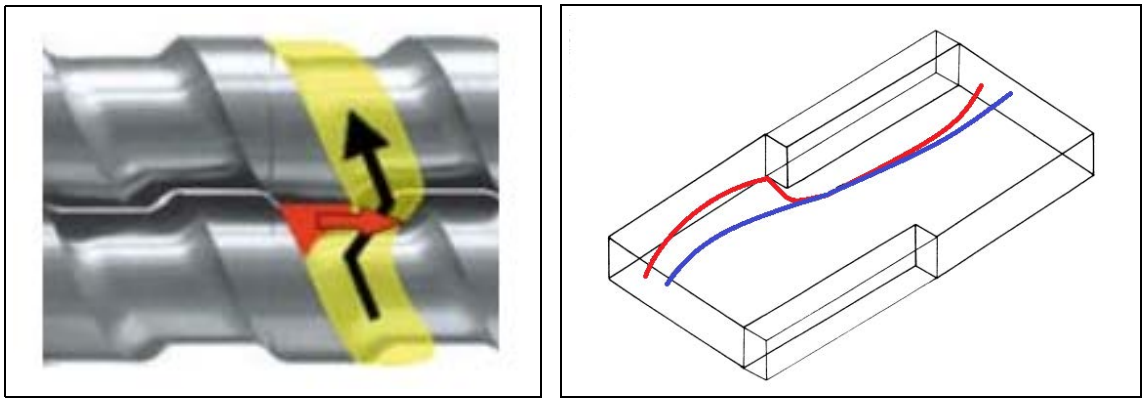

(a) *Material flow in co-rotating TSE (Kohlgrüber, 2008, p.221)*

(b) *Geometry of the nip region in co-rotating TSE (Kalyon and Sangani, 1989b, p.411)*

Figure A.13: *Flow in nip region of single flighted TSEs*

In partially intermeshing screws some flow has the ability to pass through the nip region due to a much larger space between the screw. However, the symmetry in the geometry within the nip region together with the opposing velocities of the screws means that this region does not contribute to pressure generation (Booy, 1978). As well as being able to pass through the nip, the flow is split by a flight between two chambers allowing for

greater distributive mixing, see Figure A.14. Partially intermeshing designs are considered to be '*axially open*', allowing for forward and backward flows in the axial direction as well as in the channel direction, as opposed to fully intermeshing designs that are '*axially closed*' and only allow flow from screw to screw. Conveying elements wipe the barrel surface preventing leakage flows, but as the wear on the screws increases leakage flows also increase. Substantial wear in the intermeshing regions will result in the polymer being able to flow through the region.

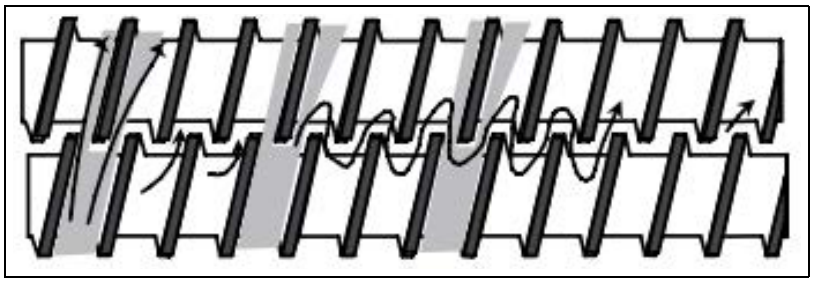

Figure A.14: *Flow in partially intermeshing axially open co-rotating TSE; from Giles et al. (2005, p.97)*

It should be noted that as a twin screw extruder is operated in starve fed mode, most of the elements will only be partially filled. This means that the rotation of the screw will force the material to accumulate on the leading edge of the pushing flight and free space to be present by the trailing flight, see Figure A.15. There will always be polymer present in the flight clearance above the pushing flight as the friction between the polymer and the barrel causes the polymer to be dragged over the pushing flight.

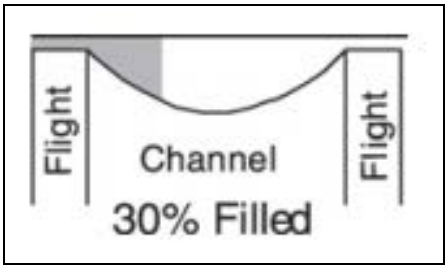

Figure A.15: *Flow in partially full channels of co-rotating TSE; from Giles et al. (2005, p.100)*

The number of threads in on the screw determine the number of partial flows existing

within the geometry. This is given by $2p - 1$ where p is the number of individual flights. This is illustrated by Figure A.16. As discussed previously, most of the twin screw extruders have two flights leading to three partial flows being present in such systems.

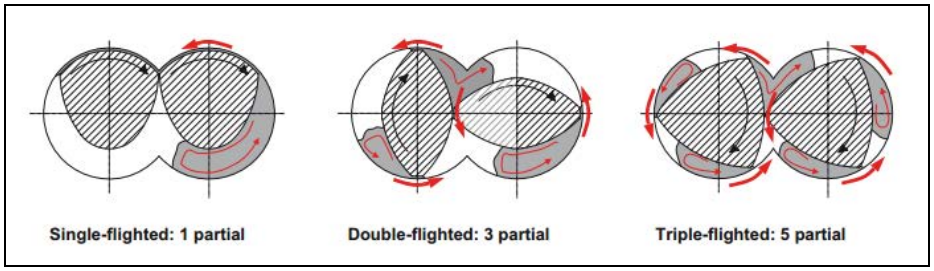

Figure A.16: *Number of partial flows in co-rotating TSE; from Kohlgrüber (2008, p.163)*

A.2.2 Flow pattern in kneading blocks

Individual kneading disks have a mild flow restricting action and lack any conveying effect. These are grouped and oriented relative to each other in order to make up kneading block sections. Depending on the orientation of the disks they can either provide a weak conveying effect in forward or reverse direction or a static mixing action (Gautam and Choudhury, 1999). The mechanism of flow within kneading blocks is well described by Kalyon et al., 1991 and Gogos et al., 1996.

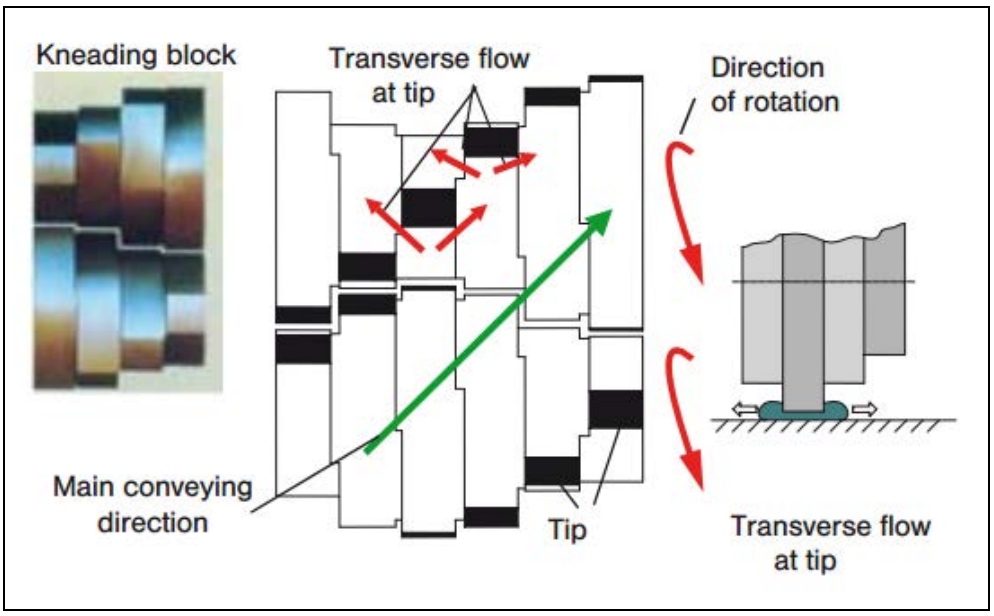

Figure A.17: *Nature of flows in kneading blocks; from Kohlgrüber (2008, p.154)*

As the kneading block rotates, the varying volume between the individual disk and the barrel as well as that in the intermeshing region leads to the squeezing of the melt. This locally pressurises the material making it flow via the path of the lowest resistance; that is in the axial direction. In the case of a forward conveying configuration the melt is blocked from moving backwards by the presence of another disk and it instantaneously flows in the forwards direction into the open channel. The opposite is true for the reverse kneading blocks where the presence of another disk in front forces the material to flow backwards. In the 90 ° kneading block configuration the areas open to flow in forward and backward direction are equal thus an upstream pressure (typically generated by an upstream conveying element) is required to push the material forward. As a result under operation this configuration is fully filled just like the reverse kneading block configurations.

As the material moves forward or backwards it is intersected by other disks within the block resulting in leakage flows around the individual disks; as indicated by red arrows in Figure A.17. The leakage flows combined with the periodic changes caused by rotation of the disks continuously alter the flow lines of the melt resulting in good distributive mixing. The material passing over the tip of the disk experiences high shear rates and stresses due to the small gap between the tip and the barrel which constitutes the high dispersive action of the kneading blocks. Dispersion is further enhanced by the elongational flows generated as the material passes over the tip, shown in Figure A.10, due to lower stresses being required to break down agglomerates under elongational flow.

Emin and Schuchmann, 2013 performed computational fluid dynamics analysis to better understand the nature of flows that occur within the kneading blocks. The author utilised a mixing index to denote the types of flow with 0 being that for pure rotational, 0.5 for simple shear and 1 for elongational flow. Interestingly, no pure elongational flows were demonstrated with mainly simple shear flows being observed. The flow becomes more extensional in nature in the intermeshing region where the tips of the kneading blocks located on separate shafts meet and more rotational close to the kneading block surface;

see Figure A.18a. The flows which are more extensional in nature tend to occur close to the kneading block tips; see Figure A.18b. Interestingly, the figure also illustrates that the nature of flows in kneading block is similar to that in the conveying element.

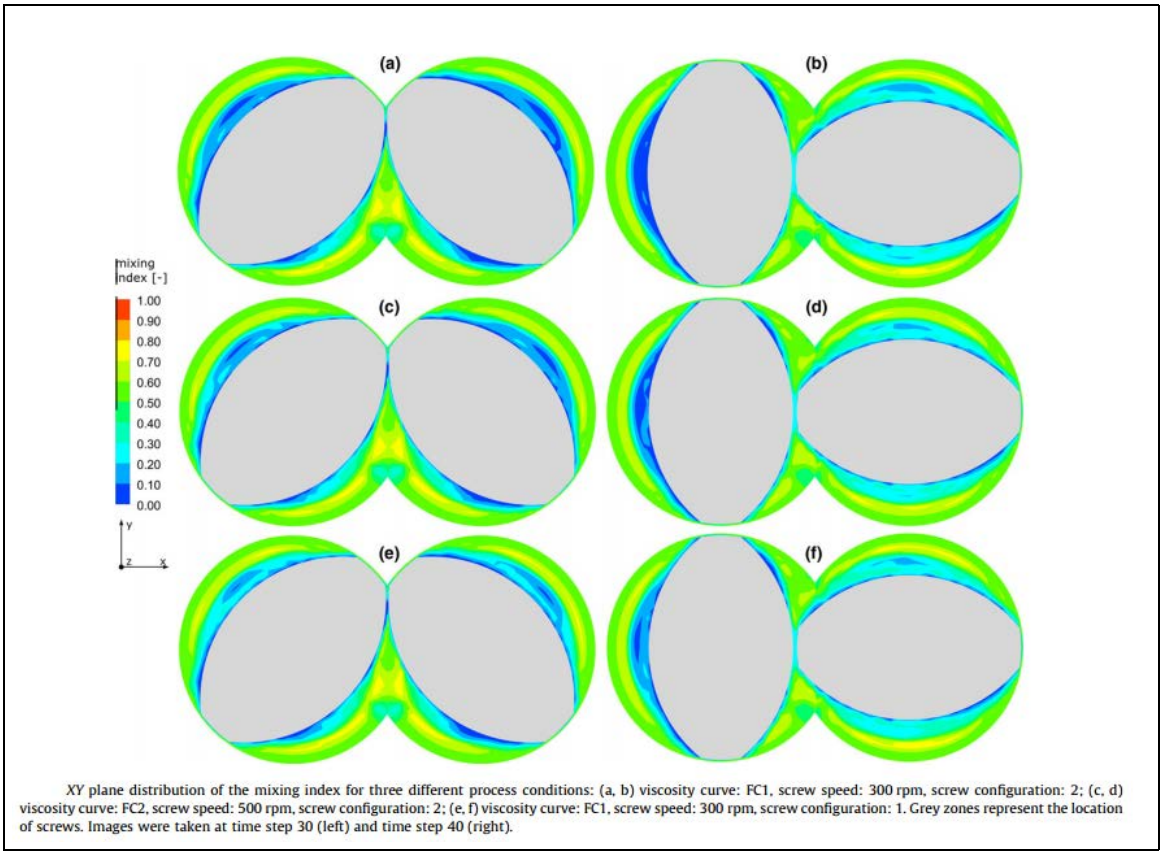

XY plane distribution of the mixing index for three different process conditions: (a, b) viscosity curve: FC1, screw speed: 300 rpm, screw configuration: 2; (c, d) viscosity curve: FC2, screw speed: 500 rpm, screw configuration: 2; (e, f) viscosity curve: FC1, screw speed: 300 rpm, screw configuration: 1. Grey zones represent the location of screws. Images were taken at time step 30 (left) and time step 40 (right).

(a) *Vertical cross section though a TSE*

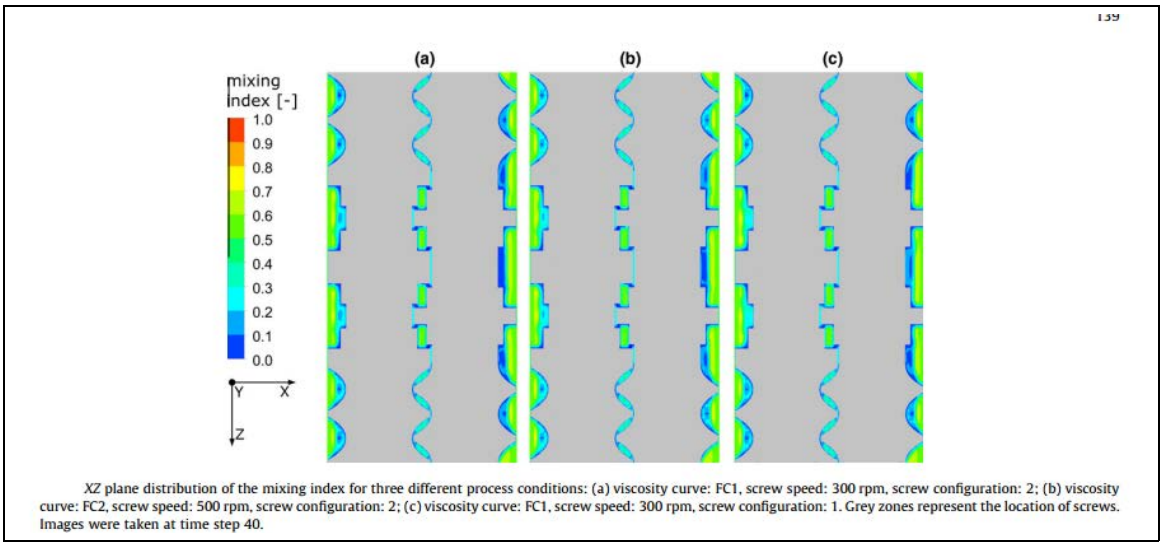

XZ plane distribution of the mixing index for three different process conditions: (a) viscosity curve: FC1, screw speed: 300 rpm, screw configuration: 2; (b) viscosity curve: FC2, screw speed: 500 rpm, screw configuration: 2; (c) viscosity curve: FC1, screw speed: 300 rpm, screw configuration: 1. Grey zones represent the location of screws. Images were taken at time step 40.

(b) *Horizontal cross section through a TSE*

Figure A.18: *Nature of flows in kneading block region of a TSE; from Emin and Schuchmann, 2013*

Changes in the geometry of the individual disk or in their configuration within the block affect the level of dispersive and distributive mixing offered by the block. The width of the disk is responsible for the balance between dispersive and distributive mixing. Narrower disks, provide better distributive mixing as they promote flows around the disk but not through the high shear clearance region Giles et al., 2005. As the width is increased the probability that an agglomerate is forced to flow through the tight clearance is also increased thus increasing the dispersive mixing effect Kohlgrüber, 2008. It is important to note, as said by Giles et al., that a configuration with wider disks provides a greater opportunity for dispersive mixing; however whether appropriate dispersive mixing for a given system is reached requires testing.

An increased staggering angle between the kneading disks leads to a more axially open configuration intensifying the axial mixing at the expense of conveying capacity. Kalyon and Sangani, 1989b performed an extensive study on the effect of stagger angle; this is discussed in Chapter J. The influence of changes in kneading block design on mixing is summarised in Figure A.19.

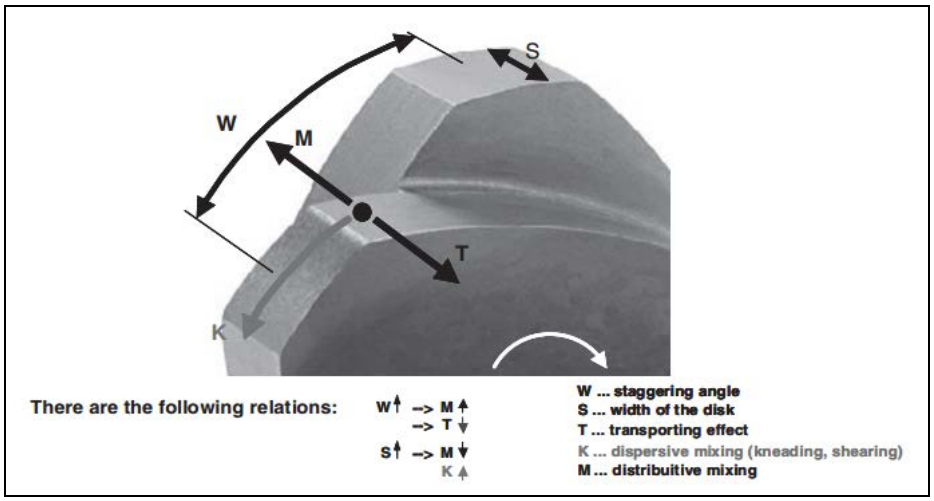

Figure A.19: *Impact of kneading block design on mixing; from Wiedmann and Holzel, 2009, p.246*

A.2.3 Flow pattern in reverse conveying elements

Backward conveying elements are also a type of axially open element. However, as they are designed to pump the material in opposite direction to the rest of the conveying elements within the TSE through the use of a flight wound in reverse direction they offer the highest resistance to flow and operate fully filled. High pressure is required to overcome this resistance; this is generated in the upstream elements causing them to operate at increased degree of fill or in some cases fully filled. Reversing elements are often utilised within the configuration to generate a 'melt plug' seal prior and/or after a degassing section allowing a vacuum to be pulled, to retard the flow and thus increase the free volume in the downstream elements or increase the degree of fill in upstream mixing elements; see Figure A.20.

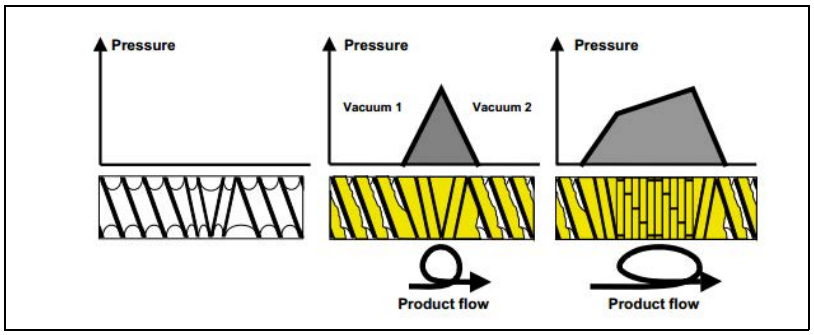

Figure A.20: *Flow in reverse conveying elements; from Kohlgrüber, 2008, p.228*

With the aid of positron emission particle tracking Diemert et al., 2011 were able to demonstrate that the use of reverse conveying elements after a forward conveying element configuration increased the average residence time significantly. At the same time the tail of the distribution was shifted to the left reducing the maximum residence time by increasing the flow through the clearance between the screw and the barrel; see Figure A.21a. This promotion of flow though the high shear region should aid the dispersion of agglomerates. The use of reversing elements downstream of a 90 ° kneading block significantly increased the residence time distribution in the element at the start of that mixing zone suggesting that the dispersive mixing capacity was increased as a result of increased number of passes through the high shear clearance regions.

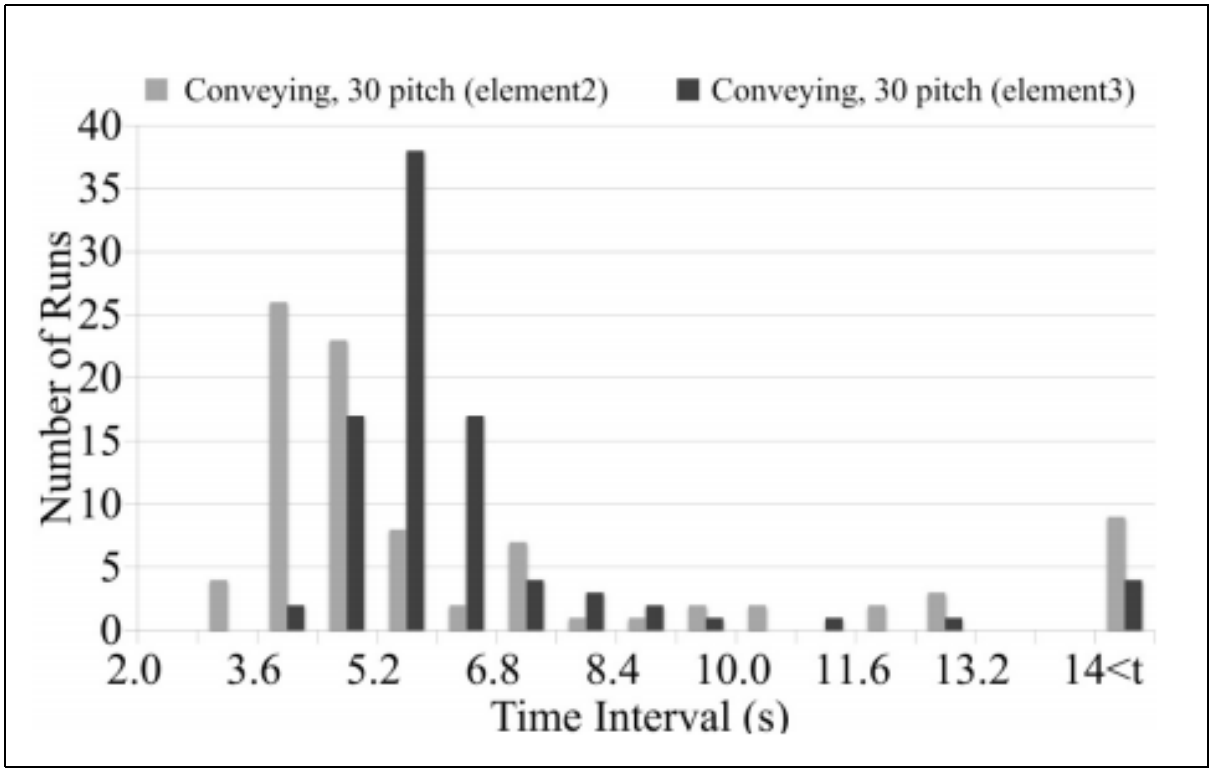

(a) *Conveying elements*

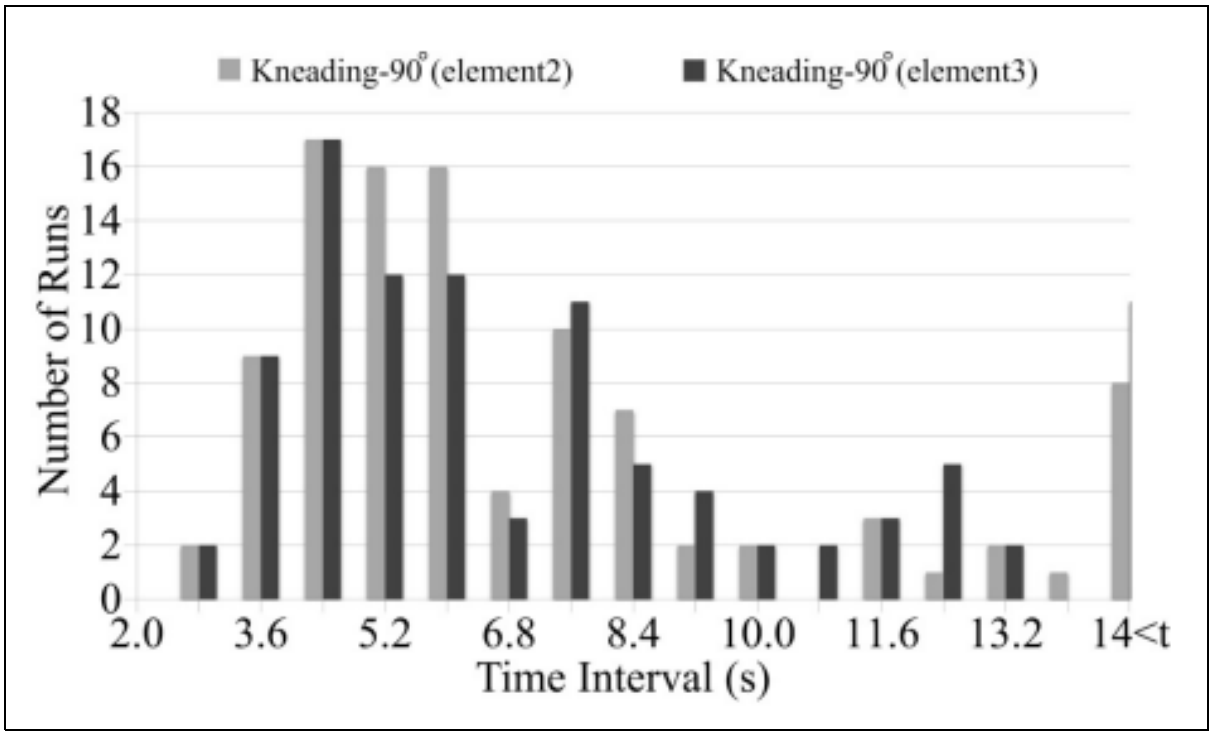

(b) *Kneading blocks*

Figure A.21: *Residence time distribution in the two elements located prior to the reversing element; from Diemert et al., 2011*

A.2.4 Flow patterns in other mixing elements

Screw and toothed mixing elements are the two other types of commonly utilised mixing elements; see Figure A.22. Screw mixing elements are based on self wiping conveying element profile with slots cut into the flight in order to promote back flow and enhance distributive mixing. These type of elements operate best against a back pressure as this ensures that they are fully filled and promotes flow through the slots.

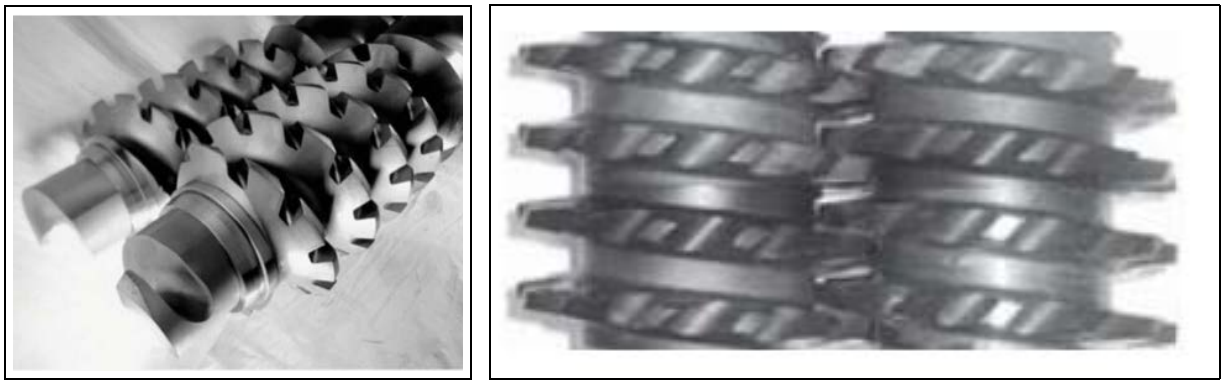

(a) *Screw mixing elements* ***(b)*** *Toothed mixing elements*

Figure A.22: *Mixing elements; from Kohlgrüber, 2008*

Toothed mixing elements, sometimes referred to as gear elements, are base on rings of the same diameter as the outer diameter of the screw. These have no pitch associated with them and have slots machined into them to leave behind 'teeth'. The rings are staggered on the shafts; see Figure A.22b which makes them effective at splitting and recombining the flows. The slots can provide a forward, backward and neutral conveying action (Kohlgrüber, 2008). The number of slots together with their height and width can also be varied. The elements split the melt stream in numerous places and recombine it the other side of the gear providing very good distributive mixing efficiency. These types of elements are particularly useful when mixing liquid additives into a polymer melt stream (Giles et al., 2005).

Numerous other types of elements exist, with each aiming to promote a particular action. This includes providing greater extensional flows, more uniform shear conditions or high dispersive action by passing material though extremely high shear such as blister rings.

Kohlgrüber, 2008 provides a good overview of the different elements that are available. Examining the flows in each type of element was deemed beyond the scope of this work.

B | Experimental methods for studying mixing in extrusion

It is inherently difficult to examine the fundamental processes occurring during polymer extrusion due to the high temperatures (ca. 280 °C for PET) and pressures associated with the running of the machines. Over the years a number of different techniques have been attempted to better understand the fundamentals of mixing in extrusion; particularly twin screw processes. Some techniques are better suited for developing the understanding of distributive and other dispersive mixing mechanisms.

With respect to distributive mixing, the residence time distribution can offer a significant insight into the nature of flows within the machine which help to better understand the mechanisms governing the distributive mixing process. Typically a pulse of a tracer material (which has a unique property such as colour, high conductivity, or infra red absorption) is injected into the feed pocket of the extruder. The concentration of the material at the die is monitored and from this the residence time distribution can be construed. This method was used as early as 1975 by Todd and is still in use within recent research e.g. Zhang et al., 2008 who developed the technique further to examine the residence time for a single element within a screw configuration.

Another commonly utilised method, is the 'dead stop' experiment. Here, the extruder is suddenly stopped during a steady state operation, material within the extruder is allowed to cool and the screws are later removed enabling samples to be collected along the length of the screw. The samples collected can be utilised to examine the degree of distributive or dispersive mixing achieved. This is a particularly useful tool when a 'clamshell' barrel design is available. The design enables the top section of the barrel to be swung open on hinges away from the bottom section thus exposing the screws and the material contained within. This set up is ideal for visualising the degree of fill within different extruder

configurations. Kalyon et al., 1991 used the technique to investigate the degree of fill within different types of kneading blocks.

More recent techniques reported by Kajiwara and Nakayama, 2011 include the use of particle image velocimetry to track the flow within the extruder. This was made possible by the use of a transparent barrel coupled with high viscosity oil to simulate polymer flow allowing the experiment to be conducted at lower pressures. The use of laser doppler velocimetry through a transparent barrel section was also reported. However, even with these more modern techniques the intermeshing region is still difficult to study. Another novel technique involved the use of positron emission particle tracking to study the nature of flows within the TSE. Diemert et al., 2011 and Lee et al., 2012 successfully utilised this method to examine the changes in residence time distribution induced by the screw configuration changes as well as examine the degree of flows through the intermeshing region and the screw tip to barrel clearance.

Most commonly used techniques for studying mixing are the indirect measures of mixing gained from the structural evaluation of the materials produced with the extruder. These include examining the degree of mixing via optical/electron microscopy, ultrasound and rheological measurements as well as analysis of the mechanical properties. Although these methods are industrially very useful (Kalyon and Sangani, 1989b), the challenge with this approach lies in correctly inferring information about mixing mechanisms. Kajiwara and Nakayama, 2011 went as far as saying that this can not be done and only the degree of mixing can be established.

As pointwise information of the mixing processes occurring within extrusion is hard to obtain, modelling of the mixing process plays a key role. Models proposed for studding the residence time distribution are discussed in Oberlehner et al., 1994. There also have been several models proposed for the dispersion of additives in polymer composites. Most of these are based on the assumption that the agglomerate ruptures when the forces imposed on it by the polymer flow exceed the cohesive forces holding it together (Flecke et al.,

2002). Kasaliwal, 2011 offer an in depth overview of these.

C An overview of twin screw extruder models in literature and 'off the shelf' software packages

Although the geometry of intermeshing co-TSEs can be described by a relatively simple set of mathematical equations, the modelling of flow in co-TSEs is complex. This is a direct result of the numerous processes occurring during extrusion (conveying, melting and mixing) as well as the changing nature of the flow geometry induced by the screw rotation. Existing models range from 1-D to 3-D; each with their advantages and disadvantages. A 1-D system calculates the changes in parameters such as temperature, pressure and DOF along the length axis of the extruder. Such an approach allows rapid comparison between differing screw configurations or operating conditions at the expense of understanding the exact nature of polymer flow around a particular screw element. An increase in computing power and reduction in its cost has led to the rising use of 3-D models; namely Computational Fluid Dynamics (CFD). These enable the visualisation of the variation in flow and shear conditions in the x, y and z-axis, however at present they can only be utilised in the fully filled sections of the extruder.

C.1 An outline of the twin screw extruder models in literature

A number of authors have published their methods for modelling flows in a TSEs, a sample of which is outlined here:

- 1-D Simulations
  - Tayeb et al., 1988 developed a 'black box' model for application in food ex-

trusion to calculate temperature, pressure and residence time of material in a TSE.

  - Potente et al., 1994 formulated equations describing the geometry of twin screw extruders and modelled them as an *'unwound channel'*; a similar ideology is used for single screw extruders. The model calculates the melting and temperature profile as well as the conveying rate of material and degree of fill.

  - Eitzlmayr et al., 2014 developed a model for use in hot melt extrusion (HME) within the pharmaceuticals sector. It calculates the degree of fill, pressure, temperature, power, torque and residence time distribution. Most notably the model looks at flow through the cross section of an extruder along its length (z - axis); it does not rely on the *'unwound channel'* assumption as others do. Two key parameters need to be determined, either experimentally or via CFD simulations, for each unique element before the model can be used.

- 2-D Simulations

  - Kalyon et al., 1988b simulated polymer flow in intermeshing co-TSEs using the Finite Element Method (FEM). The model ignored the flow though the intermeshing region and assumed all the material was purely transferred from one screw to the other. They were able to predict the temperature of the material and strain distribution through the cross section of the channel. The growth of a secondary phase interface was also tracked. This has limited application as the majority of the interfacial area increase in TSEs occurs when polymer flows over the kneading blocks which is neglected.

  - Lawal et al., 1993 used 2-D simulation to track the flow of material around a kneading block; in particular visualising the velocity vectors and the tracking of path-lines illustrating the flow through the intermeshing region and transfer of material from one screw to another.

  - Gotsis and Kalyon, 1989 attempted to simulate mixing in TSEs by a combi-

nation of 2-D and 3-D modelling. A 2-D approach was utilised to model the flow in the channel of the conveying elements whilst 3-D FEM was utilised to analyse flow in the kneading blocks. The author was able to determine the x - and y- axis velocity vectors for the kneading blocks and plot the magnitude of stress tensors.

- 3-D Simulations
  - The majority of the 3-D models focus on the flow of melted material.
  - Lawal and Kalyon, 1995 modelled flow through the kneading block elements; particularly focusing on understanding the behaviour within the intermeshing region by examining the stress and velocity distributions. They examined the effect of kneading disc stagger angle and tracked the motion of two adjacent points as they flow through kneading blocks.
  - Emin and Schuchmann, 2013 used CFD to analyse flow of plasticised maize starch; focusing on determining regions of high shear flow as well as regions of elongational and simple shear flow, considering the impact of operating conditions on these parameters.

Modelling of TSEs is becoming more widespread; but these cannot fully replace the data gathered by experiments due to limitations of each modelling method. They can however be used to minimise the number of experiments which need to be conducted and to develop a more in depth understanding of the TSE process at given set of conditions. The choice between the different modelling strategies remains a difficult one as there is no *one size fits all* solution available. Lawal and Kalyon, 1995 stated that the findings of analytical solutions when compared to computational fluid dynamics (CFD) are somewhat irrelevant since they do not provide information on the kinematics of mixing. In reality CFD is being utilised in unison with 1-D analysis to provide the detail which 1-D analysis misses; as illustrated by a number of commercial 1-D packages available on the market today. Durin et al., 2009 investigated the differences in 1-D and 3-D modelling approaches

to conclude that 1-D analysis is sufficient for simple configurations such as conveying elements. However, 3-D analysis offers better predictions for complex geometries such as kneading blocks. It is more accurate in evaluating the effects of stagger angle and is able to predict temperature hotspots which could act as potential sites for material degradation.

C.2 A brief outline of the 'off the shelf' software packages

A number of commercial modelling tools are available on the market for simulating the flows in co-rotating TSEs. Markarian, 2002; 2005 provide a good overview of the most common solutions; a brief description of which is given here.

Akro-Co-Twin-Extrusion was developed by Akron University in 1985 with the first commercial release being made available in 1990. The model provides a 1-D solution to extrusion theory by calculating the equations governing solids conveying, melting, melt conveying and temperature. The software has an internal database for screw elements based for a number of suppliers and can be used to ensure effective scale up of the process and calculation of energy consumption. The latest additions include modules for reactive extrusion and polymer molecular weight reduction with a module for dispersion of solid fillers in development.

Twin Screw Simulator, TXS was first released in 1996 by PolyTech and also provides a 1-D solution whilst taking into account the effect of clearances between the barrel and the screws. *Ludovic* was released in 1998 by the Centre for Material Forming to allow calculation of temperature pressure, fill ratio, specific mechanical energy (SME) input and residence time with the latest addition also catering for reactive extrusion. *Sigma* was developed by the Polymer Engineering Department at the University of Paderborn, Germany. It models flow in a unwound channel geometry and accounts for the nip region

by a reduction in channel width. The latest incarnation of the software calculates the degree of dispersion for filler whilst accounting for the rheological changes in the polymer as a result of filler addition. It is possible to integrate *Sigma* with *Extrud3D* package which can be used to perform 3-D simulations of the fully filled zones.

A 3-D Finite Element Method solution is offered by *PolyFlow* which uses a mesh superimposition technique to account for the transient flows. With this software it is possible to visualise the pressure, velocity, temperature and shear distributions as well as calculate both dispersive and distributive mixing indices.

D | Details of the current DTF's 'in-house' TSE model

The model provides a basis for determining pressure, degree of fill, residence time and flow velocity within each element of a given screw configuration for a the TSE running at a specified set of operating conditions. The governing equation for the model is shown below, see Equation D.1.

$$\frac{\partial P}{\partial z} = \frac{\eta\left(\alpha 60N - \frac{\dot{m}}{\rho}\right)}{\beta} \tag{D.1}$$

where P is melt pressure in bar, z is the axial distance along the extruder in m, η is the melt viscosity in Pa s, N is screw speed in rpm, $\dot{m}$ is the throughput in kg h^{-1}, ρ is density in kg m^{-3} and α & β are constants with units of m^3 rpm^{-1} and m^4 Pa s bar^{-1} h^{-1} respectively.

The model was originally developed at DuPont Corporate Labs in Wilmington by Hoffman based on extruder with 2 threads and $^{H_{CH}}/_{D_o}$ ratio of 0.155. The α and β constants in Equation D.1 are related to the properties of a given element. For conveying elements these constants are defined by diameter, pitch and channel depth and for the kneading elements by stagger angle and disc width. Ellam, from whom the model was inherited, enhanced model with scaling of the α and β constants allowing the model to be applied to extruders with different $^{H_{CH}}/_{D_o}$. The model has originally been used to determine the flood onset conditions and from experience the predicted pressure and fill profile are known to be accurate in the melt sections; but are only approximations for non molten material.

The calculations utilised within the model are presented below. For the purpose of this description n will denote the element number with $n = i$ and $n = j$ representing the

initial and final elements. In addition KB_{mi} and KB_{mj} denote the element number of the first and the last kneading block of the melt zone respectively. The model performs the following calculations.

D.1 Determining α and β

D.1.1 Two lobe conveying elements

The α and β constants in $\mathrm{m^3\,rev^{-1}}$ and $\mathrm{m^4\,Pa\,s\,bar^{-1}\,h^{-1}}$ are scaled parameters based on α_0 and β_0 in $\mathrm{in^3\,rev^{-1}}$ and $\mathrm{in^6\,P\,lb^{-1}\,min^{-1}}$. These are calculated for each element in a given screw configuration within the model. The constant α is determined as follows for elements $n = 1$ to $n = j$:

$$\alpha_n = \frac{H_{CH}/D_o}{0.155} \cdot \frac{\alpha_{0,n}}{39.37^3} \tag{D.2}$$

where

$$\alpha_{0,n} = 2.1 \times 10^{-5} \cdot t_n \cdot \cos^2\phi_n \cdot D_o^2 \cdot 0.7 \cdot \left(\frac{t_n}{D_o}\right)^{0.601} + 1.9897 \times 10^{-6} \cdot t_n \cdot D_o^2 \tag{D.3}$$

Similarly, β is determined as follows:

$$\beta_n = \frac{H_{CH}/D_o}{0.155} \cdot \frac{\beta_{0,n} \cdot 14.5 \cdot 60}{10 \cdot 39.37^4} \tag{D.4}$$

where

$$\beta_{0,n} = 2.7 \cdot 0.48 \cdot \left(\frac{t_n}{D_o}\right)^{0.805} \cdot H_{CH}^3 \cdot 0.43 \cdot t_n \cdot \cos\phi_n \cdot \sin\phi_n \tag{D.5}$$

D.1.2 Kneading block elements

The α and β constants in $\mathrm{m^3\,rev^{-1}}$ and $\mathrm{m^4\,Pa\,s\,bar^{-1}\,h^{-1}}$ are scaled parameters based on α_0 and β_0 in $\mathrm{in^3\,rev^{-1}}$ and $\mathrm{in^6\,P\,lb^{-1}\,min^{-1}}$. These are calculated for each kneading block in a given screw configuration within the model based on the kneading block equivalent pitch, t_{KB} where the disk stagger angle, ω is in rad.

$$t_{KB,n} = \frac{2\pi}{\omega_n} \cdot \frac{L_{KB,n}}{j_{KD,n}} \tag{D.6}$$

The constant α is determined as follows:

$$\alpha_n = \frac{\alpha_{0,n}}{39.37^3} \tag{D.7}$$

where

$$\alpha_{0,n} = 1.26 \times 10^{-5} \cdot t_{KB,n} \cdot \cos^2\phi_n \cdot D_o^2 \cdot FP_{\alpha,n} + 1.14 \times 10^{-6} \cdot t_{KB,n} \cdot D_o^2 \tag{D.8}$$

where FP_α and x are defined as follows

$$FP_{\alpha,n} = 0.7012 + 0.0511x_n - 0.674x_n^2 + 2.665x_n^3 - 1.426x_n^4 \tag{D.9}$$

and

$$x_n = \frac{0.298 \cdot t_{KB,n} \cdot \cos\phi_n}{H_{CH}} \tag{D.10}$$

The constant β is determined as follows:

$$\beta_n = \beta_{0,n} \cdot \frac{14.5 \cdot 60}{10 \cdot 39.37^4} \tag{D.11}$$

where

$$\beta_{0,n} = FP_{\beta,n} \cdot 1.28 \cdot \sin\phi_n \cdot H_{CH}^3 \cdot \cos\phi_n \cdot t_{KB,n} \tag{D.12}$$

where FP_β and x are defined as follows

$$FP_{\beta,n} = 0.5556 - 0.1712x_n - 0.5816x_n^2 + 0.394x_n^3 - 0.0339x_n^4 \tag{D.13}$$

and

$$x_n = \frac{0.298 \cdot t_{KB,n} \cdot \cos\phi_n}{H_{CH}} \tag{D.14}$$

D.2 Determining pressure and degree of fill

Once α and β constants have been determined for each element in the configuration other parameters can be calculated. It is vital to note that the calculations are performed starting from the extruder exit as opposed to feed throat of the machine. It is the exit pressure that determines the degree if fill in the conveying elements located immediately prior to the extruder exit.

- **Pressure**, P in bar;

  For $n = j$:

$$P_n = \max\left(P_e - \Delta P_{Actual,n}, 0\right) \tag{D.15}$$

  For $n = j - 1$ to i:

$$P_{n-1} = \max\left(P_n - \Delta P_{Actual,n-1}, 0\right) \tag{D.16}$$

- **Actual pressure drop**, ΔP_{Actual} in bar where L_F denotes filled length in mm;

  For $n = j$ to i:

$$\Delta P_{Actual,n} = \frac{L_{F,n}}{100} \cdot \Delta P_{Max,n} \tag{D.17}$$

- **Filled length**, L_F in %;

  For $n = j$:

$$L_{F,n} = \text{If}\,(P_e - \Delta P_{Max,n}) > 0 \quad \text{Then} \quad 100 \quad \text{Else} \quad \frac{P_e \cdot 100}{\Delta P_{Max,n}} \tag{D.18}$$

  For $n = j - 1$ to i:

$$L_{F,n-1} = \text{If}\,(P_n - \Delta P_{Max,n-1}) > 0 \quad \text{Then} \quad 100 \quad \text{Else} \quad \frac{P_n \cdot 100}{\Delta P_{Max,n-1}} \tag{D.19}$$

- **Maximum pressure drop**, ΔP_{Max} in bar where L_{EL} denotes element length in mm and δP denotes pressure gradient in bar mm^{-1};

$$\Delta P_{Max,n} = \delta P_n \cdot L_{EL,n} \tag{D.20}$$

- **Pressure gradient**, δP in bar mm^{-1} where F_{press} is pressure flow, N is screw speed, ρ_m is melt density, η is viscosity and β is the value calculated in previous section;

$$\delta P_n = \text{If} \quad \beta_n > 0 \quad \text{Then} \quad -\frac{F_{press,n} \cdot N}{\rho_m} \cdot 10^{-3} \cdot \frac{\eta_n}{\beta_n} \quad \text{Else} \quad 0 \tag{D.21}$$

- **Viscosity**, η in Pa s and SVF is the solids viscosity factor (1.8);

  For $n = j$ to $KB_{mj} + 1$:

$$\eta_n = \eta_m \tag{D.22}$$

  where

$$\eta_m = 10^{\left(5 \cdot \frac{Ln([\eta])}{2.30259} + \frac{2953}{273+T} - 0.9508\right) \cdot 0.1} \tag{D.23}$$

  For $n = KB_{mj}$ to KB_{mi}:

$$\eta_n = \eta_m \cdot SVF - (\eta_m \cdot SVF - \eta_m) \cdot \frac{n - KB_{mi}}{KB_{mn} - KB_{mi}} \tag{D.24}$$

For $n = KB_{mi} - 1$ to i:

$$\eta_n = \eta_m \cdot SVF \tag{D.25}$$

- **Pressure flow**, F_{press} in $\mathrm{kg\,h^{-1}\,rpm^{-1}}$ where F_{drag} is the drag flow;

$$F_{press,n} = \frac{\dot{m}}{N} - F_{drag,n} \tag{D.26}$$

- **Drag flow**, F_{drag} in $\mathrm{kg\,h^{-1}\,rpm^{-1}}$ where direction, Z is 1, 0, and -1 for positively conveying, neutral and backward pumping elements respectively;

  For $n = j$ to $KB_{mj} + 1$:

$$F_{drag,n} = \alpha_{melt,n} \cdot Z_n \tag{D.27}$$

  For $n = KB_{mj}$ to KB_{mi}:

$$F_{drag,n} = \alpha_{feed,n} + (\alpha_{melt,n} - \alpha_{feed,n}) \cdot \frac{n + 1 - KB_{mi}}{KB_{mj} + 1 - KB_{mi}} \cdot Z_n \tag{D.28}$$

  For $n = KB_{mi} - 1$ to i:

$$F_{drag,n} = \alpha_{feed,n} \cdot Z_n \tag{D.29}$$

- **Feed alpha**, $\alpha_{feed,n}$ in $\mathrm{kg\,h^{-1}\,rpm^{-1}}$ and α is the value calculated in previous section;

$$\alpha_{feed,n} = \alpha_n \cdot \rho_s \cdot 60 \tag{D.30}$$

- **Melt alpha**, $\alpha_{melt,n}$ $\mathrm{kg\,h^{-1}\,rpm^{-1}}$ and α is the value calculated in previous section;

$$\alpha_{melt,n} = \alpha_n \cdot \rho_m \cdot 60 \tag{D.31}$$

- **Channel fill**, DOF in %;

$$DOF_n = \text{If} \quad L_{F,n} < 100 \quad \text{Then} \quad -\frac{\frac{\dot{m}}{N} \cdot 100}{F_{drag,n}} \quad \text{Else} \quad 100 \tag{D.32}$$

- **Mean velocity**, $\bar{u}$ in $\mathrm{mm\,s^{-1}}$ where Q_m and Q_s are the volumetric flow rate for melt and solid phase respectively in $\mathrm{m^3\,h^{-1}}$;

  For $n = j$ to KB_{mi}:

$$\bar{u}_n = \frac{Q_m \times 10^9}{1.66 \cdot \pi \cdot D_o \cdot H_{CH} \cdot 3600 \cdot \frac{DOF_n}{100}} \tag{D.33}$$

  For $n = KB_{mi} - 1$ to i:

$$\bar{u}_n = \frac{Q_s \times 10^9}{1.66 \cdot \pi \cdot D_o \cdot H_{CH} \cdot 3600 \cdot \frac{DOF_n}{100}} \tag{D.34}$$

- **Residence time**, τ in s;

$$\tau_n = \frac{L_{EL,n}}{\bar{u}_n} \tag{D.35}$$

- **Filled residence time**, τ_F in s;

$$\tau_{F,n} = \frac{L_{EL,n} \cdot L_{F,n}}{\bar{u}_n \cdot 100} \tag{D.36}$$

- **Inventory**, I in kg;

$$I_n = \frac{\dot{m} \cdot \tau_n}{3600} \tag{D.37}$$

- **Length/Diameter** ratio is calculated for all elements as $L_{EQ,n}/D_o$.

D.3 Concluding remarks

This model has been used internally within DTF in order to better understand the behaviour of the polymer within the extruder. Although many useful parameters are calculated the ones of most interest are pressure and degree of fill. A typical output of the model is illustrated below.

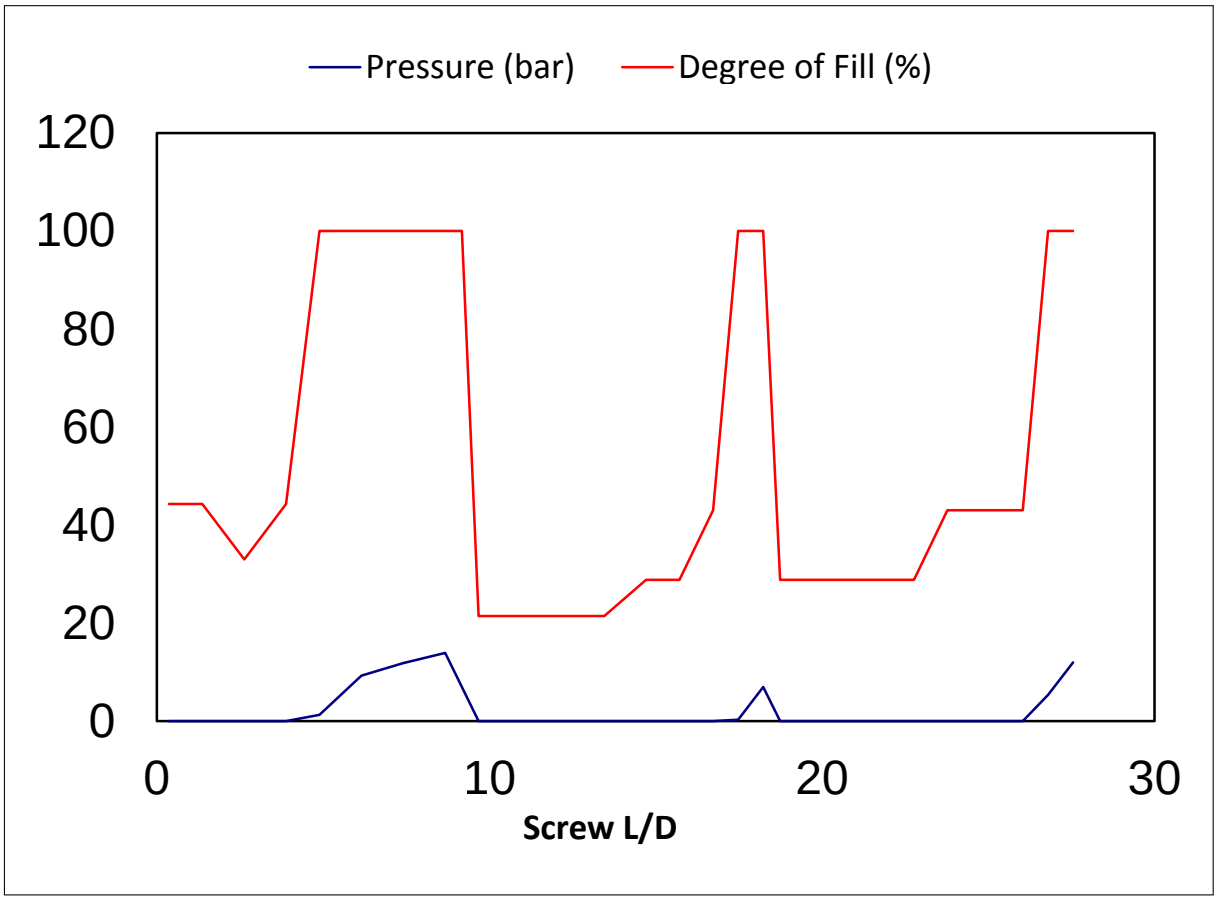

Figure D.1: *Pressure and degree of fill along the length of the extruder*

E | A review of mechanical chain scission in polymers

There is very little information in the literature on the notion of mechanically induced polymer chain scission during extrusion of PET or other polymers. The majority of reported work is from several decades ago and focuses on the shear induced molecular weight loss of polymers in solution. These include the works of Bestul, 1954; 1956; Goodman and Bestul, 1955; Goodman, 1957; Ram and Kadim, 1970 who examined the effect of shear on solutions containing polyisobutenes. Yu et al., 1979 went a step further by examining the changes in the molecular weight distribution of polyisobutenes and compared them with the effects on monodisperse polystyrene. More recently D'Almeida and Dias, 1997 considered the effect of shear on solution containing polyethylene oxide and carboxymethylcelulose to find that the prior showed a reduction in the molecular weight but the latter did not. The work on polymers in solution remains an active field with recent publications such as Brun et al., 2016; Shanshool et al., 2011 focusing on the oil and gas sector.

Some studies have been performed on polymers directly such as that of Larsen and Drickamer, 1957 who examined polyethylene and found that the amorphous regions played a much more significant role in mechanically induced chain scission compared to crystalline regions. Schott and Kaghan, 1963 performed studies on polypropylene and Rideal and Padget, 1976 on high density polyethylene. With regards to PET, Romão et al., 2009 considered the effects on the molecules during reprocessing cycles. The author suggested that mechanically induced scission of polymer chains leads to the formation of linear low molecular weight oligomer. The oligomer content increased from 0.06 $\%_{wt}$ to 4 $\%_{wt}$ when examining bottle grade PET after 5 extrusion cycles; potentially indicating that larger chains do not break in the middle during mechanical chain scission. Schöppner et al.,

2014, who examined the effect of a single extrusion run, eludes to the affect of shear by the intriguing observation that as the screw speed increases (the residence time decreases) the IV loss also increases. However, the author proposes no information on the mechanism of such molecular weight loss. Attempts to describe the mechanism of the mechanically induced chain scission have been made with the works of Bestul, 1956; Yu et al., 1979 and Brostow, 1983 with Bueche, 1960 going as far as proposing a mathematical model.

The influence of shear rate on the final molecular weight of the polymer was observed by Bestul, 1954 who saw that at low shear rate the MW of the polymer was largely unaffected, but as the shear rate increased the reduction in the MW also increased. This perhaps suggests some critical value of shear stress which induces scission of the polymer chains. A strong dependence on shear stress was observed by Ram and Kadim, 1970 where the viscosity of the processed material reduced with increasing shear stress. A similar observation was made by D'Almeida and Dias, 1997, who proposed that as the shear stress increases smaller molecules become prone to mechanical scission of the chains.

Since the shear stress is a function of the material viscosity as well as the shear rate, then it is logical that the temperature would play a key role in the mechanically induced molecular weight loss. As the temperate increases the viscosity of the polymer reduces leading to a reduction in shear stress at a given shear rate. This should result in less molecular weight loss by mechanically induced scission; as observed by Bestul, 1954; Goodman and Bestul, 1955. In their investigations Ram and Kadim, 1970 and D'Almeida and Dias, 1997 found no dependence on temperature. This is explained by the fact that the authors maintained the shear stress constant as opposed to the shear rate as was done in the prior two studies that in turn resulted in a varying stress.

On the contrary to the work on polymers in solution, when Schott and Kaghan, 1963 considered the effect of shear stress on polypropylene exposing it to repeated extrusion cycles they found that the final viscosity decreased with increased processing temperature. This perhaps, is a result of longer residence times and increased thermal degradation of the

material. This would coincide with the author's observations of increased rate of degradation at a lower throughput. Rideal and Padget, 1976 took temperature investigations a step further by attempting to separate the effects of shear and temperature. The author considered the effect of temperature by holding the sample at elevated temperature without the application of shear and comparing it to a sample which was subjected to shear at the same temperature. In this study the molecular weight distributions obtained by gas phase chromatography did not show a significant change for purely thermal reactions, but did narrow when the material was subjected to shear; indicating the preferential scission towards the middle of the polymer chains.

As the majority of these studies were performed on polymers in solution an effect of concentration has been observed. As the concentration increases the molecular weight reduction increases Bestul, 1954; this is often related to the increased number of entanglements within the system. Goodman, 1957 found that at very low concentrations there was a decreased efficiency in polymer molecules concentrating the mechanical energy supplied to them leading to a lower rate of degradation. When considering constant stress applied to the system, Ram and Kadim, 1970 found that as concentration increased the reduction in the molecular weight was less effective. A critical concentration below which no degradation occurred was identified by the authors. D'Almeida and Dias, 1997 agrees with others in acknowledging a critical concentration above which entanglements will be present, however the author did identify that molecular weight loss can occur even without entanglements being present in the system.

Perhaps of greater importance to the extrusion of polymers is the impact of the initial molecular weight of the material and corresponding distribution. One would envisage that, if entanglements played a critical role in the scission of the chains, a larger initial molecular weight resulting in more long chains (hence greater chances of entanglements) would lead to greater IV loss upon the application of shear forces. Ram and Kadim, 1970 found that the initial MW had no impact on the final MW achieved, but it did increase the rate of

chain scission. Yu et al., 1979 reported that in the case of polydisperse polyisobutenes the higher MW chains were preferentially broken leading to a polydispersity index $\left(\frac{M_w}{M_n}\right)$ of 1.5 suggesting that the chains preferentially break in the middle. An index of 2 would be indicative of a random process. In the monodisperse polystyrene system the molecular weight distribution widened upon the breaking of some of the polymer chains. The work of D'Almeida and Dias, 1997 is in agreement with that of Yu et al., 1979, reporting the preference for the higher molecular weight fractions to be broken down first. In solutions these fractions have a larger hydrodynamic radius meaning that more energy is applied to them. Yu et al., 1979 reported that the molecular weight loss under application of shear stress did not depend on the initial molecular weight of the material. It is important to note that for the same processing condition in the extruder (screw speed, output and temperature) the polymer with larger initial molecular weight would have a higher viscosity. This leads to the application of larger stresses to the molecules hence it is likely that a greater extent of mechanically induced chain scission would be seen.

Several mechanisms for mechanically induced chain scission have been proposed. Bestul, 1956 discussed the notion that the proportion of the mechanical energy applied to the system is temporarily stored within the bonds of the polymers as potential energy in a random and non-uniform fashion. When this potential energy combined with any thermal energy possessed by the molecule is more than the energy required for the bond rupture then scission will occur. If rupture does not occur then the stored potential energy is dissipated as heat into the system. Since, the energy required for bond rupture is high then it would need to be drawn in from the surrounding volume by Van der Waal's forces and secondary intermolecular interactions. As the initial molecular weight of the polymer increases, the molecular entanglements become increasingly effective in localizing mechanically applied shearing energy into the molecular bonds as temporarily stored potential energy leading to more scission.

Bueche, 1960 opted to derive a mathematical model to predict mechanically induced chain

scission based on the following proposed mechanism. When a molecule is subjected to shear it rotates at a frequency equal to one half of the applied shear rate. This action causes the molecule to be stretched in one direction and compressed in another. As the shear rate is increased the number of compressions and expansion cycles increase however if the molecule is 'free' it does not break as the time period of the changes is very small. However, if the molecule is entangled, for flow to occur the molecule must become disentangled very quickly which is difficult and hence may lead to a break in the chain. For a larger chain more entanglements will be present and a greater tension force will be exerted on the molecule. The stretching force is zero at either end of the chain and maximum in the middle with roughly a parabolic distribution across the chain (Caruso et al., 2009). This will lead to scission occurring towards the middle of the chain. Data reported by Yu et al., 1979 and D'Almeida and Dias, 1997 are in agreement with this. The model assumes that there will be a critical chain length below which the molecule will not break at a given stress. This was observed by Yu et al., 1979 and can be explained by the increased mobility of the smaller molecules allowing them to orient themselves in the direction of flow. The authors also proposed a stretching mechanism for bond breaking in addition to entanglements mechanism.

More recently, Brostow, 1983 proposed another model for mechanically induced scission. The author concluded that the scission was neither random nor set in the middle of the chain and suggested that entanglements did not play a great role in the breaking of the chain. Instead the molecules were treated as bundles with a bundle possessing the properties somewhere between that of a freely jointed and a rigid chain. Given time, both of types of chain will align themselves in flow, but the freely jointed one will take longer to do so and the alignment may not be as good. When a bundle is subjected to shear, if it is relaxed then the bundle can flow freely, however if it is rigid and compact then the energy supplied leads to scission of polymer chains. As the shear stress is increased the critical molecular weight of the chain in which a break will occur decreases.

With regard to the rate of chain scission Larsen and Drickamer, 1957 observed that the final to initial molecular weight ratio decreased almost linearly with time. Goodman and Bestul, 1955 proposed an equation to describe the rate of scission, where k is the rate, C is a pre-exponential factor, E is the energy required to break the bond, a is a constant and J represents the rate of energy input. The rate of energy input in turn depends on the wall shear stress, S_w and the nominal shear rate, D.

$$k = Ce^{E/aJ} \qquad where \qquad J = \frac{4}{9} \cdot S_w D \tag{E.1}$$

The authors estimated a rise in the minimum energy requirements with a rise in temperature which is explained by the reduced efficiency of entanglements. The data presented by Goodman, 1957 seems to support such a relationship.

An extensive set of equations was published by Bueche, 1960, who related the probability that a chain will break in a given time to the energy needed to break the bond, the tension force on the bond, the distance that the bond will stretch before breaking and the vibrational frequency of the bond. The author also indicates that the presence of oxygen increases the shear induced chain scission especially at high temperatures and leads to more random locations for chain scission. This was supported by Rideal and Padget, 1976 who observed that the presence of oxygen promoted chain scission.

As discussed in Chapter 7, the chemically induced changes in the molecular weight of PET during melt processing are well understood. Although some idea of the mechanically induced chain scission mechanisms can be obtained from the studies on polymers in solutions discussed above, there exists little experimental data that would allow the prediction of the changes in the molecular weight of PET during extrusion processing. Within DTF, there is some evidence for mechanically induced chain scission however the mechanism is not well understood.

F | A review of the impact of material properties on the level of mixing

In the the manufacture of polymer composites material properties can play a significant role in determining the level of mixing achieved within the composite. These include the inherent properties of the polymer such as molecular weight and hence viscosity as well as the inherent properties of the additive including the particle size, surface area and importantly shape. In addition to the characteristics of the polymer and the additive on their own, the way these two entities interact is vital for an effective mixing process.

F.1 Impact of the polymer properties

As a precursor to a dispersive mixing process the additive needs to be fully wetted and distributed through the polymer matrix. This is typically achieved in a twin screw extruder through the use of narrow kneading discs, ca. 0.5 $^{L}/_{D}$ (Young et al., 2013), in partially filled section which allow the air to escape (Kohlgrüber, 2008). The properties of the polymer matrix play a vital role in determining the wetting characteristics as well as the magnitude of the shear stress applied at a given shear rate. Once the outer surface of the agglomerate is wetted, it infiltrates the outer edges of the agglomerate weakening the interactions between particles and enabling a better transfer of stress to the agglomerate structure allowing much more efficient dispersion. Kasaliwal, 2011 discusses how the rate of polymer infiltration into the pores of the agglomerate is influenced by the surface energy of the melt, polymer viscosity, molecular weight, and branching. The degree of infiltration in a given time can be estimated through the Washburn equation, see Equation F.1:

$$L = \left[\frac{r \cdot t \cdot \Gamma_{LV} \cdot \cos\theta}{2\eta}\right]^{\frac{1}{2}} \tag{F.1}$$

where L is the length of pore penetration in m, r is the pore radius in m, t is time in

s, Γ_{LV} is the surface free energy (surface tension) of polymer melt in $\mathrm{N\,m\,m^{-1}}$, θ is the contact angle in $^\circ$ and η is the viscosity in Pa s.

Kasaliwal, 2011 discusses the notion that at a given shear rate for the best dispersion of the additive an optimal polymer viscosity will exist, which will balance the rate of infiltration with the hydrodynamic forces achieved at the given condition.

F.1.1 Molecular weight

Both the number average and the weight average molecular weights are used in industry as an indicator of polymer chain length. The weight average is utilised to illustrate the changes in the numbers of longer chains. Increased chain length leads to a reduction in chain mobility and a greater number of entanglements resulting in the increase in polymer viscosity. The effects of viscosity are examined separately in the next section.

In the literature whereas there are a number of studies on the impact of viscosity, there is limited information on the impact of chain length. Kasaliwal et al., 2011 examined the impact of chain length by altering the processing temperatures of different molecular weight polycarbonate in order to match the viscosity of the material. The author found that in the higher molecular weight polymer matrix the size of undispersed agglomerates was larger than in the lower molecular weigh material. The size of agglomerates increased with increasing molecular weight at both low viscosity and high viscosity conditions (Kasaliwal, 2011). This is likely a direct result of a reduction in the mobility of the polymer chains, where the increased number of entanglements and the larger hydrodynamic radius prevent the polymer chains from penetrating into the agglomerate pores. This limits the interaction between the agglomerate and the matrix lowering the ability of the matrix to effectively transfer stress to the agglomerate thus inhibiting both the agglomerate rupture process and the erosion mechanism.

F.1.2 Viscosity

The viscosity of the polymer has two competing effects. At lower viscosity, the polymer chains are more mobile allowing them to infiltrate the outer layers of agglomerate. This disrupts the interparticle interactions reducing the cohesive forces and under applied shear leads to flows within the porous agglomerate structure. As a result the agglomerates can be ruptured at lower stresses and dispersion via the erosion mechanism is enhanced. On the contrary, the increasing viscosity of the polymer matrix increases the shear stress within the fluid and thus the hydrodynamic stress experienced by the agglomerate. This increases the rupture mechanism and allows for smaller agglomerates to be broken up as these have a higher tensile stress. In the case of direct to melt addition, it is vital that the viscosity of the polymer matrix is high enough to enable effective dispersion and not simply wet out the additive (Young et al., 2013).

Vaia et al., 1995 reported that a faster intercalation of the nanoclay was achieved in a polymer matrix of a lower viscosity and molecular weight. Villmow et al., 2008 discussed the affect of viscosity on the erosion and rupture dispersion mechanisms. Those authors found that the erosion was facilitated by lower melt viscosity as the polymer was able to infiltrate the outer layer of agglomerates more easily. The rupture mechanism was enhanced by higher viscosity polymer matrix due to the higher shear stress. Le et al., 2009 (as cited in Kasaliwal et al., 2011) reported that lowering of the viscosity increased the dispersion of MWCNTs in a rubber matrix until an optimum value was reached.

Kasaliwal et al., 2009; Kasaliwal, 2011 performed extensive systematic studies on dispersing MWCNTs in a polycarbonate matrix in a micro-compounder. They reported that at lower screw speeds (low shear rates) the lower viscosity matrix delivered much better dispersion of the MWCNTs compared to a higher viscosity matrix. However, as the screw speed was increased the difference diminished with very similar levels of dispersion being achieved at high screw speeds. This result is interesting, as at the higher shear rates the stresses achieved in the higher polymer matrix are much larger.

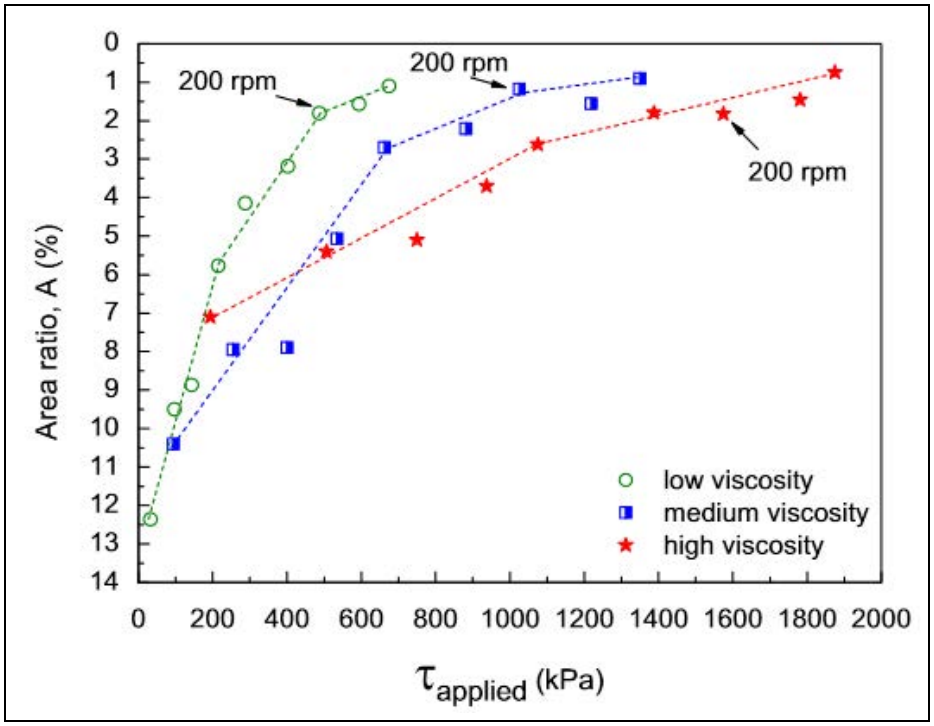

Figure F.1: *Dispersive mixing as function of shear stress (Fig. 6, p. 1031, Kasaliwal et al., 2011)*

Kasaliwal et al., 2011 reported that at the same applied shear stress, the level of dispersion achieved with a lower viscosity polymer matrix was much better than that with a higher viscosity matrix; see Figure F.1. This was attributed to the role of polymer infiltration into the agglomerate structure, which is much more prominent at a lower viscosity and has the net result of weakening the agglomerate structure as well as increasing mixing through erosion mechanism. The authors also found that irrespective of viscosity, the change in mixing achieved at different screw speeds was the same. Although there is a compromise with the lower viscosity matrix allowing better infiltration of agglomerates and the higher viscosity transferring larger stresses, Kasaliwal et al. went on to conclude that in the lower viscosity matrix erosion is a much more dominant process of dispersion and at higher viscosity the rupture mechanism was the dominant process. Considering that the erosion mechanism is much slower, the optimum viscosity will be a function the rate of infiltration, ability to transmit the shear stress and the residence time within the extruder which in turn would determine the contribution of the erosion mechanism.

From a processing prospective, the polymer viscosity also plays a vital role in determining the flow of materials through the mixing zones, the residence time and degree of fill. As the viscosity increases the degree of fill increases as a larger pressure has to be generated to pump the material forward, thus resulting in a longer residence time (Gautam and Choudhury, 1999). Kalyon et al., 1988a reported that the viscosity of the material changes as a function of specific energy input. Once the additive has been introduced, the viscosity also changes as the result the level of mixing along the length of the extruder which determines the interactions between the matrix and the polymer (Kalyon et al., 1988a).

For a PET extrusion system, the viscosity of material changes along the axis of the extruder as a result of chemical reactions and mechanical scission of the polymer chains. This is an important aspect to consider when deciding upon an additive injection point or the molecular weight of the polymer to be utilised for the manufacture of a product. It also poses a challenge in calculating the hydrodynamic stress being experienced by the particle at any stage of the extruder as the viscosity can at best only be estimated. The challenge of estimating the viscosity becomes harder with increasing molecular weight of the polymer as this increases the overall viscosity which leads to more localised viscous heating resulting in variations in temperature (Todd, 1975) and thus viscosity.

F.2 Impact of the additive properties

As well as the polymer properties, the properties of the additive also play a vital role in determining the ease of mixing. The strength of the agglomerate is determined through the inter-particle forces which bind the primary particles together. These can be separated into surface and field forces, mechanical interlocking, and material bridges (Stevens and Covas, 1995); see Figure F.2.

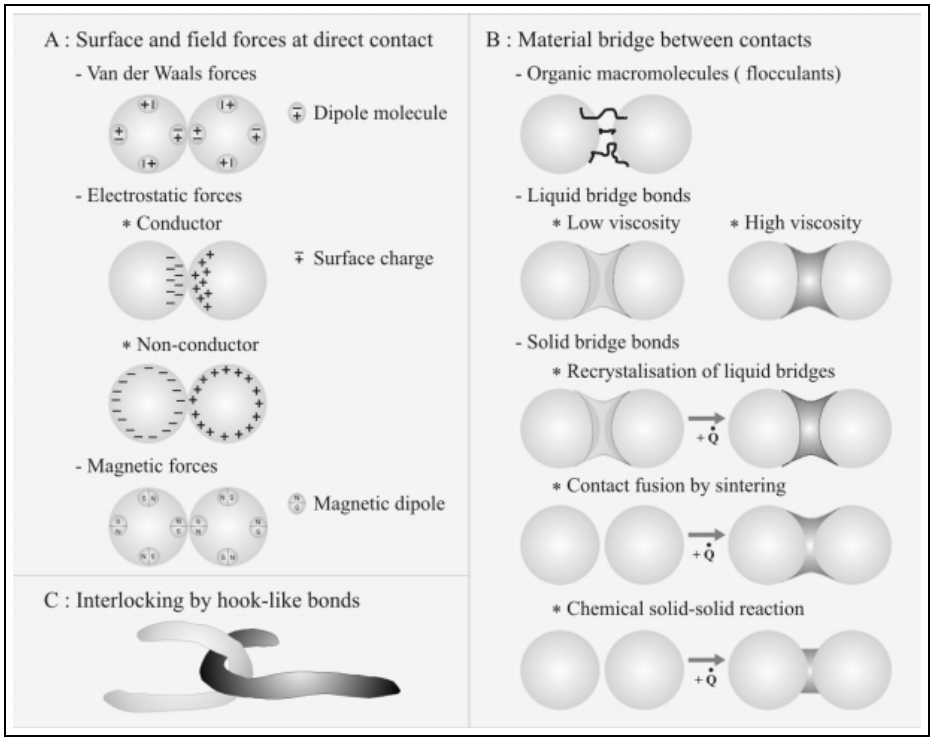

Figure F.2: *Inter-particle interactions (Fig. 1, p. 1999, Tomas, 2007)*

Table F.1: *Magnitude of attractive and separating forces for 100* µm *particles; (p.148 Bart, 2006)*

Nature	**Force**	**Type**	**Magnitude** (N)
Adhesive	*Adhesive*		10^{-4}
	Viscous		10^{-5} to 10^{-6}
	Capillary	Surface tension	10^{-5} to 10^{-6}
		Hydrostatic	10^{-5} to 10^{-6}
	Electrostatic	Coulomb	10^{-7}
		Dipole	10^{-8}
		Image charge	10^{-7}
		Space charge	10^{-8}
Separating	*Hydrodynamic*		10^{-3}
	Electrostatic		10^{-8}

Bart, 2006 provides an indication of the magnitude for the different forces experienced by 100 µm particles in a compounding process; see Table F.1. In this case, as the hydrodynamic forces are an order of magnitude larger than the adhesive forces there should be good dispersion of the filler. The inherent additive properties such as particle, shape, size, porosity and surface characteristics effect the agglomerate strength which in turn deter-

mines the hydrodynamic stresses that need to be applied to the agglomerate in order to rupture it. These are discussed below.

F.2.1 Particle size and surface area

The tensile stress of the agglomerate was discussed in detail by Tadmor and Gogos, 2006 and can be evaluated with the Rumpf model; described in Equation F.2.

$$\sigma_A = \frac{9}{8}\left(\frac{1-\varepsilon}{\varepsilon}\right)\frac{F}{D_p^2} \quad \text{where} \quad F = \frac{A \cdot R}{12z^2} \tag{F.2}$$

where σ_A is the tensile strength of the agglomerate in $\mathrm{N\,m^{-2}}$, ε is voidage, F is the force of the single bond in N, D_p is particle diameter in m, A is Hamaker constant (typically 5×10^{-20} to 5×10^{-19} J), R is particle radius in m and z is the minimum separation distance for adhering spheres (typically 0.4 nm).

The cohesive force of the agglomerate can be obtained by multiplying σ_A by the cross sectional area of the agglomerate, S.

$$F_c = \frac{9}{8}\left(\frac{1-\varepsilon}{\varepsilon}\right)\frac{F}{D_p^2} \cdot S \tag{F.3}$$

From Equation F.3 it is evident that as the diameter of the particles decreases the cohesive force of the agglomerate will increases linearly; thus making dispersion more difficult as larger hydrodynamic forces are required to rupture the agglomerates. Kwang-Jea and White, 2000 observed that silica agglomerates became more difficult to break with decreasing size of particles when he examined their dispersion in ethylene-polypropylene-diene-terpolymer (EPDM) matrix in a Brabander PL2000 Plasticorder.

Another important effect to consider is the change in surface area. As the base particle size decreases, for the same additive loading of non porous particles, the surface area of the particles increases. In a system where there is poor interaction between the additive

and the polymer matrix this in turn increases the energy required to generate effective wetting as a much larger interface area now has to be created and stabilised. Kwang-Jea and White, 2000 found that the size of agglomerates for silica and carbon black particles dispersed was proportional to the surface area of the particles. Interestingly, they found the size of agglomerates for calcite, talc, zinc oxide and carbon black with the same specific surface area was very similar when the additives were processed under the same conditions.

In a similar manner, in the case of open and large pores the increased porosity of the particles would also lead to increase in the energy required for mixing as this would raise the specific surface area of the additive. This effect is much more likely to be evident at low viscosity short chain length polymer matrix where the polymer would have the ability to penetrate deep into the pores of the particles. Although this would increase the interaction between the polymer and the particle it would theoretically allow for smaller loading of the material within the composite as there would be less polymer available for coating of the outer surface of the particle.

From Equation F.3 it is also evident that the packing density of the agglomerate structure plays a critical role in determining the cohesive forces. As the voidage within the agglomerate increases (packing density decreases) the cohesive force of the agglomerate becomes smaller. This effect is further exaggerated by the increased ability of the polymer melt to penetrate into the larger pores which in turn interrupts the inter particle interactions and promotes a better transfer of force from the fluid to the agglomerate structure.

F.2.2 Particle shape

The shape of the particles also play a role in determining the ease of dispersion. Bart, 2006 discusses the importance of particle shape concluding that the round particles tend to exhibit good flow behaviour and disperse well. On the other hand, non circular, fibrous or platelet like shapes are much harder to disperse. Fibrous particles have a high number of

entanglements within the agglomerate which gives it a very high cohesive strength. One would envisage that the increasing aspect ratio would make the particles much harder to disperse due to the increased number of entanglements. Although Young et al., 2013 acknowledge the need for different processing parameters to disperse long and short aspect ratio additives. The authors reported that it is the low aspect ratio filler which require the highest degree of dispersion in order to break up the agglomerates and the higher aspect ratio fillers require much gentler profile to minimise the breaking of the fibres.

Kasaliwal et al., 2010 concluded that for larger aspect ratio particles the dispersion process is governed by the much faster rupture mechanism. The rupture mechanism can lead to the undesired effect of breakages of the long aspect ratio particles, which mainly tends to occur at 'defect' locations within the particle. The erosion process would eliminate this drawback, but it is much slower then the rupture mechanism.

F.2.3 Moisture content

The moisture content of the additive is an important consideration especially in the manufacture of PET composites. The moisture increases the strength of agglomerates, as seen in Figure F.2B, making them harder to disperse. It also increases the cohesive nature of the particles leading to stickiness and bridging of the powder inhibiting their flowability making them much harder to maintain the accuracy of the feed (Giles et al., 2005).

Although at DTF, the PET is not normally dried prior to being extruded on the TSE, the moisture is removed rapidly from the PET with the aid of vacuum degassing section which is located straight after the melting section. This minimises any unnecessary hydrolysis of the PET chains. In the case of the direct to melt addition process, the moisture carried in by the particle will lead to the hydrolysis of PET (if not removed rapidly) decreasing the melt viscosity and thus reducing the effectiveness of the rupture mechanisms by reducing the hydrodynamic stresses which the agglomerate would experience. The issue with direct addition process is that an extra vacuum port to remove the moisture contained within

the particles can not be located directly in the zone where the additive is introduced as the particles would be removed as well. Instead the additive initially has to be gently wetted and then a melt seal has to be created prior to the second vacuum section.

If the additive is porous and the moisture is contained within the pores of the additive the challenge increases even further, as the moisture effectively becomes locked in within the particle whilst it is wetted out by the polymer. The moisture is unlikely to be removed by the vacuum port due to the polymer film layer around the particle not experiencing any interface renewal. Instead the moisture is likely to slowly diffuse out leading to the hydrolysis of the PET throughout the length of the melt system. This can be mitigated slightly by preheating the powder storage hopper and locating an atmospheric degassing section close to the additive injection point. Typically due to the porosity of the particles, the bulk density of such materials is very low which makes them very difficult to dry in standard fan operated drying ovens.

F.3 Importance of the additive-polymer interaction

The interactions between the additive and the polymer are key as they influence not only the infiltration of the polymer into the agglomerate but also the initial wetting of the particles. More information on wetting, contact angles and surface energies is provided in Appendix G. A number of substances can be introduced into the system in order to modify the nature of these interactions. These include wetting agents, compatibilisers (dispersants) and dispersive aids.

Wetting agents work by lowering the surface energy of the liquid phase promoting the wetting of the higher surface energy solid. These can be added directly into the liquid, or more commonly in compounding coated/bonded onto the surface of the particles. Surface treatment of the particles involves the addition of functional groups onto the surface of the additive which can interact or even react with the polymer matrix. This is often

undertaken in compounding of fibres (Tadmor and Gogos, 2006).

Once dispersion is achieved within a TSE extruder, there is a a tendency for the materials to re-agglomerate as the particles collide and pass through the high pressure sections. Compatilbilisers have a different role and work to prevent re-agglomeration (flocculation) of the particles once dispersion has been achieved.

The last method used to ease the task of dispersion is through dispersive aids. These are typically much lower viscosity then the polymer matrix and are introduced together with the particles (typically premixed). They work by wetting the surface of the particle and minimising inter-particle interactions which reduces the hydrodynamic stresses required to break the agglomerate (Kohlgrüber, 2008). In effect this process removes the need of the 'wetting' stage during the TSE process so that dispersion can occur almost immediately. Dispersive aids can include materials such as amides, polypropylene waxes, polyethylene waxes, fatty acids, and their esters, polyacrylates, fluorocarbon polymers as well as metal carboxylates (Bart, 2006; Kohlgrüber, 2008).

Fortunato et al., 2014 examined the dispersion of titanium dioxide in PET at various extrusion conditions and found that the addition of PVA lead to big improvements in the level of dispersion as the PVA bound the particles to the polymer matrix. Gao et al., 2011 examined the dispersion of barium sulphate in PET matrix in an in-situ polymerisation. The particle surface was modified with steric acid to generate a hydrophobic surface which in turn deliverd much better level of dispersion when compared to the original hydrophilic particles. Young et al., 2013, also commented on the good interaction between hydrophobic talc surface and the organic compounds. Kimura et al., 2000 examined the interactions between silica and PET matrix as well as modified silica particles with coatings including ethylene glycol, butanol and a number of other compounds. The coating acted to lower the dispersive component of the surface energy of the filler. The strength of interaction between the silica and the PET correlated well with the basicity of the filler (and not its acidity) suggesting that the carboxyl end group of the PET interacts strongly

with the electron donating groups of the filler coating.

One of the challenges with utilising such compounds apart from potential safety concerns and unfavourable affects on the material properties is the need to find a system specific molecule. This means that the same compatibiliser, dispersive aid or wetting agent can not be used on clay, silica or titanium dioxide filled systems; instead its a big advantage if the same functional molecule can be utilised for a single sub group and cater for a variety of clays. This is not guaranteed.

F.4 Concluding Remarks

Both the additive and the matrix properties can have a significant impact on the level of dispersion achieved within polymer composites. Perhaps the role of the matrix properties is understood in more quantifiable way than that of the filler. Kasaliwal et al., 2011; Villmow et al., 2008 examined the influence of polymer molecular weight and viscosity on the errosion adn rupture dispersion mechanisms. Regarding the additive, an established theory exists enabling the calculation of the cohesive strength of the agglomerate. As discussed by Gogos et al., 1996, this is a function of the primary particle to particle interactions, their size, and the agglomerate porosity. However, less quantitative literature exists on the role of particle shape in determining the extent of mixing achieved.

Focusing on a PET matrix, the moisture contained within the particles is expected to play a significant role due to facilitating the hydrolysis reaction. Drying the additive is not likely to be possible in standard equipment, particularly when dealing with very low bulk density materials. Similarly, it is difficult to address the issue within the extrusion process as the a vacuum degassing section can only be located after the additive has been fully wetted by the melt to prevent it being extracted from the extruder but this introduces the extra resistance when considering the moisture diffusion as it now has to diffuse through the film around the particle.

Some work has been undertaken by Fortunato et al., 2014; Kimura et al., 2000 to evaluate the effect of modifying the interactions between the additive and the PET matrix through either the use of a dispersive aids or the modification of the particle surface. However, there is almost no link between the strength of the interaction and the modifications performed.

G | Wetting, contact angle and surface energy

The strength of the interaction between the additive and the polymer in a given system can be determined by considering the work of adhesion, W_{AdP} and the interfacial tension, Γ_{AdP}. The affinity of a given polymer for a set additive can be evaluated by examining the wetting behaviour, which can be quantitatively established though the use of the contact angle, θ_{AdP}.

G.1 Work of adhesion and cohesion

Thermodynamic work of adhesion, W_{AB} is the work required to separate surface AB into two new surfaces A and B, see Figure G.1.

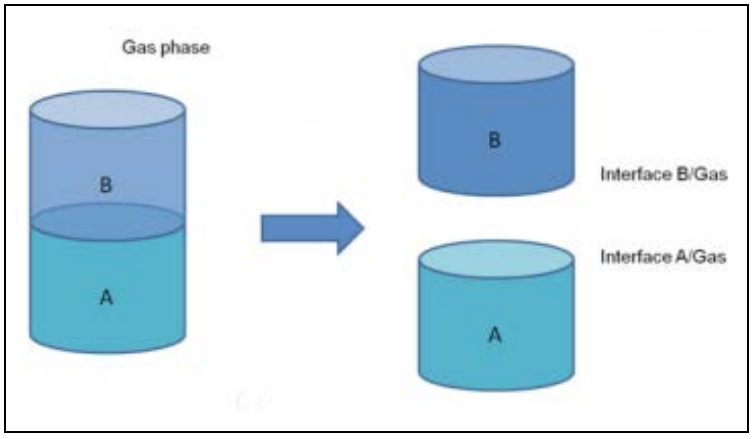

Figure G.1: *Thermodynamic work of adhesion (Biolin Scientific, 2014a)*

This can be described mathematically by Dupre's equation shown in Equation G.1; where W_{AB} is the work of adhesion between substance A and B, Γ_{AV} is the surface tension at the interface between substance A and vapour phase V, Γ_{BV} is the surface tension at the interface between substance B and vapour phase, Γ_{AB} is the interfacial tension between substance A and B.

$$W_{AB} = \Gamma_{AV} + \Gamma_{BV} - \Gamma_{AB} \tag{G.1}$$

The work of cohesion can be defined in a similar manner, as the work required to separate surface AA into two new surfaces A and A, see Figure G.2

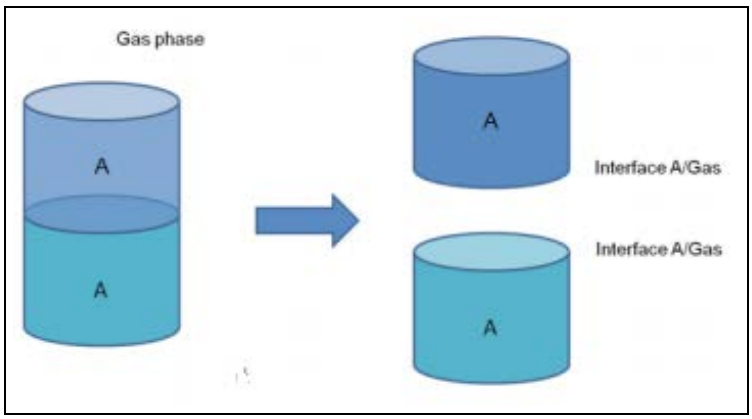

Figure G.2: *Thermodynamic work of cohesion (Biolin Scientific, 2014a)*

Mathematically this can be described by Equation G.2 which reduces to Equation G.3 as the interfacial tension within a substance, Γ_{AA} is equal to zero.

$$W_{AA} = \Gamma_{AV} + \Gamma_{AV} - \Gamma_{AA} \tag{G.2}$$

$$W_{AA} = 2\Gamma_{AV} \tag{G.3}$$

G.2 Surface tension, surface free energy and interfacial tension

In a liquid state the molecules experience forces of attraction in all directions, which on average equal each other. On the surface, technically the liquid-vapour interface, out of balance forces result in a net inward pull which results in a line tension acting perpendicular to a unit length of the interface, see Figure G.3. This force, termed *surface tension*, is measured in $\mathrm{mN\,m^{-1}}$ and denoted by Γ_{LV}.

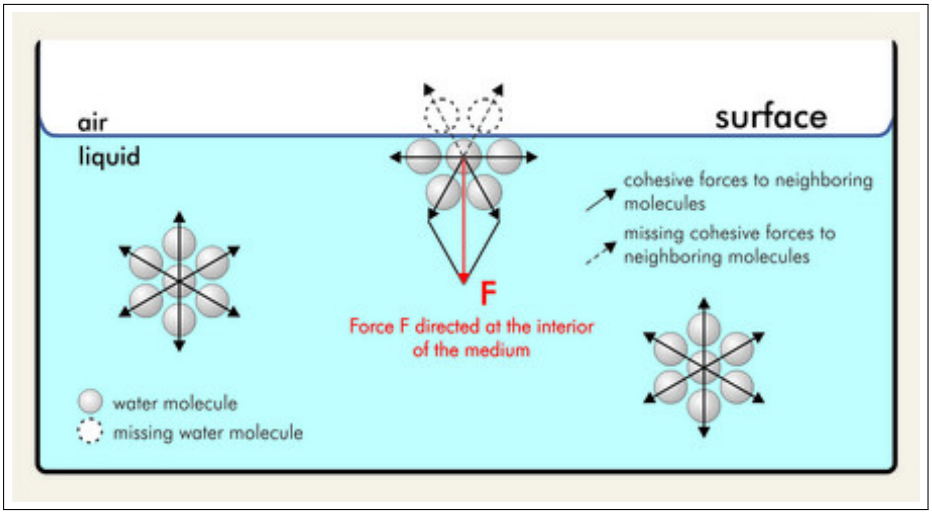

Figure G.3: *Origin of surface tension (SITA Process Solutions, 2015)*

Equivalently the term *surface free energy* denoted by Γ_{SV} measured in $\mathrm{mJ\,m^{-2}}$ is used when dealing with solids rather than liquids which is defined as the thermodynamic work required to increase the area of a surface by a unit amount reversibly under isothermal conditions (Bowen, 2013a).

The forces acting at the surface do so almost independently. Fowke's Theory states that the total force can be approximated by adding the individual components as shown in Equation G.4 (Hansen, 2004).

$$\Gamma_{LV} = \sum \Gamma^{i}_{LV} \quad \text{or} \quad \Gamma_{SV} = \sum \Gamma^{i}_{SV} \tag{G.4}$$

where the individual components, i include dispersion, polar, hydrogen, induction and acid-base interactions.

The surface tension parameter can also be related to the macroscopic properties with the help of Equation G.5, where A is the Hamaker Constant in J and a is the cut-off distance in m with 0.165 nm typically being used (Bowen, 2013a). However, as the Hamaker constant is purely a dispersive term, the relationship has limited accuracy in predicting the surface tension of polar compounds where hydrogen bonding contributes significantly to the total surface tension.

$$\Gamma = \frac{A}{24\pi a^2} \tag{G.5}$$

Interfacial tension, Γ_{AB} is the energy change required for expanding the interface between two immiscible liquids denoted as A and B by a unit area. This can be considered in a hypothetical two stage process where initially two unit areas of the separate media are generated and then brought into contact, described mathematically in Equation G.6 (Bowen, 2013a).

$$\Gamma_{AB} = \frac{1}{2}W_{AA} + \frac{1}{2}W_{BB} - W_{AB} \tag{G.6}$$

where W_{AA} and W_{BB} is the work of cohesion for substance A and B respectively and W_{AB} is the work of adhesion between the two components.

By substituting for work of cohesion, Equation G.3 one arrives at a rearranged form of Dupre's equation.

G.2.1 Wetting

Wetting examines how two substances interact with each other. For a solid - liquid phase system contact angle, θ at the solid - liquid - vapour interface is measured in order to evaluate the affinity of the liquid for the solid phase, see Figure G.4. If there is a favourable interaction between the liquid and the solid, the liquid will spread on the surface of the solid and for a thin film leading to $\theta \rightarrow 0°$. Poor affinity between the liquid and a solid would result in a bead of the liquid on the surface of the solid leading to a contact angles $>90°$ with very incompatible systems approaching 180°.

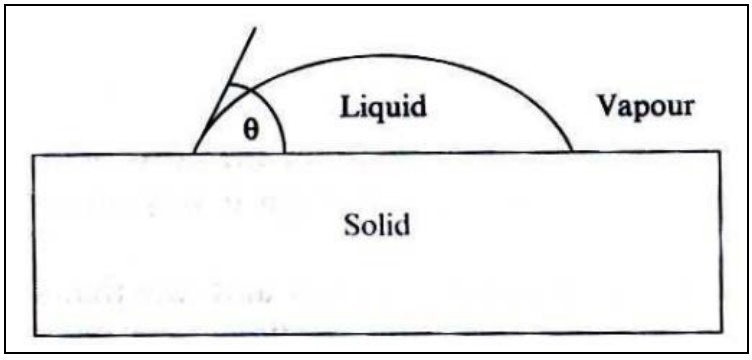

Figure G.4: *Contact angle measurement (Bowen, 2013b)*

A force balance, shown in Figure G.5, at the solid - liquid - vapour interface leads to the equation relating the surface free energy of the solid, Γ_{SV} to the surface tension of the liquid, Γ_{LV} and the interfacial tension between the solid and the liquid, Γ_{SL}.

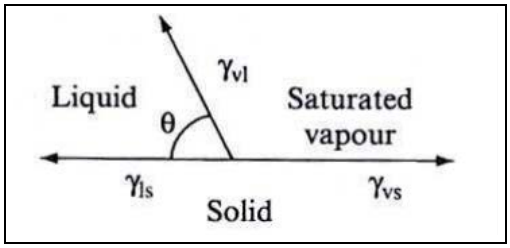

Figure G.5: *Force balance at the solid - liquid - vapour interface (Bowen, 2013b)*

The mathematics of the system in the above figure are described by the Young's equation, shown in Equation G.7.

$$\Gamma_{SV} = \Gamma_{SL} + \Gamma_{LV} \cos\theta \tag{G.7}$$

By rearranging Equation G.7 for $\cos\theta$ it can be seen that good wetting (as $\cos\theta \to 1$) is favoured by high solid surface free energy, low liquid surface tension and low interfacial tension between the liquid and the solid (Owens and Wendt, 1969).

G.3 Additive - polymer system

If the surface free energy of the additive, Γ_{AdV}, the surface tension of the polymer, Γ_{PV} and the interfacial tension between the additive and the polymer, Γ_{AdP} is known then

the Dupre equation shown in Equation G.4 can be used to calculate the work of adhesion between the additive and the polymer, W_{AdP}; see EquationG.8.

$$W_{AdP} = \Gamma_{AdV} + \Gamma_{PV} - \Gamma_{AdP} \tag{G.8}$$

Note: The surface tension of the polymer, Γ_{PV} is being considered, instead of the surface free energy as one is interested in the value for Γ_{PV} at the temperature of ca. 285 °C, where the polymer is in the melt state.

Even though it may be possible to obtain the surface free energy of the additive from the manufacturer, the direct measurement of the interfacial tension between the additive and the polymer would be very difficult and the calculation would require the knowledge of the work of adhesion. By considering the wetting of the polymer on the additive surface, one can derive a Young's equation for the system, shown below.

$$\Gamma_{AdV} = \Gamma_{AdP} + \Gamma_{PV} \cos\theta_{AdP} \tag{G.9}$$

Equation G.9 can be combined with the Dupre equation, shown in Equation G.8, to produce a Dupree - Young equation which eliminates the Γ_{AdV} and Γ_{AdP} terms resulting the work of adhesion between additive and the polymer as a function of the contact angle.

$$W_{AdP} = \Gamma_{PV} (1 + \cos\theta_{AdP}) \tag{G.10}$$

The measurement of the contact angle between the additive and the polymer, θ_{AdP} utilising the set up illustrated in Figure G.4 would not be possible as a flat surface is required for the measurement which would not be feasible to achieve with a powdered additive. The experiment would also have to be conducted at elevated temperature of ca. 285 °C to achieve a polymer melt and account for the extrusion conditions.

The Washburn method is typically utilised for determining the contact angle of the liquid with the powdered solid (Biolin Scientific, 2014b; Zenkiewicz, 2007), see Figure G.6. In

the experiment the rise of the liquid up the capillary filled with powder is monitored and can be related to the contact angle by the Washburn equation; see below (Biolin Scientific, 2014b).

$$h^2 = \frac{r\Gamma_{PV}\cos\theta_{AdP}}{2\eta}\, t \quad \text{where} \quad r = \frac{R_D^2}{R_S} \tag{G.11}$$

where h is the height of liquid in the capillary, η is the viscosity of the liquid, t is time and R_D and R_S are the mean hydrodynamic and static radius of the capillary respectively.

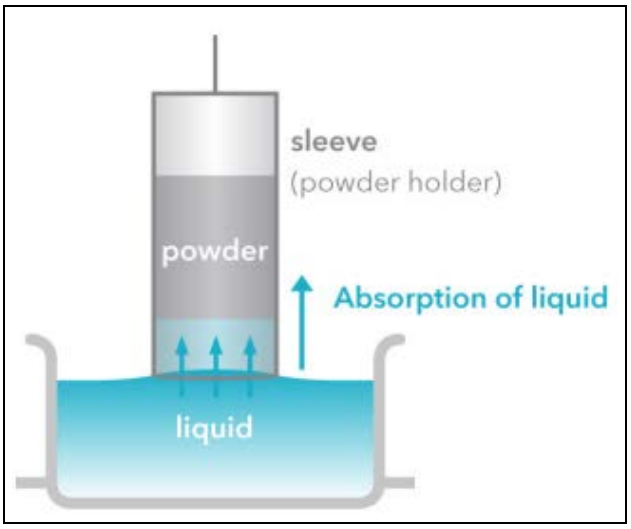

Figure G.6: *Schematic of Washburn method (Biolin Scientific, 2014b)*

The weight of the liquid within the capillary is given by Equation G.12 where ϵ is the porosity of the additive in the capillary, ρ is the polymer melt density and R is the radius of the capillary.

$$w = \epsilon\rho\pi R^2 h \tag{G.12}$$

Using this, an equation relating the weight of the liquid absorbed by the powdered additive to the time can be constructed as shown in Equation G.13, where C can be considered a material constant (Biolin Scientific, 2014b).

$$w^2 = C\,\frac{\rho^2\Gamma_{PV}\cos\theta_{AdP}}{2\eta}\, t \quad \text{where} \quad C = r\epsilon^2\pi^2 R^4 \tag{G.13}$$

For a given material, the value of C can be determined by performing an experiment with a liquid that fully wets out the solid additive, thus one can assume $\cos\theta = 1$. Typically, such liquids include hexane, heptane and octane (Biolin Scientific, 2014b).

Unfortunately this set up is also impractical for the measurement of the contact angle between the additive and the polymer. The high viscosity of the polymer would result in the need to run the experiment over a long period of time and the need for elevated temperature to maintain the molten state of the polymer would make maintaining temperature uniformity very difficult hence potentially undermining the accuracy of the data gathered. As a result, it is not possible to measure the contact angle between the polymer and the additive directly.

According to Fowkes theory the work of adhesion can be estimated by considering the individual components of the surface tensions for each material. Geometric mean can be used to estimate the interfacial properties based on the properties of the individual material, as shown in Equation G.14 (Hansen, 2004).

$$W_{AdP} = \sum 2\sqrt{\Gamma^i_{Ad}\Gamma^i_P} \quad \text{such that} \quad W_{AdP} = 2\sqrt{\Gamma^d_{Ad}\Gamma^d_P} + 2\sqrt{\Gamma^p_{Ad}\Gamma^p_P} + ... \tag{G.14}$$

where the individual components, i include dispersion, polar, hydrogen, induction and acid-base interactions.

To enable the calculation of work of adhesion Fowkes assumed that for a simplified system the surface tension can be represented by the dispersive component only and the other interactions can be neglected (Owens and Wendt, 1969); see Equation G.15.

$$W_{AdP} = 2\sqrt{\Gamma^d_{Ad}\Gamma^d_P} \tag{G.15}$$

Owens and Wendt took the work further by stating that all of the other components apart from dispersion can be considered under the polar component umbrella, resulting in the following estimate as shown in Equation G.16 (Owens and Wendt, 1969).

$$W_{AdP} = 2\sqrt{\Gamma^d_{Ad}\Gamma^d_P} + 2\sqrt{\Gamma^p_{Ad}\Gamma^p_P} \tag{G.16}$$

Wu carried on the work further by agreeing with the assumptions of Owens and Wendt but focusing utilising a harmonic mean approximation method rather than the geometric mean. Equation G.17 is more applicable for use in polar - polar systems, and can accurately predict the work of adhesion for between polymers or polymers and other liquids.

$$W_{AdP} = 4\left[\frac{\Gamma^d_{AdV}\Gamma^d_{PV}}{\Gamma^d_{AdV} + \Gamma^d_{PV}} + \frac{\Gamma^p_{AdV}\Gamma^p_{PV}}{\Gamma^p_{AdV} + \Gamma^p_{PV}}\right] \tag{G.17}$$

Once the dispersive and the polar components of the additive surface free energy and polymer surface tension are known the work of adhesion, W_{AdP} can be estimated. Based on this estimate the Equation G.10 can be utilised to calculate the contact angle which can be used to evaluate the degree of wetting. Similarly, Equation G.8 can be utilised to calculate the interfacial tension between the additive and the polymer.

G.3.1 Determining dispersive and polar components of the polymer surface free energy

A method illustrated in Figure G.4, where drop of liquid is placed onto the surface of the polymer film at ambient conditions, can be used to measure the contact angle formed at the polymer-liquid-vapour interface for liquids $L1$ and $L2$. By choosing the liquids such that their dispersive and the polar components of the surface tensions are known the dispersive, Γ^d_{PV} and the polar components, Γ^p_{PV} of the surface free energy of the polymer at ambient conditions can be estimated. This can be achieved by solving Equation G.18 and G.19 simultaneously with the equations below being derived by combining the Equation G.17 and G.10.

$$4\left[\frac{\Gamma^d_{L1V}\Gamma^d_{PV}}{\Gamma^d_{L1V} + \Gamma^d_{PV}} + \frac{\Gamma^p_{L1V}\Gamma^p_{PV}}{\Gamma^p_{L1V} + \Gamma^p_{PV}}\right] = \Gamma_{L1V}\left(1 + \cos\theta_{L1P}\right) \tag{G.18}$$

$$4\left[\frac{\Gamma^d_{L2V}\Gamma^d_{PV}}{\Gamma^d_{L2V}+\Gamma^d_{PV}}+\frac{\Gamma^p_{L2V}\Gamma^p_{PV}}{\Gamma^p_{L2V}+\Gamma^p_{PV}}\right]=\Gamma_{L2V}\left(1+\cos\theta_{L2P}\right) \tag{G.19}$$

Typically water, W is chosen as a polar liquid and methylene iodide, MI is selected as a non-polar liquid for analysis (Hansen, 2004; Owens and Wendt, 1969; Wu, 1971). Owens and Wendt reports the following values for the polar and dispersive components and polar components of the surface tensions for aforementioned liquids: $\Gamma^d_W = 21.8 \pm 0.7$ mN m^{-1}, $\Gamma^p_W = 51.0$ mN m^{-1} and $\Gamma^d_{MI} = 49.5$ mN m^{-1}, $\Gamma^p_{MI} = 1.3$ mN m^{-1}. Slightly different values, calculated on the basis of the harmonic mean equation were reported by Wu: $\Gamma^d_W = 22.1 \pm 0.6$ mN m^{-1}, $\Gamma^p_W = 50.7$ mN m^{-1} and $\Gamma^d_{MI} = 44.1$ mN m^{-1}, $\Gamma^p_{MI} = 6.7$ mN m^{-1}. Diiodomethane, DI can also be utilised as a non-polar liquid where typically it is assumed not to poses a polar component hence $\Gamma_{DI} = \Gamma^d_{DI} = 50.8$ mN m^{-1}, although values of $\Gamma^d_{MI} = 48.5$ mN m^{-1}, $\Gamma^p_{MI} = 2.3$ mN m^{-1} have been reported in literature (Zenkiewicz, 2007).

Owens and Wendt reports values for the surface free energy of PET in the solid state calculated by two liquids method and the geometric mean approximation at $\Gamma^d_{PET} = 43.2$ mJ m^{-2}, $\Gamma^p_{PET} = 4.1$ mJ m^{-2}, thus $\Gamma_{PET} = 47.3$ mJ m^{-2}. These differ from those reported by Wu: $\Gamma^d_{PET} = 32.8$ mJ m^{-2}, $\Gamma^p_{PET} = 9.3$ mJ m^{-2}, thus $\Gamma_{PET} = 42.1$ mJ m^{-2}; who use the same two liquids but combined with the harmonic mean approximation. Generally, the harmonic mean approximation is considered to be more theoretically correct (Biolin Scientific, 2014b). Measurements on PEN film conducted by Elisa Koponen at DTF reveal values not to dissimilar to that reported for PET: $\Gamma^d_{PEN} = ca.\ 40$ mJ m^{-2}, $\Gamma^p_{PEN} = ca.\ 5.6$ mJ m^{-2}, thus $\Gamma_{PEN} = ca.\ 45.6$ mJ m^{-2}. These were calculated using the harmonic mean equation by the application of the two liquid analysis, with water and diiodomethane being utilised.

Once the dispersive and the polar components of the polymer surface free energy have been established the total surface free energy can be calculated using Equation G.4. The

value at the ambient temperature can be related to that at any temperature with the relationship provided by the integral of Equation G.20 shown in Equation G.21 (Cardinaud, 2013):

$$-\frac{d\Gamma}{dT} = \frac{9}{11}\frac{\Gamma_0}{T_C}\left(1-\frac{T}{T_C}\right)^{\frac{2}{9}} \tag{G.20}$$

$$\Gamma = \Gamma_0\left(1-\frac{T}{T_C}\right)^{\frac{11}{9}} \tag{G.21}$$

where Γ is the surface free energy, Γ_0 is the surface free energy at temperature of 0 K, T is temperature in K, T_C is the critical temperature (ca. 1000 K for most polymers).

With the knowledge of the value for $-\frac{d\Gamma}{dT}$, which for PET is 0.065 mN m^{-1} K^{-1} (Cardinaud, 2013), one can calculate the Γ_0. This in turn can be utilised in Equation G.21 to calculate the surface tension at the extrusion temperature of 285 °C. By assuming that polarity is independant of temperature, hence the ratio of $\frac{\Gamma^p}{\Gamma}$ remains constant the value for the polar and dispersive component at any temperature can be determined using Equation G.4. The ratio $\frac{\Gamma^p}{\Gamma} = 0.221$ for PET polymer (Cardinaud, 2013).

G.3.2 Determining dispersive and polar components of the additive surface free energy

The Washburn method illustrated in Figure G.6, where the weight of liquid absorbed onto the powder stored in the capillary tube with respect to time is measured, can be used to determine the contact angle formed at the additive-liquid-vapour interface for liquids $L1$ and $L2$. By choosing the liquids such that their dispersive and the polar components of the surface tensions are known the dispersive, Γ^d_{AdV} and the polar components, Γ^p_{AdV} of the surface free energy of the additive at ambient conditions can be estimated. This can be achieved by solving Equation G.22 and G.23 simultaneously, with the equations below being derived by combining the Equation G.17 and G.10.

$$4\left[\frac{\Gamma^d_{L1V}\Gamma^d_{AdV}}{\Gamma^d_{L1V}+\Gamma^d_{AdV}}+\frac{\Gamma^p_{L1V}\Gamma^p_{AdV}}{\Gamma^p_{L1V}+\Gamma^p_{AdV}}\right]=\Gamma_{L1V}\left(1+\cos\theta_{L1Ad}\right) \tag{G.22}$$

$$4\left[\frac{\Gamma^d_{L2V}\Gamma^d_{AdV}}{\Gamma^d_{L2V}+\Gamma^d_{AdV}}+\frac{\Gamma^p_{L2V}\Gamma^p_{AdV}}{\Gamma^p_{L2V}+\Gamma^p_{AdV}}\right]=\Gamma_{L2V}\left(1+\cos\theta_{L2Ad}\right) \tag{G.23}$$

The harmonic mean approximation is said to be the most appropriate to use on surfaces with low surface free energy. For higher energy surfaces such as mercury, glass, oxides and graphite an approximation based on combination of means has been proposed (Hansen, 2004):

$$2\sqrt{\Gamma^d_{L1V}\Gamma^d_{AdV}}+\frac{4\Gamma^p_{L1V}\Gamma^p_{AdV}}{\Gamma^p_{L1V}+\Gamma^p_{AdV}}=\Gamma_{L1V}\left(1+\cos\theta_{L1Ad}\right) \tag{G.24}$$

$$2\sqrt{\Gamma^d_{L2V}\Gamma^d_{AdV}}+\frac{4\Gamma^p_{L2V}\Gamma^p_{AdV}}{\Gamma^p_{L2V}+\Gamma^p_{AdV}}=\Gamma_{L2V}\left(1+\cos\theta_{L2Ad}\right) \tag{G.25}$$

Ideally, one would like to be able to calculate the surface free energy of the additive at any temperature using the relationship provided in Equation G.20 and G.21. However, finding values for the $-\frac{d\Gamma}{dT}$ and $-\frac{\Gamma^p}{\Gamma}$ ratio for the additives is likely to be problematic for several reasons. These include the application of unknown coatings to the additive surface as well as the novelty of some of the additives meaning that no research would have been published on them. Thus it will be necessary to assume that the additive surface free energy does not change with temperature. This is a reasonable assumption based on the system being considered as in most cases the additive is introduced into the extrusion at ambient temperature and is wetted out by hot molten polymer; especially true for the direct addition via a stuffer feeder. It is the wetting behaviour at this initial condition which is likely to significantly impact the degree if additive dispersion seen in the finished film product. Although the importance of the change in the interfacial properties as the additive heats up should not be completely dismissed as it is these new conditions that

will govern the wetting of the additive particles when agglomerates are broken up by the shear stresses in the extruder.

H A review of the impact of operating conditions on the level of mixing

Some studies have been performed to determine the influence of machine operating conditions on the level of additive mixing (mainly filler dispersion) achieved in the final product; however, very few of these have focused on the extrusion of composites based on a PET substrate. The most notable is that of Fortunato et al., 2014 who examined the influence of screw speed and temperature in the compounding of titanium dioxide (TiO_2). The work of Gao et al., 2011 considered the dispersion of standard and surface modified barium sulphate ($BaSO_4$) particles in nanocomposites produced via in situ polymerisation.

Villmow et al., 2008; 2010 examined the affect of operating conditions on the dispersion of multi-walled carbon nanotubes (MWCNTs) in polylactic acid (PLA) and polycaprolactone (PCL) substrates respectively extruded using a Berstorff ZE25 machine. While the first study examined the influence of directly controllable parameters, the second focused on the impact of screw configuration, residence time and specific mechanical energy input (SME). Domenech et al., 2011; 2013 took a similar approach focusing initially on the effect of directly controllable parameters and then on the importance of SME. They manufactured organomodified montmorillonite layered clay (OMMT)/polypropylene (PP) nanocomposites on a ThermoFisher Rheomex PTW24 co-TSE.

Kasaliwal et al., 2009; 2010; 2011a; 2011b delivered a comprehensive parametric study on dispersion of MWCNTs in a polycarbonate (PC) polymer matrix examining a number of aspects from screw speed, residence time to polymer viscosity and molecular weight. The majority of the their work focused on the manufacture of samples using a micro-

compounder. This is a batch process where the screw speed and residence time can be controlled independently, unlike in a co-TSE process.

These and others are discussed within this section. An attempt has been made to group the relevant studies by the parameters of interest.

H.1 Effect of changes in screw speed

Screw speed is one of the most important parameters in twin screw extrusion as it defines the minimum and the maximum shear rate experienced by the polymer in a given geometry as well as partially determining the average shear rate. These in turn determine the shear stresses to which the polymer and the agglomerates are exposed, which govern dispersion. An increase in screw speed at a given output leads to an increase in all three shear rates and the number of times the polymer passes through the high shear region between the flight and the barrel theoretically increasing dispersive mixing.

A rise in screw speed also increases the shear heating of the material leading to a reduction in its viscosity which offsets some of the potential gains in the hydrodynamic stress transferred to the agglomerates. Rauwendaal, 2016 specifies an equation for the viscous heating, see Equation H.1:

$$\Delta T = \frac{1.8 \cdot f \cdot b \cdot L_s \cdot \bar{H} \cdot K \left[\frac{\pi \cdot D_o \cdot N}{\bar{H}+H_{CL}}\right]^{n+1}}{C_p \cdot \dot{m}} \tag{H.1}$$

where T is temperature in °C, f is the degree of fill (fraction), b is the channel width in mm, L_s is the length of screw in consideration (melt only), $\bar{H}$ is the average channel depth excluding clearance in mm, K is the consistency index, D_o is the outside screw diameter in mm, N is the screw speed in rpm, H_{CL} is the clearance height in mm, n is the power law index, C_p the specific heat capacity in J kg^{-1} °C and $\dot{m}$ is the throughput in kg h^{-1}.

Donoian and Christiano, 1999 reported a melt temperature increase of around 15 °C for

PP when doubling the screw speed from 500 rpm. This was more significant for the higher viscosity HDPE with a temperature rise of ca. 30 °C being reported. These demonstrate the average melt temperature; locally in the high shear regions the temperature increases will be more severe reducing the viscosity even further. They showed that reducing the kneading block clearance from 2 to 0.5 mm increased the melt temperature rise by a further 10 °C in the case of HDPE. If the material is shear thinning then the viscosity will reduce further with rising screw speed. PET is considered to be Newtonian (Champion, 2015).

A rise in screw speed is accompanied by a reduction in the degree of fill, lowering both the machine torque and the residence time. Lee et al., 2012 found that the rise in screw speed causes the residence time distribution (RTD) curve to move to the left (becoming shorter) but also become narrower theoretically leading to worse distributive mixing and more akin to plug flow. Perhaps surprisingly, by considering normalised RTD curves and Peclet number they concluded that the level of distributive mixing is similar irrespective of operating conditions.

Even though the torque and the residence time decrease the SME increases linearly with increase in screw speed (Domenech et al., 2013), theoretically leading to better dispersive mixing. They calculated the changes in the SME delivered to the polymer in the melt phase (excluding feeding and melting zones) and also observed a linear increase in SME with rising screw speed. Villmow et al., 2010 reported a non-linear increase in SME with screw speed which was attributed to shear thinning and thermal degradation of the polycaprolactone. In the case of PET, a linear trend was observed for the standard film grade IV PET (S-PET) and a non-linear trend for high IV PET (H-PET) which was attributed to the reducing molecular weight of the material due to mechanically induced chain scission; see Figure H.1.

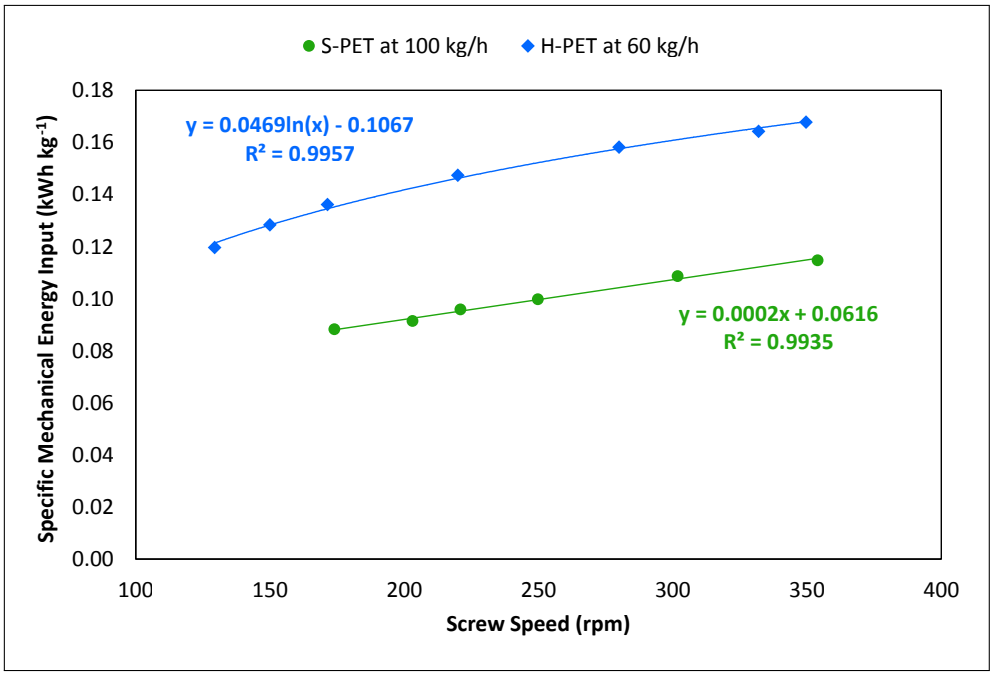

Figure H.1: *SME vs screw speed for S-PET and H-PET extruded on the Semi-Tech machine*

Any material molecular weight loss during extrusion process should also be considered. Schöppner et al., 2014 suggests that such losses should increase at lower screw speeds due the increased dwell times. However, since the material is subjected to lower shear and melt temperatures at lower speeds this is not guaranteed. Schöppner et al. found that higher screw speeds lead to greater material degradation in a PET system. This was associated with the increased melt temperatures caused by the higher shear. Schöppner et al. states that the positive effect of reduced residence time is not enough to offset the hugely negative effect of running at higher melt temperature. Such reaction driven losses would occur gradually through the extrusion process and hence gradually reducing the material viscosity and the hydrodynamic stresses transferred to agglomerates thus reducing dispersive mixing. In certain cases with PET the increase in screw speed can lead to mechanically induced chain scission of the polymer chains reducing the viscosity of the material even further; see Chapter 7. This is thought to be much more instantaneous, primarily occurring in the melting section, and thus much more detrimental to effective dispersion process.

Focusing on dispersive mixing, Kasaliwal et al., 2010; Villmow et al., 2008 found a reduction in the MWCNT agglomerate size with increasing screw speed at any mixing time, which Villmow et al., 2008 partially attributed to shortening of the carbon nanotubes leading to easier dispersion of agglomerates. Interestingly, Villmow et al., 2010 observed similar increase in dispersions with screw speed extruders set up with kneading blocks and slotted mixing elements. These should deliver quite different shear stress distributions to the material. Similarly, Domenech et al., 2011 found that an increase in screw speed led to better dispersion of layered organoclay composites; however this was only true below a certain screw speed. In later work, Domenech et al., 2013 found that beyond a certain speed a partial collapse in the interlayer spacing between sheets of clay inhibited further exfoliation. Fortunato et al., 2014 also observed a clear dependence of agglomerate size on screw speed when manufacturing PET masterbatches containing titanium dioxide.

H.2 Effect of changes in extruder output

While the screw speed directly influences the shear rate and stress, changes in extruder output can influence the average shear rate by changing the degree of fill (DOF) within the extruder. The changes in throughput also control the residence time, torque demand and hence the SME input. In a TSE, the output of the machine can be controlled almost independently of screw speed. An increase in output at the same screw speed would increase the DOF resulting in an increased torque demand. A rise in DOF also leads to the reduction of the average shear rate due to the increase in polymer flow though low shear regions found close to the centre of the channel; see Chapter 6. At the same time an increase in output would reduce the residence time leading to a reduction in the SME input. A reduction in average shear and energy input hinders effective dispersion.

During TSE operation, the output and screw speed are balanced to prevent the machine overtorquing (Giles et al., 2005), with torque values of around 90 % being targeted. If the process is not torque limited, then the feed rate has to be carefully selected to ensure that

it does not exceed the conveying capacity of the screw at a given screw speed, which would result in material accumulating in the feed pocket. In order to have the most efficient use of equipment, the manufacturer would prefer to run at the maximum machine capacity. In the case of direct addition, this may be limited by downstream equipment when targeting a certain film thickness or the upstream feeding equipment when trying to achieve a certain loading of additive within the film.

A higher machine output lowers the total shear load that the polymer experiences and leads to an overall better distribution of the shear energy (Schöppner et al., 2014). This in turn minimises any hotspots in the melt and any unwanted material molecular weight reduction. Schöppner et al., 2014 found that increasing the throughput minimises the polymer degradation at a given screw speed, and decreases the melt temperature slightly. However, the higher degree of fill reduces the surface available for devolatilisation (Schöppner et al., 2014; Todd, 1975) leading to poorer performance of the degassing zone and in the case of PET excess moisture within the melt resulting in the increased molecular weight reduction due to the hydrolysis reaction. This limits dispersion by reducing the shear stress transmitted to the agglomerates.

Focusing on dispersion, as well as a reduction in the average shear rate, the increase in output reduces the number of passes through the high shear region between the screw tip and barrel surface. This limits the opportunity for any agglomerates to pass through and reduces the chances of agglomerate dispersion by rupture mechanism. The reduced residence time also limits dispersion through erosion mechanism. Diemert et al., 2011 found that increasing the output reduces the residence time in the kneading bloc section of the extruder (typically fully filled) which reduced its distributive mixing efficiency.

Villmow et al., 2010 reported that an increase in throughput leads to a reduction in SME and hence in mixing efficiency. The author saw a significant increase in the number of agglomerates being observed with increased machine output. Interestingly, the author reported a similar decrease in mixing efficiency for screws containing mixing element

compared to those containing kneading blocks. Similarly, Domenech et al., 2011 reported that an increase in throughput lead to the reduction in the degree of dispersion achieved with the thickness of the organoclay tactoids increasing with increasing feed rate indicating that exfoliation of these is sensitive to residence time.

H.3 Effect of changes in extruder torque

Machine operating torque is a function of the screw speed, extruder output (energy required for melting and DOF), as well as material properties at the processing temperature. The torque which a machine can deliver is limited by the cross section of the shafts and their design (Martin, 2014) as well as the motor, gearing and coupling designs. Twin screw machine manufacturers have begun to deliver machines with higher torque, higher installed power and higher speed capabilities (Donoian and Christiano, 1999). These improve the flexibility of the machines by allowing them to run at higher screw speed, thus resulting in higher melt temperatures if a larger output is being targeted. For the same output, the machine is able to operate at lower screw speed minimising the melt temperature and potential unwanted reactions within the polymer. However, this is at a cost to dispersive mixing due to the reduced shear stresses being transferred to the agglomerates as result of reduction in speed and increase in degree of fill.

Although generally a manufacturer prefers to run at high torque values (ca. 90 %), a machine can be operated at lower torque values leading to a reduced degree of fill and thus potentially improved dispersion due to the higher average shear stresses transmitted to the agglomerates.

H.4 Effect of changes in degree of fill and specific output

The degree of fill within TSE is influenced by a number of factors including screw speed, extruder output, element design and screw configuration (Padmanabhan and Jayanth, 2008). In a typical TSE, the DOF is a function of length within the extruder which normally have some partially filled and some fully filled sections. Degree of fill is often quoted as an average for the whole machine; and since its calculation is somewhat complex, the more common specific output is used as a reflection of this parameter. Specific output (in $\mathrm{kg\,h^{-1}\,rpm^{-1}}$) is a measure of extruder output per revolution of screw and can be directly related to DOF via a linear relationship (see Figure 7.11). Gasner et al., 1999 stated that operating conditions at the same specific throughput have the same mean residence time and mean residence volume. Zhang et al., 2008 claims that the residence time distribution curves were different for operating conditions at given specific throughput, however when the curves were normalised by the mean residence time they overlayed each other showing that each individual specific throughput does have a unique residence time distribution (RTD).

As discussed briefly previously, and in more detail in Chapter 6, running the extruder at lower specific output and thus lower average degree of fill increases the average shear rate experienced by the material leading to higher hydrodynamic shear stresses and increased likelihood of dispersing the agglomerates. Donoian and Christiano, 1999 reported that running the extruder at lower specific output lead to better mixing, even in configurations with increased gap between the kneading block tip and barrel surface. Similarly, by operating the extruder at lower DOF the amount of shear to which the polymer is subjected to is increased resulting in the increase in the melt temperature of the material.

H.5 Effect of residence time

In a TSE process each fluid element of the polymer may undergo different temporal, thermal and mechanical history (Zhang et al., 2008). The residence time distribution provides information on the flow patterns within the machine as well as the level of axial mixing. Vergnes et al., 1992 established that TSEs behaves closer to a perfect mixer as opposed to plug flow; however TSEs are modelled as both a series of continuously stirred tank reactors (CSTRs) and plug flow reactors (PFRs). Intermeshing co-TSEs have one of the narrowest residence time distributions that can only be bettered by counter rotating intermeshing machines (Giles et al., 2005). This implies that the majority of the material flows via very similar flow paths, providing uniform exposure to shear and thus uniform dispersive mixing capabilities. Depending on configuration and operating conditions mean residence time can range from 5 s to 10 min with typical ranges being between 20 s and 2 min (Martin, 2014).

The mean residence time in co-TSE process decreases with increasing throughput and increasing screw speed. Gasner et al., 1999 reports that the mean residence time decreased non linearly as a function of output at a given screw speed. The same holds true for residence time as function of screw speed.

The throughput is key in determining the shape of the RTD curve. If the throughput is increased at a given speed, this results in a sharper RTD curve with a reduced mean residence time (Gao et al., 2000; Zhang et al., 2008). Interestingly, Diemert et al., 2011 showed that the shape of the RTD curves does not change significantly in the conveying elements when the throughput is increased, since the screws are not fully filled at this point. This highlights that any changes in the throughput will directly impact the fully filled sections associated with the higher shear inducing elements such as kneading blocks, mixing and reversing elements. On the other hand, if the throughput remains the same and the screw speed is altered the shape of the RTD curve remains similar (Gao et al., 2000; Zhang et al., 2008).

Villmow et al., 2010 reported that an increase in screw speed decreased the residence time by 25 to 40 % represented by an exponential decay function. Similarly, increases in output from 5 to 25 $\mathrm{kg\,h^{-1}}$ on a 25 mm machine decrease mean residence time by 50 to 60 %. In addition to screw speed and output, the barrel temperatures can have a potential impact by influencing the material viscosity. Gao et al., 2000 reported that an increase in barrel temperature reduced the viscosity and thus resulted in a longer mean residence time. Gautam and Choudhury, 1999 disagrees with the finding stating that the higher viscosity material would have a longer mean residence time as a result of higher pressure drops and thus higher degree of fill within the machine. In his work, Zhang et al., 2008 worked out RTD for a given element by deconvolution of the overall extruder RTD and the RTD prior the element of interest.

Figures H.2a and H.2b illustrate the change in mean residence time as a function of screw speed and output for polymers with different intrinsic viscosity values and processing temperatures respectively. The results were generated utilising the model developed in Chapter 6. Here, the plateaus at low screw speeds and high outputs are conditions when the extruder is predicted to be fully filled. It appears that the intrinsic viscosity has little impact on the mean residence time. Similarly, the changes in temperature also show little difference between conditions, but agreeing with the findings reported in Gao et al., 2000 where the higher temperature results in a slightly longer mean residence time.

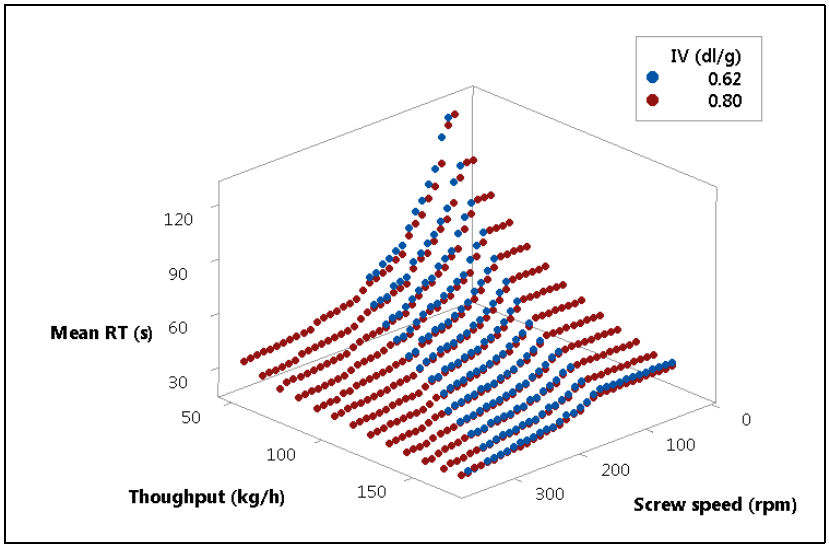

(a) Impact of IV

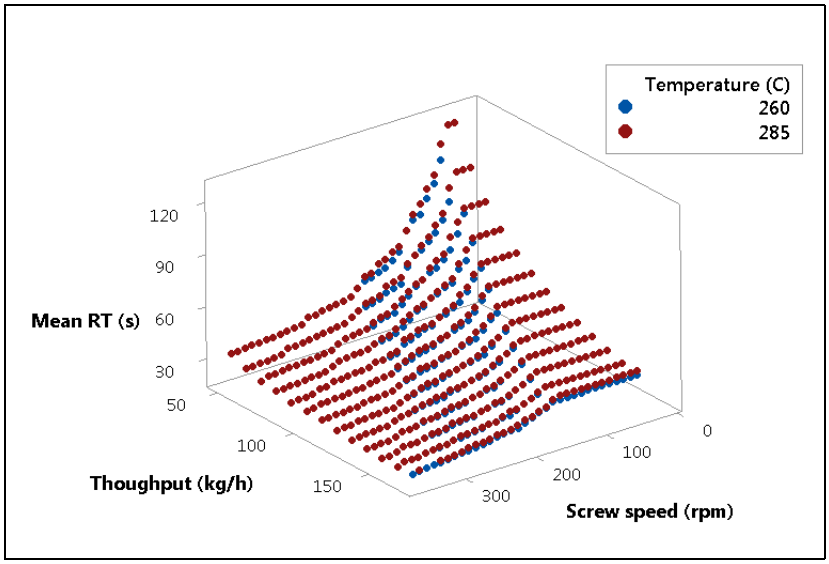

(b) Impact of temperature

Figure H.2: *Mean residence time as function of screw speed and output, as predicted by the model developed in Chapter 6*

Theoretically a longer residence time would aid dispersive mixing (assuming no material viscosity changes). A larger mean residence time would allow for more of the smaller fragments to be pealed from the parent agglomerates structure through a prolonged exposure to shear enhancing erosion mechanism. Similarly, increased dwell times in the sections fitted with kneading blocks and/or mixing elements would see the number of passes through the high shear regions increasing the probability of agglomerate rupture.

Kasaliwal et al., 2010 observed that the size and the number of agglomerates decreased with the increase in dwell time, but the effect was much more pronounced at lower screw speeds. This suggests that residence time plays a greater role in the effectiveness of the erosion mechanism. Interestingly, the author also reports an existence of a plateau where above a certain residence time no further gains can be achieved. This plateau was reached faster at higher speeds suggesting that there is a critical size of agglomerate which can not be broken down further. A potential explanation for this is the increased cohesive strength of the agglomerates with a reduction in size which makes them inherently more difficult to break down; see Section F.2.1.

Vergnes et al., 1992 modelled the residence time in reversing screw elements. His experimental results illustrated that 25 % of the tracer experienced a relatively short residence time of less than 10 % of the maximum. Although, 20 % of the tracer experienced a relatively long residence time, 60 % of the tracer material experiences a residence time less than the mean value. This has a direct effect on the specific mechanical energy delivered to the material. They found that the increase in throughput significantly reduced the mean residence time whilst narrowing the RTD distribution; thus one can say that lower outputs are best for effective back mixing. The addition of a second reversing element was found to significantly broaden the residence time distribution as well as increasing the mean value, increasing the amount of energy delivered to the material. Assuming no polymer degradation such a change would facilitate better mixing.

H.6 Effect of specific mechanical energy input

Specific mechanical energy (SME) depends on the screw speed, output, degree of fill (governs torque) within the extruder as well as the melt temperature. Changes to SME as a function of screw speed and throughput were discussed previously. These can be related to SME by Equation H.2; as described by Domenech et al., 2013:

$$SME = \frac{P_w}{\dot{m}} \times \frac{N}{N_{max}} \times \frac{F}{100} \tag{H.2}$$

Here, SME is in $\mathrm{kW\,h\,kg^{-1}}$, P_w is the motor power in kW, $\dot{m}$ is the throughput in $\mathrm{kg\,h^{-1}}$, N and N_{max} are the operating and maximum screw speed in rpm and F is machine torque in %. Martin, 2013 includes an additional multiplier of 0.97 in the equation to account for energy losses through the gearbox.

Vergnes et al., 1992 related the residence time distribution to the distribution of energy which the product receives. The author showed that 65 % of the product received a total amount of energy less than the average value with only 5 % of the product receiving the high energy input. From Equation H.2 it is evident that the parameter is dependant on feedrate and decreases with increasing output. Although the mean SME is reduced, the narrowing residence time distribution at higher feedrate should theoretically lead to a narrower SME distribution and thus more uniform mixing.

Gotsis and Kalyon, 1989 employed SME as a measure of combined dispersive and distributive mixing. Since then a number of recent studies tried to relate the SME input to the degree of dispersion achieved. Kasaliwal et al., 2010 found that the degree of mixing (as measured by area fractions) could be correlated to the total energy delivered to the polymer. An exponential decay curve (similar to Figure H.3) for reducing area fraction (indicating increased mixing) vs increasing SME for all the different screw speeds tested was observed. Further work was carried out by Kasaliwal, 2011 showing this curve holding true when measuring volume resistivity of the polymer composites manufactured.

Similarly, Villmow et al., 2010 reported that an increase in throughput leads to a reduction in SME and hence mixing efficiency as measured by an increase in the number of agglomerates. The author also reported that the increase in mixing can be described by a power law relationship where as energy input increased initially the mixing increases rapidly and then less so as SME is increased further. Interestingly, a similar decay profile

was observed for configurations with mixing and kneading block elements. A similar trend was observed for an increase in screw speed by Kasaliwal et al., 2010. Domenech et al., 2011 went a step further and showed that mixing as a function of SME could be plotted on a single master curve, regardless of whether the screw speed or the output were being changed; see Figure H.3.

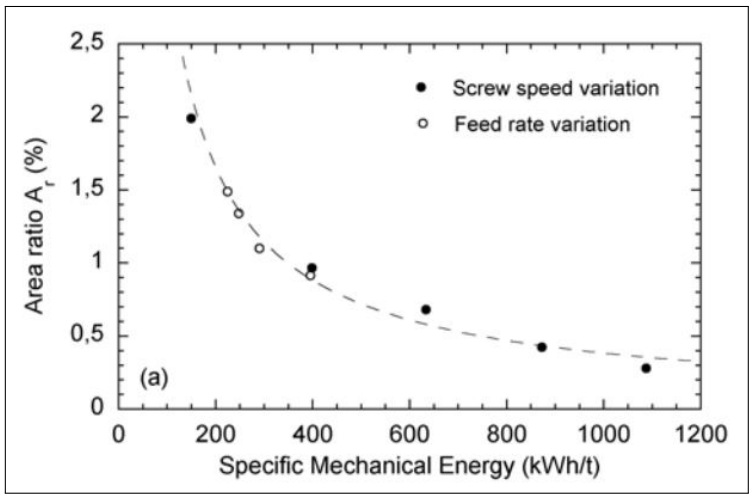

Figure H.3: *Area fraction vs specific mechanical energy input; from Domenech et al. (2011, p.9)*

Domenech et al., 2013 considered the level of dispersion as a function of SME delivered to the melt only, SME_{melt}, ignoring the energy required for transporting and melting the solids. The model indicated that the majority of the SME_{melt} was dissipated in the kneading block sections as opposed to the conveying section. The author found that even though increasing the screw speed reduces the torque demand, the linear increase in SME_{melt} still exists. Although an increase in output leads to an increase in torque there is a reduction in SME_{melt} as a result of shorter residence time. The parameter was found to reduce linearly with barrel temperature increase which was attributed to the change in polymer viscosity. They found that the area fraction of agglomerates, representing the level of mixing, decreased with increase in SME_{melt}. However when considering the melt yield strength, they found that beyond a certain value of SME_{melt} there was no increase in strength indicating that the exfoliation of the clay did not increase beyond this point.

H.7 Effect of barrel temperature

The barrel temperatures are an important parameter within the extruder as they directly influence the melt viscosity as well as the feeding characteristics. As a rule of thumb, DTF, consider melt temperature to change by 20 % of the change in barrel temperature. The effect of barrel temperatures on the melt temperature can be measured at the extruder exit with an immersed melt thermocouple or at the die exit utilising a pyrometer. Melt thermocouples often yeild elevated readings due to shearing at the tip, but can provide an accurate indication of the trends (Steward, 2000).

Villmow et al., 2008 reported that a temperature profile with cooler temperatures in the mixing zones (post melting) and warmer temperatures in the conveying zones at the end of the extruder produced marginally better mixing than a profile with warmer mixing zones and a cooler metering section. This is in agreement with Kasaliwal, 2011 who reported an increase in mixing with a reduction of melt temperature; although the effect was only seen at low screw speeds. Similarly, Domenech et al., 2013 observed SME_{melt} linearly decrease with increasing barrel temperature which would suggest conditions that lead to poorer mixing. Fortunato et al., 2014 found no impact of melt temperature on the mixing of titanium dioxide in PET composites even though the SME varied by ca. 200 $\mathrm{kJ\,kg^{-1}}$.

Aside from mixing, (Schöppner et al., 2014) reported that running with lower barrel temperatures in a PET extrusion process lead to a reduction in molecular weight loss with a linear relationship for the intrinsic viscosity and barrel temperatures being observed. One would argue that the IV loss is a direct result of the moisture content of the polymer, the degree of fill in the degassing section and the screw speed (shear) to which the polymer is subjected; see Chapter 7.

H.8 Effect of additive loading and injection point

Typical configurations of a TSE compounding processes are discussed in Giles et al., 2005 and see p. 57-89 in Kohlgrüber, 2008. In bi-axially oriented film manufacture the additive is introduced in a form of compounded masterbatch containing the pre-dispersed additive that has been uniformly distributed in the polymer at 5 to 10 times the final loading. As alternative to masterbatches, there are several options for the introduction of additives. These include:

1. *Premix* - dry blended additive and polymer fed into the main feed throat of the extruder;
2. *Split feed* - additive and polymer fed via separate streams into the main feed pocket;
3. *Direct to melt* - additive injected directly into the polymer melt (in one or several locations);
4. *Direct to melt premixed* - additive dry blended with polymer (chip or powder) and then directly injected into the polymer melt (in one or several locations).

Depending on the additive physical characteristics each of these methods has its advantages and disadvantages. Although both additive loading and the injection point in their own right will have an influence on degree of mixing, the loading of the additive is especially key in the direct to melt addition processes. Here, combined with the degree of fill in the injection zone, it directly governs the wetting of the additive; which in itself is a precursor to dispersion.

Considering the masterbatch route initially, Villmow et al., 2008 reported that when manufacturing MWCNTs in PLA composites the 15 $\%_{wt}$ masterbatch contained mean agglomerates size 2.3 times higher than the masterbatch with a loading of 7.5 $\%_{wt}$. Domenech et al., 2013 investigated the dispersion of layered silicate in a masterbatch itself and reported the presence of agglomerates of up to 170 µm in size, almost 4 times the maximum characteristic size of the additive. They state that the majority of the macro scale dispersion occurs in the melting zone as this is where the viscosity of the polymer is the highest and the highest shear stresses are delivered. In agreement, Lafleur et al., 2000 found that

injection of the material into the feed pocket of the extruder achieved better dispersion of the additive due to the increased specific energy input that is experienced by the additive compared to direct to melt addition.

Although this is a major advantage for a masterbatch process, it can be a severe disadvantage for *split feed* process where the high compaction stresses generated by the kneading elements (often found in the melting zone) will lead to compaction of any un-wetted additive (termed cold agglomeration). This in turn makes the newly formed compacted agglomerates much harder to disperse further down the extruder. Padmanabhan and Jayanth, 2008 discussed this type of re-agglomeration in carbon black and titanium dioxide systems. In the case of titanium dioxide, the author reported agglomerates of around 10 µm being present in poorly dispersed system compared to well dispersed system which contained titanium dioxide around its base crystal size of 200 nm.

Cold agglomeration is somewhat mitigated by the *premix* process where the dry blending ensures that the additive particles are in the vicinity of the polymer when they are fed into the extruder. Softening the polymer prior to dry blending (Giles et al., 2005) helps ensure that segregation does not occur before the melt section; but even with this method care has to be taken so that the polymer does not sinter. Kohlgrüber, 2008 reports that up to 10 $\%_{\mathrm{wt}}$ can be incorporated directly into the feed pocket of the extruder. This method of addition is particularly difficult with low bulk density powders which can be entrained in the escaping air from the feed pocket. The powder can be introduced in the form of a compressed pellet mitigating the issue; however this increases material costs (Kohlgrüber, 2008) as well as the risk of cold agglomeration. In addition, having a dry blending operation on a continuous process running at several tonnes per hour is extremely difficult without significant investment into specialised dry blending equipment.

Highly abrasive materials are often added directly to the melt in order to minimize the wear of the machine. Similarly, long aspect ratio particles are incorporated into the polymer through direct to melt addition in order to avoid the attrition of the filler (Giles

et al., 2005). In such cases, for a single point of addition up to 40 $\%_{wt}$ of filler can be incorporated with *premixed direct to melt* process being preferred over *direct to melt* process (Kohlgrüber, 2008). At high loadings caution has to be taken to ensure that the temperature of the polymer does not drop below the its melting temperature once the cold additive is introduced. Hensen, 1988 discussed the difficulty in designing a *'one for all'* system to handle a variety of additive properties, especially at loadings of 20 - 80 $\%_{wt}$.

Focusing on mixing, Schöppner et al., 2014 showed that the IV of PET increases post vacuum degassing port during its extrusion theoretically raising its viscosity and helping dispersive mixing. Although, this effect is likely to be very limited if at all visible due to the short residence times in the extruder. To the contrary to what one might expect, Kwang-Jea and White, 2000 found that the agglomerates were larger in size when the additive loading was 10 $\%_{vol}$ compared to 20 $\%_{vol}$. This was attributed to the increased effectiveness of dispersion via the collision mechanism; although it could also be associated with the changes in the melt rheology where an increase in the overall viscosity would deliver larger shear stresses. One would expect the dispersion performance to decrease with loading due to the increased chances of re-agglomeration and the much higher demands placed on the wetting process; this was observed by Lafleur et al., 2000.

H.9 Concluding Remarks

Twin screw extrusion is a complex process with a change in a single controllable parameters affecting several dependant (calculated) parameters simultaneously; this makes it difficult to evaluate the role of the individual parameters. Nevertheless, attempts to quantify the role of the controllable parameters have been made; although the vast majority of these deal with non PET systems.

Focusing on controllable parameters initially, Fortunato et al., 2014; Kasaliwal et al., 2010; Villmow et al., 2008 all considered the role of screw speed and found that the

level of mixing increases with increase in speed. Interestingly, Domenech et al., 2011 reported that the effect is only true below a certain screw speed. Such limitation would be expected in PET systems, where the increase in shear rate is likely to induce mechanical degradation (see Chapter 7) which coupled with localised temperature variations will reduce the viscosity of the material and inhibit the dispersion via rupture mechanism. Donoian and Christiano, 1999 found that using larger clearances significantly reduced the viscous heating of the melt. Diemert et al., 2011 considered the impact of throughput reporting that higher output lead to reduced residence time in the fully filled kneading block sections and thus resulted in poorer dispersion. Within a PET matrix, the higher throughput will equate to smaller energy input per unit polymer and thus may minimise degradation of the material potentially resulting in better mixing.

Impact of calculated parameters has also been considered. Donoian and Christiano, 1999 reported that lower degree of fill (specific output) led to better dispersion. Kasaliwal et al., 2010 the role of residence time, reporting that increased residence time (up to a limiting value) leads to better mixing. Most interestingly, both Kasaliwal et al., 2011 and Domenech et al., 2011 reported the existence of an exponential decay type curve for the level of mixing as function of the specific mechanical energy input. Here, the increased SME leads to much improved mixing initially with the gains diminishing as the SME is increased further. As the changes in the SME are largely driven by changes screw speed, it is envisaged that the same type of behaviour is likely within the PET based system; however these would be due to the sensitivities to high shear.

I Supporting data for Chapter 9

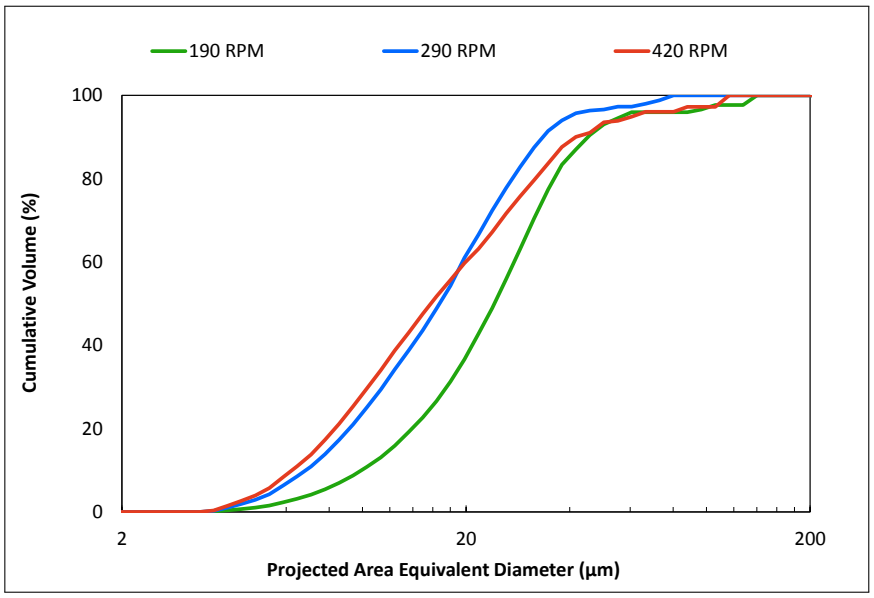

Figure I.1: *Effect of screw speed on mixing in FR-3/H-PET composites containing additive at 5 $\%_{wt}$ manufactured on the Dr Collin ZK25 machine at 6 $\mathrm{kg\,h^{-1}}$ using premix method*

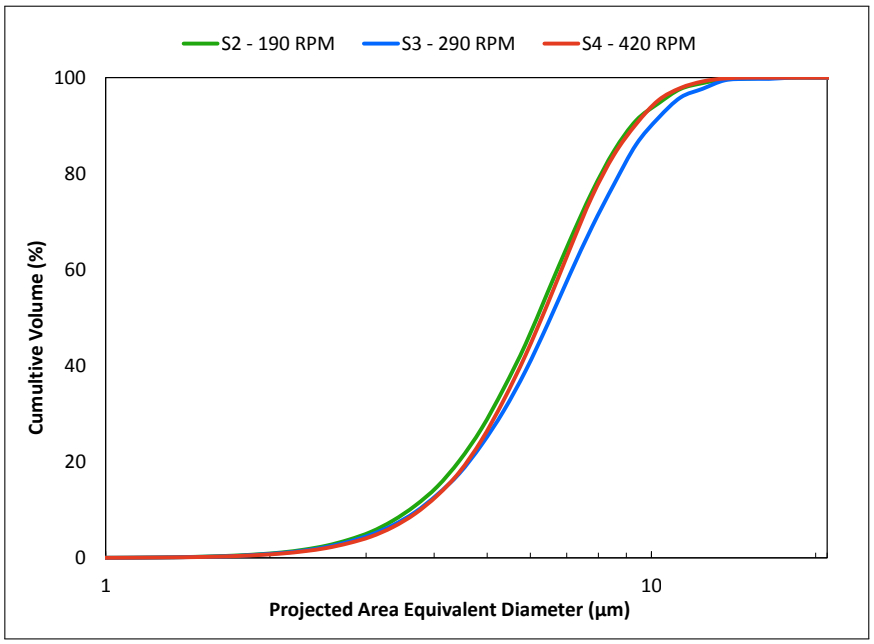

Figure I.2: *Effect of screw speed on mixing in S-PET composites containing S-3 additive at 5 $\%_{wt}$ manufactured on the Dr Collin ZK25 machine at 4.75 $\mathrm{kg\,h^{-1}}$ using direct to melt addition method*

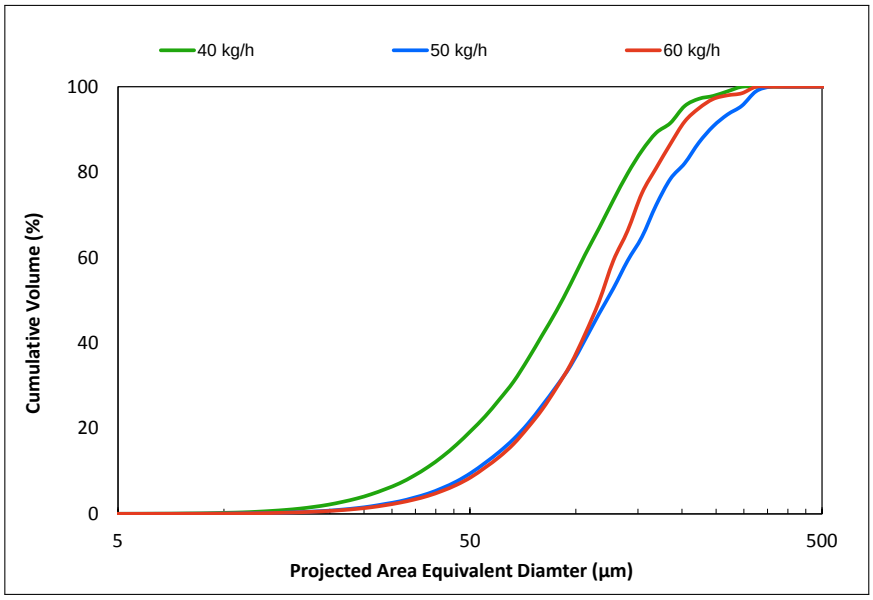

Figure I.3: *Effect of extruder output on mixing in H-PET composites containing FR-1 additive at 5* $\%_{wt}$ *manufactured on the Berstorff ZE40A machine at 122* rpm *using split feed addition method*

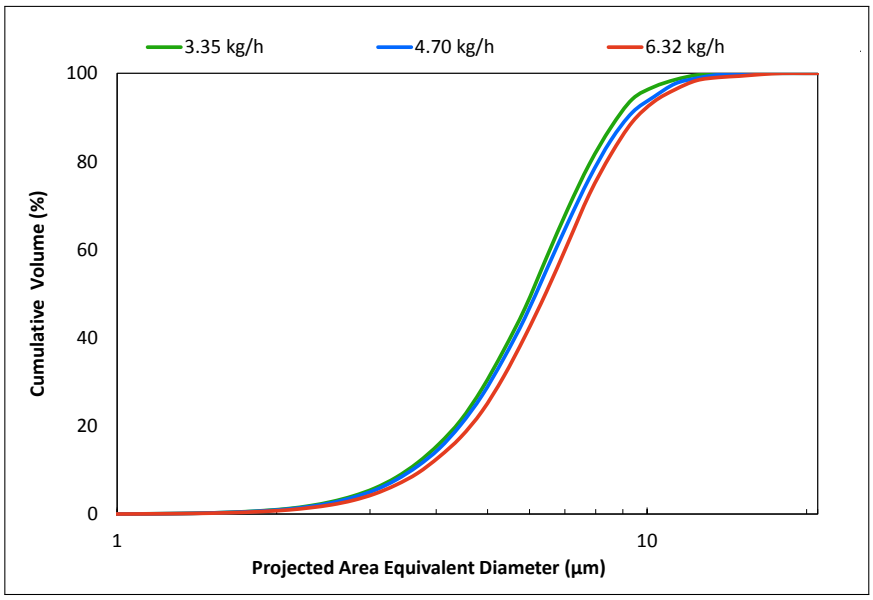

Figure I.4: *Effect of extruder output on mixing in S-PET composites containing S-3 additive at 5* $\%_{wt}$ *manufactured on the Dr Collin ZK25 machine at 190* rpm *using direct to melt addition method*

J | Modifying screw design for improved dispersive mixing capacity

In order for extensive (distributive) and intensive (dispersive) mixing operations to be effective different requirements have to be met. The details of the mixing mechanisms was discussed in Section 2.4. The main focus of this work is on achieving good intensive mixing whilst maintaining effective distributive mixing that the current masterbatch process possesses. Efficient dispersive mixing requires the fluid to pass through a high shear region where the agglomerates contained within it would be exposed to high shear stresses (preferentially elongational in nature). Ideally, such exposure would be very short and repeated a number of times. This would enable effective rupture of the agglomerates but ensure that the negative effects on the polymer matrix such as mechanically induced chain rupture and temperature rise are minimized. It is important to note that there is a minimum time which has to be satisfied for exposure to high shear stress to be effective in achieving dispersion. Rauwendaal, 1986 discusses work on carbon black dispersion where exposure for less than 0.2 s lead to no dispersion irrespective of the magnitude for the shear.

J.1 Importance of screw design in achieving dispersion

The modular design of TSEs enables the extruder to be configured in accordance with the mixing requirements of the product (Kalyon et al., 1991). An optimized screw configuration is vital in ensuring the correct nature of flows within the machine. The purpose of the individual zones found in a co-TSE was discussed in Section A.1 together with the nature of the flow fields in the different types of elements. This subsection deals with the ability of each element type to deliver the desired dispersive mixing.

Although much of the work on the effect of different screw configurations on dispersive

mixing goes unpublished and remains the proprietary knowledge of institutions preforming the research, a small number of studies have been published. These include that of Villmow et al., 2008 who examined the dispersive mixing of multiwalled carbon nanotubes (MWCNTs) in polylactic acid on a Berstorff ZE25 fitted with a typical kneading block (KB) configuration and toothed mixing elements (TME) set up. The author reported better mixing with the TME configuration and later conducted a more detailed study examining the use of reversing elements and the impact of increased extruder length (see Villmow et al., 2010). Emin and Schuchmann, 2013 examined the effectiveness of kneading block section in dispersing droplets of a secondary phase in the polymer matrix though computational fluid dynamics (CFD) simulations. Results based on CFD are likely to dominate the literature in the future as they do not require expensive equipment and trial time on the lines. Although Young et al., 2013 does not report experimental data, the author provides suggestions on the configurations required by a mineral and glass fibre compounding processes.

Some earlier research on the distributive mixing within co-TSEs should not be ignored when attempting to derive an optimum screw configuration. Studies such as that of Kalyon and Sangani, 1989b examining the growth of interfacial area though the nip regions of the different kneading blocks and Kalyon et al., 1991 looking at the degree of fill within the different kneading block designs provide an important insight into the nature of flow fields within the different types of elements. Works of Carneiro et al., 1999; Diemert et al., 2011; Lee et al., 2012; Yerramilli and Karwe, 2004 examine the flow patterns within various elements through differing techniques. These have been discussed in Section A.2.

J.1.1 Effect of the overall geometry

In setting the screw geometry, through specifying both of the diameters, the D_o/D_i ratio is set and as a result the free volume of the machine and maximum torque transmission through the shafts is also determined. The free volume itself determines the cross sectional

area available for flow which in turn sets the minimum and the average shear rates at a given output and screw speed that the polymer and agglomerates experiences and hence determines the corresponding shear stresses. The maximum shear rate and the corresponding stress is largely determined by the clearance between the screw flight tip and the barrel surface. A machine with a larger ratio has an increased free volume and reduced torque capacity. Thummert, 2013 reported that a higher D_o/D_i delivers a lower shear rate in the axial direction and inputs less specific energy into the polymer leading to poorer mixing being observed.

At a given output and screw speed the screw configuration and element design (e.g. stagger angle/pitch) determine the local parameters such as pressure drop (Domenech et al., 2013; Gautam and Choudhury, 1999). This in turn determines the degree of fill within each element and hence the residence time, average shear rate and to a degree melt temperature. As the polymer flows though each screw element each of the fluid elements travel via a different path leading to a residence time and specific energy distribution (Vergnes et al., 1992). Hence, the type and length of each element as well as its location are key in determining these distributions.

A higher residence time in the high shear zones will normally lead to a better dispersion of the additive (Lafleur et al., 2000). However, this can also lead to some re-agglomeration and more importantly in the case of PET a higher polymer chain scission lowering the matrix viscosity and the stresses experienced by the agglomerates. Screw profiles with longer mean residence time and broader distributions are deemed more severe. Gao et al., 2000 reported that the use of kneading blocks and reverse conveying elements increased the mean residence time distribution. The location of these elements is critical. As these elements are moved further away from the exit of the extruder the mean residence time increases (Gautam and Choudhury, 1999). The author also reports the increase in mean residence time with enlarged spacing between such elements.

Villmow et al., 2010 examined the impact of residence time by considering the changes to

agglomerate size along the length of the screw. The authors report a fast rate of dispersion initially which decreased towards the end of the screw; a likely result to changes in polymer matrix viscosity. It was found that via the split feed method of addition the size of the largest agglomerates detected in the product was similar to that just after the melt section indication that the majority of agglomerate rapture occurs in this zone as the highest shear stresses are found here due to the high polymer viscosity.

J.1.2 Mixing in conveying elements

The main role of the fully flighted conveying elements is to transport the materials forward whilst pressurising them where required. Some mixing does occur in this type of elements. The majority of distributive mixing takes place through the growth of interfacial area when the material is transferred from one screw onto the next in the nip region, although some area growth does occur in the channel as well. Dispersive mixing mainly happens in the high shear region over and close to the flight clearance as well as the nip section.

The helix angle and the pitch determine the flight width, which then sets the duration of exposure for the material to the high shear. The shear rate and hence stress is determined by the flight clearance. Combined, the flight width and the clearance determine the pressure drop over the flight which then governs the amount of leakage flow and the proportion of material which is exposed to the high shear conditions. All of these factors influence the dispersive ability of the elements.

These type of elements provide very little axial mixing along the length of the extruder, particularly when the helix angle is low (Todd, 1975). Another parameter describing this type of element is the pitch. As it decreases the mean residence time increases since the material must complete more revolutions prior to exiting the extruder (Giles et al., 2005). Average residence time in the conveying elements is about one half of that in the neutral kneading block (Diemert et al., 2011).

J.1.3 Mixing in reverse conveying elements

Reverse conveying elements are similar in design to forward conveying elements. They are characterised by the opposing direction of the flight to the rest of the elements in the configuration which pushes the material backwards towards the feed pocket of the extruder. The high pressure drop associated with material flow through these elements means that they operate completely full (Vergnes et al., 1992). The high pressure drop also causes an increase in degree of fill within the elements located prior to the reversing element increasing the residence time in those elements. This is their main function with regards to mixing; as well as generating melt seals e.g. prior to degassing sections. As the reverse conveying elements are more restrictive to flow than the equivalent reversing kneading blocks, a greater amount of specific mechanical energy can be introduced into the polymer (Gautam and Choudhury, 1999). These elements can have slots cut into the flights in order to facilitate flow towards the die (Vergnes et al., 1992).

With the use of reversing elements located after elements which are forward conveying in nature the residence time distribution can be changed significantly. Diemert et al., 2011 found through positron emission particle tracking that although the number of long passage times decreased caused by the increased flow though the flight clearances the average residence time increased drastically. The broad residence time distribution with an increased mean residence time was observed in cases when the reversing element was placed in front of a conveying element and a kneading block. Gautam and Choudhury, 1999 from their experimental work on rice flour report that the use of reversing elements increased the mean residence time by 63.5 to 100 % depending on location from the die when compared to a forward screw configuration with just conveying elements. They also found that increasing the length of the conveying element broadened the residence time distribution as well as reduced the frequency of the modal time (height of distribution).

It is the changes in the residence time in the mixing elements located prior to the reverse conveying element that are expected to lead to better mixing in these mixing elements.

Emin and Schuchmann, 2013 from their modelling work stated the that use of reversing elements increases the mixing in the elements prior to the reversing element due to more material passing through the high shear regions. Villmow et al., 2010 on the other hand reported that in the case of dispersion, the use of backward conveying elements post kneading blocks (KBs) lead to the broadening of the particle size distribution with larger fragments being detected. This was observed at both low and high screw speeds. A potential explanation lies in the increased pressures leading to re agglomeration of the additive within the fully filled kneading blocks.

J.1.4 Kneading blocks

Typically, kneading blocks consisting of 5 individual discs are utilised for dispersive and distributive mixing operations. They can deliver high stresses required for intensive mixing as well as introduce complex flow fields required for distributive mixing. Complex velocity distributions are observed near the kneading block tip, especially at the nip region where the two discs are moving in opposite directions. Such complex flows mean that two adjacent points can have very different paths (Lawal et al., 1993).

Oberlehner et al., 1994 demonstrated that the residence time distribution in the conveying elements was the narrowest with the shortest mean residence time. The addition of kneading blocks broadens the distribution whilst reducing the height of the peak. This theoretically leads to better mixing as the material can spend more time in the high shear regions. Gautam and Choudhury, 1999 showed that the addition of kneading blocks does leads to increased mixing.

The individual kneading discs are characterised by their width. These are mild flow restricting devices that have no conveying effect. Typically, the discs are grouped into a kneading block where the stagger angle and direction determine the conveying capacity of the block. It is these parameters coupled with the clearance between the tip of the disc and the barrel that determine their mixing ability.

J.1.4.1 Impact of stagger angle

Typical stagger angle configuration for the kneading blocks include 30 °, 45 ° and 60 ° forward conveying, 90 ° neutral conveying as well as 60 °, 45 ° and 30 ° reverse conveying. As the angle of stagger is increased from 30 ° forward conveying to 90 ° neutral element there is a reduction in material exchange between the two screws leading to a reduction in the positive axial transport (Diemert et al., 2011). This means that more revolutions of the screw are required to convey the material forwards. Similarly, as the angle degreases from 60 ° to 30 ° in the reverse kneading discs they generate more back pressure hence increasing the residence time. Such transitions improve the mixing performance due to the increased number of leakage flows as well as the increased residence time within the element (Kohlgrüber, 2008).

Kalyon and Sangani, 1989b reported from dead stop experiments that in the 30 ° forward and reverse configurations large proportion of the tracer material was found in the centre channel indicating that the materials were being pumped as opposed to mixed. This type of flow segregation was not observed in the 60 ° and 90 ° configurations. Carneiro et al., 1999 reported observation of flow subdivision in 90 ° as well as 60 ° forward and backward conveying elements, thus supporting Kalyon and Sangani. This is in agreement with Zhang et al., 2008 who found that the axial mixing quality as characterised by the width of residence time distribution, increased with increasing angle of stagger from 30 ° to 90 °; this is in agreement with Diemert et al., 2011; Lee et al., 2012.

The mean residence time in the element is a direct function of the degree fo fill within that element. This in itself is the function of the pressure drops and the conveying capacity of the elements. Kalyon et al., 1991 found that the degree of fill for 30 ° forward conveying kneading block was around 25 %, which increased to 55 % for the 60 ° and 100 % for 90 ° and the reverse configurations. In addition to this Carneiro et al., 1999 reported that 90 ° kneading blocks did not influence degree of fill in the elements upstream, however reversing variants combined with reverse conveying elements resulted in several turns of

screw prior to those elements being filled.

Kalyon et al., 1991 reported mean element residence time for the 30 ° forward configuration to be ca. 60 % of the 60 ° forward block and ca. 33 % of that in the 90 ° block. The mean residence time in the 90 ° degree block is very similar to that of the mean residence time in the reversing configurations as all of these operate fully filled. Gautam and Choudhury, 1999 reported that the mean residence time of the material in the extruder was 44 to 58 % larger for a configuration contained kneading blocks than that containing conveying elements depending on the location of the kneading element. Villmow et al., 2010 reported that the screws configurations containing backward conveying kneading blocks had a significantly larger residence time compared to those containing 90 ° kneading blocks. This was particularly evident at high screw speed of 500 rpm where the difference was 30 % as compared to 10 % at 100 rpm.

With regards to distributive mixing, the quality largely depends on the extent of melt reorientation and interfacial area growth, which depends on the angle of stagger. The kneading blocks become increasingly better mixers as the angle of stagger is increased from 30 ° forward to reverse configurations. This was observed by Kalyon and Sangani, 1989b who examined the growth of interfacial area directly. Similarly, the increase in residence time with increased angle of stagger should mean that a greater proportion of the material can be exposed to higher stresses and as a result this should make kneading blocks more effective as dispersive mixers. However, this is based on the assumption that the polymer matrix viscosity does not change. By exposing the polymer to high shear forces for prolonged period of time the risk of viscosity reduction through viscous heating or more importantly mechanical chain scission is greatly increased. Thus it may be that the smaller stagger angle would prove more effective in dispersing the agglomerates.

J.1.4.2 Impact of disc width

The land length of the kneading block can be increased to improve the dispersive mixing performance (Todd and Baumann, 1978) with the wider kneading discs generating extensive back flow compared to the narrower discs. Yerramilli and Karwe, 2004 examined the shear rates achieved at 90 rpm in a 31 mm extruder with a channel depth of 4.7 mm using laser Doppler anemometry. They found that the wider discs provided broader range of shear rates ranging from 7 to 74 s^{-1} where as the narrower discs generally offered a tighter range which was also smaller in magnitude ranging from 16 to 40 s^{-1}. This is in agreement with the work of Fukuda et al., 2013 who evaluated the stress distribution within the different kneading elements by monitoring the rupture of polymer spheres (provided by CAMES) that were rated at 92, 119 and 158 kPa. The author found that at every operating condition more beads were broken with the use of wider kneading discs. In addition, the author reports that as the critical strength of the bead was increased the number of beads broken decreased, showing that the quantity of material experiencing higher magnitude of stress reduces. Schöppner et al., 2014 also stated that wider discs have a higher magnitude of shear stress making them better for dispersive mixing and melting applications. The narrow kneading discs introduce a lower magnitude shear stress they have increased downstream conveying action and are able to generate higher strains due to increased leakage flows which aid distributive mixing (Fukuda et al., 2013; Kohlgrüber, 2008). This type of mixing is key in delivering a uniform product.

Schöppner et al., 2014 reported that the wider kneading discs did not seem to increase the molecular weight loss in extrusion of film grade PET; perhaps not surprising as the viscosity of such material is relatively low. From the work in Chapter 7 one would expect that the wide discs would lead to greater mechanical scission of the polymer chains due to the exposure to higher shear leading to a loss in viscosity. This would then translate into a loss in the magnitude of the shear stress transmitted to the agglomerates thus reducing dispersive mixing ability of the system. However, such losses may be mitigated

by the increase in the melt temperature in the clearances leading to lower viscosity of the material. Eitzlmayr et al., 2014 discussed how the melt temperature increases for the material in the clearances can be around 20 °C higher than the bulk depending on the material viscosity and screw speed. In the high screw speed experiments discussed in Chapter 7, the barrel cooling was not able to maintain the temperatures at the set point thus indicating significant viscous heating. As the temperature increase is not instantaneous, significant mechanically induced scission could still be observed.

Perhaps, Young et al., 2013 summarised the selection process for the elements the best in saying that the optimum combination of kneading blocks depends on the polymer - filler system in question. Typically narrow kneading blocks are utilised to first distribute the filler in the melt with the wider discs being used to disperse the agglomerates. When processing long aspect ratio fillers e.g. glass fibres the element selection is narrower to avoid attrition of the fibres.

J.1.4.3 Impact of clearance gap and tip design

In addition to the parameters discussed above, Donoian and Christiano, 1999 investigated the impact of the kneading block tip to barrel clearance (0.5 and 2 mm) on the level of mixing and melt temperature at different screw speeds and outputs using ethylene vinyl alcohol copolymer (EVOH), high density polyethylene (HDPE) and polypropylene (PP) matrix. They found that as the clearance increased the melt temperature and the specific mechanical energy input reduced in all cases independent of throughput or screw speed. The most noticeable change was in the case of the higher viscosity of HDPE matrix with changes from 5 to 15 °C being measured. This is a significant reduction considering that the majority of the motor power is used up in the melting process. The HDPE produced on screws with larger tip clearance had better material properties as a result of minimized cross-linking.

There are two competing effects when considering the impact of tip clearance on dispersive

mixing. From one perspective the larger clearance reduces the shear rate in that zone leading to potentially lower stresses. In the case of PET this may be offset by a reduction in the melt temperature and mechanical chain scission which in turn would result in higher material viscosity in this region. The increased clearance also allows more material to flow though the region and has an effect of broadening the residence time distribution. Donoian and Christiano, 1999 evaluated the impact on mixing in EVOH/PP, EVOH/HDPE and carbon black/HDPE systems. The increase in clearance was found to result in slight deterioration in mixing for all systems. In the carbon black system, high screw speed, low specific output and tight tip clearance generated the best mixing results. In practice, at a given screw speed, if the material viscosity of polymer in the flight clearance region was known the size of the gap could be designed to generate hydrodynamic stresses that will over come the critical stresses for a given additive. Although, this would lead to an optimised system in the case of one additive (and those with lower critical stresses) this type of product specific design is unlikely to be beneficial on an extrusion line which deals with a variety of additive-polymer systems.

J.1.5 Mixing in other types of elements

The most common other types of elements include the toothed mixing element which rapidly split and rearrange flow elements as well as the slotted mixing element which provide a degree of back flow. Both of these are typically utilised to provide distributive mixing capability. Zhang et al., 2008 reported that a wider residence time distribution was achieved with a toothed mixing element compared to a number of different kneading block set ups indicating much better axial mixing. Thummert, 2013 considered various extruder screw profiles and the impact on the specific mechanical energy input. He found that these types of mixing elements were not as good as kneading blocks but they enabled significant increase in mixing ability with minimal increase in the energy delivered into the polymer. Interestingly Villmow et al., 2010 reported that the screw configurations containing toothed mixing elements lead to better dispersion in the case of multi walled

carbon nanotubes. This was explained by the improved mixing efficiency of the element. Young et al., 2013 recommends the use of toothed mixing elements in fibre compounding as the attrition of the fibres is minimised producing longer length than that achieved with wide or even narrow kneading blocks.

Other types of element designs with improved dispersive mixing ability have been proposed. Emin and Schuchmann, 2013 discuss how the complex geometric nature of twin screw extruders poses challenges particularly with inhomogeneous stress distribution. This is something that has been examined by Padmanabhan and Jayanth, 2008. The authors commented on the difference in magnitude of the axial shear rate which can reach the value of up to 250 s^{-1} and the radial shear rate which can be 10 to 20 times of this in magnitude. As not all of the melt will experience the maximum radial shear rate, he proposed a novel element design which provides a much more uniform exposure to shear; see Figure J.1.

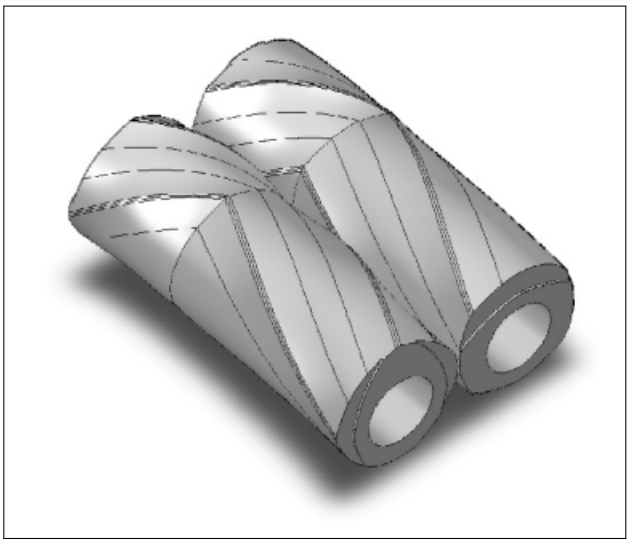

Figure J.1: *Fractional lobed mixing elements; see Fig. 7 in Padmanabhan and Jayanth, 2008*

Uphus et al., 2000 examined the level of dispersion of carbon black in rubber. The authors reported that much better level of dispersion , particularly at low screw speeds, was achieved using a Farrel Asymmetric Modular Mixing Element (FAMME) in comparison to a kneading block configuration. FAMME offer a larger clearance between the tip and

the barrel and thus generate lower shear rates in that clearance. However, the smaller pressure drop in the clearance allows more material to flow though it and the lower shear rate is offset by the very high viscosity of the rubber. It is important to note that these elements are not self cleaning.

Nakayama et al., 2011 considered modifications to the kneading block design. The authors examined the impact of kneading block tip design though CFD modelling and proposed the use of a 'pitch tip' on the kneading block; see Figure J.2. This yields four possible configurations: backward stagger angle and forward tip (Bs-Ft), forward stager angle and forward tip (Fs-Ft), backward stagger angle and backward tip (Bs-Bt) as well as forward stagger angle and backward tip (Fs-Bt).

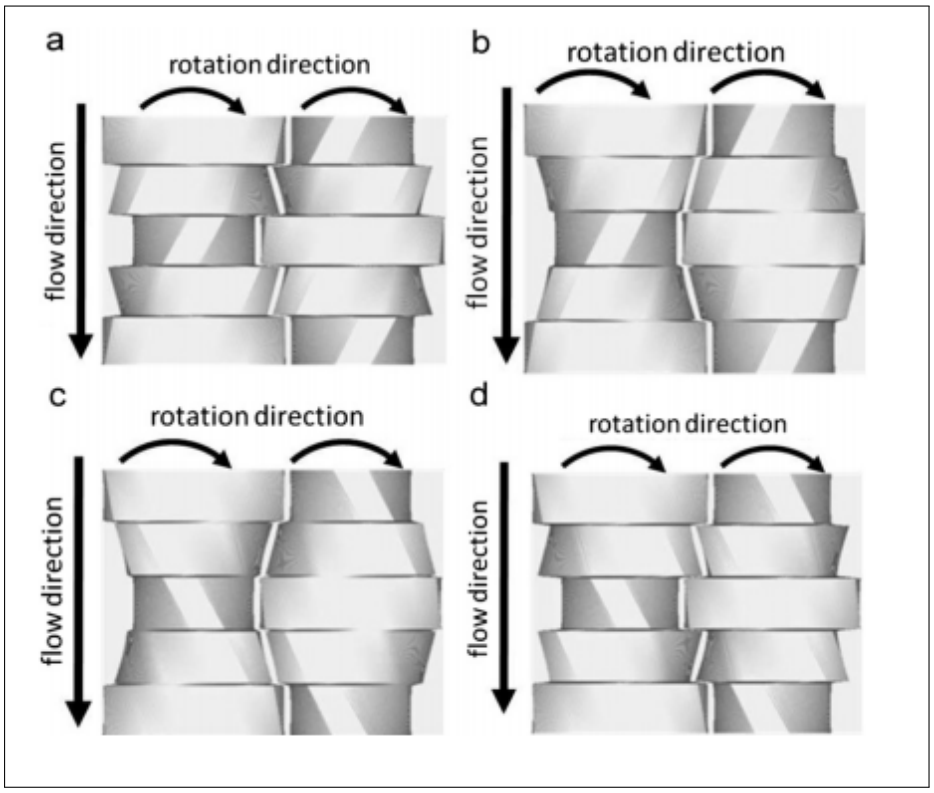

Figure J.2: *Pitched tip kneading discs: a - backward stagger angle and forward tip (Bs-Ft) b - forward stager angle and forward tip (Fs-Ft) c - backward stagger angle and backward tip (Bs-Bt) d - forward stagger angle and backward tip (Fs-Bt); see Fig. 1, p. 104 in Nakayama et al., 2011*

Nakayama et al., 2011 found that when the tip angle was in the opposite direction to

the stagger angle of the kneading discs (in Fs-Bt and Bs-Ft cases) the residence time distribution was broadened and the stress fluctuation was reduced. In the Fs-Ft and Bs-Bt combinations the residence time was very in-homogeneous and large portion of population had a residence time and shear history smaller then the average indicating pipeline flows. The authors proposed that such elements could be utilised to achieve an optimum balance between dispersive and distributive mixing.

Recently the idea of specialised extensional flow elements has been proposed since the dispersion of agglomerates is twice as effective in extensional flows as that in simple shear flow. Carson et al., 2015 proposed elements which are static on their shafts and can be located in any position along the shafts of the twin screw extruder; shown in Figure J.3. These have shown promising results in dispersing of polypropylene/polystyrene blends (Carson et al., 2016).

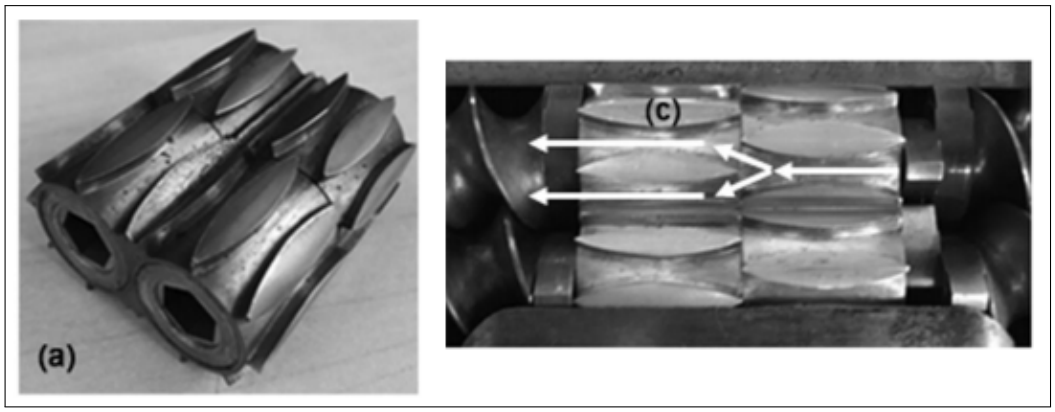

Figure J.3: *Extensional flow mixing elements; see Fig. 1, p. 3 in Carson et al., 2015*

Although the design of new elements is far beyond the scope of this research, it is important to note that potentially significant improvements may be realised by utilising novel element designs. On production scale, the choice of elements will likely be limited to that provided by the machine supplier for the given machine. Often, across different sites and even various production lines on a particular site the extruders may be from different manufacturers; thus the choice of elements may differ. However, should the financial benefits of the technology prove attractive investment into new technology is always possible.

J.2 Results

In order to develop an understanding of how different screw configurations affect the level of dispersion achieved in manufacturing of PET composites an extensive set of experiments was undertaken on 6 different screw configurations. The composites were manufactured on the *Dr Collin ZK25* machine via direct to melt addition. Three screw speeds of 100, 240 and 400 rpm were utilised to understand the impact of increased shear rate and stress together with two outputs of 3 and 6 $\mathrm{kg\,h^{-1}}$ at each speed to evaluate the impact of the degree of fill. The results presented here are those for 6 $\mathrm{kg\,h^{-1}}$ and 240 rpm which aim to provide a balance between energy input into the polymer and high shear for dispersion. These conditions were established in Chapter 9.

Three types of composites were manufactured at each condition containing 5 $\%_{\mathrm{wt}}$ of additive. The first contained the flame retardant additive (FR-1), which was shown to yield significant difference in the level of dispersion depending on the operating conditions and the severity of the screw configuration as seen by the differences in mixing achieved on the *Dr Collin ZK25* and *Berstorff ZE40A* machines; see Chapter 9. The second additive tested was the tubular clay (C-1), which from previous work in Chapter 8 was show to deliver very poor mixing with the '*existing*' configuration which is deemed as 'severe'. For details of the configuration see Section 5.3. The final additive tested was the W-5 whitener, which yielded a very good dispersion on the '*existing*' configuration for the *Dr Collin ZK25* machine. This was included in order to see if the level of dispersion achieved will reduce when processed on less severe configurations.

The six screw configurations evaluated can be subdivided into two sets. The first set is shown in Figure J.4, through which a quantitative difference was determined for the level of mixing achieved with the same length of narrow and wide kneading blocks as well as slotted mixing elements. Each of these configurations start with undercut conveying elements to aid with feeding, which then transition to self wiping profile of the same pitch followed by a reduced pitch conveying elements to compact the pellets prior to the

melting section. The melting section itself consists of two narrow kneading blocks and two slotted mixing elements to homogenise the newly formed melt. The powder additives were introduced in zone 3 onto large pitch conveying elements that offer a large free volume whilst maintaining the self wiping function. Two kneading blocks consisting of narrow discs were utilised to distribute the powder within the polymer melt at the beginning of zone 4. The remainder of this zone was configured with large pitched elements to allow the air which was drawn in with the powder and did not return via the side feeder to be removed under an atmospheric vent. This was closed at the time of the experiments. Zone 5 was designated the dispersive mixing zone which for the purpose of this analysis consisted of mixing element, 2.4 $^{L}/_{D}$ in length. It is in this zone where configurations C3, C5 and C51 differ with narrow kneading disks being utilised in C3, wide kneading disks in C5 and slotted mixing elements in C5a; as shown in Figures J.4a, J.4b and J.4c. Zone 6 simulates an existing mixing section of the DTF's extrusion process which should be maintained and zone 7 utilises an array of conveying elements to pump and pressurise the melt in order to push the material through the lace die at the end of the extruder.

Figure J.5 shows the second set of screw configurations that aims to compare the level of mixing achieved in a base case configuration with two mixing configurations. The base case configuration (Figure J.5a) contains mainly conveying elements with 1.6 $^{L}/_{D}$ of mixing elements towards the end of the extruder that aim to replicate and conserve an existing DTF process. The severe mixing screw configuration (Figure J.5b) contains 13 $^{L}/_{D}$ of mixing elements with 10.8 $^{L}/_{D}$ of the that as a continuous block. The last configuration (Figure J.5c) is less severe with 9.4 $^{L}/_{D}$ of mixing elements which includes conveying elements in between the mixing elements which aim to lower the degree of fill within the mixing elements. Potente et al., 1994 and Dhakal et al., 2017 suggest that operating mixing elements partially filled leads to much better level of mixing.

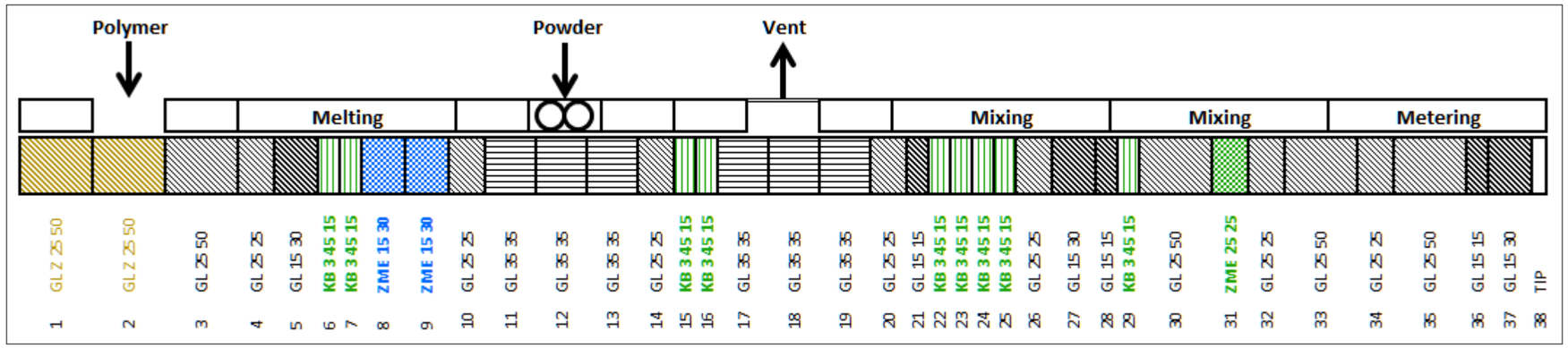

(a) *Configuration C3 - narrow kneading discs*

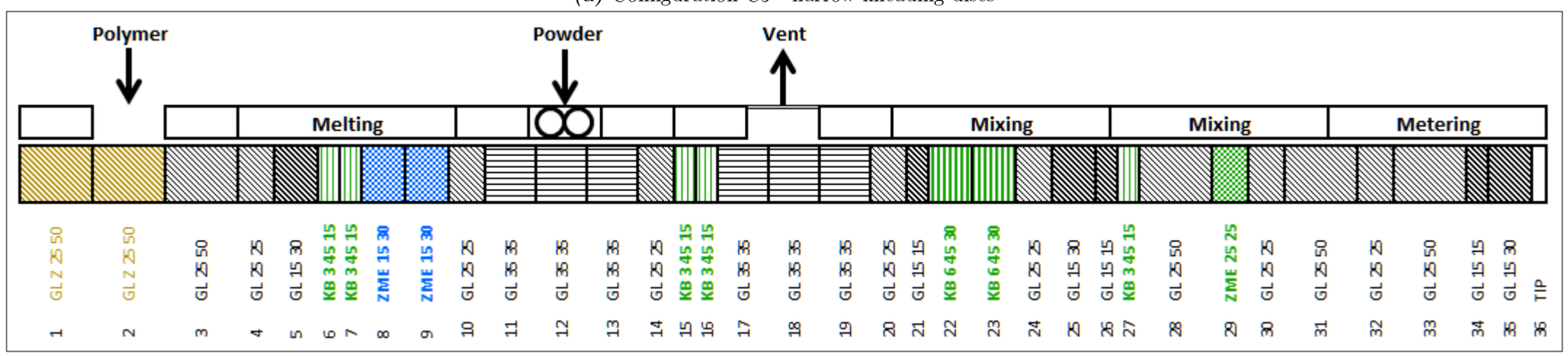

(b) *Configuration C5 - narrow kneading discs*

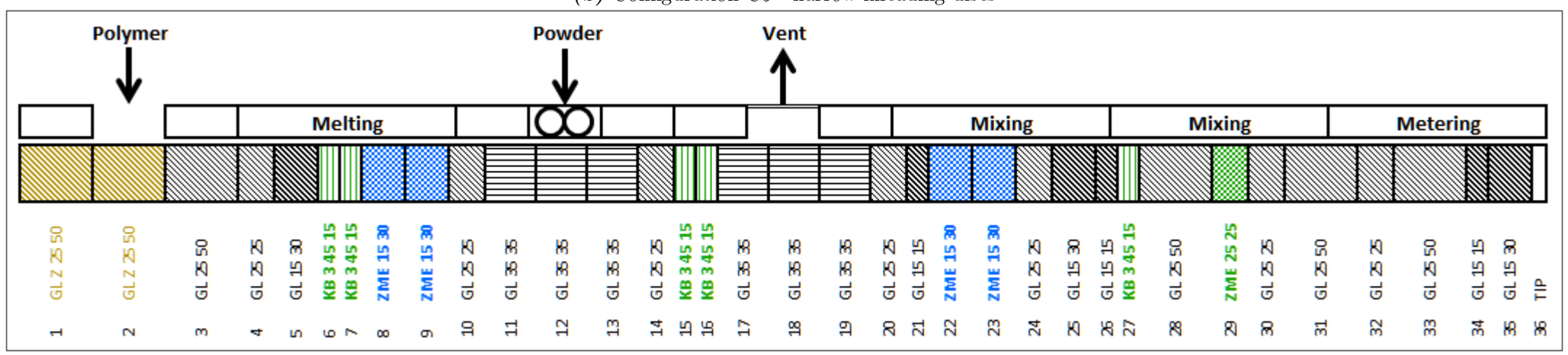

(c) *Configuration C5a - slotted mixing elements*

Figure J.4: *Screw configurations comparing the level of mixing achieved with different elements; where green indicates the least severe, blue moderate and red the most severe mixing elements*

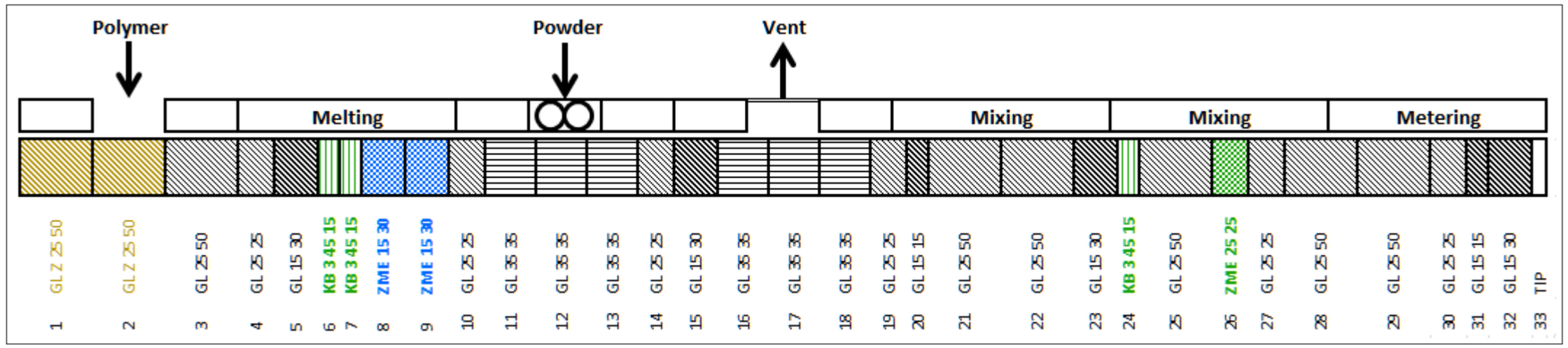

(a) Configuration BC - base case; no mixing elements apart from zone to maintain existing DTF extrusion process

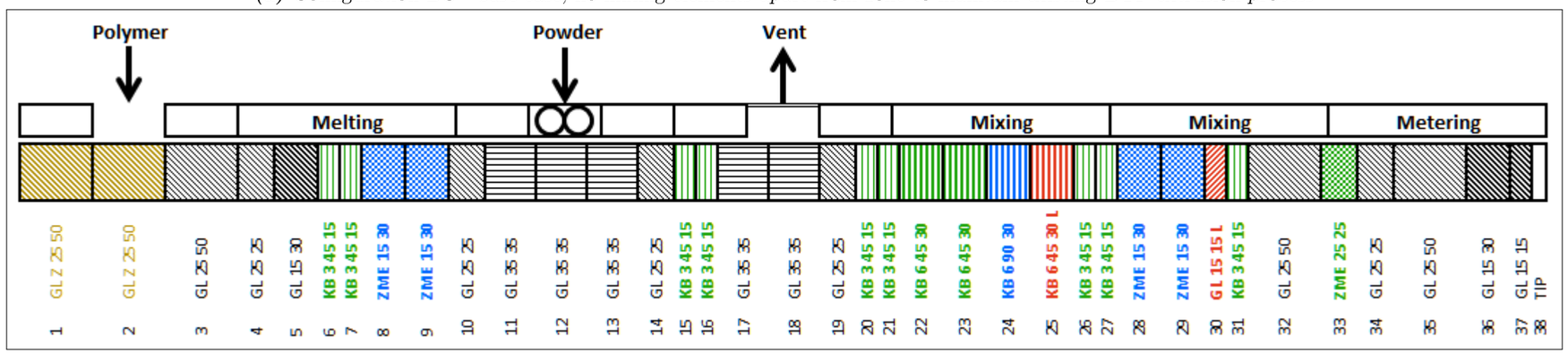

(b) Configuration C6 - most severe mixing configuration

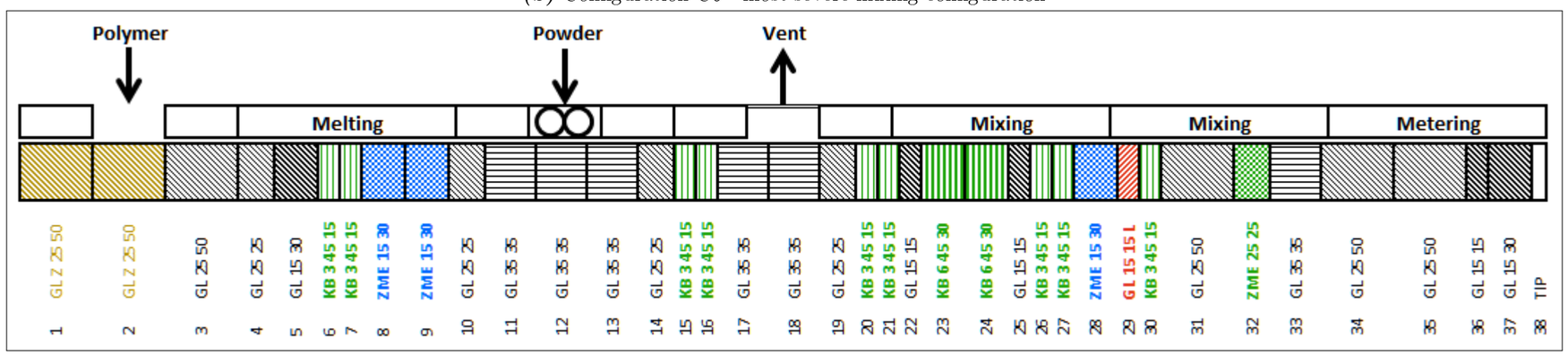

(c) Configuration C7 - mixing configuration with reduced degree of fill in the mixing elements

Figure J.5: *Screw configurations comparing the level of mixing achieved with different elements; where green indicates the least severe, blue moderate and red the most severe mixing elements*

These configurations have the same set up within the first three zones of the extruder as the previous set, with the differences beginning at the end of zone 4. The mixing zone within the most severe configuration (C6) begins with a set of two narrow kneading blocks, which follow two narrow kneading blocks at start of zone 4, that aim to further distribute the additive within the melt. The narrow kneading blocks are followed by a dispersive mixing section consisting of wide kneading blocks that increase in severity from a set of two 45 ° forward conveying blocks, one neutral 90 ° block followed by a 45 ° reverse conveying block. The dispersive mixing section is followed by a set of two narrow kneading blocks combined with two slotted mixing elements to further distribute the powder within the melt. A reverse conveying element at the end of the mixing section ensures that the slotted mixing elements are fully filled and operate against a pressure head resulting in back flow of material through the slots in the flight. Although some dispersion is likely to take place in the narrow kneading elements and in the slotted mixing elements, the majority of intensive mixing is likely to occur in the 4.8 $^{L}/_{D}$ wide kneading blocks.

Configuration C7, is a sightly gentler mixing configurations. It also has two narrow kneading blocks at the end of zone 4 to further distribute the additive through the melt. This is followed by a narrow pitch conveying element that conveys the material into the dispersive mixing section that consists of two wide 45 ° forward conveying kneading blocks. A narrow pitch conveying element conveys the material into the distributive portion of the mixing zone which in this case consists of two narrow kneading blocks, a slotted mixing element and a reversing element which ensures that the distributive mixing section is fully filled.

Figure of J.6a shows the degree of fill for this set of configurations as a function of extruder length. In the calculation of the degree of fill, the slotted mixing elements were assumed to not have the ability to generate pressure and thus any conveying capacity. Although this behaviour is true for toothed mixing elements (Kohlgrüber, 2008), it is harder to quantify for slotted mixing elements which are likely to have some ability to generate pressure due

to the area of the slots being a small fraction of the overall flight area. From Figure J.6a it is evident that the reduction in DOF in the mixing section was not fully achieved with the use of narrow pitch conveying elements. In order to achieve this a longer length of larger pitch conveying elements has to be utilised.

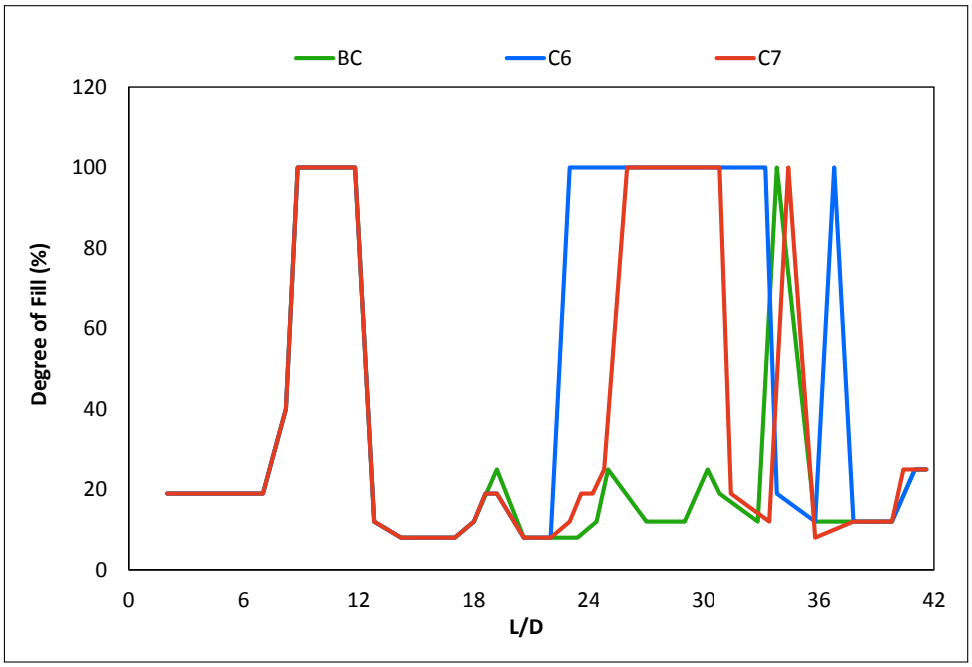

(a) *Degree of fill as function of length for configurations BC, C6 and C7*

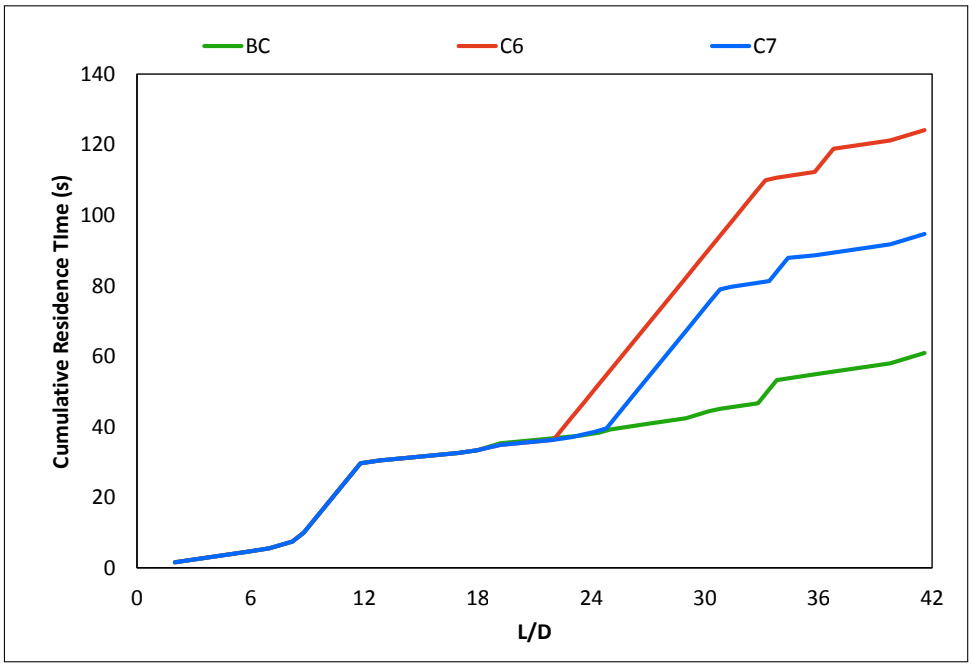

(b) *Cumulative residence time as function of length for configurations BC, C6 and C7*

Figure J.6: *Key parameters as function of length for configurations BC, C6 and C7*

This in turn would diminish the length of the metering zone potentially reducing the ability of the extruder to pressurise the melt and achieve stable conveying. Such sacrifice can be made when a melt pump is fitted on the end of the extruder to stabilise the flow, however this was not available on the *Dr Collin ZK25* machine. Figure J.6b however shows that the reduced number of mixing elements considerably lowers the cumulative residence time within the extruder. This coupled with a potential of reduced mechanical degradation achieved through the use of 'gentler' mixing element may lead to improvement in dispersion for certain systems.

J.2.1 Comparing dispersion in narrow and wide kneading blocks as well as slotted mixing elements

Figure J.7 shows the level of mixing achieved within tubular clay and flame retardant composites manufactured in H-PET matrix using the first set of screw configurations; see Figure J.4. It is evident that the level of dispersion achieved with the use of narrow kneading blocks was considerably better than that achieved with wide kneading blocks and slotted mixing elements for both of the composites. The trends remain true even though the level of mixing in FR-1 composites was significantly better than that in the clay composites. In these configurations the forward conveying nature of the elements combined with the lack of reversing element located directly after means that the elements are likely to be partially filled. It is hard to estimate the degree of fill within the slotted mixing element; however these were assumed to be fully filled.

The notion that narrow kneading discs provide better dispersive capacity than the wider alternative is surprising. It is possible that the slightly longer residence time associated with the same length of narrower kneading discs versus the wider discs contributed to better mixing. As the narrow kneading block configuration has twice the number of paddles in the same length, it is likely that the increased sectioning of the melt which induces elongational flows explains the results obtained.

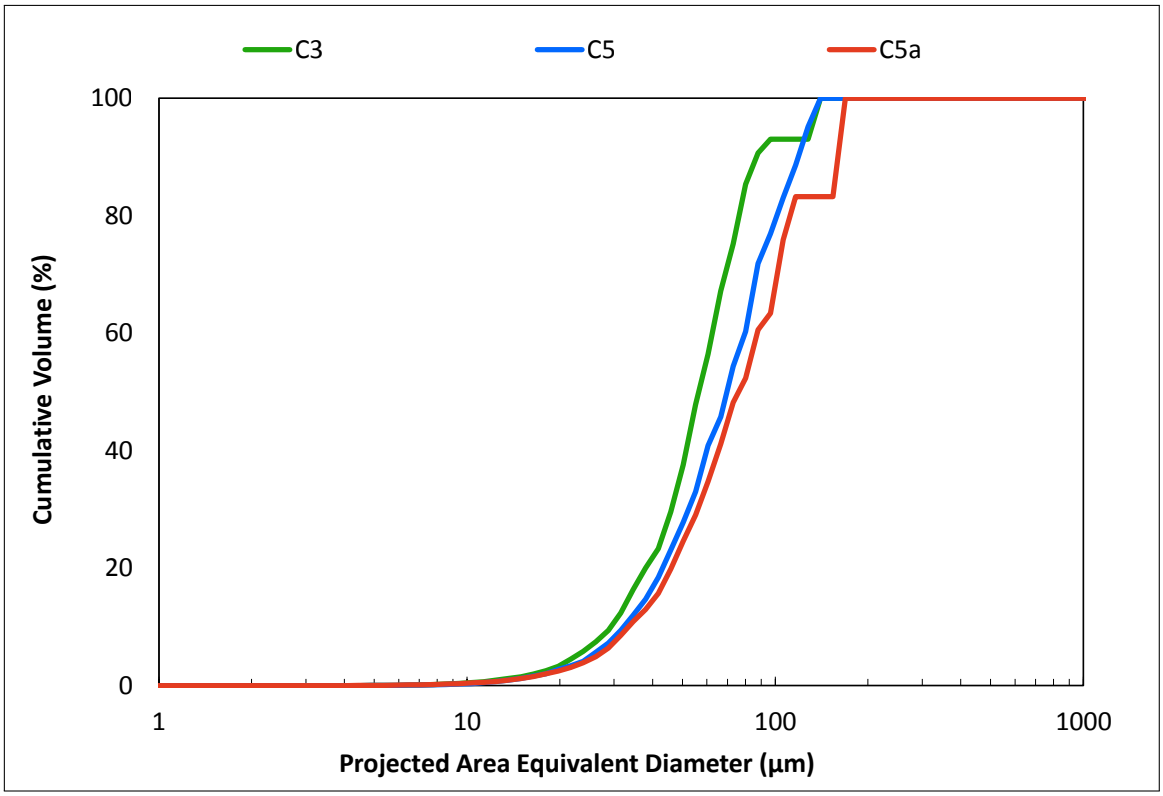

(a) Tubular clay C-1

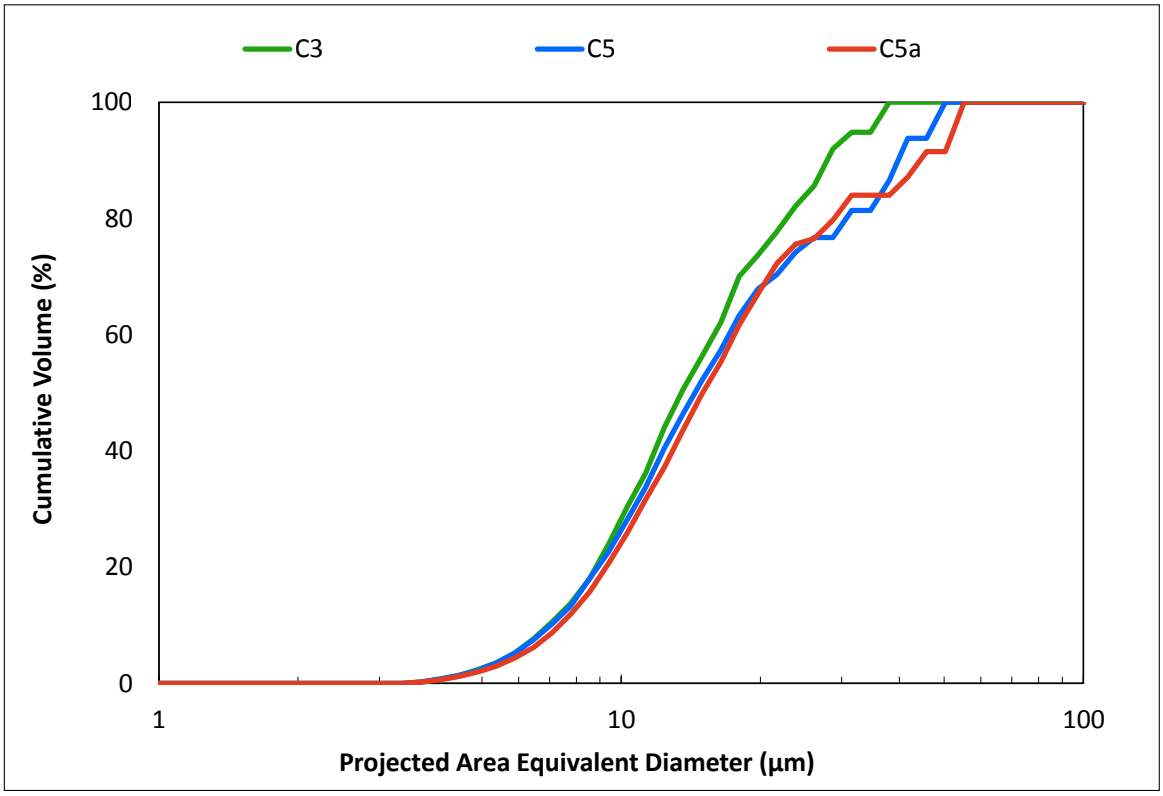

(b) Flame retardant FR-1

Figure J.7: *Mixing in C-1 and FR-1 composites processed on configuration C3, C5 and C5a; manufactured at 6* $\mathrm{kg\,h^{-1}}$ *and 240* rpm

In the case of whitener (W-5) composites a different trend is observed; see Figure J.8. The plot is based on the 'Feret' diameter which is the longest length of the particle in order to reflect the long aspect ratio nature and monitor the particle attrition. Similarly, the cumulative volume was calculated on the basis of the particles having a cylindrical shape as opposed to the spherical shape assumed for the FR-1 additive and C-1 agglomerates.

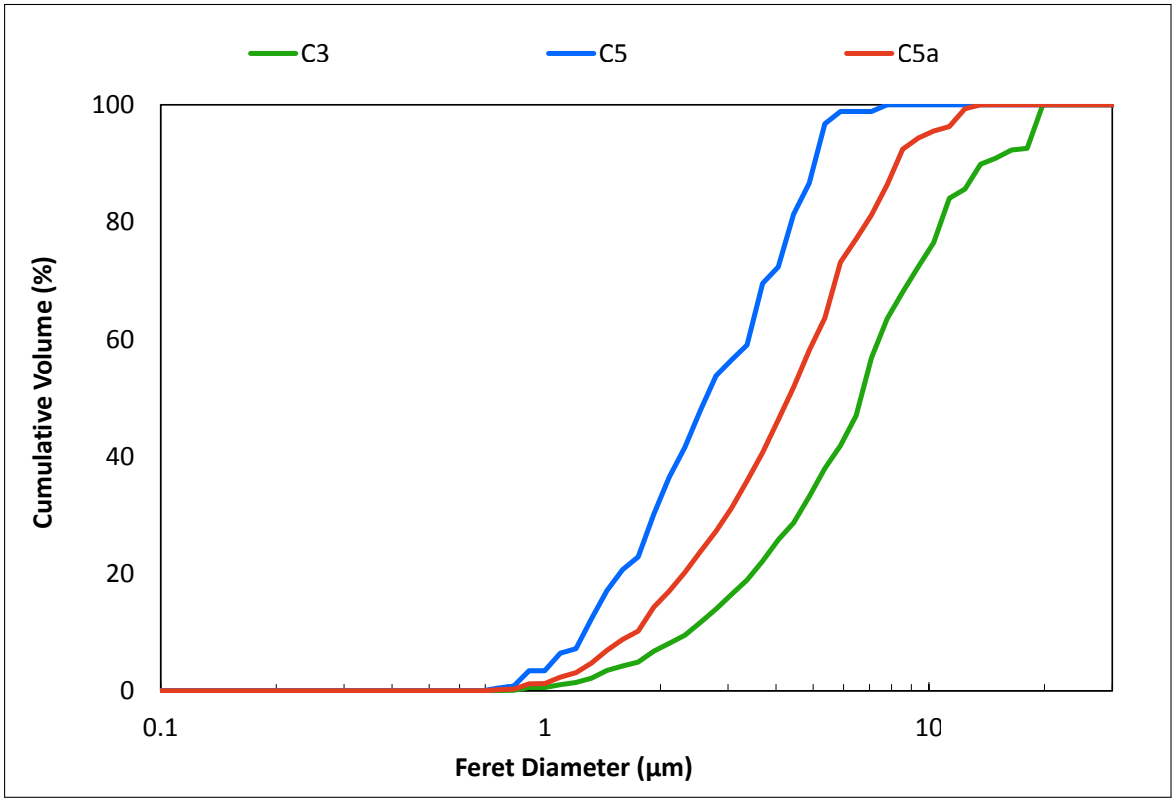

Figure J.8: *Mixing in whitener composites processed on configuration C3, C5 and C5a; manufactured at 6* $\mathrm{kg\,h^{-1}}$ *and 240* rpm

From J.8, it is clear that within the *W-5* composite manufactured on the C5 configuration there were no particles larger than 3µm in length detected, which compared to the specification length of ca. 5 µm suggests attrition of the additive. This was not seen on the C3 or C5a configuration. However, a closer inspection of the SEM images in Figure J.9 reveals that there are fewer particles detected in Figure J.9b (corresponding to W-5 whitener manufactured on C5 configuration) relative to other images in Figure J.9 (corresponding to W-5 whitener manufactured on other configuration). This suggests that operator error is likely and potentially the sampling of the material was mistimed.

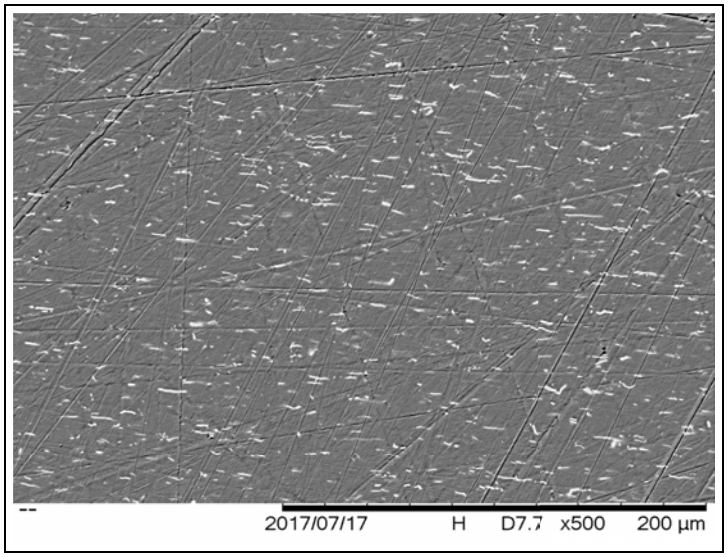

(a) Whitener W-5 manufactured on C3 configuration

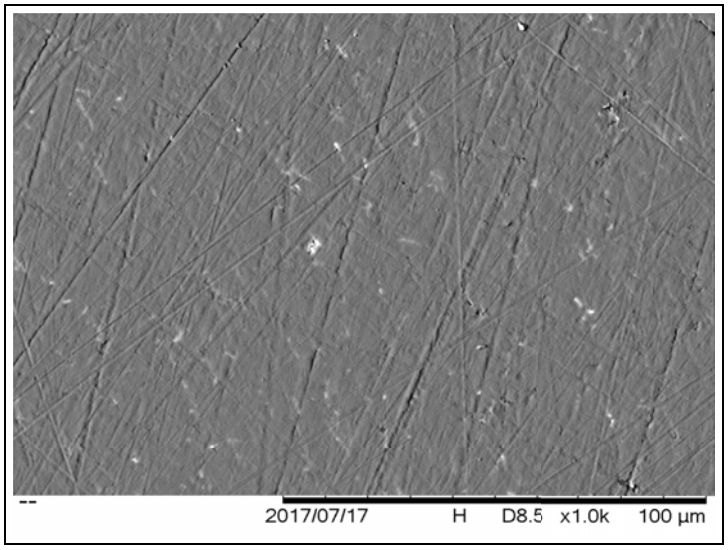

(b) Whitener W-5 manufactured on C5 configuration

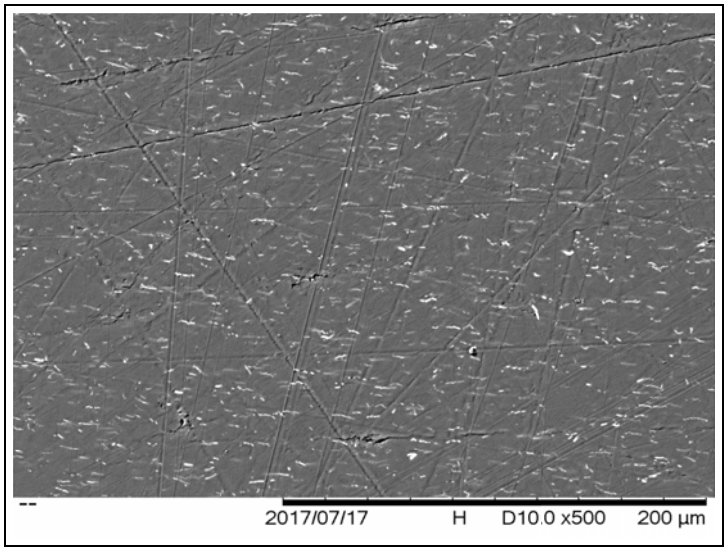

(c) Whitener W-5 manufactured on C5a configuration

Figure J.9: *Mixing in W-5 composites processed on configuration C3, C5 and C5a; manufactured at 6* $\mathrm{kg\,h^{-1}}$ *and 240* rpm

The finding that the slotted mixing element configuration (C5a) delivers better dispersion compared to the narrow kneading disc configuration (C3) agrees with the work of Villmow et al., 2010 who reported that toothed mixing elements delivered better mixing as opposed to kneading discs in processing of MWCNTs. However, the increased IV losses in the composites processed on the C3 configuration (see Table J.1) could explain the slightly deteriorated mixing as a result of lower shear hydrodynamic stresses being transferred to the filler in order to disperse it. As this trend does not correlate to the other composites, it is likely that the increased loss is associated with a higher initial moisture content of the polymer as opposed to the effect of the screw configuration itself.

In both the tubular clay and the flame retardant composites, the IV loss increased when the materials were processed with wider kneading discs or slotted mixing elements. This suggests that these configurations are more detrimental to the polymer molecular weight than an equal length of the narrow kneading discs.

Table J.1: *IV losses in % for composites manufactured via direct to melt addition and premix routes at 6* $\mathrm{kg\,h^{-1}}$ *and 240* rpm *on the Dr Collin ZK25 machine using C3, C5 and C5a configuration; error according to student-t distribution at 90 % CI*

Configuration	C3	C5	C5a
C-1/H-PET composites	27.6 ± 2.8	32.5 ± 0.8	34.5 ± 3.4
FR-1/H-PET composites	25.9 ± 1.6	41.4 ± 5.4	29.9 ± 14.0
W-5/H-PET composites	29.3 ± 2.9	22.0 ± 0.9	21.2 ± 0.9

J.2.2 Comparing entire screw configurations

In the case of the tubular clay, processing the materials with the mixing configurations yielded better mixing as expected. Interestingly, the less severe of the two mixing configurations provided better dispersion through the erosion mechanism as indicated by the distribution for configuration C7 being further to the left than that for C6; see Figure J.10a. The maximum size of agglomerates detected is very similar indicating that the magnitude of peak shear stress experienced was very close in both configurations.

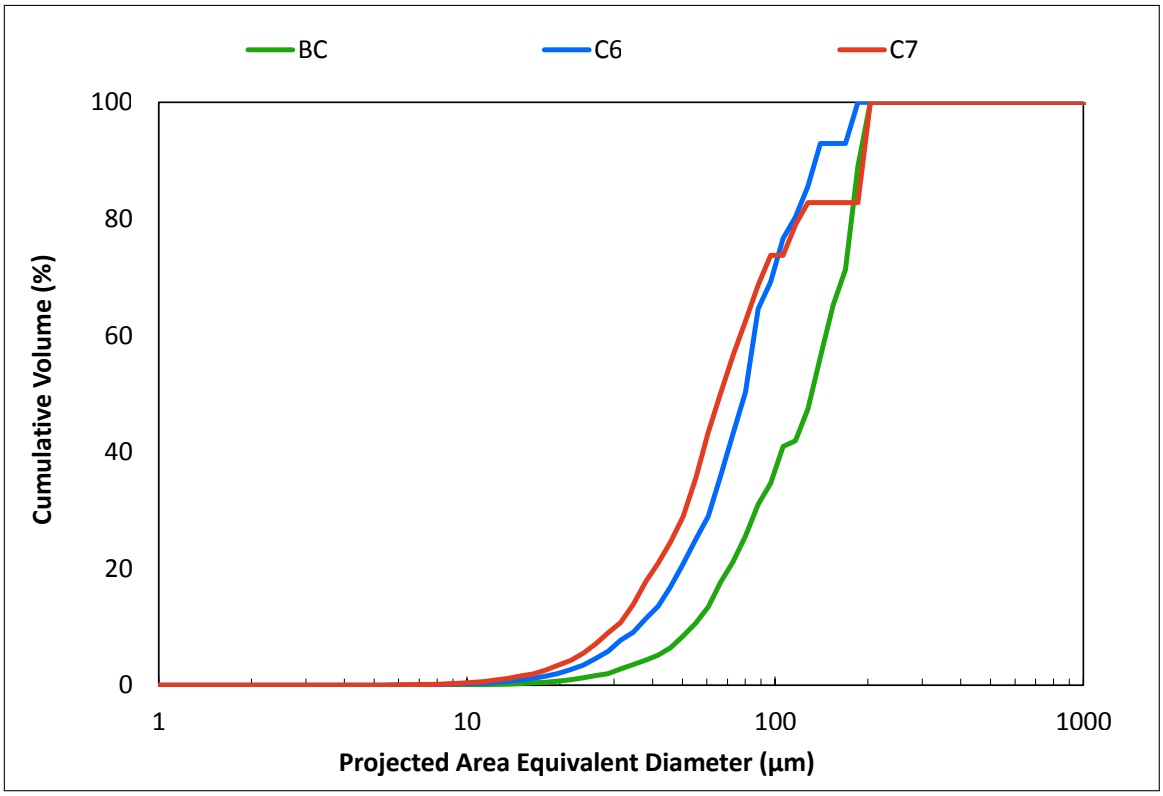

(a) Tubular clay C-1

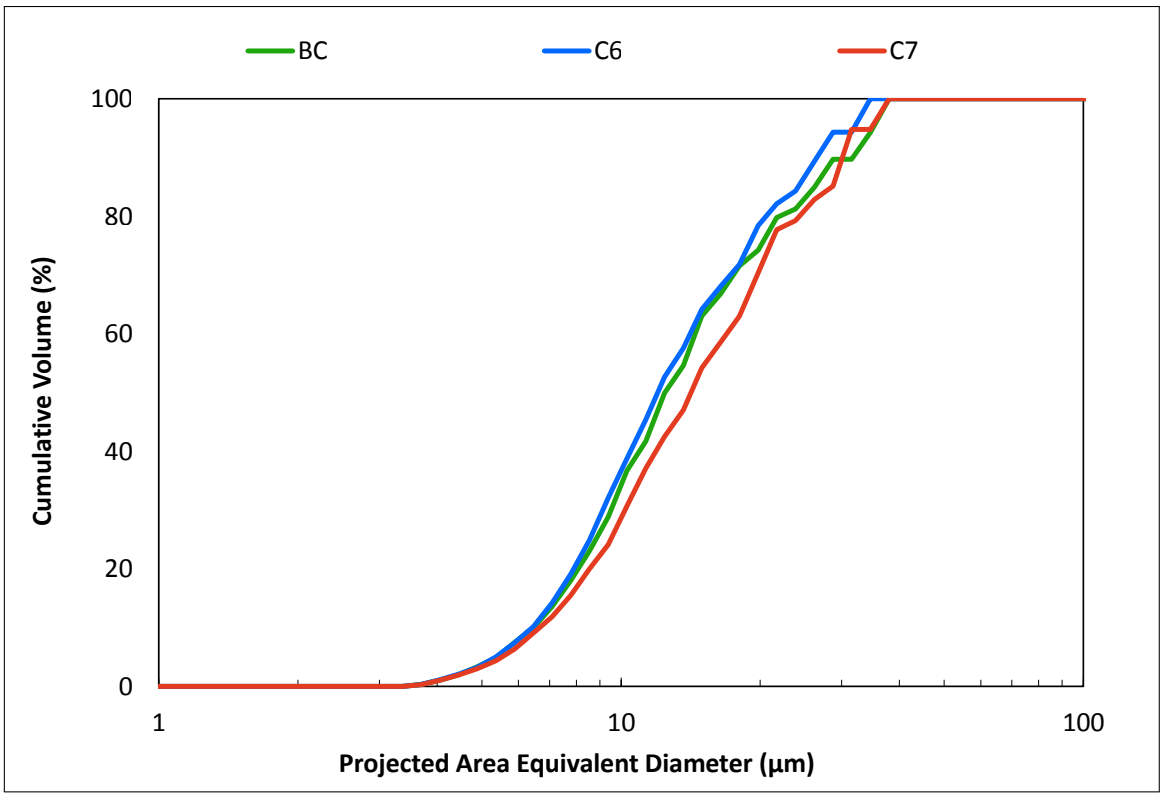

(b) Flame retardant FR-1

Figure J.10: *Mixing in C-1 and FR-1 composites processed on configuration BC, C6 and C7; manufactured at 6* $\mathrm{kg\,h^{-1}}$ *and 240* rpm

The level of mixing achieved in the case of FR-1 additive appears to be very similar irrespective of the configurations. The reflected light microscopy analysis of the chip has been confirmed using transmitted light microscopy which yielded distributions that were much closer together and hence are not shown herein. This is surprising as in the previous work the level of mixing observed on the *Berstorff ZE40A* machine versus that on the *Dr Collin ZK25* machine have been significantly different suggesting the importance of screw configuration. It is possible that the level of mixing achieved on the *Dr Collin ZK25* machine is significantly higher due to the higher magnitude shear stresses found in screw tip to barrel clearance. This raises a concern for scale up.

Figure J.11 shows the level of mixing achieved with the W-5 whitener grade when manufacturing composites on various screw configurations.

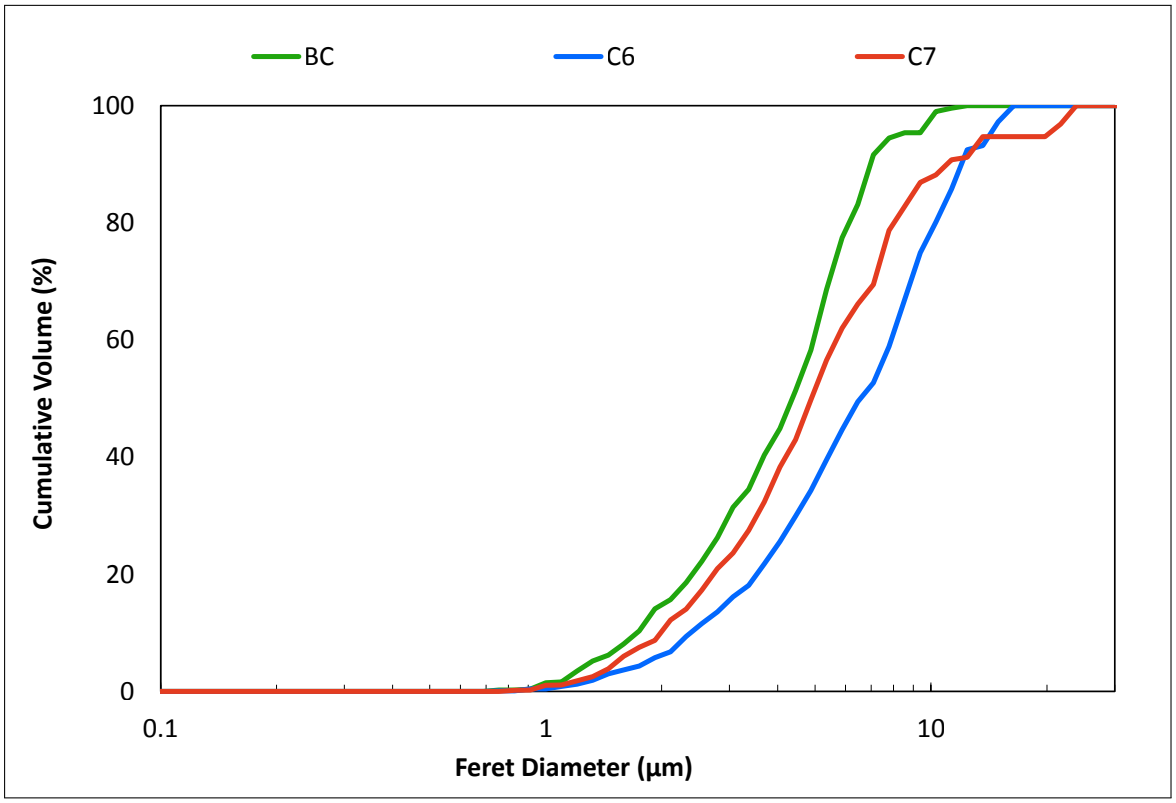

Figure J.11: *Mixing in whitener composites processed on configuration C3, C5 and C5a; manufactured at 6* $\mathrm{kg\,h^{-1}}$ *and 240* rpm

Different patterns are observed here with the base case configuration BC providing the best level of dispersion which is followed by the less severe C7 configuration and then

the most severe C6 configuration. The most likely explanation for such a result is the extremely good affinity between the additive and the polymer. This means that there is no large demand for dispersive mixing zones that promote mixing via rupture mechanism. Instead gentler mixing through erosion mechanisms at the lower average degree of fill is satisfactory to disperse this additive to its primary particle size. The average degree of fill in the BC, C7 and C6 configuration was calculated to be 24.5, 36.8 and 47.6 % respectively.

Regarding the IV loses for the polymer matrix, the most severe mixing configuration C6 delivered the largest losses. This was particularly evident in the flame retardant and the whitener composite systems; see Table J.2. The gentle mixing configuration C7 delivered IV losses slightly higher than those obtained through processing by the mainly conveying screw set up. Since the polymers were pre-dried in all of the experiments, this demonstrates that a significant portion of the total IV loss occurs in the melt zone; as proposed in Chapter 7.

Table J.2: *IV losses in % for composites manufactured via direct to melt addition and premix routes at 6* $\mathrm{kg\,h^{-1}}$ *and 240* rpm *on the Dr Collin ZK25 machine using BC, C6 and C7 configuration; error according to student-t distribution at 90 % CI*

Configuration	BC	C6	C7
C-1/H-PET composites	26.1 ± 4.2	33.7 ± 1.7	33.9 ± 1.3
FR-1/H-PET composites	34.9 ± 0.5	54.8 ± 8.4	33.9 ± 1.3
W-5/H-PET composites	27.4 ± 0.5	29.3 ± 3.0	18.7 ± 4.7

J.2.3 Impact of operating condition on the base case and severe mixing configurations

As well as considering different screw configurations the impact of operating conditions on the base case configuration BC and the most severe mixing set up C6 was examined; see Figure J.12. The role of screw configuration on the influence of screw speed is very significant.

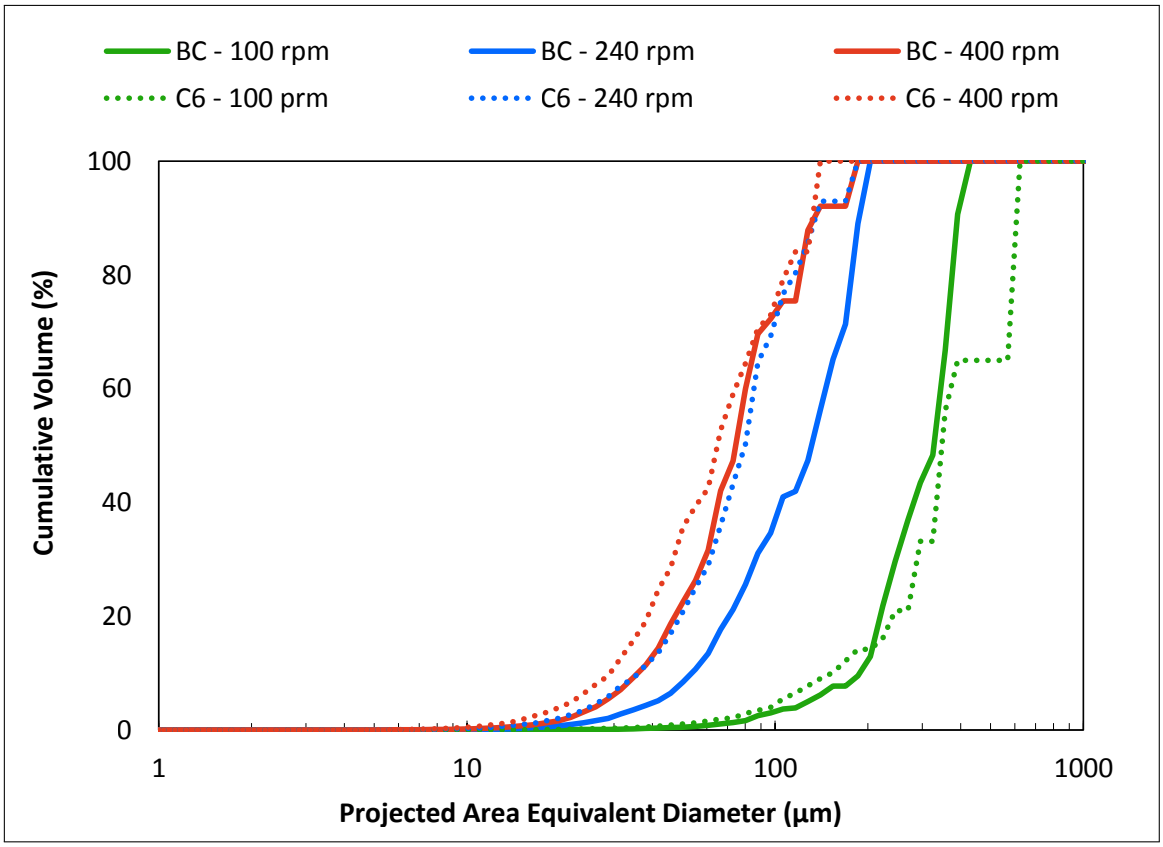

(a) Screw speed

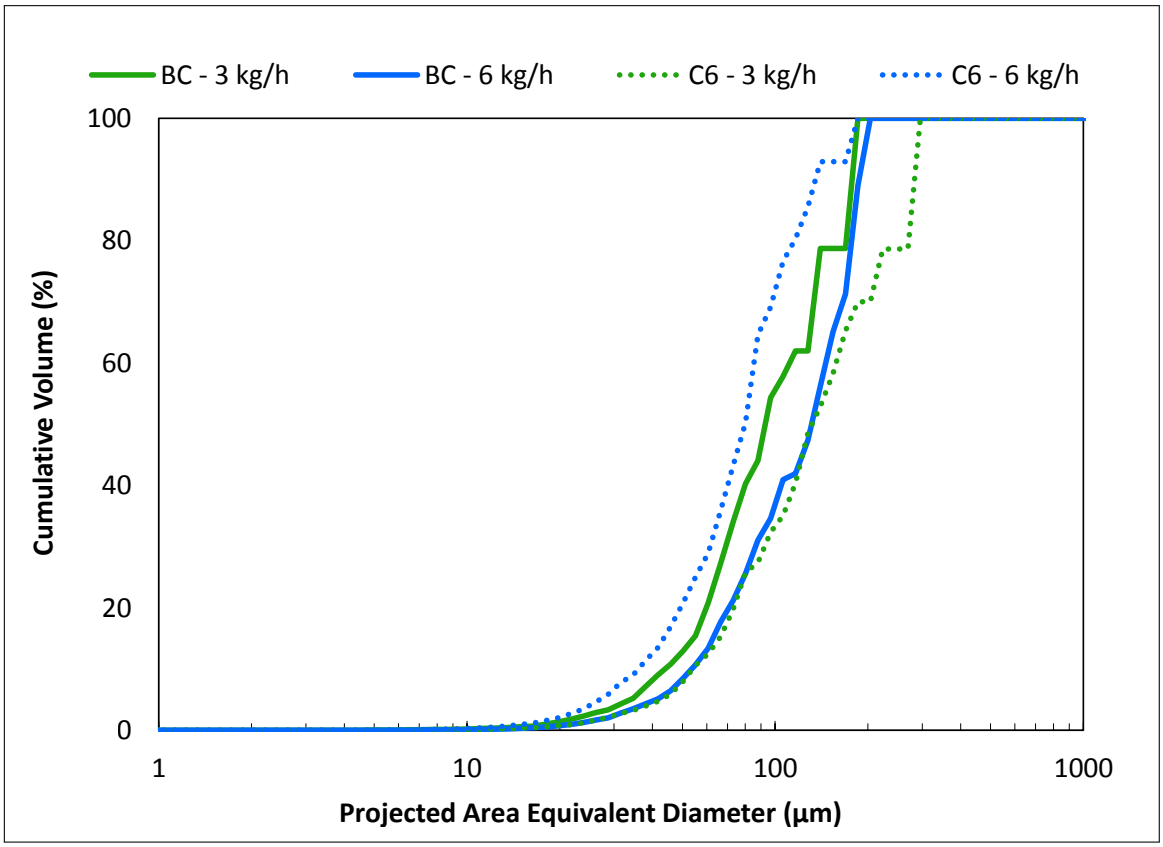

(b) Output

Figure J.12: *Impact of operating conductions on mixing of tubular clay composites processed on configuration BC and C6*

As the screw speed increased for composites manufactured on the base case configuration, there is a gain in the effectiveness of the erosion mechanism. The increase in rupture mechanism is also evident, but it diminishes rapidly past screw speed of 240 rpm due to little change in the D_{90} of the distributions.

A significantly different behaviour is observed with the most severe configuration (C6). As the speed is increased from 100 to 240 rpm there is a highly significant rise in the level of mixing achieved via both the erosion and rupture mechanisms as illustrated by the shift of the distribution to the left. However, as the speed is increased from 240 to 400 rpm almost no further gains are realised. Importantly the distributions of additive size for composites manufactured on configuration BC and C6 are reasonably similar and most importantly the distribution from configuration BC at 400 rpm and that of C6 at 240 rpm are almost identical. This shows that similar level of mixing can be achieved at lower speeds using a more severe screw configuration. Critically, as the peak shear stress achieved in the most severe configuration at 240 rpm is far less than that in the base case at 400 rpm this suggests an existence for a state of dispersion beyond which no further reduction can be achieved without altering the properties of the materials being processed.

In the case of the output, different effects occur in the base case and the most severe mixing configuration; see Figure J.12b. Focusing on the base case configuration, as the output is reduced the degree of fill reduces resulting in larger average shear rates and stresses and yields better mixing. In this case the IV losses of 25.5 ± 1.1 and 26.1 ± 4.2 % were obtained at outputs of 3 and 6 $\mathrm{kg\,h^{-1}}$ respectively. A different behaviour is observed on the severe mixing configuration. Here, the increase in output leads to a significant increase in the level of dispersion achieved. This is a likely result of the reduction in the IV loss experienced at the higher output with 33.7 ± 1.7 % being measured at 6 $\mathrm{kg\,h^{-1}}$ and 38.2 ± 4.0 at 3 $\mathrm{kg\,h^{-1}}$.

J.2.4 Premix versus direct to melt addition route

Figure J.13 compares the differences in dispersion achieved within tubular clay (C-1) and the flame retardant (FR-1) composites processed via the direct to melt and premix addition routes on the base case configuration with no mixing elements and the most severe mixing configuration (C6). The distributions shown are based on a number of images captured at each sample condition via reflected light microscopy on the chip surface at five times magnification for clay and ten times magnification for FR-1.

The results suggest the existence of two scenarios, one where the additive has a poor interaction with the polymer matrix and the other where the interaction is much stronger. In the case of poor interaction, as demonstrated by C-1/PET composites in Figure J.13a, there is a tendency for the additive to naturally form large agglomerates when it is introduced to the polymer. In such a case, the premix method of addition performs better than the direct to melt addition on both configurations as larger stresses can be applied in the melt zone leading to more efficient rupture and longer residence time associated with this route lead to better erosion.

In the composites manufactured via the premix method, the more severe mixing configuration delivered better mixing than the base case due to the larger residence times enabling effective erosion. For the composites manufactured via the direct addition route, which theoretically had larger agglomerates present upon entry into zone 4, best mixing was achieved on the base case configuration. This is the direct result of the lower degree of fill within zones 3 to 7 leading to higher magnitude average shear rates which in turn enable much more efficient rupture of the large agglomerates. Based on the model developed in Chapter 6, the residence time weighted average shear rate for zone 3 to 7 was calculated at of 391 s^{-1} and 188 s^{-1} for configuration BC and C6 respectively.

In the second scenario, as illustrated by FR-1/PET composites in Figure J.13b, where good interaction between the polymer and the additive exists there is much lower tendency

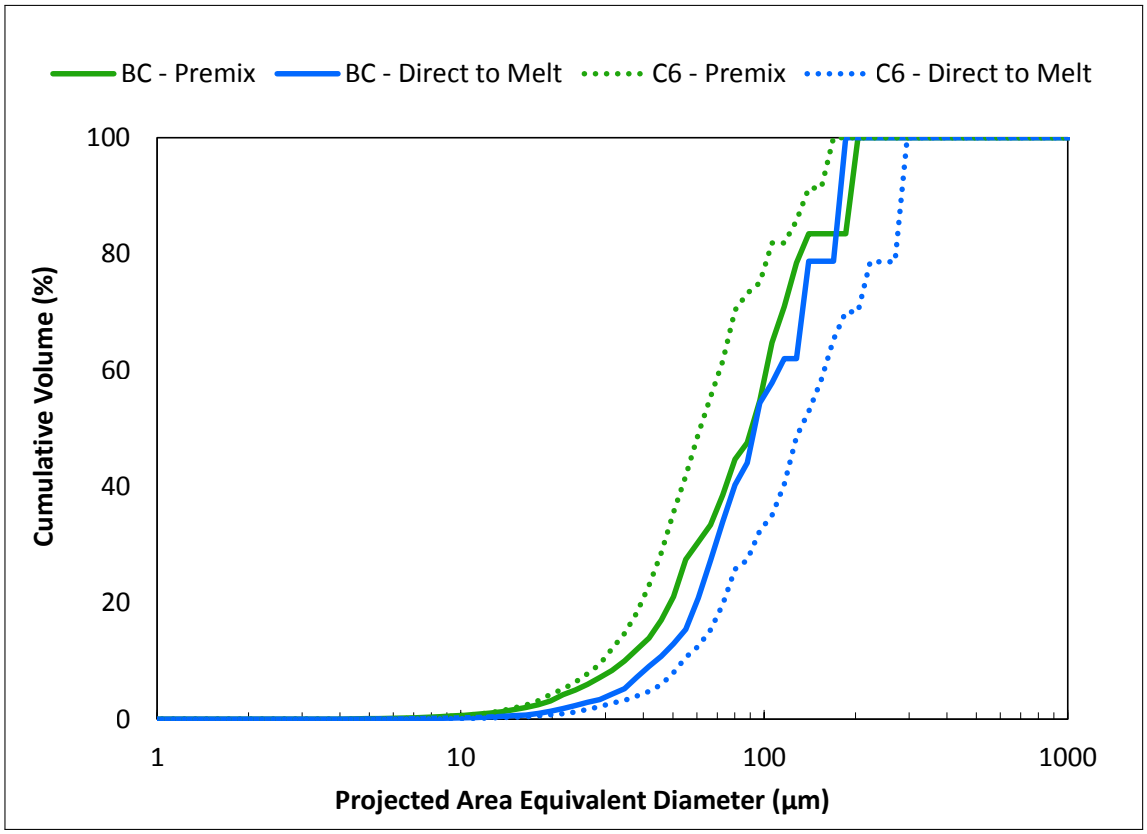

(a) Tubular clay C-1: premix vs direct to melt addition on BC and C6 configurations

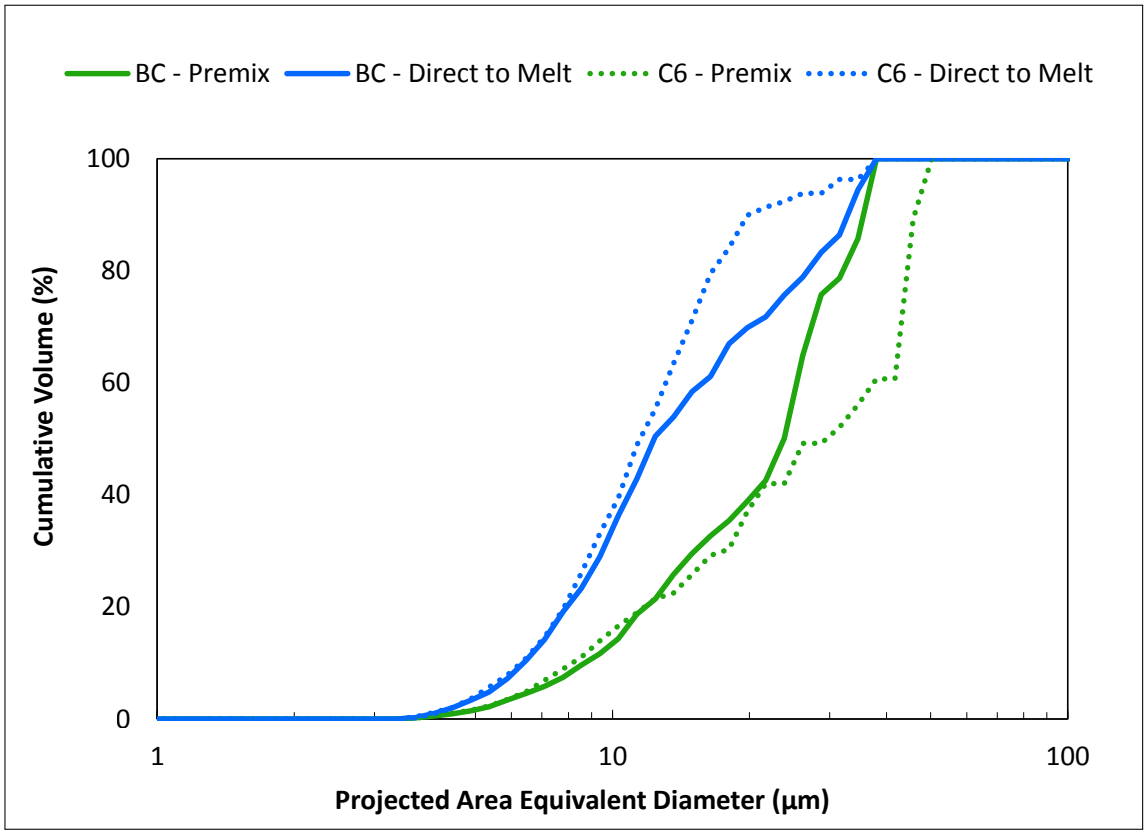

(b) Flame retardant FR-1: premix vs direct to melt addition on BC and C6 configurations

Figure J.13: *Premix versus direct to melt addition for C-1 and FR-1 processed on configuration BC and C6; manufactured at 3* $\mathrm{kg\,h^{-1}}$ *and 240* rpm

for agglomeration upon addition of the additive. In this case the direct to melt addition yielded better mixing on both configurations as there are no large agglomerates which require the large stresses in the melt section to be broken. Instead, when the additives are processed via the premix section any agglomerates present are compacted by the high pressures within the zone making them harder to rupture later in the process.

Within the direct to melt subset, the mixing configuration provides better dispersion as the result of increased residence time which increases the number of passes through the high shear regions enabling effective rupture. In the case of the composites manufactured via the premix method the base case provides better mixing. This is again the result of the lower degree of fill which leads to higher shear rates and stresses that in turn are better able to rupture the compacted agglomerates.

Table J.3: *IV losses in % for composites manufactured via direct to melt addition and premix routes at 3* $\mathrm{kg\,h^{-1}}$ *and 240* rpm *on the Dr Collin ZK25 machine using BC and C6 configuration; error according to student-t distribution at 90 % CI*

Configuration	BC		C6	
Process	Premix	Direct to melt	Premix	Direct to melt
C-1/H-PET composites	30.9 ± 5.5	25.5 ± 1.1	40.1 ± 1.4	38.2 ± 4.0
FR-1/H-PET composites	38.2 ± 2.8	40.4 ± 6.5	30.9 ± 1.3	46.6 ± 7.8

The IV losses calculated are shown in Table J.3. In the case of direct to melt addition and yield no conclusive trends as some of the errors are relatively large. More analysis has to be undertaken in order to be able to see conclusive difference.

J.3 Concluding remarks

In this chapter the impact of different screw configurations on the level of dispersion achieved in tubular clay, flame retardant and whitener filled PET composites. A total of six configurations were considered with three of them focusing on understanding the differences between element types and the other three looking at the role of the whole

configuration. A number of operating conditions have been considered for each of the screw set ups.

In systems with spherical particles (flame retardant) or agglomerates (as in case of tubular clay) for the same total length of the screw the narrow kneading elements showed better dispersion then the kneading blocks composed of wider discs. This was associated with the narrower configuration having twice the number of paddles and thus generating more extensional flows which are more efficient in dispersing fillers. Both of the kneading configurations were better than the slotted mixing elements; however the difference between the mixing elements and the wider kneading configuration was relatively small. In the case of longer aspect ratio fillers that do not have a tendency to agglomerate the use of slotted mixing elements yielded better level of dispersion than the kneading blocks composed of narrow discs.

In considering the role of the entire configuration for the tubular clay system where the additive has poor interaction with the matrix the gentler mixing configuration generated better level of dispersion, particularly an increase in the number of smaller particles when compared to the more severe mixing set up. Both of these were better than the base case configuration that consisted almost entirely of conveying elements. In the manufacture of the flame retardant composites there was surprisingly little difference between the configurations. This is despite a considerable difference between gentler *Berstorff ZE40A* and more severe *Dr Collin ZK25* configurations being observed in the previous work. This finding raises a concern for the scale up process. As the clearances within the machines change the peak shear stresses applied alter so there is a need to ensure that the same peak shear stresses are delivered to guarantee the same level of dispersion. As for the whitener system, the best level of mixing was achieved with the base case configuration which was attributed to the very good affinity between the polymer and the additive. These results do reiterate that at the same processing conditions even the most severe configuration delivers a variation in dispersive mixing with the maximum particles for tubular clay

being hundreds of microns in size and that for the long aspect ratio whitener in single figures. This reiterates the possible need to use effective dispersive aids, as discussed in Chapter 8.

As well as changes to the configurations, the impact of operating condition on the different configurations was also considered. In the case of a tubular clay composites, the same level limiting state of dispersion was achieved on the most severe screw set up and the base case configuration. For the base case this was achieved at a screw speed of 400 rpm and the most severe configuration of 240 rpm. This shows that a more severe screw geometry can be utilised in order to decrease the speed at which the material is being processed.

The optimum injection point also depends on the level of additive interaction with the polymer matrix. In the case of poor interaction the optimum dispersion was achieved via the premix route where the most severe configuration generated the optimum mixing. Within a system where good interaction is present the best dispersion was achieved on the most severe configuration via the direct to melt addition process.

The results from these studies clearly identify the need to have an understanding of the level of interaction between the additive and the polymer prior to any design of the screw configuration. These also pose a challenge for the direct to melt addition process on the film lines. Currently, the products on different manufacturing lines are grouped based on some inherent property of the final product such as thickness or colour. This work identifies the need to segregate the extrusion process by the level of interaction between the additive and the polymer. Thus implying the need to either switch screw configurations more regularly (increases down time), have separate extruders for the same manufacturing line (increases capital investment) or select the products manufactured on a given line by the level of additive to polymer interactions.

K | Prediction of the intrinsic viscosity reduction from Polyhand

Polyhand is an internal software package utilised within DTF to predict the intrinsic viscosity (IV) reduction of the polymer under given process conditions. More information on the model and the parameters used within the calculations can be found in Chapter 7. In the extrusion process the parameters of interest such as temperature, residence time screw speed etc. are dependant on each other. For example the change in screw speed will induce a change in residence time as well as the polymer melt temperature. *Polyhand* can be utilised to analyse the hypothetical situations where only one parameter is changed at a time. For example, Figure K.1 shows the role that the initial moisture content plays in determining the IV loss (*note: no degassing taking place in this simulated case*). Figure K.2 shows the influence of the polymer temperature on the IV reduction and thus the molecular weight of the extrudate.

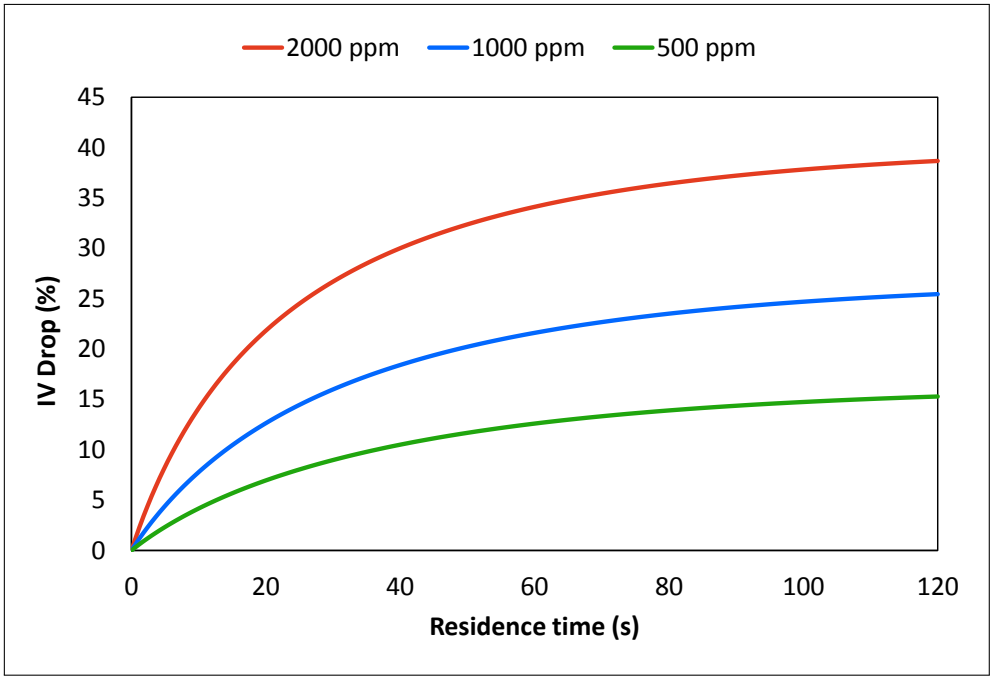

Figure K.1: *Effect of initial moisture concentration on IV drop at temperature of 275 °C and residence time of 120 s*

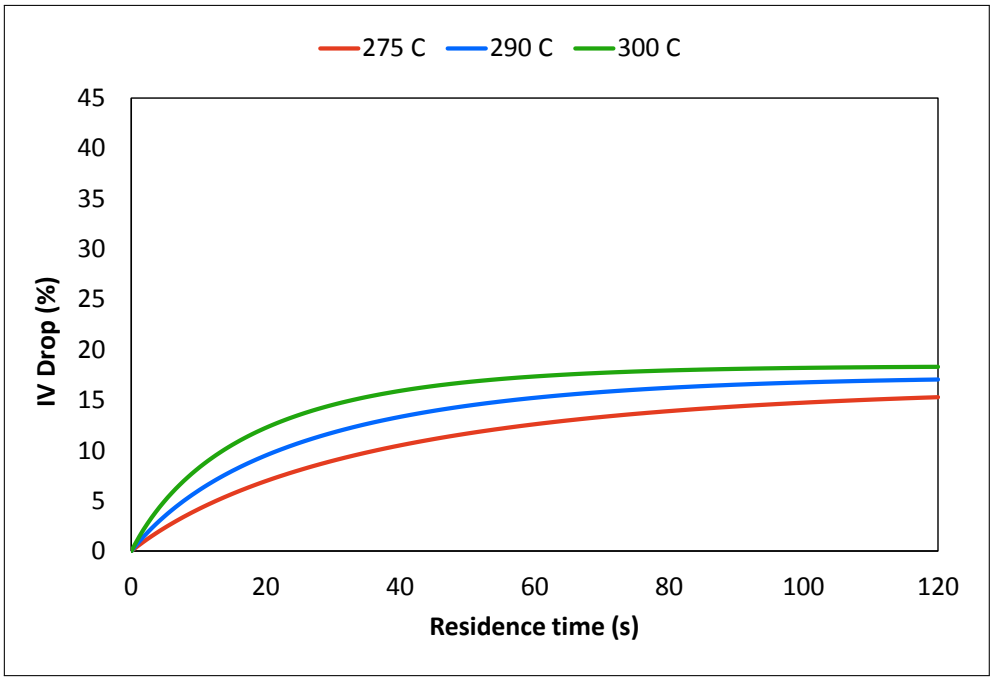

Figure K.2: *Effect of polymer and medium temperature on IV drop at initial moisture content of 500 ppm and residence time of 120 s*

References

Albalak, R. (1996), *Polymer Devolatilization*, Plastics Engineering, Taylor and Francis, ISBN: 9780824796273.

Altinkaynak, A., M. Gupta, M. A. Spalding, and S. L. Crabtree (2006), "Three-Dimensional Finite Element Simulation of Polymer Melting in a Single-Screw Extruder", in: *Annual Meeting of Polymer Processing Society*.

Ammala, A., C. Bell, and K. Dean (2008), Poly(ethylene terephthalate) clay nanocomposites: Improved dispersion based on an aqueous ionomer, *Composites Science and Technology*, **68** (6), pp. 1328 –1337, ISSN: 0266-3538.

AMPEF [Association of Manufacturers of Polyester Film] (2002a), *Polymer Structure*, URL: http://www.ampef.com/polystruc.html (visited on June 12, 2015).

AMPEF [Association of Manufacturers of Polyester Film] (2002b), *Process Flow*, URL: http://www.ampef.com/technology2.html (visited on June 12, 2015).

Bart, J. C. J (2006), *Polymer additive analytics - industrial practice and case studies*, Firenze: Firenze University Press.

Beckman Coulter (2009), *Meeting and exceeding the standard for laser diffraction particle size analysis*.

Bell, T. and J. Bloom (2014), *Increased bulk density powders and polymers containing them*, US Patent 8,623,507.

Bestul, A. B. (1954), Composition of Apparent Shearing Forces During Shear Degradation of Polymers, *Journal of Applied Physics*, **25** (9), pp. 1069–1074.

Bestul, A. B. (1956), Kinetics of Capillary Shear Degradation in Concentrated Polymer Solutions, *The Journal of Chemical Physics*, **24** (6), pp. 1196–1201.

Biolin Scientific (2014a), *Theory note 4: surface free energy - theory and calculations*, Tietäjäntie 2 fin-02130 Espoo, Finland.

Biolin Scientific (2014b), *Washburn Method*, Tietäjäntie 2 fin-02130 Espoo, Finland.

Booy, M. L. (1978), Geometry of fully wiped twin-screw equipment, *Polymer Engineering & Science*, **18** (12), pp. 973–984, ISSN: 1548-2634.

Bowen, J., ed. (Nov. 11, 2013a), *Liquid-Gas and Liquid-Liquid Interfaces*, Colloids & Rheology Course, (School of Chemical Engineering, University of Birmingham).

Bowen, J., ed. (Nov. 11, 2013b), *Solid-Liquid-Gas Interfaces*, Colloids & Rheology Course, (School of Chemical Engineering, University of Birmingham).

Brostow, W. (1983), Drag reduction and mechanical degradation in polymer solutions in flow, *Polymer*, **24** (5), pp. 631 –638, ISSN: 0032-3861.

Brun, N. L., I. Zadrazil, L. Norman, A. Bismarck, and C. N. Markides (2016), On the drag reduction effect and shear stability of improved acrylamide copolymers for enhanced hydraulic fracturing, *Chemical Engineering Science*, **146**, pp. 135 –143, ISSN: 0009-2509.

Bueche, F. (1960), Mechanical degradation of high polymers, *Journal of Applied Polymer Science*, **4** (10), pp. 101–106, ISSN: 1097-4628.

Campanelli, J. R., M. R. Kamal, and D. G. Cooper (1993), A kinetic study of the hydrolytic degradation of polyethylene terephthalate at high temperatures, *Journal of Applied Polymer Science*, **48** (3), pp. 443–451, ISSN: 1097-4628.

Cardinaud, R. (2013), Localization of MWCNTs in PET/LDPE blends, *European Polymer Journal*, (49), pp. 1287–1297.

Carneiro, O. S., G. Caldeira, and J. A. Covas (1999), Flow patterns in twin screw extruders, *Journal of Material Processing Technology*,

Carson, S. O., J. Covas, and J. Maia (Nov. 2015), A New Extensional Mixing Element for Improved Dispersive Mixing in Twin-Screw Extrusion, Part 1: Design and Computational Validation.

Carson, S. O., J. Maia, and J. A. Covas (2016), A New Extensional Mixing Element for Improved Dispersive Mixing in Twin-Screw Extrusion, Part 2: Experimental Validation for Immiscible Polymer Blends, *Advances in Polymer Technology*, ISSN: 1098-2329.

Caruso, M. M., D. A. Davis, Q. Shen, S. A. Odom, N. R. Sottos, S. R. White, and J. S. Moore (2009), Mechanically-Induced Chemical Changes in Polymeric Materials, *Chemical Reviews*, **109** (11), pp. 5755–5798.

Champion, J. (2015), *Use of Computational Fluid Dynamics to improve the layer thickness control of polyester based multilayered films*, Doctor of Engineering, University of Birmingham.

Connelly, R. K. and J. L. Kokini (2007), Examination of the mixing ability of single and twin screw mixers using 2D finite element method simulation with particle tracking, *Journal of Food Engineering*, **3** (79), pp. 956–969.

Coperion & K-tron (2014), *Application Example: High Performance Compounding*, URL: http://www.ktron.com/industries_served/Plastics/HiPerfCompounding.cfm (visited on June 18, 2015).

Cubeddu, A., C. Rauh, and A. Delgado (2014), 3D Thermo-Fluid Dynamic Simulations of High-Speed-Extruded Starch Based Products, *Open Journal of Fluid Dynamics*, **4**, pp. 103–114.

Cullen, P. (2009), *Food Mixing: Principles and Applications*, Wiley, ISBN: 9781444309881.

Cunha, S., A. Gaspar-Cunha, and J. A. Covas (2008), "Melting of PP/PA6 Polymer Blends in Single Screw Extruders–An Experimental Study", in: *Materials Science Forum*, vol. 587, Trans Tech Publ, pp. 505–509.

D'Almeida, A. R. and M. L. Dias (1997), Comparative study of shear degradation of carboxymethylcellulose and poly(ethylene oxide) in aqueous solution, *Polymer Degradation and Stability*, **56** (3), pp. 331 –337, ISSN: 0141-3910.

Darnell, W. H. and E. A. J. Mol (1956), Solids conveying in extruders, *SPE Journal*,

Davidson, M. W. (2017), *Resolution*, URL: https://www.microscopyu.com/microscopy-basics/resolution.

Dhakal, P., S. R. Das, H. Poudyal, and A. J. Chandy (2017), Numerical simulations of partially-filled rubber mixing in a 2-wing rotor-equipped chamber, *Journal of Applied Polymer Science*, **134** (2), ISSN: 1097-4628.

Diemert, J., C. Chilles, J. Colbert, T. Miri, A. Ingram, P. David, A. S. Fard, and P. D. Anderson (2011), Flow Visualisation in Co-rotating Twin Screw Extruders: Positron Emission Particle Tracking and Numerical Particle Trajectories, *International Polymer Processing*, **26** (5), pp. 540–550.

Domenech, T., E. Peuvrel-Disdier, and B. Vergnes (2011), "Influence of twin-screw processing conditions on structure and properties of polypropylene - organoclay nanocomposites", in: *27th World Congress of the Polymer Processing Society*, Marrakech, Morocco: Polymer Processing Society, pp. 1–10.

Domenech, T., E. Peuvrel-Disdier, and B. Vergnes (2013), The importance of specific mechanical energy during twin screw extrusion of organoclay based polypropylene nanocomposites, *Composites Science and Technology*, **75** (0), pp. 7 –14, ISSN: 0266-3538.

Donoian, G. S. and J. P. Christiano (1999), "Effect of Kneading Block Tip Clearance on Performance of Co-Rotating Twin-Screw Extruders", in: *ANTEC 1999 Plastics: Bridging the Millennia, Volume 1: Processing*, Annual Technical Conference, Society of Plastics Engineers, ISBN: 978-1-56676-805-4.

Dr Collin GmbH (2018), *Sportparkstrasse 2, D-85560 Ebersberg*.

DTF [DuPont Teijin Films U.K. Ltd.] (Aug. 2011), "Polyester Science Background", Wilton, U.K., DTF Internal Document.

DTF [DuPont Teijin Films U.K. Ltd.] (2013), *Innovation for Life*.

DuPont [DuPont Titanium Technologies] (2003), *DuPont Ti-Pure, Titanium Dioxide*, Wilmington, DE, USA.

Durin, A., P. D. Micheli, H. Nguyen, C. David, R. Valette, and B. Vergnes (2009), Comparison between 1D and 3D Approaches for Twin-Screw Extrusion Simulation, *nternational Polymer Processing Journal of the Polymer Processing Society*, (5).

Eitzlmayr, A., G. Koscher, G. Reynolds, Z. Huang, J. Booth, P. Shering, and J. Khinast (2014), Mechanistic modeling of modular co-rotating twin-screw extruders, *International Journal of Pharmaceutics*, (147), pp. 157–176.

Ellam, M. (2013a), *Extrusion Models*, Report, DuPont Teijin Films.

Ellam, M. (2013b), "TS Pressure Fill General Model".

Ellam, M. (Apr. 17, 2007), "Twin Screw Extrusion Overview", Wilton, U.K., DTF Internal Document.

Ellam, M. (Dec. 9, 2010), "Extrusion Technologies for PET - An Overview", Wilton, U.K., DTF Internal Document.

Emin, M. and H. Schuchmann (2013), Analysis of the dispersive mixing efficiency in a twin-screw extrusion processing of starch based matrix, *Journal of Food Engineering*, **115** (1), pp. 132 –143, ISSN: 0260-8774.

Eslami, H. (2015), *Understanding Screw Design for Film Extrusion Process*, version White Paper, MACRO Advanced Extrusion Systems, URL: http://www.macroeng.com/understanding-screw-design-for-film-extrusion-process.php (visited on June 15, 2015).

Flecke, J., H. Potente, and K. Kretschmer (2002), A Physico-Mathematical Model for the Dispersion Process in a Co-Rotating Intermeshing Twin Screw Extruder, *Journal of Reinforced Plastics and Composites*, **21** (6), pp. 507–515.

Fortunato, G., A. Tenniche, L. Gottardo, and R. Hufenus (2014), Development of poly-(ethylene terephthalate) masterbatches incorporating highly dispersed TiO2 nanoparticles: Investigation of morphologies by optical and rheological procedures, *European Polymer Journal*, **57**, pp. 75 –82, ISSN: 0014-3057.

Fukuda, G., R. Adnew, H. B. 2nd, J. Kim, and D. I. Bigio (2013), "An Expanded Residence Stress Distribution Study in a Twin-Screw Extruder: The Effect of Stress Bead Strength", in: *ANTEC 2013 - Proceedings of the Technical Conference & Exhibition, Cincinnati, Ohio, USA April 22-24, 2013*, Society of Plastics Engineers.

Gao, J., G. C. Walsh, D. Bigio, R. M. Briber, and M. D. Wetzel (2000), Mean residence time analysis for twin screw extruders, *Polymer Engineering & Science*, **40** (1), pp. 227–237, ISSN: 1548-2634.

Gao, W., B. Zhou, X. Ma, Y. Liu, Z. Wang, and Y. Zhu (2011), Preparation and characterization of BaSO4/poly(ethylene terephthalate) nanocomposites, *Colloids and Surfaces A: Physicochemical and Engineering Aspects*, **385**, pp. 181–187.

Gasner, G. E., D. Bigio, C. Marks, F. Magnus, and C. Kiehl (1999), A new approach to analyzing residence time and mixing in a co-rotating twin screw extruder, *Polymer Engineering & Science*, **39** (2), pp. 286–298, ISSN: 1548-2634.

Gautam, A. and G. S. Choudhury (1999), Screw configuration effects on starch breakdown during twin-screw extrusion of rice flour, *Journal of Food Processing and Preservation*, **23** (5), pp. 355–375, ISSN: 1745-4549.

Giles Jr., H. F., J. R. Wagner Jr., and E. M. Mount 3rd. (2005), *Extrusion: The Definitive Processing Guide and Handbook*, New York: William Andrew Publishing.

Gogos, C. G., M. Esseghir, D. B. Todd, and D. W. Yu (1996), Dispersive mixing in immiscible polymer blends, *Macromolecular Symposia*, **101** (1), pp. 185–198, ISSN: 1521-3900.

Goodman, P. and A. B. Bestul (1955), Temperature dependence of mechanical shear degradation, *Journal of Polymer Science*, **18** (88), pp. 235–244, ISSN: 1542-6238.

Goodman, P. (1957), Dependence of mechanical shear degradation of polymers in solution on rate of energy application and on concentration, *Journal of Polymer Science*, **25** (110), pp. 325–331, ISSN: 1542-6238.

Gotsis, A. D. and D. M. Kalyon (1989), "Simulation of mixing in co-rotaing twin screw extruders", in: *ANTEC : Society of Plastics Engineers Annual Technical Papers*, Annual Technical Conference.

Hansen, F. K. (2004), *The Measurement of Surface Energy of Polymers by Means of Contact Angles of Liquids on Solid Surfaces*, Department of Chemistry, University of Oslo.

Hensen, F. and H. Bongaerts (1979), title, *Plastverarbeiter*, **30** (618).

Hensen, F. (1988), *Plastics Extrusion Technology*, Munich: Hanser Publishers, ISBN: 3-446-14589-3.

Huang, H. X. and Y. C. Peng (1993), Fluid flow aspects of twin-screw extruder process: numerical simulations of TSE rheomixing, *Advances in Polymer Technology*, **12**, p. 343.

Huntsman (Jan. 2002), *A guide to Tioxide*, Calais, France.

Huntsman (Oct. 2007), *Tioxide, The new reference*, Billingham, U.K.

IVL (Oct. 10, 2017), *IVL Acquires DuPont Teijin Films: Delivering Value Through HVA and World - Class Culture of Innovation*, Presentation, Indorama Ventures.

Jaffer, S. A. (1998), *Experimental studies of static mixers and twin screw extruders*, Doctor of Philosophy (Chemical Engineering), McMaster University.

Kajiwara, T. and Y. Nakayama (2011), Capturing the Efficiency of a Melt-Mixing Process for Polymer Processing, *JOURNAL OF CHEMICAL ENGINEERING OF JAPAN*, **44** (11), 831–839", ISSN: 0021-9592.

Kalyon, D. M. and H. Sangani (1989a), "Characterization of distributive mixing in fully-intermeshing, co-rotating twin screw extruders", in: *ANTEC : Society of Plastics Engineers Annual Technical Papers*, Annual Technical Conference, pp. 124–128.

Kalyon, D. M. (1989), "{CHAPTER} 8 - Applications of continuous mixers", in: *Handbook of Polymer Science and Technology*, ed. by N. P. Cheremisinoff, vol. 3, New York: Marcel Dekker, pp. 373 –417.

Kalyon, D. M. and H. N. Sangani (1989b), An experimental study of distributive mixing in fully intermeshing, co-rotating twin screw extruders, *Polymer Engineering and Science*, **29** (15), pp. 1018–1026, ISSN: 1548-2634.

Kalyon, D. M., A. D. Gotsis, U. Yilmazer, C. G. Gogos, H. Sangani, B. Aral, and C. Tsenoglou (1988a), Development of experimental techniques and simulation methods to analyze mixing in co-rotating twin screw extrusion, *Advances in Polymer Technology*, **8** (4), pp. 337–353, ISSN: 1098-2329.

Kalyon, D. M., A. D. Gotsis, C. G. Gogos, and C. Tsenoglou (1988b), "Simulation Of The Mixing Of Highly Filled Suspensions In The Co-Rotating Twin Screw Extrusion Process", in: vol. 0872, pp. 71–78.

Kalyon, D. M., C. Jacob, and P. Yaras (1991), An experimental study of the degree of fill and melt densification in fully-intermeshing, co-rotating twin screw extruders, *Plastics, Rubber and Composites Processing and Applications*, **16**, pp. 193–200.

Kasaliwal, G., A. Göldel, and P. Pötschke (2009), Influence of processing conditions in small-scale melt mixing and compression molding on the resistivity and morphology of polycarbonateâĂŞMWNT composites, *Journal of Applied Polymer Science*, **112** (6), pp. 3494–3509, ISSN: 1097-4628.

Kasaliwal, G. R., S. Pegel, A. Göldel, P. Pötschke, and G. Heinrich (2010), Analysis of agglomerate dispersion mechanisms of multiwalled carbon nanotubes during melt mixing in polycarbonate, *Polymer*, **51** (12), pp. 2708–2720.

Kasaliwal, G. R., A. Göldel, P. Pötschke, and G. Heinrich (2011), Influences of polymer matrix melt viscosity and molecular weight on MWCNT agglomerate dispersion, *Polymer*, **52** (4), pp. 1027–1036.

Kasaliwal, G. R. (Mar. 1, 2011), *Analysis of multiwalled carbon nanotube agglomerate dispersion in polymer melts*, PhD Thesis, Technischen Universität Dresden.

Kelly, A., ed. (2013), *Fundamentals of Extrusion Processing*, (University of Bradford), IRC in Polymer Engineering.

Kimura, M., S. Kataoka, and K. Tsutsumi (2000), A study on the surface free energy of modified silica fillers and poly(ethylene terephthalate) fibers by inverse gas chromatography, *Colloid and Polymer Science*, **278** (9), pp. 848–854.

Kohlgrüber, K. (2008), *Co-Rotating Twin Screw Extruders - Fundamentals, Technology and Applications*, Munich: Hanser Publishers.

KraussMaffei Berstorff GmbH (1989), *An der Breiten Wiese 3-530625, Hannover.*

Kutz, M. (2011), *Applied Plastics Engineering Handbook: Processing and Materials*, Oxford: William Andrew.

Kwang-Jea, K. and J. L. White (2000), Breakdown of Silica Agglomerates and Other Particles during Mixing in an Internal Mixer and Their Procesing Character, *Journal of Industrial and Engineering Chemistry*, **6** (4), pp. 262–269.

Lafleur, P. G., F. Berzin, M. Grmela, S. R. Tremblay, and B. Vergnes (2000), "Simulation of CaCO3 Dispersion in a PP Matrix during Twin Screw Extrusion", in: *ANTEC 2000 Plastics: The Magical Solution, Volume 1: Processing*, Annual Technical Conference, Society of Plastics Engineers, ISBN: 978-1-56676-957-0.

Larsen, H. A. and H. G. Drickamer (1957), Mechanical Degradation and Cross Linking of Polymers by Plastic Deformation at High Pressure, *The Journal of Physical Chemistry*, **61** (12), pp. 1643–1646.

Launay, A., F. Thominette, and J. Verdu (1994), Hydrolysis of poly(ethylene terephthalate): A kinetic study, *Polymer Degradation and Stability*, **46** (3), pp. 319–324.

Lawal, A. and D. M. Kalyon (1995), Mechanisms of mixing in single and co-rotating twin screw extruders, *Polymer Engineering & Science*, **35** (17), pp. 1325–1338, ISSN: 1548-2634.

Lawal, A., D. M. Kalyon, and Z. Ji (1993), Computational study of chaotic mixing in co-rotating two-tipped kneading paddles: Two-dimensional approach, *Polymer Engineering & Science*, **33** (3), pp. 140–148, ISSN: 1548-2634.

Lee, K. T., A. Ingram, and N. A. Rowson (2012), Twin screw wet granulation: The study of a continuous twin screw granulator using Positron Emission Particle Tracking (PEPT) technique, *European Journal of Pharmaceutics and Biopharmaceutics*, **81** (3), pp. 666 –673, ISSN: 0939-6411.

Leistritz GmbH (Dec. 18, 2014), *Refreshing extrusion technology.*

Levresse, P, I Manas-Zloczower, D. Feke, Y Bomal, and D Bortzmeyer (1999), Observation and analysis of the infiltration of liquid polymers into calcium carbonate agglomerates, *Powder Technology*, **106** (1 - 2), pp. 62 –70, ISSN: 0032-5910.

Liang, W. and M. P. Enright (2012), Estimating the probabilistic size and shape distributions of 3D anomalies from sectioning measurements using the stereological unfolding approach, *Journal of engineering for gas turbines and power*, **134** (5), p. 052506.

Liestritz (Oct. 10, 2015), *Refreshing extrusion technology.*

Linjie, Z. and G. Xiaozheng (2000), "Physical Model of Polymer Pellets Melting in Co-Rotating Twin-Screw Extrusion", in: *ANTEC 2000 Plastics: The Magical Solution, Volume 1: Processing*, Annual Technical Conference, Society of Plastics Engineers, pp. 149–155, ISBN: 978-1-56676-957-0.

Looney, K., G. Williams, K. Soulsby, J. Lewis, and D. Li (Aug. 1, 2016), "Polyhand - A Polymer Handling Model", Wilton, U.K., DTF Internal Document.

Lopez-Sanchez, M. A. (Mar. 23, 2016), *GrainSizeTools script*, URL: http://dx.doi.org/10.6084/m9.figshare.1383130.

Lopez-Sanchez, M. A. (Aug. 4, 2017), *Grain Size Tools*.

MacDonald, W. A. (2002), *Polyester Films*, in: *Encyclopedia of Polymer Science and Technology*, John Wiley and Sons, Inc., ISBN: 9780471440260.

MacDonald, W. A., M. K. Looney, D. MacKerron, R. Eveson, R. Adam, K. Hashimoto, and K. Rakos (2007), Latest advances in substrates for flexible electronics, *Journal of the Society for Information Display*, **15** (12), pp. 1075–1083, ISSN: 1938-3657.

MacKerron, D. (2013), Wilton, U.K., DTF Internal Document.

Maddock, B. H. (1959), A visual analysis of flow and mixing in extruder screws, *SPE Journal*, **15**, pp. 383–389.

Manas-Zloczower, I. (2009), *Mixing and Compounding of Polymers: Theory and Practice*, Hanser, ISBN: 9783446407732.

Manas-Zloczower, I. and H. Cheng (1996), Analysis of mixing efficiency in polymer processing equipment, *Macromolecular Symposia*, **112** (1), pp. 77–84, ISSN: 1521-3900.

Markarian, J. (2002), Twin screw extruder simulation programs - what can they offer?, *Plastics Additives & Compounding*,

Markarian, J. (2005), Compounders look to simulation software for savings in time and costs, *Plastics Additives & Compounding*,

Martin, C. (2013), *Twin Screw Extrusion for Pharmaceutical Processes*, in: Repka, M. A., N. Langley, and J. DiNunzio, *Melt Extrusion*.

Martin, C. (Feb. 22, 2012), "Twin screw extrusion systems to process PLA more efficiently", in: Innovation takes root 2012, Leistritz.

Martin, C. (July 16, 2014), "Devolatilization via Twin screw Extrusion: Theory, Tips and Test Results", in: Plastics Extrusion Asia 2014, Leistritz.

Morton-Jones, D. H. (1989), *Polymer Processing*, London: Chapman and Hall.

Murphy, J. (2001), "{CHAPTER} 21 - Background Information: Equipment âĂŞ Mixing, Compounding, and Dosing", in: *Additives for Plastics Handbook (Second Edition)*, ed. by J. Murphy, Second Edition, Amsterdam: Elsevier Science, pp. 245 –255, ISBN: 978-1-85617-370-4.

Nakayama, Y., E. Takeda, T. Shigeishi, H. Tomiyama, and T. Kajiwara (2011), Melt-mixing by novel pitched-tip kneading disks in a co-rotating twin-screw extruder, *Chemical Engineering Science*, **66** (1), pp. 103 –110, ISSN: 0009-2509.

Natarajan, V., C. L. Wilson, S. L. Hayward, and S. Kidambi (Aug. 7, 2015), Titanium Dioxide Nanoparticles Trigger Loss of Function and Perturbation of Mitochondrial Dynamics in Primary Hepatocytes, *PLOS ONE*,

Oberlehner, J., P. Cassagnau, and A. Michel (1994), Local residence time distribution in a twin screw extruder, *Chemical Engineering Science*, **49** (23), pp. 3897 –3907, ISSN: 0009-2509.

Owens, D. K. and R. C. Wendt (1969), Estimation of the Surface Free Energy of Polymers, *Journal of Applied Polymer Science*, **13**, pp. 1741 –1747.

Padmanabhan, B. and C. C. Jayanth (Mar. 2008), Understanding the extruder processing zones: the heart of a twin screw extruder, *Plastics Additives & Compounding*, pp. 30–35.

Potente, H., J. Ansahl, and B. Klarholz (1994), Design of Tightly Intermeshing Co-Rotating Twin Screw Extruders, *International Polymer Processing*, **9** (1), pp. 11–25.

Powder and Bulk Solids (Mar. 2016), *Loss-in-Weight Screw Feeders: Screw Trough Agitation and Screw Alternatives*, URL: http://www.powderbulksolids.com/article/Loss-in-

Weight-Screw-Feeders-Screw-Trough-Agitation-and-Screw-Alternatives-03-28-2016 (visited on Sept. 3, 2017).

Rakos, K. (Apr. 28, 2016), "Meeting with Grace".

Ram, A. and A. Kadim (1970), Shear degradation of polymer solutions, *Journal of Applied Polymer Science*, **14** (8), pp. 2145–2156, ISSN: 1097-4628.

Ramos, E., W. A. Pardo, M. Mir, and J. Samitier (2017), Dependence of carbon nanotubes dispersion kinetics on surfactants, *Nanotechnology*, **28** (13), p. 135702.

Rauwendaal, C. (1986), *Polymer Extrusion*, Munich: Hanser Publishers, ISBN: 3-446-14196-0.

Rauwendaal, C. (1996a), Comparison of two melting models, *Advances in Polymer Technology*, **15** (2), pp. 135–144, ISSN: 1098-2329.

Rauwendaal, C. (1996b), The geometry of self-cleaning twin-screw extruders, *Advances in Polymer Technology*, **15** (2), pp. 127–133, ISSN: 1098-2329.

Rauwendaal, C. (2010), *Understanding Extrusion*, 2nd ed., Munich: Hanser Publishers, ISBN: 978-3-446-41686-4.

Rauwendaal, C. (2016), Heat transfer in twin screw compounding extruders, *AIP Conference Proceedings*, **1779** (1), p. 030014.

Remmler, T., ed. (Oct. 15, 2015), *Understanding the Link between Particle Properties and Rheology of Suspensions*, testXpo.

Reynolds, A., ed. (2004), *The World Masterbatch Market*, AMI Conference Masterbatch 2004, Cologne.

Rideal, G. R. and J. C. Padget (1976), The thermal-mechanical degradation of high density polyethylene, *Journal of Polymer Science: Polymer Symposia*, **57** (1), pp. 1–15, ISSN: 1936-0959.

Romão, W., M. F. Franco, Y. E. Corilo, M. N. Eberlin, M. A. Spinacé, and M.-A. D. Paoli (2009), Poly (ethylene terephthalate) thermo-mechanical and thermo-oxidative degradation mechanisms, *Polymer Degradation and Stability*, **94** (10), pp. 1849 –1859, ISSN: 0141-3910.

Ross, J. (Nov. 13, 2009), *ImageJ Seminar: Introduction to Image Analysis*, Guide, The University of Auckland.

Rudersdorf, T., ed. (Nov. 4, 2014), *Compounding of $CaCO_3$ Formulation, Liestritz compounding workshop*, Nuremberg, Germany.

Saltikov, S. A. (1967), *The Determination of the Size Distribution of Particles in an Opaque Material from a Measurement of the Size Distribution of Their Sections*, in: *Stereology: Proceedings of the Second International Congress for STEREOLOGY, Chicago—April 8–13, 1967*, ed. by H. Elias, Berlin, Heidelberg: Springer Berlin Heidelberg, pp. 163–173, ISBN: 978-3-642-88260-9.

Schöppner, V., T. Herken, and N. Fecke (2014), "Experimental Analysis of the Material Degradation of PET on a Co-Rotating Twin-Screw Extruder", in: *ANTEC 2014 - Proceedings of the Technical Conference & Exhibition, Las Vegas, Nevada, USA April 28-30, 2014*, Society of Plastics Engineers, ISBN: 978-0-9850112-4-6.

Schott, H. and W. S. Kaghan (1963), Viscous flow and degradation of molten polypropylene, *Polymer Engineering and Science*, **3** (2), pp. 145–151, ISSN: 1548-2634.

Schulze, D. (2008), *Powder and Bulk Solids - Characterization, Storage and Flow*, 3rd ed., Heidelberg.

Seyvet, O. and P. Navard (2000), Collision-induced dispersion of agglomerate suspensions in a shear flow, *Journal of Applied Polymer Science*, **78** (5), pp. 1130–1133, ISSN: 1097-4628.

Shah, A. and M. Gupta (2004), "Comparison of the flow in co-rotating and counter-rotating twin-screw extruders", in: *ANTEC 2004 : Society of Plastics Engineers Annual Technical Papers*, Annual Technical Conference, Society of Plastics Engineers, pp. 444–447.

Shanshool, J., M. F. A. Jabbar, and I. N. Slaiman (2011), The influence of mechanical effects on degradation of polyisobutylenes as drag reducing agents, *Petroleum and Coal*, **53** (3), pp. 218–222, ISSN: 1337-7027.

Shortall, S. (Nov. 13, 2015), *Determination of Intrinsic Viscosity by 8 % w/v o-Chlorophenol Solution*.

Siebold, A., M. Nardin, J. Schultz, A. Walliser, and M. Oppliger (2000), Effect of dynamic contact angle on capillary rise phenomena, *Colloids and Surfaces A: Physicochemical and Engineering Aspects*, **161** (1), pp. 81 –87, ISSN: 0927-7757.

SITA Process Solutions (2015), *Process parameter surface tension*, URL: http://www.sita-process.com/information-service/process-parameter-surface-tension/ (visited on Mar. 23, 2015).

Stevens, M. J. and J. A. Covas (1995), *Extruder principles and operation*, 2nd ed., London: Chapman and Hall.

Steward, E. (2000), "Melt Temperature Considerations for Extrusion", in: *ANTEC 2000 Plastics: The Magical Solution, Volume 1: Processing*, Annual Technical Conference, Society of Plastics Engineers, ISBN: 978-1-56676-957-0.

Tadmor, Z. (1966), Fundamentals of plasticating extrusion. I. A theoretical model for melting, *Polymer Engineering and Science*, **6** (3), pp. 185–190, ISSN: 1548-2634.

Tadmor, Z. and C. G. Gogos (2006), *Principles of Polymer Processing*, 2nd ed., New Jersey: John Wiley & Sons.

Tang, H, L. C. Wrobel, and Z Fan (2003), Fluid flow aspects of twin-screw extruder process: numerical simulations of TSE rheomixing, *Modelling and Simulation in Materials Science and Engineering*, **11** (5), p. 771.

Tarverdi, K., P. Allan, and S. Sentikaew (2014), "Using Twin Screw Extrusion Technology to Determine the Effects of Surfactant Concentrations by Melt Blending Organoclays with PET Nanocomposites", in: *ANTEC 2014 - Proceedings of the Technical Conference & Exhibition, Las Vegas, Nevada, USA April 28-30, 2014*, Society of Plastics Engineers, ISBN: 978-0-9850112-4-6.

Tayeb, J., B. Vergnes, and G. D. Valle (1988), A Basic Model for a Twin Screw Extruder, *Journal of Food Science*, **53** (4), pp. 1047–1056.

TDSC [Titanium Dioxide Stewardship Council] (Aug. 2012), *About Titanium Dioxide*, Washington, D.C., USA.

Thummert, M. (2013), "Comparing high screw energy input (HSEI) twin screw extruders with 1.5 and 1.66 OD/ID ratios", in: EUROTEC.

Todd, D. B. and D. K. Baumann (1978), Twin screw reinforced plastics compounding, *Polymer Engineering & Science*, **18** (4), pp. 321–325, ISSN: 1548-2634.

Todd, D. B. (1975), Residence time distribution in twin-screw extruders, *Polymer Engineering & Science*, **15** (6), pp. 437–443, ISSN: 1548-2634.

Tomas, J. (2007), Adhesion of ultrafine particles a micromechanical approach, *Chemical Engineering Science*, **62** (7), pp. 1997 –2010, ISSN: 0009-2509.

Tomiyama, H., S. Takamoto, H. Shintani, and S. Inoue (2009), Devolatilization Analysis in a Twin Screw Extruder by using the Flow Analysis Network (FAN) Method, *Seikei-Kakou*, **19**, pp. 565–574.

Töpfer, O. and S. Fraas, eds. (Nov. 4, 2014), *Ideal compounding of flame-retardant formulations*, *Liestritz compounding workshop*, Nuremberg, Germany.

Uphus, R., O. Skibba, R. H. Schuster, and U. Gorl (2000), Continious Mixing of powder rubber on twin screw extruders, *Machinery and Equipment*, **53** (5), pp. 279–289.

Vaia, R. A., K. D. Jandt, E. J. Kramer, and E. P. Giannelis (1995), Kinetics of Polymer Melt Intercalation, *Macromolecules*, **28** (24), pp. 8080–8085.

Venkatachalam, S., S. G. Nayak, J. V. Labde, P. R. Gharal, K. Rao, and A. K. Kelkar (Sept. 26, 2012), *Degradation and Recyclability of Poly (Ethylene Terephthalate)*, in: *Polyester*, pp. 75–98.

Vergnes, B., C. Barrès, and J. Tayeb (1992), Computation of residence time and energy distributions in the reverse screw element of a twin-screw extrusion-cooker, *Journal of Food Engineering*, **16** (3), pp. 215 –237, ISSN: 0260-8774.

Villmow, T., P. Pötschke, S. Pegel, L. Häussler, and B. Kretzschmar (2008), Influence of twin-screw extrusion conditions on the dispersion of multi-walled carbon nanotubes in a poly(lactic acid) matrix, *Polymer*, **49** (16), pp. 3500 –3509, ISSN: 0032-3861.

Villmow, T., B. Kretzschmar, and P. PÃűtschke (2010), Influence of screw configuration, residence time, and specific mechanical energy in twin-screw extrusion of polycaprolactone/multi-walled carbon nanotube composites, *Composites Science and Technology*, **70** (14), pp. 2045 –2055, ISSN: 0266-3538.

Wagner, H. L. (1985), The Mark - Houwink - Sakurada Equation for the Viscosity of Linear Polyethylene, *Journal of Physical Chemistry*, **14** (2), pp. 611 –617.

Wang, N. H. (2001), Polymer Extrusion Devolatilization, *Chemical Engineering and Technology*, **24** (9), pp. 957–961, ISSN: 1521-4125.

Weinmann, M. (2007), Masterbatch production on co-rotating twin screw extruders, *Plastics, Additives & Compounding*, **March**, pp. 36–39.

White, J. a. (1990), *Twin Screw Extrusion: Technology and Principles*, Hanser Publishers.

Wiedmann, W. and M. Holzel (2009), *Twin-Screw Extruders in Ceramic Extrusion*, in: *Extrusion in Ceramics*, ed. by F. Handle, Berlin: Springer.

Wilczynski, K., A. Nastaj, K. J. Wilczynski, and A. Lewandowski (2013), Melting in starve-fed single screw extrusion, *SPE Plastics Research Online*,

Williams, A. M., C. P. Garner, and J. G. Binner (2008), Measuring Pore Diameter Distribution of Gelcast Ceramic Foams from Two-Dimensional Cross Sections, *Journal of the American Ceramic Society*, **91** (9), pp. 3113–3116.

Wu, S. (1971), Calculation of interfacial tension in polymer systems, *Journal of Polymer Science, Part C*, (34), pp. 19 –30.

Yamada, H, I Manas-Zloczower, and D. Feke (1997), Influence of matrix infiltration on the dispersion kinetics of carbon black agglomerates, *Powder Technology*, **92** (2), pp. 163 –169, ISSN: 0032-5910.

Yamada, H., I. Manas-Zloczower, and D. L. Feke (1998), The Influence of Matrix Viscosity and Interfacial Properties on the Dispersion Kinetics of Carbon Black Agglomerates, *Rubber Chemistry and Technology*, **71** (1), pp. 1–16.

Yerramilli, L and M. Karwe (2004), Velocity distributions and mixing in the translational region of a kneading section in a co-rotating twin-screw extruder, *Food and bioproducts processing*, **82** (1), pp. 5–12.

Young, K., A. Lim, and P. G. Anderson (Mar. 15, 2013), Techniques and options for improved twin screw compounding of reinfirced polyolefins, *Plastics Technology*,

Yu, J. F. S., J. L. Zakin, and G. K. Patterson (1979), Mechanical degradation of high molecular weight polymers in dilute solution, *Journal of Applied Polymer Science*, **23** (8), pp. 2493–2512, ISSN: 1097-4628.

Zenkiewicz, M. (2007), Methods for the calculation of surface free energy of solids, *Journal of Achievements in Materials and Manufacturing Engineering*, **24** (1), pp. 137 –145.

Zhang, X.-M., L.-F. Feng, S. Hoppe, and G.-H. Hu (2008), Local residence time, residence revolution, and residence volume distributions in twin-screw extruders, *Polymer Engineering & Science*, **48** (1), pp. 19–28, ISSN: 1548-2634.

Zimmerman, H. and N. T. Kim (1980), Investigations on thermal and hydrolytic degradation of poly(ethylene terephthalate), *Polymer Engineering and Science*, **20** (10), pp. 680–683, ISSN: 1548-2634.